The *XYZ* states: experimental and theoretical status and perspectives

Nora Brambilla[l,m], Simon Eidelman[b,k,h], Christoph Hanhart[f,*], Alexey Nefediev[h,i,j], Cheng-Ping Shen[e,a,*], Christopher E. Thomas[d], Antonio Vairo[l], Chang-Zheng Yuan[g,c]

[a]*School of Physics and Nuclear Energy Engineering, Beihang University, Beijing 100191, China*
[b]*Budker Institute of Nuclear Physics, SB RAS, Novosibirsk 630090, Russia*
[c]*University of Chinese Academy of Sciences, Beijing 100049, China*
[d]*DAMTP, University of Cambridge, Wilberforce Road, Cambridge CB3 0WA, UK*
[e]*Key Laboratory of Nuclear Physics and Ion-beam Application and Institute of Modern Physics, Fudan University, Shanghai 200433, China*
[f]*Institute for Advanced Simulation, Institut für Kernphysik and Jülich Center for Hadron Physics, Forschungszentrum Jülich, Jülich D-52425, Germany*
[g]*Institute of High Energy Physics, Chinese Academy of Sciences, Beijing 100049, China*
[h]*P.N. Lebedev Physical Institute of the Russian Academy of Sciences, Leninskiy Prospect 53, Moscow 119991, Russia*
[i]*Moscow Institute of Physics and Technology, Institutsky lane 9, Dolgoprudny, Moscow Region 141700, Russia*
[j]*National Research Nuclear University MEPhI, Kashirskoe highway 31, Moscow 115409, Russia*
[k]*Novosibirsk State University, Novosibirsk 630090, Russia*
[l]*Physik Department, Technische Universität München, Garching D-85748, Germany*
[m]*Institute for Advanced Study, Universität München, Lichtenbergstrasse 2 a, Garching D-85748, Germany*

Abstract

The quark model was formulated in 1964 to classify mesons as bound states made of a quark-antiquark pair, and baryons as bound states made of three quarks. For a long time all known mesons and baryons could be classified within this scheme. Quantum Chromodynamics (QCD), however, in principle also allows the existence of more complex structures, generically called exotic hadrons or simply exotics. These include four-quark hadrons (appearing, e.g., as compact tetraquarks or hadronic molecules), five-quark hadrons (pentaquarks) and states with active gluonic degrees of freedom (hybrids), and even states of pure glue (glueballs). Exotic hadrons have been systematically searched for in numerous experiments for many years. Remarkably, in the past fifteen years, many new hadrons that do not exhibit the expected properties of ordinary (not exotic) hadrons have been discovered in the quarkonium spectrum. These hadrons are collectively known as *XYZ* states. Some of them, like the charged states, are undoubtedly exotic. Parallel to the experimental progress, the last decades have also witnessed an enormous theoretical effort to reach a theoretical understanding of the *XYZ* states. Theoretical approaches include not only phenomenological extensions of the quark model to exotics, but also modern non-relativistic effective field theories and lattice QCD calculations. The present work aims at reviewing the rapid progress in the field of exotic *XYZ* hadrons over the past few years both in experiments and theory. It concludes with a summary on future prospects and challenges.

Keywords: Quarkonium, exotic hadrons, *B* factories, LHC experiments, BES, potential models, effective field theories, lattice QCD

Contents

---

*Corresponding author
Email addresses: `nora.brambilla@ph.tum.de` (Nora Brambilla), `eidelman@mail.cern.ch` (Simon Eidelman), `c.hanhart@fz-juelich.de` (Christoph Hanhart), `nefediev@lebedev.ru` (Alexey Nefediev), `shencp@fudan.edu.cn` (Cheng-Ping Shen), `C.E.Thomas@damtp.cam.ac.uk` (Christopher E. Thomas), `antonio.vairo@ph.tum.de` (Antonio Vairo), `yuancz@ihep.ac.cn` (Chang-Zheng Yuan)

1. Introduction

1.1. Some generalities

Hadrons are described in the Standard Model by Quantum Chromodynamics (QCD), the theory of the strong interactions. QCD is based on the gauge symmetry group SU(3), whose quantum number is called 'color'. At the most fundamental level its degrees of freedom are quarks (q)[1], antiquarks $(\bar{q})$ and gluons (g), the last ones being the SU(3) gauge bosons [1]. The fact that SU(3) is a non-Abelian group makes QCD a very different theory from Quantum Electrodynamics (QED), the theory of the electromagnetic interactions, and accordingly the phenomenology of hadrons is very different from the one of atoms. Gluons, in contrast to photons, carry a (color) charge, self-interact, antiscreen the vacuum, and are at the origin of such highly nontrivial phenomena in QCD as asymptotic freedom and color confinement. Asymptotic freedom guarantees that high-energy properties of QCD can be computed in weak-coupling perturbation theory [2, 3]. On the other hand, color confinement, which implies that all detected hadrons are singlets (neutral) under color SU(3), sets in at low energies, where weak-coupling perturbation theory fails. Both energy scales are relevant for the formation of heavy hadrons.

The simplest color-singlet quark combinations that can be formed are $\bar{q}q$ and qqq. For a long time, all known hadrons could be explained in terms of the quark model where mesons are bound states of a constituent quark and antiquark, and baryons are bound states of three constituent quarks. However, the requirement of color neutrality still allows for more complicated structures, as was already recognised by Gell-Mann in one of the first publications on the quark model [4], like $\bar{q}\bar{q}qq$, $\bar{q}\bar{q}\bar{q}qqq$, $\bar{q}qqqq$, and so on. In QCD additional states are, in principle, possible like hybrids whose quantum numbers are determined by their quark, antiquark and gluon content: as gluons carry a color charge they can play a much more active role in the formation of a state than photons in atoms. One even expects 'glueballs' whose quantum numbers are determined exclusively by their gluonic content. We will refer to any state which does not appear to fit with the expectations for an ordinary $\bar{q}q$ or qqq hadron in the quark model as 'exotic'.

Some of these exotics have quantum numbers that cannot be reproduced by ordinary hadrons. In this case, the identification of these states as exotic is straightforward. In the other cases, the distinction requires a careful analysis of experimental observations and theoretical predictions as will be also discussed in some detail in this review.

There are various candidates for exotics in the light-quark sector, e.g., the light scalar mesons. Nevertheless, at the beginning of the century, no candidates for states beyond ordinary hadrons containing heavy quarks had been found. This was even more the case for mesons made of a heavy quark and a heavy antiquark, called quarkonia: The quark model showed excellent agreement with the data both in the charmonium ($\bar{c}c$ quarkonia) and in the bottomonium ($\bar{b}b$ quarkonia) sectors. The situation changed dramatically in 2003 when Belle observed a structure in the $\pi\pi J/\psi$ final state [5], the $X(3872)$. The properties of the new state did not fit those of an ordinary quarkonium, although it definitely contained a charm-anticharm pair. The assumption that the $X(3872)$ contains the charm-anticharm pair observed in the final state is motivated by the strong suppression of the heavy quark-antiquark pair creation within QCD. After the discovery of the $X(3872)$, many more hadrons were found in processes with final states containing a heavy quark and antiquark, but with properties at odds with those expected for ordinary quarkonia. Among these new states, those that carry an electric charge stick out. Since they must contain, in addition to a heavy quark-antiquark pair, at least a light quark-antiquark pair, they immediately qualify as exotics. For states that from their quantum numbers could be quark-antiquark mesons, but show properties inconsistent with expectations from established quark models, sometimes the term crypto-exotic is used.

The candidates for exotic states were dubbed by the experimental collaborations either X(mass), or Y(mass), or Z(mass), and are usually referred to collectively as XYZ states. Y(mass) is usually used for exotics with vector quantum numbers, i.e., $J^{PC} = 1^{--}$ where J is the spin, P is the parity and C is the charge-conjugation quantum number. Meanwhile, the Particle Data Group (PDG) has proposed a new naming scheme [6] which is briefly reviewed in Sec. 1.2.

The spectrum in the $\bar{c}c$ sector is shown in Fig. 1. Only states with known quantum numbers are included in the figure and, in all cases, the primary name according to the PDG is used. In addition, we also show with dotted lines some thresholds for decays into open-flavour states. To not overload the figure, thresholds with hidden strangeness are not shown. States that show quantum numbers incompatible with the quark model are clearly exotic. For the states

---

[1]For a heavy quark a capital letter Q $(\bar{Q})$ for the (anti)quark may be used in what follows to stress its large mass.
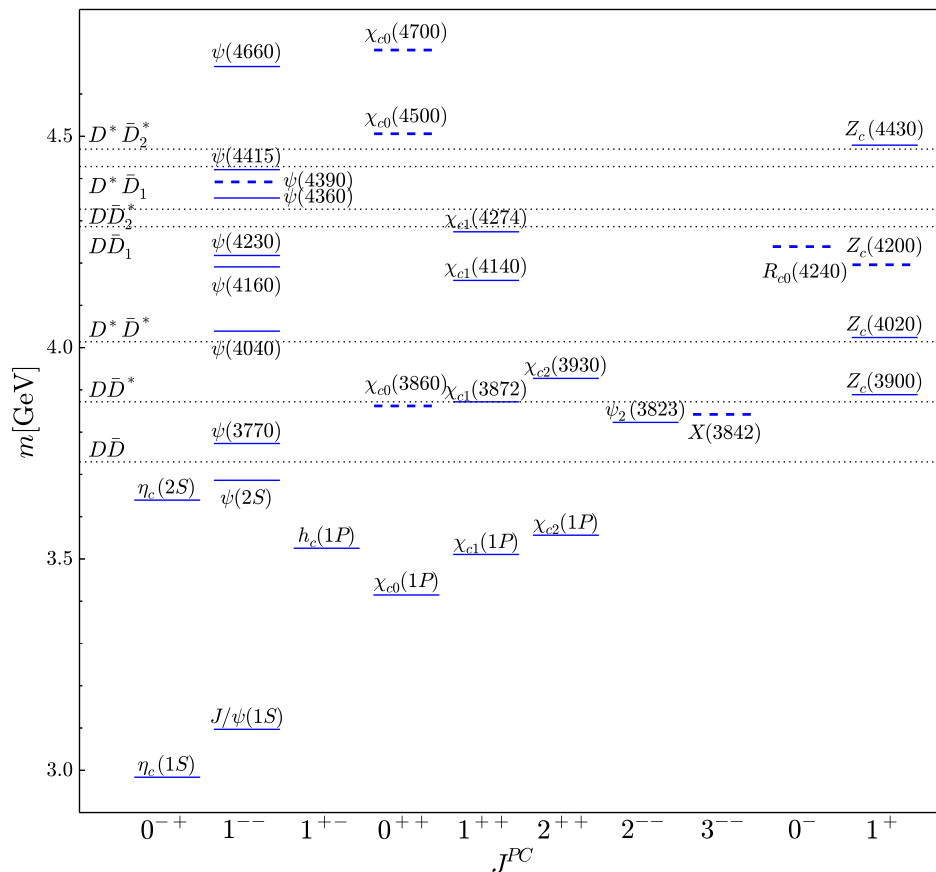
Figure 1: The spectrum of states in the $\bar{c}c$ sector as of July 2019. Thin solid lines represent the states established experimentally and dashed lines are for those that are claimed but not (yet) established (following the approach used by PDG, we regard a state as established if it is seen in different modes). States whose quantum numbers are undetermined are not shown. States in the plot are labeled according to the PDG primary naming scheme — see Sec. 1.2 for further details and for the correspondence with the *XYZ* naming scheme. Dashed lines show some relevant thresholds that open in the considered mass range; here D_1 stands for $D_1(2420)$ and D_2^* for $D_2^*(2460)$. Thresholds with hidden strangeness or involving broad states are not shown. The states shown in the two columns to the right are isovectors containing a $\bar{c}c$ pair; they are necessarily exotic.

in Fig. 1, this applies to the isovector states displayed in the two rightmost columns. In the other cases, there is no general rule when a state should carry the label exotic and when it is an ordinary $\bar{c}c$ state. However, there is consensus that all states below the lowest open-flavour threshold ($\bar{D}D$) are ordinary states. Moreover, also the properties of the vector states $\psi(3770)$, $\psi(4040)$ and $\psi(4160)$ and of the tensor state $\psi_2(3823)$ appear to agree with those of ordinary quarkonia. All the other states may or may not be exotic and will be discussed in this report. As of today, in the charmonium sector the number of experimentally established exotic candidates is similar to the number of ordinary states. In the bottomonium sector, on the other hand, only two exotics are established and they are both charged. The states in the $\bar{b}b$ spectrum are shown in Fig. 2.

Some of the exotic candidates reside rather close to open-flavour thresholds, however, the impact these thresholds have on the states is not clear yet. A possibility is that they induce kinematic enhancements, so that not all of the observed signals may correspond to new states in the QCD spectrum. Nevertheless, as we will argue in this review, most of them certainly do correspond to new states. From a comparison of Figs. 1 and 2 one can see that
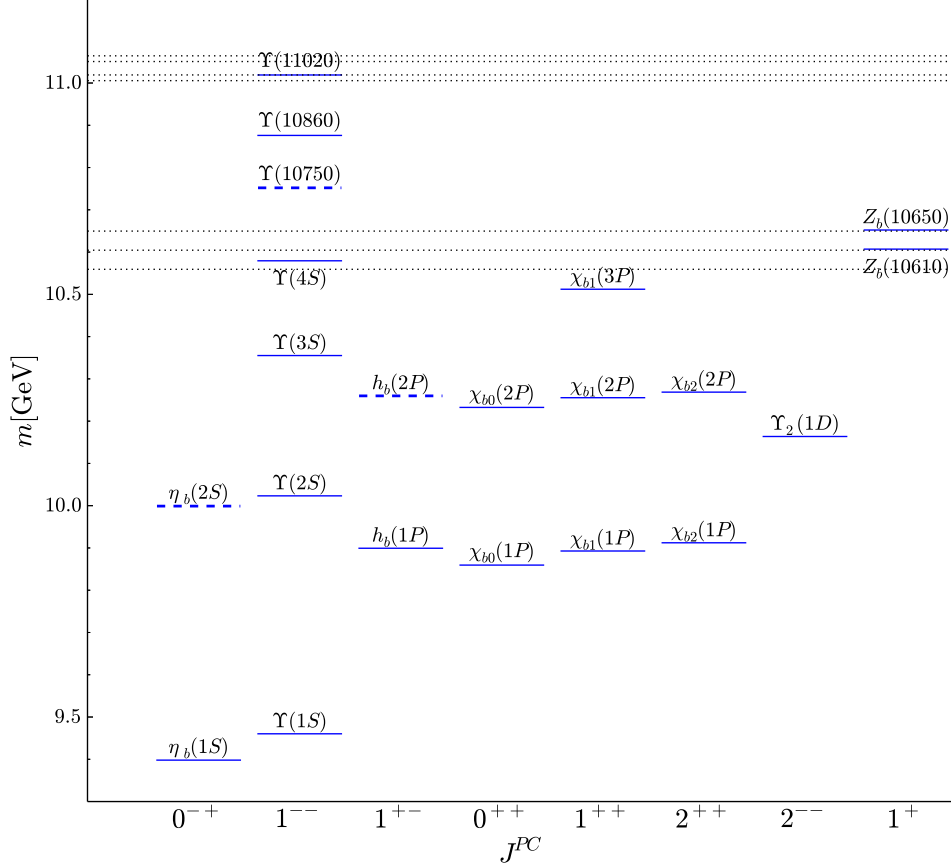
4

Figure 2: The same as in Fig. 1 but for the states in the $\bar{b}b$ spectrum. Dashed lines show the open-bottom thresholds (from the lowest upwards) $\bar{B}B$, $\bar{B}B^*$, $\bar{B}^*B^*$, $\bar{B}B_1(5721)$, $\bar{B}B_2^*(5747)$, $\bar{B}^*B_1(5721)$, and $\bar{B}^*B(5747)$. Given its large statistical significance (6.7 standard deviations) we have included the $\Upsilon(10750)$ signal recently seen by the Belle Collaboration [7], although it is not in the current PDG list (see also Sec. 4.4.4).

the distribution of states and thresholds in the charmonium sector and in the bottomonium sector is, at present, rather different. If this hints to some physical differences in the two heavy-quark sectors or just reflects our limited knowledge of the bottomonium spectrum is one of the challenges that future theoretical and experimental studies will have to face.

Exotic states may originate dynamically from different possible structures. These can be grouped into two classes: (i) structures with active gluons and (ii) multiquark states. The former class contains hybrids and glueballs. The latter class contains exotics made of a heavy quark and its antiquark together with at least one light quark-antiquark pair. *A priori* the simplest system consisting of only two quarks and two antiquarks (generically called tetraquarks) is already a very complicated object and it is unclear whether or not any kind of clustering occurs in it. However, to simplify the problem it is common nowadays to focus on certain substructures and investigate their implications: (i) In hadroquarkonia the heavy quark and antiquark form a compact core surrounded by a light-quark cloud. (ii) In compact tetraquarks the relevant degrees of freedom are compact diquarks and antidiquarks. In this review we restrict ourselves to this definition of a compact tetraquark which is quite common in the contemporary literature. It should be mentioned, however, that in the older literature sometimes the phrase "diquonium" was used to refer directly to the assumed diquark clustering [8, 9]. For a comprehensive review of diquarks we refer to Ref. [10] while for a critical

5

discussion of the diquark clustering in heavy exotics we refer to Ref. [11]. (iii) In hadronic molecules the building blocks are color-neutral hadrons. Obviously a complete picture may include some of or even all these configurations in the final description of the exotic state; nevertheless, the question remains of what is the dominant configuration. Finally, even an ordinary hadron, which has a dominant $\bar{q}q$ or qqq configuration, will have subleading configurations with additional quark-antiquark pairs and active gluons. Depending on the state, they may turn out to be more or less relevant to describe its properties.

<div align="center">*   *   *</div>

This report is devoted to exotic states in the charmonium and bottomonium spectrum, i.e. the XYZ states, and also discusses related states in this energy region, such as double-charm/bottom systems, and pentaquarks containing heavy quarks. Its aim is to review the experimental information we have gained on these states over the last fifteen years, and to summarize our theoretical understanding of them.

Data have been collected originally mostly at the B factories (Belle, BaBar, CLEO) and also at the Tevatron experiments, and later at BES and LHCb. They have led to the discovery of several new states (see Figs. 1 and 2) and to the collection of an impressive amount of measurements in production and decay channels. This clean and clear amount of data has no match with the few controversial exotic states in the light-hadron sector.

From the theoretical viewpoint, the study of quarkonium in the last few decades has witnessed two major developments: (i) the establishment of non-relativistic effective field theories and (ii) progress in dynamical lattice QCD calculations of excited states and resonances, and calculations with light-quark masses at or close to the physical point. Both allow for precise and systematically improvable computations that are (to a large extent) model-independent. Although in many cases phenomenological quark models remain a useful resource, it is the advancement in our understanding of quarkonium and quarkonium-like systems due to non-relativistic effective field theories and lattice QCD that makes quarkonium exotica particularly valuable. In fact, today we are not only confronted with a huge amount of high-quality data, which have provided for the first time uncontroversial evidence for the existence of exotic hadrons, but also have modern theoretical tools that allow us to explore in a controlled way these new forms of matter and get a unique insight into the low-energy dynamics of QCD.

The new quarkonium revolution that started in 2003 with the discovery of the $X(3872)$, with all its experimental and theoretical developments and challenges, has been chronicled over the past years in several comprehensive reviews [12–14]. The present report focuses on the XYZ states and aims at portraiting, as precisely as possible, the status of the subject in the year 2019. It is organized in the following main sections. In Sec. 2, we review the main experimental facilities participating to the XYZ searches. The status of these searches and the relevant data that have been collected are summarized in Sec. 3. Theoretical methods, ranging from phenomenological quark models to effective field theories of QCD and lattice QCD, and theoretical results and predictions are discussed in Sec. 4. Finally, in Sec. 5 some future prospects both for experiments and theory are highlighted. We close with a short summary.

As was explained above, in recent years the field of exotic hadrons in general and especially those containing heavy quarks has attracted a lot of experimental and theoretical efforts. As an interesting fact it is worth mentioning that, despite a very rich physics programme at the Belle experiment and many interesting and exciting results obtained by this collaboration for the entire history of its operation, the paper on the discovery of the exotic $X(3872)$ charmonium-like state turns out to be its most cited publication. Thus it should not come as a surprise that the number of papers on the subject, both experimental and theoretical, including various reviews, grows fast. It is therefore important to make it clear from the very beginning what one will find here that has not been previously discussed. A unique feature of the present review is that it contains simultaneously the most recent experimental information and updates on the exotic states, and a discussion of various aspects of the theoretical interpretation of the existing and foreseen experimental data. In the theoretical part, although various models for exotic states presented in the literature are mentioned and discussed in some detail, the main emphasis is on model-independent approaches based on effective field theories and lattice QCD.

1.2. Remarks on the naming scheme of the Particle Data Group

Exotic states that do not seem to fit with expectations of ordinary quarkonia have been dubbed X, Y, and Z in their discovery publications, without any special naming criterion. These names have been used so far in most of the literature on the subject. With the number of XYZ states growing, this way of naming the new states has become increasingly inadequate. For this reason the PDG has recently developed a new naming scheme [6] with the intent

to extend the scheme used for ordinary quarkonia, and based on the quark model, to the newly discovered states. The new names carry the information on the J^{PC} quantum numbers of the states. In addition, aside from the ground states, a mass label is added in brackets behind the name symbol. This mass label may deviate from the actual mass whenever updated measurements give shifted mass values compared to the earlier measurements. They do not say anything about the nature of the state, as this is in many cases controversial. For instance, even the $X(3872)$ is not unanimously accepted as an exotic quarkonium. The only exception are the charged states, which clearly require at least a four-quark structure.

	PC	$-+$	$+-$	$--$	$++$
Isospin	heavy quark content				
$I = 0$	with $c\bar{c}$	η_c	h_c	ψ	χ_c
$I = 0$	with $b\bar{b}$	η_b	h_b	Υ	χ_b
$I = 1$	with $c\bar{c}$	(Π_c)	Z_c	(R_c)	(W_c)
$I = 1$	with $b\bar{b}$	(Π_b)	Z_b	(R_b)	(W_b)

Table 1: The PDG naming scheme for quarkonium and quarkonium-like states. For $I = 1$, C refers to the charge-conjugation quantum number of the neutral state. The quark model for ordinary quarkonia only allows even values of J for the states in the first column, and odd values of J for those in the second one. Moreover, it does not allow a 0^{--} state – see Sec. 4.2. Aside from the η_Q states with $J = 0$ and h_Q, ψ and Υ states with $J = 1$, the value of J is added to the name as a subscript. E.g., a state containing a $\bar{c}c$ pair with the quantum numbers 1^{-+} is called η_{c1}. Aside from the ground states a mass label is added in brackets to the name symbol. In this table names in brackets indicate that there is no experimentally established state (yet) with the corresponding quantum numbers.

The naming scheme adopted by the PDG is shown in Tab. 1 and explained in the caption. It serves the purpose of allowing an unambiguous identification of the quantum numbers of a given state from its name. States whose quantum numbers are not yet fixed are named X(mass). It is important to remark that, even if in this way a state may get the name of an ordinary quarkonium, this is not meant to imply that the nature of the state is that of an ordinary quarkonium. So far, only for the charged quarkonium-like states new names have been introduced — here the names already used in the literature are used, namely Z_c(mass) and Z_b(mass) for states containing a charm-anticharm and a bottom-antibottom pair, respectively, with the isospin 1 and $J^{PC} = 1^{+-}$ (where C refers to the charge-conjugation quantum number of the neutral member of the isotriplet).

To keep track of the names used so far in the literature, those are added in the listings with the remark 'also known as', abbreviated as 'aka'. For instance, the states known as $X(3872)$ and $Y(4660)$ appear as

$$\chi_{c1}(3872) \text{ aka } X(3872) \quad \text{and} \quad \psi(4660) \text{ aka } Y(4660).$$

In this report, we use the XYZ-names for the states most of the time, but in various places we remind the reader of the PDG naming scheme, especially in the headings.

2. Experiments

As a hot topic in experimental particle physics, exotic hadrons containing heavy quarks are studied in all experiments where their production is possible. This includes not only experiments dedicated to hadron physics such as BESIII, GlueX and CLEO-c, but also experiments designed for completely different purposes such as ATLAS and CMS for precision eletroweak physics and beyond, and the B factories, BaBar, Belle, and LHCb, for CP violation. Sometimes the study of exotic states is originally only a byproduct of some other measuremnts, but it becomes more and more significant as more and more candidates for exotic hadrons are observed.

Most of the exotic hadron studies are from e^+e^- annihilation experiments such as BESIII, Belle, BaBar, and CLEO, because of the very clean experimental environment and various production mechanisms. Exotic hadrons are produced directly in e^+e^- annihilation and in association with another charmonium production (double charmonium production), two-photon processes, initial-state radiation (ISR) processes, bottomonium decays and B decays.

More and more results are being reported from the LHCb experiment where long-lived b hadrons (B and B_s mesons as well as the Λ_b baryon) produced in pp collisions are used as a source of exotic hadrons. Essential information on
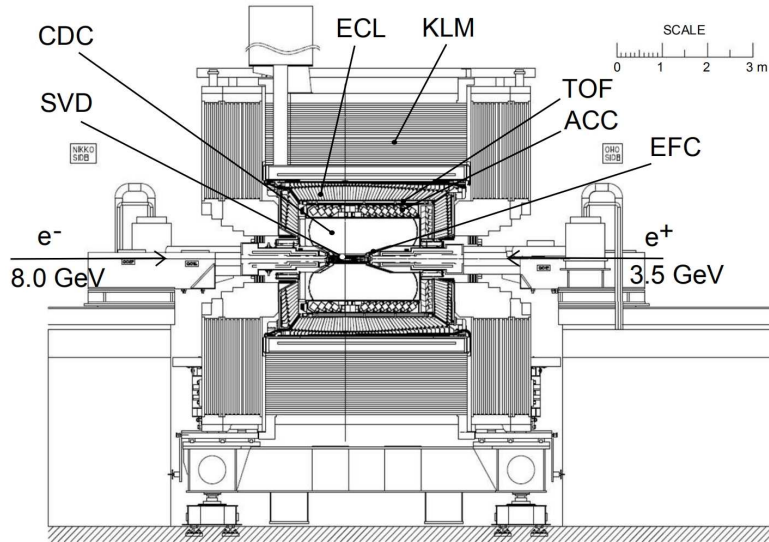
Figure 3: Belle detector longitudinal section from Ref. [15].

production of exotic hadrons directly in parton fusion and in b-hadron decays is also coming from the ATLAS and CMS experiments at the LHC pp collider, and came from CDF and D0 at the Tevatron $p\bar{p}$ collider.

In this section, we give a short introduction to the experiments which are involved in the studies of exotic hadrons discussed in this review, including a description of the detector components, data samples, and production mechanisms of exotic hadrons. New experiments being built or planned which can contribute to the study of exotic states in the future, along with those which have recently started taking data such as GlueX and Belle II, will be discussed in Sec. 5.1.

2.1. Experiments at e^+e^- colliders

The first state that triggered studies of the new hadron spectroscopy is the $X(3872)$ observed by the Belle experiment in 2003. All the e^+e^- annihilation experiments operating at that time joined the effort immediately, if their energy could reach the production threshold of charmonium states. The BaBar experiment with data samples comparable with Belle could do the same study. The CLEO experiment also had data in the bottomonium energy region but with much smaller statistics, whereas somewhat later the CLEO-c detector could run directly in the charmonium energy region allowing for new specific studies. The BES experiment running at the BEPC had small data samples only, originally taken for measurements of the R value, and a focused study of the XYZ states became possible only after its upgrade to the BESIII experiment at BEPCII with its first data sample taken in 2011.

2.1.1. The Belle experiment

The Belle detector [15] operating at the KEKB asymmetric-energy e^+e^- collider [16] is a large solid-angle magnetic spectrometer that consists of a silicon vertex detector (SVD), a 50-layer central drift chamber (CDC), an array of aerogel threshold Cherenkov counters (ACC), a barrel-like arrangement of time-of-flight (TOF) scintillation counters, and an electromagnetic calorimeter (EMC) comprised of CsI(TI) crystals located inside a superconducting solenoid coil that provides a 1.5 T magnetic field. Information from specific ionization in the CDC, time measurements in the TOF and the response of the ACC is combined to perform the charged particle identification (PID). An iron flux-return yoke instrumented with resistive plate chambers (RPC) located outside the coil is used to detect K_L^0 mesons and to identify muons. A detailed description of the Belle detector can be found in Refs. [15, 17]. Figure 3 shows the structure of the Belle detector.

The Belle detector as described above took data from 1999-2010 that are partially still under analysis. Since the beginning of 2019 the successor experiment Belle II, which is described in Sec. 5.1 of this review, has been in
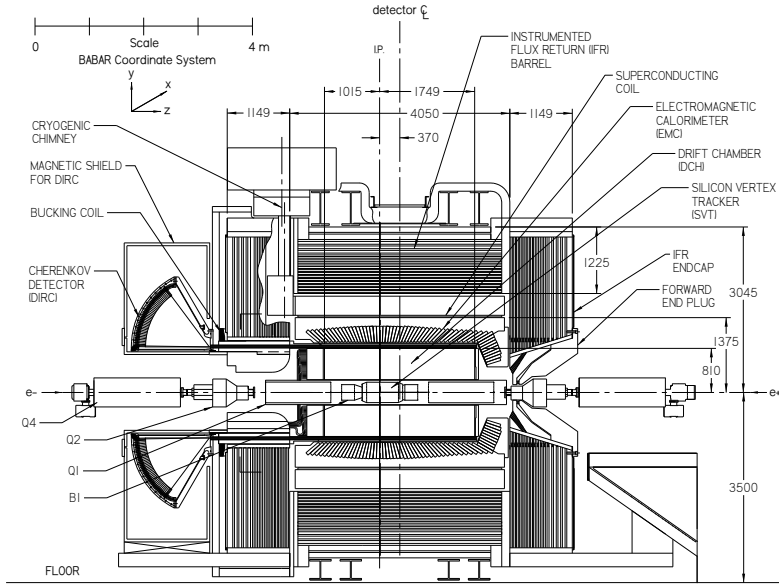
Figure 4: BaBar detector longitudinal section from Refs. [18].

operation. The analyses from Belle utilize one or more of the following data samples: 5.74 fb^{-1} of data collected at the $\Upsilon(1S)$ peak [102 million $\Upsilon(1S)$ events], 24.91 fb^{-1} collected at the $\Upsilon(2S)$ peak [158 million $\Upsilon(2S)$ events], 89.5 fb^{-1} collected at $\sqrt{s}$ = 10.52 GeV, 702.6 fb^{-1} data collected at $\sqrt{s}$ = 10.58 GeV [$\Upsilon(4S)$ peak], and 121.1 fb^{-1} data collected at $\sqrt{s}$ = 10.867 GeV [$\Upsilon(5S)$ peak]. There are also some data points between $\Upsilon(4S)$ and $\Upsilon(6S)$ with low statistics for a measurement of the inclusive hadronic cross sections.

2.1.2. The BaBar experiment

The PEP-II B Factory was an asymmetric e^+e^- collider designed to operate at a center-of-mass (c.m.) energy of 10.58 GeV, the mass of the $\Upsilon(4S)$ resonance. The BaBar detector was the experiment running at this collider. Figure 4 shows a longitudinal section through the detector center [18, 19].

The charged particle tracking system was made of two components: the silicon vertex tracker (SVT) and the drift chamber (DCH). Pulse height information from the SVT and DCH was also used to measure ionization losses for charged PID. The SVT was composed of five layers of double-sided silicon strip detectors and the DCH of 40 layers of small, hexagonal cells. The Detector of Internally Reflected Cherenkov light (DIRC) provides separation of pions and kaons up to the kinematic limit of 4.5 GeV. Cherenkov light was produced in 4.9-m long bars of synthetic fused silica of rectangular cross section, and transported to a large array of photomultiplier tubes (PMT). The EMC was a finely segmented array of CsI(Tl) crystals of projective geometry to detect electromagnetic showers with excellent energy and angular resolution over the energy range from 20 MeV to 4 GeV. The instrumented flux return was designed to identify muons and to detect neutral hadrons. The BaBar experiment took data from 1999-2008, however, some analyses are still ongoing.

The analyses from BaBar utilize one or more of the following data samples: 13.6 fb^{-1} of data collected at the $\Upsilon(2S)$ peak, 27.96 fb^{-1} collected at the $\Upsilon(3S)$ peak, 424.7 fb^{-1} collected at the $\Upsilon(4S)$ peak, and 43.9 fb^{-1} collected at $\sqrt{s}$ = 10.54 GeV.

2.1.3. The CLEO(-c) experiment

The CLEO experiment ran successfully for nearly thirty years, from 1979 to 2008, recording particles produced in electron-positron collisions at the Cornell Electron-positron Storage Ring (CESR). The experiment took data in the bottomonium energy region before 2003 and CLEO-c, a modified version of the CLEO III detector, accumulated data in the charmonium energy region between 2004 and 2008. The main differences between CLEO III and CLEO-c
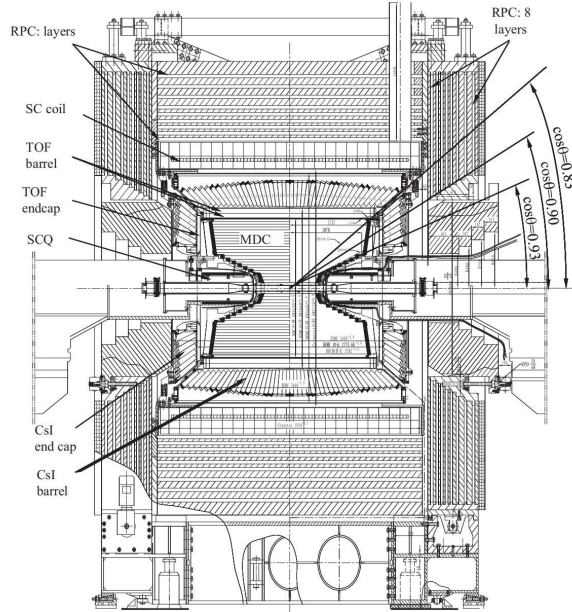
9

Figure 5: Schematic drawing of the BESIII detector from Ref. [20].

detectors are the SVD replaced with a wire vertex chamber and the magnetic field reduced from 1.5 T to 1.0 T to maintain high efficiency for low momentum tracks and reasonably high momentum resolution.

The CLEO-c detector was equipped to measure the momenta and directions of charged particles, identify charged hadrons, detect photons, and determine with good precision their directions and energies. The muons above $p = 1.1$ GeV could also be identified with the muon detector. The detector was almost cylindrically symmetric with everything but the muon detector inside a superconducting magnet coil supplying 1.0 T field. The charged tracks were reconstructed using the 47-layer drift chamber and the coaxial 6-layer vertex drift chamber. For tracks that traverse all layers of the drift chamber, the root-mean-square (rms) momentum resolution was approximately 0.6% at $p = 1$ GeV. In the whole of this review we set $c = 1$. Photons were detected in an EMC containing about 7800 CsI(Tl) crystals, whose rms photon energy resolution was 2.2% at $E_\gamma = 1$ GeV, and 5% at $E_\gamma = 100$ MeV. The solid angle for detection of charged tracks and photons was 93% of 4π. PID information to separate kaon from pion was provided by measurements of ionization (dE/dx) in the CDC and by a cylindrical ring-imaging Cherenkov (RICH) detector.

The CLEO experiment had 22.2 fb^{-1} of e^+e^- data taken in the $\Upsilon(1S - 5S)$ region, which were used for XYZ and charmed meson studies. The CLEO-c experiment accumulated 27 million $\psi(2S)$ events, 818 pb^{-1} of data at the $\psi(3770)$ peak, 586 pb^{-1} collected at 4.17 GeV, and 60 pb^{-1} of data between 3.97 and 4.26 GeV (including 13 pb^{-1} of data at 4.26 GeV) – these data were also used for XYZ studies.

2.1.4. The BESIII experiment

The BESIII experiment [20] at the BEPCII storage ring started its first collisions in the tau-charm energy region in 2008. The BESIII detector has an effective geometrical acceptance of 93% of 4π. It contains a small cell helium-based multilayered drift chamber (MDC) that provides momentum measurements of charged particles; a TOF based on plastic scintillator which helps to identify charged particles; an EMC made of CsI(Tl) crystals which is used to measure the energies of photons and provide trigger signals; and a muon system (MUC) made of RPCs. The momentum resolution of the charged particles is 0.5% at 1 GeV in a 1 T magnetic field; the energy loss measurement provided by the MDC has a resolution better than 6% for electrons from Bhabha scattering; the photon energy resolution can reach 2.5% (5%) at 1 GeV in the barrel (endcaps) of the EMC; and the time resolution of TOF is 80 ps in the barrel and 110 ps in the endcaps. In 2015, the endcap TOF was replaced with a Multigap Resistive Plate Chamber (MRPC), and the time resolution improved to 60 ps.

After a few years of running at energies of the J/ψ, $\psi(2S)$, and $\psi(3770)$ peaks [21], the BESIII experiment started

collecting data for the study of *XYZ* particles. At the moment the maximum c.m. energy point that BESIII can reach is 4.6 GeV. In a data sample of 525 pb^{-1} collected during one month from December 14, 2012 to January 14, 2013 at the c.m. energy of 4.26 GeV, the charged charmonium-like state $Z_c(3900)$ was discovered [22]. This motivated BESIII to focus on c.m. energies above 4 GeV resulting in the largest data sample above 4 GeV for *XYZ* studies.

The data samples for the *XYZ* study ("*XYZ* data" hereafter) are presented in Table 2.1.4, which lists the nominal c.m. energy, measured c.m. energy (when it is available), and integrated luminosity at each energy point. These data were used for all the analyses presented in this report. BESIII also did a fine scan between 3.8 and 4.6 GeV at more than 100 energy points ("*R*-scan data" hereafter) in 2014, with a total integrated luminosity of about 800 pb^{-1}. This data sample is also used for *XYZ* studies although the statistics are low [23].

Data sample	c.m. energy (MeV)	$\mathcal{L}$ (pb^{-1})
3810	3807.65±0.10±0.58	50.54±0.03
3900	3896.24±0.11±0.72	52.61±0.03
4009	4007.62±0.05±0.66	481.96±0.01
4090	4085.45±0.14±0.66	52.63±0.03
4130	–	∼ 400
4160	–	∼ 400
4180	4178	∼ 3190
4190	4188.59±0.15±0.68	43.09±0.03
4190	–	∼ 500
4200	–	∼ 500
4210	4207.73±0.14±0.61	54.55±0.03
4210	–	∼ 500
4220	4217.13±0.14±0.67	54.13±0.03
4220	–	∼ 500
4230	4226.26±0.04±0.65	1091.74±0.15
4237	–	∼ 500
4245	4241.66±0.12±0.73	55.59±0.04
4246	–	∼ 500
4260	4257.97±0.04±0.66	825.67±0.13
4270	–	∼ 500
4280	–	∼ 200
4290	–	∼ 500
4310	4307.89±0.17±0.63	44.90±0.03
4315	–	∼ 500
4340	–	∼ 500
4360	4358.26±0.05±0.62	539.84±0.10
4380	–	∼ 500
4390	4387.40±0.17±0.65	55.18±0.04
4400	–	∼ 500
4420	4415.58±0.04±0.72	1073.56±0.14
4440	–	∼ 570
4470	4467.06±0.11±0.73	109.94±0.04
4530	4527.14±0.11±0.72	109.98±0.04
4575	4574.50±0.18±0.70	47.67±0.03
4600	4599.53±0.07±0.74	566.93±0.11

Table 2: The measured c.m. energy [23] and integrated luminosity $\mathcal{L}$ [24] of each data sample collected for the BESIII study of *XYZ* states. The uncertainties on the c.m. energies are statistical and systematic. The uncertainties on the integrated luminosities are statistical only; a 1% systematic uncertainty common to all the data points is not listed. "–" means not available yet and numbers without error are rough estimates.

Compared with the *B* factories, BaBar and Belle, BESIII has some advantages in the study of the *XYZ* states,

especially those Y states with vector quantum numbers. BESIII collects e^+e^- annihilation data at c.m. energies that go directly into the production of Y states, while the B factories use data produced via ISR, so BESIII has a much higher detection efficiency and can take more data at any energy of interest [for example, the efficiency is 46% at BESIII [22] and about 10% at Belle [25] for selecting $Y(4260) \to \pi^+\pi^- J/\psi \to \pi^+\pi^- \ell^+\ell^-$ ($\ell = e$, or μ) events]. This makes the study of the Z_c states from the Y decays also more efficient at BESIII than at the B factories. However, B factories can measure the cross sections in a wide energy range since all the events are produced at the same time, while BESIII needs to tune the c.m. energy point by point to collect data, thus can only cover a limited energy range. Finally, the B factories can study the XYZ states with B decays, two-photon fusion, double-charmonium production, and $\Upsilon(nS)$ ($n = 1 - 6$) decays, while BESIII is limited to e^+e^- annihilation.

2.2. Experiments at proton-antiproton colliders

The Tevatron was a synchrotron at Fermilab that accelerated protons and antiprotons in a 6.28 km ring to energies of up to 1 TeV. First collisions were in 1986 and it ran until 2011. The maximum luminosity achieved was 4×10^{32} cm^{-2} s^{-1}. Two large general-purpose detectors, CDF [26] and D0 [27], shown in Fig. 6, were taking data. The CDF detector consists of: a silicon detector used to track the paths of charged particles and composed of seven layers of silicon arranged in a barrel shape around the beam pipe; the central outer tracker used to track the paths of charged particles and located within a 1.5 T solenoidal magnetic field; the combined electromagnetic and hadronic calorimeter that has approximately uniform granularity in rapidity-azimuthal angle and extends down to 2° from the beam direction to measure the energy of light particles and hadrons; the muon detector with four layers of planar drift chambers, each with the capability of detecting muons with a transverse momentum $p_T > 1.4$ GeV. The D0 detector consists of three major subsystems: central tracking detectors, uranium/liquid-argon calorimeters, and a muon spectrometer. The central tracking system includes a silicon microstrip tracker and a scintillating-fiber tracker located within a 2 T solenoidal magnet to identify displaced vertices for b-quark tagging. The magnetic field enables measurement of the energy-to-momentum ratio for electron identification and calorimeter calibration. The calorimeters were designed to provide energy measurements for electrons, photons, and jets in the absence of a central magnetic field, as well as assist in identification of electrons, photons, jets, and muons and measure the transverse energy balance in events. The outermost layer of the D0 detector is the muon spectrometer consisting of a central muon system proportional drift tubes and toroidal magnets, central scintillation counters, and a forward muon system.
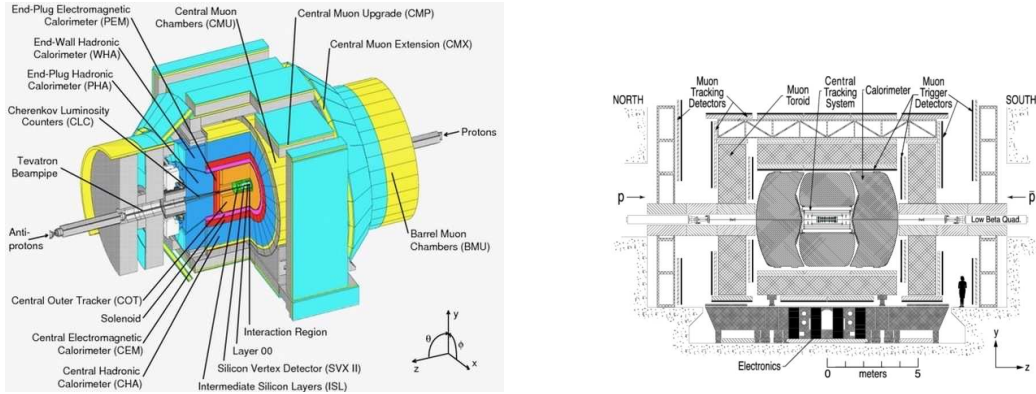
Figure 6: General layout of the CDF (left) and D0 (right) detectors from Refs. [26, 27].

In 1995, the CDF and D0 Collaborations announced the discovery of the top quark [28, 29] and then systematically studied its characteristics. By now the combination of their measurements of the top quark mass gives (172.9 ± 0.4) GeV, a precision of about 0.23% [30]. In 2006, the CDF Collaboration reported the first measurement of B_s oscillations [31] and both detectors observed for the first time various heavy baryons. In addition to that, CDF and D0 have also contributed to studies of exotic states using data samples of 9.0 fb^{-1} and 10.4 fb^{-1} of proton-antiproton collisions taken at $\sqrt{s} = 1.96$ TeV. For example, after the discovery of the $\chi_{c1}(3872)$ aka $X(3872)$ both groups worked on determining its characteristics and the most precise measurement of its mass still belongs to CDF [32]. In 2009 CDF

was the first to report an observation of the $\chi_{c1}(4140)$ aka $X(4140)$ [33] while in 2016 D0 announced an observation of the $X(5568)$ [34].

2.3. Experiments at proton-proton colliders

The Large Hadron Collider (LHC) is the world largest and most powerful particle accelerator. It started operation on September 10, 2008. The LHC consists of a 27-kilometer ring of superconducting magnets with a number of accelerating structures to boost the energy of the particles up to 6.5 TeV. The maximum luminosity achieved so far is 2.06×10^{34} cm^{-2} s^{-1}. Four large detectors, ALICE, ATLAS, CMS, and LHCb, are taking data.

2.3.1. The LHCb experiment

The LHCb detector shown in Fig. 7 investigates properties of the charm and bottom quarks [35]. It has contributed a lot to various studies of mesons and baryons with open charm and bottom, and has also succeeded in investigating exotics, e.g. discovering pentaquarks [36], determining the quantum numbers of the $X(3872)$ [37] and $Z(4430)$ [38], and disentangling the complicated structure of the $J/\psi\phi$ system around 4140 MeV [39].
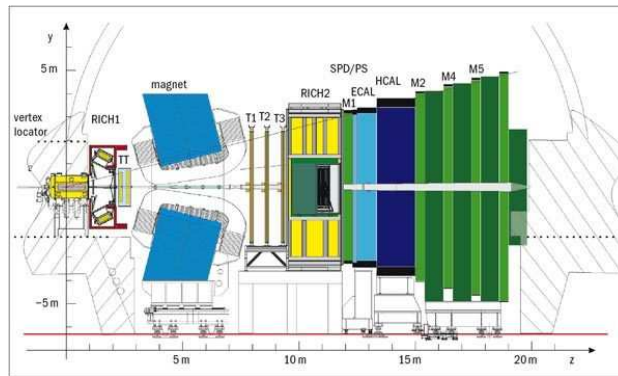
Figure 7: General layout of the LHCb detector from Ref. [40].

The LHCb detector is a single-arm spectrometer with a forward angular coverage from approximately 15 mrad to 300 (250) mrad in the bending (non-bending) plane [40]. The spectrometer magnet is a warm dipole magnet providing an integrated field of about 4 Tm, which deflects charged particles in the horizontal plane. The tracking system consists of the vertex locator, and four planar tracking stations: the Tracker Turicensis (TT) upstream of the dipole magnet, and tracking stations T1–T3 downstream of the magnet. Charged particles require a minimum momentum of 1.5 GeV to reach the tracking stations, T1–T3. Charged hadron identification in the momentum range from 2 to 100 GeV is achieved by two RICHs (RICH1 and RICH2). The calorimeter system is composed of a scintillating pad detector, a preshower, a shashlik type EMC and a hadronic calorimeter. The muon detection system provides muon identification and contributes to the L0 trigger of the experiment. The minimum momentum that a muon must have to traverse the five stations is approximately 6 GeV.

The LHCb detector started its data taking in 2008. The integrated luminosity recorded is 1.11 fb^{-1} at 7 TeV in 2011, 2.08 fb^{-1} at 8 TeV in 2012, and 5.9 fb^{-1} at 13 TeV from 2015 up to now.

Due to the large production cross sections, more B mesons and other particles are produced at LHCb than at other experiments like BaBar and Belle. However, to avoid background from direct pp collision, many of the studies looked for XYZ states in the decays of a mother particle which has a long decay length. So far, most of the results related to the XYZ particles are from B decays. The large B sample makes the determination of the quantum numbers and the decay dynamics of the XYZ states possible via partial wave analysis (PWA) of the B decays.

2.3.2. The ATLAS and CMS experiments

In 2012, the ATLAS and CMS Collaborations announced the discovery of the Higgs boson – a fundamental particle with a mass around 125 GeV predicted by the Standard Model as manifestation of the mechanism generating

13

the masses of the elementary particles [41, 42]. These detectors, shown in Fig. 8, extensively study its properties and simultaneously search for various possible manifestations of new physics beyond the Standard Model. They are also involved in looking for new heavy states.
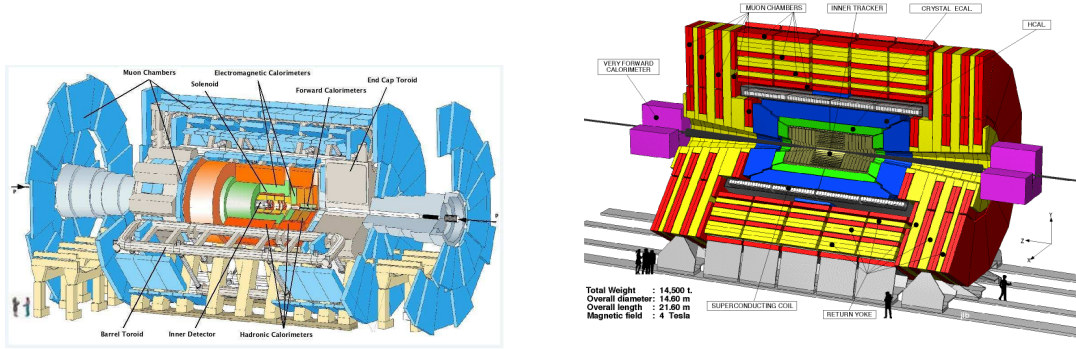

Figure 8: General layout of the ATLAS (left) and CMS (right) detectors from Refs. [41, 42].

The CMS detector is built around a huge solenoid magnet. It is a cylindrical coil of superconducting cables that generates a field of 3.8 T. The complete detector is 21 meters long, 15 meters wide, and 15 meters high. The subdetectors which constitute the CMS detector from inner to outer are inner tracking system to measure the trajectories of charged particles and reconstruct secondary vertices; EMC to measure the energy of electrons and photons; hadronic calorimeter to measure the energy of hadrons; superconducting magnet providing a 3.8 T magnetic field parallel to the beam axis to bend the tracks of charged particles; muon system to identify and measure the trajectories of muons. The ATLAS detector has cylindrical geometry with its central axis coinciding with the beamlines. It is 44 meters in length and 25 meters along the diameter of the transverse round plane, and provides almost full 4π solid angle coverage around the collision point. The subdetectors which constitute the ATLAS detector from inner to outer are inner tracking detector which consists of a silicon pixel detector, silicon microstrip tracker and transition radiation tracker to provide good charged-particle tracking reconstruction as well as vertex reconstruction; EMC surrounded by the hadronic calorimeter; solenoid superconducting magnetic system providing a 2 T axial magnetic field; muon spectrometer with a whole coverage up to $|\eta| < 2.4$.

The integrated luminosity recorded by the CMS/ATLAS detectors is 45.0/45.0 pb^{-1} at 7 TeV in 2010, 6.1/5.1 fb^{-1} at 7 TeV in 2011, 23.3/21.3 fb^{-1} at 8 TeV in 2012, and 162.9/147.0 fb^{-1} at 13 TeV from 2015 up to now.

3. Exotic hadron candidates

In this section, experimental evidence for the candidates for exotic states is collected. While some comments are already given about why those states might most probably not be regular quark-model states, a detailed discussion of their nature is postponed to the subsequent sections — for all states the relevant theory sections are mentioned below.

3.1. Isoscalar states

Most of the states discovered recently in the quarkonium mass range are isoscalar states and we will begin the discussion with those. Isoscalar states could in principle be regular quarkonia — the arguments for why most authors still regard them as exotics are presented in this article. The isovector states that call for going beyond the most naive realisation of the quark model are presented in section 3.2.

3.1.1. Neutral X states

• *The $\psi_2(3823)$*

In the charmonium spectrum, the $\psi_2(1^3D_2)$ is expected to dominantly decay into $\gamma\chi_{c1}$, while the $\psi_3(1^3D_3)$ is expected to decay into $\gamma\chi_{c2}$ with a large branching fraction besides its dominant open charm decay into $D\bar{D}$. To
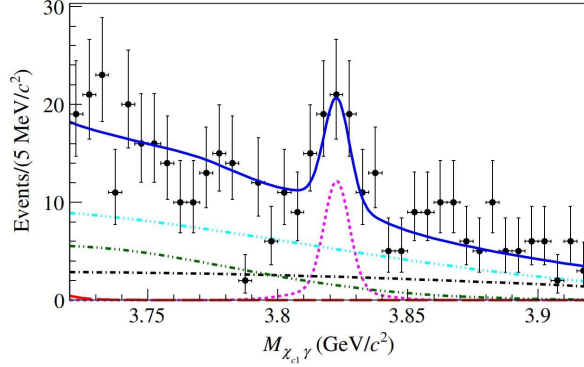
14

Figure 9: The simultaneous fit projection on the $\gamma\chi_{c1}$ mass spectrum to the selected $B^\pm \to K^\pm \gamma\chi_{c1}$ and $B^0 \to K^0_S \gamma\chi_{c1}$ signal candidates [43], where the solid blue line is the best fit. The curves show the signal [large-dashed red line for $\psi(2S)$, short-dashed magenta line for $\psi_2(3823)$, and dotted violet line for $\chi_{c1}(3872)$ aka $X(3872)$] and the background components [dot-dashed black line for combinatorial, two-dot-dashed dark green line for $B \to K\psi(2S)(\nrightarrow \gamma\chi_{c1})$, and cyan three-dot-dashed for peaking component].

search for them, Belle measured the reactions $B \to K\gamma\chi_{c1} \to K\gamma\gamma J/\psi$ and $B \to K\gamma\chi_{c2} \to K\gamma\gamma J/\psi$ using a data sample of 772×10^6 $B\bar{B}$ events [43]. In this analysis, the most important technique is a correction of the photon energy from B decays by scaling the energy of the photon so that the ΔE (the energy difference between the beam energy and the reconstructed B candidates) is equal to zero. This improves the $\gamma\chi_{cJ}$ mass resolution a lot. In the $\gamma\chi_{c1}$ mass spectrum for the selected $B^\pm \to K^\pm \gamma\chi_{c1}$ signal candidates, besides the clear $\psi(2S)$ signal, there is a significant narrow peak at 3823 MeV, denoted as $\psi_2(3823)$. No signal of $X(3872) \to \gamma\chi_{c1}$ is seen. After using a Breit-Wigner (BW) function convolved with a mass resolution to parameterize the $\psi_2(3823)$ signal shape, the mass obtained from a simultaneous fit to the selected $B^\pm \to K^\pm \gamma\chi_{c1}$ and $B^0 \to K^0_S \gamma\chi_{c1}$ signal candidates is $(3823.1 \pm 1.8 \pm 0.7)$ MeV with a significance of 4.0σ with systematic uncertainties included, see Fig. 9. The upper limit at 90% confidence level (C.L.) on its width is estimated to be 24 MeV. The $\psi_2(3823)$ mass agrees well with the potential model expectations for $\psi_2(1^3D_2)$. Besides the mass, the measured product of branching fractions $\mathcal{B}[B \to K\psi_2(3823)]\mathcal{B}[\psi_2(3823) \to \gamma\chi_{c1}]$ is approximately two orders of magnitude lower than for the $\psi(2S)$, which also supports the interpretation of the $\psi_2(3823)$ as the $\psi_2(1^3D_2)$ state [44, 45]. In the $\gamma\chi_{c2}$ mass spectrum, no evidence is found for $\psi_2(3823) \to \gamma\chi_{c2}$.

Later BESIII searched for the $\psi_2(3823)$ in the $e^+e^- \to \pi^+\pi^-\psi_2(3823) \to \pi^+\pi^-\gamma\chi_{c1}$ process using data samples at c.m. energies of 4.23, 4.26, 4.36, 4.42, and 4.60 GeV corresponding to a total luminosity of 4.67 fb^{-1} [46]. In the $\pi^+\pi^-$ recoil mass distribution for events in the χ_{c1} signal region, the $\psi_2(3823)$ signals are observed clearly with a statistical significance of 6.2σ, while no evidence for the $\psi_2(3823)$ signal can be seen for events in the χ_{c2} signal region. The fit yields 19 ± 5 $\psi_2(3823)$ signal events in the $\gamma\chi_{c1}$ mode, with a measured mass of $(3821.7 \pm 1.3 \pm 0.7)$ MeV. The upper limit on its width is estimated to be 16 MeV at 90% C.L. The measured parameters of $\psi_2(3823)$ are consistent with those from the Belle measurement [43]. The products of $\sigma[e^+e^- \to \pi^+\pi^-\psi_2(3823)]\mathcal{B}[\psi_2(3823) \to \gamma\chi_{c1}]$ are measured at the above mentioned c.m. energies, as shown in Fig. 10 with dots with error bars. Fitting this distribution using a $Y(4360)$ shape or $\psi(4415)$ shape with their resonant parameters fixed to the PDG values [6] can describe the data well in both cases. The fit results are shown in Fig. 10 with the solid and dot-dashed lines. Larger data samples with more energy points are needed to separate these two fits or more possibilities.

According to the measurements from BESIII and Belle, the narrow $\psi_2(3823)$ resonance is a good candidate for the $\psi_2(1^3D_2)$ charmonium state. According to potential models [47–51], the mass of $\psi_2(1^3D_2)$ is in the 3.810 ∼ 3.840 GeV range, which is above the $D\bar{D}$ mass threshold but below the $D\bar{D}^*$ and $D\bar{D}\pi$ thresholds. Since the decay $\psi_2(1^3D_2) \to D\bar{D}$ needs to proceed in a D–wave which would violate parity, the $\psi_2(1^3D_2)$ state is expected to be narrow, and $\psi_2(1^3D_2) \to \gamma\chi_{c1}$ should be the dominant decay mode [47–52]. All agree well with the experimental observations. From the cross section measurement, BESIII obtained the ratio

$$\frac{\mathcal{B}[\psi_2(3823) \to \gamma\chi_{c2}]}{\mathcal{B}[\psi_2(3823) \to \gamma\chi_{c1}]} < 0.42$$

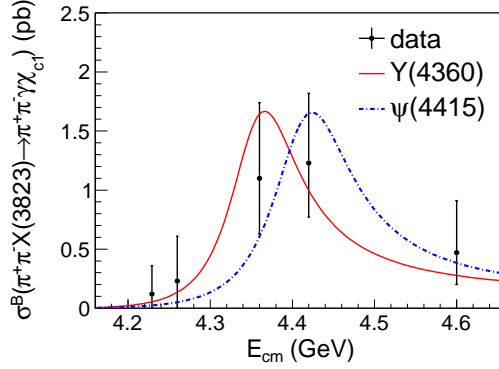at the 90% C.L., which also agrees with expectations for the $\psi_2(1^3D_2)$ state [52].

15

Figure 10: The fits to the products of $\sigma[e^+e^- \to \pi^+\pi^-\psi_2(3823)]\mathcal{B}[\psi_2(3823) \to \gamma\chi_{c1}]$ from the BESIII measurement [46] using a $\psi(4360)$ aka $Y(4360)$ or $\psi(4415)$ line shape. Dots with error bars are data, and the red solid/blue dot-dashed curve shows the best fit with a $Y(4360)/\psi(4415)$ line shape.

It should be noted that the spin-parity of this state were not determined, although the BESIII measurement of the angular distribution supports a $J^P = 2^-$ assignment. With much larger data samples at BESIII and Belle II in the near future, the determination of the spin-parity and precise measurements of the width and decay ratio between $\gamma\chi_{c1}$ and $\gamma\chi_{c2}$ are needed to confirm the $\psi_2(3823)$ as the conventional $\psi_2(1\,^3D_2)$ charmonium state.

Very recently LHCb observed a new narrow charmonium state, the $X(3842)$ resonance, in the decay modes $X(3842) \to D^0\bar{D}^0$ and $X(3842) \to D^+D^-$ with its measured mass and width consistent with the unobserved spin-3 $\psi_3(1^3D_3)$ charmonium state using an integrated luminosity of 9 fb^{-1} proton-proton collision data [53]. This state can be checked in other experiments in the near future.

• *The $\chi_{c1}(3872)$ aka $X(3872)$ and its counterpart X_b*

The $X(3872)$ was first observed in $B^\pm \to K^\pm\pi^+\pi^-J/\psi$ decays by Belle in 2003 [5], and subsequently was confirmed by several other experiments [54–56]. The spin-parity quantum numbers J^P of the state were restricted to two possibilities, 1^+ or 2^-, by the CDF experiment via an analysis of the angular correlations in the $\pi^+\pi^-J/\psi \to \pi^+\pi^-\mu^+\mu^-$ final state [57]. Using 1.0 fb^{-1} of pp collision data, LHCb rules out $J^P = 2^-$ by analyzing the angular correlations in the same decay chain, with the $X(3872)$ state produced in $B^+ \to K^+X(3872)$ decays [37]. Twelve years after the $X(3872)$ was discovered, its spin-parity quantum numbers were finally determined in the LHCb experiment by performing a five-dimensional angular correlation analysis in $B^+ \to K^+X(3872)$, $X(3872) \to \rho^0J/\psi$, $\rho^0 \to \pi^+\pi^-$, $J/\psi \to \mu^+\mu^-$ decays with 1011 ± 38 events selected from 3 fb^{-1} data at 7 and 8 TeV [58]. This analysis determined the J^{PC} values to be 1^{++} for the $X(3872)$ which thus could be a candidate for the not yet identified quark model state $\chi_{c1}(2^3P_1)$.

So far the $X(3872)$ is one of the best studied exotic meson candidates with a $c\bar{c}$ content. Some properties including the enhancement of isospin-violating ρ^0J/ψ decays, the mass right at the $D^0\bar{D}^{*0}$ threshold, and the spin-parity quantum numbers J^{PC} are well established. Due to its mass at the $D^0\bar{D}^{*0}$ threshold and large decay rate to $D^0\bar{D}^{*0}$, a natural explanation of this state is a loosely bound molecule. However, its large prompt production rates at the Tevatron [55] and the LHC [59–61] might point at a compact component. Its preferred decay mode of $\gamma\psi(2S)$ over $\gamma J/\psi$ matches the expectation for the $\chi_{c1}(2P)$ state. The various possible interpretations of the $X(3872)$ are discussed in detail in various subsections of Sec. 4.

In order to better understand the nature of $X(3872)$ experimentally, one might either look for more production mechanisms, or find more decay modes.

(1) Production mechanisms of $\chi_{c1}(3872)$ aka $X(3872)$

Since the quantum numbers of $X(3872)$ are $J^{PC} = 1^{++}$, it can be produced through the radiative transition of excited vector charmonium/bottomonium or charmonium-like/bottomonium-like states. Belle reported the searches
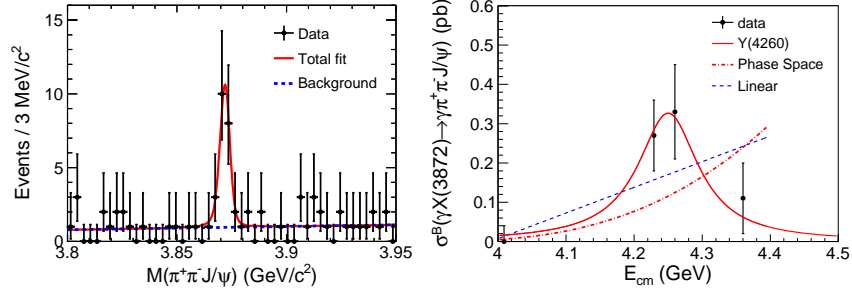
Figure 11: Left panel: a fit to the $M(\pi^+\pi^- J/\psi)$ distribution observed at BESIII [65]. Dots with error bars are data, and the red solid curve is the best fit. Right panel: a fit to $\sigma[e^+e^- \rightarrow \gamma X(3872)]\mathcal{B}[X(3872) \rightarrow \pi^+\pi^- J/\psi]$ measured by BESIII [65] (dots with error bars) with a $Y(4260)$ resonance (red solid curve), a linear continuum (blue dashed curve), or an $E1$-transition phase-space term (red dotted-dashed curve).

for the $X(3872)$ as well as the $X(3915)$ and $X(4140)$ using 102×10^6 $\Upsilon(1S)$ and 158×10^6 $\Upsilon(2S)$ events [62, 63]. Belle also searched for the $X(3872)$ in $\Upsilon(1S)$ inclusive decays [64]. In all these attempts, no apparent $X(3872)$ signal was observed and 90% C.L. upper limits of the production rates in $\Upsilon(1S, 2S)$ decays were set.

BESIII reported evidence for $X(3872)$ in $Y(4260)$ radiative decay [65]. It searched for the process $e^+e^- \rightarrow \gamma X(3872) \rightarrow \gamma\pi^+\pi^- J/\psi$ with data collected at c.m. energies of 4.01, 4.23, 4.26, and 4.36 GeV [65]. The $M(\pi^+\pi^- J/\psi)$ distribution summed over all energy points, as shown in Fig. 11 (left plot), is fitted to extract the mass and signal yield of $X(3872)$. The solid line shows the best fit with the measured mass of $(3871.9 \pm 0.7 \pm 0.2)$ MeV and the width of less than 2.4 MeV at the 90% C.L. for the $X(3872)$. The statistical significance of $X(3872)$ is 6.3σ. The measured Born cross sections[2] are shown in Fig. 11 (right plot) with dots with error bars, together with the comparison with a $Y(4260)$ resonance (parameters fixed to PDG [6] values), linear continuum, or $E1$-transition phase space ($\propto E_\gamma^3$) term. The $Y(4260)$ resonance describes the data better than the other two options, which supports the existence of the radiative transition $Y(4260) \rightarrow \gamma X(3872)$. Together with the hadronic transition to the charged charmonium-like state $Z_c(3900)$ [22, 68, 69], this suggests that there might be some common nature of $X(3872)$, $Y(4260)$, and $Z_c(3900)$, and so models developed to interpret any one of them should also consider the other two — in fact both the compact tetraquark model, discussed in Sec. 4.3.3, as well as the molecular model, discussed in Sec. 4.3.4, are consistent with this request. The radiative decay of $Y(4260)$ to the $X(3872)$ was even predicted within the latter model as a necessary consequence of the observation of the reaction $Y(4260) \rightarrow \pi Z_c(3900)$, if all the three mentioned states are hadronic molecules [70]. Recently BESIII updated the analysis of $e^+e^- \rightarrow \gamma X(3872) \rightarrow \gamma\pi^+\pi^- J/\psi$ using an about 9 fb^{-1} data sample at c.m. energies above 4 GeV [71]. Clear $X(3872)$ signals are observed with a signal significance of 16.1σ, which confirms the previous observation [65]. Besides the discovered channel, Belle also observed clear $X(3872)$ signals in $B^0 \rightarrow K^+\pi^- X(3872)$ and $B^+ \rightarrow K_S^0\pi^+ X(3872)$ using 772×10^6 $B\bar{B}$ events [72], where the fraction of the $K^*(892)^0$ signal component in the $K^+\pi^-$ system is 34%.

Combining the measured $e^+e^- \rightarrow \pi^+\pi^- J/\psi$ cross sections at c.m. energies of 4.23 and 4.26 GeV from BESIII [73], we obtain $\sigma[e^+e^- \rightarrow \gamma X(3872)]\mathcal{B}[X(3872) \rightarrow \pi^+\pi^- J/\psi]/\sigma(e^+e^- \rightarrow \pi^+\pi^- J/\psi) = (3.7 \pm 0.9) \times 10^{-3}$, under the assumption that $X(3872)$ and $\pi^+\pi^- J/\psi$ are only produced from $Y(4260)$ decays. If we take $\mathcal{B}[X(3872) \rightarrow \pi^+\pi^- J/\psi] = 5\%$ as an estimate, then we have

$$\mathcal{R} = \frac{\mathcal{B}[Y(4260) \rightarrow \gamma X(3872)]}{\mathcal{B}[Y(4260) \rightarrow \pi^+\pi^- J/\psi]} \sim 10\% \,,$$

which is quite sizeable given the suppression from the small electromagnetic coupling present in the numerator.

---

[2] The Born cross section for $e^+e^- \rightarrow \gamma X(3872) \rightarrow \gamma\pi^+\pi^- J/\psi$ at each c.m. energy point is given by the formula $\sigma[e^+e^- \rightarrow \gamma X(3872)] \times \mathcal{B}[X(3872) \rightarrow \pi^+\pi^- J/\psi] = \sigma^{\text{dressed}}[e^+e^- \rightarrow \gamma X(3872)] \times \mathcal{B}[X(3872) \rightarrow \pi^+\pi^- J/\psi] \times |1 - \Pi|^2 = \sigma^{\text{vis}}[e^+e^- \rightarrow \gamma X(3872)] \times \mathcal{B}[X(3872) \rightarrow \pi^+\pi^- J/\psi] \times |1 - \Pi|^2/(1 + \delta)_{\text{ISR}} = N^{\text{obs}} \times |1 - \prod|^2/[\mathcal{L} \times \mathcal{B}(J/\psi \rightarrow \ell^+\ell^-) \times \varepsilon \times (1 + \delta)_{\text{ISR}}]$, where σ^{dressed} and σ^{vis} are called dressed cross section and visible cross section, N^{obs} is the number of $X(3872)$ signal events obtained from the fit to the $\pi^+\pi^- J/\psi$ mass spectrum, $\mathcal{L}$ is the integrated luminosity of the data sample, $\mathcal{B}(J/\psi \rightarrow \ell^+\ell^-)$ is the branching fraction of J/ψ to lepton pair, ε is the detection efficiency. $(1 + \delta)_{\text{ISR}}$ is the radiative-correction factor, calculated using the formula given in Ref. [66], and $|1 - \prod|^2$ is the vacuum polarization factor, calculated according to Ref. [67]. For other processes, the calculation is similar.
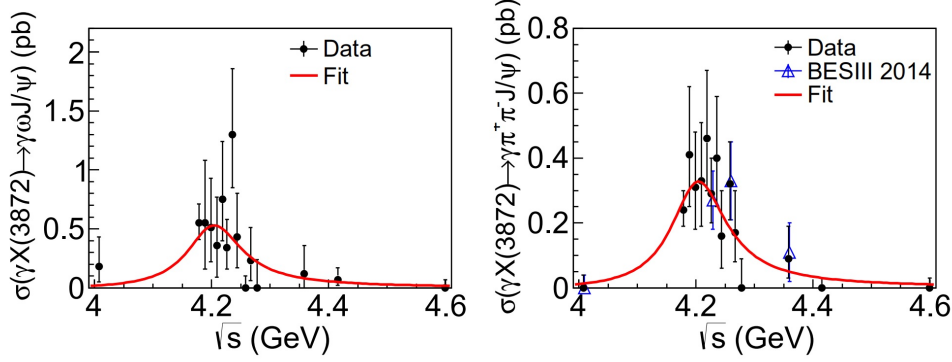
17

Figure 12: The distributions of $\sigma[e^+e^- \to \gamma X(3872)]\mathcal{B}[X(3872) \to \omega J/\psi]$ (left) and $\sigma[e^+e^- \to \gamma X(3872)]\mathcal{B}[X(3872) \to \pi^+\pi^- J/\psi]$ (right) from the BESIII measurement [74]. The solid lines are from a simultaneous fit to these two distributions assuming a single BW resonance.

Since the $X(3872)$ can be produced in $e^+e^- \to \gamma X(3872)$, very recently BESIII studied the $e^+e^- \to \gamma \omega J/\psi$ process using 11.6 fb^{-1} of data at c.m. energies from $\sqrt{s} =$4.008 to 4.600 GeV [74], where a signal peak consistent with the $X(3872)$ resonance is observed in the $\omega J/\psi$ mass spectrum. The measured $\sigma[e^+e^- \to X(3872)]\mathcal{B}[X(3872) \to \omega J/\psi]$ cross section is shown in Fig. 12 (left panel). Meanwhile, using the same analysis method as in Ref. [65], BESIII updated the measurement of $\sigma[e^+e^- \to \gamma X(3872)]\mathcal{B}[X(3872) \to \pi^+\pi^- J/\psi]$ as well, as shown in the right panel of Fig. 12. A simultaneous maximum-likelihood fit is performed to these two distributions with a single BW resonance. The fit gives its mass $M = (4200.6^{+7.9}_{-13.3} \pm 3.0)$ MeV and width $\Gamma = (115^{+38}_{-26} \pm 12)$ MeV, the values of which are consistent with the $\psi(4160)$ or $Y(4230)$. The ratio $\mathcal{B}[X(3872) \to \omega J/\psi]/\mathcal{B}[X(3872) \to \pi^+\pi^- J/\psi]$ as a free parameter in the simultaneous fit is obtained to be $1.6^{+0.4}_{-0.3} \pm 0.2$.

Besides a few more $X(3872)$ production modes discovered by BESIII, the first observation of the $X(3872)$ in the Λ_b^0 decay $\Lambda_b^0 \to X(3872)pK^- \to J/\psi\pi^+\pi^- pK^-$ with $J/\psi \to \mu^+\mu^-$ was reported very recently by LHCb based on data collected in proton-proton collisions corresponding to 1.0, 2.0 and 1.9 fb^{-1} of integrated luminosity at c.m. energies of 7, 8 and 13 TeV [75], respectively.

After event selection, clear Λ_b^0 signals in $J/\psi\pi^+\pi^- pK^-$ mass spectrum, and $\psi(2S)$ and $X(3872)$ signals in $J/\psi\pi^+\pi^-$ mass spectrum are observed. To obtain the $\psi(2S)$ and $X(3872)$ signal yields from Λ_b^0 decay, a 2D unbinned extended maximum-likelihood fit to the $J/\psi\pi^+\pi^- pK^-$ and $J/\psi\pi^+\pi^-$ mass spectra was performed with four components included: $\psi(2S)$ or $X(3872)$ signals from Λ_b^0 decay ($\Lambda_b^0 \to \psi_{\pi\pi} pK^-$); a nonresonant (NR) component from Λ_b^0 decay with on $\psi(2S)$ or $X(3872)$ intermediate state; a component with $\psi(2S)$ or $X(3872)$ describing random combinations that are not from Λ_b^0 decay ($\psi_{\pi\pi} pK^-$); and a combinatorial $J/\psi\pi^+\pi^- pK^-$ component. The fit yields 610 ± 30 and 55 ± 11 $\psi(2S)$ and $X(3872)$ signal events with a statistical significance of 7.2σ for the $X(3872)$. The projection to $J/\psi\pi^+\pi^-$ mass distribution from the 2D fit in the $X(3872)$ signal region is shown in Fig. 13 (left panel) with fitted components indicated. The background-subtracted pK^- mass spectrum for the $X(3872)$ channel is shown in Fig. 13 (right panel), where a clear peak associated with the $\Lambda(1520)$ state is seen. An unbinned maximum-likelihood fit with a $\Lambda(1520)$ signal and a nonresonant component was performed. The fraction of the $\Lambda(1520)$ is $(58 \pm 15)\%$, where the uncertainty is statistical only. The fitted results are shown in Fig. 13 (right panel) with fitted components indicated. Using the $\Lambda_b^0 \to \psi(2S)pK^-$ decay as a normalization channel, the ratio of the branching fractions is measured to be

$$R = \frac{\mathcal{B}[\Lambda_b^0 \to X(3872)pK^-]}{\mathcal{B}[\Lambda_b^0 \to \psi(2S)pK^-]} \times \frac{\mathcal{B}[X(3872) \to J/\psi\pi^+\pi^-]}{\mathcal{B}[\psi(2S) \to J/\psi\pi^+\pi^-]} = (5.4 \pm 1.1 \pm 0.2)\%,$$

where the first uncertainty is statistical and the second is systematic. This the first time that the $X(3872)$ was observed in the Λ_b^0 decay.

A search for exotic charmonium-like states in exclusive photoproduction reactions was proposed in Refs. [76–78]. Recently COMPASS, a fixed-target experiment at CERN, analyzed the full set of data collected with a muon beam between 2002 and 2011, covering the range from 7 to 19 GeV in the c.m. energy of the virtual photon-nucleon
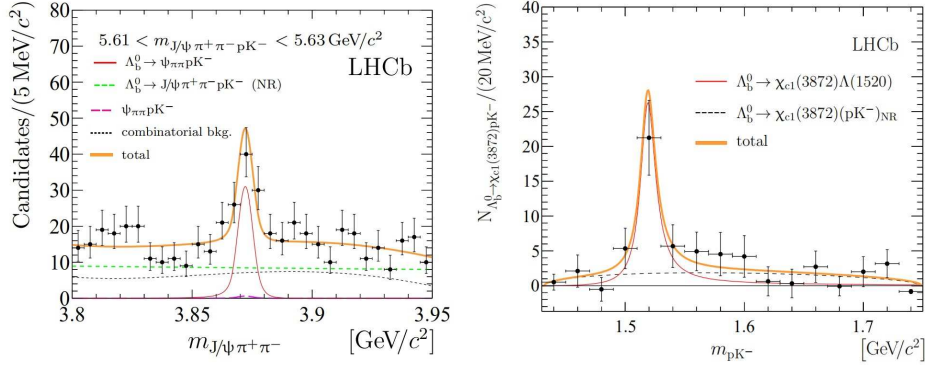
Figure 13: The $J/\psi\pi^+\pi^-$ and background-subtracted pK^- mass spectra within the $X(3872)$ signal region from $\Lambda_b^0 \to J/\psi\pi^+\pi^- pK^-$ decay, together with fitted results described in the text [75].

system, to search for the $X(3872)$ in photoproduction reactions. The $X(3872)$ was searched for in the charge-exchange reaction $\mu^+ N \to \mu^+ J/\psi\pi^+\pi^-\pi^\pm N'$, where N denotes the target nucleon and N' the unobserved recoil system. The resulting $\pi^+\pi^- J/\psi$ invariant mass distribution is shown in Fig. 14 (left plot), where two peaks with positions and widths consistent with the $\psi(2S)$ and $X(3872)$ are evident. The significance of the second peak is 4.1σ with systematic effects included. However, the shape of the $\pi^+\pi^-$ mass distribution corresponding to the second peak shows disagreement with previous observations for $X(3872)$ and is inconsistent with quantum numbers $J^{PC} = 1^{++}$, as shown in Fig. 14 (right plot) where the squares with error bars are from the COMPASS measurement and the dots with error bars from the ATLAS data set [61] for comparison. Due to this critical difference, the COMPASS Collaboration concluded that the observed signal is not the well-known $X(3872)$ giving possible evidence for a new charmonium-like state denoted $\tilde{X}(3872)$. The measured mass and width of the $\tilde{X}(3872)$ are $M[\tilde{X}(3872)] = (3860.0 \pm 10.4)$ MeV and $\Gamma[\tilde{X}(3872)] <$ 51 MeV at 90% C.L., and the product of the cross section and branching fraction of the $\tilde{X}(3872)$ into $\pi^+\pi^- J/\psi$ is determined to be $(71 \pm 28 \pm 39)$ pb. An independent confirmation of the observed $\tilde{X}(3872)$ signal from high-precision experiments with high-energy virtual or real photons is required.
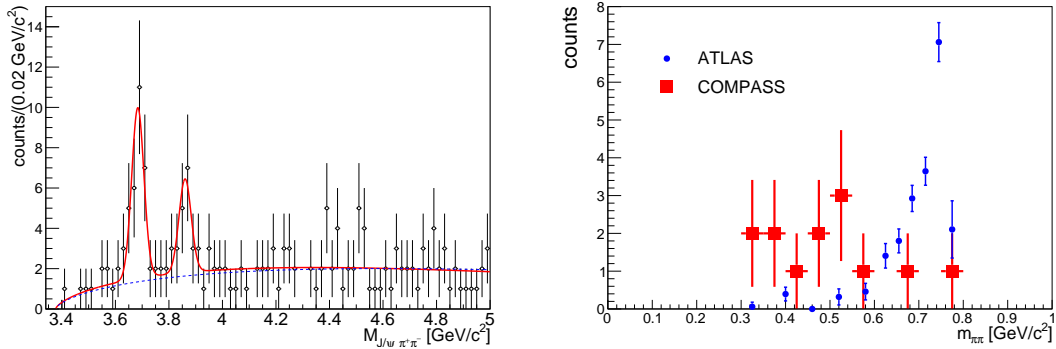
Figure 14: The $M(\pi^+\pi^- J/\psi)$ distribution (left) and the corresponding $\pi^+\pi^-$ mass spectrum with $M(\pi^+\pi^- J/\psi)$ within the $X(3872)$ signal region shown with the squares with error bars (right) from the selected $\mu^+ N \to \mu^+ J/\psi\pi^+\pi^-\pi^\pm N'$ candidates [79]. The dots with error bars in the right plot are from the decays of $X(3872) \to \pi^+\pi^- J/\psi$ observed by ATLAS for comparison [61].

Lepto(photo-)production of the $X(3872)$ was also searched for in the neutral reaction $\mu^+ N \to \mu^+ J/\psi\pi^+\pi^- N'$ [79]. Except for a peak from photodiffractive production of $\psi(2S)$ in the $\pi^+\pi^- J/\psi$ invariant mass spectrum, no statistically significant signal at around 3872 MeV can be seen. The 90% C.L. upper limit of the $X(3872)$ production cross section in this reaction multiplied by the branching fraction for the decay $X(3872) \to J/\psi\pi^+\pi^-$ was set to be 2.9 pb.

19

(2) Decay patterns of $\chi_{c1}(3872)$ aka $X(3872)$

The transition $X(3872) \to \gamma J/\psi$ was measured by BaBar [80] with a statistical significance of 3.6σ, Belle [81] with a statistical significance of 5.5σ, and LHCb clearly [82]. So the decay mode $X(3872) \to \gamma J/\psi$ is well established, while for $X(3872) \to \gamma\psi(2S)$, the results from some measurements are not consistent. Evidence for it was first reported by BaBar with a statistical significance of 3.5σ using $(465 \pm 5) \times 10^6$ $B\bar{B}$ pairs [80]. The ratio of the branching fractions is measured to be $R = \mathcal{B}[X(3872) \to \gamma\psi(2S)]/\mathcal{B}[X(3872) \to \gamma J/\psi] = 3.4 \pm 1.4$, where statistical and systematic uncertainties are combined. Using a 3 fb^{-1} data sample at $\sqrt{s} = 7$ and 8 TeV, LHCb reported strong evidence for the decay $X(3872) \to \gamma\psi(2S)$ with a statistical significance of 4.4σ [82]. The measured value of the ratio R is $2.46 \pm 0.64 \pm 0.29$, which is in good agreement with the BaBar's measurement [80]. In contrast, the negative result was reported by Belle using 772×10^6 $B\bar{B}$ pairs and an upper limit of $R < 2.1$ was set at the 90% C.L. [81]. Using the information from Ref. [81], we obtain $R = 0.6 \pm 1.4$ as an estimation of the central value and uncertainty. Although there is no serious disagreement between the measurements from BaBar, LHCb, and Belle, there is some tension in the values for the decay rates of $X(3827) \to \gamma\psi(2S)$. Using the above mentioned results, a weighted average gives

$$\overline{R} = \frac{\mathcal{B}[X(3872) \to \gamma\psi(2S)]}{\mathcal{B}[X(3827) \to \gamma J/\psi]} = 2.31 \pm 0.57$$

without considering a possible small correlation. Since BESIII has observed clear $e^+e^- \to \gamma X(3872) \to \gamma\pi^+\pi^- J/\psi$ signals [65, 74], we also expect the results for $e^+e^- \to \gamma X(3872) \to \gamma\gamma\psi(2S)$ from this experiment soon.

A relatively large branching fraction for $X(3872) \to \gamma\psi(2S)$ was claimed to be inconsistent with a purely $D^0\bar{D}^{*0}$ molecular interpretation of the $X(3872)$ based on a model calculation presented in Ref. [83]. In the meantime, it is consistent with expectations if the $X(3872)$ is a pure charmonium or a mixture of a molecule and a charmonium [13, 82, 84]. However, Ref. [85] argues that the results of Ref. [83] are model dependent and that an effective field theory approach allows for the mentioned ratio even within a molecular approach — we come back to this issue in Secs. 4.3.4 and 4.4.5.

A measurement of pionic transitions of the $X(3872)$ to the χ_{cJ} ($J = 0, 1, 2$) has been proposed to be one way to distinguish between various interpretations. If the $X(3872)$ is a conventional $c\bar{c}$ state, transition to the $\pi^0\chi_{c1}$ should be suppressed compared to $\pi^+\pi^-\chi_{c1}$ due to isospin breaking by the light quark masses. If the $X(3872)$ is a compact tetraquark or molecular state, on the other hand, these rates are expected to be enhanced [86–88]. In the search for $X(3872) \to \pi^+\pi^-\chi_{c1}$ with negative results, the Belle Collaboration determined the branching fraction $\mathcal{B}[B^+ \to K^+X(3872)]\mathcal{B}[X(3872) \to \pi^+\pi^-\chi_{c1}] < 1.5 \times 10^{-6}$ at 90% C.L. [89]. Recently BESIII reported the first observation of the decay $X(3872) \to \pi^0\chi_{c1}$ in $e^+e^- \to \gamma X(3872)$ with a statistical significance of 5.2σ using data at the c.m. energies above 4 GeV corresponding an integrated luminosity of 9 fb^{-1} [71]. To calculate the ratio

$$R^X_{\chi_{cJ}/\psi} \equiv \frac{\mathcal{B}[X(3872) \to \pi^0\chi_{cJ}]}{\mathcal{B}[X(3872) \to \pi^+\pi^- J/\psi]} = \left\{ 6.6^{+6.5}_{-4.5} \pm 1.1(19),\ 0.88^{+0.33}_{-0.27} \pm 0.10,\ 0.40^{+0.37}_{-0.27} \pm 0.04(1.1) \right\},$$

for $J = 0, 1,$ and 2, respectively, where the numbers in brackets are 90% C.L. upper limits. The normalization channel was $e^+e^- \to \gamma X(3872)$ with $X(3872) \to \pi^+\pi^- J/\psi$ updated at the same time. In the BESIII measurement, after initial event selection, a clear signal for the $X(3872)$ can be seen in the data of 4.15 to 4.30 GeV, while no evidence for the $X(3872)$ is seen at other c.m. energy points. A fit to the invariant mass distribution of $\pi^0\chi_{cJ}$ with a first-order polynomial background and a signal shape from the signal MC simulation directly yields $16.9^{+5.2}_{-4.5}$ $X(3872)$ events with a statistical significance of 4.8σ. After requiring the $\gamma J/\psi$ mass within the χ_{cJ} ($J = 0, 1, 2$) mass region respectively, the resulting distributions for $M(\pi^0\chi_{cJ})$ with $J = 0, 1, 2$ are shown in Fig. 15. The fits to each $M(\pi^0\chi_{cJ})$ distribution with a constant background and a signal shape from MC simulation give $1.9^{+1.9}_{-1.3}$, $10.8^{+3.8}_{-3.1}$, and $2.5^{+2.3}_{-1.7}$ $X(3872)$ signal events with signal significances of 1.6σ, 5.2σ, and 1.6σ for $J = 0, 1,$ and 2, respectively. No significant $X(3872)$ signal is found in the $M(\pi^0\chi_{c0,c2})$ distributions. This is the first observation of a decay of the $X(3872)$ to a P-wave charmonium state and it supports the non-$c\bar{c}$ interpretations of the $X(3872)$ [86–88]. This BESIII observation can be cross-checked by other experiments like Belle. Previously, Belle measured $B^+ \to K^+\pi^0\chi_{c1}$ and provided the background-subtracted $\pi^0\chi_{c1}$ mass distribution without any structure at the $X(3872)$ mass [89], but the bin width of that mass spectrum is too large to claim a contradictory result. Considering this, very recently Belle updated the analysis of $B^+ \to \chi_{c1}\pi^0 K^+$ decays to focus on the $X(3872)$ mass region [90] using 772×10^6 $B\bar{B}$ events.

No statistically significant $X(3872)$ signal at around 3872 MeV can be seen in the $\chi_{c1}\pi^0$ mass spectrum even with a much narrower bin width. An upper limit $R^X_{\chi_{c1}/\psi} < 0.97$ at 90% C.L. is set, which does not contradict the BESIII result [71]. In the future Belle II can utilize a similar study to provide improved results for the ratio $R^X_{\chi_{cJ}/\psi}$.
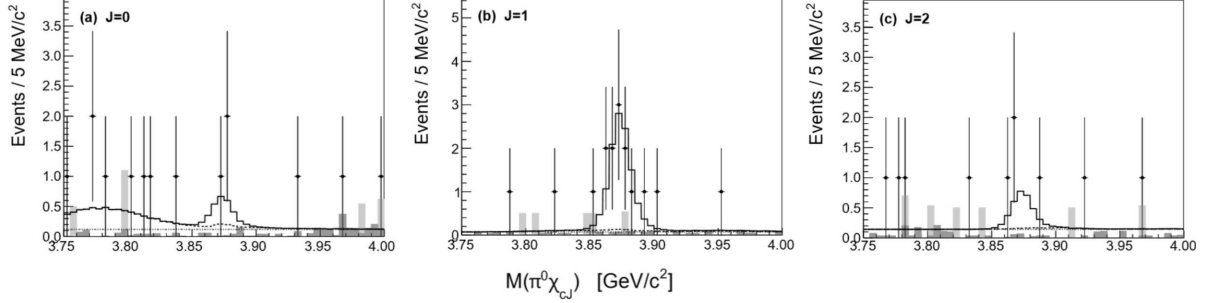

Figure 15: The $\pi^0\chi_{cJ}$ mass distributions, $M(\pi^0\chi_{cJ})$, from the process $e^+e^- \to \gamma\pi^0\chi_{cJ}$ for (a) $J = 0$, (b) $J = 1$, and (c) $J = 2$ [71]. Points are data; lines are fits (solid is the total, the dotted is the polynomial background, and the dashed line is the total background); the darker histogram is a MC estimate of peaking J/ψ backgrounds; the lighter stacked histogram is an estimate of non-peaking backgrounds using J/ψ sidebands from data.

The hadronic decay $X(3872) \to \omega J/\psi$ was reported by the Belle and BaBar Collaborations with less than 5σ evidence in B decays based on 275 million and 467 million $B\bar{B}$ pairs, respectively [91, 92]. Recently the $X(3872) \to \omega J/\psi$ decay was firmly observed with a more than 5σ significance by the BESIII Collaboration in the process $e^+e^- \to \gamma\omega J/\psi$ with a total integrated luminosity of about 11.6 fb^{-1} at c.m. energies from $\sqrt{s} =$4.008 to 4.600 GeV [74]. The $\omega J/\psi$ invariant mass distribution from the BESIII measurement is shown in Fig. 16 as the dots with error bars, where a signal peak consistent with the $X(3872)$ resonance is observed together with a broad structure from irreducible $e^+e^- \to \omega\chi_{c0}$ background events. In addition, there are evident structures above 3.9 GeV. Two fit scenarios were adopted for an approximation of the $\omega J/\psi$ mass spectrum: (1) the incoherent sum of three BW resonances (denoted as $X(3872)$, $X(3915)$, and $X(3960)$, respectively); (2) the incoherent sum of the $X(3872)$ and $X(3915)$. The corresponding fit results are shown in Fig. 16 with red solid lines. In both fits, the signal significance of the $X(3872)$ is larger than 5σ and the $X(3872)$ mass was measured to be $(3873.3 \pm 1.1 \pm 1.0)$ MeV. The low statistics of the BESIII experiment prevent us from drawing a solid conclusion about the states above 3.9 GeV.
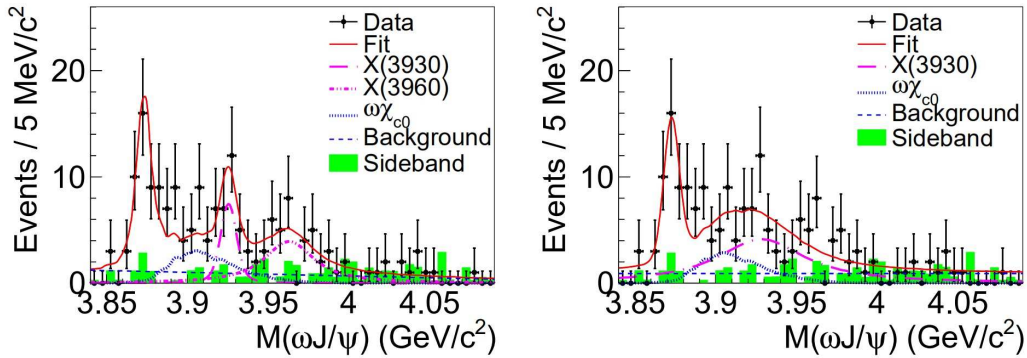
Figure 16: The $\omega J/\psi$ mass distributions with results of two fit scenarios described in the text. Dots with error bars are data [74], the red solid curves show the total fit results, the green shaded histograms are the normalized contribution from the J/ψ- and ω-mass sidebands, and other components included in the fits are indicated in the plots.

With a data sample containing 447M $B\bar{B}$ events, Belle observed a near-threshold $D^0\bar{D}^0\pi^0$ mass enhancement in $B \to KD^0\bar{D}^0\pi^0$ decays that, when interpreted as $X(3872) \to D^0\bar{D}^0\pi^0$, gave an $X(3872)$ mass of $(3875.4 \pm 0.7^{+1.2}_{-2.0})$ MeV [93]. BaBar studied $B \to KD^{*0}\bar{D}^0$ with a sample of 383M $B\bar{B}$ pairs and found a similar near-threshold

enhancement that, if considered to be due to the $X(3872) \to D^{*0} \bar{D}^0$, gave a mass of $(3875.1^{+0.7}_{-0.5} \pm 0.5)$ MeV [94]. Originally this state has been considered to be a state different from the $X(3872)$ in literature. However, a subsequent Belle study of $B \to K D^{*0} \bar{D}^0$ based on 657M $B\bar{B}$ pairs found for the near-threshold peak a mass of $(3872.9^{+0.6+0.4}_{-0.4-0.5})$ MeV [95] by fitting the peak with a phase-space modulated BW function, much closer to the value determined from the $\pi^+\pi^- J/\psi$ decay channel. Now those data are taken as the open charm decay mode of the $X(3872)$.

LHCb searched for the $X(3872) \to p\bar{p}$ using a 3 fb^{-1} pp collision data sample [96]. No signals of the $X(3872)$ are seen, and a 95% C.L. upper limit is obtained

$$\frac{\mathcal{B}[B^+ \to K^+ X(3872)]\mathcal{B}[X(3872) \to p\bar{p}]}{\mathcal{B}(B^+ \to K^+ J/\psi)\mathcal{B}(J/\psi \to p\bar{p})} < 0.25\% \,.$$

LHCb also searched for the $X(3872) \to \phi\phi$, but no signals of the $X(3872)$ are seen either [97]. An upper limit for the inclusive production of $X(3872)$ at 90% C.L. is obtained on

$$\frac{\mathcal{B}[b \to X(3872)X]\mathcal{B}[X(3872) \to \phi\phi]}{\mathcal{B}(b \to \chi_{c1}X)\mathcal{B}(\chi_{c1} \to \phi\phi)} < 0.34 \,.$$

(3) Other studies related to $\chi_{c1}(3872)$ aka $X(3872)$

So far, all the $X(3872)$ related measurements are product branching fractions or relative branching ratios since the absolute production rate of the $X(3872)$ is unknown in any of the experiments. The only attempt to measure the production rate of the $X(3872)$ is via inclusive B decays into a $X(3872)$ and a kaon in the BaBar and Belle experiments. But due to the high multicombinational background level, no evidence for the $X(3872)$ can be seen. BaBar set an upper limit of the $X(3872)$ production rate in the B-meson decays by measuring the momentum distribution of the inclusive kaons from B-meson decays with 210 fb^{-1} $\Upsilon(4S)$ data [98]: $\mathcal{B}[B^- \to K^- X(3872)] < 3.2 \times 10^{-4}$ at the 90% C.L.

A recent update comes from the Belle experiment with the full sample of 772×10^6 $B\bar{B}$ pairs [99]. No significant $X(3872)$ signal is observed, and Belle sets a more stringent upper limit of $\mathcal{B}[B^- \to K^- X(3872)] < 2.7 \times 10^{-4}$ at the 90% C.L., and the central value is $\mathcal{B}[B^- \to K^- X(3872)] = (1.2 \pm 1.1 \pm 0.1) \times 10^{-4}$. Together with all the other measurements on the product branching fractions $\mathcal{B}[B^- \to K^- X(3872)]\mathcal{B}[X(3872) \to \text{exclusive}]$ [exclusive = $\pi^+\pi^- J/\psi$, $\pi^+\pi^-\pi^0 J/\psi$, $\gamma J/\psi$, $\gamma \psi(2S)$, $D^0 \bar{D}^{*0} + c.c.$] [6], one obtains

$$2.9\% < \mathcal{B}[X(3872) \to \pi^+\pi^- J/\psi] < 10\%,$$

$$0.9 \times 10^{-4} < \mathcal{B}[B^- \to K^- X(3872)] < 2.7 \times 10^{-4},$$

at the 90% C.L. [100]. We find that the decay width of the $X(3872)$ to $\pi^+\pi^- J/\psi$ is larger and the production rate of the $X(3872)$ is smaller than for conventional charmonium states such as η_c, $\psi(2S)$, and χ_{c1} [6]. In the forthcoming Belle II experiment, to measure the absolute branching fraction of $X(3872)$, the inclusive decays $B \to KX(3872)$ may be still the only way. In order to observe the $X(3872)$ signals, we need to improve the B tagging efficiency and suppress the multicombinatorial backgrounds.

An axial-vector χ_{c1} state should also be produced directly in the e^+e^- annihilation, however, the corresponding probability is suppressed by an additional power of the fine structure constant α because positive-parity states cannot be produced in a single-photon annihilation of an electron-positron pair. Theoretical predictions for such a direct production of the generic $c\bar{c}$ charmonium χ_{c1} can be found in Refs. [101–103] while a similar estimate for the $X(3872)$ was made in Ref. [104]. The result obtained, $\Gamma_{ee}[X(3872)] > 0.03$ eV, is not in contradiction with the upper limit on the probability of this production established experimentally — the most recent result is $\Gamma_{ee}[X(3872)]\mathcal{B}[X(3872) \to \pi^+\pi^- J/\psi] < 0.13$ eV at the 90% C.L. [105]. It, therefore, remains to be seen whether or not necessary statistics can be collected in future experiments to observe the $X(3872)$ directly in e^+e^- annihilation.

In a short summary, after 16 years of studies, the knowledge on the $X(3872)$ is still very limited: We know it is an isoscalar with $J^{PC} = 1^{++}$, a very precise mass close to the $D^0 \bar{D}^{*0}$ threshold, and a very small width. Significant decays into $D^0 \bar{D}^{*0}$, $\pi^+\pi^- J/\psi$, $\omega J/\psi$, $\pi^0 \chi_{c1}$, and $\gamma J/\psi$ have been observed, while the significances of other modes such as $\gamma\psi(2S)$ and light hadrons are still less than 5σ. The absolute decay rates to the above modes are unknown. Although an isoscalar partner of $X(3872)$ was observed by COMPASS, further confirmation is needed.

Since more data have been accumulated at LHCb, some of the measurements can be improved, such as the study of $X(3872) \to \gamma\psi(2S)$ and possibly of $X(3872) \to \pi^+\pi^-\pi^0 J/\psi$, if the π^0 background can be handled properly. The BESIII experiment accumulated more data close to the $Y(4260)$ peak, which can be used to measure all the final states since the background level is very low as has been shown in the $\pi^+\pi^- J/\psi$ and $\omega J/\psi$ cases [65, 74]. Since the production cross section of $e^+e^- \to \gamma X(3872)$ is at a few pb level [65, 74], the $X(3872)$ sample has about 10^4 events, which allows measurements of final states with branching fractions at the percent level only.

A very interesting proposal for a precise $X(3872)$ mass measurement was put forward recently [106]. It exploits the interplay of a triangle singularity and the pole of the $X(3872)$ on the resulting line shapes in this way enhancing tremendously the sensitivity to the mass. For this method to work it is necessary that the source of the reaction generates a large number of low-energy $D^*\bar{D}^*$ pairs which appears possible, e.g., at LHCb.

(4) Search for the X_b state

Many theoretical works have been carried out in order to understand the nature of $X(3872)$. It is also natural to search for a similar state with $J^{PC} = 1^{++}$ (called X_b hereafter) in the bottomonium system [107, 108]. The search for X_b supplies important information about the discrimination of a compact multiquark configuration and a loosely bound hadronic molecule configuration for the $X(3872)$. The existence of the X_b is predicted in both the compact tetraquark model [109] and those involving a molecular interpretation [110, 111], although employing heavy quark flavor symmetry within a common hadronic effective field theory for states containing $b\bar{b}$ and $c\bar{c}$ appears not to be possible [112].

The production of X_b at LHC and Tevatron [113] has been extensively investigated. Since the mass of X_b may be very large, a search at LHC should be promising. The X_b state can also be searched for at B-factories with radiative decays $\Upsilon(5S, 6S) \to \gamma X_b$, and the production rates are predicted at the orders of 10^{-5} under the assumption that the X_b is a $B\bar{B}^*$ molecular state [114]. As for the X_b decay modes, partial widths of the radiative decays of $X_b \to \gamma\Upsilon(nS)$ ($n = 1, 2, 3$) with X_b being a candidate for the $B\bar{B}^*$ molecular state are found at about 1 keV level [115], and the partial width of the hadronic decay of $X_b \to \omega\Upsilon(1S)$ is about tens of keVs [116].

The ATLAS and CMS Collaborations searched for the X_b decaying to $\pi^+\pi^-\Upsilon(1S)$ based on a sample of pp collisions at $\sqrt{s} = 8$ TeV, corresponding to an integrated luminosity of 16.2 fb^{-1} and 20.7 fb^{-1}, respectively [117, 118]. Figure 17 (left plot) shows the $\pi^+\pi^-\Upsilon(1S)$ invariant mass distribution in CMS data [118]. Except the clear $\Upsilon(2S)$ signal, no evidence for an X_b signal was observed. However, unlike the $X(3872)$, whose decays exhibit large isospin violation, the X_b should decay preferably into $\pi^+\pi^-\pi^0\Upsilon(1S)$ rather than $\pi^+\pi^-\Upsilon(1S)$ if it exists [110, 111, 113]. So Belle performed a search for an X_b signal decaying to $\omega\Upsilon(1S)$ in $e^+e^- \to \gamma X_b$ at a c.m. energy of 10.867 GeV using a 118 fb^{-1} data sample [119]. Figure 17 (right plot) shows the $\omega\Upsilon(1S)$ invariant mass distribution in a range from 10.55 to 10.65 GeV. The dots with error bars are from data, the solid histogram is from the normalized contribution of $e^+e^- \to \omega\chi_{bJ}$ ($J = 0, 1, 2$). No obvious X_b signal is observed, and 90% C.L. upper limits on the product branching fraction $\mathcal{B}[\Upsilon(5S) \to \gamma X_b]\mathcal{B}[X_b \to \omega\Upsilon(1S)]$ vary smoothly from 2.6×10^{-5} to 3.8×10^{-5} between 10.55 and 10.65 GeV. We also note that the absence of the X_b state in ATLAS, CMS, and Belle experiments may be understood in a few theoretical models. For example, in Ref. [120] the X_b is regarded as a virtual state about 10 MeV below the BB^* threshold, which means that it has no significant observable effects.

● *The $X(3915)$ and $X(3860)$*

The Belle experiment studied the process $\gamma\gamma \to \omega J/\psi$ using an integrated luminosity of 694 fb^{-1} [121]. The obtained $\omega J/\psi$ mass spectrum is shown in Fig. 18(a), where a prominent resonance-like peak around 3.92 GeV is observed. Using an S-wave BW function with a variable width for the resonant component, the obtained resonance parameters are: $M = (3915 \pm 3 \pm 2)$ MeV and $\Gamma = (17 \pm 10 \pm 3)$ MeV. This structure is called $X(3915)$. Subsequently, the $X(3915)$ was confirmed by BaBar using a data sample of 519.2 fb^{-1} in the same process [122]. Besides the confirmation of the existence of $X(3915)$, BaBar also did a spin-parity analysis, which supports the assignment $J^{PC} = 0^{++}$. Therefore, BaBar identified the $X(3915)$ as the $\chi_{c0}(2P)$ resonance.

Actually, the $X(3915)$ was firstly observed by Belle in $B \to J/\psi\omega K$ decays [124] with an original name of $Y(3940)$, and then was confirmed by BaBar [125]. However, in 2010 BaBar restudied the decays $B^{0,+} \to J/\psi\pi^+\pi^-\pi^0 K^{0,+}$ using 467×10^6 $B\bar{B}$ pairs [91]. Considering the phase space limitation, with a less restrictive $\pi^+\pi^-\pi^0$ mass region requirement a detailed study on the $\omega J/\psi$ mass spectrum revealed that the original $Y(3940)$ was made up of two structures, the
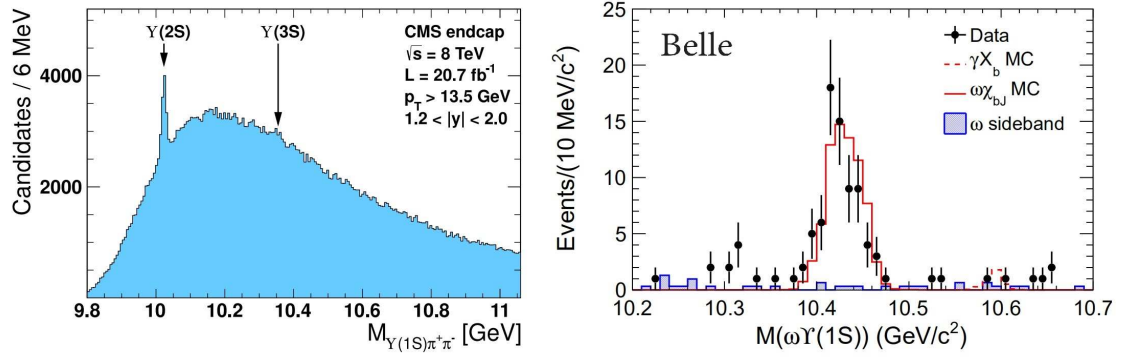
Figure 17: Results on the search of the X_b state from CMS in the $M[\pi^+\pi^-\Upsilon(1S)]$ distribution [118] and Belle in the $M[\omega\Upsilon(1S)]$ distribution [119].
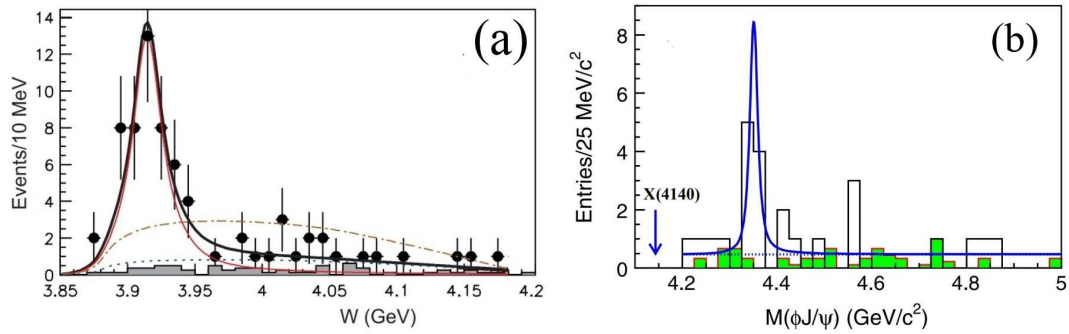
Figure 18: Distributions of $\omega J/\psi$ and $\phi J/\psi$ invariant mass spectra from the selected (a) $\gamma\gamma \to \omega J/\psi$ [121] and (b) $\phi J/\psi$ [123] candidates at Belle. The dots with error bars in (a) and the open histogram in (b) are from experimental data. The shaded histograms are from non-$\omega J/\psi$ and non-$\phi J/\psi$ backgrounds. The solid curves are the best fits with an (a) $X(3915)$ and (b) $X(4350)$ signal component. The dot-dashed curve in (a) is the fit without a resonance.

24

$X(3915)$ and $X(3872)$. As mentioned above, due to the assignment of $J^{PC} = 0^{++}$ for the $X(3915)$, it was identified as the $\chi_{c0}(2P)$ in the 2014 PDG tables. However, this assignment has some problems [126, 127]. Moreover, in Ref. [128] it was shown that the data for the $X(3915)$ could even be consistent with the $\chi_{c2}(3930)$, if the helicity-1-dominance constraint is relaxed in the analysis. As a result of these considerations, the $X(3915)$ is no longer identified as the $\chi_{c0}(2P)$ in the more recent PDG tables.

Some theoretical models explained the $X(3915)$ as a $D_s\bar{D}_s$ molecule, a compact tetraquark state, a $c\bar{c}$-gluon hybrid, etc. If $X(3915)$ were a compact $cs\bar{c}\bar{s}$ tetraquark, although the decay $X(3915) \to \omega J/\psi$ is allowed, the decay rate should be much lower than the mode of $\eta\eta_c$ considering the η meson has a relative large $s\bar{s}$ component. Experimental search for $X(3915) \to \eta\eta_c$ was done by Belle in $B^{\pm} \to K^{\pm}\eta\eta_c$, but a negative result was reported [129]. This disfavors the interpretation of the $X(3915)$ as a compact $cs\bar{c}\bar{s}$ tetraquark. If $X(3915)$ were a $c\bar{c}$-gluon hybrid, for a 0^{++} state, the $X(3915)$ mass would however not be a good match for a light hybrid [130, 131]. Therefore none of the above explanations is satisfactory and the nature of the $X(3915)$ is still unknown.

A promising process that is suitable for a search for the $\chi_{c0}(2P)$ and other charmonium states with positive C-parity is double-charmonium production in association with a J/ψ. The $X(3940)$ state was observed by Belle in the inclusive $e^+e^- \to J/\psi X$ spectrum and in the process $e^+e^- \to J/\psi D^*\bar{D}$ [132, 133], and the $X(4160)$ was observed in the process $e^+e^- \to J/\psi D^*\bar{D}^*$ [133]. Recently, Belle performed a full amplitude analysis of the process $J/\psi D\bar{D}$ ($D=D^0$ or D^+) based on a 980 fb^{-1} data sample [134]. A new charmonium-like state $X(3860)$ that decays to $D\bar{D}$ is observed with a significance of 6.5σ. Its mass is (3862^{+26+40}_{-32-13}) MeV and width is $(201^{+154+88}_{-67-82})$ MeV. The $J^{PC} = 0^{++}$ hypothesis is favored over the 2^{++} hypothesis at the level of 2.5σ and the new state is now called $\chi_{c0}(3860)$ by the PDG. Its mass is close to the potential model expectations for the $\chi_{c0}(2P)$, so it is a better candidate for the $\chi_{c0}(2P)$ charmonium state than the $X(3915)$. Figure 19 shows the projection of the signal fit results onto the $M(D\bar{D})$ distribution. The points with error bars are the data, the hatched histogram is the background, the blue solid line is the fit with the new resonance with $J^{PC} = 0^{++}$, and the red dashed line is the fit with a nonresonant amplitude only.
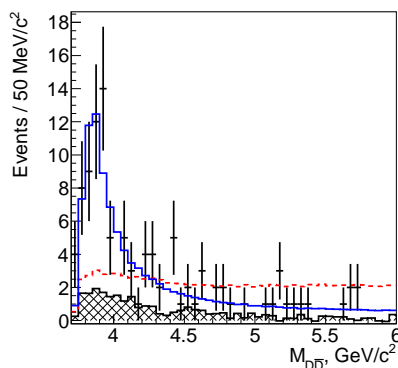
Figure 19: Projection of the signal fit results onto $M(D\bar{D})$ in the analysis of $e^+e^- \to J/\psi D\bar{D}$ by Belle [134]. The points with error bars are the data, the hatched histogram is the background, the blue solid line is the fit with a new X^* resonance with $J^{PC} = 0^{++}$, and the red dashed line is the fit with a nonresonant amplitude only.

The resonant parameters of the $X(3860)$ are very close to the phenomenological analyses [126, 135] of the Belle [136] and BaBar [137] data on $\gamma\gamma \to D\bar{D}$ where the $\chi_{c2}(3930)$ was observed. Further experimental investigation is needed to check the angular distribution of the two-photon process and to confirm the resonant nature of the events. The search for $\chi_{c0}(3860)$ and $\chi_{c2}(3930)$ in the radiative transitions of the excited ψ states is also very helpful to understand whether they are charmonium 2P states.

• *The $\chi_{c1}(4140)$ aka $X(4140)$ and other related states*

In 2008 the CDF experiment claimed a 3.8σ evidence for a near-threshold $X(4140) \to J/\psi\phi$ in $B^+ \to J/\psi\phi K^+$ decays using a data sample corresponding to an integrated luminosity of 2.7 fb^{-1} [33]. The mass and width of this

structure are measured to be (4143.0 ± 2.9 ± 1.2) MeV and $(11.7^{+8.3}_{-5.0} \pm 3.7)$ MeV, respectively. Much larger widths are expected for charmonium states in this mass range because of open-flavor decay channels, which makes the observation of the $X(4140)$ very interesting. It has been suggested that the $X(4140)$ structure could be a molecular state, a $\chi_{c1}(3P)$ state, a compact tetraquark state, a hybrid state, a rescattering effect and so on.

Searches for the $X(4140)$ did not confirm its presence in the analyses of the same B decays performed by the Belle [138] (unpublished) and BaBar [139] experiments. With a much larger data sample, LHCb did not find evidence for the narrow $X(4140)$ peak in the same B decays either [140]. Later CDF updated the analysis of $B^+ \to J/\psi\phi K^+$ using a larger data sample of 6.0 fb^{-1} [141]. This time, besides the confirmation of the $X(4140)$ with a mass of $(4143.4^{+2.9}_{-3.0} \pm 0.6)$ MeV and a width of $(15.3^{+10.4}_{-6.1} \pm 2.5)$ MeV, evidence for another structure with a mass of $(4274.4^{+8.4}_{-6.7} \pm 1.9)$ MeV and a width of $(32.3^{+21.9}_{-15.3} \pm 7.6)$ MeV is reported. The significance of this structure is estimated to be approximately 3.1σ. The $X(4140)$ was seen by CMS and D0 in both $B^+ \to J/\psi\phi K^+$ decays with a greater than 5.0σ and 3.1σ significance, respectively [142, 143]. The second peak observed in the updated analysis of $B^+ \to J/\psi\phi K^+$ by CDF [141] was also seen by CMS [142], but the measured mass was higher by 3.2σ.

Looking for more production modes will undoubtedly help us to understand the $X(4140)$. The first evidence for the prompt production of $X(4140) \to \phi J/\psi$ was presented by D0 based on 10.4 fb^{-1} of $p\bar{p}$ collision data [144]. The measured mass and width are $(4152.5 \pm 1.7^{+6.2}_{-5.4})$ MeV and $(16.3 \pm 5.6 \pm 11.4)$ MeV, respectively. BESIII searched for the $X(4140)$ via $e^+e^- \to \gamma\phi J/\psi$ at $\sqrt{s} =$4.23, 4.26, 4.36, and 4.60 GeV, but no significant $X(4140)$ signal was observed in any of these data samples [145, 146]. The upper limits of the product of the cross section and branching fraction $\sigma[e^+e^- \to \gamma X(4140)]B[X(4140) \to \phi J/\psi]$ are determined to be 0.35, 0.28, 0.33, and 1.2 pb at $\sqrt{s} =$4.23, 4.26, 4.36, and 4.60 GeV, respectively, at the 90% C.L.

To search for the $X(4140)$, Belle did a two-photon analysis of $\gamma\gamma \to \phi J/\psi$ [123]. The $\phi J/\psi$ mass spectrum is shown in Fig. 18(b), where the open histogram shows the experimental data, and the shaded histogram is from normalized ϕ and J/ψ mass sidebands. The arrow shows the expected position of the $X(4140)$. Instead of observation of the $X(4140)$, Belle found a 3.2σ evidence for a narrow $\phi J/\psi$ peak at $(4350.6^{+4.6}_{-5.1} \pm 0.7)$ MeV with a width of $(13^{+18}_{-9} \pm 4)$ MeV [123]. This structure is called $X(4350)$. The fit results are shown in Fig. 18(b) with the solid curve for the best fit and the dashed line for the backgrounds. It should be noted that the production of the $X(4140)$ in two-photon fusion is forbidden by the Landau–Young theorem if its spin is one as described below.

Considering the complicated structures and confusing experimental situation concerning the $\phi J/\psi$ mass spectrum, LHCb did a full amplitude analysis of the selected 4289 ± 151 $B^+ \to K^+\phi J/\psi$ events using 3 fb^{-1} data collected at c.m. energies 7 and 8 TeV [39]. This analysis offers the best sensitivity to study the resonant structures in the $\phi J/\psi$ system. The data requires not only two $J^{PC} = 1^{++}$ states, the $\chi_{c1}(4140)$ aka $X(4140)$ and $\chi_{c1}(4274)$ aka $X(4274)$ observed by CDF and CMS before, but also two new broad $J^{PC} = 0^{++}$ states, $X(4500)$ and $X(4700)$. Figure 20 shows the $\phi J/\psi$ invariant mass distribution for the selected signal candidates, where four $\phi J/\psi$ structures, $X(4140)$, $X(4274)$, $X(4500)$, and $X(4700)$, are needed [39]. These resonance parameters including signal significance, J^{PC} values, and the measured mass and width are listed in Table 3.

A comparison of the resonant parameters of $X(4140)$ reported from the different measurements [33, 39, 141–144, 147] is shown in Fig. 21, where the filled (open) circles indicate the significance of the $X(4140)$ signals greater (less) than 5σ. Note that Ref. [148] finds that the LHCb data are in fact compatible with a narrow $X(4140)$ as long as a broad $X(4160)$ state, a candidate for a $D_s^*\bar{D}_s^*$ molecular state, as well as the cusp for the $D_s^*\bar{D}_s^*$ threshold are included in the analysis. Confirmation, especially of the $X(4500)$ and $X(4700)$, from other experiments and further experimental investigation of them are needed. In the near future, the Belle II experiment can reanalyze the $B^+ \to K^+\phi J/\psi$ decays.

States	Significance	J^{PC}	Mass (MeV)	Width (MeV)
$X(4140)$	8.4σ	1^{++}	$4146.5 \pm 4.5^{+4.6}_{-2.8}$	$83 \pm 21^{+21}_{-14}$
$X(4274)$	6.0σ	1^{++}	$4273.3 \pm 8.3^{+17.2}_{-3.6}$	$56 \pm 11^{+8}_{-11}$
$X(4500)$	6.1σ	0^{++}	$4506 \pm 11^{+12}_{-15}$	$92 \pm 21^{+21}_{-20}$
$X(4700)$	5.6σ	0^{++}	$4704 \pm 10^{+14}_{-24}$	$120 \pm 31^{+42}_{-33}$

Table 3: Results for significances, masses, and widths of the $\phi J/\psi$ components in $B^+ \to J/\psi\phi K^+$ from the LHCb experiment [39].
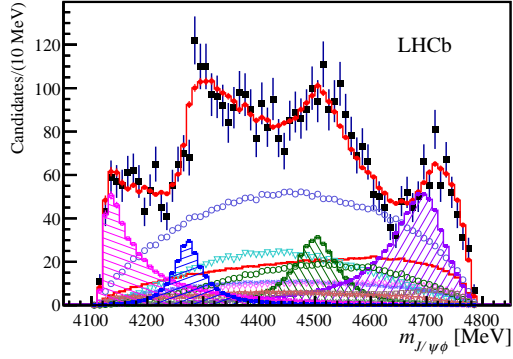
Figure 20: Distributions of $\phi J/\psi$ invariant mass for the $B^+ \rightarrow J/\psi\phi K^+$ candidates (black data points) compared with the fit containing eight $K^{*+} \rightarrow \phi K^+$ and five $X \rightarrow J/\psi\phi$ contributions [39]. The total fit is given by the red points with error bars. Individual fit components are also shown.
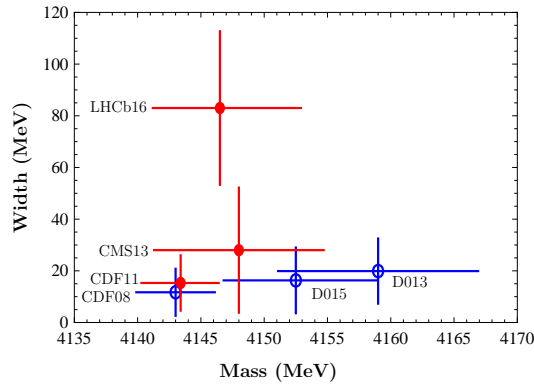
Figure 21: A comparison of the resonant parameters of $\chi_{c1}(4140)$ aka $X(4140)$ reported from different measurements [33, 39, 141–144, 147]. The filled (open) circles indicate the significance of the $X(4140)$ signals greater (less) than 5σ.

3.1.2. The Y states

Among the charmonium-like states, there are many vectors with quantum numbers $J^{PC} = 1^{--}$ that are usually called Y states, and according to the new PDG naming scheme (see Sec. 1.2) should be called $\psi(\text{mass})$, like the $\psi(4260)$ aka $Y(4260)$ [149], $\psi(4360)$ aka $Y(4360)$ [150, 151], and $\psi(4660)$ aka $Y(4660)$ [151]. The Y states show strong coupling to hidden-charm final states in contrast to the vector charmonium states in the same energy region, $\psi(4040)$ and $\psi(4160)$, which couple dominantly to the ground state open-charm meson pairs [6]. These Y states are good candidates for new types of exotic particles and stimulated many theoretical interpretations, including compact tetraquarks, molecules, hybrids, or hadrocharmonia (see, e.g., Ref. [13] and references therein).

The first Y state, the $Y(4260)$, was observed by BaBar via the ISR process $e^+e^- \to \pi^+\pi^- J/\psi$ using data samples of 211 fb^{-1} at $\sqrt{s} = 10.58$ GeV and 22 fb^{-1} at 10.54 GeV [149]. After that, a few Y states were discovered at B factories using ISR technology. The idea of utilizing ISR from a high-mass state to explore electron-positron processes at all energies below that state was outlined in Ref. [152]. With ISR events the whole hadron spectrum is visible so that the line shape of the resonance and fine structures can be investigated, while the effective luminosity and detection efficiency are relatively low. To study the Y states, a method complementary to the ISR is to take data via direct e^+e^- annihilation in the charmonium energy region. In particular, BESIII has collected large data samples above 4 GeV in recent years [20], which allow accurate determinations of the cross sections for some final states. The drawback is that since the data are taken at fixed energy points, one might miss narrow structures.

● *The $\psi(4230)$ aka $Y(4230)$ state*

The process $e^+e^- \to \pi^+\pi^- J/\psi$ via ISR at c.m. energies up to 5.0 GeV was first studied by BaBar, where an unexpected structure at about 4.26 GeV was observed clearly [149]. It is the first observed Y state, which is referred to as $Y(4260)$. Subsequently, although the $Y(4260)$ was confirmed by Belle in the same process, Belle found that $Y(4260)$ alone cannot describe the line shape satisfactorily [25]. Besides the $Y(4260)$, Belle also observed a broad excess near 4 GeV, called $Y(4008)$ [25]. Improved measurements with both BaBar [153] and Belle [68] full data samples confirmed the existence of a component in addition to $Y(4260)$ in $e^+e^- \to \pi^+\pi^- J/\psi$ but the line shape was parametrized with different models.

BESIII reported a precise measurement of $e^+e^- \to \pi^+\pi^- J/\psi$ cross sections from 3.77 to 4.60 GeV using data samples with an integrated luminosity of 9 fb^{-1} [73]. While the nature of the events at around 4 GeV is still ambiguous, the dominant resonant structure, the so called $Y(4260)$, was found to have a mass of $(4222.0 \pm 3.1 \pm 1.4)$ MeV and a width of $(44.1 \pm 4.3 \pm 2.0)$ MeV. In addition, a new resonance with a mass of around 4.32 GeV is needed to describe the high precision data. Its mass and width are $(4320.0 \pm 10.4 \pm 7.0)$ MeV and $(101.4^{+25.3}_{-19.7} \pm 10.2)$ MeV with a statistical significance larger than 7.6σ. This resonance is called $Y(4320)$. However, it should be mentioned that the analysis mentioned above was performed using BW functions that generate symmetric line shapes — however, already the analysis of the older data based on the molecular picture, which naturally generates asymmetric line shapes even from a single state only, found a mass for the $Y(4260)$ close to 4230 MeV [154] that is also qualitatively consistent with the new data as discussed in Sec. 4.3.4 (see Fig. 81). Figure 22(a) shows the measured $e^+e^- \to \pi^+\pi^- J/\psi$ cross sections, where one can see clearly the $Y(4260)$ structure observed by BaBar and Belle experiments, but its peaking position is at around 4.22 GeV rather than 4.26 GeV from the previous fits [68, 153]. Since both mass and width of $Y(4320)$ are consistent with those of the $Y(4360)$ resonance observed in $e^+e^- \to \pi^+\pi^- \psi(2S)$ by BaBar and Belle [155, 156], they could be the same state, which needs to be confirmed with precise measurements of these two resonant parameters in the future. It is worth pointing out that the lower mass structure [called $\psi(4230)$ aka $Y(4230)$ hereafter] is the main component of the $Y(4260)$ structure with an improved measurement of the resonant parameters. But we also note that an accurate measurement of the cross section at 4.32 GeV is very important since its size will determine how to describe the line shape of $e^+e^- \to \pi^+\pi^- J/\psi$ cross sections, in particular if there is one or two resonances.

Besides the $\pi^+\pi^- J/\psi$ final states, the neutral process $e^+e^- \to \pi^0\pi^0 J/\psi$ was measured by BESIII from 4.19 to 4.42 GeV corresponding to an integrated luminosity of 2.8 fb^{-1} [157]. The measured cross sections are shown in Fig. 22(b), where the $Y(4260)$ signals are clear. Although the covered energy range is narrower than in the charged mode, the measured line shape is in good agreement with that in Fig. 22(a). In the future, BESIII is able to improve the measurements by using more data points.

From the BESIII data, one can see that besides the $Y(4230)$ peak, the $\pi^+\pi^- J/\psi$ cross section is at the 10–15 pb level. Whether the cross section is due to the pure continuum process or from the decays of other charmonium or

28
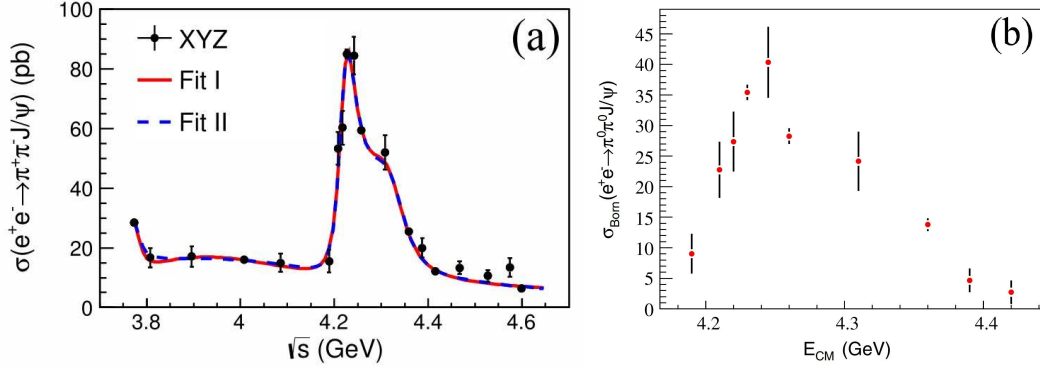
Figure 22: Measured cross sections of (a) $e^+e^- \to \pi^+\pi^- J/\psi$ [73] and (b) $e^+e^- \to \pi^0\pi^0 J/\psi$ [157]. In (a), the solid and dashed lines are the fits with the coherent sum of three BW functions (Fit I, red solid curve) and the coherent sum of an exponential continuum and two BW functions (Fit II, blue dashed curve).
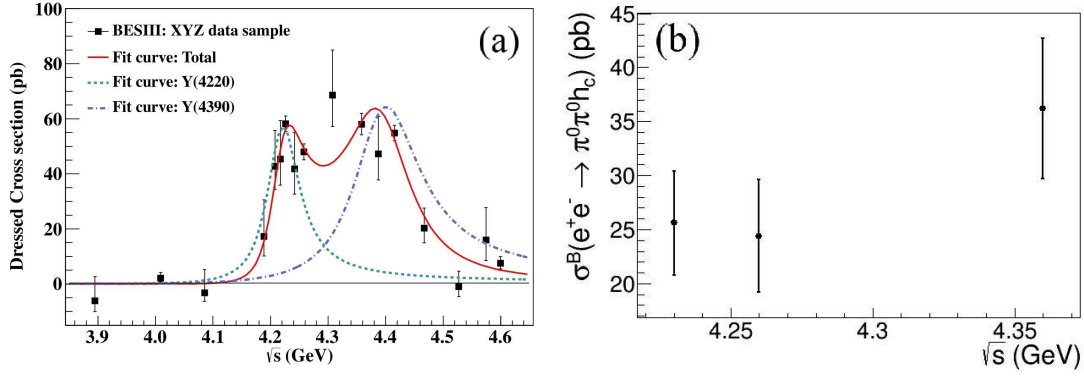
Figure 23: Measured cross sections of (a) $e^+e^- \to \pi^+\pi^- h_c$ [159] and (b) $e^+e^- \to \pi^0\pi^0 h_c$ [157]. In (a), the solid curve is the fit with the coherent sum of two BW functions, and the dashed and dash-dotted curves show the contributions from the two structures $\psi(4230)$ aka $Y(4230)$ and $Y(4390)$.

charmonium-like states is still not clear. Once more data samples are available at BESIII or Belle II in the future, one can try to fit the cross sections by adding coherent $\psi(4040)$ and $\psi(4160)$ resonances to check their couplings to the $\pi^+\pi^- J/\psi$ final state.

Replacing the J/ψ with an h_c, BESIII reported the cross section measurement of $e^+e^- \to \pi^+\pi^- h_c$ at 13 c.m. energies from 3.9 to 4.4 GeV and found the magnitude of the cross sections is about the same as that of $e^+e^- \to \pi^+\pi^- J/\psi$ but with a different line shape [158]. Although no quantitative results were given in interpreting the $\pi^+\pi^- h_c$ line shape, the resonant structure at around 4.22 GeV is obvious [158]. A follow-up measurement of $e^+e^- \to \pi^+\pi^- h_c$ cross sections at c.m. energies from 3.9 to 4.6 GeV was done in 2017 with improved precision [159]. The cross sections of the neutral process $e^+e^- \to \pi^0\pi^0 h_c$ were also measured by BESIII at $\sqrt{s}$ =4.23, 4.26, and 4.36 GeV [157]. In all the above measurements, the h_c is reconstructed via its electric-dipole transition $h_c \to \gamma\eta_c$ with η_c to 16 exclusive hadronic final states. The measured cross sections are shown in Fig. 23. The Born cross sections of $e^+e^- \to \pi^0\pi^0 h_c$ are found to be about half of those of $e^+e^- \to \pi^+\pi^- h_c$ within less than 2σ.

The cross sections of $e^+e^- \to \pi^+\pi^- h_c$ indicate that there are possibly two resonant structures in the studied energy range although the error bar at around 4.3 GeV is large and it seems very important to understand the line shape. Assuming that there are two interfering resonances, BESIII performed a fit to the distribution of the $e^+e^- \to \pi^+\pi^- h_c$ cross sections and obtained the parameters of the two resonances: $M = (4218.4^{+5.5}_{-4.5} \pm 0.9)$ MeV, $\Gamma = (66.0^{+12.3}_{-8.3} \pm 0.4)$ MeV, and the product of the electronic partial width and the decay branching fraction $\Gamma_{e^+e^-}\mathcal{B}[Y(4230) \to \pi^+\pi^- h_c] =$

$(4.6^{+2.9}_{-1.4} \pm 0.8)$ eV for $Y(4230)$, and $M = (4391.5^{+6.3}_{-6.8} \pm 1.0)$ MeV, $\Gamma = (139.5^{+16.2}_{-20.6} \pm 0.6)$ MeV, and $\Gamma_{e^+e^-}\mathcal{B}[Y(4390) \rightarrow \pi^+\pi^- h_c] = (11.6^{+5.0}_{-4.4} \pm 1.9)$ eV for $Y(4390)$, with a relative phase of $\phi = (3.1^{+0.7}_{-0.9} \pm 0.2)$ rad. The parameters of the $Y(4230)$ are consistent with those of the resonance observed in $e^+e^- \rightarrow \pi^+\pi^- J/\psi$ [73] discussed above and in $e^+e^- \rightarrow \omega\chi_{c0}$ [160] discussed below. The high mass structure is different from the $Y(4360)$ [155, 156] (discussed below) and $\psi(4415)$ [6]. In the future, the precision of the cross section at around 4.3 GeV needs to be improved in order to better understand the line shape of $e^+e^- \rightarrow \pi^+\pi^- h_c$.

A possible strong coupling of the $Y(4230)$ to the $\omega\chi_{cJ}$ ($J = 0, 1, 2$) final state was proposed by a few authors [161, 162]. In 2014, BESIII reported the cross section measurement of $e^+e^- \rightarrow \omega\chi_{c0}$ at 9 c.m. energies from 4.21 to 4.42 GeV, where χ_{c0} candidates are reconstructed via a pair of $\pi^+\pi^-$ or K^+K^- [160]. The Born cross sections are measured to be $(55.4 \pm 6.0 \pm 5.9)$ pb and $(23.7 \pm 5.3 \pm 3.5)$ pb at $\sqrt{s} = 4.23$ and 4.26 GeV, respectively, which are comparable to those of the $\pi^+\pi^- J/\psi$ process [73]. Later BESIII updated the measurement of $e^+e^- \rightarrow \omega\chi_{c0}$ with higher energy data up to 4.6 GeV included [163]. Besides the energy points at 4.23 and 4.26 GeV, no significant signals are found at other energy points, and the upper limits on the cross sections at the 90% C.L. are determined [163]. The cross sections are shown in Fig. 24 (left plot), where a clear peaking structure close to the threshold is observed although there are only two statistically significant measurements available. Assuming the $\omega\chi_{c0}$ signals come from a single resonance, the cross sections of $e^+e^- \rightarrow \omega\chi_{c0}$ are fitted with a BW function as shown in Fig. 24 (left plot). The fitted mass and width are $(4226 \pm 8 \pm 6)$ MeV and $(39 \pm 12 \pm 2)$ MeV, respectively, with a statistical significance of more than 9σ.
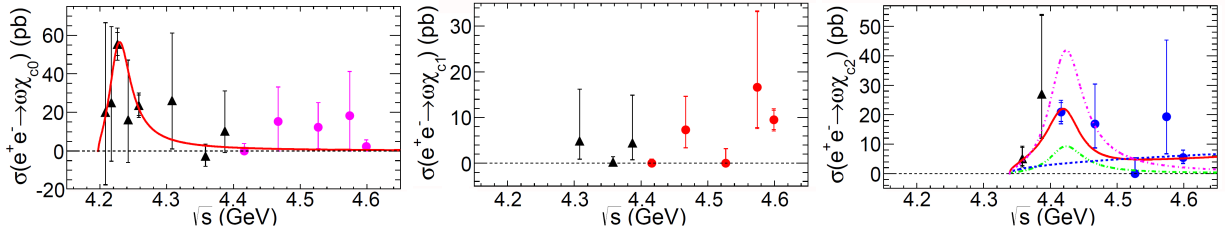
Figure 24: Measured Born cross section for $e^+e^- \rightarrow \omega\chi_{cJ}$ ($J = 0, 1, 2$) as a function of c.m. energy [160, 163]. The smaller error bars are statistical and the larger error bars are the combined statistical and systematic errors. The solid curves show the fit results.

Very recently the cross section of the process $e^+e^- \rightarrow \omega\chi_{c0}$ was again updated by BESIII at c.m. energies $\sqrt{s}$ from 4.178 to 4.278 GeV using a data sample of 7 fb^{-1} [164]. The event selection is almost the same as before [160, 163]. The updated $e^+e^- \rightarrow \omega\chi_{c0}$ cross section as a function of the c.m. energy is shown in Fig. 25, where the blue points are from the updated measurement [164] and the black square points are from previous measurements [160, 163]. As expected, the $Y(4230)$ signal is observed clearly. By assuming that all the $\omega\chi_{c0}$ signals come from this resonance, the fit result is shown in Fig. 25 with a solid red line and the fitted mass and width are $M = (4218.5 \pm 1.6 \pm 4.0)$ MeV and $\Gamma = (28.2 \pm 3.9 \pm 1.6)$ MeV. The updated measurement confirms and statistically improves upon the previous observation [160, 163]. The parameters of this state are consistent with those of the narrow structure in the $e^+e^- \rightarrow \pi^+\pi^- h_c$ [159, 161], $\pi^+\pi^- J/\psi$ [73], $D^0 D^{*-}\pi^+ + c.c.$ [165], and $\pi^+\pi^-\psi(2S)$ [166] (discussed below) processes.

For the $Y(4230)$, one of the big puzzles is that there is a dip at around 4.22 GeV in the distribution of cross sections of the charm meson pairs, instead of a peak. Therefore, whether or not this state can couple to open charm channels is a crucial issue for understanding its nature. Utilizing the measured cross sections of $e^+e^- \rightarrow D^*\bar{D}^*$ and $D_s^*\bar{D}_s^*$ by Belle [167, 168], the authors of Ref. [169] performed fits using $\psi(4040)$, $\psi(4160)$, and $\psi(4415)$ together with the $Y(4230)$ allowing for an interference between them [169]. The cross sections can be well described by these states, and the interference between the $Y(4230)$ and the other charmonia produces a dip around 4.22 GeV in the $e^+e^- \rightarrow D^*\bar{D}^*$ cross section line shape. However, the errors of current Belle measurements are large especially for $e^+e^- \rightarrow D_s^*\bar{D}_s^*$ cross sections. More precise measurements should be done at BESIII to clarify the role played by the $Y(4230)$.

Motivated by the absence of open-charm decay channels for the Y states, Belle did the first measurement of the exclusive cross section for $e^+e^- \rightarrow D^0 D^{*-}\pi^+ + c.c.$ as a function of c.m. energy from the $D^0 D^{*-}\pi^+ + c.c.$ threshold to 5.2 GeV with ISR using an integrated luminosity of 695 fb^{-1} data sample at the $\Upsilon(4S)$ resonance [170]. The measured
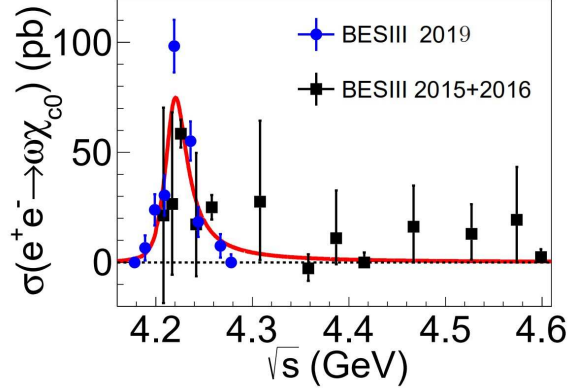
Figure 25: The $e^+e^- \to \omega\chi_{c0}$ cross section as a function of the c.m. energy from BESIII. The blue points are from the updated measurement [164] and the black square points are from previous measurements [160, 163]. The red solid line is the fit result assuming all the $\omega\chi_{c0}$ signals come from a single resonance.

cross sections are shown in Fig. 26(a). No evidence for the $Y(4230)$, $Y(4360)$, $\psi(4415)$, $Y(4630)$, or $Y(4660)$ was found with the limited statistics. Belle performed a likelihood fit with a possible $\psi(4415)$ signal contribution plus a threshold function. The fit yields $14.4 \pm 6.2^{+1.0}_{-9.5}$ signal events for the $\psi(4415)$ state with a statistical significance of 3.1σ. A 90% C.L. upper limit on the peak cross section for the $e^+e^- \to \psi(4415) \to D^0 D^{*-}\pi^+ + c.c.$ process at $\psi(4415)$ nominal mass is obtained to be 0.76 nb.

Recently BESIII reported an improved measurement of the cross section of $e^+e^- \to D^0 D^{*-}\pi^+ + c.c.$ at c.m. energies from 4.05 to 4.60 GeV at 15 energy points with integrated luminosity larger than 40 pb^{-1} for each point and 69 "R-scan data" points with integrated luminosity smaller than 20 pb^{-1} for each point [165], where the D^0 meson is reconstructed via $D^0 \to K^-\pi^+$ and the bachelor π^+ is also reconstructed, while the D^{*-} is inferred from energy-momentum conservation in order to increase the statistics. The measured cross sections are shown in Fig. 26(b). Two resonant structures in good agreement with the $Y(4230)$ and $Y(4390)$ observed in $\pi^+\pi^- h_c$ [159] are identified over a smoothly increasing non-resonant term which can be parametrized with a three-body phase-space amplitude. Therefore, a fit to the cross section from BESIII measurement is performed to determine the parameters of the two resonant structures.
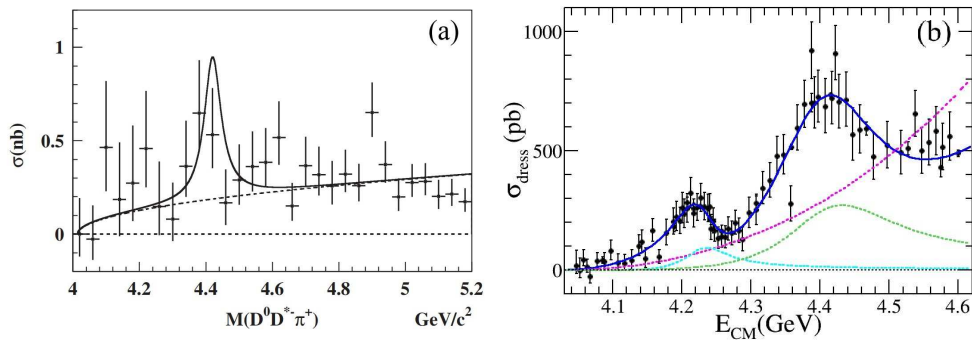
Figure 26: Measured cross sections of $e^+e^- \to D^0 D^{*-}\pi^+ + c.c.$ from (a) Belle [170] and (b) BESIII [165] experiments. Belle did a fit to cross sections with a $\psi(4415)$ signal plus a threshold function, while BESIII did a fit with the coherent sum of a direct three-body phase-space term and two BW functions for the $Y(4230)$ and $Y(4390)$. The solid lines are the total fit results.

The total amplitude is described by the coherent sum of a direct three-body phase-space term for $e^+e^- \to D^0 D^{*-}\pi^+ + c.c.$ and two BW functions, representing the two resonant structures. The fit yields a mass of $(4228.6 \pm 4.1 \pm 6.3)$ MeV and a width of $(77.0 \pm 6.8 \pm 6.3)$ MeV for the lower mass structure. As for the higher mass structure,

31

there are complicated effects which require further detailed amplitude analysis since a few excited ψ states and Y charmonium-like states may overlap in this wide mass region. Models including one additional known resonance, either $Y(4320)$, $Y(4360)$, or $\psi(4415)$ with their masses and widths fixed to the world average values [6], can improve the fit quality. However, the statistical significance of any additional resonance is less than 2σ. Since the lower mass resonance is in good agreement with the $Y(4230)$ observed in $\pi^+\pi^- J/\psi$, $\pi^+\pi^- h_c$, and $\omega\chi_{c0}$ modes [73, 159], this indicates the first observation of the $Y(4230)$ decays into an open-charm final state $D^0 D^{*-}\pi^+ + c.c..$ The measured Born cross section of $e^+e^- \rightarrow D^0 D^{*-}\pi^+ + c.c.$ at the $Y(4230)$ peak is higher than the sum of the known hidden-charm channels, which tells us the $D^0 D^{*-}\pi^+ + c.c.$ final state may be the dominant decay mode of the $Y(4230)$ state.

An obvious feature in the above four channels $e^+e^- \rightarrow \omega\chi_{c0}$, $\pi^+\pi^- h_c$, $\pi^+\pi^- J/\psi$, and $D^0 D^{*-}\pi^+ + c.c.$ from the BESIII measurements is that there is a common structure at around 4.22 GeV, i.e., the $Y(4230)$. Considering this, the authors of Ref. [171] did a simultaneous fit to the cross sections of these four processes. The measured mass and width of the $Y(4230)$ are $(4219.6 \pm 3.3 \pm 5.1)$ MeV and $(56.0 \pm 3.6 \pm 6.9)$ MeV, respectively.

The leptonic decay width for a vector state is an important quantity for discriminating various theoretical interpretations of its nature. As current measurements only give the product of the leptonic decay width and the strong decay widths, the magnitude of the leptonic decay width determines how the strong decay widths sum up to the total width. Smaller leptonic decay width means that the strong decay widths will be relatively enhanced and vice versa. The estimate of quenched[3] lattice QCD for the leptonic decay width of the $Y(4230)$ is about 40 eV [172] assuming it to be a hybrid meson and neglecting its coupling to meson-meson decay channels; the predicted upper limit of the $Y(4230)$ leptonic decay width is about 500 eV if the $Y(4230)$ is a hadronic molecule dominated by $D\bar{D}_1(2420)$ [173]; the leptonic decay width is only about 23 eV for the $\omega\chi_{c0}$ molecule interpretation [162], where no contributions from the open charm decay channel are included in the analysis.

By considering the isospin symmetric modes of the measured channels, the authors of Ref. [171] estimated the lower limit on the leptonic partial width of the $Y(4230)$ decays for the first time: $\Gamma_{e^+e^-}[Y(4230)] > (29.1\pm2.5\pm7.0)$ eV. This lower limit is close to quenched lattice QCD result for a hybrid vector charmonium state [172]. By considering other $Y(4230)$ decay modes, such as $\pi^+\pi^-\psi(2S)$, ηh_c discussed below, the above estimation can be refined.

In an analysis of $e^+e^- \rightarrow \pi^+\pi^-\psi(2S)$, Belle found evidence for the contribution from the $Y(4230)$ [155] while high-statistics BESIII data confirmed the observation of this mode together with a measurement of the resonant parameters [166]. Figure 27 shows the measured mass and width of the $Y(4230)$ from the processes $\pi^+\pi^- J/\psi$ [73], $e^+e^- \rightarrow \pi^+\pi^- h_c$ [159], $D^0 D^{*-}\pi^+ + c.c.$ [165], $\pi^+\pi^-\psi(2S)$ [166], and $\omega\chi_{c0}$ [164] from the BESIII Collaboration. Although the measured masses are consistent with each other, the widths from the processes $e^+e^- \rightarrow \pi^+\pi^- h_c$, $\pi^+\pi^-\psi(2S)$, and $D^0 D^{*-}\pi^+ + c.c.$ are larger than those from the processes $e^+e^- \rightarrow \pi^+\pi^- J/\psi$ and $\omega\chi_{c0}$. At the moment, we cannot draw a conclusion on whether the structure observed in these processes is the same state or whether the inconsistencies are caused by the BW parametrization. Further experimental studies with higher statistics are needed to draw a more reliable conclusion on the nature of this structure.

The compact tetraquark model [174] predicted a sizeable isospin-violating process $Y(4230) \rightarrow \eta\pi^0 J/\psi$ with Z_c^0 decaying into $\pi^0 J/\psi$ and possibly $\eta J/\psi$. The molecular model [175] predicted a peak in the cross section of $e^+e^- \rightarrow \eta\pi^0 J/\psi$ at the $D_1\bar{D}$ threshold and a narrow peak in the $\eta J/\psi$ mass spectrum at the $D\bar{D}^*$ threshold. Therefore, using data samples collected at c.m. energies of $\sqrt{s}$ =4.009, 4.226, 4.257, 4.358, 4.416, and 4.599 GeV with a total luminosity of 4.5 fb^{-1}, BESIII searched for such an isospin-violating decay process [176]. No $Y(4230)$ signal is observed, and upper limits on the cross sections $e^+e^- \rightarrow \eta\pi^0 J/\psi$ at the 90% C.L. are determined to be 3.6, 1.7, 2.4, 1.4, 0.9, and 1.9 pb for $\sqrt{s}$ =4.009, 4.226, 4.257, 4.358, 4.416, and 4.599 GeV, respectively.

Under the assumption of $Y(4230)$ being a hybrid meson, the quenched lattice study [177] suggested that the rate of decay to $\gamma\eta_c$ may be enhanced relative to $\gamma\chi_{c0}$. Finding evidence for $Y(4230) \rightarrow \gamma\eta_c$ could thus give additional support to the hybrid interpretation. BESIII searched for the process $e^+e^- \rightarrow \gamma\eta_c$ at six c.m. energies between 4.01 and 4.60 GeV corresponding to a total integrated luminosity of 4.6 fb^{-1} [178]. The final distribution of $\sigma(e^+e^- \rightarrow \gamma\eta_c)$ is shown as the points in Fig. 28. The lines in Fig. 28 show the different assumptions of resulting cross sections as a function of energy, where (1) σ_{FLAT}: the cross section is constant, (2) σ_{BELLE}: the cross section follows the Belle parametrization of $\sigma(e^+e^- \rightarrow \pi^+\pi^- J/\psi)$ [68], (3) $\sigma_{Y(4230)}$: the cross section follows a non-relativistic BW distribution for the $Y(4260)$ with mass and width values from the PDG [6], and (4) $\sigma_{Y(4360)}$: the cross section follows a non-relativistic BW distribution for the $Y(4360)$ with mass and width values from the PDG [6]. With current statistics,

---

[3]i.e., not including the effects of sea quarks and so leading to a non-unitary theory and an unknown systematic uncertainty — see Sec. 4.5.
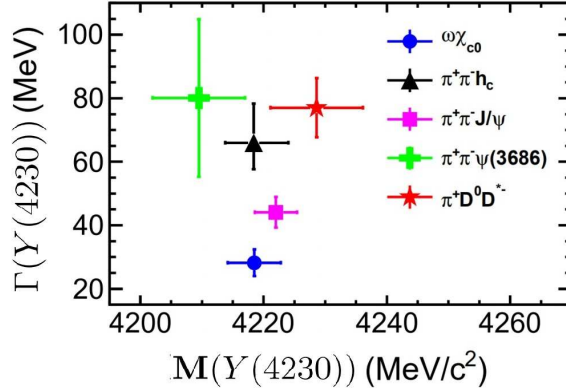
Figure 27: The measured mass and width of the $Y(4230)$ from the processes $\pi^+\pi^-J/\psi$ [73], $e^+e^- \to \pi^+\pi^-h_c$ [159], $D^0D^{*-}\pi^+ + c.c.$ [165], $\pi^+\pi^-\psi(2S)$ [166], and $\omega\chi_{c0}$ [164] from the BESIII Collaboration.

different assumptions for the energy dependence of the cross section can not be distinguished, but the cross section is somewhat better explained by $\sigma_{Y(4230)}$. The expected rates of $e^+e^- \to \psi(4040)/\psi(4415) \to \gamma\eta_c$ are also shown in Fig. 28 as solid lines. Both significances are 1.9σ. Much larger data samples are required to confirm the existence of the $Y(4230) \to \gamma\eta_c$ process.
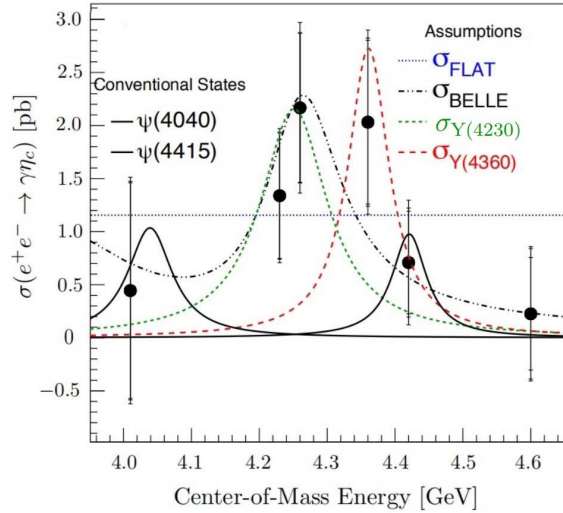
Figure 28: Measured Born cross section for $e^+e^- \to \gamma\eta_c$ as a function of c.m. energy [178] and comparison with different assumptions about the energy-dependence of the cross section (broken lines). The predicted cross sections for $e^+e^- \to \psi(4040)/\psi(4415) \to \gamma\eta_c$ are shown as solid lines.

Some light-hadron final states are also searched for by BESIII for the $Y(4230)$ decays including $K_S^0K^\pm\pi^\mp$ [179], $K_S^0K^\pm\pi^\mp\pi^0$, and $K_S^0K^\pm\pi^\mp\eta$ [180]. The Born cross sections of e^+e^- to these final states are measured up to 4.6 GeV. In fitting these cross sections, besides the continuum component, a $Y(4230)$ signal is added. No clear signal is observed, thus the 90% C.L. upper limits on the cross sections of $e^+e^- \to Y(4230)$ times the branching fractions of the $Y(4230)$ to these final states are set.

The $Y(4230)$ was also searched for in the charged B decay $B^+ \to K^+\pi^+\pi^-J/\psi$ by the BaBar Collaboration based on 232×10^6 $B\bar{B}$ pairs and a signal with a statistical significance of 3.1σ was observed [181]. Very recently, Belle did the same search in both charged and neutral B decays $B^+ \to K^+\pi^+\pi^-J/\psi$ and $B^0 \to K^0\pi^+\pi^-J/\psi$ by fully reconstructing

the final states from B decays based on 771.58 million $B\bar{B}$ pairs [182]. The obtained $\pi^+\pi^- J/\psi$ mass spectra after subtracting the combinatorial background from charged and neutral B decays are shown in Fig. 29, where no clear $Y(4230)$ signal can be seen. The signal significances of the $Y(4230)$ taking into account the systematic uncertainties are 2.1σ and 0.9σ by an unbinned extended maximum-likelihood fit to these two $\pi^+\pi^- J/\psi$ mass spectra with a sum of two Gaussians as a $Y(4230)$ signal shape. The blue solid lines in Fig. 29 are the best fits. The upper limits on the product branching fractions $\mathcal{B}[B^+ \to K^+ Y(4230)]\mathcal{B}[Y(4230) \to \pi^+\pi^- J/\psi]$ and $\mathcal{B}[B^0 \to K^0 Y(4230)]\mathcal{B}[Y(4230) \to \pi^+\pi^- J/\psi]$ at the 90% C.L. are determined to be 1.4×10^{-5} and 1.7×10^{-5}, respectively. In a search for the $Z_c(3900)$ in b-hadron decays, the D0 experiment reported evidence for the $Y(4230)$ production associated with its $\pi Z_c(3900)$ decay mode [183] (discussed in Sec. 3.2). These studies will obviously benefit from much larger data samples.
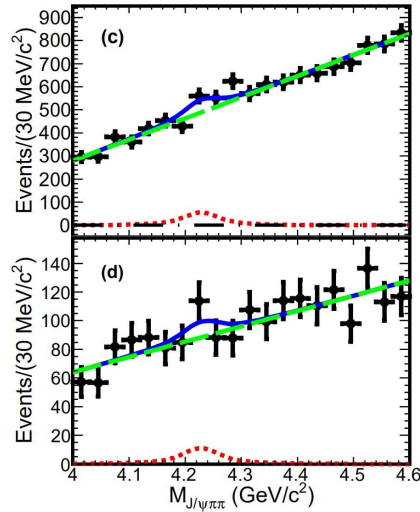
Figure 29: The $\pi^+\pi^- J/\psi$ mass spectra from charged (top) and neutral (bottom) B decays $B^+ \to K^+\pi^+\pi^- J/\psi$ and $B^0 \to K^0\pi^+\pi^- J/\psi$ [182]. The blue solid lines are the best fits, the green dashed curves are the fitted backgrounds, and the red dotted curves are the signals.

Further studies of $Y(4230)$ decays in experiments are needed with larger data statistics. Being well above the thresholds of many final states with η_c, such as $\pi\rho\eta_c$, $\omega\eta_c$, and $\phi\eta_c$, and final states like ηh_c, $K\bar{K}J/\psi$, $\eta^{(\prime)}J/\psi$, and $\eta^{(\prime)}\psi(2S)$, $Y(4230)$ may decay into such final states with substantial rates. In addition, the decays into open charm final states other than $D\bar{D}^*\pi$ such as $D\bar{D}$, $D\bar{D}^* + c.c.$, $D^*\bar{D}^*$, $D_s^+D_s^-$, $D_s^+D_s^{*-} + c.c.$ are also possible, even if the charmed mesons are in a relative P-wave. The $Y(4230)$ is very close to the $D_s^{*+}D_s^{*-}$ threshold, a possible coupling to this mode should also be investigated. Whether the $Y(4230)$ can decay into the light-hadron final states is also interesting. Further information on these final states will be important for deeper understanding of the nature of the $Y(4230)$.

For the $Y(4230)$, popular theoretical interpretations include a $D\bar{D}_1(2420)$ molecule [154, 184, 185], a $c\bar{c}$-gluon hybrid [186–188], a compact tetraquark state [189], a hadrocharmonium [190, 191]. If $Y(4230)$ is a $D\bar{D}_1(2420)$ molecule, the binding energy is about 66 MeV which is rather large but not excluded. If $Y(4230)$ is a $c\bar{c}$-gluon hybrid, its mass is about 180 MeV below current predictions from lattice QCD [131], but consistent with the mass determined from combining non-relativistic EFTs and lattice QCD data of the hybrid static energies [192, 193] (see also Sec. 4.4.4), all of which neglect the resonant nature of the $Y(4230)$. If it were a compact tetraquark state, it would have isospin- and SU(3)-multiplet partner states. However, none of them has been observed in experiments so far. If it is a hadrocharmonium, its decay rate to non-$J/\psi(h_c)$ charmonium states should be suppressed, which is not supported by the data although a possible mixing of two hadrocharmonia with spin 1 and spin 0 compact $\bar{c}c$ cores can make the scenario consistent [191]. At this point in time the nature of this lightest negative parity exotic candidate is not yet fully settled.

There have been a number of different interpretations proposed for the $Y(4320)$ and $Y(4390)$, including a $\psi(3^3D_1)$ state [194, 195], a compact tetraquark state [196, 197], a hadrocharmonium [198], a $D^*\bar{D}_1(2420)$ molecule [199–201], a state formed from dynamical diquarks [202], a hybrid state [193] and so on. In addition to the above explanations, a

special explanation is that the $Y(4320)$ and $Y(4390)$ may not exist at all. The authors of Ref. [203] found that the fits to the distributions of $e^+e^- \to \pi^+\pi^- J/\psi$ and $\pi^+\pi^- h_c$ cross sections measured by BESIII with three interfering resonances $Y(4230)$, $\psi(4160)$, and $\psi(4415)$ can also describe the data well with a goodness of the fit of $\chi^2/ndf = 118/153$ and $18/69$, respectively, where ndf is the number of degrees of freedom. Based on the fit qualities, the authors argued that two newly reported charmonium-like states, $Y(4320)$ and $Y(4390)$, are not genuine resonances. However, it should be stressed that the analysis of Ref. [203] needs to implement a huge amount of spin-symmetry violation as well as very large non–resonant couplings at odds with our current understanding of the role of the heavy quark spin symmetry in doubly-heavy systems (see also Sec. 4.4).

• *The $\psi(4360)$ aka $Y(4360)$ and $\psi(4660)$ aka $Y(4660)$ states*

Replacing the J/ψ with a $\psi(2S)$, BaBar studied the ISR process $e^+e^- \to \pi^+\pi^-\psi(2S)$ to search for the exotic state found previously, namely $Y(4260)$ [150]. Instead of the $Y(4260)$, a clear structure around 4.32 GeV was observed [150]. Subsequently, Belle checked this process and found that there are actually two resonant structures at 4.36 and 4.66 GeV, denoted as the $Y(4360)$ and $Y(4660)$ [151].

The BaBar experiment reported the update of the study of $e^+e^- \to \pi^+\pi^-\psi(2S)$ with ISR events with the full data sample recorded at and near the $\Upsilon(nS)$ (n=2, 3, 4) resonances with an integrated luminosity of 520 fb^{-1} [156]. The cross sections for $e^+e^- \to \pi^+\pi^-\psi(2S)$ from 3.95 to 5.95 GeV have been measured. A fit to the $\pi^+\pi^-\psi(2S)$ mass distribution yields a mass of $(4340 \pm 16 \pm 9)$ MeV and a width of $(94 \pm 32 \pm 13)$ MeV for the $Y(4360)$, and a mass of $(4669 \pm 21 \pm 3)$ MeV and a width of $(104 \pm 48 \pm 10)$ MeV for the $Y(4660)$ [156]. The results are in good agreement with the Belle measurement and confirm the $Y(4660)$ observed by the Belle experiment [151]. In both the Belle and BaBar measurements, the $\pi^+\pi^-$ mass distribution appears to differ from the phase-space expectation. For the $Y(4660) \to \pi^+\pi^-\psi(2S)$ decays, there is an indication of an accumulation of events in the vicinity of the $f_0(980)$ state.

The $Y(4360)$ and $Y(4660)$ parameters were measured with improved precision with the full 980 fb^{-1} data sample of Belle [155]. Fitting the mass spectrum of $\pi^+\pi^-\psi(2S)$ with two coherent BW functions (see Fig. 30 (left)), Belle obtained $M[Y(4360)] = (4347 \pm 6 \pm 3)$ MeV, $\Gamma[Y(4360)] = (103 \pm 9 \pm 5)$ MeV, $M[Y(4660)] = (4652 \pm 10 \pm 8)$ MeV, and $\Gamma[Y(4660)] = (68 \pm 11 \pm 1)$ MeV. Belle also noticed that there are a number of events in the vicinity of the $Y(4230)$ mass. The fit with the $Y(4230)$ included is also performed. In the fit, the mass and width of the $Y(4230)$ are fixed to the latest measured values at Belle [68]. The signal significance of the $Y(4230)$ is found to be only 2.4σ. In this fit, one obtains $M[Y(4360)] = (4365 \pm 7 \pm 4)$ MeV, $\Gamma[Y(4360)] = (74 \pm 14 \pm 4)$ MeV, $M[Y(4660)] = (4660 \pm 9 \pm 12)$ MeV, and $\Gamma[Y(4660)] = (74 \pm 12 \pm 4)$ MeV. By comparing the fitted results in these two fits, one can find that the resonant parameters depend strongly on whether there is an additional $Y(4230)$.
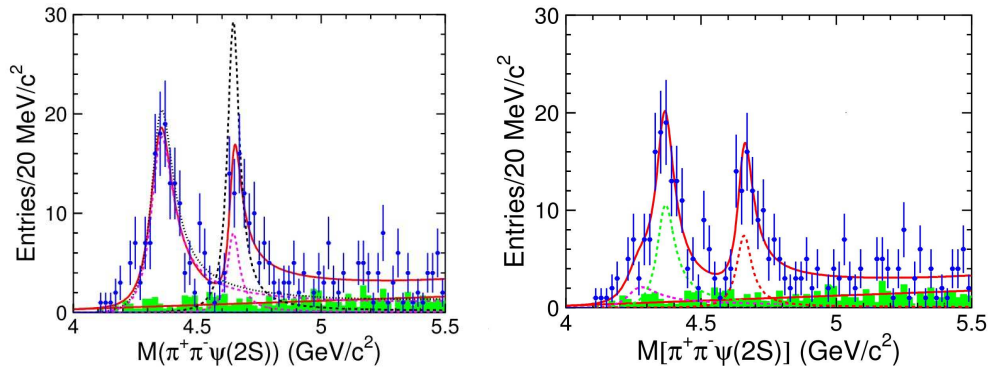
Figure 30: The $\pi^+\pi^-\psi(2S)$ invariant mass distributions from the Belle experiment [155] and the fit results with the coherent sum of two BW functions (left panel) and with the coherent sum of three BW functions (right panel). The points with error bars are data while the shaded histograms are the normalized $\psi(2S)$ mass sideband backgrounds. The curves show the best fits and the dashed curves show the contributions from different BW components.

BESIII measured $e^+e^- \to \pi^+\pi^-\psi(2S)$ cross sections at 16 c.m. energies from 4.0 to 4.6 GeV using 5.1 fb^{-1} of data in total, where the $\psi(2S)$ candidates are reconstructed via two decay modes $\psi(2S) \to \pi^+\pi^- J/\psi$ and $\psi(2S) \to$

neutrals + J/ψ (neutral=$\pi^0\pi^0$, π^0, η, and $\gamma\gamma$) [166]. After event selection criteria were applied, a prominent $\psi(2S)$ signal over a small background is observed in both $\psi(2S)$ decay modes. The measured cross sections are shown in Fig. 31 together with the comparisons from the Belle and BaBar measurements [155, 156]. The results are in good consistency with former BaBar and Belle results [155, 156], and have much improved precision. A binned χ^2 fit with the coherent sum of three BW amplitudes for the $Y(4230)$, $Y(4360)$, and $Y(4660)$ is applied to describe the $e^+e^- \to \pi^+\pi^-\psi(2S)$ cross section in a energy range from 4.085 to 4.600 GeV. As the BESIII data can only reach 4.6 GeV, the parameters of the $Y(4660)$ are fixed to the Belle measurement [155] in the fit. The fit results in a mass $M = (4383.8 \pm 4.2 \pm 0.8)$ MeV and a width $\Gamma = (84.2 \pm 12.5 \pm 2.1)$ MeV for the $Y(4360)$. By comparing to the fit with the coherent sum of two BW amplitudes, $Y(4360)$ and $Y(4660)$, the data require a lower-mass resonance with a mass $M = (4209.5 \pm 7.4 \pm 1.4)$ MeV and a width $\Gamma = (80.1 \pm 24.6 \pm 2.9)$ MeV with a statistical significance of 5.8σ. This is the first observation of the new decay mode $Y(4230) \to \pi^+\pi^-\psi(2S)$. The fit results with the coherent sum of three BW amplitudes and two BW amplitudes are shown in Fig. 31 with solid and dashed lines.
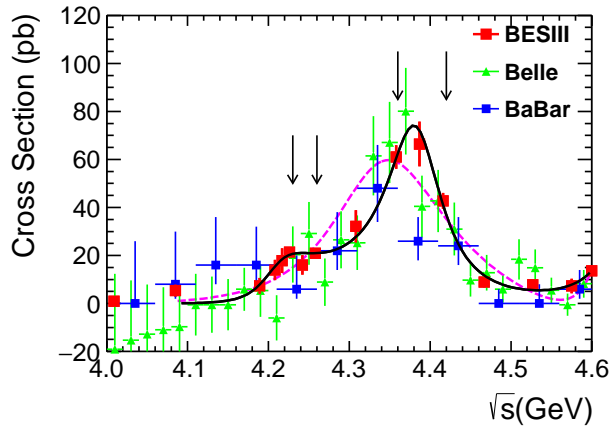
Figure 31: Cross sections of $e^+e^- \to \pi^+\pi^-\psi(2S)$, where the large red squares, green triangles, and small blue squares are from BESIII [166], Belle [155], and BaBar [156] measurements, respectively. The solid (dashed) curve is the fit to the BESIII measurement with the sum of three (two) BW functions. The arrows indicate the locations of four energy points with large integrated luminosities.

The $Y(4630)$ was first observed by Belle in the $\Lambda_c^+\bar{\Lambda}_c^-$ invariant mass distribution in the ISR process $e^+e^- \to \Lambda_c^+\bar{\Lambda}_c^-$ [204] with a measured mass of (4634^{+8+5}_{-7-8}) MeV and a width of (92^{+40+10}_{-24-21}) MeV. The measured cross sections are shown in Fig. 32(a), where the $Y(4630)$ peak is evident near the $\Lambda_c^+\bar{\Lambda}_c^-$ threshold with a statistical significance of 8.8σ. The measured $Y(4630)$ parameters are consistent within errors with the mass and width of $Y(4660)$, that was found in $\pi^+\pi^-\psi(2S)$ decays via ISR [151, 155, 156].

Recently BESIII performed a measurement of $e^+e^- \to \Lambda_c^+\bar{\Lambda}_c^-$ using data samples at $\sqrt{s} = 4574.5$, 4580.0, 4590.0, and 4599.5 MeV [205]. Figure 32(b) shows the measured $e^+e^- \to \Lambda_c^+\bar{\Lambda}_c^-$ cross sections from BESIII [205] together with those from Belle [204] near the $\Lambda_c^+\bar{\Lambda}_c^-$ mass threshold. The non-zero cross section from BESIII near the $\Lambda_c^+\bar{\Lambda}_c^-$ production threshold is evident. This means that when the cross sections are fitted, the effect of the threshold should be considered, which will affect the parameters of $Y(4630)$. Due to a large uncertainty in the Belle measurement, such a threshold effect was not considered. Unfortunately, the maximum energy point that BESIII can achieve is 4.6 GeV. In the future, with much larger data samples accumulated by Belle II, the $Y(4630)$ parameters can be measured more precisely.

As the $Y(4630)$ mass is very close to that of the $Y(4660)$ observed by Belle and BaBar in the process $e^+e^- \to \pi^+\pi^-\psi(2S)$ [151, 155, 156], many theoretical explanations assume they are the same state [206–208]. In Refs. [209, 210], where the $Y(4660)$ is modeled as an $f_0(980)\psi(2S)$ bound state, the authors predicted that it should have a spin partner—a $f_0(980)\eta_c(2S)$ bound state denoted as the Y_η—with a mass and width of (4613 ± 4) MeV and around 30 MeV, respectively, and a large partial width into $\Lambda_c^+\bar{\Lambda}_c^-$ [208, 210].

To search for Y_η in the $\Lambda_c^+\bar{\Lambda}_c^-$ system, Belle performed an updated measurement of $B^- \to K^-\Lambda_c^+\bar{\Lambda}_c^-$ using a sample of $(772 \pm 11) \times 10^6 B\bar{B}$ pairs [211]. The obtained $M_{\Lambda_c^+\bar{\Lambda}_c^-}$ spectrum is shown in Fig. 33, in which no clear Y_η or $Y(4660)$

36
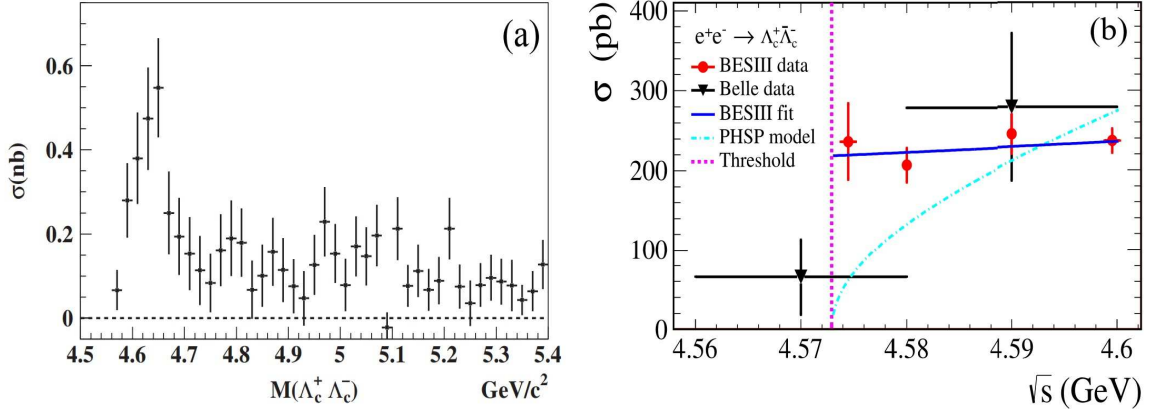
Figure 32: The measured $e^+e^- \to \Lambda_c^+\Lambda_c^-$ cross sections from (a) Belle [204] and (b) BESIII [205] together with those from Belle from threshold to 4.6 GeV.

signal is seen. The 90% C.L. upper limits for the $Y(4660)$ and its theoretically predicted spin partner Y_η are set to be $\mathcal{B}[B^- \to K^- Y(4660)]\mathcal{B}[Y(4660) \to \Lambda_c^+\bar\Lambda_c^-] < 1.2\times10^{-4}$ and $\mathcal{B}[B^- \to K^- Y_\eta]\mathcal{B}[Y_\eta \to \Lambda_c^+\bar\Lambda_c^-] < 2.0\times10^{-4}$ respectively. Subsequently, Belle also searched for the $Y(4660)$ and Y_η in $\bar{B}^0 \to K_S^0\Lambda_c^+\bar\Lambda_c^-$ decays [212]. Similarly, no evidence of Y_η or $Y(4660)$ is seen in the $\Lambda_c^+\bar\Lambda_c^-$ mass spectrum. The 90% C.L. upper limits are $\mathcal{B}[\bar{B}^0 \to \bar{K}^0 Y(4660)]\mathcal{B}[Y(4660) \to \Lambda_c^+\bar\Lambda_c^-] < 2.3 \times 10^{-4}$ and $\mathcal{B}[\bar{B}^0 \to \bar{K}^0 Y_\eta]\mathcal{B}[Y_\eta \to \Lambda_c^+\bar\Lambda_c^-] < 2.2 \times 10^{-4}$.
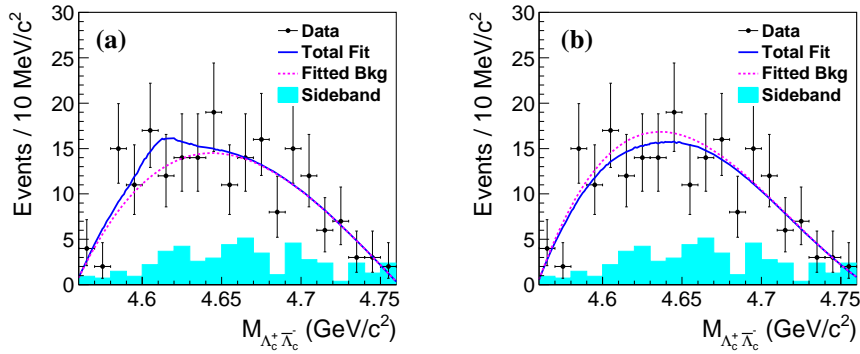
Figure 33: The $\Lambda_c^+\bar\Lambda_c^-$ invariant mass spectra in $B^- \to K^-\Lambda_c^+\bar\Lambda_c^-$ decays from Belle [211] with (a) Y_η and (b) Y(4660) signals included in the fits. The shaded cyan histograms are from the normalized Λ_c^+ and $\bar\Lambda_c^-$ mass sidebands.

• *Possible Y structures in other final states*

Besides the e^+e^- annihilation final states discussed above in the study of the $Y(4230)$, $Y(4360)$, and $Y(4660)$ states, many other final states are studied to search for the new decay modes of these Y and the excited ψ states, and new Y states.

1) $e^+e^- \to K^+K^-J/\psi$ and $K_S^0K_S^0J/\psi$

Evidence (3.7σ) for $e^+e^- \to K^+K^-J/\psi$ signal was observed by CLEO using a 13.2 pb^{-1} data sample at $\sqrt{s} = 4.26$ GeV [213]. Belle measured for the first time the cross section of $e^+e^- \to K^+K^-J/\psi$ for c.m. energies between threshold and 6.0 GeV using 673 fb^{-1} of data [214]. No significant signal for $Y(4230) \to K^+K^-J/\psi$ is observed. At the same time, Belle found evidence for $e^+e^- \to K_S^0K_S^0J/\psi$ in the same data sample. A few years

later, Belle updated the measurements of the cross sections of $e^+e^- \to K^+K^- J/\psi$ and $K_S^0 K_S^0 J/\psi$ using a data sample of 980 fb^{-1} [215] (Fig. 34, left panel). No significant signal for $Y(4230) \to K^+K^- J/\psi$ is observed either, and $\mathcal{B}[Y(4230) \to K^+K^- J/\psi]\Gamma[Y(4230) \to e^+e^-] < 0.85$ eV at a 90% C.L. is set. Belle tried to fit the $e^+e^- \to K^+K^- J/\psi$ cross sections using either a single BW function or using the $\psi(4415)$ plus a second BW function, but found that both are inadequate to describe the data.

Very recently, BESIII measured the cross sections of the processes $e^+e^- \to K^+K^- J/\psi$ and $K_S^0 K_S^0 J/\psi$ at c.m. energies from 4.189 to 4.600 GeV using 4.7 fb^{-1} of data [216]. The measured Born cross sections of $e^+e^- \to K^+K^- J/\psi$ and $K_S^0 K_S^0 J/\psi$ are shown in the right panel of Fig. 34, where the energy dependence of the cross section for $e^+e^- \to K^+K^- J/\psi$ obviously differs from that for $\pi^+\pi^- J/\psi$ in the region around the $Y(4230)$. The combined ratio of the cross sections of $e^+e^- \to K_S^0 K_S^0 J/\psi$ and $e^+e^- \to K^+K^- J/\psi$ over all energies is $0.370^{+0.064}_{-0.058} \pm 0.018$, which is consistent with the expected value of 0.5 according to isospin symmetry.
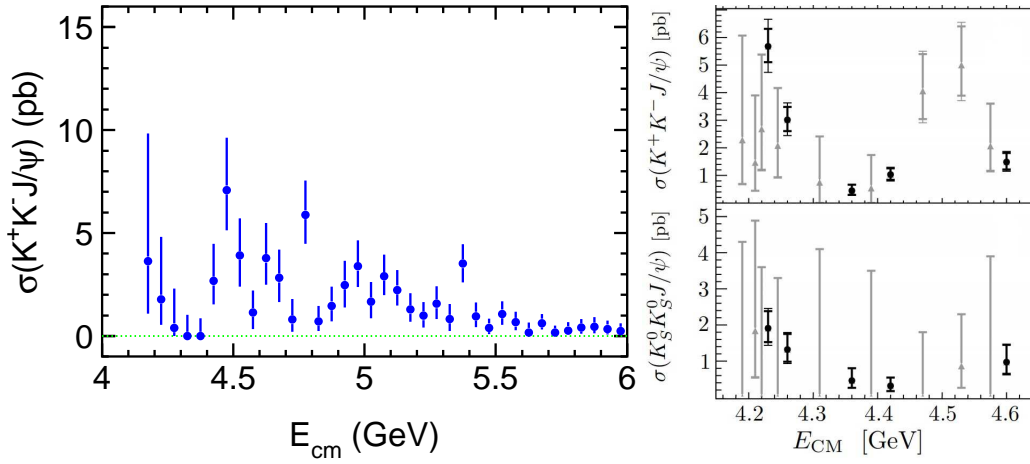
Figure 34: The measured Born cross sections of $e^+e^- \to K^+K^- J/\psi$ from Belle (left panel), and those of $e^+e^- \to K^+K^- J/\psi$ and $K_S^0 K_S^0 J/\psi$ from BESIII (right panel). For the left panel, the errors are statistical; a 7.8% systematic error that is common for all data points is not included. For the right panel, the black circular points are for data sets with high integrated luminosities; the gray triangular points are for smaller data sets. Thicker error bars are for statistical uncertainties only; thinner error bars are for combined statistical and systematic uncertainties. In the bottom plot, the large error bars with no central point are 90% C.L. upper limits.

If we combine the measurements of $e^+e^- \to K^+K^- J/\psi$ from Belle and BESIII experiments, it seems that there is a contribution from the $Y(4230)$ with a peak cross section of about 5 pb. In addition, there is evidence for a structure at around 4.5 GeV with a width of about 100 MeV. It is not clear whether it is a new structure, or the contribution from the known Y structures.

2) $e^+e^- \to \eta J/\psi$, $\eta' J/\psi$, ηh_c, and $\pi \rho \eta_c$

An important way to search for Y states is the investigation of the $\eta J/\psi$ system. Belle first reported an investigation of the $e^+e^- \to \eta J/\psi$ process using ISR events. The integrated luminosity used is 980 fb^{-1} [217]. After event selection, two distinct peaks are observed in the $\eta J/\psi$ mass spectrum above 3.8 GeV, one at 4.0 GeV and the other at 4.2 GeV. A fit to the signal events with two coherent P-wave BWs for $\psi(4040)$ and $\psi(4160)$ and an incoherent second-order polynomial background can describe the data well. The statistical significance is 6.5σ for $\psi(4040)$ and 7.6σ for $\psi(4160)$. The branching fractions of $\psi(4040) \to \eta J/\psi$ and $\psi(4160) \to \eta J/\psi$ are obtained to be $(0.56 \pm 0.10 \pm 0.17)\%$ and $(1.30 \pm 0.15 \pm 0.24)\%$, respectively, which correspond to about 1 MeV partial widths to $\eta J/\psi$ for these two states. Possible contributions from other excited charmonium-like states are examined, including the $Y(4230)$, $Y(4360)$, and $Y(4660)$. None of their significance is larger than 3σ, and 90% C.L. upper limits of their production rates in e^+e^- annihilation are determined. The measured Born cross sections are shown in the left panel of Fig. 35.

Using data samples at c.m. energies from 3.810 to 4.600 GeV, BESIII also performed a study of $e^+e^- \to \eta J/\psi$ [219]. The measured cross sections are shown in Fig. 35 (right plot) as blue squares together with a measurement at
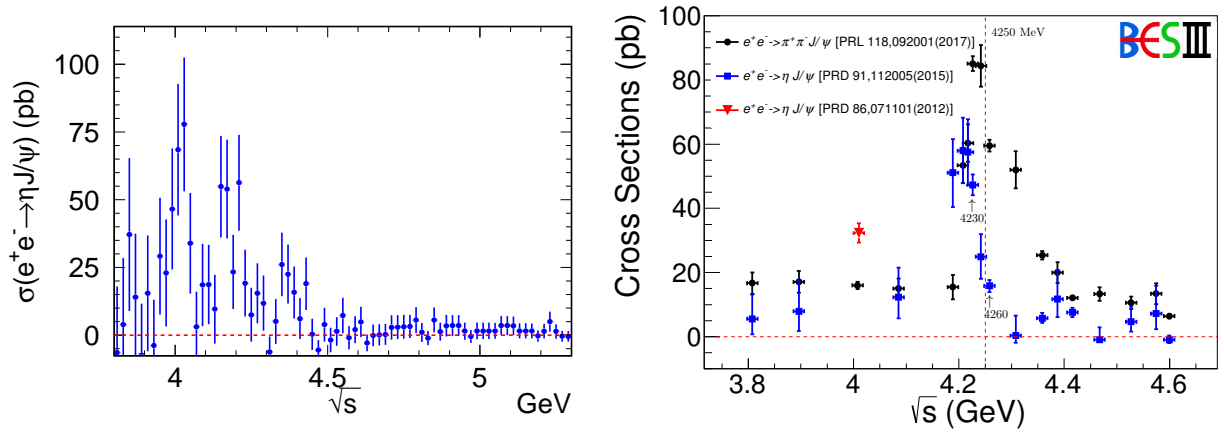
Figure 35: The measured Born cross sections of $e^+e^- \to \eta J/\psi$ from Belle [217] (left panel) and BESIII [218, 219] (right panel) together with the cross sections of $e^+e^- \to \pi^+\pi^- J/\psi$ from BESIII [73] (right panel). In the left panel, the errors are the summed statistical errors of the numbers of signal and background events. A systematic error of 8.0% common to all the data points is not shown. In the right panel, the errors are combined statistical and systematic errors.

$\sqrt{s}$ = 4.009 GeV [218]. These measurements are compatible with the measurement by Belle, but with a significantly improved precision at certain energies. The measured Born cross sections are also compared to those of $e^+e^- \to \pi^+\pi^- J/\psi$ obtained from BESIII [73] as shown in Fig. 35 with the dots with error bars. Obviously the processes $e^+e^- \to \eta J/\psi$ and $\pi^+\pi^- J/\psi$ have different line shapes including the peaking position, which indicates the existence of a rich spectrum of Y and excited ψ states in this energy region with different coupling strengths to the various decay modes. More data samples are needed to do an accurate measurement and describe better the shape of the cross section.

After the observation of strong $\psi(4040)$ and $\psi(4160)$ decays into $\eta J/\psi$, it is natural to perform the measurement of $e^+e^- \to \eta' J/\psi$ process. BESIII did such a measurement to search for potential $\eta' J/\psi$ transitions from charmonium and charmonium-like states using data samples of about 4.5 fb^{-1} in total at c.m. energies from 4.189 to 4.600 GeV [220], where the η' is reconstructed in two decay channels, $\eta' \to \eta\pi^+\pi^- \to \gamma\gamma\pi^+\pi^-$ and $\eta' \to \gamma\pi^+\pi^-$. Figure 36 shows the measured Born cross sections for $e^+e^- \to \eta' J/\psi$. Two alternative fits are taken to fit the cross section distribution: one is the fit with a $\psi(4160)$ resonance with the BW parameters fixed to PDG values [6], and the other is the fit with an additional $\psi(4415)$ resonance. The fitted results are shown in Fig. 36 as the red and green curves. The statistical significance of $\psi(4415)$ is 2.6σ only. No interesting charmonium-like states are observed with current statistics.
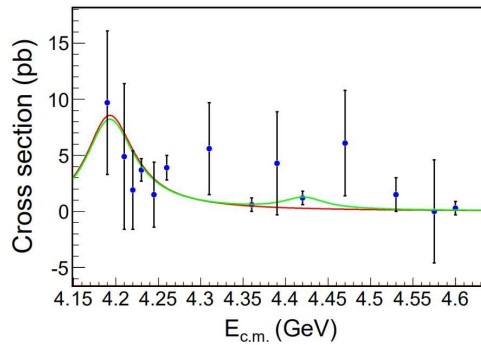
Figure 36: The measured Born cross sections of $e^+e^- \to \eta' J/\psi$ by BESIII [220]. The red curve is the fit with a $\psi(4160)$ resonance, and the green curve is the fit with an additional $\psi(4415)$ resonance.

Some Y states are observed decaying into spin-triplet charmonium states with a large rate since the spin alignment of the c and $\bar{c}$-quarks does not need to be changed between initial and final states. However, the cross section for the spin-flip process may not be small, for example the $Y(4230)$ and $Y(4390)$ are reported by BESIII in $e^+e^- \to \pi^+\pi^- h_c$ [159]. This suggests a more complicated structure of the states containing both heavy-quark spin-0 and 1 components or a milder heavy-quark spin suppression mechanism as discussed in the theory sections below. Consequently, searching for the reaction of e^+e^- to final states with an h_c or η_c is very important.

BESIII measured $e^+e^- \to \eta h_c \to \eta\gamma\eta_c$ with η_c reconstructed with 16 hadronic final states using data samples of about 4.7 fb^{-1} in total at c.m. energies from 4.085 to 4.600 GeV [221]. Figure 37 shows the energy-dependent $e^+e^- \to \eta h_c$ cross sections together with the measurement at 4.17 GeV from CLEO [222]. Clear signals and evidence for $e^+e^- \to \eta h_c$ are observed at $\sqrt{s}$ = 4.226 and 4.358 GeV for the first time, and the Born cross sections are measured to be $(9.5^{+2.2}_{-2.0} \pm 2.7)$ and $(10.0^{+3.1}_{-2.7} \pm 2.6)$ pb, respectively. A fit to the cross section distribution using the coherent sum of three BW functions, the $Y(4360)$ and other two resonances with parameters free, is shown in Fig. 37 with the solid line. The fitted parameters of the free BWs are: M_1 = (4204±6) MeV, Γ_1 = (32±22) MeV, and M_2 = (4496±26) MeV, Γ_2 = (104 ± 69) MeV, where the uncertainties are statistical only. Due to the limited statistics, a further update is needed to determine the line shape of the c.m. energy dependent cross section precisely.
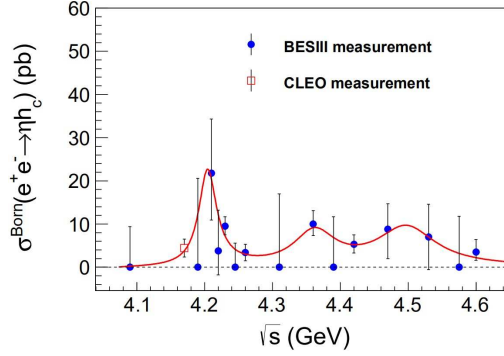
Figure 37: The measured Born cross sections of $e^+e^- \to \eta h_c$ by BESIII [221] and CLEO [222]. The solid line is the fit using the coherent sum of three BW functions.

BESIII searched for $e^+e^- \to \pi^+\pi^-\pi^0\eta_c$ with data at c.m. energies above 4 GeV corresponding to an integrated luminosity of about 4.1 fb^{-1} [223]. In this analysis, the η_c is reconstructed with nine hadronic final states: $p\bar{p}$, $2(K^+K^-)$, $K^+K^-\pi^+\pi^-$, $K^+K^-\pi^0$, $p\bar{p}\pi^0$, $K^0_S K^\pm\pi^\mp$, $\pi^+\pi^-\eta$, $K^+K^-\eta$, and $\pi^+\pi^-\pi^0\pi^0$. A clear signal of $e^+e^- \to \pi^+\pi^-\pi^0\eta_c$ is observed at $\sqrt{s}$ = 4.23 GeV. From the fit to the η_c mass spectrum, 333^{+83}_{-80} η_c signal events are obtained with a statistical significance of 4.2σ. No significant signals are observed at other c.m. energy points. The cross section is measured as $\sigma(e^+e^- \to \pi^+\pi^-\pi^0\eta_c) = (46^{+12}_{-11} \pm 10)$ pb at $\sqrt{s}$ = 4.226 GeV. It is still not clear whether the signal is from the $Y(4230)$ decays.

3) $e^+e^- \to \omega\chi_{c1,2}$

The processes $e^+e^- \to \omega\chi_{c1,2}$ were observed for the first time by BESIII [163]. Here, the $\chi_{c1,2}$ are reconstructed via their $\gamma J/\psi$ decays. The measured cross sections for $e^+e^- \to \omega\chi_{c1,2}$ are shown in Fig. 24 (middle and right plots). A significant $\omega\chi_{c2}$ signal is found at $\sqrt{s}$ =4.42 GeV with an integrated luminosity of 1074 pb^{-1}, and the cross section is measured to be $(20.9 \pm 3.2 \pm 2.5)$ pb. With 567 pb^{-1} data near $\sqrt{s}$ = 4.6 GeV, a clear $\omega\chi_{c1}$ signal is seen, and the cross section is measured to be $(9.5 \pm 2.1 \pm 1.3)$ pb. Due to low luminosity or low cross section at other energies, no significant signals are observed. A coherent sum of the $\psi(4415)$ BW function and a phase-space term can well describe the $\omega\chi_{c2}$ line shape, and the branching fraction $\psi(4415) \to \omega\chi_{c2}$ is found to be of the order of 10^{-3}. The solid line in Fig. 24 (right plot) shows the fit result. Further studies based on more data samples at higher energy points will be helpful to clarify the nature of charmonium(like) states decaying to $\omega\chi_{cJ}$ final states.

3.1.3. Searches for glueballs with exotic quantum numbers

The existence of bound states of gluons (so-called "glueballs"), with a rich spectroscopy and a complex phenomenology, is one of the early predictions of the non-Abelian nature of QCD. Due to the mixing between glueballs and conventional mesons, the lack of solid information on the glueball production mechanism, and the lack of knowledge about glueball decay properties, none of these gluonic states have been established unambiguously experimentally.

Recently Belle utilized the 102M $\Upsilon(1S)$ and 158M $\Upsilon(2S)$ event data samples to search for 0^{--} glueballs (G_{0--}), called oddballs, with quantum numbers incompatible with quark-antiquark bound states [224]. Two 0^{--} oddballs are predicted using QCD sum rules [225] with masses of (3.81 ± 0.12) GeV and (4.33 ± 0.13) GeV, while the lowest-lying state calculated using distinct bottom-up holographic models of QCD [226] has a mass of 2.80 GeV. Belle searched for such G_{0--} in $\Upsilon(1S, 2S) \rightarrow \chi_{c1} + G_{0--}$, $\Upsilon(1S, 2S) \rightarrow f_1(1285) + G_{0--}$, $\chi_{b1} \rightarrow J/\psi + G_{0--}$, and $\chi_{b1} \rightarrow \omega + G_{0--}$ processes. No evident signal is found at the three theoretically-predicted masses in all the studied processes, and 90% C.L. upper limits are set on the branching fractions for these processes. Figure 38 shows the 90% C.L. upper limits on the branching fractions of $\Upsilon(1S)/\Upsilon(2S) \rightarrow \chi_{c1} + G_{0--}$ as a function of the 0^{--} glueball width as an example. Interestingly, a signal with a significance of 3.7σ at 3.92 GeV is observed in $\Upsilon(1S) \rightarrow f_1(1285) + G_{0--}$, which will need special attention and inspection at Belle II with much larger data samples.
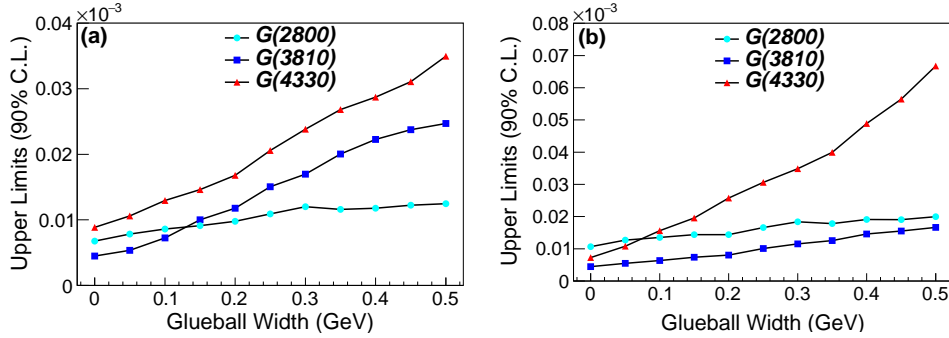
Figure 38: The upper limits on the branching fractions for (a) $\Upsilon(1S) \rightarrow \chi_{c1} + G_{0--}$ and (b) $\Upsilon(2S) \rightarrow \chi_{c1} + G_{0--}$ as a function of the assumed G_{0--} width [224].

3.2. Isovector states

While the states discussed in the previous section could, in principle, be interpreted as conventional heavy quark-antiquark bound states distorted, e.g., by threshold or unitarization effects, the isovector states discussed in this section clearly require going beyond the most naive quark-antiquark picture — at least if these states indeed exist as poles in the S-matrix. Some authors claimed, however, that these states might be simply threshold cusps. This issue is discussed at the beginning of Sec. 4. In this section, we present the experimental evidence for structures in the heavy quarkonium mass range with isovector quantum numbers.

3.2.1. The $X(5568)$ state

The D0 Collaboration reported evidence for a narrow structure, $X(5568)$, in the hadronic decay $X(5568) \rightarrow B_s^0 \pi^\pm$ with $B_s^0 \rightarrow J/\psi\phi$ with a signal significance greater than 3.9σ in proton-antiproton collisions at a c.m. energy of 1.96 TeV [34]. The measured mass and width are $M = (5567.8 \pm 2.9^{+0.9}_{-1.9})$ MeV and $\Gamma = (21.9 \pm 6.4^{+5.0}_{-2.5})$ MeV. Since the state can be interpreted as a compact tetraquark with four different valence quark flavors, b, s, u, d, it has received extensive attention from theoretical and experimental physicists. Later the $X(5568)$ signal was confirmed by the D0 Collaboration in the semileptonic decay of $B_s^0 \rightarrow \mu^\mp D_s^\pm X$ with a statistical significance greater than 4.3σ [227]. Figure 39 shows the $M(B_s^0\pi^\pm)$ distributions for the hadronic (red squares) and semileptonic (black circles) data (a) with and (b) without the cone requirement $\Delta R = \sqrt{\Delta\eta^2 + \Delta\phi^2} < 0.3$, where the cone is the angle between the B_s^0 and $\pi^\pm$ for hadronic decay, the angle between the $\mu^\mp D_s^\pm$ system and $\pi^\pm$ for semileptonic decay, $\eta = -\ln[\tan(\theta/2)]$ is the pseudorapidity (θ is the polar angle between the track momentum and the proton beam direction), and ϕ is the

azimuthal angle of the track. A combined fit is performed to the selected hadronic and semileptonic signal candidates, and the fitted results are shown in Fig. 39 as solid lines. The fitted mass and width are $M = (5566.9^{+3.2+0.6}_{-3.1-1.2})$ MeV and $\Gamma = (18.6^{+7.9+3.5}_{-6.1-3.8})$ MeV. The signal significance with the systematic uncertainties included is $6.7\,\sigma$ with the cone requirement, and $4.7\,\sigma$ without it.
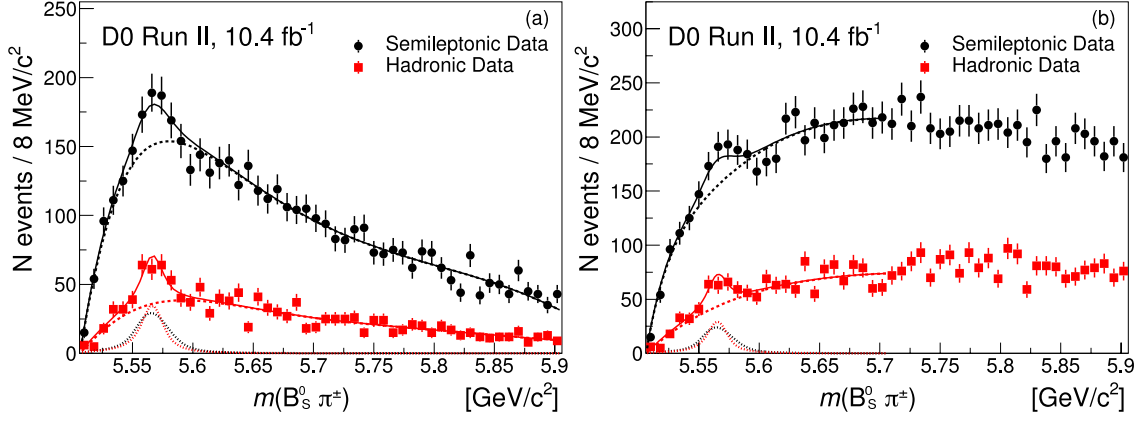
Figure 39: The $M(B_s^0\pi^\pm)$ distributions for the hadronic (red squares) and semileptonic (black circles) data (a) with and (b) without the cone requirement [227]. The solid lines are the best fits.

While the D0 Collaboration reported the $X(5568)$ in both hadronic and semileptonic decays, negative results were obtained in the LHCb [228], CDF [229], CMS [230], and ATLAS [231] experiments. LHCb first provided negative results using a 3 fb^{-1} data sample of pp collision data at $\sqrt{s} = 7$ and 8 TeV [228], where the B_s^0 mesons are reconstructed through the decays $B_s^0 \to D_s^\pm\pi^\mp$ and $J/\psi\phi$. The reconstructed B_s^0 yield is approximately 20 times larger than that used by D0. No significant signal is seen in the $B_s^0\pi^\pm$ invariant mass distribution in the range of about 5.5 GeV to 6 GeV, and upper limits on $\sigma(pp \to X + \text{anything})\mathcal{B}(X \to B_s^0\pi^\pm)$ are set as a function of the mass and width of a possible exotic meson decaying to the $B_s^0\pi^\pm$ final state. Recently, CDF, CMS, and ATLAS also searched for the $X(5568)$ in hadronic decays using data samples of 9.6 fb^{-1} from $p\bar{p}$ collisions at $\sqrt{s} = 1.96$ TeV, 19.7 fb^{-1} from pp collisions at $\sqrt{s} = 8$ TeV, and 4.9 fb^{-1} at $\sqrt{s} = 7$ TeV and 19.5 fb^{-1} at $\sqrt{s} = 8$ TeV from pp collisions, respectively [229–231]. Figure 40 shows the reconstructed $M(B_s^0\pi^\pm)$ distributions from the CDF [229] (left plot), CMS [230] (middle plot), and ATLAS [231] (right plot) measurements for $B_s^0\pi^\pm \to J/\psi\phi\pi^\pm$ candidates with $p_T(B_s^0) > 10$ GeV, respectively. No statistically significant peaks can be seen in either of them. Upper limits of 6.7% from CDF, 1.1% from CMS, and 1.5% from ATLAS on the fraction of B_s^0 produced through the $X(5568) \to B_s^0\pi^\pm$ process at the 95% C.L. are set for $p_T(B_s^0) > 10$ GeV, respectively.
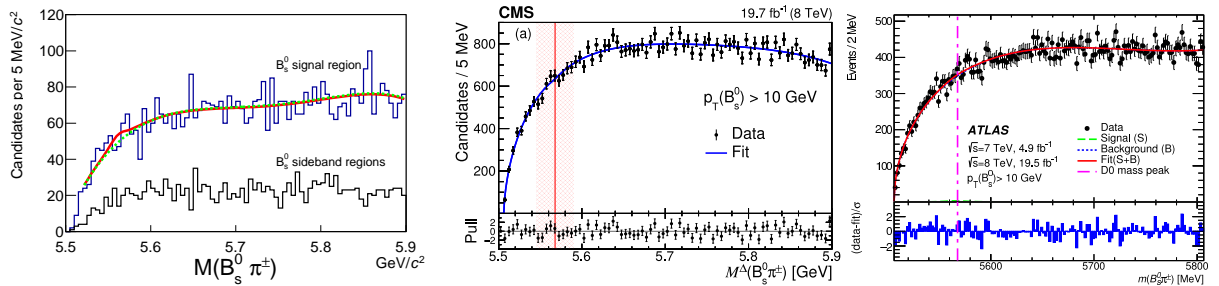
Figure 40: The $M(B_s^0\pi^\pm)$ distributions from the CDF [229] (left plot), CMS [230] (middle plot), and ATLAS [231] (right plot) measurements for $B_s^0\pi^\pm \to J/\psi\phi\pi^\pm$ candidates with $p_T(B_s^0) > 10$ GeV. The solid lines are the best fits. The bottom panels in the middle and right plots show the difference between each data point and the fit divided by the statistical uncertainty of that point.

The $X(5568)$ state, if confirmed, would differ from any previously observed state, as it must have constituent quarks with four different flavors (b, s, u, d). So far, however, only the D0 experiment observed signals, while other experiments with larger statistics reported negative results, especially the CDF experiment from the same proton-antiproton collisions. Therefore, the urgent task in the future is to confirm or definitely exclude the existence of the $X(5568)$ with larger data samples and to look for possible similar exotic states in the $B_s^* \pi$, $D_s \pi$, and $D_s^* \pi$ systems.

From the theoretical side, many explanations on the $X(5568)$ being a compact tetraquark state [232–243] or a meson molecule [244, 245] have been proposed. At the same time, there have also been theoretical analyses that do not support the interpretation as a compact tetraquark state [246], as a molecular state [247–251], or as any of the two [252, 253]. In Ref. [254] all the possible interpretations, such as compact tetraquark, hadronic molecule, threshold effect from the meson loop, and so on, have been found unable to provide a consistent explanation of the $X(5568)$. Finally, due to the inconsistency of the interpretations in both the compact tetraquark and hadronic molecular scenarios, the authors of Refs. [255–257] have suggested that the state might originate from a mixing of these two scenarios.

3.2.2. Charmonium-like charged Z_c states

Searching for charged charmonium-like states is one of the most promising ways of studying exotic hadrons, since such a state must contain at least four quarks and thus cannot be a conventional quark-antiquark meson. Searches were performed in the combination of one charged pion/kaon/proton and a charmonium state, like η_c, J/ψ, $\psi(2S)$, χ_c, and h_c.

The first charged charmonium-like state, $Z_c(4430)^-$, was reported in the $\pi^- \psi(2S)$ mass spectrum in $B \to K\pi^- \psi(2S)$ decays in the Belle experiment [258, 259], and it was confirmed by the LHCb experiment seven years later [38]. The $Z_c(3900)^-$ was observed in $\pi^- J/\psi$ invariant mass distribution in the study of $e^+ e^- \to \pi^+ \pi^- J/\psi$ at BESIII [22] and Belle [68] experiments, and the $Z_c(4020)^-$ was observed in the $\pi^- h_c$ system in $e^+ e^- \to \pi^+ \pi^- h_c$ [158] only at BESIII. There are other Z_c states observed in different processes, such as the two structures at 4050 and 4250 MeV in the $\pi^- \chi_{c1}$ system in $B \to K\pi^- \chi_{c1}$ decays [260]; and the $Z_c(4200)^-$ in the $\pi^- J/\psi$ invariant mass distribution in $B \to K\pi^- J/\psi$ decays [261] from the Belle experiment. There is also evidence for Z_c structures in the $\pi \psi(2S)$ system at Belle [155] and BESIII [166] in $e^+ e^- \to \pi^+ \pi^- \psi(2S)$, and in the $\pi \eta_c$ system at LHCb [262] in $B^0 \to K^+ \pi^- \eta_c$.

These states indicate that a new class of hadrons has been observed. As they are made by at least four quarks, they have been interpreted either as compact tetraquark states, molecular states of two charmed mesons ($\bar{D}D^*$, $\bar{D}^*D^*$, $\bar{D}D_1$, $\bar{D}^*D_1$, etc.), hadroquarkonium states, or other configurations [13, 84].

• *The $Z_c(4430)$ state*

A feature that clearly distinguishes multiquark states from hybrids or charmonia is the possibility to have charmonium-like mesons with nonzero electric charge. Thus, Belle studied exclusive $B \to K\pi^- \psi(2S)$ decays to search for a charged charmonium-like state in the $\pi^- \psi(2S)$ system using 657×10^6 $B\bar{B}$ pairs [258]. In the Dalitz plot of $M^2(K\pi^-)$ vs. $M^2[\pi^- \psi(2S)]$, two clear bands corresponding to $K^*(892)$ and $K_2^*(1430)$ decays to $K\pi$ final states can be seen. After vetoing these events, the $\pi^- \psi(2S)$ mass spectrum is shown in Fig. 41, where a strong enhancement is evident near 4.43 GeV. A fit with a relativistic S-wave BW function to model the peak plus a smooth phase-space-like function yields a mass $M = (4433 \pm 4 \pm 2)$ MeV and a width $\Gamma = (45^{+18+30}_{-13-13})$ MeV with a signal significance of 6.5σ.

After Belle claimed that a charged $Z_c(4430)$ particle was discovered, BaBar analyzed the same process using an integrated luminosity of 413 fb^{-1} $\Upsilon(4S)$ data [263]. BaBar found that the $\pi \psi(2S)$ mass distribution can be well described by the reflection of the known $K\pi$ resonances. Although BaBar did not confirm the existence of the $Z_c(4430)$, its results did not contradict the Belle observation due to low statistics. To take into account the interference effect between the $Z_c(4430)^-$ and the K^* intermediate states in $B \to K\pi^- \psi(2S)$ decays, Belle updated their $Z_c(4430)^-$ results with a four-dimensional (4D) amplitude analysis [259]. The $Z_c(4430)^-$ is observed with a significance of 5.2σ, a much larger mass of $(4485 \pm 22^{+28}_{-11})$ MeV, and a large width of (200^{+41+26}_{-46-35}) MeV. The product branching fraction is measured to be $\mathcal{B}[B^0 \to Z_c(4430)^- K^+]\mathcal{B}[Z_c(4430)^- \to \pi^- \psi(2S)] = (6.0^{+1.7+2.5}_{-2.0-1.4}) \times 10^{-5}$, and spin-parity $J^P = 1^+$ is favored over the other assignments by more than 3.4σ. The inconsistent results on the $Z_c(4430)^-$ between BaBar and Belle measurements have been an open question for a very long time since there were no new data available until recently.

Since LHCb has large B-samples, the same process $B^0 \to K^+ \pi^- \psi(2S)$ with $\psi(2S) \to \mu^+ \mu^-$ was analyzed to
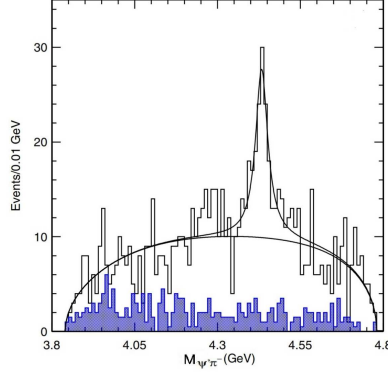
Figure 41: The $M[\pi^-\psi(2S)]$ distribution by Belle for events in the selected B signal region and with the $K^*(892)$ and $K_2^*(1430)$ signals veto applied [258]. The shaded histogram is from non-B backgrounds. The solid curves show the best fit results with a relativistic $\tilde{S}$-wave BW function to model the peak plus a smooth phase-space-like function.

search for resonant structures using pp collision data corresponding to 3 fb^{-1} [38]. After event selection, 25176 ± 174 $B^0 \rightarrow K^+\pi^-\psi(2S) \rightarrow K^+\pi^-\mu^+\mu^-$ candidates were selected. The order-of-magnitude increase in the signal yield over the Belle measurement [259] improved the sensitivity of $Z_c(4430)^-$ searches and allowed a measurement of quantum numbers and Argand plot. Thus, a 4D model-dependent amplitude fit with $M^2_{K^+\pi^-}$, $M^2_{\pi^-\psi(2S)}$, $\cos\theta_{\psi(2S)}$, and ϕ as variables, was performed to the selected signal candidates, where $\theta_{\psi(2S)}$ is the $\psi(2S)$ helicity angle and ϕ is the angle between the K^* and $\psi(2S)$ decay planes in the B^0 rest frame. In the amplitude fit, all known K^* resonances, a nonresonant term, and a Z_c^- amplitude represented by a BW function are included. The fit yields a mass of $(4475 \pm 7^{+15}_{-25})$ MeV and a width of $(172 \pm 13^{+37}_{-34})$ MeV, which are consistent with, but more precise than, the Belle results [259]. The lowest significance for the $Z_c(4430)^-$ signal is 13.9σ. It means the data cannot be described with $K^+\pi^-$ resonances alone, thus confirming the existence of the $Z_c(4430)^-$. The projection of the 4D amplitude fit on the $M_{\pi^-\psi(2S)}$ is shown in Fig. 42, where the red solid (brown dashed) histogram represents the total amplitude with (without) the Z_c^- component, the upper (lower) blue points represent the Z_c^- component removed (taken alone), and the orange, magenta, cyan, yellow, green, and red points represent the $K^*(892)$, total S-wave, $K^*(1410)$, $K^*(1680)$, $K_2^*(1430)$, and background terms, respectively. Relative to $J^P = 1^+$, the 0^-, 1^-, 2^+, and 2^- hypotheses are ruled out by at least 9.7σ, thus the spin-parity of the $Z_c(4430)$ is established to be 1^+ unambiguously. In addition, LHCb measures the Argand plot of the Z_c^- amplitude as a function of $M_{\pi\psi(2S)}$, which is consistent with a rapid change of the $Z_c(4430)^-$ phase when its magnitude reaches the maximum, expected behavior of a resonance. This is the first time an Argand plot is obtained for an exotic charmonium-like state.

In the amplitude fit, LHCb also tried to add an additional resonance Z_c^- and found the p-value of the χ^2 test improves from 12% to 26%, corresponding to a 6σ signal significance. The measured mass and width of this additional Z_c^- state are $(4239 \pm 18^{+45}_{-10})$ MeV and $(220 \pm 47^{+108}_{-74})$ MeV and 0^- is preferred over other J^P assignments by 8σ. This is the state dubbed $R_{c0}(4240)$ in the spectrum shown in Fig. 1. Although the signal significance is large for this state, Argand diagram studies are inconclusive. Therefore, its characterization as a resonance will need further confirmation.

In a full amplitude analysis of $B^0 \rightarrow K^+\pi^- J/\psi$ decay based on a 711 fb^{-1} $\Upsilon(4S)$ data sample at Belle [261], the $Z_c(4430)^- \rightarrow \pi^- J/\psi$ is observed as a 4.0σ signal, while BaBar's earlier model-independent analysis of the same mode did not find this process [263]. Very recently, an angular analysis of $B^0 \rightarrow K^+\pi^- J/\psi$ with $J/\psi \rightarrow \mu^+\mu^-$ decays was performed by LHCb, although non-K^* events must exist, whether there is a contribution from the $Z_c(4430)$ is not clear [264].

• *The $Z_{c1}(4050)$ and $Z_{c2}(4250)$ states*

Replacing the $\psi(2S)$, Belle subsequently checked the $\pi^-\chi_{c1}$ system in exclusive $B^0 \rightarrow K^+\pi^-\chi_{c1}$ using 657×10^6 $B\bar{B}$ pairs [260]. After signal selections, the Dalitz plot distribution exhibits some distinct features: two clear bands corresponding to $K^*(892)$ and $K^*(1430)$ decays to $K\pi$; a distinct band at $M^2(\pi^-\chi_{c1}) \approx 17$ GeV^2 corresponding to a

44
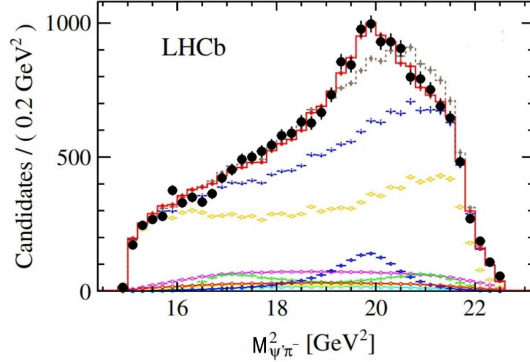
Figure 42: The projection of the 4D amplitude fit on the $M_{\pi^-\psi(2S)}$ [38]. The red solid (brown dashed) histogram represents the total amplitude with (without) the Z_c^- component, the upper (lower) blue points represent the Z_c^- component removed (taken alone), and the orange, magenta, cyan, yellow, green, and red points represent the $K^*(892)$, total S-wave, $K^*(1410)$, $K^*(1680)$, $K_2^*(1430)$, and background terms, respectively.

structure in the $\pi^-\chi_{c1}$ channel. To obtain such structure parameters, a 6D Dalitz plot analysis was performed, where all the known $K^+\pi^-$ resonances below 1900 MeV and a single exotic $\pi^-\chi_{c1}$ resonance are included. Such a fit gives the confidence level of 0.5%, which indicates that the shape of the structure is not well reproduced by a single BW. Motivated by this, an additional resonance decaying to $\pi^-\chi_{c1}$ is added to the above fit model. The masses and widths of the two Z_c^- resonances from the fit are $M_1 = (4051 \pm 14^{+20}_{-41})$ MeV, $\Gamma_1 = (82^{+21+47}_{-17-22})$ MeV, $M_2 = (4248^{+44+180}_{-29-35})$ MeV, and $\Gamma_2 = (177^{+54+316}_{-39-61})$ MeV. They are denoted as $Z_{c1}(4050)$ and $Z_{c2}(4250)$ with signal significances greater than 5σ for both. The confidence level for this fit is 42%.

The invariant mass distribution $M(\pi^-\chi_{c1})$ with 1.0 GeV^2 < $M^2(K^+\pi^-)$ < 1.75 GeV^2 is shown in Fig. 43, where the solid (dashed) histogram is the Dalitz plot fit result for the fit model with all known K^* and two (without any) $\pi^-\chi_{c1}$ resonances, the dotted histograms represent the contribution of the two $Z_{c1}(4050)$ and $Z_{c2}(4250)$ states. These two charged resonances represent additional candidate states of similar characteristics to the $Z_c(4430)^-$.
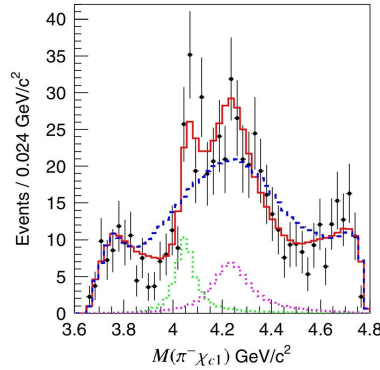
Figure 43: The invariant mass distribution $M(\pi^-\chi_{c1})$ with 1.0 GeV^2 < $M^2(K^+\pi^-)$ < 1.75 GeV^2 [260]. The solid (dashed) histogram is the Dalitz plot fit result for the fit model with all known K^* and two (without any) $\pi^-\chi_{c1}$ resonances, the dotted histograms represent the contribution of the two $Z_{c1}(4050)$ and $Z_{c2}(4250)$ states.

After Belle claimed the observation of the $Z_{c1}(4050)$ and $Z_{c2}(4250)$ states, the BaBar experiment analyzed the same process using an integrated luminosity of 429 fb^{-1} [265]. In this analysis, BaBar fitted the background-subtracted and efficiency-corrected $\pi^-\chi_{c1}$ mass distribution using the $K\pi$ mass distribution and the corresponding normalized $K\pi$ Legendre-polynomial moments, and found that the fit can describe the data well without the need of any charged Z_c resonance in the $\pi^-\chi_{c1}$ system. So their conclusion is: Neither $Z_{c1}(4050)$ nor $Z_{c2}(4250)$ is evident, leading to 90% C.L. upper limits on the branching fractions for the corresponding B-meson decay modes. Given the large uncertainties, the

upper limits are still compatible with the branching fraction values from the Belle measurement [260]. Thus, further confirmation of the existence of the $Z_{c1}(4050)$ and $Z_{c2}(4250)$ states at LHCb and Belle II is needed in the future.

- *The $Z_c(4200)$ state*

After the charged charmonium-like states of $Z_c(4430)$, $Z_{c1}(4050)$, and $Z_{c2}(4250)$ were observed in B decays by Belle, a full amplitude analysis was performed to the $B^0 \rightarrow K^+\pi^- J/\psi$ decay with J/ψ decaying to a lepton pair to search for possible charged charmonium-like states in the $\pi^- J/\psi$ system based on a 711 fb^{-1} $\Upsilon(4S)$ data sample [261]. After event selection, the total number of signal events is $29\,990 \pm 190 \pm 50$. For these selected signal candidates, the amplitude of the decay $B^0 \rightarrow K^+\pi^- J/\psi$ is represented as the sum of BW contributions for different intermediate two-body states calculated using the helicity formalism in a four-dimensional parameter space, defined as $\Phi = (M^2_{K\pi}, M^2_{J/\psi\pi}, \theta_{J/\psi}, \varphi)$, where $\theta_{J/\psi}$ is the J/ψ helicity angle [the angle between the momenta of the $(K^+\pi^-)$ system and the ℓ^- in the J/ψ rest frame; $\ell^-\ell^+$ is the leptonic pair from the J/ψ decay] and φ is the angle between the planes defined by the $(\ell^+\ell^-)$ and $(K^+\pi^-)$ momenta in the B^0 rest frame. The known resonances included in the default model are $K_0^*(700)$, $K^*(892)$, $K^*(1410)$, $K_0^*(1430)$, $K_2^*(1430)$, $K^*(1680)$, $K_3^*(1780)$, $K_0^*(1950)$, $K_2^*(1980)$, $K_4^*(2045)$, and $Z_c(4430)^-$; a search for additional exotic Z_c^- resonances is performed. An unbinned maximum-likelihood fit over the four-dimensional space Φ was performed. The considered spin-parity hypotheses of a possible Z_c^- resonance are $J^P = 0^-$, 1^-, 1^+, 2^- and 2^+. The best fit gives a global 6.2σ significance of a Z_c^- resonance with a mass of (4196^{+31+17}_{-29-13}) MeV and a width of $(370^{+70+70}_{-70-132})$ MeV. Thus, a new charged Z_c state, $Z_c(4200)^-$, is observed. The preferred quantum numbers assigned to this state are $J^P = 1^+$. Projections of the fit results onto the $M^2_{J/\psi\pi}$ axis in different $K^+\pi^-$ mass regions for the model with the $Z_c(4200)$ ($J^P = 1^+$) are shown in Fig. 44.
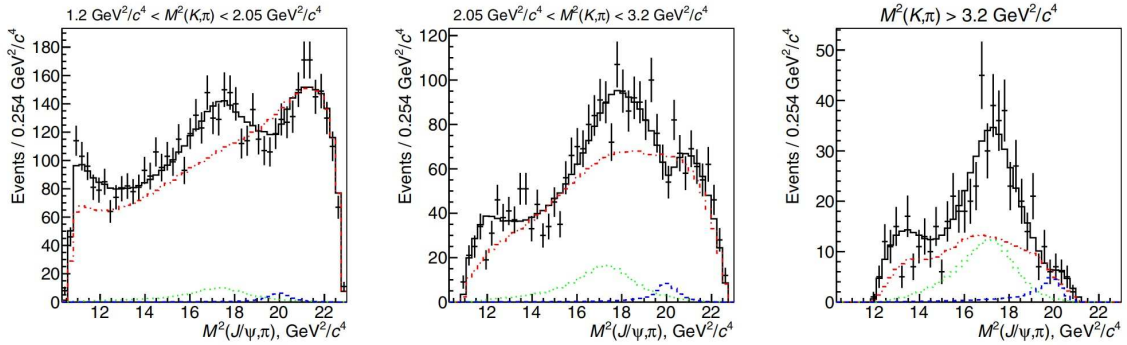
Figure 44: Projections of the fit results onto the $M^2_{J/\psi\pi}$ axis with the $Z_c(4200)$ ($J^P = 1^+$) in different $K^+\pi^-$ mass regions [261]. The points with error bars are data; the solid histograms are fit results, the dashed histograms are the $Z_c(4430)^-$ contributions, the dotted histograms are the $Z_c(4200)^-$ contributions and the dash-dotted histograms are contributions of all K^* resonances.

Note that similar to the $Z_c(4430)$, BaBar's earlier model-independent analysis of $B^0 \rightarrow K^+\pi^- J/\psi$ decays did not find the $Z_c(4200)^-$ in the $\pi^- J/\psi$ system using an integrated luminosity of 413 fb^{-1} $\Upsilon(4S)$ data [263]. BaBar made minimal assumptions about the K_J^* spectrum, using two-dimensional moments in the variables $M(K^+\pi^-)$ and the K^+ helicity angle. Within uncertainties, the $M(J/\psi\pi^-)$ spectrum in the BaBar data was found to be adequately described using just K_J^* states, without a need for exotic contribution. The inconsistent results on the $Z_c(4200)$ between BaBar and Belle measurements have been recently solved by LHCb as is described below.

LHCb performed an angular analysis of $B^0 \rightarrow K^+\pi^- J/\psi$ with $J/\psi \rightarrow \mu^+\mu^-$ decays using proton-proton collision data corresponding to an integrated luminosity of 3 fb^{-1} [264]. After event selection, 554500 ± 800 signal candidates are obtained in the mass region $745 < M(K^+\pi^-) < 1545$ MeV. This selected data sample is divided into 35 fine bins in $M(K^+\pi^-)$ and a four-dimensional angular analysis is performed in each mass bin. The four variables, $M(K^+\pi^-)$, θ_V, θ_l, and χ, fully describe the decay topology, where θ_V is the K^+ helicity angle defined as the K^+ momentum direction in the $K^+\pi^-$ helicity frame with respect to the B^0 rest frame, θ_l is the similar lepton helicity angle, and χ is the the azimuthal angle between the $(\mu^+\mu^-)$ and $(K^+\pi^-)$ decay planes. To maximise the sensitivity to any exotic component, an angular analysis is performed in the $M(K^+\pi^-) \in [1085, 1445]$ MeV region, where J_{max}^k, the allowed spin of the highest

partial wave for the $K^-\pi^+$ system (K_J^*), is 3. Figure 45 shows the comparison of the $M(J/\psi\pi^-)$ distributions between the background-subtracted data and weighted simulated events with the $J_{max}^k = 2$ model taken in the $M(K^+\pi^-) \in [1085, 1265]$ MeV region. The $J_{max}^k = 2$ model clearly can not describe the peaking structures in the data around $M(J/\psi\pi^-) \approx 4200$ and 4600 MeV, which strongly indicates presence of exotic components. The significance for exotic components is in excess of 6σ with systematic uncertainties included. The structure at $M(J/\psi\pi^-) \approx 4200$ MeV is close to the exotic state reported by Belle [261]. To interpret these structures as exotic tetraquark resonances and measure their properties will require a future model-dependent amplitude analysis of the data.
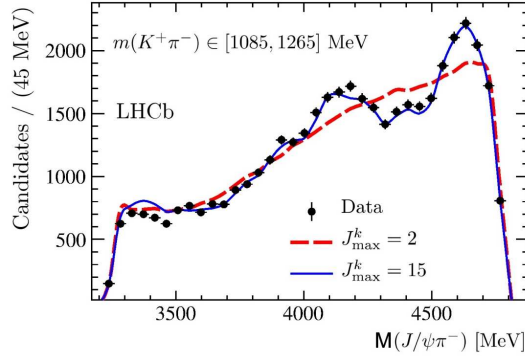
Figure 45: Comparison of $M(J/\psi\pi^-)$ distributions in the $M(K^+\pi^-) \in [1085, 1265]$ MeV region between the background-subtracted data and simulated events weighted by moment models with $J_{max}^k = 2$ and $J_{max}^k = 15$ [264].

• *The $Z_c(3900)$ and $Z_c(4020)$ states*

To understand the intermediate states in $Y(4230) \to \pi^+\pi^- J/\psi$, the BESIII experiment collected a 525 pb^{-1} data sample in 2013 at c.m. energy of 4.26 GeV, the peak of the $Y(4230)$ [22]. The cross section of $e^+e^- \to \pi^+\pi^- J/\psi$ at $\sqrt{s} = 4.26$ GeV is measured to be $(62.9 \pm 1.9 \pm 3.7)$ pb based on the selected 1477 signal candidates, which agrees with the previous results from the BaBar [153] and Belle [25] experiments. Using this selected signal sample, the Dalitz plot is drawn to check for possible intermediate states, as shown in Fig. 46 (left panel). At the same time, Belle updated the measurement of the cross section of $e^+e^- \to \pi^+\pi^- J/\psi$ from 3.8 to 5.5 GeV using the ISR method with a 967 fb^{-1} data sample [68]. The Dalitz plot for events in the $Y(4230)$ signal region (4.15 GeV $< M(\pi^+\pi^- J/\psi) < 4.45$ GeV) is also investigated, as shown in Fig. 46 (right panel).

Figures 47 and 48 show the projections of the $M(\pi^+\pi^-)$ and $M_{max}(\pi^\pm J/\psi)$ [the maximum value out of $M(\pi^+ J/\psi)$ and $M(\pi^- J/\psi)$] distributions for the signal events, as well as the background events estimated from the normalized J/ψ mass sidebands. A parametrization for the $\pi^+\pi^-$ mass spectrum that includes $f_0(980)$, $f_0(500)$ (σ), and a non-resonant
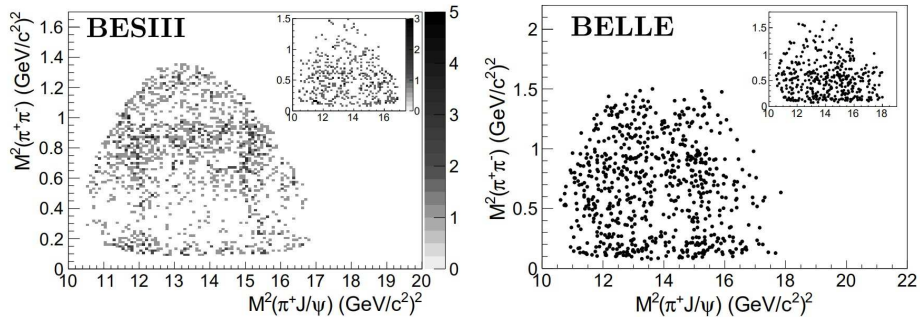
Figure 46: Dalitz plots for selected $e^+e^- \to \pi^+\pi^- J/\psi$ events in the J/ψ signal region from BESIII [22] and Belle [68] experimental data. The insets show background events from the J/ψ mass sidebands (not normalized).
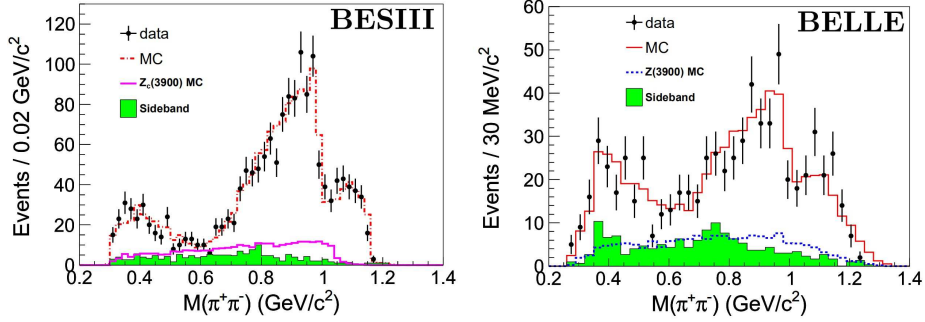
Figure 47: Invariant mass distributions of $\pi^+\pi^-$ for events in the J/ψ signal region from BESIII [22] and Belle [68] experimental data. Points with error bars represent data, shaded histograms are the normalized background estimates from the J/ψ-mass sidebands, red histograms represent MC simulation results from $\sigma(500)$, $f_0(980)$, and non-resonant $\pi^+\pi^-$ amplitudes, and lower histograms are MC simulation results for a $Z_c(3900)$ signal.

amplitude can describe the data well, but does not generate any peaking structure in the $\pi^\pm J/\psi$ mass projection. The $\pi^+\pi^-$ mass spectrum shows complicated structures. Unbinned maximum-likelihood fits are applied to the distributions of $M_{\max}(\pi^\pm J/\psi)$ from Belle and BESIII measurements. The signal shape is parameterized as an S-wave BW function convolved with a Gaussian function with a mass resolution fixed at the MC simulated value. Figure 48 shows the fit results. The measured masses are $(3899.0 \pm 3.6 \pm 4.9)$ MeV and $(3894.5 \pm 6.6 \pm 4.5)$ MeV and the measured widths are $(46 \pm 10 \pm 20)$ MeV and $(63 \pm 24 \pm 26)$ MeV from the Belle and BESIII experiments, respectively. They are consistent with each other within the uncertainties. The signal significance is greater than 5σ in both measurements. This structure is now referred to as the $Z_c(3900)$. The production ratios of $Z_c(3900)$ are measured to be

$$\frac{\sigma[e^+e^- \to \pi^\pm Z_c(3900)^\mp \to \pi^+\pi^- J/\psi]}{\sigma(e^+e^- \to \pi^+\pi^- J/\psi)} = (21.5 \pm 3.3 \pm 7.5)\% \text{ and } (29.0 \pm 8.9)\%$$

in the BESIII and Belle experiments, respectively, where the error in the Belle measurement is statistical only. As the $Z_c(3900)$ state has a strong coupling to charmonium and is charged, it cannot be a conventional $c\bar{c}$ state. Actually, since the final state is an isovector, the Z_c state should be an isovector as well.
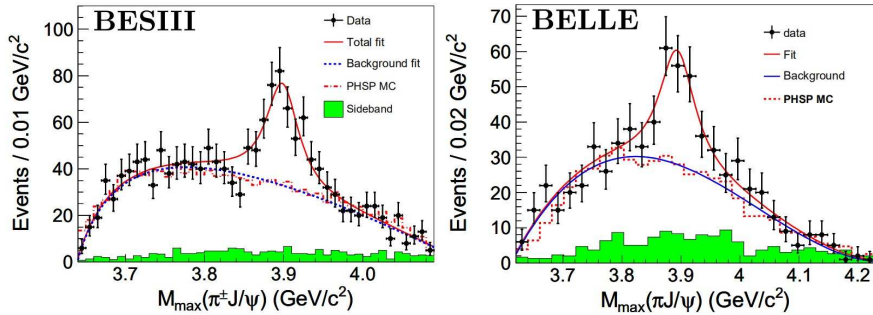
Figure 48: Unbinned maximum-likelihood fits to the distributions of the $M_{\max}(\pi J/\psi)$ from BESIII [22] and Belle [68] experimental data. Dots with error bars are data, the solid curves are the best fits, the dashed histograms represent the results of the phase-space distribution, and the shaded histograms are the normalized J/ψ sideband events.

The $Z_c(3900)$ state was confirmed shortly after with CLEO-c data at a c.m. energy of 4.17 GeV [69], and the mass and width agreed very well with the BESIII and Belle measurements. In addition, a 3.5σ evidence for $Z_c(3900)^0$ in the CLEO-c data was also reported in the $e^+e^- \to \pi^0\pi^0 J/\psi$ process [69].

BESIII measured the cross sections of $e^+e^- \to \pi^0\pi^0 J/\psi$ with data in the c.m. energy ranges from 4.19 to 4.42 GeV [157]. A neutral state $Z_c(3900)^0 \to \pi^0 J/\psi$ with a significance of 10.4σ was observed, with the mass and width measured to be $(3894.8 \pm 2.3 \pm 3.2)$ MeV and $(29.6 \pm 8.2 \pm 8.2)$ MeV, respectively, which are close to

those of $Z_c(3900)^{\pm}$. Thus, it is interpreted as the neutral partner of the $Z_c(3900)^{\pm}$. The measured production rate of $e^+e^- \to \pi^0 Z_c(3900)^0$ is about half of that for $e^+e^- \to \pi^+ Z_c(3900)^- + c.c.$, which is consistent with the expectation from isospin symmetry. This confirms that the $Z_c(3900)$ is an isovector state.

As the $Z_c(3900)$ mass is close to the $D\bar{D}^*$ mass threshold, it is natural to check the $D\bar{D}^*$ mass spectrum in $e^+e^- \to \pi^{\pm}(D\bar{D}^*)^{\mp}$, which was studied by BESIII using the data sample at $\sqrt{s} = 4.26$ GeV [266]. The $e^+e^- \to \pi^+(D\bar{D}^*)^- + c.c.$ events are selected by a so-called single-tag technique in which only the bachelor $\pi^{\pm}$ and one final-state D meson are reconstructed, and the $\bar{D}^*$ is inferred from energy-momentum conservation. In this analysis, both isospin channels $\pi^+ D^0 D^{*-} + c.c.$ and $\pi^+ D^- D^{*0} + c.c.$ are studied and the D mesons are reconstructed in the $D^0 \to K^-\pi^+$ and $D^+ \to K^-\pi^+\pi^+$ decay channels. As expected, a structure close to the $D\bar{D}^*$ mass threshold is observed in the $(D\bar{D}^*)^{\pm}$ invariant mass distributions, as shown in Fig. 49 for the selected $e^+e^- \to \pi^+(D\bar{D}^*)^- + c.c.$ candidates. Using a BW function with a mass-dependent width as a signal shape to fit the $(D\bar{D}^*)^{\pm}$ invariant mass distributions, the pole mass and width are determined to be $(3883.9 \pm 1.5 \pm 4.2)$ MeV and $(24.8 \pm 3.3 \pm 11.0)$ MeV, respectively. The fit results are shown in Fig. 49 with solid lines. The production rate is measured to be $\sigma[e^+e^- \to \pi^{\mp} Z_c(3900)^{\pm}]\mathcal{B}[Z_c(3900)^{\pm} \to (D\bar{D}^*)^{\pm}] = (83.5 \pm 6.6 \pm 22.0)$ pb.
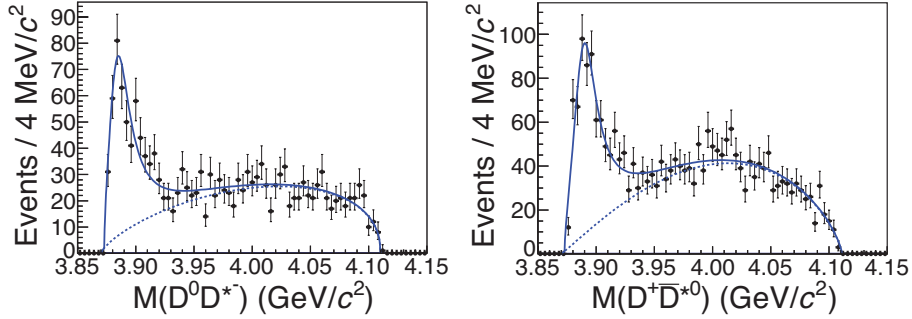
Figure 49: The $M(D^0 D^{*-})$ (left) and $M(D^+\bar{D}^{*0})$ (right) distributions for selected signal candidates at $\sqrt{s}$ = 4.26 GeV in the single-tag analysis [266]. The solid curves show the best fits.

The processes $e^+e^- \to \pi^+ D^0 D^{*-} + c.c.$ and $\pi^+ D^- D^{*0} + c.c.$ are reanalyzed using a double-tag technique with data samples at $\sqrt{s}$=4.23 and 4.26 GeV [267]. The bachelor π^+ and the D-meson pair are reconstructed, with the π from D^{*-} and D^{*0} decays inferred using energy-momentum conservation. The D^0 candidates are reconstructed in four decay modes ($K^-\pi^+$, $K^-\pi^+\pi^0$, $K^-\pi^+\pi^+\pi^-$, and $K^-\pi^+\pi^+\pi^-\pi^0$), and the D^- in six decay modes ($K^+\pi^-\pi^-$, $K^+\pi^-\pi^-\pi^0$, $K_S^0\pi^-$, $K_S^0\pi^-\pi^0$, $K_S^0\pi^+\pi^-\pi^-$, and $K^+K^-\pi^-$). With both D candidates reconstructed, the background level is greatly suppressed. Similarly, a structure close to the $D\bar{D}^*$ mass threshold is observed in the $(D\bar{D}^*)^{\pm}$ invariant mass distributions for the two processes at $\sqrt{s}$=4.23 and 4.26 GeV. A simultaneous fit with a BW function for the $Z_c(3900)$ signal and a phase-space distribution for the background to the $(D\bar{D}^*)^{\pm}$ invariant mass distributions yields a mass of (3890.3 ± 0.8) MeV and a width of (31.5 ± 3.3) MeV, with a statistical significance greater than 10σ, where the errors are statistical only. The corresponding pole mass and width are $(3881.7 \pm 1.6 \pm 1.6)$ MeV and $(26.6 \pm 2.0 \pm 2.1)$ MeV, respectively. The production rates are measured to be $\sigma[e^+e^- \to \pi^{\mp} Z_c(3900)^{\pm}]\mathcal{B}[Z_c(3900)^{\pm} \to (DD^*)^{\pm}] = (141.6 \pm 7.9 \pm 12.3)$ pb and $(108.4 \pm 6.9 \pm 8.8)$ pb for $\sqrt{s}$=4.23 GeV and 4.26 GeV, respectively. The pole position of the $Z_c(3900)$ and the production rate are consistent with those from the single-tag analysis with improved precision. Figure 50 shows the $M(D^0 D^{*-})$ and $M(D^-D^{*0})$ distributions for selected signal candidates at $\sqrt{s}$ = 4.23 GeV and 4.26 GeV together with the projection of of the simultaneous fit. The double-tag analysis only has ~9% events in common with the single-tag analysis, so the two analyses are almost statistically independent and can be combined into a weighted average. The combined pole mass and width are $(3882.2 \pm 1.1 \pm 1.5)$ MeV and $(26.5 \pm 1.7 \pm 2.1)$ MeV, respectively. The combined production rate $\sigma[e^+e^- \to \pi^{\mp} Z_c(3900)^{\pm}]\mathcal{B}[Z_c(3900)^{\pm} \to (DD^*)^{\pm}]$ is $(104.4 \pm 4.8 \pm 8.4)$ pb at $\sqrt{s}$=4.26 GeV. In an analysis of $e^+e^- \to \pi^0(D\bar{D}^*)^0$, the $Z_c(3900)^0 \to (D\bar{D}^*)^0$ is also observed [268] and all the results agree with the expectations from isospin symmetry.

Determination of the spin-parity of the $Z_c(3900)$ is undoubtedly a crucial issue. In both the single-tag and double-tag analyses of $Z_c(3900) \to D\bar{D}^* + c.c.$ [266, 267], by checking the angular distribution of the π accompanying the $Z_c(3900)$, BESIII found that the spin-parity $J^P = 1^+$ of the $Z_c(3900)$ is favored over $J^P = 0^-$ and 1^- assumptions,
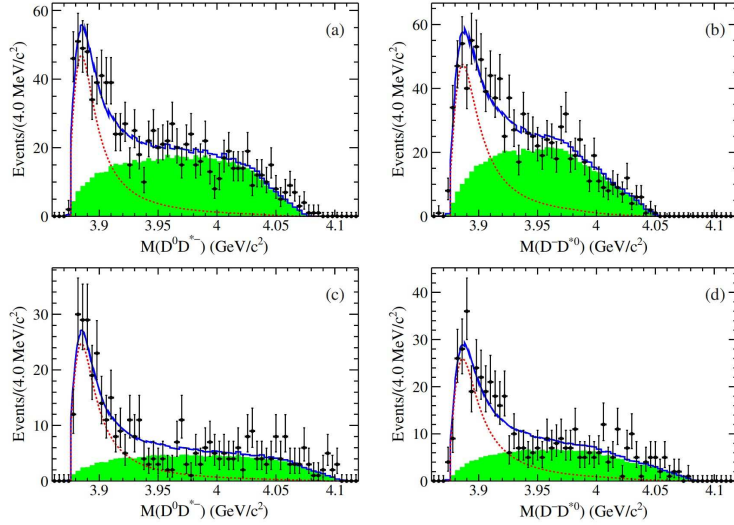
Figure 50: The $M(D^0 D^{*-})$ (a,c) and $M(D^- D^{*0})$ (b,d) distributions for selected signal candidates at $\sqrt{s} = 4.23$ GeV (a,b) and 4.26 GeV (c,d) in the double-tag analysis [267]. The solid curves show the total fits, the dashed lines are the signal shapes, and the green shaded histograms describe the background shapes estimated by phase space MC simulation.

but $J > 1$ cannot be ruled out by simply checking one angular distribution. The quantum numbers $J^P = 0^+$ are not allowed due to spin-parity conservation in $Z_c(3900) \to \pi J/\psi$ decays. To determine the J^P values of $Z_c(3900)$ precisely, BESIII performed a PWA to the selected $e^+e^- \to \pi^+\pi^- J/\psi$ candidates at $\sqrt{s} = 4.23$ and 4.26 GeV [269]. With the same event selection as in Ref. [22], the numbers of selected signal events are 4154 at $\sqrt{s} = 4.23$ GeV and 2447 at $\sqrt{s} = 4.26$ GeV, with 365 and 272 background events, respectively, estimated by using the normalized J/ψ mass sidebands.

Amplitudes of the PWA are constructed with the helicity-covariant method [270–272]. The process $e^+e^- \to \pi^+\pi^- J/\psi$ is assumed to proceed via the $Z_c(3900)$ resonance, i.e., $e^+e^- \to \pi^\pm Z_c(3900)^\mp$, $Z_c(3900)^\mp \to \pi^\mp J/\psi$, and via the non-$Z_c(3900)$ decay $e^+e^- \to RJ/\psi$, $R \to \pi^+\pi^-$, with $R = \sigma$, $f_0(980)$, $f_2(1270)$, and $f_0(1370)$. In the fit, the $Z_c(3900)$ line shape is described with a Flatté-like formula taking into account the fact that the $Z_c(3900)^\pm$ decays are dominated by the $(D\bar{D}^*)^\pm$ [266, 267] and $\pi^\pm J/\psi$ [22] final states. All processes are added coherently to obtain the total amplitude. The fit indicates that the spin-parity $J^P = 1^+$ of the $Z_c(3900)$ are favored by more than 7σ over other quantum numbers (0^-, 1^-, 2^-, and 2^+). Figure 51 shows projections of the simultaneous fit results with $J^P = 1^+$ for the $Z_c(3900)$ state at $\sqrt{s} = 4.23$ and 4.26 GeV, where contributions from fitted components are indicated in the plots. The pole mass and width are determined to be $(3881.2 \pm 4.2 \pm 52.7)$ MeV and $(51.8 \pm 4.6 \pm 36.0)$ MeV, respectively. The Born cross sections for $e^+e^- \to \pi^+ Z_c(3900)^- + c.c. \to \pi^+\pi^- J/\psi$ are measured to be $(21.8 \pm 1.0 \pm 4.4)$ pb at $\sqrt{s} = 4.23$ GeV and $(11.0 \pm 1.2 \pm 5.4)$ pb at $\sqrt{s} = 4.26$ GeV. If the $Z_c(3900)^\pm$ would be parametrized with a constant-width BW function, a simultaneous fit would disfavor the BW parametrization with a significance of 6.6σ.

Although the $Z_c(3900)$ has been clearly observed at e^+e^- colliders, it is still necessary to check if it can be produced in other processes, such as in B decays or at hadron colliders. This will also add more experimental information to our understanding of its inner structure. For example, the $Z_c(3900)^\pm$ may be produced in b-hadron decays. Recently the D0 experiment looked for the $Z_c(3900)$ using 10.4 fb^{-1} of $p\bar{p}$ collision data and found evidence for the decay $Z_c(3900)^\pm \to \pi^\pm J/\psi$ [183]: For the selected $\pi^+\pi^- J/\psi$ candidates, D0 performed binned maximum-likelihood fits to the $\pi^\pm J/\psi$ mass distribution in six $\pi^+\pi^- J/\psi$ mass intervals, (4.1–4.2), (4.2–4.25), (4.25–4.3), (4.3–4.4), (4.4–4.7), and (4.7–5.0) GeV, with roughly equal numbers of signal plus background events. Figure 52 (left plot) shows the fit to the invariant mass distribution of $\pi^\pm J/\psi$ candidates in the $4.2 < M(\pi^+\pi^- J/\psi) < 4.25$ GeV region as an example. A clear enhancement near the $Z_c(3900)^\pm$ mass can be seen, which is consistent with the decays of the $Y(4230)$. The significances are smaller but nonvanishing in other $\pi^+\pi^- J/\psi$ mass regions between 4.25 and 4.7 GeV, while no significant signal is seen in the bins $4.1 < M(\pi^+\pi^- J/\psi) < 4.2$ GeV or $4.7 < M(\pi^+\pi^- J/\psi) < 5.0$ GeV. The measured
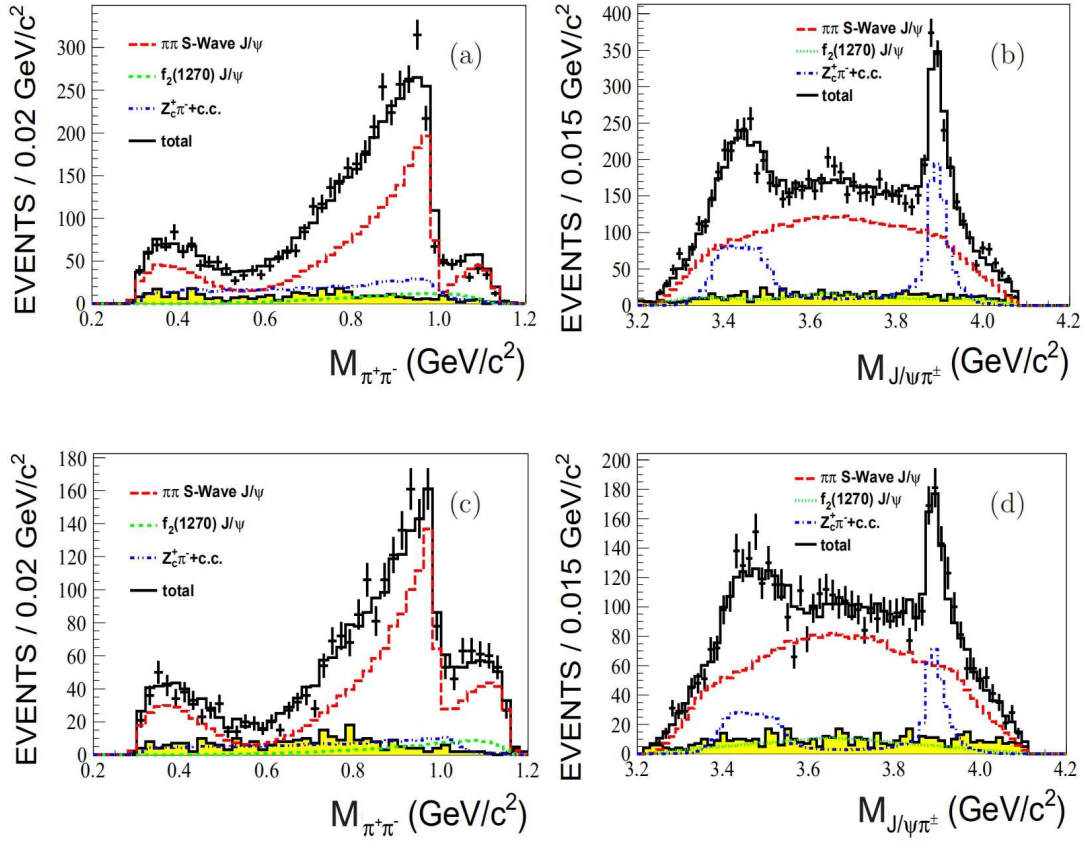
Figure 51: Projections to $M_{\pi^+\pi^-}$ (a, c) and $M_{\pi^\pm J/\psi}$ (b, d) of the fit results with $J^P = 1^+$ for the $Z_c(3900)$, at $\sqrt{s} = 4.23$ GeV (a, b) and 4.26 GeV (c, d) from BESIII PWA [269]. The points with error bars are data, and the black histograms are the total fit results. The shaded histograms denote the backgrounds. Plots (b) and (d) are filled with two entries per event. The contributions from fitted components are indicated in the plots.
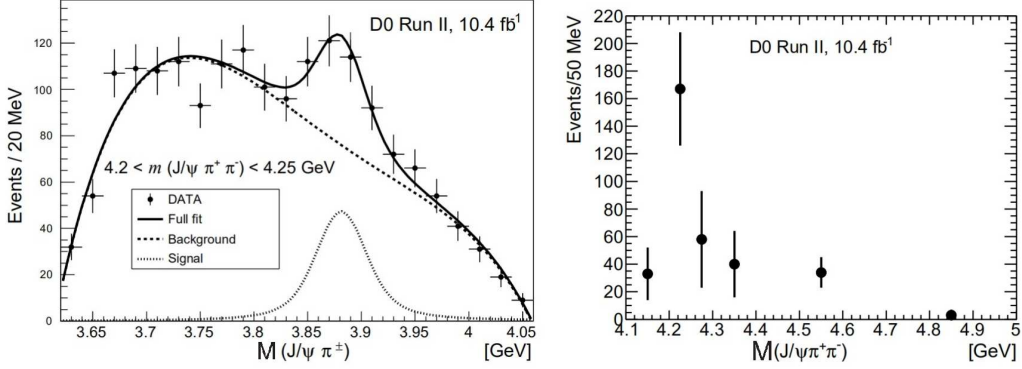
Figure 52: The fit to the invariant mass distribution of $\pi^\pm J/\psi$ candidates in $4.2 < M(\pi^+\pi^- J/\psi) < 4.25$ GeV range (left plot) and the resulting differential distribution of the $Z_c(3900)^\pm$ signal yield versus $M(\pi^+\pi^- J/\psi)$ (right plot) [183].
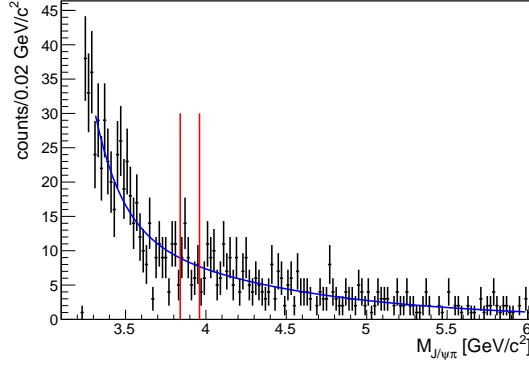
Figure 53: The fit to the mass spectrum of the $\pi^\pm J/\psi$ candidates obtained by the COMPASS Collaboration in the $\mu^+ N \to \mu^+ Z_c^\pm(3900) N \to \mu^+\pi^\pm J/\psi N \to \mu^+\mu^+\mu^-\pi^\pm N$ process [274]. The red solid lines show the expected $Z_c(3900)^\pm$ signal region.

mass is $M = (3895.0 \pm 5.2^{+4.0}_{-2.7})$ MeV and the significance is 4.6σ with systematic uncertainties included from a fit to the data in the mass range $4.2 < M(\pi^+\pi^- J/\psi) < 4.7$ GeV. The resulting differential distribution of the $Z_c(3900)^\pm$ signal yield is shown in Fig. 52 (right plot). It reveals that a $Z_c(3900)^\pm$ signal is correlated with the $\pi^+\pi^- J/\psi$ system in the invariant mass range $4.2-4.7$ GeV including the $Y(4230)$ and $Y(4360)$ states. There is also an indication that some $Z_c(3900)^\pm$ signal events come from b-hadron decays to an intermediate $J/\psi\pi^+\pi^-$ combination with mass above that of the $Y(4360)$. This is the first evidence for the $Z_c(3900)$ production at a hadron collider.

Based on the vector meson dominance model, the authors of Ref. [273] predicted a sizable cross section of the reaction $\gamma N \to Z_c(3900)^\pm N$ for $\sqrt{s_{\gamma N}} \sim 10$ GeV, where a $Z_c(3900)^\pm$ can be produced by the interaction of an incoming photon with a virtual charged pion provided by the target nucleon. Using the data obtained by scattering positive muons of 160 GeV (2002-2010) or 200 GeV momentum (2011) off solid ^{6}LiD (2002-2004) or NH$_3$ targets (2006-2011), COMPASS searched for the process $\mu^+ N \to \mu^+ Z_c(3900)^\pm N \to \mu^+\pi^\pm J/\psi N \to \mu^+\mu^+\mu^-\pi^\pm N$ [274]. The mass spectrum for the selected $\pi^\pm J/\psi$ candidates is shown in Fig. 53, where no statistically significant resonant structure around 3.9 GeV can be seen. An upper limit for the ratio $\mathcal{B}[Z_c(3900)^\pm \to \pi^\pm J/\psi]\sigma[\gamma N \to Z_c(3900)^\pm N]/\sigma(\gamma N \to J/\psi N)$ of 3.7×10^{-3} was established at the 90% C.L.

As mentioned in Sec. 3.1.2, BESIII measured cross sections of $e^+e^- \to \pi^+\pi^- h_c$ at c.m. energies of 3.90–4.42 GeV with $h_c \to \gamma\eta_c$ and η_c decays into 16 hadronic final states [158]. The h_c signal is selected using 3.518 GeV $< M_{\gamma\eta_c} <$ 3.538 GeV, and $\pi^+\pi^- h_c$ samples of 859 events at 4.23 GeV, 586 events at 4.26 GeV, and 469 events at 4.36 GeV are obtained with purities of about ~65%. The Dalitz plot of the selected $\pi^+\pi^- h_c$ candidate events to check for possible

intermediate states is shown in Fig. 54. There are no clear structures in the $\pi^+\pi^-$ system, while there is distinct evidence in the $\pi^\pm h_c$ system at about 4.02 GeV. Figure 55 (left) shows the projection of the $M(\pi^\pm h_c)$ (two entries per event) distribution for the signal events summed over the three c.m. energy points, as well as the background events estimated from the normalized h_c mass sidebands. There is a significant peak at around 4.02 GeV [$Z_c(4020)$], and there are also some events at around 3.9 GeV which could be $Z_c(3900)$ as shown in the inserted plot.
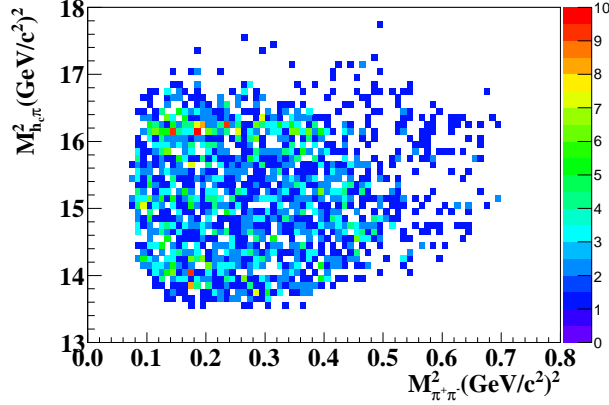
Figure 54: Dalitz plot of $M^2_{\pi^+ h_c}$ versus $M^2_{\pi^+\pi^-}$ for the selected $e^+e^- \to \pi^+\pi^- h_c$ events summed over the 4.23, 4.26, and 4.36 GeV c.m. energy points [158].

Assuming there are both $Z_c(4020)$ and $Z_c(3900)$ contributions with the mass and width of the latter fixed to the BESIII measurements [22], an unbinned maximum-likelihood fit is applied to the $M(\pi^\pm h_c)$ distribution summed over the 16 η_c decay modes. As the $Z_c(3900)$ signal overlaps with the reflection of the $Z_c(4020)$ at $\sqrt{s}$ = 4.36 GeV, the data at 4.23, 4.26, and 4.36 GeV are fitted simultaneously to the same $Z_c(4020)$ signal function only with common mass and width from 3.95 to 4.25 GeV, while the data at 4.23 and 4.26 GeV are fitted simultaneously with both of the $Z_c(3900)$ and $Z_c(4020)$ signals from 3.8 to 4.15 GeV. The fitted results are shown in Fig. 55 (left), where the inset shows the sum of the simultaneous fit at 4.23 and 4.26 GeV with $Z_c(3900)$ and $Z_c(4020)$. The fit yields a mass of $(4022.9 \pm 0.8 \pm 2.7)$ MeV and a width of $(7.9 \pm 2.7 \pm 2.6)$ MeV, with a statistical significance greater than 8.9σ for the $Z_c(4020)$. The cross sections are calculated to be $\sigma[e^+e^- \to \pi^\pm Z_c(4020)^\mp \to \pi^+\pi^- h_c] = (8.7 \pm 1.9 \pm 2.8 \pm 1.4)$ pb at 4.23 GeV, $(7.4 \pm 1.7 \pm 2.1 \pm 1.2)$ pb at 4.26 GeV, and $(10.3 \pm 2.3 \pm 3.1 \pm 1.6)$ pb at 4.36 GeV, where the first errors are statistical, the second ones systematic, and the third ones from the uncertainty in $\mathcal{B}(h_c \to \gamma\eta_c)$ [6]. Since the statistical significance of $Z_c(3900)$ is only 2.1σ, the upper limits on the production cross sections $\sigma[e^+e^- \to \pi^\pm Z_c(3900)^\mp \to \pi^+\pi^- h_c]$ are determined to be 13 pb and 11 pb at $\sqrt{s}$ = 4.23 and 4.26 GeV, respectively, at 90% C.L., which are lower than those of $Z_c(3900) \to \pi^\pm J/\psi$ [269].

As mentioned in Sec. 3.1.2, BESIII measured cross sections of $e^+e^- \to \pi^0\pi^0 h_c$ at $\sqrt{s}$ = 4.23, 4.26, and 4.36 GeV for the first time [157]. The intermediate state of $Z_c(4020)^0$, the neutral isospin partner of the $Z_c(4020)^\pm$, is observed in the $\pi^0 h_c$ invariant mass distribution, as shown in Fig. 55 (right). This observation indicates that there is no anomalously large isospin violation in $\pi^+\pi^- h_c$ and $\pi Z_c(4020)$ systems, and $Z_c(4020)$ is an isovector state.

Since the $Z_c(4020)$ mass is close to the $D^*\bar{D}^*$ mass threshold, it may have a strong coupling to the $D^*\bar{D}^*$ final state. The process $e^+e^- \to (D^*\bar{D}^*)^\pm \pi^\mp$ [$(D^*\bar{D}^*)^\pm = D^{*+}\bar{D}^{*0}$ and $D^{*-}D^{*0}$] was studied by BESIII using a 827 pb^{-1} data at $\sqrt{s}$ = 4.26 GeV to check the $D^*\bar{D}^*$ system [275]. In this analysis, a partial reconstruction technique is used, i.e., taking $\pi^- D^{*+}\bar{D}^{*0}$ as an example, only the bachelor π^-, a charged D^+, and at least one soft π^0 from D^* decays are reconstructed. By identifying the D^+ particle, the charges of its mother particle D^{*+} and the bachelor π^- are also unambiguously identified. The $Z_c(4020)$ state is searched for in the bachelor $\pi^\pm$ recoil mass spectrum. The final $\pi^\pm$ recoil mass spectrum is shown in Fig. 56 (left), where a structure near the $(D^*\bar{D}^*)^\pm$ threshold is observed and the shaded histogram is from the combinatorial backgrounds estimated by combining a reconstructed $D^\pm$ with a pion of the wrong charge. Since the signal events from phase space (dot-dashed line) and combinatorial backgrounds (dotted
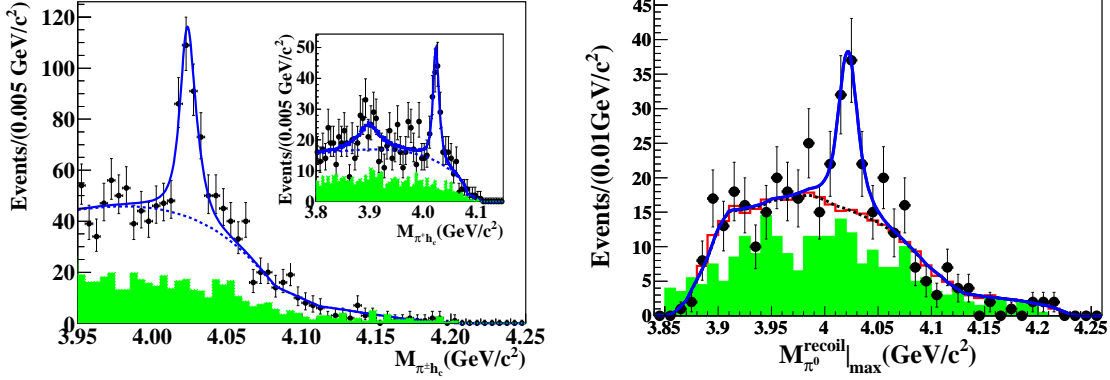
Figure 55: Sum of the simultaneous fits to the $M(\pi^\pm h_c)$ [158] (left panel) and $M(\pi^0 h_c)$ [158] (right panel) distributions from $e^+e^- \to \pi^+\pi^- h_c$ and $\pi^0\pi^0 h_c$, respectively, at 4.23, 4.26, and 4.36 GeV in the BESIII data; the inset in the left panel shows the sum of the simultaneous fit to the $M(\pi^\pm h_c)$ distributions at 4.23 and 4.26 GeV with $Z_c(3900)$ and $Z_c(4020)$. Dots with error bars are data; shaded histograms are normalized sideband background; the solid curves show the total fits, and the dotted curves are the backgrounds from the fits.

line) cannot describe the data, assuming the enhancement is due to $Z_c(4020)$, an unbinned maximum-likelihood fit to the $\pi^\pm$ recoil mass spectrum is performed with an S-wave BW shape to parameterize the structure. The fit yields a mass of $(4026.3 \pm 2.6 \pm 3.7)$ MeV and a width of $(24.8 \pm 5.6 \pm 7.7)$ MeV, with a statistical significance of 13σ. The fit results are shown in Fig. 56 (left). The Born cross section of $e^+e^- \to (D^*\bar{D}^*)^\pm\pi^\mp$ is measured to be $(137 \pm 9 \pm 15)$ pb at $\sqrt{s}$ =4.26 GeV. From the fit results, 401 ± 47 $Z_c(4020)$ signal events are obtained, and the associated ratio of the production rates is determined to be

$$\frac{\sigma[e^+e^- \to Z_c(4020)^\pm\pi^\mp \to (D^*\bar{D}^*)^\pm\pi^\mp]}{\sigma[e^+e^- \to (D^*\bar{D}^*)^\pm\pi^\mp]} = 0.65 \pm 0.09 \pm 0.06.$$
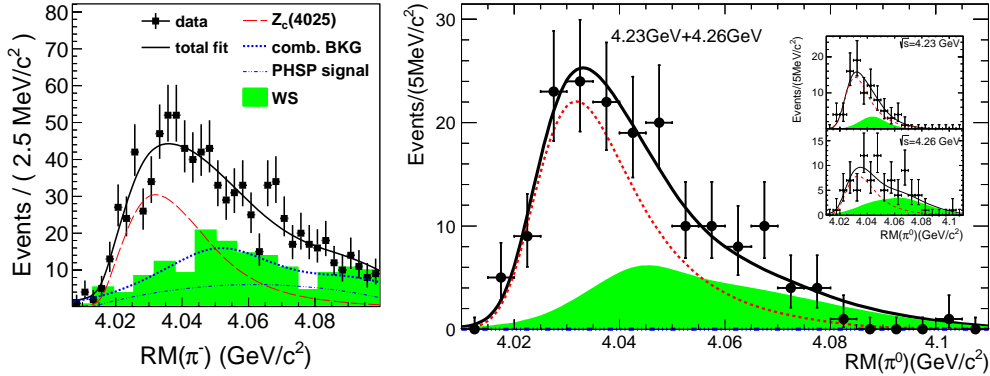
Figure 56: Unbinned maximum-likelihood fits to the $\pi^\mp$ recoil mass spectrum in $e^+e^- \to (D^*\bar{D}^*)^\pm\pi^\mp$ at $\sqrt{s}$ = 4.26 GeV [275] (left), and to the π^0 recoil mass spectrum in $e^+e^- \to (D^*\bar{D}^*)^0\pi^0$ at $\sqrt{s}$ = 4.23 and 4.26 GeV [276] (right) at BESIII.

The processes $e^+e^- \to (D^{*0}\bar{D}^{*0})\pi^0$ and $(D^{*+}D^{*-})\pi^0$ are also studied at BESIII to search for the neutral partner of the $Z_c(4020)$ with integrated luminosities of 1092 pb^{-1} at $\sqrt{s}$ = 4.23 and 826 pb^{-1} at $\sqrt{s}$ =4.26 GeV [276]. In this analysis, two D mesons are reconstructed together with the bachelor π^0. The recoil mass distribution of the bachelor π^0 is shown in Fig. 56 (right), together with the distributions at $\sqrt{s}$ =4.23 GeV and 4.26 GeV in the inset plots. The points with error bars are the data and the shaded histograms represent the inclusive backgrounds. Enhancements over the inclusive backgrounds estimated using the inclusive MC samples for both data samples can

54

be seen, which cannot be explained by three-body nonresonant processes either. A simultaneous unbinned maximum-likelihood fit to the bachelor π^0 recoil mass spectra at $\sqrt{s}$ =4.23 GeV and 4.26 GeV is performed with BW functions with a mass-dependent width as $Z_c(4020)$ signal shapes. The solid lines show the fit results and the dotted red lines stand for the $Z_c(4020)^0$ signals. The fit determines the mass and width of the $Z_c(4020)$ pole position to be $(4025.5^{+2.0}_{-4.7} \pm 3.1)$ MeV and $(23.0 \pm 6.0 \pm 1.0)$ MeV, respectively. From the simultaneous fit, 69.5 ± 9.2 and 46.1 ± 8.5 $Z_c(4020)^0$ signal events are obtained at 4.23 and 4.26 GeV, respectively, with a statistical significance of 5.9σ. The Born cross section $\sigma[e^+e^- \rightarrow Z_c(4020)^0\pi^0 \rightarrow (D^{*0}\bar{D}^{*0} + D^{*+}D^{*-})\pi^0]$ is measured to be $(61.6 \pm 8.2 \pm 9.0)$ pb at 4.23 GeV and $(43.4 \pm 8.0 \pm 5.4)$ pb at 4.26 GeV. BESIII also obtained the ratio

$$\frac{\sigma[e^+e^- \rightarrow Z_c(4020)^0\pi^0 \rightarrow (D^*\bar{D}^*)^0\pi^0]}{\sigma[e^+e^- \rightarrow Z_c(4020)^+\pi^- \rightarrow (D^*\bar{D}^*)^+\pi^-]} \approx 1$$

at $\sqrt{s}$ = 4.26 GeV, which is expected from isospin symmetry. This also confirms that the isospin of the $Z_c(4020)$ is one.

As mentioned before, to determine the J^P values of $Z_c(3900)$, BESIII did the PWA to the selected $e^+e^- \rightarrow \pi^+\pi^-J/\psi$ events at $\sqrt{s}$ =4.23 and 4.26 GeV [269]. In the PWA, BESIII also searched for the process $e^+e^- \rightarrow \pi^-Z_c(4020)^+ + c.c. \rightarrow \pi^+\pi^-J/\psi$, with the $Z_c(4020)^\pm$ assumed to be a 1^+ state added in the global fit. Its mass is taken from Ref. [158] and width is taken as the observed value. The fit yields a 3σ statistical significance for $Z_c(4020)^\pm \rightarrow \pi^\pm J/\psi$ in the combined data. The Born cross sections are measured to be (0.2 ± 0.1) pb at $\sqrt{s}$ = 4.23 GeV and (0.8 ± 0.4) pb at $\sqrt{s}$ = 4.26 GeV, and the corresponding upper limits at the 90% C.L. are estimated to be 0.9 and 1.4 pb, respectively.

Although the observations of the $Z_c(3900)$ and $Z_c(4020)$ indicate that they are not conventional mesons consisting of a quark-antiquark pair, their exact quark configuration is still unknown. There are many models developed to interpret their inner structure, including loosely bound hadronic molecules of two charmed mesons, compact tetraquarks, hadroquarkonium, and so on. Therefore, how to discriminate between the molecule and compact tetraquark scenarios experimentally is an important research topic that will be discussed in some depth in various subsections of Sec. 4. It has recently been suggested that the relative decay rate of $Z_c(3900) \rightarrow \rho\eta_c$ to $\pi J/\psi$ [or $Z_c(4020) \rightarrow \rho\eta_c$ to πh_c] can be used to discriminate them [277]. In the compact tetraquark scenario, the predicted ratio of $\mathcal{B}[Z_c(3900) \rightarrow \rho\eta_c]/\mathcal{B}[Z_c(3900) \rightarrow \pi J/\psi]$ is 230 or 0.27, depending on whether or not the spin-spin interaction outside the diquarks is kept [277–282]. In the molecular framework, on the other hand, this ratio is only 0.046. Similarly, the predicted ratio of $\mathcal{B}[Z_c(4020) \rightarrow \rho\eta_c]/\mathcal{B}[Z_c(4020) \rightarrow \pi J/\psi]$ is 6.6 in the compact tetraquark model, but only 0.01 in the meson molecule model [277]. Therefore, a search for the decays $Z_c(3900)/Z_c(4020) \rightarrow \rho\eta_c$ offers an important opportunity to understand the internal structure of the $Z_c(3900)$ and $Z_c(4020)$.

BESIII searched for $e^+e^- \rightarrow \pi^+\pi^-\pi^0\eta_c$ and intermediate states decaying into $\rho\eta_c$ with data at c.m. energies above 4 GeV corresponding to an integrated luminosity of about 4.1 fb^{-1} [223]. In this analysis, η_c is reconstructed with 9 hadronic final states: $p\bar{p}$, $2(K^+K^-)$, $K^+K^-\pi^+\pi^-$, $K^+K^-\pi^0$, $p\bar{p}\pi^0$, $K^0_S K^\pm\pi^\mp$, $\pi^+\pi^-\eta$, $K^+K^-\eta$, and $\pi^+\pi^-\pi^0\pi^0$. A clear signal of $e^+e^- \rightarrow \pi^+\pi^-\pi^0\eta_c$ is observed at $\sqrt{s}$ = 4.23 GeV. From the fit to the η_c mass spectrum, 333^{+83}_{-80} η_c signal events are obtained with a statistical significance of 4.2σ. No significant signals are observed at other c.m. energy points. The $Z_c(3900/4020)^\pm \rightarrow \rho^\pm\eta_c$ signals are examined after requiring that the invariant mass of an η_c candidate is within the η_c signal region [2.95, 3.02] GeV and the invariant mass of $\pi^\pm\pi^0$ is within the $\rho^\pm$ signal region [0.675, 0.875] GeV. The recoil mass of the remaining $\pi^\mp$ (equivalent to the invariant mass of $\rho^\pm\eta_c$) is shown in Fig. 57 for the data at $\sqrt{s}$ = 4.23 GeV, together with the contribution from the η_c mass sideband events (the shaded histogram). In Fig. 57, the $Z_c(3900)^\pm$ signal is apparent, but there is no statistically significant $Z_c(4020)^\pm$ signal. The $\rho^\pm\eta_c$ invariant mass distribution is fitted with the contributions from $Z_c(3900)$ and $Z_c(4020)$ together with a smooth background. In the fit, a possible interference between the signal and the background is neglected. The solid line in the left plot of Fig. 57 shows the best fit, while the right plot is the background-subtracted distribution. The total $Z_c(3900)^\pm$ signal yield is 240^{+56}_{-54} events with a statistical significance of 4.3σ, and that of the $Z_c(4020)^\pm$ is 21^{+15}_{-11} events with a statistical significance of 1.0σ. The $Z_c(3900)$ signals at other c.m. energies and the $Z_c(4020)$ signals at all the c.m. energies are not statistically significant. The cross section is measured as $\sigma[e^+e^- \rightarrow \pi^\mp Z_c(3900)^\pm \rightarrow \pi^\mp\rho^\pm\eta_c] = (48 \pm 11 \pm 11)$ pb at $\sqrt{s}$ = 4.23 GeV. This result is equal within errors to the cross section of $e^+e^- \rightarrow \pi^+\pi^-\pi^0\eta_c$, which is $(46^{+12}_{-11} \pm 10)$ pb. This indicates that the $e^+e^- \rightarrow \pi^+\pi^-\pi^0\eta_c$ process is saturated by the process $e^+e^- \rightarrow \pi^\mp Z_c(3900)^\pm \rightarrow \pi^\mp\rho^\pm\eta_c$. No signal is observed at $\sqrt{s}$ =4.26, 4.36, 4.42, and 4.6 GeV, and the upper limits of the production cross sections at the 90% C.L. are determined to be 62 pb, 36 pb, 44 pb, and 14 pb, respectively. The upper limits of the production cross

section $\sigma[e^+e^- \to \pi^{\mp} Z_c(4020)^{\pm} \to \pi^{\mp}\rho^{\pm}\eta_c]$ at the 90% C.L. are determined to be 14 pb, 6 pb, 14 pb, 11 pb, and 21 pb, respectively, at $\sqrt{s}$ = 4.23, 4.26, 4.36, 4.42, and 4.6 GeV.
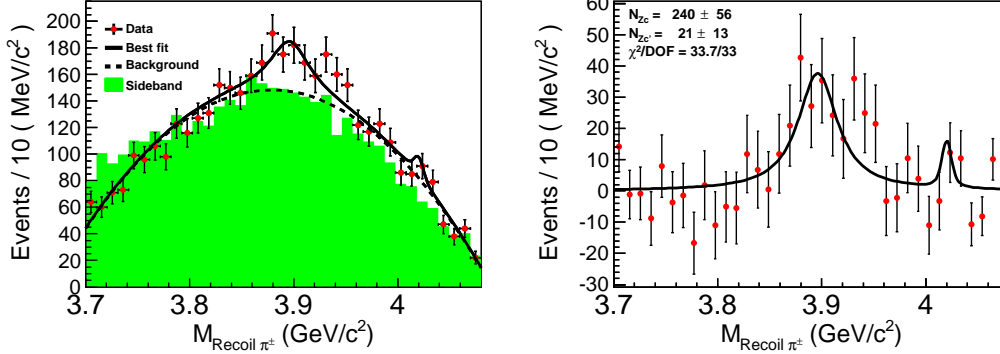
Figure 57: The $\pi^{\pm}$ recoil mass distribution summed over 9 η_c decay channels in $e^+e^- \to \pi^{\pm}\rho^{\mp}\eta_c$ at $\sqrt{s}$ = 4.23 GeV and fit with $Z_c(3900/4020)^{\pm}$ signals (left panel), and the same plot with background subtracted (right panel) [223]. Dots with error bars are data, the shaded histogram is from η_c mass sidebands, normalized to the number of backgrounds from the fit, the solid lines are the total fits, and the dotted line is the background.

Using the results from Refs. [158, 269], the ratio $R_{Z_c(3900)} = \mathcal{B}[Z_c(3900) \to \rho\eta_c]/\mathcal{B}[Z_c(3900) \to \pi J/\psi]$ is 2.2 ± 0.9 at $\sqrt{s}$ = 4.23 GeV and less than 5.6 at $\sqrt{s}$ = 4.26 GeV at the 90% C.L., while the ratio $R_{Z_c(4020)} = \mathcal{B}[Z_c(4020)^{\pm} \to \rho^{\pm}\eta_c]/\mathcal{B}[Z_c(4020)^{\pm} \to \pi^{\pm}h_c]$ is less than 1.6, 0.9, and 1.4 at c.m. energies of 4.23, 4.26, and 4.36 GeV, respectively, at the 90% C.L. For the $R_{Z_c(3900)}$, the current result seems to favor the compact tetraquark interpretation, while $R_{Z_c(4020)}$ is somewhat more consistent with the molecular one. A clear discrimination is not yet possible because of both the experimental and theoretical uncertainties.

From the above studies, we conclude that the $Z_c(3900)$ has been observed at both e^+e^- and hadron colliders. It is an isovector state with positive G-parity and spin-parity $J^P = 1^+$. It decays into $\pi J/\psi$ and $D\bar{D}^*$, and it may also decay into $\rho\eta_c$ and πh_c final states. The neutral $Z_c(3900)$ has a negative C-parity. Although the reported masses and widths are consistent with each other in many measurements, in most of the cases the possible interference between the $Z_c(3900)$ and other amplitudes is neglected. A PWA to the selected $e^+e^- \to \pi^+\pi^- J/\psi$ events has been done by BESIII [269], giving a pole mass of $(3881.2 \pm 4.2 \pm 52.7)$ MeV and a width of $(51.8 \pm 4.6 \pm 36.0)$ MeV, where the large errors are dominated by the uncertainties in the parametrization of the $\pi^+\pi^-$ S-wave amplitudes. In this PWA, a drawback is the assumption of $Z_c(3900)$ decaying dominantly into $\pi J/\psi$ and $D\bar{D}^*$ modes, which may introduce bias, as the $\rho\eta_c$ mode has been observed with a larger decay rate than $\pi J/\psi$. There could be other decay modes such as πh_c, $\pi\psi(2S)$ and so on. This needs to be checked with larger data samples in the future. The reported production cross section for $e^+e^- \to \pi^+ Z_c(3900)^- + c.c.$ suffers from the same problems mentioned above. The only reliable measurement is the product cross section of $e^+e^- \to \pi^+ Z_c(3900)^- + c.c. \to \pi^+\pi^- J/\psi$ determined from PWA which is $(21.8 \pm 1.0 \pm 4.4)$ pb at $\sqrt{s}$ = 4.23 GeV and $(11.0 \pm 1.2 \pm 5.4)$ pb at $\sqrt{s}$ = 4.26 GeV [269]. The former at 4.23 GeV is twice as big as the latter at 4.26 GeV. It would be very important to measure the $Z_c(3900)$ production cross sections at other c.m. energies, to check if the line shape of $e^+e^- \to \pi Z_c(3900)$ is the same as that of $e^+e^- \to \pi^+\pi^- J/\psi$. This will be an important piece of information in understanding the nature of the $Z_c(3900)$ and the production mechanism.

As for the $Z_c(4020)$, we conclude that it is an isovector state with positive G-parity, similar to the $Z_c(3900)$ state. The spin-parity quantum numbers of the $Z_c(4020)$ are not measured yet, but $J^P = 1^+$ are assumed in all the analyses. The currently observed decay modes are πh_c and $D^*\bar{D}^*$. With current statistics at BESIII, the possible decay modes of $\pi J/\psi$ and $\rho\eta_c$ have not been observed yet. The neutral $Z_c(4020)$ has a negative C-parity. The reported masses and widths in both analyses of $\pi^+\pi^- h_c$ and $D^*\bar{D}^*$ final states may have bias, since the reported values depend on different assumptions on the signal shape and the possible interference between the $Z_c(4020)$ and other amplitudes is neglected. In the analyses of $e^+e^- \to \pi D^*\bar{D}^*$ [275, 276], the $Z_c(4020)^{\pm}$ and $Z_c(4020)^0$ are parameterized with different line shapes and the pole mass and width are reported in the latter case. In addition, the fractions of non-$Z_c(4020)$ events in $e^+e^- \to \pi D^*\bar{D}^*$ are quite different in charged and neutral modes. All these suggest that improved measurements of $e^+e^- \to \pi D^*\bar{D}^*$, both charged and neutral modes, using more D-tag modes and data at other c.m. energies are necessary. The most reliable measurement is probably from $e^+e^- \to \pi^+\pi^- h_c$ mode [158] due to the

very narrow width. The mass and width are measured to be $(4022.9 \pm 0.8 \pm 2.7)$ MeV and $(7.9 \pm 2.7 \pm 2.6)$ MeV, respectively, in this mode. Of course, a combined analysis of $\pi^+\pi^- h_c$ and $\pi D^* \bar{D}^*$ modes will give more reliable measurements of the resonant parameters. The production cross section for $e^+e^- \to \pi Z_c(4020)$ suffers from the same problems mentioned in the $Z_c(4020)$ mass and width determination. It would be very important to measure the $Z_c(4020)$ production cross sections as a function of the c.m. energy with PWA, to check if the $e^+e^- \to \pi Z_c(4020)$ process is from continuum production or from decays of some resonant structures, such as the $Y(4230)$ and $Y(4390)$ observed in $e^+e^- \to \pi^+\pi^- h_c$ [159]. This will be an important piece of information in understanding the nature of the $Z_c(4020)$ and the production mechanism.

• *The $Z_c(4050)$ state*

Belle updated the measurement of $e^+e^- \to \pi^+\pi^- \psi(2S)$ via ISR using the 980 fb^{-1} full data sample [155]. Two distinct resonances, $Y(4360)$ and $Y(4660)$, are observed. Possible charged charmonium-like structures in $\pi^{\pm}\psi(2S)$ final states from the $Y(4360)$ or $Y(4660)$ decays are searched for by checking the Dalitz plot of the selected candidate events. Figure 58 (left) shows the $M_{\max}[\pi^{\pm}\psi(2S)]$ distribution, the maximum of $M[\pi^-\psi(2S)]$ and $M[\pi^+\psi(2S)]$, in $Y(4360)$ decays $(4.0 < M[\pi^+\pi^-\psi(2S)] < 4.5$ GeV), where an excess evidence at around 4.05 GeV can be seen. An unbinned maximum-likelihood fit is performed on the distribution of $M_{\max}[\pi^{\pm}\psi(2S)]$. The excess is parameterized with a BW function and the non-resonant non-interfering background with a second-order polynomial function. The fit yields a mass of $(4054 \pm 3 \pm 1)$ MeV and a width of $(45 \pm 11 \pm 6)$ MeV, as shown in Fig. 58 (left). The statistical significance of the signal is 3.5σ with systematic uncertainties included. Due to limited statistics in $Y(4660)$ decays $(4.5 < M_{\pi^+\pi^-\psi(2S)} < 4.9$ GeV), no significant structure in the $\pi^{\pm}\psi(2S)$ system is observed.
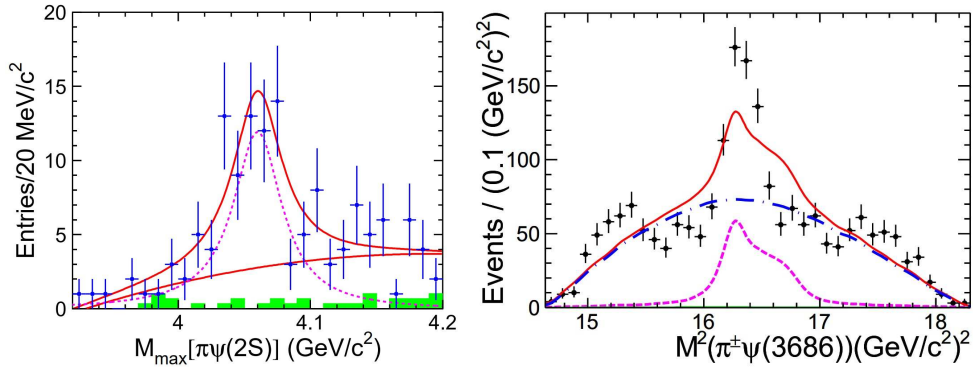
Figure 58: The distributions of (a) $M_{\max}[\pi^{\pm}\psi(2S)]$ from $\psi(4360)$ aka $Y(4360)$ decays from Belle [155] and (b) $M^2[\pi^{\pm}\psi(2S)]$ at $\sqrt{s}$=4.416 GeV (two entries per event) from BESIII [166]. The points with error bars represent the data; the shaded histogram is from the $\psi(2S)$ mass sidebands, the solid curves are the best fits, and the dashed curves show the shapes of the intermediate states.

As mentioned before, BESIII studied the process $e^+e^- \to \pi^+\pi^-\psi(2S)$ using 5.1 fb^{-1} of data at c.m. energies from 4.0 to 4.6 GeV [166]. Intermediate states are investigated in the data samples that have large integrated luminosity. For data at $\sqrt{s}$ =4.416 GeV, a prominent narrow structure is observed around 4030 MeV in the $M[\pi^{\pm}\psi(2S)]$ spectrum, as shown in Fig. 58 (right). For data at $\sqrt{s}$ =4.358 GeV, there is no obvious structure observed in the $M[\pi^{\pm}\psi(2S)]$ spectrum. For data at $\sqrt{s}$ =4.258 GeV, the possible structures with masses of 3900 and 4030 MeV in the $M[\pi^{\pm}\psi(2S)]$ spectrum have kinematic reflections at each other mass positions. For data at $\sqrt{s}$ =4.226 GeV, no structure is clearly seen, which is very different from the behavior at the nearby energy point of 4.258 GeV. From the above, we see the structures in the $M[\pi^{\pm}\psi(2S)]$ spectrum are correlated with $M(\pi^+\pi^-)$ and $M[\pi^+\pi^-\psi(2S)]$. A dedicated PWA is needed to extract reliable resonance parameters.

To characterize the structure observed in the $M[\pi^{\pm}\psi(2S)]$ spectrum for data at $\sqrt{s}$ = 4.416 GeV, an unbinned maximum-likelihood fit to the Dalitz plot is applied. Assuming an intermediate Z_c state in the $\pi\psi(2S)$ system with spin-parity $J^P = 1^+$, the Dalitz plot is parameterized by the coherent sum of the process $e^+e^- \to \pi Z_c \to \pi^+\pi^-\psi(2S)$ and the direct process $e^+e^- \to \pi^+\pi^-\psi(2S)$. The fit yields a mass of $M = (4032.1 \pm 2.4)$ MeV and a width of $\Gamma = (26.1 \pm 5.3)$ MeV for the intermediate state with a significance of 9.2σ. The fit projection on $M^2[\pi^{\pm}\psi(2S)]$ is shown

in Fig. 58 (right). Since the overall fit curve does not match the peaking structure and the corresponding C.L. of the fit is 8% only, the reported errors are statistical only for the parameters of the Z_c structure.

The authors of Ref. [283] reported their preliminary PWA results on $e^+e^- \to \pi^+\pi^-\psi(2S)$ at the Charm 2018 meeting by using BESIII published results. A similar PWA method used in the analysis of $\Upsilon(5S) \to \pi Z_b \to \pi^+\pi^-\Upsilon(nS)$ ($n = 1,\ 2,\ 3$) [284] is taken to refit $e^+e^- \to \pi^+\pi^-\psi(2S)$ events from BESIII at $\sqrt{s}$ = 4.416 GeV [166]. In the fit, the interference effect between the $\pi^+\pi^-$ amplitude and the Z_c amplitude is taken into account properly. The fit quality is much improved. It is found that the structure can be described well with a charged state with a mass of (4019.0 ± 1.9) MeV and a width of (29 ± 4) MeV, or the $Z_c(4020)$ state observed in $\pi^+\pi^-h_c$ final state [158]. The ratio $\sigma[e^+e^- \to \pi^+ Z_c(4020)^- + c.c. \to \pi^+\pi^-\psi(2S)]/\sigma[e^+e^- \to \pi^+\pi^-\psi(2S)]$ from the fit is $(12.0 \pm 3.7)\%$, corresponding to $\sigma[e^+e^- \to \pi^+ Z_c(4020)^- + c.c. \to \pi^+\pi^-\psi(2S)] = (5.1 \pm 1.6)$ pb. If such PWA results are confirmed in the future, it means a new decay mode of $Z_c(4020) \to \pi\psi(2S)$ is found. Thus, both $\pi^+\pi^-\psi(2S)$ and $\pi^+\pi^-h_c$ final states need to be further investigated to understand the intermediate structures.

• *The $Z_c(4100)$ state*

Motivated by a series of discovered Z_c states, and a prediction from the diquark model [285] of a possible exotic state decaying to the $\pi\eta_c$ system, the LHCb Collaboration recently performed a Dalitz plot analysis of $B^0 \to K^+\pi^-\eta_c$ using data samples of 4.7 fb^{-1} pp collisions at c.m. energies of $\sqrt{s}$ = 7, 8, and 13 TeV [262].

After event selection, there are 2105 ± 75 $B^0 \to K^+\pi^-\eta_c$ signal candidates, and the measured branching fraction $\mathcal{B}(B^0 \to \eta_c K^+\pi^-)$ is $(5.73 \pm 0.24 \pm 0.13 \pm 0.66) \times 10^{-4}$, where the first uncertainty is statistical, the second systematic, and the third is due to the limited knowledge of the external branching fractions. For these selected signal candidates, an isobar model is used to perform the Dalitz plot analysis, where seven components [$K^*(892)^0$, $K^*(1410)^0$, $K_0^*(1430)^0$, $K_2^*(1430)^0$, $K^*(1680)^0$, $K_0^*(1950)^0$, and non-resonant] states are taken to describe the $K^+\pi^-$ system and an additional exotic $Z_c^- \to \eta_c\pi^-$ component is assumed. Satisfactory description of the data is achieved when including a contribution representing an exotic $\pi^-\eta_c$ resonant state with χ^2/ndf = 1.3. The parameters of such a charged charmonium-like resonance are $M_{Z_c^-} = (4096 \pm 20\ ^{+18}_{-22})$ MeV and $\Gamma_{Z_c^-} = (152 \pm 58\ ^{+60}_{-35})$ MeV with a significance of 3.2σ with systematic errors considered. The projections of the data and amplitude fit onto the $\pi^-\eta_c$ system are shown in Fig. 59, where the contributions from each included component are shown. The spin-parity assignments $J^P = 0^+$ and $J^P = 1^-$ are both consistent with the data.
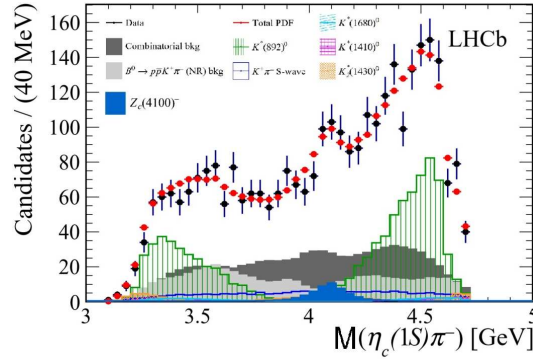
Figure 59: The projections of the data and amplitude fit onto the $\pi^-\eta_c$ system from a Dalitz plot analysis of $B^0 \to K^+\pi^-\eta_c$ performed by the LHCb Collaboration [262], where the contributions from each included component are shown and a charged charmonium-like resonance is needed for a satisfactory description of the data with a significance of 3.2σ with systematic errors considered.

Some phenomenological models have been developed to explain the nature of the charged $Z_c(4100)$, including an effect arising from an S-wave $D^*\bar{D}^*$ rescattering with $I^G J^{PC} = 1^- 0^{++}$, a resonance produced by the P-wave $D^*\bar{D}^*$ interaction of which the neutral partner has exotic quantum numbers $I^G J^{PC} = 1^- 1^{-+}$ [286], a four-quark state of the hadrocharmonium type [287], and a compact tetraquark state [288]. However, by constructing a diquark-antidiquark current in QCD sum rules, the predicted mass in Ref. [289] is (4.24 ± 0.1) GeV, which agrees with the $Y(4230)$ mass and disfavors assigning the $Z_c(4100)$ as a compact tetraquark state. Due to low signal significance of $Z_c(4100)$ in

LHCb data, more data will be required to confirm this state. The $Z_c(4100)^-$ and its neutral partner can be searched for at Belle and Belle II in $B \to K\pi\eta_c$ to conclusively determine the nature of the $Z_c(4100)$ resonance.

• *Search for Z_c pair production*

Considerable efforts in theory have been devoted to interpret the charged charmonium-like states as compact tetraquarks, molecules, or hadrocharmonia [13, 14, 290]. To distinguish among these explanations, more experimental or theoretical input is needed. A new idea in this respect is presented in Refs. [291, 292], where for double $Z_c^\pm$ production in $e^+e^- \to Z_c^+ Z_c^-$ the dependence on s (the e^+e^- c.m. energy squared) of the electromagnetic form factor, $F_{Z_c^+ Z_c^-}$ is claimed to be related to the number of active constituents in the states. However, it remains unclear from which values of s onwards this scaling is applicable.

Belle searched for doubly charged charmonium-like state production with 102 million $\Upsilon(1S)$ events, 158 million $\Upsilon(2S)$ events, 89.5 fb^{-1} data collected at $\sqrt{s}$ = 10.52 GeV, 711.0 fb^{-1} data collected at $\sqrt{s}$ = 10.58 GeV, and 121.4 fb^{-1} data collected at $\sqrt{s}$ = 10.867 GeV. No significant signals are observed in any of the studied modes, and the 90% C.L. upper limits on $\mathcal{B}[\Upsilon(1S, 2S) \to Z_c^+ Z_c^{(\prime)-}]\mathcal{B}(Z_c^+ \to \pi^+ + c\bar{c})$ [$c\bar{c} = J/\psi, \chi_{c1}(1P), \psi(2S)$] and $\sigma[e^+e^- \to Z_c^+ Z_c^{(\prime)-}]\mathcal{B}(Z_c^+ \to \pi^+ + c\bar{c})$ at $\sqrt{s} = 10.52, 10.58$, and 10.867 GeV are in the range of $(1.8 - 45.5) \times 10^{-6}$ and $(1.3 - 143.9)$ fb, respectively. Here, Z_c refers to the $Z_c(3900)$ and $Z_c(4200)$ observed in the $\pi J/\psi$ final state, the $Z_{c1}(4050)$ and $Z_{c2}(4250)$ in the $\pi\chi_{c1}(1P)$ final state, and the $Z_c(4050)$ and $Z_c(4430)$ in the $\pi\psi(2S)$ final state.

3.2.3. Bottomonium-like charged Z_b states

Although the processes $\Upsilon(5S) \to \pi^+\pi^-\Upsilon(nS)$ ($n = 1, 2, 3$) were observed [293] at Belle in 2008 with 21.7 fb^{-1} data collected near the $\Upsilon(5S)$ peak, the Dalitz plots of the processes were only investigated in 2012 together with the processes $\Upsilon(5S) \to \pi^+\pi^- h_b(mP)$ ($m = 1, 2$) with 121.4 fb^{-1} data collected in the vicinity of the $\Upsilon(5S)$ resonance [284]. Amplitude analyses of the three-body $\Upsilon(5S) \to \pi^+\pi^-\Upsilon(nS)$ decays with $\Upsilon(nS) \to \mu^+\mu^-$ are performed by means of unbinned maximum likelihood fits to two-dimensional $M^2[\pi^+\Upsilon(nS)]$ versus $M^2[\pi^-\Upsilon(nS)]$ Dalitz distributions [284]. One-dimensional invariant mass projections for events in the $\Upsilon(nS)$ signal regions are shown in Fig. 60, where two peaks are observed in the $\pi\Upsilon(nS)$ system near 10.61 GeV and 10.65 GeV [named as $Z_b(10610)$ and $Z_b(10650)$]. The combined statistical significance of the two peaks exceeds 10σ for all $\pi^+\pi^-\Upsilon(nS)$ channels. The yields of $\Upsilon(5S) \to \pi^+\pi^- h_b(1P)$ and $\pi^+\pi^- h_b(2P)$ as a function of π missing mass are shown in Fig. 61, where the $Z_b(10610)$ and $Z_b(10650)$ signals are clear although the available phase-space is smaller for $\pi h_b(2P)$. The histograms in Fig. 61 are the fit results with interfering $Z_b(10610)$ and $Z_b(10650)$ signals. Analyses of charged pion angular distributions favor the $J^P = 1^+$ spin-parity assignment for both the $Z_b(10610)$ and $Z_b(10650)$. Their π^0 transition modes were measured to confirm their isospin [294], and the open bottom decay modes were studied to understand the couplings to various final states [295]. Note that their decay modes fix the isospin of the Z_b states to one.
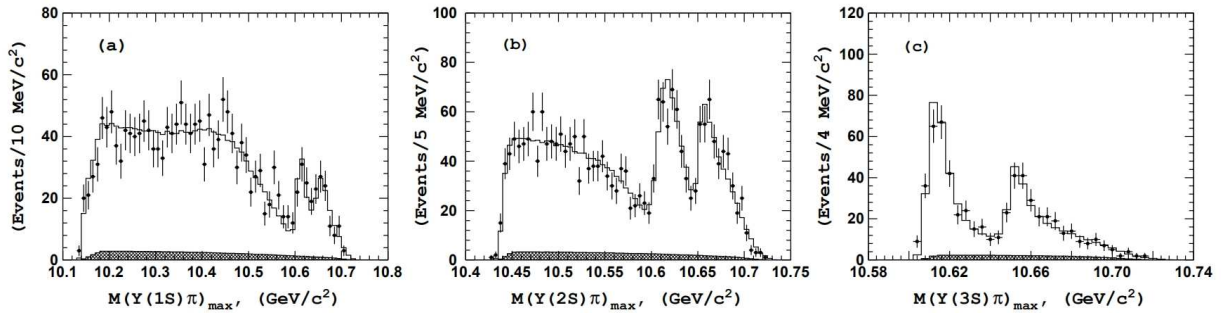
Figure 60: Comparison of fit results (open histogram) with experimental data (points with error bars) for events in the (a) $\Upsilon(1S)$, (b) $\Upsilon(2S)$, and (c) $\Upsilon(3S)$ signal regions [284]. The hatched histogram shows the background component.

The cross sections of $e^+e^- \to \pi^+\pi^-\Upsilon(nS)$ ($n = 1, 2, 3$) at the $\Upsilon(5S)$ peak and 22 energy points between 10.63 and 11.02 GeV with approximately 1 fb^{-1} of the collected luminosity each are measured by Belle [296]. Can-
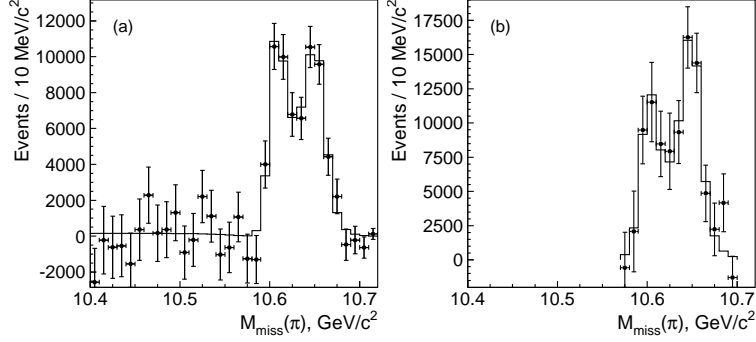
Figure 61: The yields of (a) $\pi^+\pi^- h_b(1P)$ and (b) $\pi^+\pi^- h_b(2P)$ as a function of π missing mass (points with error bars) and results of the fit (histogram).

didate $\pi^+\pi^-\Upsilon(nS)(\to \mu^+\mu^-)$ events are selected for the measurement. Figure 62 shows $R_{\pi^+\pi^-\Upsilon(nS)} \equiv \sigma[e^+e^- \to \pi^+\pi^-\Upsilon(nS)]/\sigma^0(e^+e^- \to \mu^+\mu^-)$. The cross sections are fit for the masses and widths of the $\Upsilon(5S)$ and $\Upsilon(6S)$ resonances. It is found that $e^+e^- \to \pi^+\pi^-\Upsilon(nS)$ is dominated by the two resonances. With $e^+e^- \to \pi^+\pi^-\Upsilon(nS)$, Belle measured $M_{\Upsilon(10860)} = (10891.1 \pm 3.2^{+0.6}_{-1.7})$ MeV and $\Gamma_{\Upsilon(10860)} = (53.7^{+7.1}_{-5.6}{}^{+0.9}_{-5.4})$ MeV, and reported the first measurements $M_{\Upsilon(11020)} = (10987.5^{+6.4}_{-2.5}{}^{+9.0}_{-2.1})$ MeV, $\Gamma_{\Upsilon(11020)} = (61^{+9}_{-19}{}^{+2}_{-20})$ MeV, and the relative phase $\phi_{\Upsilon(11020)} - \phi_{\Upsilon(10860)} = (-1.0 \pm 0.4^{+1.0}_{-0.1})$ rad.
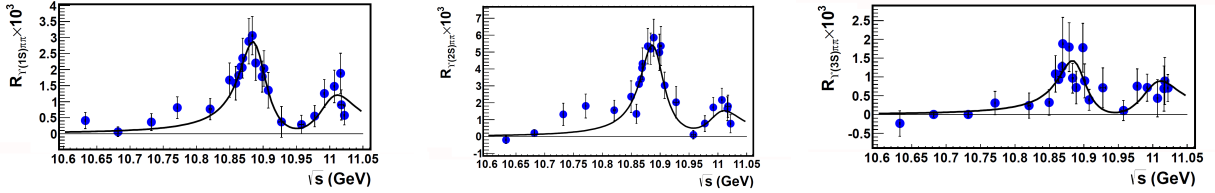
Figure 62: Cross sections of $e^+e^- \to \pi^+\pi^-\Upsilon(1S)$ (left), $\pi^+\pi^-\Upsilon(2S)$ (middle), and $\pi^+\pi^-\Upsilon(3S)$ (right) [296], and the fits with a coherent sum of two BW functions. Error bars are statistical only.

The large statistics at the $\Upsilon(5S)$ peak make a study of the intermediate states of $e^+e^- \to \pi^+\pi^-\Upsilon(nS)$ possible [284]. After event selection, 1905, 2312, and 635 candidate events are left for the $\pi^+\pi^-\Upsilon(1S)$, $\pi^+\pi^-\Upsilon(2S)$, and $\pi^+\pi^-\Upsilon(3S)$ final states, respectively. Belle performed a full amplitude analysis of three-body $e^+e^- \to \pi^+\pi^-\Upsilon(nS)$ transitions and determined the relative fractions of various quasi-two-body components of the three-body amplitudes as well as the spin and parity of the two observed Z_b states. The favored quantum numbers are $J^P = 1^+$ for both $Z_b(10610)$ and $Z_b(10650)$ states, and the alternative $J^P = 1^-$ and $J^P = 2^\pm$ combinations are rejected at confidence levels exceeding six standard deviations. Results of the amplitude analysis are summarized in Table 4, where fractions of individual quasi-two-body modes, masses and widths of the two Z_b states, the relative phase (ϕ_Z) between the two Z_b amplitudes, and fraction $c_{Z_b(10610)}/c_{Z_b(10650)}$ of their amplitudes are given.

The processes $\Upsilon(5S) \to \pi^0\pi^0\Upsilon(nS)$ are observed at Belle with the 121.4 fb^{-1} data sample too [294], and the measured cross sections, $\sigma[e^+e^- \to \pi^0\pi^0\Upsilon(1S)] = (1.16 \pm 0.06 \pm 0.10)$ pb, $\sigma[e^+e^- \to \pi^0\pi^0\Upsilon(2S)] = (1.87 \pm 0.11 \pm 0.23)$ pb, and $\sigma[e^+e^- \to \pi^0\pi^0\Upsilon(3S)] = (0.98 \pm 0.24 \pm 0.19)$ pb, are consistent with the expectations from isospin conservation based on $\sigma[e^+e^- \to \pi^+\pi^-\Upsilon(nS)]$ measured at the same c.m. energy. The Dalitz analyses of the processes $e^+e^- \to \pi^0\pi^0\Upsilon(2S)$ and $\pi^0\pi^0\Upsilon(3S)$ indicate that the neutral partner of the $Z_b(10610)$ is observed in its $\pi^0\Upsilon(2S)$ and $\pi^0\Upsilon(3S)$ decay modes with a significance of 6.5σ including systematic uncertainties [294]. Its measured mass, $(10609 \pm 4 \pm 4)$ MeV, is consistent with the mass of the corresponding charged state, the $Z_b(10610)$. The $Z_b(10650)$ signal is not significant in any of the $\pi^0\pi^0\Upsilon(nS)$ channels with the limited statistics.

Belle measured $e^+e^- \to \pi^+\pi^- h_b(nP)$ ($n =1, 2$) with on-resonance $\Upsilon(5S)$ data of 121.4 fb^{-1}, and energy scan data

Parameter	$\pi^+\pi^-\Upsilon(1S)$	$\pi^+\pi^-\Upsilon(2S)$	$\pi^+\pi^-\Upsilon(3S)$
$f_{Z_b^\mp(10610)\pi^\pm}$, %	$4.8 \pm 1.2^{+1.5}_{-0.3}$	$18.1 \pm 3.1^{+4.2}_{-0.3}$	$30.0 \pm 6.3^{+5.4}_{-7.1}$
$Z_b(10610)$ mass, MeV	$10608.5 \pm 3.4^{+3.7}_{-1.4}$	$10608.1 \pm 1.2^{+1.5}_{-0.2}$	$10607.4 \pm 1.5^{+0.8}_{-0.2}$
$Z_b(10610)$ width, MeV	$18.5 \pm 5.3^{+6.1}_{-2.3}$	$20.8 \pm 2.5^{+0.3}_{-2.1}$	$18.7 \pm 3.4^{+2.5}_{-1.3}$
$f_{Z_b^\mp(10650)\pi^\pm}$, %	$0.87 \pm 0.32^{+0.16}_{-0.12}$	$4.05 \pm 1.2^{+0.95}_{-0.15}$	$13.3 \pm 3.6^{+2.6}_{-1.4}$
$Z_b(10650)$ mass, MeV	$10656.7 \pm 5.0^{+1.1}_{-3.1}$	$10650.7 \pm 1.5^{+0.5}_{-0.2}$	$10651.2 \pm 1.0^{+0.4}_{-0.3}$
$Z_b(10650)$ width, MeV	$12.1^{+11.3+2.7}_{-4.8-0.6}$	$14.2 \pm 3.7^{+0.9}_{-0.4}$	$9.3 \pm 2.2^{+0.3}_{-0.5}$
ϕ_Z, degrees	$67 \pm 36^{+24}_{-52}$	$-10 \pm 13^{+34}_{-12}$	$-5 \pm 22^{+15}_{-33}$
$c_{Z_b(10650)}/c_{Z_b(10610)}$	$0.40 \pm 0.12^{+0.05}_{-0.11}$	$0.53 \pm 0.07^{+0.32}_{-0.11}$	$0.69 \pm 0.09^{+0.18}_{-0.07}$
$f_{\Upsilon(nS)f_2(1270)}$, %	$14.6 \pm 1.5^{+6.3}_{-0.7}$	$4.09 \pm 1.0^{+0.33}_{-1.0}$	–
$f_{\Upsilon(nS)(\pi^+\pi^-)_S}$, %	$86.5 \pm 3.2^{+3.3}_{-4.9}$	$101.0 \pm 4.2^{+6.5}_{-3.5}$	$44.0 \pm 6.2^{+1.8}_{-4.3}$
$f_{\Upsilon(nS)f_0(980)}$, %	$6.9 \pm 1.6^{+0.8}_{-2.8}$	–	–

Table 4: Summary of results of fits to $\Upsilon(5S) \to \pi^+\pi^-\Upsilon(nS)$ events in the signal regions.

in the range from about 10.77 to 11.02 GeV taken at 19 points of about 1 fb^{-1} each [297]. The processes $e^+e^- \to \pi^+\pi^- h_b(np)$ are reconstructed inclusively using the missing mass of $\pi^+\pi^-$ pairs, $M^{\text{miss}}_{\pi^+\pi^-} = \sqrt{(\sqrt{s} - E^*_{\pi^+\pi^-})^2 - p^{*2}_{\pi^+\pi^-}}$, where $E^*_{\pi^+\pi^-}$ and $p^*_{\pi^+\pi^-}$ are the energy and momentum of the $\pi^+\pi^-$ pair measured in the c.m. frame. The resulting cross sections are shown in Fig. 63. Belle performed a simultaneous fit to the energy dependence of the $e^+e^- \to \pi^+\pi^- h_b(nP)$ ($n = 1, 2$) cross sections. The fit function is a coherent sum of two BW amplitudes and (optionally) a constant with an energy continuum contribution:

$$A_n\, f(s) \left| BW(s, M_5, \Gamma_5) + a\, e^{i\phi} BW(s, M_6, \Gamma_6) + b\, e^{i\delta} \right|^2,$$

where $f(s)$ is the phase space function, which is calculated numerically taking into account the measured Z_b line shape, $BW(s, M, \Gamma)$ is a BW amplitude $BW(s, M, \Gamma) = M\Gamma/(s - M^2 + iM\Gamma)$. The parameters A_1, A_2, M_5, Γ_5, M_6, Γ_6, a, ϕ and (optionally) b, δ are floated in the fit. The significance of the non-resonant continuum contribution from the fit is found to be 1.5σ only. Thus the default fit function does not include the continuum contribution. The fit results for the default model are given in Table 5.
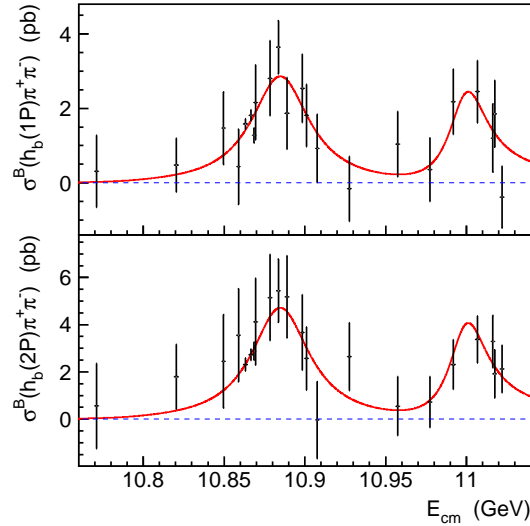
Figure 63: Cross sections for the $e^+e^- \to \pi^+\pi^- h_b(1P)$ (top) and $e^+e^- \to \pi^+\pi^- h_b(2P)$ (bottom) processes as a function of c.m. energy measured by Belle [297]. Points with error bars are the data and red solid curves are the fit results.

Parameter	Results
M_5 (MeV)	$10884.7^{+3.2+8.6}_{-2.9-0.6}$
Γ_5 (MeV)	$44.2^{+11.9+2.2}_{-7.8\ -15.8}$
M_6 (MeV)	$10998.6 \pm 6.1^{+16.1}_{-1.1}$
Γ_6 (MeV)	29^{+20+2}_{-12-7}
$A_1/10^3$	$4.8^{+2.7}_{-0.8}$
$A_2/10^3$	$8.0^{+4.6}_{-1.3}$
a	$0.64^{+0.37+0.13}_{-0.11-0}$
(ϕ/π)	$0.1^{+0.3}_{-0.5}$

Table 5: Fit results to the measured $e^+e^- \to \pi^+\pi^- h_b(nP)$ ($n = 1, 2$) cross sections [297].

The efficiency-corrected $\pi h_b(1P)$ and $\pi h_b(2P)$ invariant mass distributions are shown in Fig. 64 [297]. The data do not follow a phase-space distribution, but populate the mass region of the $Z_b(10610)$ and $Z_b(10650)$ states. Belle found that the transitions are dominated by the intermediate $Z_b(10610)$ and $Z_b(10650)$ states, but the limited statistics do not allow a measurement of the contribution from each mode.
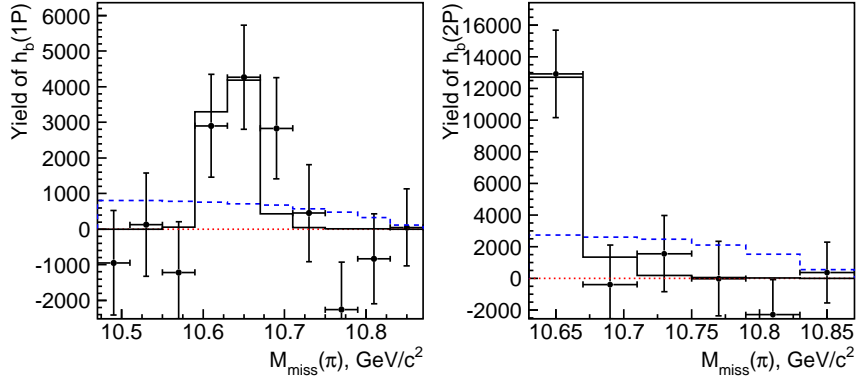
Figure 64: The efficiency-corrected yields of $\pi^+\pi^- h_b(1P)$ (left) and $\pi^+\pi^- h_b(2P)$ (right) as a function of π missing mass [297]. Points represent data, the black solid histogram represents the fit result with the shape fixed from the $\Upsilon(5S)$ analysis, the blue dashed histogram is the result of the fit to the phase-space distribution.

Evidence for the three-body $\Upsilon(5S) \to B\bar{B}^*\pi$ decay has been reported previously by Belle, based on a data sample of 23.6 fb^{-1} [298]. The analysis is updated with a data sample of 121.4 fb^{-1} on the $\Upsilon(5S)$ resonance [295]. For brevity, $B^+\bar{B}^0\pi^-$ and $B^-B^0\pi^+$ final states are referred to as $B\bar{B}\pi$; $B^+\bar{B}^{*0}\pi^-$, $B^-B^{*0}\pi^+$, $B^0B^{*-}\pi^+$, and $\bar{B}^0B^{*+}\pi^-$ final states are referred to as $B\bar{B}^*\pi$; and $B^{*+}\bar{B}^{*0}\pi^-$ and $B^{*-}B^{*0}\pi^+$ final states are denoted as $B^*\bar{B}^*\pi$. The inclusion of the charge-conjugate mode is implied here. The B mesons are reconstructed in 18 decay channels: $B^+ \to J/\psi K^{(*)+}$, $B^+ \to \bar{D}^{(*)0}\pi^+$, $B^0 \to J/\psi K^{(*)0}$, and $B^0 \to D^{(*)-}\pi^+$. The B candidates are identified by their reconstructed invariant mass $M(B)$ as shown in Fig. 65(a). The requirement $P(B) < 1.35$ GeV, where $P(B)$ is the momentum of B candidates in the c.m. frame, is applied to retain B mesons produced in both two-body and multibody processes.

Reconstructed B^+ or $\bar{B}^0$ candidates are combined with π^-'s and the missing mass, $M_{\text{miss}}(B\pi)$, is calculated as $M_{\text{miss}}(B\pi) = \sqrt{(\sqrt{s} - E_{B\pi})^2 - P_{B\pi}^2}$, where $E_{B\pi}$ and $P_{B\pi}$ are the measured energy and momentum of the reconstructed $B\pi$ combination. Signal $e^+e^- \to B\bar{B}^*\pi$ events produce a narrow peak in the $M_{\text{miss}}(B\pi)$ spectrum around the nominal $\bar{B}^*$ mass, while $e^+e^- \to B^*\bar{B}^*\pi$ events produce a peak at $m_{\bar{B}^*} + \Delta m_{B^*}$, where $\Delta m_{B^*} = m_{B^*} - m_B$, due to the missed photon from the $B^* \to \gamma B$ decay. To remove the correlation between $M_{\text{miss}}(B\pi)$ and $M(B)$ and to improve the resolution, $M_{\text{miss}}^* = M_{\text{miss}}(B\pi) + M(B) - m_B$ instead of $M_{\text{miss}}(B\pi)$ is used. The M_{miss}^* distribution is shown in Fig. 65(b), where peaks corresponding to the $B\bar{B}^*\pi$ and $B^*\bar{B}^*\pi$ signals are evident. The fit to the M_{miss}^* distribution yields $N_{B\bar{B}\pi} = 13 \pm 25$, $N_{B\bar{B}^*\pi} = 357 \pm 30$, and $N_{B^*\bar{B}^*\pi} = 161 \pm 21$ signal events. The statistical significances of the observed $B\bar{B}^*\pi$ and $B^*\bar{B}^*\pi$ signals are 9.3σ and 8.1σ, respectively.
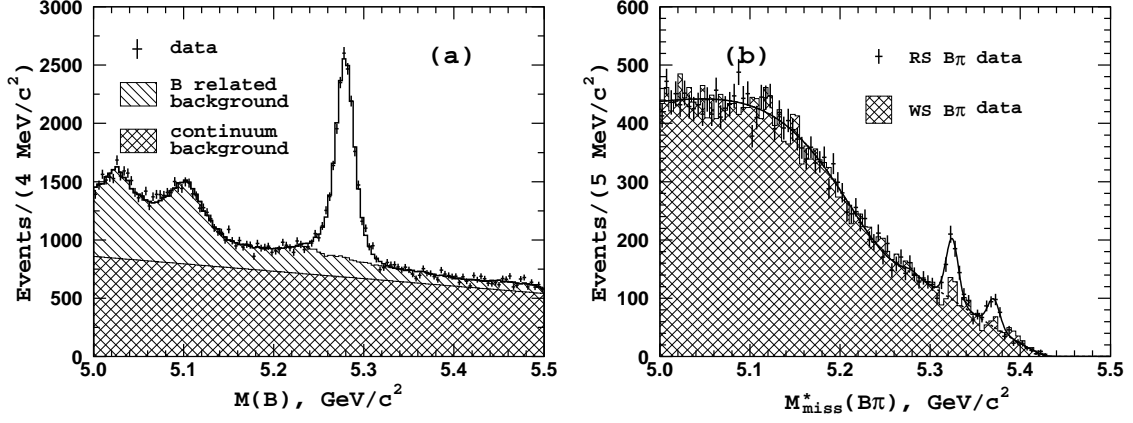
Figure 65: The invariant mass (a) and $M^*_{\text{miss}}(B\pi)$ (b) distributions for B candidates in the B signal region from the analysis of $\Upsilon(5S) \to B^{(*)}\bar{B}^{(*)}\pi$ decay by Belle [295]. Points with error bars are data. The open histogram in (a) is the fit to data. The solid line in (b) is the fit to the $B\pi$ missing mass; the dashed line is the background level.

The π missing mass $M_{\text{miss}}(\pi) = \sqrt{(\sqrt{s} - E_\pi)^2 - P_\pi^2}$ distributions are shown in Fig. 66 for selected $B\bar{B}^*\pi$ ($|M^*_{\text{miss}} - m_{\bar{B}^*}| < 15$ MeV/c^2) and $B^*\bar{B}^*\pi$ candidate events [$|M^*_{\text{miss}} - (m_{\bar{B}^*} + \Delta m_B)| < 12$ MeV/c^2 with $\Delta m_B = m_{B^*} - m_B$]. Here E_π and P_π are the reconstructed energy and momentum, respectively, of the charged pion in the c.m. frame. It is found that $e^+e^- \to B\bar{B}^*\pi$ is dominated by $Z_b(10610)$ and $e^+e^- \to B^*\bar{B}^*\pi$ is dominated by $Z_b(10650)$. The fits to the π missing mass distributions with different models parameterizing the line shapes are also shown in Fig. 66, where Model-0 is the fit with only $Z_b(10610)$ for $B\bar{B}^*\pi$ events and $Z_b(10650)$ for $B^*\bar{B}^*\pi$ events, Model-1 is the fit with an additional non-resonant component for $B\bar{B}^*\pi$ events, Model-2 is the fit with a combination of two Z_b amplitudes for $B\bar{B}^*\pi$ events, and Model-3 is the fit with only a pure non-resonant amplitude for both of $B\bar{B}^*\pi$ and $B^*\bar{B}^*\pi$ events.
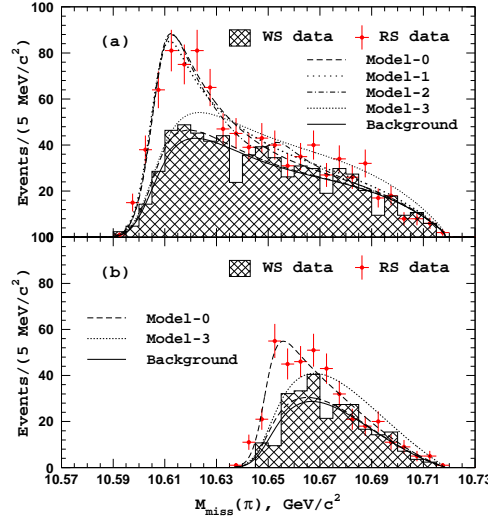
Figure 66: The $M_{\text{miss}}(\pi)$ distributions for the (a) $B\bar{B}^*\pi$ and (b) $B^*\bar{B}^*\pi$ candidate events from the analysis of $\Upsilon(5S) \to B^{(*)}\bar{B}^{(*)}\pi$ decay by Belle [295].

The relative fractions for Z_b decays, assuming that they are saturated by the already observed $\pi\Upsilon(nS)$, $\pi h_b(mP)$, and $B^{(*)}\bar{B}^*$ channels, are listed in Table 6. However, this assumption needs to be further checked. For example, the decay mode of $Z_c(3900) \to \rho\eta_c$ is observed with a similar rate as $Z_c(3900) \to \pi J/\psi$ in the BESIII experiment; hence $Z_b \to \rho\eta_b$, as its counterpart in the bottom sector, is expected to happen with a possible rate of a few percent.

Channel	Fraction, %	
	$Z_b(10610)$	$Z_b(10650)$
$\pi^+\Upsilon(1S)$	$0.54^{+0.16+0.11}_{-0.13-0.08}$	$0.17^{+0.07+0.03}_{-0.06-0.02}$
$\pi^+\Upsilon(2S)$	$3.62^{+0.76+0.79}_{-0.59-0.53}$	$1.39^{+0.48+0.34}_{-0.38-0.23}$
$\pi^+\Upsilon(3S)$	$2.15^{+0.55+0.60}_{-0.42-0.43}$	$1.63^{+0.53+0.39}_{-0.42-0.28}$
$\pi^+ h_b(1P)$	$3.45^{+0.87+0.86}_{-0.71-0.63}$	$8.41^{+2.43+1.49}_{-2.12-1.06}$
$\pi^+ h_b(2P)$	$4.67^{+1.24+1.18}_{-1.00-0.89}$	$14.7^{+3.2+2.8}_{-2.8-2.3}$
$B^+\bar{B}^{*0} + \bar{B}^0 B^{*+}$	$85.6^{+1.5+1.5}_{-2.0-2.1}$	–
$B^{*+}\bar{B}^{*0}$	–	$73.7^{+3.4+2.7}_{-4.4-3.5}$

Table 6: Branching fractions for the $Z_b(10610)$ and $Z_b(10650)$ decays [295]. The first uncertainties are statistical and the second systematic.

While the mass determinations reported above for both the $Z_b(10610)$ and $Z_b(10650)$ are above the nearby open-flavor thresholds, more refined analyses seem to prefer lower masses — typically below the threshold [299]. When, however, the pion dynamics is included fully dynamically like in Ref. [300], this leads to an additional energy dependence that pushes the $Z_b(10650)$ pole a little above the $B^*\bar{B}^*$ threshold. These remarks illustrate that amplitudes consistent with unitarity and analyticity should be used to extract parameters of very near-threshold states reliably (see discussion in Sec. 4.2).

3.3. Isospin-half states

3.3.1. Searches for multi-quark states with strangeness

After the discovery of the Z_c states, it is natural to search also for their possible strange partners, Z_{cs}, by looking at $K^\pm$ associated with a charmonium state. The lowest $J^P = 1^+$ Z_{cs} state has been predicted to have a mass of (3.97 ± 0.08) GeV [301] and its decay widths to $K^+ J/\psi$, $K^{*+}\eta_c$, $D_s^+\bar{D}^{*0}$, and $\bar{D}^0 D_s^{*+}$ have been calculated using QCD sum rules [302]. The Z_{cs} has also been predicted in the single-kaon emission model [303, 304].

Similar to the process $e^+e^- \rightarrow Y(4230) \rightarrow \pi^+\pi^- J/\psi$ in which the $Z_c(3900)$ is observed [22, 68], the $e^+e^- \rightarrow K^+K^- J/\psi$ process is a suitable process to search for the Z_{cs}. Belle has updated the cross sections of $e^+e^- \rightarrow K^+K^- J/\psi$ via ISR at c.m. energies between the threshold and 6.0 GeV using a data sample of 980 fb^{-1} [215]. Possible intermediate states for the selected $e^+e^- \rightarrow K^+K^- J/\psi$ events have been investigated by examining the Dalitz plot, but no clear structure has been observed in the $K^\pm J/\psi$ system. A larger data sample seems therefore necessary to obtain more information about possible structures in the $K^+K^- J/\psi$ and $K^\pm J/\psi$ systems.

3.3.2. Pentaquark states

In 2015, LHCb reported the observation of two exotic structures, named as $P_c(4380)^+$ (9σ significance) and $P_c(4450)^+$ (12σ significance), in the $J/\psi p$ system in $\Lambda_b^0 \rightarrow J/\psi K^- p$ [36]. The $P_c(4380)^+$ has a mass of $(4380 \pm 8 \pm 29)$ MeV and a width of $(205 \pm 18 \pm 86)$ MeV, while the $P_c(4450)^+$ is much narrower with a mass of $(4449.8 \pm 1.7 \pm 2.5)$ MeV and a width of $(39 \pm 5 \pm 19)$ MeV. The results of the fit to the $J/\psi p$ invariant mass distribution are shown in Fig. 67, where the purple hatched and blue hatched histograms, labeled as "1" and "2", are from the $P_c(4380)^+$ and $P_c(4450)^+$ contributions, respectively. Since the valence structure of $J/\psi p$ is $c\bar{c}uud$, the newly discovered particles consist of at least five quarks.

Considering the complicated Λ^* spectroscopy in the amplitude analysis of $\Lambda_b^0 \rightarrow J/\psi K^- p$, LHCb checked the level of consistency of the data with minimal assumptions about the spin and lineshape of possible Λ^* contributions. It is demonstrated that at more than 9 standard deviations $\Lambda_b^0 \rightarrow J/\psi K^- p$ decays cannot be described with $K^- p$ contributions alone, and that $J/\psi p$ contributions play a dominant role. These model-independent results support the existence of the $P_c(4380)^+$ and $P_c(4450)^+$ [305]. Based on the measured fractions of the $P_c(4380)^+$ and $P_c(4450)^+$ [36] and the measured $\mathcal{B}(\Lambda_b^0 \rightarrow J/\psi K^- p)$ [306], the branching fractions $\mathcal{B}(\Lambda_b^0 \rightarrow P_c^+ K^-)\mathcal{B}(P_c^+ \rightarrow J/\psi p)$ are determined to be $(2.66 \pm 0.22 \pm 1.33^{+0.48}_{-0.38}) \times 10^{-5}$ for $P_c(4380)^+$ and $(1.30 \pm 0.16 \pm 0.35^{+0.23}_{-0.18}) \times 10^{-5}$ for $P_c(4450)^+$ [306], respectively, where the first uncertainty is statistical, the second is systematic, and the third is due to the systematic uncertainty on $\mathcal{B}(\Lambda_b^0 \rightarrow J/\psi K^- p)$.
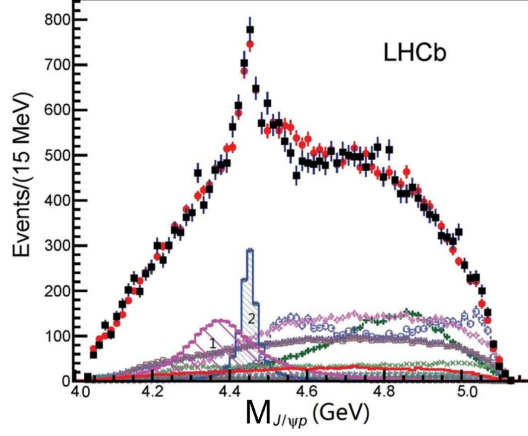
Figure 67: Distribution of the $J/\psi p$ invariant mass and the fit with two P_c^+ states [36]. The purple hatched histogram is the $P_c(4380)^+$ and the blue hatched histogram is the $P_c(4450)^+$ signal.

Many theoretical interpretations of these two P_c states have been developed, including a pentaquark doublet, hadronic molecules composed of an anticharm meson and a charm baryon, a $\chi_{c1}p$ resonance and so on. The structure of these two states is still an open question, and none of the explanations in the literature have been accepted unanimously [84].

Very recently, the LHCb Collaboration updated the same analysis with more data [307] and discovered a new state $P_c(4312)^+$ in the $J/\psi p$ invariant mass spectrum. At the same time they found that the $P_c(4450)^+$ is composed of two narrow overlapping structures, $P_c(4440)^+$ and $P_c(4457)^+$, with the following resonant parameters:

$$P_c(4312)^+ : \quad M = (4311.9 \pm 0.7^{+6.8}_{-0.6})\,\text{MeV}\,, \ \Gamma = (9.8 \pm 2.7^{+3.7}_{-4.5})\,\text{MeV}\,,$$
$$P_c(4440)^+ : \quad M = (4440.3 \pm 1.3^{+4.1}_{-4.7})\,\text{MeV}\,, \ \Gamma = (20.6 \pm 4.9^{+8.7}_{-10.1})\,\text{MeV}\,,$$
$$P_c(4457)^+ : \quad M = (4457.3 \pm 0.6^{+4.1}_{-1.7})\,\text{MeV}\,, \ \Gamma = (6.4 \pm 2.0^{+5.7}_{-1.9})\,\text{MeV}\,.$$

All these values are obtained by fitting the $J/\psi p$ invariant mass spectrum directly without doing PWA, so the numbers are subject to change in a more sophisticated analysis and the spin-parities are not determined. It should be noticed that the $P_c(4312)$, $P_c(4440)$, and $P_c(4457)$ are just below the $\Sigma_c^+ \bar{D}^0$ and $\Sigma_c^+ \bar{D}^{*0}$ thresholds of 4318 and 4460 MeV, respectively, so that it is natural to interpret them as bound states composed of charmed baryons and anticharmed mesons. On the other hand, the two-peak structure of the $P_c(4450)$ was predicted in Ref. [308] after LHCb reported the discovery of the two first pentaquarks. In the interpretation of Ref. [308], however, the $P_c(4450)$ is a bound state of a charmonium $\psi(2S)$ and a nucleon consisting of two almost degenerate pentaquark states with $J^P = (1/2)^-$ and $J^P = (3/2)^-$.

There should exist other processes leading to the production of pentaquark states that can be accessed by experiments. Moreover, if pentaquark states exist, we should be able to observe more than just a few of them. One would expect more states with either different spin-parity, or different flavor content. To confirm the existence of the found pentaquark states and search for new ones, LHCb did the following analyses: (1) A full amplitude analysis of $\Lambda_b^0 \to J/\psi p\pi^-$ was performed using an integrated luminosity of 3 fb^{-1} [309]. Besides the nucleon excitations, the $P_c(4380)^+ \to J/\psi p$, $P_c(4450)^+ \to J/\psi p$, and $Z_c(4200)^- \to J/\psi \pi^-$ states are also needed for a better description of the data with a significance of more than 3σ. (2) The pentaquark states containing a single b (anti)quark decaying weakly into four specific final states $J/\psi K^+ \pi^- p$, $J/\psi K^- \pi^- p$, $J/\psi K^- \pi^+ p$, and $J/\psi \phi p$ were searched for, using an integrated luminosity of 3 fb^{-1} [310]. No evidence for these decays was found. Upper limits at 90% C.L. on the ratios of the production cross sections of these states times the branching fractions into the searched modes, with respect to the production and decay of the Λ_b^0 baryon in the mode $J/\psi K^- p$, were set at the 10^{-3} level. (3) The Cabibbo-suppressed decay $\Lambda_b^0 \to \psi(2S)p\pi^-$ was observed for the first time and the $\psi(2S)p$ and $\psi(2S)\pi^-$ mass spectra were investigated, but no evidence for contributions from exotic states was found [311]. With a larger data sample, a detailed amplitude

analysis of this decay could be performed to search for possible exotic states. (4) Clear signals of $\Lambda_b^0 \to \psi(2S)pK^-$, $J/\psi\pi^+\pi^- pK^-$ [312], $\chi_{c1}pK^-$, and $\chi_{c2}pK^-$ [313] were observed, but no intermediate states were investigated. For these processes, LHCb may be conducting further analyses of intermediate states.

One of the most promising ways to independently confirm the pentaquarks is the J/ψ photoproduction off a nucleon using the $\gamma p \to J/\psi p$ reaction, as suggested in Ref. [314]. Similar ideas were also presented in Refs. [315–321]. J/ψ photoproduction can benefit from the experimental fact that the pentaquark states are coupled to $J/\psi p$. Note that S-channel pentaquark productions via high energy photon-nucleon scattering can be understood in the framework of the vector meson dominance model for photon-J/ψ coupling. The strong production and decay of the pentaquarks can be connected to their couplings to $J/\psi p$.

If a pentaquark state P_c does exist, the P_c production would manifest itself as a peak in the cross sections of $\gamma p \to J/\psi p$ [$\sigma(E_\gamma)$]. Figure 68 (left) shows the expected line shapes and cross sections of pentaquark states with different assumptions for the J^P values, $\mathcal{B}(P_c \to J/\psi p)$, and width from the Joint Physics Analysis Center (JPAC) predictions [319]. Recently the cross sections of $\gamma p \to J/\psi p$ were measured by GlueX at $8.2 < E_\gamma < 11.8$ GeV using about 25% of the total data accumulated by the GlueX experiment from 2016 to date, where clear J/ψ signals are observed [322]. The measured total cross section in bins of beam energy is shown in Fig. 68 (right), and compared to the earlier measurements at Cornell [323] and SLAC [324]. The measured cross sections do not favor either pure two- or three-hard-gluon exchange predicted by the Brodsky et $al.$ model [325], and a combination of the two processes is required to fit the data adequately as shown in Fig. 68 (right) assuming no interference between the two contributions. The total cross section calculations of Kharzeev et $al.$ [326] multiplied by a factor 2.3 agree well with the measurements implying large gluonic contribution to the nuclear mass and are shown in Fig. 68 (right). The $P_c(4312)^+$, $P_c(4440)^+$, and $P_c(4457)^+$ states are expected to appear as structures at $E_\gamma = 9.44$, 10.04, and 10.12 GeV in the cross-section results shown in Fig. 68 (right). Thus, no evidence for the P_c state can be seen. The expected $P_c(4440)^+$ contribution from the JPAC model-predicted yield with assumption of $\mathcal{B}(P_c(4440)^+ \to J/\psi p) = 1.6\%$ is also shown in Fig. 68 (right). GlueX is planning to analyze the full data sample including data taken in 2018, therefore a higher sensitivity is expected in the near future.
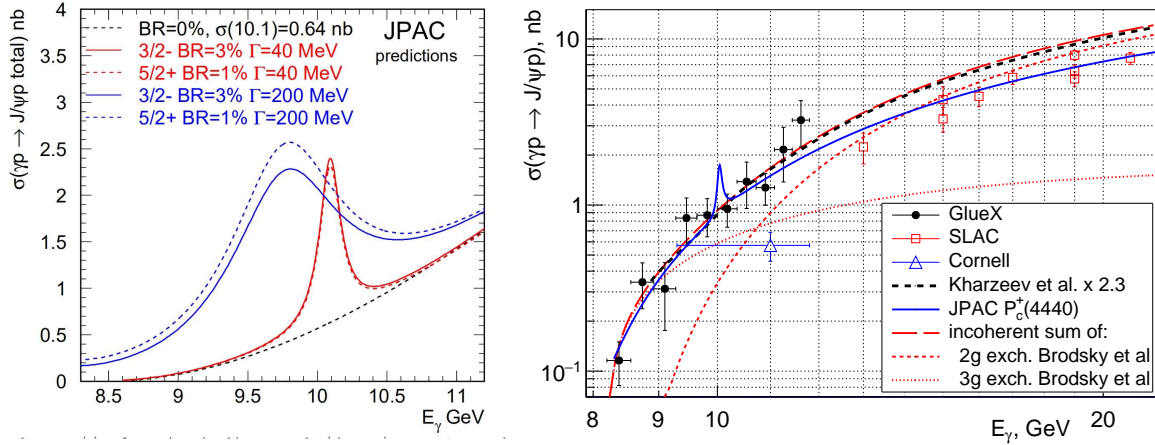
Figure 68: The theoretical predictions on the cross sections of $\gamma p \to P_c \to J/\psi p$ with different assumptions of J^P values, $\mathcal{B}(P_c \to J/\psi p)$, and width for P_c states [319] (left plot), and the measured cross sections of $\gamma p \to J/\psi p$ by GlueX [322] together with the comparison to the Cornell [323] and SLAC [324] data, the theoretical predictions [325, 326], and the JPAC model [319] corresponding to $\mathcal{B}(P_c(4440)^+ \to J/\psi p) = 1.6\%$ for the $J^P = 3/2^-$ case as discussed in the text.

Many theoretical models precisely predicted the masses and decay widths of the multiquark states, but the internal structure of these states is still uncertain. The magnetic moments of a particle are fundamental parameters, which are directly related to the charge and current distributions in the hadrons and these parameters are directly connected to the spatial distributions of quarks and gluons inside the hadrons. Therefore, the magnetic moments provide copious information on the underlying quark structure and can be used to distinguish the preferred configuration from various

theoretical models and deepen our understanding of the underlying dynamics. However, works on the magnetic moments of the exotic particles *XYZ* are rare. Recently, under the assumption of $Z_c(3900)$ being a compact tetraquark state, the magnetic moment of the $Z_c(3900)$ (μ_Z) was calculated to be $|\mu_Z| = (0.35^{+0.24}_{-0.19}) \mu_N$ or $(0.47^{+0.27}_{-0.22}) \mu_N$ based on different sets of input parameters with the QCD sum rules [327], and $|\mu_Z| = (0.67 \pm 0.32) \mu_N$ with the light-cone QCD sum rules [328], where μ_N is the nucleon magneton. Also in Refs. [329, 330] the electromagnetic multipole moments of pentaquarks were calculated exploiting the flavor structure or with the light-cone QCD sum rule mentioned above, respectively, by assuming, e.g., a diquark-diquark-antiquark and $\bar{D}^* \Sigma_c$ molecular structure with different quantum numbers $J^P = \frac{3}{2}^-$. The obtained values of the electromagnetic multipole moments under the two different assumptions show large differences from each other. The magnetic moments of the $Z_c(3900)$ and $P_c(4380)^+$ can be measured in future experiments, for example the electromagnetic multipole moments of $P_c(4380)^+$ can be extracted through the process $\gamma^{(*)} p \rightarrow P_c(4380)^+ \rightarrow P_c(4380)^+ \gamma \rightarrow J/\psi\, p\, \gamma$ in the GlueX experiment. Measurements and comparisons with predictions may provide valuable knowledge on the internal structure of these multiquark states.

To understand the pentaquark states better, further experimental research should be pursued with the currently available and the forthcoming experimental data. There have been many suggestions on the discovery channels for these and other exotic pentaquarks, such as (1) in *B* decays: $B^0 \rightarrow p\bar{p}K^0$, $\bar{B}^0 \rightarrow D^0 p\bar{p}$; (2) in baryon decays: $\Lambda_c^+ \rightarrow pK^0\bar{K}^0$, $\Lambda_b^0 \rightarrow K^- \chi_{c1} p$; (3) in quarkonium decays: $\Upsilon(nS) \rightarrow J/\psi\, p + X, \chi_{cJ} p + X$, and $D^{(*)-} p + X$ ($n = 1, 2, 3$); (4) in e^+e^- continuum processes: $e^+e^- \rightarrow J/\psi\, p + X, \chi_{cJ} p + X, D^{(*)-} p + X$, and $D^{(*)} \Lambda + X$. It is clear that a systematic search for baryon-meson resonances should be pursued in various processes, where the baryon could be $p, \Lambda, \Sigma, \Xi, \Omega, \Sigma_c, ...$, and the meson $\pi, \eta, \omega, \phi, K, D, J/\psi, \chi_{cJ}, ...$.

4. Theoretical foundations

Quantum Chromodynamics is the sector of the Standard Model that describes the strong interaction. It depends on only one coupling, α_s. Once renormalized, the coupling becomes small at high energies — a phenomenon known as asymptotic freedom [2, 3]. Asymptotic freedom allows weak-coupling perturbative calculations of high-energy processes in terms of quarks and gluons, the fundamental degrees of freedom of QCD. Equivalently, instead of α_s, one may use the intrinsic energy scale, Λ_{QCD}. The precise value of Λ_{QCD} depends on the adopted renormalization scheme: in the $\overline{\mathrm{MS}}$ scheme with three flavors, $\Lambda_{\overline{\mathrm{MS}}} = (332 \pm 17)$ MeV [6].

At low energies, i.e., at energies of the order of Λ_{QCD} or smaller, the coupling becomes large and weak-coupling perturbative calculations are no longer an available tool for computing observables. Also, the right low-energy degrees of freedom of the strong interaction are hadrons rather than quarks and gluons, as the former are detected in the experiments and not the latter. This phenomenon goes under the name of color confinement, because hadrons are color singlets, while quarks and gluons transform as triplet and octet representations, respectively, under the color SU(3) group underlying QCD. QCD is the only sector of the Standard Model that exhibits a strongly-coupled low-energy regime.

Since non relativistic bound states are characterized by a momentum transfer and a binding energy that is much smaller than the mass, even the study of hadrons made of heavy quarks requires at some point the use of methods for QCD at low energies. Because low-energy QCD cannot be addressed with weak-coupling perturbation theory, alternative approaches have been developed. Most of the approaches can be grouped in the following categories: phenomenological approaches, which will be discussed in Sec. 4.3, effective field theories, which will be presented in Sec. 4.4, and lattice QCD numerical computations, whose main results will be listed in Sec. 4.5. A full description of each of these approaches would deserve a review by itself and would go far beyond the scope of the present one. Hence we will present them with a focus mostly on their applications to the *XYZ* states.

The connection of phenomenological approaches to QCD is at most plausible, but they provide a framework for the classification of the states, offer some valuable physics insights for observables where more rigorous alternatives are not available and have the potential to pave the way towards more systematic approaches. Sum rules supply rigorous results, but are limited in their applications, accuracy and also in the insights they offer into the physical problem. A detailed discussion of such phenomenological approaches lies beyond the scope of the present paper, especially given that there exist recent reviews dedicated to all of them — in each subsection devoted to a particular approach we provide the corresponding reference together with a brief introduction to the subject. On the contrary, in this review we put most emphasis on the discussion of effective field theories and lattice QCD, which are rigorous
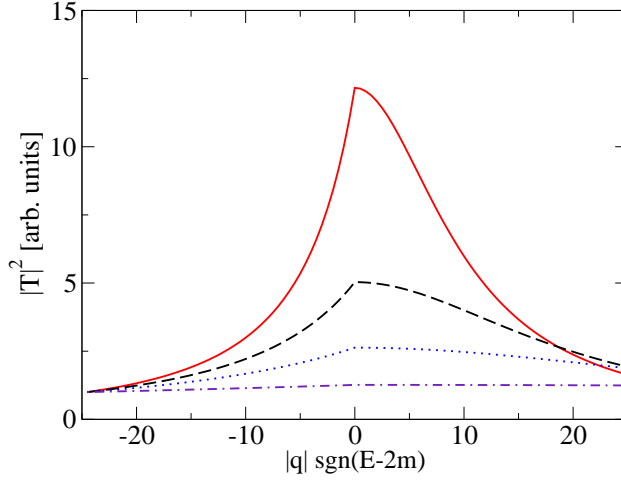
Figure 69: Threshold structure of the T-matrix of Eq. (1) as a function of the scattering length a. Shown is the absolute square of the amplitude for $a = 20$ fm (red solid), 10 fm (black dashed), 5 fm (blue dotted), and 1 fm (magenta dot-dashed). Note that in the sign convention employed here positive scattering lengths refer to virtual states.

and systematic approaches. Their common feature is that the calculations have a sound connection to QCD and can be improved systematically. Of the highest relevance for the subject of this report are heavy quark effective theory — see Sec. 4.4.1 — and potential non-relativistic QCD — see Secs. 4.4.3 and 4.4.4 — both operating fundamentally at the quark-gluon level, and chiral perturbation theory and its non-perturbative version — see Sec. 4.4.5 — operating at the hadron level.

4.1. Threshold effects without new states

Before examining the different approaches in detail, it is necessary, however, to comment on alternative explanations for the structures found in the various data sets, namely those that try to describe them without nearby poles and accordingly without any states. In these explanations the structures are usually generated by the branch points that emerge whenever the energy crosses a threshold related to a new channel. As will be shown below those are of particular importance for thresholds of two (near-)stable particles in a relative S-wave, for then they can induce pronounced non-analyticities of the production amplitudes. Clearly this kind of explanation is quite appealing, since not only does it provide a reason why many of the additional structures are located right at the thresholds, but also, if confirmed, would remove many states from the particle listings. There are also attempts to explain some structures as interference phenomena. Both concepts will now be examined critically.

We begin with the former. It should be stressed that whenever the total energy (or a subsystem energy) or, more appropriately for relativistic systems, the Mandelstam variable s crosses an N-particle threshold, the corresponding scattering amplitude develops a branch point in the energy plane. The corresponding phase space scales as $(s - M_{\text{thr.}}^2)^{(3N-5)/2}$, where the threshold mass is denoted by $M_{\text{thr.}} = \sum_{i=1}^{N} m_i$ with m_i for the mass of particle i. The "-5" term comes from the four-dimensional delta function present in the expression for the phase space acknowledging that energy integration counts as two powers of the momentum. As a consequence of unitarity the phase space not only enters the expressions for cross sections but also scales the imaginary parts of the corresponding loop diagrams and in this way enters the amplitudes. This allows for a pronounced non-analyticity at threshold, driven by a diverging, discontinuous derivative, of the amplitude only for $N = 2$. Accordingly we will now focus on two-body reactions. We may write the partial-wave-projected elastic $2 \to 2$ T-matrix generically for small momenta as

$$T(s) \propto \frac{q^{2L} F^2(s)}{1/a - iq^{(2L+1)} F^2(s) + O(q^4)} \, , \tag{1}$$

where q is the particle momentum in the rest frame of the system — e.g., for $m_1 = m_2 = m$ we may write $q = \sqrt{s/4 - m^2 + i\epsilon}$. Here the term $+i\epsilon$ ensures that the square root is chosen positive for real valued $s > 4m^2$, which

refers to the physical sheet. Accordingly one may move to the unphysical sheet by choosing the $-i\epsilon$-prescription, or, equivalently, the negative square root. In Eq. (1) L denotes the angular momentum of the particle pair and a is the scattering length. With the sign convention employed in Eq. (1), positive and negative values of a lead to poles on the unphysical and the physical sheet, respectively. The former are called virtual states, the latter bound states. To allow for resonances one would need to add an effective range term, $+1/2\, rq^2$, to the denominator, however, this is not necessary for the kind of reasoning we are after here [4]. As done in many analyses, in addition, a form factor, denoted here as $F(s)$ with $F(0) = 1$, is introduced for convenience. It mimics the internal structure of interacting particles and becomes operative as soon as the momentum transferred is large enough ($q \gtrsim \Lambda$ with a suitable Λ depending on the particular system at hand) to resolve the latter. From Eq. (1) one reads off immediately that the mentioned pronounced structure emerging from a discontinuity in the first derivative of the scattering amplitude — called a cusp — appears only for $L = 0$. A cusp is always present when a threshold related to a pair of stable particles in a relative S-wave opens, however, one also sees that its significance depends very sensitively on the value of the scattering length a. In this discussion let us focus on positive values of a since bound states leave a clear imprint in observables and are connected to physical states beyond any doubt. The dependence of the cusp on the value of a is shown in Fig. 69 where, for the illustration purpose, we employ

$$F(s) = \exp(-q^4/\Lambda^4)\,, \tag{2}$$

with $\Lambda = 0.33$ GeV. The result is given for $a = 20, 10, 5$, and 1 fm, respectively. One can clearly see that a pronounced structure appears only for the two larger values while, for example, for $a = 1$ fm the amplitude shows only a very small kink that cannot generate any structure in data. Neglecting the effect of $F(s)$, the value of a can be translated directly into the location of the corresponding pole below the threshold on the second sheet: One finds $E = -E_v = -1/(2\mu a^2)$. Using $2\mu = M_D = 1865$ MeV for illustration, one finds $E_v \approx 0.05, 0.2, 1$, and 20 MeV for $a = 20, 10, 5$, and 1 fm, respectively. Thus, the presence of a pole on the unphysical sheet very close to the threshold is necessary to have a pronounced cusp effect. Since a pole is to be identified with a state, a pronounced cusp in the data is also a signature of a near-threshold state.

In view of the reasoning of the previous paragraph the claim of Refs. [303, 332–338] that various near-threshold states are simply cusp effects without any nearby pole does not look justified. However, in all these works production reactions were studied with final states different from those which generate the cusps [for example, the $Z_c(3900)$ is claimed to be a $D\bar{D}^*$ cusp, but studied only in the $\pi J/\psi$ final state in Ref. [338]] — thus in this case the transition to the final state is independent of the interaction in the nearby channel. It was first pointed out in Ref. [339] that the observable most sensitive to the pole structure of the S-matrix is the final state that matches the nearby threshold. This transition (up to possible contributions from left-hand cuts) is proportional to the T-matrix in that channel. As argued above, however, a pronounced cusp in the T-matrix occurs only if there is a nearby pole. Based on this, the authors of Ref. [339] argue that at least $Z_c(3900)$, $Z_c(4020)$, $Z_b(10610)$, $Z_b(10650)$, and $\chi_{c1}(3872)$ aka $X(3872)$ should exist as states since they are all connected to signals in the nearby channels.[5] The statements of Ref. [339] were criticised in Ref. [340]. However, in the latter work, the signal in the nearby channel is not generated by the cusp itself, but by the vertex form factor, while the structures in the other channels are still assumed to be driven by the cusp. Moreover, if this explanation were correct it would imply that there should be an enhancement at every threshold, since the vertex factors should be universal.

In some cases there should be a triangle mechanism at work that can in principle mimic a resonance structure (for a recent discussion of the issue see, for example, Refs. [341, 342]). However, it is shown in Refs. [341, 343] for the case of the $Z_c(3900)$ that the triangle singularity alone cannot accommodate the data available at various energies.

Another proposal for the origin of the XYZ structures without nearby poles is that they emerge as interference effects of various nearby quarkonia. For example, in Ref. [203] it is argued that an interference of the quark states $\psi(4160)$ and $\psi(4415)$ together with a non-resonant background and only one additional resonance located at 4220 MeV can explain all available data for $e^+e^- \to \pi^+\pi^- J/\psi$, $\pi^+\pi^- h_c$, and $\pi^+ D^0 D^{*-}$. It is even shown that already without this additional resonance a reasonable fit to the data can be achieved. However, this description comes at

---

[4]For a detailed discussion of the connection of effective range parameters and pole locations we refer to Ref. [331].

[5] The logic of the presentation of Ref. [339] is somewhat different: It is shown there that, as soon as one fits the data in the nearby channel with a one-loop diagram, the size of the interaction in that channel calls for a resummation, which then necessarily generates a pole.

the price that the coupling of the photon to the $\pi\pi J/\psi$ channel is smaller than that to the $\pi\pi h_c$ channel although the latter is, contrary to the former, forbidden by spin symmetry. Moreover, in all channels studied a fine tuning of the non–resonant terms vs. the resonant contributions is necessary in order to diminish the appearance of structures near the resonance positions. In this sense the results of Ref. [203] appear not to be a very natural explanation. In Ref. [344] the Belle and BaBar data for $e^+e^- \to \pi^+\pi^- J/\psi$ in the mass range from 3.8 to 4.7 GeV are also explained as an interference of charmonium states with some very broad structure. However, the resulting line shape appears to be inconsistent with the new high-accuracy data by BESIII (see Fig. 22). Moreover, it is unclear how the $\pi\pi h_c$ final state can be understood within this picture.

From here on we will assume that at least most of the structures established in the last fifteen years correspond, indeed, to states. We will, therefore, discuss the theoretical implications of their existence in some depth.

4.2. The quark model

The quark model lies at the basis of the foundation of QCD. It allows one to identify hadrons as compound objects consisting of quarks and antiquarks and provides a framework to describe their dynamics inside hadrons employing the rich and well-developed apparatus of quantum mechanics. In particular, this framework is given by potential models that capture different aspects of this dynamics. Nowadays, the quark model has been replaced in many aspects by more rigorous treatments following directly from QCD. These are effective field theories of QCD, which we will discuss in Sec. 4.4, and lattice QCD, which we will present in Sec. 4.5. Nevertheless, the quark model is still essential for *(i)* classifying hadrons and *(ii)* describing some features of near- and above-open-flavor-threshold states, where more rigorous alternatives are missing. An important disclaimer is in order here. The presentation of the material in this subsection pretends neither to be chronological nor comprehensive. An interested reader is advised to check dedicated review papers on the quark model which are supposed to meet these criteria, for example the review [345]. On the contrary, as it has just been stated, in this review, the quark model is only used for classification purposes as well as a benchmark for the properties of hadrons containing heavy quarks, especially those regarded as candidates to exotic states. For this reason, the presentation of the basic features of the quark model contained in this subsection is rather schematic. When its predictions are exemplified, versions of the model which appear to be most recent, rather well-developed, and provide a unified description for both charmonium and bottomonium spectrum are preferred among many others. As such representative examples we choose (i) a relativistic potential model augmented with a heavy-light meson pair creation mechanism [346, 347] and (ii) a relativistic quasipotential model of Refs. [48, 348–350]. Obviously, for charmonium and especially for bottomonium systems, relativistic effects are supposed to provide only little corrections, so using the relativistic form of the dynamics may be justified by a closer connection with the light-quark sector where the same models may provide a reasonable description of the properties of hadrons.

• *Potential models and classification*

The classification of mesons in terms of bound states of a constituent (or valence) quark and antiquark, follows the same patterns as for atoms. Baryons are understood as bound states of three quarks. In this review, following the commonly accepted wisdom, we identify as exotic those hadrons which do not fit into the quark model classification of mesons and baryons. Such exotic hadrons either involve valence gluons (these are glueballs, which are bound states made of gluons only, or hybrids, which are bound states of quarks and gluons) or are made from more than three valence quarks (these are multiquark states). Nevertheless, exotic hadrons can also have the quantum numbers of ordinary hadrons and can, therefore, mix with the latter.

The quark model describes the interaction of the constituent quarks in terms of potentials which are usually phenomenologically motivated, but may also be inferred from lattice QCD computations. This description works fairly well even for light quarks (with the exception of the would-be Goldstone bosons of the chiral symmetry breaking, *in primis* the pions), but it is only for heavy quarks that potential models can be justified from first principles. We will show this rigorously in Sec. 4.4.3. The physical reason is however clear: the interaction between constituents may be described by a potential, i.e., an instantaneous interaction, only if the typical time scale is much larger than the average distance between the constituents. This happens if the typical energy of the constituents is much smaller than their relative momentum, i.e., if the quarks move non relativistically. For the latter to be true their masses should be much larger than any other scale in the system, in particular, Λ_{QCD}, that qualifies the quarks as heavy. The heavy quark masses, m_h, being much larger than any other scale justifies organizing the potential as an expansion in $1/m_h$.

In this section, we will restrict our discussion of the quark model only to quark–antiquark mesons (or quarkonia). Then a typical potential-model Hamiltonian for a quark–antiquark system has the form

$$H_0 = T + V, \tag{3}$$

where T is the kinetic energy of the constituents, and V is the potential. For heavy quarks the kinetic energy can be non relativistically expanded but it is sometimes treated exactly, see, for instance, Ref. [47]. The potential is usually also expanded in powers of $1/m_h$. If relativistic corrections are also treated exactly in V one speaks of a relativistic quark model, examples of which will be discussed later in this section. In general, potential quark models reduce the study of quark bound states to a quantum mechanical problem with the entire QCD dynamics encoded in the potential.
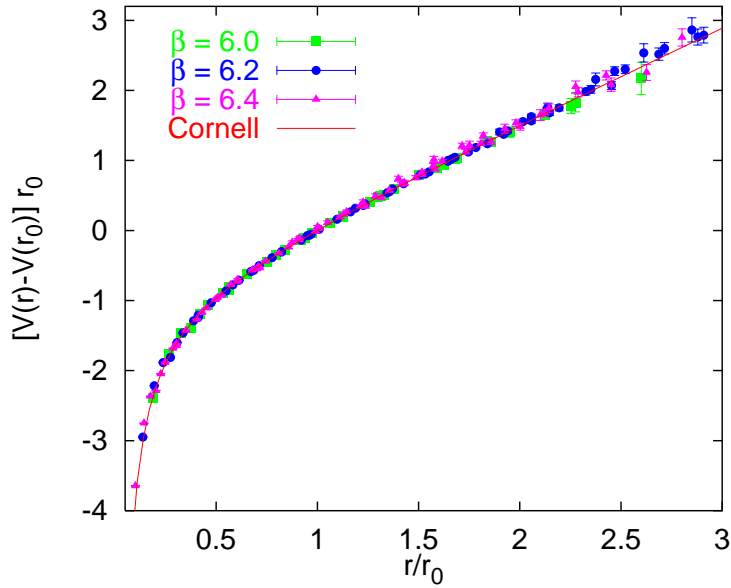
Figure 70: The static quark-antiquark energy from quenched lattice QCD for different couplings $\beta = 3/(2\pi\alpha_s)$ as a function of the quark-antiquark distance r. The lattice scale is $r_0 \approx 0.5$ fm. The red solid line corresponds to the Cornell potential of Eq. (4). Adapted from [351].

In the meson case, the potential V is a function of the distance r between the quark and the antiquark, their masses, spin, momenta and angular momenta. If it is organized as an expansion in the inverse of the masses, m_h, the leading-order term is the static potential, $V^{(0)}$, which is only a function of r. At short distances, $r \ll 1/\Lambda_{QCD}$, asymptotic freedom constrains the potential to be Coulombic. At large distances, $r \gg 1/\Lambda_{QCD}$, the potential is confining. This is confirmed by lattice simulations of the static quark-antiquark energy, see Fig. 70; for a more recent determination in 2+1 flavor lattice QCD see, for instance, Ref. [352]. Lattice simulations also indicate that the confining part of the static potential grows linearly with the distance r. A simple parameterization of the static potential consists, then, in the sum of a Coulombic and a linear potential,

$$V^{(0)}(r) = -\frac{\kappa}{r} + \sigma r + C. \tag{4}$$

This parameterization goes under the name of Cornell potential [353]. The parameter κ would be $4\alpha_s/3$ plus higher-order corrections at very short distances, if the linear term was subtracted from the lattice data; the coefficient 4/3 is the Casimir of the fundamental SU(3) representation and the coupling α_s is the strong coupling of QCD. The parameter σ, whose typical value varies in the range 0.16-0.2 GeV^2, is known as the string tension. It may be understood as a constant force that prevents color charges from separating. The emergence of a string tension at long distances is suggestive of a description of the long-range interaction between heavy quark-antiquark pairs in terms of the effective string theory [354]. The constant C is a normalization constant of the dimension of an energy; as we will discuss later

71

in the section, it may also serve to mimic the effect of hadronic loops. These parameters can be determined from fits to lattice QCD data, see e.g. Fig. 70, as well as from phenomenological approaches.

At higher orders in the $1/m_h$ expansion, the potential V exhibits also spin- and momentum-dependent terms. Like in Eq. (4) for the static potential, also higher-order potentials in the $1/m_h$ expansion may be parameterized by summing a short distance part with a long distance confining one. The short-distance part may be computed in perturbation theory — see Eqs. (68)-(70) below for the leading-order expressions. The long-distance part may be derived from the effective string theory, see, for instance, Ref. [355]. Spin-dependent terms show up at order $1/m_h^2$. In the quark model this just reflects the smallness of the fine and hyperfine splittings. We will see in Sec. 4.4 that, in the framework of non relativistic effective field theories, the suppression in $1/m_h$ of the spin-dependent potentials is a consequence of the heavy quark spin symmetry. The first derivation of the spin-dependent potentials goes back to Refs. [356–358] and played a crucial role in establishing the nature of the confining interaction in QCD. Finally, we remark that kinetic energy and potential in the Hamiltonian (3) depend on the heavy quark masses. In the quark model, masses are just free parameters like σ and κ. They are sometimes called constituent masses. Their values are related to the constant C and fixed through fits to the data (typically, to the mass spectrum). If the Hamiltonian is derived and defined in the context of the effective field theory of Sec. 4.4.3, then the mass acquires a precise meaning. If no constant is added/subtracted from the static potential, it is the pole mass, whereas different constants define masses in different subtraction schemes, see Sec. 4.4.1.

A review of the determination of the potential in lattice QCD from the year 2000 is given in Ref. [351]. More recent determinations can be found, for example, in Refs. [352, 359–361]. We discuss these lattice results, along with analogous results for the quark-quark potential and the quark-antiquark potential in the presence of a gluonic excitation, later in this review — see Secs. 4.4.3, 4.4.4 and 4.5. The potential may also be computed through models of the QCD low-energy dynamics and the agreement/disagreement of the model predictions with data or lattice determinations will then provide useful insight in the QCD low-energy dynamics. Most of the models share the basic features of the Cornell model discussed above. In the short range, they agree with perturbative QCD, as a result of asymptotic freedom, and, in the long range, they agree with the expectations of the effective string theory. In the intermediate range they show different behaviours. Examples of model determinations of the quarkonium potential can be found in Refs. [362–367].

Finally, we add a few comments on the quantum numbers of quark-antiquark states. In practical applications, the Hamiltonian of the quark model is diagonalized in the J^{PC} basis, where J is the total angular momentum, $\boldsymbol{J} = \boldsymbol{L} + \boldsymbol{S}$, $\boldsymbol{L}$ the total orbital angular momentum, $\boldsymbol{S}$ the total spin, while $P = (-1)^{L+1}$ and $C = (-1)^{L+S}$ are the spatial and charge parity, respectively, of the corresponding quark-antiquark state. While the Hamiltonian commutes with $\boldsymbol{J}$, it does not commute neither with $\boldsymbol{S}$ nor with $\boldsymbol{L}$ separately, that is, generally speaking, neither $\boldsymbol{S}$ nor $\boldsymbol{L}$ are good quantum numbers for describing a quark-antiquark system. The same is true also for atomic systems.

The case $J = L$ is trivial, as the angular wave function is simply given by the spherical harmonic $Y_{JM}(\boldsymbol{n})$ or by the spherical vector $\boldsymbol{Y}_{JLM}(\boldsymbol{n})$ for a spin-singlet $[P = (-1)^{J+1}, C = (-1)^J]$ or a spin-triplet $[P = (-1)^{J+1}, C = (-1)^{J+1}]$, respectively. Here M is the magnetic quantum number and $\boldsymbol{n}$ is the unit vector in the direction of the radius $\boldsymbol{r}$ or momentum $\boldsymbol{p}$, depending on whether the eigenstate problem is formulated in coordinate or momentum space. Details of the formalism of the spherical harmonics and vectors can be found, for instance, in the book [368].

The case $L = J \pm 1$ $[P = (-1)^J, C = (-1)^J]$ is more involved (with the obvious exception of the 0^{++} scalar meson case, where $J = 0$ and $L = 1$). The reason is that, because of the spin-dependent potential, the wave function mixes terms proportional to $\boldsymbol{Y}_{J(J-1)M}(\boldsymbol{n})$ and $\boldsymbol{Y}_{J(J+1)M}(\boldsymbol{n})$. For example, a vector state 1^{--} is a mixture of $^3S_1$ and $^3D_1$ wave functions, with the coefficients which depend on the dynamics. It is commonly accepted, however, that some quarkonium vector states are predominantly $^3S_1$ states [for example, $\psi(3686) = \psi(2S)$], while others are predominantly $^3D_1$ states [for example, $\psi(3770)$]. Sometimes the relative coefficient between the two wave functions can be fixed from additional symmetry-based arguments. For example, if chiral symmetry is effectively restored (i.e., becomes manifest) in the spectrum of highly excited quarkonia [369, 370], then the latter fills approximate multiplets of the $\mathrm{SU}(2)_L \times \mathrm{SU}(2)_R$ chiral group. As a consequence, there must exist two types of vectors,

$$|\bar{q}\gamma^i q\rangle = \sqrt{\frac{2}{3}}|^3S_1\rangle + \sqrt{\frac{1}{3}}|^3D_1\rangle, \tag{5}$$

$$|\bar{q}\sigma^{0i} q\rangle = \sqrt{\frac{1}{3}}|^3S_1\rangle - \sqrt{\frac{2}{3}}|^3D_1\rangle, \tag{6}$$

where the interpolating currents are written in the kets on the left-hand side, and the mixing coefficients between the states on the right-hand side are completely fixed by chiral symmetry.[6] Here q is a generic quark field, $\sigma^{\mu\nu} = (i/4)[\gamma^\mu \gamma^\nu]$ and the γ's are the Dirac matrices. The corresponding chiral basis for all quantum numbers is built in Ref. [372].

S-D mixing takes place not only between quark-antiquark states with the same radial quantum numbers, but also between states with different ones [373]. Moreover, since states with similar masses mix more strongly it may happen that higher radially excited S-wave states play an important role in the mixing with D-states that are heavy due to the large orbital angular momentum. There exist claims in the literature that such a mixing may allow, for instance, to get more realistic values of the leptonic widths of vector charmonium and bottomonium states and even to treat some Y states [in particular, $Y(4230)$ and $Y(4360)$] as generic $\bar{c}c$ quarkonia — see Refs. [374–377] and references therein. It is important to notice, however, that the underlying mechanism for this mixing involves creation of heavy-light meson pairs, and, as such, lies beyond the scope of the potential models discussed so far. The effect of hadronic loops and above-threshold states on the quarkonium spectrum will be discussed below. Besides that, although the suggested mixing mechanism is interesting by itself, its reliable implementation requires, *inter alia*, a better understanding of the mixing patterns between states with different angular momenta within the quark model scheme.

● *Coupling to an open-flavor threshold*

The quark model discussed above relies upon the assumption that only the heavy constituent quark and antiquark of the quarkonium are relevant degrees of freedom at scales comparable with the typical momentum transfer and binding energy inside the bound state. This is not the case anymore, however, when the quark-antiquark distance becomes so large that the energy stored in the string formed between the heavy quark-antiquark pair exceeds twice the mass of the lightest heavy-light, $(\bar{Q}q)$, meson ($\sigma r \gtrsim 2M_{\bar{Q}q}$, where Q and q denote the heavy and the light quarks, respectively). At this distance it is energetically favorable for the string to break, which means that the heavy quark-antiquark pair decays strongly as $(\bar{Q}Q) \to (\bar{Q}q)+(\bar{q}Q)$. The open-flavor mesons created in this way are clearly degrees of freedom not accounted for by the naive potential models discussed so far.

The phenomenon of the string breaking is sometimes incorporated effectively into potential models through the flattening of the static quark-antiquark potential at relatively large quark-antiquark distances [378–381]. Moreover, the constant parameter C in Eq. (4) can be related to the real part of the hadronic loops. If in this adaptation of the Cornell potential the constant C is taken as a universal parameter of the model, the accuracy of predictions appears to be rather low. Some attempts to relate the constant C with the light-quark content of the meson were made in Ref. [382], while in Ref. [383] this parameter was directly related to the quark selfenergies and evaluated using the field correlator method [366].

The effects of hadronic loops were studied in many theoretical works — see, for example, Refs. [49, 353, 373, 384–416] to mention some. These studies were triggered by the discovery of the narrow charm-strange mesons $D_{s0}^*(2317)$ [417] and $D_{s1}(2460)$ [418], which appear to have much lower (~ 100 MeV) masses than predicted by quark models. Such a discrepancy was explained by a strong coupling of these states to the DK [400, 419] and D^*K channel [400, 420], respectively. Thus, one has to proceed beyond the scope of the simple constituent quark, potential model and to treat open-flavor decays properly. Sometimes, this is described as "unquenching" the quark model.

A systematic approach to hadronic-loop effects on the spectrum of quark-antiquark states is developed in Ref. [421] and a number of loop theorems are formulated and proved there. In particular, to incorporate hadronic-loop effects in the quark model a physical hadron is modeled as a bare valence state $|A\rangle$ augmented by two-hadron continuum components, $|BC\rangle$,

$$|\Psi\rangle = |A\rangle + \sum_{\{BC\}} \psi_{BC}|BC\rangle \,, \tag{8}$$

---

[6] Notice that, since the photon mediates electromagnetic interactions described by a vector current, the S-D wave function decomposition of a photoproduced fermion-antifermion pair should be given by Eq. (5). Indeed, as one can readily verify, in the ultrarelativistic limit, the differential cross section of e^+e^- annihilation into a pair of fermions shows an angular dependence consistent with the decomposition (5) [371]:

$$\frac{d\sigma}{d\Omega} \propto 1 + \cos^2\theta = \frac{16\pi}{3} \left| \sqrt{\frac{2}{3}} Y_{101}(\boldsymbol{n}) + \sqrt{\frac{1}{3}} Y_{121}(\boldsymbol{n}) \right|^2 . \tag{7}$$

and it is assumed that the Hamiltonian consists of a valence Hamiltonian H_0 [the quark model Hamiltonian (3)] and an interaction term H_I that couples the valence and continuum sectors,

$$H = H_0 + H_I. \tag{9}$$

The shift in the hadron A mass due to its coupling to the BC continuum channels can be evaluated using the second-order quantum-mechanical perturbation theory formula written in the rest frame of the decaying particle A,

$$\Delta M_{\rm A}^{\rm (BC)} = \int d^3 p \, \frac{|\langle {\rm BC}|H_I|{\rm A}\rangle|^2}{M_{\rm A} - E_{\rm BC} + i0}, \qquad E_{\rm BC} = \sqrt{p^2 + M_{\rm B}^2} + \sqrt{p^2 + M_{\rm C}^2}, \tag{10}$$

where $\boldsymbol{p} = \boldsymbol{p}_{\rm B} = -\boldsymbol{p}_{\rm C}$ and a particular microscopic model needs to be invoked to provide a form factor which regulates the integral.

If $M_{\rm A} > M_{\rm B} + M_{\rm C}$, then $\Delta M_{\rm A}^{\rm (BC)}$ acquires an imaginary part which is trivially related to the partial decay width,

$$\Gamma({\rm A} \to {\rm BC}) = -2{\rm Im}(\Delta M_{\rm A}^{\rm (BC)}). \tag{11}$$

The total hadronic shift and the total decay width for a given meson A are given by the sum over all open-flavor channels {BC},

$$\Delta M_{\rm A} = \sum_{\{{\rm BC}\}} \Delta M_{\rm A}^{\rm (BC)}, \qquad \Gamma_{\rm A} = \sum_{\{{\rm BC}\}} \Gamma({\rm A} \to {\rm BC}). \tag{12}$$

In order to proceed, one has to solve the eigenstate problem for the quark model Hamiltonian H_0 and to devise a suitable mechanism for the strong decays described by the term H_I. It was suggested long ago [422–425] that such a mechanism could be provided by the creation from the vacuum of light-quark pairs with vacuum quantum numbers $J^{PC} = 0^{++}$, that is, $^3P_0$ pairs. For this reason, this model is known nowadays as the $^3P_0$ model.[7] See also Refs. [47, 429–434] for further details. Since a quark-antiquark pair is created by the operator $b^\dagger d^\dagger$ (here b and d are the quark and antiquark annihilation operators), the $^3P_0$ model can be formulated with the help of the interaction Hamiltonian (see, for example, Refs. [434, 435])

$$H_I = g \int d^3 x \, \bar\psi\psi, \tag{13}$$

where g, or, equivalently, the dimensionless quantity $\gamma_q = g/(2m_q)$, is a free parameter of the model. A graphical representation of the quark-pair creation is in Fig. 71. The values of γ_q typically lie in the range 0.3-0.5 depending on the light-quark flavor and on the values taken by other parameters of the model — see, for example, Refs. [405, 436].
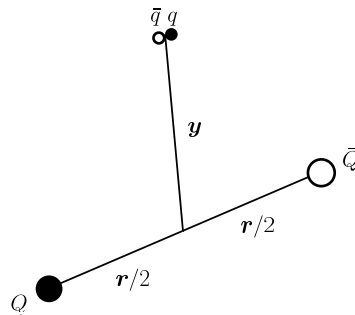
Figure 71: Graphical representation of the $(q\bar{q})$ pair creation mechanism. Adapted from Ref. [437].

For states {A} belonging to a given {n, L} multiplet, the following three theorems about hadronic loops hold [421]:

---

[7] An alternative approach, based on the $^1S_0$ pair creation, is also known in the literature — see, for example, Refs. [426, 427]. However, this model is not supported by experimental data [428].

1. The total mass shifts [see Eq. (12)] are equal.
2. The total decay widths [see Eq. (12)] are equal.
3. The mixing amplitude between any two valence basis states i and f vanishes if $L_i \neq L_f$ or $S_i \neq S_f$.

The above conclusions hold if all members of the $(Q\bar{Q})$ multiplet have equal masses and the heavy-light mesons in the loops also have identical masses. In addition, the final-state interaction in the continuum channels is neglected. Although in reality these conditions cannot be met exactly, the results of numerical calculations performed in Ref. [421] show that the claims of the theorems are fulfilled with a quite high accuracy in the spectrum of charmonium. Moreover, those numerical calculations also show that the total hadronic shifts for low-lying $\bar{c}c$ states are quite large, of the order of 400-500 MeV. Somewhat lower shifts, of the order of 200 MeV, have been obtained for the same charmonia in a similar approach in Ref. [405]. The conclusion drawn by the authors of Ref. [421] is that, although hadronic-loop effects may be largely renormalized away, their accurate description calls for further developments in the understanding of the valence-continuum coupling.

As a representative example of a typical quarkonium spectrum calculation in the framework of a quark model coupled to the open-flavor threshold, we present the results of Refs. [346, 347]. In those references, the authors use a Hamiltonian H_0 with relativistic kinetic energies and a Cornell-type potential that includes a static and a spin-dependent part (no spin-independent part, however, beyond the static potential). Moreover, they include quark-antiquark pair creation through the $^3P_0$ model described above — see Eq. (13). In addition, the creation point of the light-quark pair is smeared with a form factor of the size r_q, which takes values in the range 0.25-0.35 fm [346, 394–396, 438, 439]. Further details of the model, as well as the values of the parameters used in the actual calculations, can be found in Refs. [346, 347], while here we only quote the results obtained for the charmonium and bottomonium mass spectra — see Table 7.

We have just seen that unquenching the quark model reveals new effects related to hadronic loops. In particular, if a quarkonium state lies above an open-flavor threshold, not only its mass is shifted, as a result of its coupling to the open-flavor channel, but, in addition, the bound-state pole moves away from the real axis into the complex plane and the mass acquires an imaginary part, conventionally identified with the width of the state. The mass (energy) distribution that describes such a state is the famous BW distribution. To arrive at it let us parametrize the S-matrix element for the elastic scattering process $(\bar{Q}q) + (\bar{q}Q) \to (\bar{Q}q) + (\bar{q}Q)$ as

$$S = 1 + 2iA. \tag{14}$$

Then the unitary condition for the amplitude A,

$$AA^\dagger = \frac{1}{2i}(A - A^\dagger), \tag{15}$$

is fulfilled automatically for

$$A = K(1 - iK)^{-1}, \tag{16}$$

if the quantity K is real (in case of multichannel dynamics the corresponding K-matrix must be Hermitian, $K^\dagger = K$). If the scattering $(\bar{Q}q) + (\bar{q}Q) \to (\bar{Q}q) + (\bar{q}Q)$ proceeds through the formation of the state $(\bar{Q}Q)$ of mass M then

$$K = G(s)\frac{1}{M^2 - s}G(s) = \frac{\Gamma(s)\sqrt{s}}{M^2 - s}, \quad \Gamma(s) = \frac{G^2(s)}{\sqrt{s}}, \tag{17}$$

which gives the amplitude

$$A = \frac{\Gamma(s)\sqrt{s}}{M^2 - s - i\Gamma(s)\sqrt{s}} = G(s)\frac{1}{M^2 - s - \Sigma(s)}G(s). \tag{18}$$

The amplitude (18) describes all possible rescatterings $(\bar{Q}q)(\bar{q}Q) \to (\bar{Q}Q) \to (\bar{Q}q)(\bar{q}Q) \to (\bar{Q}Q)\dots$ in the intermediate state that result in the appearance of the selfenergy (hadronic loop) operator $\Sigma(s)$ in the denominator. The selfenergy modifies the propagator of the bare $(\bar{Q}Q)$ state. Since the amplitude is an analytic function of s, the operator $\Sigma(s)$ is defined both above and below the corresponding open-flavor threshold $(\bar{Q}q)(\bar{q}Q)$, and, therefore, it contributes in general to both the real and imaginary parts of the denominator. Therefore, indeed, the bare pole of the amplitude,

State	J^{PC}	$D\bar{D}$	$\bar{D}D^*$ $D\bar{D}^*$	$\bar{D}^*D^*$	$D_s\bar{D}_s$	$D_s\bar{D}_s^*$ $\bar{D}_sD_s^*$	$D_s^*\bar{D}_s^*$	$\eta_c\eta_c$	$\eta_c J/\psi$	$J/\psi J/\psi$	$\Sigma(M_0^2)$	M_0	M	$M_{\text{exp.}}$
$\eta_c(1^1S_0)$	0^{-+}	–	-34	-31	–	-8	-8	–	–	-2	-83	3062	2979	2984
$J/\psi(1^3S_1)$	1^{--}	-8	-27	-41	-2	-6	-10	–	-2	–	-96	3233	3137	3097
$\eta_c(2^1S_0)$	0^{-+}	–	-52	-41	–	-9	-8	–	–	-1	-111	3699	3588	3638
$\psi(2^3S_1)$	1^{--}	-18	-42	-54	-2	-7	-10	–	-1	–	-134	3774	3640	3686
$h_c(1^1P_1)$	1^{+-}	–	-59	-48	–	-11	-10	–	-2	–	-130	3631	3501	3525
$\chi_{c0}(1^3P_0)$	0^{++}	-31	–	-72	-4	–	-15	0	–	-3	-125	3555	3430	3415
$\chi_{c1}(1^3P_1)$	1^{++}	–	-54	-53	–	-9	-11	–	–	-2	-129	3623	3494	3511
$\chi_{c2}(1^3P_2)$	2^{++}	-17	-40	-57	-3	-8	-10	0	–	-2	-137	3664	3527	3556
$h_c(2^1P_1)$	1^{+-}	–	-55	-76	–	-12	-8	–	-1	–	-152	4029	3877	–
$\chi_{c0}(2^3P_0)$	0^{++}	-23	–	-86	-1	–	-13	0	–	-1	-124	3987	3863	3860
$\chi_{c1}(2^3P_1)$	1^{++}	–	-30	-66	–	-11	-9	–	–	-1	-117	4025	3908	3872
$\chi_{c2}(2^3P_2)$	2^{++}	-2	-42	-54	-4	-8	-10	0	–	-1	-121	4053	3932	3927
$\eta_{c2}(1^1D_2)$	2^{-+}	–	-99	-62	–	-12	-10	–	–	-1	-184	3925	3741	–
$\psi(3770)(1^3D_1)$	1^{--}	-11	-40	-84	-4	-2	-16	–	0	–	-157	3907	3750	3773
$\psi_2(3823)(1^3D_2)$	2^{--}	–	-106	-61	–	-11	-11	–	-1	–	-190	3926	3736	3823
$\psi_3(3842)(1^3D_3)$	3^{--}	-25	-49	-88	-4	-8	-10	–	-1	–	-185	3936	3751	3842

State	J^{PC}	$B\bar{B}$	$B\bar{B}^*$ $\bar{B}B^*$	$B^*\bar{B}^*$	$B_s\bar{B}_s$	$B_s\bar{B}_s^*$ $\bar{B}_sB_s^*$	$B_s^*\bar{B}_s^*$	$B_c\bar{B}_c$	$B_c\bar{B}_c^*$ $\bar{B}_cB_c^*$	$B_c^*\bar{B}_c^*$	$\eta_b\eta_b$	$\eta_b\Upsilon$	$\Upsilon\Upsilon$	$\Sigma(M_0^2)$	M_0	M	$M_{\text{exp.}}$
$\eta_b(1^1S_0)$	0^{-+}	–	-26	-26	–	-5	-5	–	-1	-1	–	–	0	-64	9455	9391	9399
$\Upsilon(1^3S_1)$	1^{--}	-5	-19	-32	-1	-4	-7	0	0	-1	–	0	–	-69	9558	9489	9460
$\eta_b(2^1S_0)$	0^{-+}	–	-43	-41	–	-8	-7	–	-1	-1	–	–	0	-101	10081	9980	9999
$\Upsilon(2^3S_1)$	1^{--}	-8	-31	-51	-2	-6	-9	0	0	-1	–	0	–	-108	10130	10022	10023
$\eta_b(3^1S_0)$	0^{-+}	–	-59	-52	–	-8	-8	–	-1	-1	–	–	0	-129	10467	10338	–
$\Upsilon(3^3S_1)$	1^{--}	-14	-45	-68	-2	-6	-10	0	0	-1	–	0	–	-146	10504	10358	10355
$h_b(1^1P_1)$	1^{+-}	–	-49	-47	–	-9	-8	–	-1	-1	–	0	–	-115	10000	9885	9899
$\chi_{b0}(1^3P_0)$	0^{++}	-22	–	-69	-3	–	-13	0	–	-1	0	–	0	-108	9957	9849	9859
$\chi_{b1}(1^3P_1)$	1^{++}	–	-46	-49	–	-8	-9	–	-1	-1	–	–	0	-114	9993	9879	9893
$\chi_{b2}(1^3P_2)$	2^{++}	-11	-32	-55	-2	-6	-9	0	-1	-1	0	–	0	-117	10017	9900	9912
$h_b(2^1P_1)$	1^{+-}	–	-66	-59	–	-10	-9	–	-1	-1	–	0	–	-146	10393	10247	10269
$\chi_{b0}(2^3P_0)$	0^{++}	-33	–	-85	-4	–	-14	0	–	-1	0	–	0	-137	10363	10226	10233
$\chi_{b1}(2^3P_1)$	1^{++}	–	-63	-60	–	-9	-10	–	-1	-1	–	–	0	-144	10388	10244	10255
$\chi_{b2}(2^3P_2)$	2^{++}	-16	-42	-72	-2	-6	-10	0	0	-1	0	–	0	-149	10406	10257	10269
$h_b(3^1P_1)$	1^{+-}	–	-18	-73	–	-11	-10	–	-1	-1	–	0	–	-114	10705	10591	–
$\chi_{b0}(3^3P_0)$	0^{++}	-4	–	-160	-6	–	-15	0	–	-1	0	–	0	-186	10681	10495	–
$\chi_{b1}(3^3P_1)$	1^{++}	–	-25	-74	–	-11	-10	–	0	-1	–	–	0	-121	10701	10580	10512
$\chi_{b2}(3^3P_2)$	2^{++}	-19	-16	-79	-3	-8	-12	0	0	-1	0	–	0	-138	10716	10578	–
$\Upsilon_2(1^1D_2)$	2^{-+}	–	-72	-66	–	-11	-10	–	-1	-1	–	–	0	-161	10283	10122	–
$\Upsilon(1^3D_1)$	1^{--}	-24	-22	-90	-3	-3	-16	0	0	-1	–	0	–	-159	10271	10112	–
$\Upsilon_2(1^3D_2)$	2^{--}	–	-70	-68	–	-10	-11	–	-1	-1	–	0	–	-161	10282	10121	10164
$\Upsilon_3(1^3D_3)$	3^{--}	-18	-43	-78	-3	-8	-11	0	-1	-1	–	0	–	-163	10290	10127	–

Table 7: Selfenergies due to coupling to the meson-meson continuum (meson loops) (in MeV) for various charmonium and bottomonium states as evaluated in Refs. [346, 347]. The masses M_0 are the quarkonium masses without hadronic-loop effects, i.e., the quarkonium masses computed from the valence Hamiltonian H_0. The masses $M = M_0 + \Sigma(M_0^2)$ are the final masses including hadronic-loop effects. The masses $M_{\text{exp.}}$ are the experimental masses from Ref. [6].

$s_{\mathrm{bare}} = M^2$, moves from its original location both along the real axis (mass shift) and the imaginary axis, that is, the pole position acquires also an imaginary part — the width.

In Eq. (18) we recognise the relativistic form of the BW distribution for an isolated resonance. If the form factor $G(s)$ in Eq. (17) weakly depends on s for $s \approx M^2$ ($G(s) \approx G(M^2) \equiv g$) and $\Gamma \equiv \Gamma(M^2) = g^2/\sqrt{M} \ll M$, then the amplitude (18) has a pole at

$$s_{\mathrm{pole}} = \left(M - \frac{i}{2}\Gamma\right)^2 \approx M^2 - iM\Gamma . \tag{19}$$

Therefore, the larger the coupling g of the quarkonium state to the continuum channel, the larger is its width and, consequently, the more the corresponding pole in the amplitude moves away from the real axis. Nevertheless, the single-resonance amplitude (18) is unitary by construction. Multiresonance systems, instead, have to be treated with care, since unitarisation effects may play an important and sometimes quite unexpected role. In particular, it has been argued for a long time that, when building quark models with coupled channels, unitarisation cannot be neglected, and may be even responsible for the appearance of extra, dynamically generated resonances — see, for example, Refs. [387, 437, 440–447] and references therein.

In Ref. [437], the effects of unitarisation have been studied in a simple toy model in which a scalar field φ [viewed as a $(q\bar{Q})$ meson] interacts with a set of scalar quark-antiquark fields R_n ($n \in \{1, \ldots, N\}$) associated with the n-th radial excitations of a $(Q\bar{Q})$ system. The number of excitations has been assumed to be large, $N \gg 1$. The fields φ and $\bar{\varphi}$ can be produced from R_n through some strong open-flavor decay mechanism controlled by a coupling g. The behaviour of the poles as g is varied in a wide range can be summarized as follows:

- For small values of the coupling g, unitarisation effects are negligibly small, so that all poles are independent of each other, and they deviate only slightly from their respective positions, $s_n^{(0)} = M_n^2$, found for $g = 0$. Their behaviour complies, therefore, with the one described by Eq. (19).

- For growing values of the coupling g, as soon as the selfenergy due to the loop operator becomes as large as the level spacing [$|\Sigma_n| \simeq M^2(R_{n+1}) - M^2(R_n)$], unitarisation effects become important and cannot be treated perturbatively anymore. In particular, for most states the pole trajectories bend and their widths decrease. A similar observation that quark states may become narrower as the coupling to the continuum grows was made in Ref. [443]. Such a nontrivial behaviour disproves an old prejudice that, because of the large phase space available, the states high up in the spectrum acquire large widths and, therefore, cannot be observed. However, a large width inevitably implies strong unitarisation effects, which, as a back reaction, tame it.

- At least one state possesses a pole trajectory that spans a wide (compared to the level spacing) range and acquires contributions from multiple bare poles. This behaviour has been interpreted in Ref. [437] as a sort of collective phenomenon.

The conclusion is that unitarisation effects may substantially affect the properties of hadronic states, such as the real and imaginary parts of the corresponding poles in the complex plane (conventionally interpreted as the mass and the width of the state), and, for strongly-coupled systems, result in some quite unexpected behaviour of the system, such as a decrease of the width with the increase of the coupling and a sort of collective phenomenon involving multiple poles. Such effects may manifest themselves in the line shapes of the hadronic resonances, which can depart from the simple symmetric BW form.

• *Quasipotential model*

In relativistic quark models, classes of relativistic corrections are included in the potential. The inclusion is not systematic and may miss some equally important corrections, nevertheless, the aim of these models is to capture some features of the relativistic dynamics. Hence, one possible use of relativistic quark models is to provide a checking ground for the convergence of the non relativistic expansion. This is particularly relevant for not so heavy quarks, like the charm quark.

Among the relativistic quark models, in the following we will consider the quasipotential approach of Refs. [348, 349]. In this approach a meson is described as a bound state of a quark of mass m_1 and an antiquark of mass m_2 with

the wave function satisfying a quasipotential equation [448] of the Schrödinger type [449],

$$\left(\frac{b^2(M)}{2\mu_R} - \frac{\boldsymbol{p}^2}{2\mu_R}\right)\Psi_M(\boldsymbol{p}) = \int \frac{d^3q}{(2\pi)^3} V(\boldsymbol{p}, \boldsymbol{q}; M)\,\Psi_M(\boldsymbol{q})\,, \tag{20}$$

where

$$\mu_R = \frac{E_1 E_2}{E_1 + E_2} = \frac{M^4 - (m_1^2 - m_2^2)^2}{4M^3}, \quad E_1 = \frac{M^2 - m_2^2 + m_1^2}{2M}, \quad E_2 = \frac{M^2 - m_1^2 + m_2^2}{2M}, \quad M = E_1 + E_2\,, \tag{21}$$

and the c.m. relative momentum squared on mass shell reads

$$b^2(M) = \frac{[M^2 - (m_1 + m_2)^2][M^2 - (m_1 - m_2)^2]}{4M^2}. \tag{22}$$

The kernel $V(\boldsymbol{p}, \boldsymbol{q}; M)$ in Eq. (20) is a quasipotential operator that describes the interaction between the quark and the antiquark,

$$V(\boldsymbol{p}, \boldsymbol{q}; M) = \bar{u}_1(p)\bar{u}_2(-p)\mathcal{V}(\boldsymbol{p}, \boldsymbol{q}; M)u_1(q)u_2(-q)\,, \tag{23}$$

where the u's are Dirac spinors, and the interaction,

$$\mathcal{V}(\boldsymbol{p}, \boldsymbol{q}; M) = -\frac{16\pi}{3}\alpha_s D_{\mu\nu}(\boldsymbol{k})\gamma_1^\mu\gamma_2^\nu + V_{\text{conf}}^V(\boldsymbol{k})\Gamma_1^\mu\Gamma_{2;\mu} + V_{\text{conf}}^S(\boldsymbol{k})\,, \qquad \boldsymbol{k} = \boldsymbol{p} - \boldsymbol{q}\,, \tag{24}$$

consists of a gluon exchange and a confining term [somehow providing a Lorentz-covariant version of the Cornell potential (4)]. The gluon propagator in Coulomb gauge reads

$$D^{00}(\boldsymbol{k}) = \frac{1}{\boldsymbol{k}^2}, \qquad D^{ij}(\boldsymbol{k}) = \frac{1}{\boldsymbol{k}^2}\left(\delta^{ij} - \frac{k^i k^j}{\boldsymbol{k}^2}\right), \qquad D^{0i} = D^{i0} = 0\,, \tag{25}$$

whereas the confining term consists of a scalar and a vector part:

$$V_{\text{conf}}^V(r) = (1 - \varepsilon)Ar + B\,, \qquad V_{\text{conf}}^S(r) = \varepsilon Ar\,, \qquad V_{\text{conf}}(r) = V_{\text{conf}}^S(r) + V_{\text{conf}}^V(r) = Ar + B\,. \tag{26}$$

Finally, the effective long-range vector vertex is given by

$$\Gamma_\mu(\boldsymbol{k}) = \gamma_\mu + \frac{i\kappa}{2m}\sigma_{\mu\nu}k^\nu\,, \tag{27}$$

where κ is taken as a constant and is a parameter of the model.

Expressions of the quasipotential for heavy quarkonia, expanded non relativistically (i.e., in the inverse of the heavy quark masses and for small heavy quark momenta) without and with retardation corrections to the confining potential, can be found in Refs. [348] and [349], respectively. The spin-dependent interaction reduces in this way to the spin-dependent potential of the non relativistic quark model. In particular, it agrees with the Cornell-type parameterization of Ref. [356].

The model is completely fixed by setting

$$A = 0.18 \text{ GeV}^2\,, \quad B = -0.16 \text{ GeV}\,, \quad \varepsilon = -1\,, \quad \kappa = -1\,, \quad m_b = 4.88 \text{ GeV}\,, \quad m_c = 1.55 \text{ GeV}\,, \tag{28}$$

where A can be identified with the string tension in the Cornell potential and m_b and m_c are the bottom and charm mass parameters, respectively. Predictions of the model for the mass spectrum of $\bar{c}c$ and $\bar{b}b$ quarkonia are collected in Table 8.

• *Beyond the quark model: exotic states and the $\chi_{c1}(3872)$ aka X(3872)*

It is instructive to put the charmonium states predicted by the quark model in a single plot (for definiteness we use the masses listed in Table 8; using the values from Table 7 would result in a quite similar plot) — see Fig. 72. In addition, a few observed vector states not present in the table are shown in red. It is clearly seen from Table 8

$n\,^{2S+1}L_J$	J^{PC}	$\bar{c}c$ state	Theory	Exp	$\bar{b}b$ state	Theory	Exp
$1\,^1S_0$	0^{-+}	$\eta_c(1S)$	2981	2983.9±0.5	$\eta_b(1S)$	9398	9399.0±2.3
$2\,^1S_0$	0^{-+}	$\eta_c(2S)$	3635	3637.6±1.2	$\eta_b(2S)$	9990	9999±4
$1\,^3S_1$	1^{--}	$J/\psi(1S)$	3096	3096.900±0.006	$\Upsilon(1S)$	9460	9460.30±0.26
$2\,^3S_1$	1^{--}	$\psi(2S)$	3685	3687.097±0.025	$\Upsilon(2S)$	10023	10023.26±0.31
$3\,^3S_1$	1^{--}	$\psi(4040)$	4039	4039±1	$\Upsilon(3S)$	10355	10355.2±0.5
$4\,^3S_1$	1^{--}	$\psi(4415)$	4427	4421±4	$\Upsilon(4S)$	10586	10579.4±1.2
$5\,^3S_1$	1^{--}		4837		$\Upsilon(10860)$	10869	$10889.9^{+3.2}_{-2.6}$
$6\,^3S_1$	1^{--}		5167		$\Upsilon(11020)$	11088	$10992.9^{+10.0}_{-3.1}$
$1\,^3P_0$	0^{++}	$\chi_{c0}(1P)$	3413	3414.71±0.30	$\chi_{b0}(1P)$	9859	9859.44±0.42±0.31
$2\,^3P_0$	0^{++}	$\chi_{c0}(2P)$	3870	$3862^{+50}_{-35}(*)$	$\chi_{b0}(2P)$	10233	10232.5±0.4±0.5
$1\,^3P_1$	1^{++}	$\chi_{c1}(1P)$	3511	3510.67±0.05	$\chi_{b1}(1P)$	9892	9892.78±0.26±0.31
$2\,^3P_1$	1^{++}	$\chi_{c1}(2P)$	3906	3871.69±0.17(**)	$\chi_{b1}(2P)$	10255	10255.46±0.22±0.50
$3\,^3P_1$	1^{++}	$\chi_{c1}(3P)$	4319		$\chi_{b1}(3P)$	10541	10512.1±2.3
$1\,^3P_2$	2^{++}	$\chi_{c2}(1P)$	3555	3556.17±0.07	$\chi_{b2}(1P)$	9912	9912.21±0.26±0.31
$2\,^3P_2$	2^{++}	$\chi_{c2}(2P)$	3949	3927.2±2.6	$\chi_{b2}(2P)$	10268	10268.65±0.22±0.50
$1\,^1P_1$	1^{+-}	$h_c(1P)$	3525	3525.38±0.11	$h_b(1P)$	9900	9899.3±0.8
$2\,^1P_1$	1^{+-}	$h_c(2P)$	3926		$h_b(2P)$	10260	10259.8±1.2
$1\,^3D_1$	1^{--}	$\psi(3770)$	3783	3773.13±0.35		10154	
$2\,^3D_1$	1^{--}	$\psi(4160)$	4150	4191±5		10435	
$1\,^3D_2$	2^{--}	$\psi_2(3823)$	3795	3822.2±1.2	$\Upsilon_2(1D)$	10161	10163.7±1.4

Table 8: Charmonium and bottomonium mass spectra (in MeV) obtained in Ref. [48] and updated in Ref. [350] in the framework of the relativistic quark model [348, 349]. Predictions of the model are compared with the experimental data from the PDG [6]. Only states with well established quantum numbers are considered, with the only exception made for the charmonium $\chi_{c0}(2P)$ state (marked with an asterisk) reported recently by the Belle Collaboration [134], which fits well into the quark model scheme. The charmonium $\chi_{c1}(2P)$ state (marked with a double asterisk) is identified with the $X(3872)$. However, for this state the effect of the coupling to the $D\bar{D}^*$ threshold would be very large and result in a shift downwards of the mass of the state, see discussion in the following paragraphs. The effects of the coupling to open-flavor thresholds have not been included in the results of the table. Further predictions for other $c\bar{c}$ and $b\bar{b}$ quarkonia can be found in Refs. [48, 350].

that, while most of the charmonium states are well described by the quark model, still there are some (shown in red and named X's and Y's) that do not fit into the quark model scheme. Furthermore, the charged charmonium and bottomonium states observed experimentally cannot fit into the $Q\bar{Q}$ scheme as a matter of principle, since their minimal quark content is four quarks. As detailed in Sec. 3.2, charged states are the $Z_c(3900)^\pm$, $Z_c(4020)^\pm$, and $Z_c(4430)^\pm$ in the charmonium spectrum, and the $Z_b(10610)^\pm$ and $Z_b(10650)^\pm$ in the bottomonium spectrum. Other additional states claimed in the literature, but not confirmed, have been discussed in Sec. 3. All these states are exotic states with respect to the quark model.

We conclude by adding a few comments on the spectral identification of the state $X(3872)$, which is the first and best known of the possible charmonium-like exotica. Since the properties of this state were discussed in detail in Sec. 3.1.1, we only mention here that it was observed by the Belle Collaboration in 2003 [5] and that its quantum numbers, $J^{PC} = 1^{++}$, were unambiguously determined by the LHCb Collaboration only 10 years later, in 2013 [37, 58]. The most up-to-date value of its mass given by the PDG [6] is quoted in the last column of Table 9.

Reference	[47]	[346]	[405]	[350]	[450]	[6]
Mass, MeV	3960	3908	3990	3906	3954	3871.69 ± 0.17

Table 9: Predictions of some quark models for the mass of the genuine $\chi_{c1}(2P)$ (or χ'_{c1}) charmonium. The last column contains the experimental mass of the exotic charmonium-like state $\chi_{c1}(3872)$ aka $X(3872)$.

From the point of view of the quark model, the best $c\bar{c}$ candidate for the $X(3872)$ is the radially excited $\chi_{c1}(2P)$ charmonium, since it possesses the right quantum numbers and lies nearby. However, such an identification meets
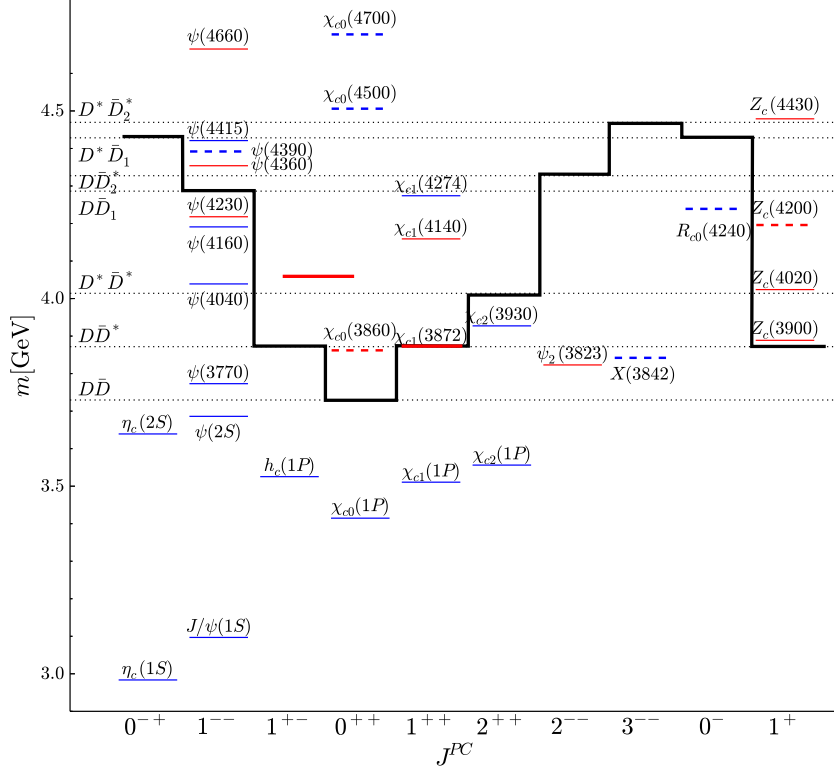
Figure 72: The spectrum of states in the $c\bar{c}$ sector as of July 2019 (see the caption of Fig.1 for the notations and further details). The red lines show exotic candidates with established quantum numbers and discussed in this review. The blue lines correspond to the experimental charmonium spectrum listed in Table 8. In each J^{PC} channel the thick black line indicates the lowest threshold energy where a pair of narrow resonances can couple to the given quantum number in an S wave. Note that the parity of the channels that contain the ground-state D and D^* in S wave can only be positive, while by replacing one of the mesons by either a D_1 or a D_2 gives a negative parity. Higher partial waves change the parity by the additional factor $(-1)^L$, with L being the angular momentum in the pair.

certain problems. In particular, the quark model is unable to explain the low mass of the X. Indeed, predictions of quark models for this state — see, for example, those collected in Table 9 — are in the range 3900-4000 MeV, that is, from a few dozen to more than a hundred MeV higher than needed. Furthermore, it is clearly seen from Fig. 72 that the mass of the $X(3872)$ is extremely close (within just 1 MeV!) to the neutral $D\bar{D}^*$ threshold — a fact that cannot be explained by the quark model other than by an accident. Such a proximity to an open-flavor threshold implies that this threshold strongly impacts the properties of the state, and that coupled channel effects need to be taken into account — see, for example, Refs. [405, 450]. In particular, it is shown in Ref. [405] that coupling of the bare 2^3P_1 charmonium state to the $D\bar{D}^*$ channel generates, together with a quarkonium of mass 3990 MeV (see Table 9), a very shallow virtual state at the $D\bar{D}^*$ threshold. This virtual state has a very small admixture of $c\bar{c}$ charmonium in the wave function and is suggested to be identified with the $X(3872)$. In Ref. [450] the peak at the neutral $D\bar{D}^*$ threshold is argued to be due to a BW resonance shifted by channel coupling from its original position of 3954 MeV (see Table 9).

In order for the $X(3872)$ to be unambiguously identified with or distinguished from the $\chi_{c1}(2P)$ on spectroscopic grounds, an interesting observation was made in Ref. [451]. The spin-dependent potential induces a splitting within spin-triplet states of the same radial excitation n and angular momentum L. The center-of-gravity mass of these states

is defined as

$$M^{\text{c.o.g.}}_{n^3 L_J} = \frac{1}{3(2L+1)} \left((2L-1)M(n^3 L_{J=L-1}) + (2L+1)M(n^3 L_{J=L}) + (2L+3)M(n^3 L_{J=L+1}) \right) . \tag{29}$$

It is well known [452] that the hyperfine splitting between the mass of the spin-singlet heavy quarkonium state h ($J^{PC} = 1^{+-}$) and the centre-of-gravity mass of the corresponding spin triplet χ ($J^{PC} = J^{++}$, $J = 0, 1, 2$),

$$\Delta_{n,1} = M_{n^1 P_1} - M^{\text{c.o.g.}}_{n^3 P_J} , \tag{30}$$

is very small both in the charm and bottom sector. Indeed, the experimental values read [6]

$$\Delta_{1,1}(c\bar{c}) = 0.08(13)\ \text{MeV} , \qquad \Delta_{1,1}(b\bar{b}) = -0.57(88)\ \text{MeV} , \qquad \Delta_{2,1}(b\bar{b}) = -0.44(1.31)\ \text{MeV} . \tag{31}$$

Thus, it was suggested in Ref. [451] that the splitting $\Delta_{n,L}$ could be used as a benchmark for the quark content of hadronic states. A large $\Delta_{n,L}$ would signal that at least one state in the quartet contains a significant non-$Q\bar{Q}$ component and, therefore, should be regarded as an exotic state. In particular, the experimental measure of the mass of the $h_c(2P)$ would allow to test the entire charmonium $2P$ quartet against the identification of the $X(3872)$ with the $\chi_{c1}(2P)$, under the assumption that $\chi_{c0}(2P)$ and $\chi_{c2}(2P)$ have been identified correctly.

4.3. Phenomenological approaches to exotic hadrons

In this section various phenomenological approaches are discussed, which are often used in the literature to classify mesons, including candidates for exotic states. As mentioned above, we define the latter to be states which demonstrate properties at odds with the predictions of the simplest quark model describing mesons as bound states of a quark and an antiquark. Amongst the exotic states there are some that carry quantum numbers that are incompatible with the simple quark model — for example, the isovector quarkonium-like states introduced in Secs. 3.2.1, 3.2.2 and 3.2.3 — and others that have quantum numbers allowed for a quark-antiquark state, but show properties at odds with the quark model predictions. Here the most famous example is the $\chi_{c1}(3872)$ aka $X(3872)$ introduced in Sec. 3.1.1.

Amongst the scenarios relevant for exotic states in the spectrum of heavy quarks, that is those containing a heavy $Q\bar{Q}$ pair, one may distinguish states with an active gluonic degree of freedom (hybrid mesons) and multiquark configurations that are distinguished on the basis of their internal quark clustering — a graphical representation of the most common scenarios for exotics is shown in Fig. 73. It is fair to note here that Gell-Mann proposed the existence of multiquark states already in 1964, when introducing his famous classification model for mesons and baryons [4].

4.3.1. Hybrids

Due to its non-Abelian nature, QCD allows for more colorless hadrons than just quark-antiquark mesons and three-quark baryons. Of relevance for the present review are quarkonium hybrids or simply hybrids, which constitute the subject of the present section, and multi-quarks, which will be discussed in the next sections. With the word "hybrid" we identify conventionally quark-antiquark mesons with excited gluonic degrees of freedom. Gluons bring a new type of excitation to the system, in addition to the rotational and radial motion of the quarks in ordinary ($Q\bar{Q}$) systems discussed in the previous section.

Predictions for various properties of hybrids with heavy quarks found in the vast literature on the subject rely on different approaches. In particular, the interested reader can find predictions from the flux-tube model in Ref. [453, 454], from the Coulomb-gauge QCD approach in Refs. [455–457], from a constituent gluon model for gluelumps (short-distance hybrids) in Ref. [458], from the constituent gluon model in Refs. [459, 460] — see also the discussion below — and from the QCD string model in Refs. [461–466]. An effective field theory description based on non-relativistic effective field theories has also been developed. This is the Born–Oppenheimer effective field theory of Refs. [192, 193, 467–472] discussed in more detail in Sec. 4.4.4, An independent source of information about the masses and splittings of hybrids comes from lattice QCD calculations [130, 131, 473–477].

Models differ substantially in the way they describe hybrids. For example, in the flux tube model [478], hybrids are described as phonon-type excitations, while in the constituent gluon model [459, 460] they carry both color and spin. Nevertheless, there is some consensus about few basic facts.

In addition, the excitation of the gluonic degrees of freedom contributes at least with approximately 1 GeV to the mass of the system, so that the mass of the ground-state hybrid can be roughly estimated to be $2m_h + 1$ GeV,
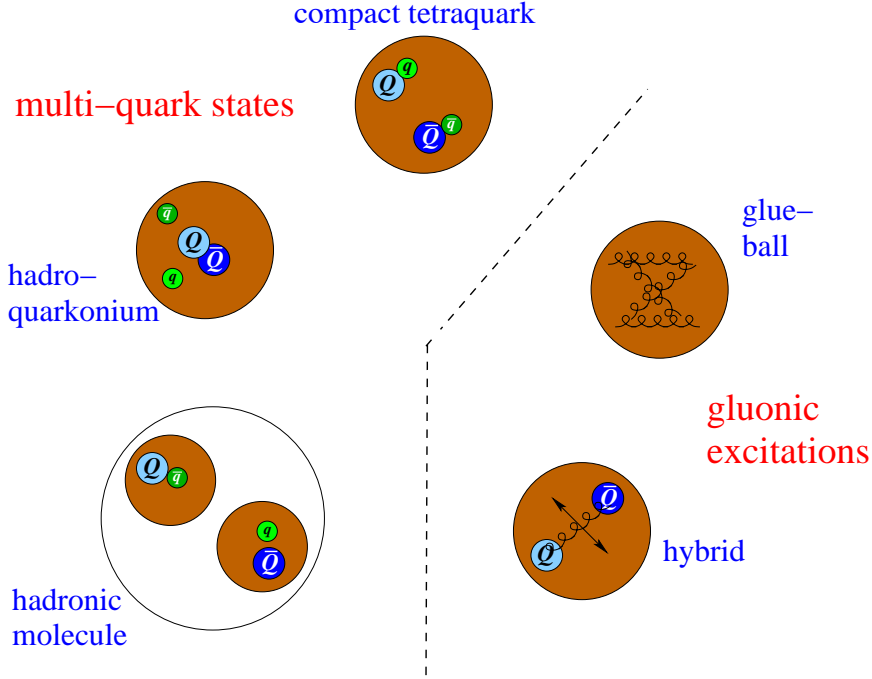
Figure 73: Graphic illustration of the most common proposals for the structure of exotic states. Details are given in the text.

where m_h is the mass of the heavy quark. This gives about 4 GeV for the mass of the lowest charmonium hybrid and 11 GeV for the one of the lowest bottomonium hybrid. Results obtained by different theoretical approaches, as well as determinations from lattice QCD (mostly in the quenched approximation, but Ref. [131] is a 2+1 flavor dynamical lattice simulation, with a pion mass of about 240 MeV, discussed in Sec. 4.5.1) for the lowest charmonium hybrid are collected in Table 10. We see that, indeed, all predictions are generally consistent with each other and with the simple estimate made above for what concerns the value of the mass of the lowest-lying hybrid. The situation for bottomonium hybrids looks similar. Indeed, the most recent calculations place the mass of the lowest bottomonium hybrid around 11 GeV, also in agreement with the simple estimate made above — see Refs. [192, 466, 468] for more details.

Clearly, as the table shows, there are also considerable differences between the different approaches. First, not all of them identify the same hybrid state as the lowest-lying one. Moreover, also the (approximate) degeneracy pattern of the different hybrid multiplets differ. These disagreements may serve to select among different approaches.

Model	Reference	Quantum numbers	Mass, GeV
Flux-tube	[454]	—	$4.1 - 4.2$
Gluelump	[458]	2^{++}	4.12
QCD string	[479]	1^{-+}	4.2 ± 0.2
	[465, 466]	$1^{--}, (0, 1, 2)^{-+}$	$4.3 - 4.5$
BOEFT	[192]	$1^{--}, (0, 1, 2)^{-+}$	4.15 ± 0.15
Lattice	[131, 473]	1^{-+}	$4.3 - 4.4$
	[131, 474, 475]	0^{-+}	$4.3 - 4.4$

Table 10: Predictions of various models, effective field theory and lattice QCD for the mass of the lowest charmonium hybrid. BOEFT stands for the Born–Oppenheimer effective field theory discussed in Sec. 4.4.4.

• *Constituent gluons and potential models*

The quark model may be extended to describe hybrids by allowing, besides constituent quarks and antiquarks, also constituent gluons. In the simplest realisation, the hybrid is a quark-antiquark pair augmented by a single gluonic excitation. The constituent gluon plays the role of an additional gluonic degree of freedom that binds with the heavy quark-antiquark pair to form the hybrid. It can be given an effective mass of about 1 GeV. As was stated above, this is the typical energy gap between the heavy quark-antiquark levels and their first gluonic excitations. Because in this picture the gluon, like the other constituents, is a massive mode, it is possible to describe the interaction among the constituents in terms of a potential and expand it in the inverse of the masses. The valence gluon, located at $\boldsymbol{r}_g$, is connected to the quark, located at $\boldsymbol{r}_Q$, and the antiquark, located at $\boldsymbol{r}_{\bar{Q}}$, by two strings with the same string tension σ as in the quark-antiquark potential of Eq. (4). Then, for a hybrid in the constituent gluon picture, the long-range, confining, static potential is

$$V_{\text{conf}}[Q\bar{Q}g] = \sigma|\boldsymbol{r}_Q - \boldsymbol{r}_g| + \sigma|\boldsymbol{r}_{\bar{Q}} - \boldsymbol{r}_g|, \tag{32}$$

and the leading-order short-range static potential reads

$$V_{\text{Coul}}[Q\bar{Q}g] = -\frac{3\alpha_s}{2|\boldsymbol{r}_Q - \boldsymbol{r}_g|} - \frac{3\alpha_s}{2|\boldsymbol{r}_{\bar{Q}} - \boldsymbol{r}_g|} + \frac{\alpha_s}{6|\boldsymbol{r}_Q - \boldsymbol{r}_{\bar{Q}}|}. \tag{33}$$

Note that at leading order the short-range potential is just the sum of three two-body Coulomb potentials in the suitable SU(3) color representation of the interacting pair: the gluon-heavy-quark pair in the fundamental representation, the gluon-heavy-antiquark pair in the complex conjugate of the fundamental representation, and the heavy quark-antiquark pair in the octet representation. The different factors in front of the Coulomb potentials are due to the different representations; the octet potential is repulsive, hence at short distances the hybrid is kept together by the bindings of the quark and antiquark with the constituent gluon alone. At higher orders in the inverse of the masses, one may establish also Cornell-like potentials similar to the static potential. In particular, one gets a spin-dependent potential of the same form as the spin-dependent potential for ordinary quarkonia — see, for example, Ref. [465]. As we will see in Sec. 4.4.4 — and, in particular, with Eq. (75) — the naive constituent gluon potential model misses, however, even the leading, only $1/m_h$ suppressed, spin-dependent potential in the hybrid system. This happens because this potential has no analog in ordinary quarkonium. As a consequence, the spin symmetry is broken more strongly in hybrids than in quarkonia.

The spatial and charge-conjugation parity of a hybrid read

$$P = (-1)^{L+K}, \qquad C = (-1)^{L+S+1}, \tag{34}$$

for a chromomagnetic gluon ($L_g = K$), and

$$P = (-1)^{L+K+1}, \qquad C = (-1)^{L+S+1}, \tag{35}$$

for a chromoelectric gluon ($L_g = K \pm 1$), where L_g is the relative angular momentum between the heavy quark-antiquark pair and the gluon, K is the total angular momentum of the gluon, L is the orbital angular momentum of the quark-antiquark pair, and S is the spin of the quark-antiquark pair. Hybrids with a chromoelectric gluon couple strongly to pairs of S-wave heavy-light mesons and, as a result, they become very broad and cannot be observed as resonances [460]. In the following, we will stick, therefore, to hybrids with a chromomagnetic gluon.

For hybrids with a chromomagnetic gluon (that is, a 1^{+-} gluon), if the heavy quark-antiquark pair is in an S-wave spin-singlet state ($S = L = 0$) and $L_g = K = 1$, then, according to Eq. (34), the quantum numbers are 1^{--}, that is, the hybrid is a vector state. If, on the contrary, the $Q\bar{Q}$ pair is in an S-wave spin-triplet state, then the hybrid may have the quantum numbers $J^{PC} = J^{-+}$ with $J = 0, 1, 2$; hence the quantum numbers include the exotic 1^{-+}. These states constitute the so-called H_1 multiplet and are (approximately) degenerate — see Table 12. This pattern of (approximate) degeneracies has been confirmed by model calculations, effective field theory analyses, and lattice simulations. Similarly, the binding of a chromomagnetic gluon with a P-wave heavy quark-antiquark pair ($L = 1$) with the quantum numbers $\{1^{+-}, (0, 1, 2)^{++}\}$ (corresponding to different spin states) gives hybrids with the quantum numbers of the $H_2 \cup H_3 \cup H_4$ multiplets — see Table 12. This (approximate) degeneracy pattern is specific of the constituent gluon picture [192, 469]. Different (approximate) degeneracy patterns show up in different approaches. We will discuss the degeneracy pattern emerging in the Born–Oppenheimer effective field theory approach in Sec. 4.4.4.

Due to the symmetry of the wave function, it was found that a selection rule exists that suppresses the decay of the vector hybrid with a chromomagnetic gluon into a pair of S-wave heavy-light mesons in the final state [188, 460, 480, 481]. Similarly to the case of ordinary quarkonia, but in the constituent gluon model, the relative strength of the strong decays of hybrids into one S-wave and one P-wave heavy-light meson has been estimated in the heavy-quark limit and the corresponding spin-recoupling coefficients have been computed [465]. Although the heavy-quark symmetry is not exact for the c and b quarks and, therefore, its predictions cannot be treated as exact results, nevertheless these recoupling coefficients set a particular pattern for the open-flavor decays of the hybrids. Transitions from hybrids to quarkonia have been considered in non-relativistic effective field theories that by construction implement the heavy quark symmetry [193]; these transitions will be reviewed in Sec. 4.4.4.

A comment on the P-wave positive-parity D_J (B_J) mesons is in order here. In the strict heavy-quark limit, the quadruplet of such P-wave heavy-light mesons turns to a pair of doubly degenerate states, P_j, with $j = 1/2$ or $j = 3/2$ being the light quark total angular momentum. Since the $P_{1/2}$ and $P_{3/2}$ mesons decay via pion emission to lower-lying heavy-light mesons in the S-wave and in the D-wave, respectively, the $P_{1/2}$ mesons appear to be much broader than the $P_{3/2}$ ones. This makes it hardly feasible to identify experimentally either of the two $P_{1/2}$ quadruplet members (D_0 and D_1 in the c-sector and B_0 and B_1 in the b-sector) in the final state, while this is possible for the other two members of the P-wave quadruplet (D_1 and D_2 in the c-sector and B_1 and B_2 in the b-sector). Then, since the most prominent decay channels of the $D_1(2420)$ and $D_2(2460)$ are the $D^{(*)}\pi$ modes, the open-flavor decays of the vector charmonium hybrid should be saturated by $D^*\bar{D}^{(*)}\pi$ final states. The situation with bottomonium hybrids is similar. At this point, it is instructive to compare the production of a heavy-light meson from the $P_{3/2}$ doublet accompanied by an S-wave meson in the decays of ordinary quarkonia and hybrids. Such a production is only possible if the produced light-quark pair has total angular momentum equal to 1. This condition cannot be fulfilled in the vector quarkonium decay, as in this case $j_{q\bar{q}} = 0$. Therefore, the amplitude for the quarkonium decay into such a final state vanishes in the strict heavy-quark limit [353, 482]. Instead, open-flavor decays of $(Q\bar{Q}g)$ hybrids proceed through the gluon conversion into a light quark-antiquark pair, which, therefore, carries the angular momentum of a vector, $j_{q\bar{q}} = 1$. This implies that there is no suppression of the amplitude for the vector hybrid decay into one S-wave and one $P_{3/2}$-wave open-flavor meson.

The heavy-quark limit is not exact in QCD. Beyond this limit, one needs to take into account corrections controlled by the ratio Λ_{QCD}/m_h, which may be sizeable in the charm sector. In particular, the physical P-wave heavy-light mesons come not as pure $P_{1/2}$ and $P_{3/2}$ states, but as mixtures governed by a mixing angle θ. The probability of the decay of an ordinary quarkonium into a final state containing one S-wave and one narrow P-wave open-flavor meson is proportional to $\sin^2 \theta$, while the same probability for the hybrid is proportional to $\cos^2 \theta$. The heavy-quark selection rule manifests itself in the data if $\theta \ll 1$. Recent estimates of the mixing angle θ in the charm and bottom systems can be found, for instance, in Ref. [466]. They show that, at least in the bottomonium sector, the heavy-quark selection rule may indeed allow one to distinguish hybrids from conventional quarkonia.

The heavy quark-antiquark pair ($Q\bar{Q}$) in a hybrid is dominantly in a color-octet state, while in an ordinary quarkonium it is dominantly in a color-singlet state. This observation leads to one more prediction for the decays of hybrids: since the color-octet quark-antiquark pair cannot annihilate into a photon, which would eventually convert into a lepton pair, the leptonic width of hybrids has to be small and, in particular, hybrids should not be seen as an enhancement in the R-ratio scan.

For what concerns hidden-flavor decays of hybrids, they can happen according to the following scheme:

$$(Q\bar{Q})_8 g \quad \begin{array}{l} \nearrow (Q\bar{Q})_1(gg) \rightarrow (Q\bar{Q}) + \text{light hadrons} \\ \searrow (ng) \rightarrow \text{light hadrons}, \quad n \geqslant 2 \end{array}, \tag{36}$$

that is, the quark-antiquark pair inside the hybrid, either converts from the color-octet state into a color-singlet one by emitting a gluon, g, or it annihilates completely into gluons. Then the gluons convert into light hadrons. In the former case, the hybrids hidden-flavor decays populate final states with hidden flavor, which may provide a clear experimental signal [483]. In the latter case, final states not containing heavy quarks are enhanced [484]. See also Ref. [485] for further details on the experimental signatures and search strategies for charmonium hybrids in B-meson decays. Various estimates of the hybrid production probability in such decays can be found in Refs. [485, 486]. In particular, it is argued that the hybrid production probability is $\approx 10^{-3}$-10^{-2}, which lies in the same ballpark as the production probability of conventional quarkonia.

• *The ψ(4230) aka Y(4230)*

Among the exotic *XYZ* states the most prominent candidate for a hybrid is the *Y*(4230) [the literature often refers to ψ(4260) aka *Y*(4260), however, the most recent BESIII data shows that the mass of the state needs to be lower — compare the discussion in Sec. 3.1.2], as it shows some features expected for a charmonium hybrid. To begin with, it has a mass [6],

$$M = (4230 \pm 8) \text{ MeV},\tag{37}$$

close to the theoretical predictions discussed above — see Table 10 and the discussion in Sec. 4.4.4, in particular Fig. 89 — and, what is more important, there are indications that it has a decay pattern that is not typical of conventional quarkonia but specific of hybrids. Indeed, the ratio $R = \sigma(e^+e^- \to \text{hadrons})/\sigma(e^+e^- \to \mu^+\mu^-)$ has a dip in the energy region around the mass 4230 MeV. Besides, measurements of the electronic width of the *Y*(4230) give small values [6] in agreement with the expectations for hybrids. Furthermore, one can see a pronounced dip in the cross sections of the e^+e^- annihilation into open-charm final states — see, for example, Fig. 74 for the most recent data from the Belle Collaboration [487]. Also, the expectation, discussed above, that the open-flavor decays of the charmonium hybrid should populate the three-body $D^*\bar{D}^{(*)}\pi$ final states is in line with the recent BESIII data — see Fig. 26. Thus, the *Y*(4230) could be a hybrid charmonium with a spin 1 [187, 192] or spin 0 [188, 465] $c\bar{c}$ core, or a mixture of both.
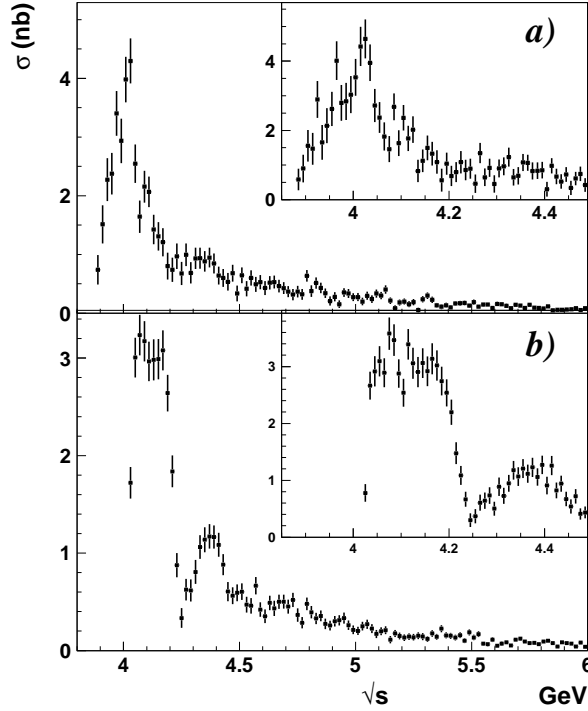
Figure 74: Recent results from the Belle Collaboration [487] on the e^+e^- annihilation into the $D\bar{D}^*$ (a) and $D^*\bar{D}^*$ (b) final states via ISR using a 951 fb^{-1} data sample.

It should be mentioned, however, that there exist alternative explanations for the established properties of the *Y*(4230). In particular, nontrivial structures in the shape of the inclusive and exclusive cross section can be explained by unitarisation effects — see, for example, Ref. [488]. Also, the proximity of the *Y*(4230) mass to the $D\bar{D}_1$ threshold hints to a large admixture of the molecular component in the wave function. Then, the experimentally observed enhancement in the three-body final state $D\bar{D}^*\pi$ just above the c.m. energy of 4.2 GeV — see Fig. 26 — is naturally explained by the dominating decay chain for the molecule, $Y(4230) \to D\bar{D}_1 \to D\bar{D}^*\pi$. A detailed discussion of the experimental situation is given in Sec. 3.1.2, and further details of the molecular model for the *Y*(4230) are collected in

Sec. 4.3.4. Finally, it is possible that a realistic picture of the $Y(4230)$ might require that both hybrid and quarkonium (short-range), and molecular (long-range) components coexist in the wave function.

4.3.2. Hadroquarkonium

Triggered by the experimental fact that all the candidates for heavy exotic states were discovered in final states that contain a quarkonium and light quarks, in Ref. [489] it was proposed that those states could be viewed as a compact quarkonium core surrounded by an excited light-quark cloud. Later the idea was worked out in depth in Ref. [190]. This structure naturally explains that in the decay the compact core simply stays intact while the light-quark cloud gets radiated off in terms of multipion states. The core and the cloud are held together by the QCD analogue of the Van der Waals force known from molecular physics (for recent studies, see [490, 491]). In Ref. [190] this picture is applied to the $\psi(4260)$ aka $Y(4260)$ [8], $\psi(4360)$ aka $Y(4360)$, $\psi(4660)$ aka $Y(4660)$ and $Z_c(4430)$. In Ref. [492] the hadrocharmonium picture is contrasted with the molecular picture for the $Z_c(3900)$. This mechanism provides a natural explanation why states like $Y(4260)$ do not decay to $D^{(*)}\bar{D}^{(*)}$ as the lower-lying vector states. Note that only the latter decay pattern is in line with the predictions from the quark model. The hadroquarkonium picture makes distinct predictions for both decay patterns and spin-partner states. Because of the heavy-quark symmetry, states with the same light-quark cloud, but the heavy-quark spin coupled differently, should be degenerate, up to terms suppressed by powers of $\Lambda_{\rm QCD}/m_h \ll 1$, where m_h denotes either the charm or the bottom mass. This also implies that the spin of the heavy quarks is conserved in decays. For a more detailed discussion of the heavy-quark symmetry as well as the symmetry breaking terms we refer to Sec. 4.4.1.

The effective Hamiltonian underlying the concept of hadroquarkonium is given by the leading term of the QCD multipole expansion:

$$H_{\rm eff} = -\frac{1}{2}\alpha^{(\bar{Q}Q)}E_i^a E_i^a \,, \tag{38}$$

where $\vec{E}^a$ is the chromoelectric field with color index a and $\alpha^{(\bar{Q}Q)}$ is the chromo-electric polarizability of the $\bar{Q}Q$ state. One may write

$$\alpha^{(\bar{Q}Q)} = \frac{1}{16}\langle(\bar{Q}Q)|\xi^a r_i \mathcal{G} r_i \xi^a|(\bar{Q}Q)\rangle \,, \tag{39}$$

where ξ^a denotes the difference of the color generators acting on the quark and the antiquark, and r_i denotes their relative position. The Green's function $\mathcal{G}$ describes the propagation of the heavy quark pair in the color octet. As pointed out in Ref. [190] this structure suggests that the most likely hadroquarkonia should emerge for higher charmonium resonances such as $\psi(2S)$ and χ_{cJ} in conjunction with some excited hight quark cloud.

To investigate the phenomenological implications of the Hamiltonian quoted above, we start with discussing the properties of $Z_c(3900)$ that would emerge if this state were a hadrocharmonium, in particular a J/ψ core surrounded by a light-quark cloud. Here we largely follow Ref. [492]. In this picture the $Z_c(4430)$ seen in the $\psi(2S)\pi$ final state can be viewed as a radial excitation of the $Z_c(3900)$ in the same way as the $\psi(2S)$ is the first excited state of the J/ψ. Spin interactions scale with the inverse of the heavy-quark mass such that the spin of heavy quarks is conserved at least in the limit of infinitely heavy quarks. For the system at hand this implies that the $Z_c(3900)$ should be found only in final states with heavy-quark spin equal to 1. This is in conflict with the presence of a $Z_c(3900)$ signal in the πh_c final state, see inset in the left panel of Fig. 55. Moreover, in this picture one should expect the decay of the $Z_c(3900)$ into open-flavor two-meson states to be suppressed compared to the decay into $\pi J/\psi$. However, this is also not the case. Thus, one needs to conclude that the $Z_c(3900)$ does not qualify as a state with a dominant $\pi J/\psi$ component.

The second example we want to discuss is the $Y(4260)$ and $Y(4360)$. Originally they were proposed to be hadrocharmonium states with a scalar-isoscalar cloud and a J/ψ and $\psi(2S)$ core, respectively [190], since they were observed in the corresponding $c\bar{c}2\pi$ final states. A model calculation performed in Ref. [494], where a state near the mass of the $Y(4260)$ emerges from non-perturbative $f_0(980)J/\psi$ interactions [9] supports this picture. However, recently the two states were also seen in the $\pi\pi h_c$ final state with a comparable rate [159] (c.f. Fig. 23), which would imply a significant amount of spin-symmetry violation if the picture mentioned above were right. To explain the simultaneous

---

[8]Although there is now striking evidence that the $Y(4260)$ is to be identified with the $Y(4230)$, in this paragraph we stick to the old mass value to keep closer contact to the connected publications.

[9]In this work, the system is treated as a three-body system with the $\pi\pi - K\bar{K}$ system interacting with the J/ψ.
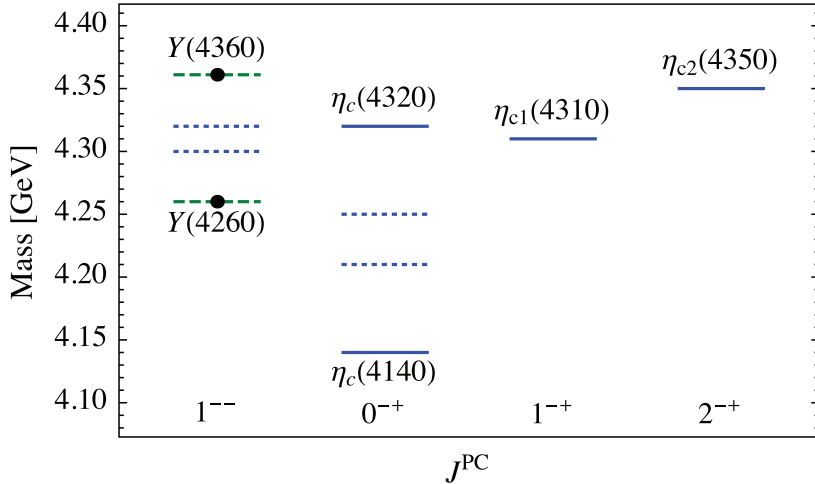
Figure 75: Family of spin partners of the $\psi(4260)$ aka $Y(4260)$ and $\psi(4360)$ aka $Y(4360)$ that should exist [493], if both states qualify as mixed hadrocharmonia as proposed in Ref. [191]. The short dashed lines show the seed states and the (green) long dashed lines show the masses used as input. The (blue) solid lines then show the predictions that emerge from imposing spin symmetry.

observation of $Y(4260)$ and $Y(4360)$ in final states with heavy-quark spin equal to 1 and 0, in Ref. [191] it was proposed that both states are mixed hadrochamonia from two different seeds: One that contains a $J^{PC} = 1^{--}$ charmonium core [to be identified with J/ψ or $\psi(2S)$ or a mixture thereof with the latter being prominent] surrounded by a 0^{++} light-quark cloud and one that contains a 1^{+-} charmonium core [to be identified with $h_c(1P)$] surrounded by a 0^{-+} light-quark cloud. In Ref. [191] it is shown that such an assignment allows one to at least qualitatively describe the data in the $\pi\pi J/\psi$, the $\pi\pi\psi(2S)$ as well as the $\pi\pi h_c$ final states, if the seed states are located at 4.30 and 4.32 GeV, respectively. While this mass difference is quite small, it is stressed in Ref. [191] that there is nothing that prohibits such a near degeneracy. In Ref. [493] it was pointed out that the mixing scheme just described allows one to predict four spin-partner states of $Y(4260)$ and $Y(4360)$: One simply has to replace the cores of the seed states by their respective spin-partner states. Accordingly, $\psi(2S)$ needs to be replaced by $\eta_c(2S)$ giving rise to a state with η_c quantum numbers when being paired with the 0^{++} cloud and h_c needs to be replaced by the triplet of $\{\chi_{c0}, \chi_{c1}, \chi_{c2}\}$ giving rise to states with quantum numbers of η_c, η_{c1} and η_{c2}. Naturally, the two η_c states will mix in the same way as their vector partners. The pattern that emerges is shown in Fig. 75. As a special feature, the scheme predicts with $\eta_c(4140)$ a relatively light η_c state that should not decay to $D^*\bar{D}$ but predominantly $\pi\pi\eta_c$ and $\pi\pi\chi_{c0}$. This highly nontrivial prediction awaits its experimental confirmation or refutation. Note that in the molecular as well as in the compact tetraquark picture the lightest 0^{-+} state is located in mass above the $Y(4260)$ as will be explained in detail in Secs. 4.3.3 and 4.3.4.

The $Y(4660)$ with quantum numbers 1^{--} is seen in the $\pi\pi\psi(2S)$ final state and is therefore a candidate for a hadrocharmonium with a 0^{++} light-quark cloud surrounding a $\psi(2S)$ core [190]. In addition, the mass of the $Y(4660)$ is very close to the threshold for the production of $f_0(980)\psi(2S)$ which led the authors of Ref. [209] to propose that the state is a $\psi(2S) - f_0(980)$ molecular state — note that in all previous cases the quarkonium–light-quark resonance threshold was far below the mass of the state such that in those cases a molecular assignment cannot be applied. The implications of spin symmetry are the same as before: If the $Y(4660)$ has a prominent $f_0(980)\psi(2S)$ substructure, there should exist a spin partner, Y_η, with similar properties as the $Y(4660)$ and $f_0(980)\eta_c(2S)$ as a prominent component [210] — this should be true in both pictures if we call the state a molecule or a hadrocharmonium, however, so far experimental searches for this state were not successful — see the discussion in Sec. 3.1. Note that the enhancement seen in $\Lambda_c\bar{\Lambda}_c$ at 4630 MeV is consistent with originating from the $Y(4660)$ [207, 208, 495].

Very recently, Ref. [287] proposed that the two charged states $Z_c(4100)$ and $Z_c(4200)$ claimed in Refs. [262] and [261], respectively, are hadrocharmonia (the experimental evidence is shown and discussed in Sec. 3.2.2). The analysis presented in this work is very similar to the one discussed in the previous paragraph, only that here at least evidence for the pair of spin-partner states is already found: The $Z_c(4100)$ is proposed to be a hadrocharmonium with

an η_c core and the $Z_c(4200)$ to have a J/ψ core — both with a light-quark cloud with pion quantum numbers. A typical prediction that emerges from this assignment is for the productions (around the same invariant mass as the resonances)

$$\frac{\Gamma[B^0 \to Z_c(4100)^- K^+]}{\Gamma[B^0 \to Z_c(4200)^- K^+]} \approx \left.\frac{\Gamma[B^0 \to \eta_c \pi^- K^+]}{\Gamma[B^0 \to J/\psi \pi^- K^+]}\right|_{M(c\bar{c}\pi) \approx M(Z_c)} \tag{40}$$

and for the decays

$$\Gamma[Z_c(4100) \to \eta_c(2S)\pi] \simeq \Gamma[Z_c(4200) \to \psi(2S)\pi] \,, \tag{41}$$

up to spin-symmetry-violating corrections. If this prediction were confirmed experimentally, it would provide strong evidence for the mentioned hadrocharmonium assignment of both $Z_c(4100)$ and $Z_c(4200)$.

4.3.3. Compact tetraquarks

Sometimes the term tetraquark is used generically for all states containing four constituent quarks irrespective of their clustering. In the older literature multi-quark states containing diquarks (a quark–quark pair) and anti-diquarks (an antiquark–antiquark pair), as subclusters were sometimes called "diquonium" [8, 9]. However, in line with the recent literature on the XYZ states, in this review, we use the term "compact tetraquark" to refer to multiquark states that show this kind of clustering. It should be stressed that so far no mechanism is identified in QCD that would lead to such clusters — this issue is discussed a little more in the following paragraph; for a more general discussion of four-quark states we refer to Ref. [11] and references therein. The first microscopic model working with diquark degrees of freedom was presented by Jaffe in 1976 [496] at that time focussing on light quarks. For a pedagogical introduction to the subject of diquark clustering we refer to Ref. [497] and for a recent book see Ref. [498]. Heavy-light diquarks were first discussed in Ref. [285]. A comprehensive discussion of further developments of these ideas and their application to the spectrum of the *XYZ* states can be found in a recent review [499]. In this review we will focus on the results that were later developed on the basis of this work. Results for compact tetraquarks obtained in the quasipotential quark model described in Sec. 4.2 can be found in Refs. [107, 500–503].

A pair of quarks can be either in the [$\bar{\mathbf{3}}$] or in the [$\mathbf{6}$] representation of the color group. There is phenomenological evidence that the former configuration is more tightly bound — for example, the one-gluon exchange is attractive in the [$\bar{\mathbf{3}}$] but repulsive in the [$\mathbf{6}$]. Accordingly, the latter is neglected in many works, although the [$\mathbf{6}$] may play an important role considering the findings of, e.g., Refs. [504, 505] for multiheavy systems, which put into question the emergence of compact diquarks as building blocks of compact hadrons.

Usually it is found that the spin-zero diquarks are more tightly bound in both the light-quark sector [496][10] as well as in the heavy-quark sector [508]. In the latter case the two spin configurations form a spin doublet in analogy to, e.g., D and D^* or B and B^*. It is therefore reasonable that the mass difference between spin-1 and spin-0 cq-diquarks, where c (q) denotes the charm (a light) quark, is within 120 MeV [189], fixed to the mass difference of $Z_c(3900)$ and $Z_c(4020)$, found to be of the order of the D-D^* mass difference. In Ref. [189] it is argued that this phenomenology follows from the condition that the spin-spin interaction is operative predominantly inside the diquarks (driving the mentioned mass difference) and not between the light quarks as assumed originally [285]. For this to happen it appears necessary that the diquark and the antidiquark do not come too close. Therefore in Ref. [509] an idea put forward in Ref. [497] was adapted to quarkonium-like states, namely that they are sitting in distinct wells of a double-well potential as shown in Fig. 76. The emerging structure is characterized by two length scales, the diquark radius, R_{Qq}, as well as the tetraquark radius, R_{4q}. In Ref. [509] it is claimed that a sensible phenomenology emerges when $R_{Qq} \ll R_{4q}$ — as possible values $R_{Qq} \sim 0.7$ fm and $R_{4q} \sim 2$ fm are advocated. Besides providing a reason for the hierarchy of the spin interactions, the potential of Fig. 76 can also provide a reason why exotics typically prefer to decay into pairs of open-flavor mesons instead of a quarkonium and a light meson as will be discussed in a little more detail below. So far, however, no mechanism was proposed that could explain the emergence of a potential of the type of Fig. 76. Its existence emerges as a phenomenological necessity to justify the diquark picture. An alternative approach trying to justify the emergence of compact diquark building blocks in compact tetraquarks was proposed in Ref. [510] and applied in Refs. [202]. However, since the emerging phenomenology of the two approaches is similar, we are reviewing here the research focussed around the work [509] by Maiani et al.

---

[10]Nevertheless also the spin-1 diquarks are found to contribute considerably, e.g., to the binding of light baryons [506, 507].
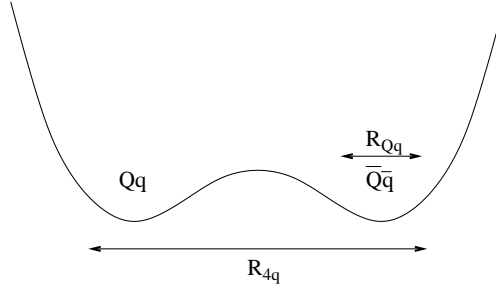
Figure 76: Proposed potential between a diquark and an antidiquark forming a compact tetraquark [509]. Here R_{Qq} denotes the size of the diquark while R_{4q} stands for the size of the whole tetraquark.

The assumption that the spin-spin interactions are active only within the diquarks and not between the light quarks influences significantly the decays of compact tetraquarks. In particular, since the heavy-quark spins within the compact tetraquarks turn out not to be correlated with each other, decays into both spin-1 and spin-0 quarkonia are allowed [189] — in line with observations. The same mechanism is at work in the molecular model described in the next section.

Furthermore it turns out that a spin-tensor force needs to be included into the Hamiltonian to avoid the appearance of the light high-spin states found in Ref. [493]. The Hamiltonian then reads [508]:

$$2m_Q + \frac{B_Q}{2}\boldsymbol{L}^2 + 2a_Y \boldsymbol{L} \cdot \boldsymbol{S} + \frac{b_Y}{4} S_{12} + 2\kappa_{Qq}\left(\boldsymbol{S_q} \cdot \boldsymbol{S_Q} + \boldsymbol{S_{\bar{q}}} \cdot \boldsymbol{S_{\bar{Q}}}\right) , \tag{42}$$

where S_{12} is the tensor operator $S_{12}/4 = 3(\boldsymbol{S_1} \cdot \hat{\boldsymbol{r}})(\boldsymbol{S_2} \cdot \hat{\boldsymbol{r}}) - (\boldsymbol{S_1} \cdot \boldsymbol{S_2})$, $\boldsymbol{S} = \boldsymbol{S_1} + \boldsymbol{S_2}$, with $\boldsymbol{S_1}$ and $\boldsymbol{S_2}$ the spins of the diquark and the antidiquark, respectively, $\hat{\boldsymbol{r}} = \boldsymbol{r}/r$ is a unit vector pointing along the radius vector, Q is the heavy quark flavor and q the light quark one. The tensor operator gives a nonvanishing contribution only for states with $S_2 = S_1 = 1$. Moreover, the terms that contain the angular momentum operator contribute only for $L \neq 0$.

The parameters in Eq. (42) are fitted to the data. To do so, one has to establish which observed exotic candidate (see Sec. 3) should be identified with which compact tetraquark. The positive-parity compact tetraquarks that emerge from the picture sketched above are discussed in some depth in Ref. [189]. In particular, using the mass difference of $Z_c(3900)$ and $Z_c(4020)$ as input allows the authors to fix $\kappa_{Qq} = 67$ MeV. In this paper, also states with 0^{++} and 2^{++} are predicted, however, those are almost 100 MeV away from the states observed with these quantum numbers.

Very interesting are the negative-parity states. In the compact tetraquark model those arise from two diquarks in a P-wave that have their constituents in a relative S-wave. Since the diquarks have either spin 1 or spin 0, in total four ground states are possible with $J^{PC} = 1^{--}$, namely $[0, 0]_0$, $[1, 0]_1$, $[1, 1]_0$, and $[1, 1]_2$, where the diquark spins are given in the bracket and the subscript denotes the total spin that resulted from their coupling. Note that $[1, 1]_1$ would produce the wrong C-parity. The preferred assignments of Ref. [508] for those four states are[11] $Y(4220)$, $Y(4330)$, $Y(4390)$, and $Y(4660)$ [12], since this pattern is consistent with the spin-spin interaction determined in the even-parity sector as well as an analysis of Ω_c states [508]. This is in contrast with the analysis of Ref. [189], where the $Y(4008)$ is taken as a genuine structure, which is not confirmed by the recent BESIII data, although the existence of a very broad state below 4.2 GeV can not be excluded (see Sec. 3.1.2). As will be explained below, the hadronic-molecule picture for the negative-parity states allows for only three ground states — thus a proper mapping of the singularity structure of the S–matrix should allow us to eventually decide how QCD structures its non-$Q\bar{Q}$ heavy mesons. Moreover, since now all parameters of Eq. (42) are fixed, it is straightforward to make predictions for negative-parity states with $J \neq 1$. The resulting spectrum is shown in Fig. 77. Clearly, Eq. (42) leads to a very rich and specific spectrum that contains

---

[11]We use here the names currently adopted by the Particle Data Group instead of those quoted in the original experimental works and in Ref. [508].

[12]As in the previous section also here we stick to the mass values used in the original publication although there is evidence that $Y(4330)$ and $Y(4390)$ could be realisations of $Y(4360)$.
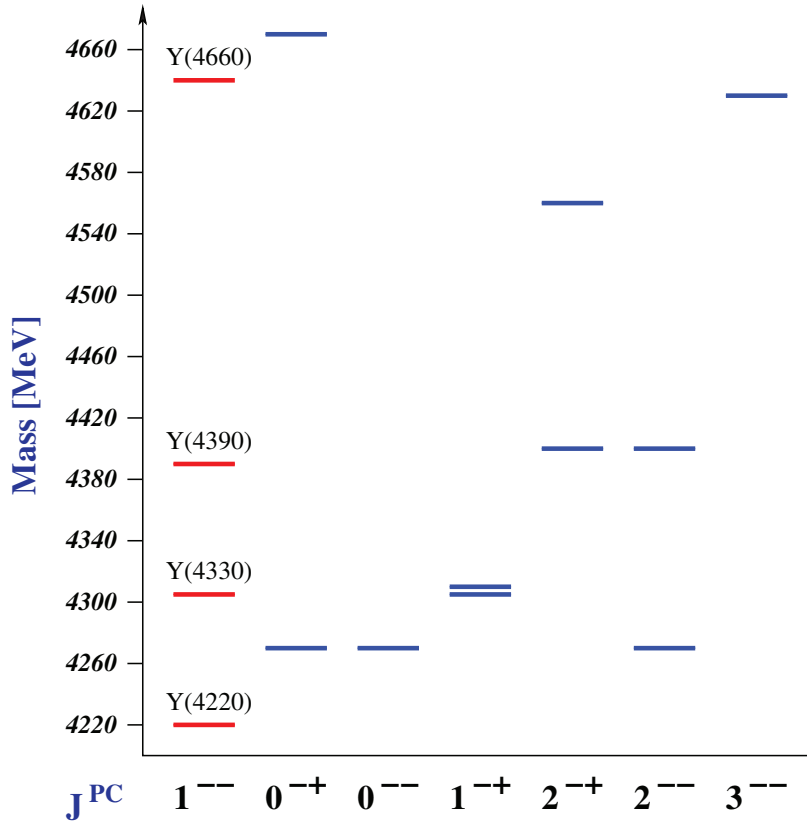
Figure 77: Spectrum of negative-parity compact tetraquarks according to the preferred solution of Ref. [508]. Note that 0^{--} and 1^{-+} are exotic quantum numbers that cannot be generated for $Q\bar{Q}$ states.

both quantum numbers that are allowed in the quark model and those that are not, like 0^{--} or 1^{-+}. This spectrum will be compared to what is expected for molecular states in the next section.

The compact tetraquark model is also capable of explaining some unexpected decay chains. For example, in the coupling scheme outlined above both the $Y(4360)$ as well as $X(3872)$ have the same heavy-quark spin structure $\sim (\bar{s} = 0, s = 1) + (\bar{s} = 1, s = 0)$, where $\bar{s}$ and s denote the spin of the antidiquark and the diquark, respectively, and thus a transition $Y(4360) \to \gamma X(3872)$ appears naturally as electric dipole transition [508]. On the other hand, this structure implies that the $Y(4360)$ has purely heavy-quark spin 1 and as such should not appear in the $\pi\pi h_c$ final state. Present data does not yet allow one to decide how many states there are in the mass region $4200 - 4400$ MeV with quantum numbers 1^{--} (see Sec. 3.1.2), however, upcoming data with improved statistics should eventually allow one to conclude whether the pattern presented is realised in nature.

Before closing this section, a few comments should be made about the decays of the compact tetraquarks. As outlined above, the candidates for exotic states typically decay to both open-flavor channels as well as hidden-flavor channels — e.g. $X(3872)$ is seen in $D^0\bar{D}^{*0}$ and amongst others in $\pi\pi J/\psi$, $3\pi J/\psi$, $Z_c(3900)$ is seen in $D\bar{D}^*$ as well as in $\pi J/\psi$, $Y(4230)$ is seen in $D\bar{D}^*\pi$ as well as in $\pi\pi J/\psi$, $Z_b(10610)$ is seen in $B\bar{B}^*$ as well as in $\pi\Upsilon(nS)$, and $\pi h_b(mP)$ and $Z_b(10650)$ is seen in $B^*\bar{B}^*$ as well as in $\pi\Upsilon(nS)$ and $\pi h_b(mP)$. Common to all these examples is that, although the open-flavor channels have a lot less phase space available, still the states decay predominantly into those. This is commonly taken as a strong indication for a molecular nature of these states, however, it may also be understood from the proposed diquark–antidiquark potential shown in Fig. 76, in which case a constituent of a diquark must tunnel

90

through the barrier to enable the decay. Since the tunnelling for heavy quarks is exponentially suppressed compared to that of the light quarks, the pattern described appears naturally [509].

In Ref. [511] it was found from an analysis of the $\pi\pi$ spectra from $e^+e^- \to \pi^+\pi^- J/\psi$ in the 4260 MeV mass range, that the source of the pion pair must contain a sizeable flavor-octet component. This observation is in line with a prominent molecular or compact tetraquark interpretation of the vector states in this mass range but poses a problem for their conventional $c\bar{c}$ or hybrid interpretation. The results of Ref. [511] could be confirmed if data became available also for $e^+e^- \to K\bar{K}J/\psi$.

An interesting ansatz to study compact tetraquarks is via the large N_c expansion first introduced by 't Hooft [512]. Under the assumptions that confinement survives the large N_c limit and that the strong coupling constant scales as $1/\sqrt{N_c}$ which provides a smooth limit for $N_c \to \infty$, rigorous conclusions about features of the QCD spectrum become accessible — e.g. in this limit there is an infinite tower of stable quark-antiquark pairs generated from an infinite sum of planar QCD diagrams. Until a few years ago there was the belief that all configurations that contain four or more quarks and survive the large N_c limit are just given by noninteracting multimeson states [513]. However, in 2013 this was questioned in Ref. [514]: There it was argued that *if* there are compact tetraquark poles present in the connected piece of the amplitude, they will also survive the large N_c limit, in particular with a width that decreases as N_c increases. This work initiated a series of publications — see, e.g., Refs. [515, 516]. In all those works the focus is still on planar diagrams. In contrast to this, Refs. [517, 518] argue that non-planar diagrams should be favored for providing the origin of very narrow compact tetraquarks. A recent critical reflection on the subject is in Refs. [519–521].

Recently the interest into $QQ\bar{q}\bar{q}$ tetraquarks, first studied in Ref. [504], has revived. There exist now studies from QCD sum rules [522] (see also Sec. 4.3.5), lattice QCD [523–525] (see also Sec. 4.5) as well as phenomenology [526–529]. Especially the last works employ the observation of doubly-heavy baryons to make predictions for doubly-heavy tetraquarks. The connection between these systems might be most compactly illustrated by the mass formula [529]

$$m(QQ\bar{q}\bar{q}) - m(QQq) \approx m(\bar{Q}\bar{q}\bar{q}) - m(\bar{Q}q) \,, \tag{43}$$

which is based on the quark-diquark symmetry, see also Sec. 4.4.1. This symmetry is realized in nature, if heavy diquarks form compact substructures in hadrons, for this would allow one to perform a systematic expansion in r_{QQ}/r_{qq}, where r_{qq} denotes the size of the light-quark cloud that may be estimated as $1/\Lambda_{\rm QCD}$. If r_{QQ}/r_{qq} is a small parameter, one may safely assume the QQ diquark to be in a color–antitriplet configuration, since for heavy quarks the QQ interaction should be largely governed by the one-gluon exchange, which is attractive only in this channel. Then Eq. (43) follows naturally. After the recent observation of the first doubly-heavy baryon [530], Eq. (43) might be also used the other way around to argue that if this (approximate) equality is not realized in nature, then QCD does not favor doubly-heavy compact diquarks. Therefore the experimental search for tetraquark structures should be performed with high priority at, e.g. Belle II and LHCb. In the bottomonium sector, the studies mentioned above find typically a deeply bound $bb\bar{u}\bar{d}$ system with $J^P = 1^+$ 100-200 MeV below the B^-B^{*0} threshold. The issue of multiquarks with two heavy quarks (in contrast to a heavy quark and its antiquark) is picked up again in Sec. 4.4.1 from the effective field theory perspective.

4.3.4. Hadronic molecules

Hadronic molecules are compound states of two hadrons. For a recent review on the subject we refer to Ref. [531]. The concept is nothing else but a generalisation of nuclei to systems of mesons. Accordingly one may derive some properties to be expected for hadronic molecules from those of light nuclei — because of this we start this section with a short review of few-nucleon systems.

It is widely accepted that nuclei are bound states of protons and neutrons. The lightest nucleus is the deuteron with a binding energy of $E_b(\text{deuteron}) = 2.22$ MeV, where $E_b(X) = m_1 + m_2 - M_X$, with m_i and M_X denoting the masses of the constituents and the mass of the state X, respectively. An important quantity for hadronic molecules is the so-called binding momentum,

$$\gamma = \sqrt{2\mu E_b}, \quad \mu = m_1 m_2/(m_1 + m_2), \tag{44}$$

which defines the size of the molecule since the large distance behaviour of a molecular state scales as $\exp(-\gamma r)$. At the same time γ is a measure of the typical momentum within the bound state. In the case of the deuteron one finds $\gamma = 45.7$ MeV. In other nuclear systems the corresponding number can be as small as 13 MeV — the Λ separation

energy of hypertriton is only $E_b = 130$ keV — and as large as the almost 200 MeV that is necessary to kick a single nucleon our of ^{4}He. Accordingly we should expect a similar range of binding momenta also for bound states of two mesons.

It should be noted, however, that while the analogy between nuclei and mesonic molecules is apparent within, e.g., potential models, it does not survive the large N_c limit: While nuclei should continue to exist in the large N_c limit [513], since a baryon contains N_c quarks and this adds to the multiplicity of the possible diagrams, mesonic molecules will most probably not [532].

In general, the internucleon interaction is the strongest in the S-waves, since S-waves do not have a centrifugal barrier (see, for example, the discussion in the beginning of section 4). Indeed, the deepest nuclear bound states that appear (if allowed by the Pauli principle) are S-wave ones. Therefore, in this section we will mainly focus on mesonic systems in the S-wave. However, also P-wave bound states are possible. For example[13]: ^{6}Li is located 1.47 MeV below the deuteron-^{4}He threshold. It may thus be viewed as a deuteron-^{4}He bound state. The first negative-parity excitation of ^{6}Li is located 18 MeV above the ground state [533] — a number of the order of the energy difference between different nuclear shells. Having this said, it is certainly not straightforward to learn something about possible P-wave states in mesonic systems from their appearance in nuclei. We come back to the proposed P-wave hadronic molecules in the XYZ-family near the end of this section.

That heavy mesons should form bound states was proposed in Ref. [534] already in 1976. The assumed binding mechanism was the exchange of vector mesons. Later, in Ref. [535] similar conclusions were drawn from calculations using one-pion exchange for the potential. In particular, both calculations predicted that, for example, the $D\bar{D}^*$ system, where the $X(3872)$ was found in 2003, should bind.

The role of one-pion exchange to molecular binding is widely discussed in the literature. It was argued in Ref. [536] that the pion cut, if kinematically accessible, should be kept in the calculations. This issue is further elaborated in Ref. [537]. In Ref. [538], it is stressed that the one-pion exchange is well defined only when being accompanied with a local counterterm. Thus it is fair to state that at present little is known about the binding potential of hadronic molecules, if they exist[14]. However, as it will become clear below, many statements can already be made without detailed knowledge of the potential.

There is an intense discussion in the literature whether a bound state as shallow as the $X(3872)$ could be produced copiously in reactions with a large momentum transfer. One can find works that conclude from the observed rates that the $X(3872)$ cannot be a shallow bound state [536, 539–541], while others argue that as soon as final-state interactions are taken into account and proper momentum ranges are considered, there is no contradiction between a molecular nature of the $X(3872)$ and its production rates [542–547]. In this review we only state that at present there is no full understanding of the production rates of shallow molecular states.

Implications of the molecular scenario are contrasted with different quark model approaches in Ref. [548].

• *The Weinberg criterion and its implications*

In order to discuss the implications of the molecular nature for a given state, we first need to define the notion of a molecule. The most popular definition goes back to Weinberg who set up a scheme that allowed him to quantify the molecular component of the deuteron [549]. In particular, in his work Weinberg showed that the residue of a bound-state pole located close to a threshold could be written as[15], using the notation of Ref. [531],

$$\frac{g_{\text{eff}}^2}{4\pi} = 4M^2 \left(\frac{\gamma}{\mu}\right)(1 - \lambda^2),\tag{45}$$

where λ^2 denotes the probability to find a non-molecular component in the bound-state wave function, μ is the reduced mass of the nearby two-hadron channel, and M is the mass of the bound state. Weinberg also showed that λ^2 could be identified with the wave function renormalisation constant. In particular, the effective coupling of the bound state to the continuum gets maximal when the state is a pure molecule ($\lambda^2 = 0$). Since, for a shallow bound state, the

---

[13]C.H. is grateful to Andreas Nogga for providing him with valuable information on nuclear level schemes.

[14]Note that there are indications that one-pion exchange leaves some imprint in the line shapes of the Z_b states [300] as is detailed below.

[15]A simple straightforward derivation of this relation in a somewhat less general form was obtained eralier by L. Landau [550].
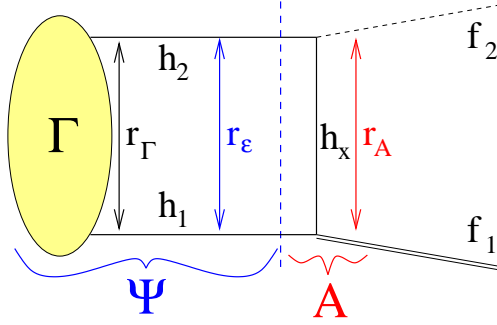
Figure 78: Illustration of the strong decay of a hadronic molecule, composed of two hadrons h_1 and h_2, into f_1 and f_2. The vertex for the transition of the molecule into its constituents is denoted by Γ, the corresponding wave function by Ψ, and the annihilation potential by A. Solid lines denote the propagation of the h_1, h_2 and the intermediate hadron h_x, whereas the double line and the dashed line denote the decay products f_1 and f_2.

low-energy scattering amplitude parameterised, for example, in terms of the scattering length and the effective range can be expressed in terms of g_{eff}, this coupling can be regarded an observable.

It is important to keep in mind, when it comes to identifying hadronic molecules, that only those observables are useful that are sensitive to the effective coupling defined in Eq. (45). If, for example, a reaction is sensitive to the short-ranged part of the wave function, no statement about the molecular admixture of the given state is possible. This observation, relevant for both the production of $X(3872)$ in large momentum transfer reactions as well as its radiative decays, will be discussed in more detail in Sec. 4.4.5.

Equation (45) acquires corrections of the order of (γ/β), where β is the mass scale of either the next higher channel or the inverse of the range of forces. Accordingly, the value of g_{eff} can only be used for shallow bound states. However, starting from Eq. (45) it appears justified to assume that a state with $\lambda^2 \to 0$ is characterised by a large effective coupling to the two-hadron channel that forms the molecule. As will be illustrated below, the prominence of these two-hadron channels has important phenomenological implications, even in cases where the quantitative connection of Eq. (45) is lost because of a too large binding momentum γ. Weinberg's argument was generalised to resonances in Refs. [551, 552]. Coupled channels are discussed in Ref. [553]. Some related ideas for inferring that a resonance in coupled-channel scattering is dominated by molecular configurations, based on the presence and position of poles on unphysical sheets, are discussed in Refs. [554–556].

The observation that in a molecular state the coupling to its constituents gets large has direct implications on how decays of molecules are calculated: The most natural decay chain runs via its constituents. Accordingly, it appears natural to calculate these decays in analogy to those of the positronium via a factorisation into the wave function at the origin times an on-shell annihilation amplitude. However, this ansatz is in general not justified [557] and a careful study of the scales involved appears to be necessary. Those are illustrated in Fig. 78: The length scale of the decay vertex is typically controlled by the mass of the lightest exchange meson that contributes to the molecular binding — thus we have $r_\Gamma \sim 1/\beta$ — and the size of the wave function is controlled by the binding momentum, as was explained above, $r_\epsilon \sim 1/\gamma$. The length scale r_A is controlled by either the cut $f_2 h_x h_1$ or the cut $f_1 h_x h_2$. For example, the former may be written as

$$r_A \sim \frac{1}{M - E_{f_2} - E_{h_x} - E_{h_1}} = \frac{1}{E_{f_1} - E_{h_x} - E_{h_1}},$$

where M denotes the mass of the molecular state and E_n denotes the energy of the state n. The aforementioned factorisation of the decay amplitude is justified only if $r_A \ll r_\epsilon$ and $r_A \ll r_\Gamma$. Such a hierarchy of scales holds, for example, for the positronium, where $r_\Gamma \sim r_\epsilon \sim 1/(\alpha_{\text{QED}} m_e)$ and $E_{f_1} \simeq E_{h_x} \simeq E_{h_1} \simeq m_e$, such that $r_A/r_\epsilon \simeq \alpha_{\text{QED}}$, where $\alpha_{\text{QED}} = 1/137$ is the electromagnetic fine structure constant. However, if the decay $f_1 \to h_x h_1$ is (nearly) allowed kinematically, r_A can become very large. In fact, by assumption we have a large r_ϵ since we study shallow bound states, and therefore $r_A \simeq r_\epsilon$ can even imply the proximity of a so-called triangle or Landau singularity [558] which can lead to a significant enhancement of the transition rates. We come back to this discussion in section 4.4.3. In a possible decay $X(3872) \to \pi^0 \chi_{cJ}$ which is of direct relevance for this review, the factorisation method is contrasted

93

with the full evaluation of the hadronic loop in Ref. [88]. The role of the triangle singularities in the decays of heavy quarkonium-like states is discussed in Ref. [341].

- *General considerations*

Before discussing examples of molecular candidates and some model descriptions for the *XYZ*-states, some general remarks are in order. First of all, it should be stressed that relatively narrow, shallow molecular states can only be formed from similarly narrow constituents, since the width of the molecular state is strongly correlated with the width of the constituents [559]. Stated differently, the constituents must be sufficiently long-living to allow the molecular state to form [560]. Focusing on states containing a $c\bar{c}$ pair and no strange quarks, this implies that only the ground-state spin doublet $\{D, D^*\}$, with the quantum numbers 0^- and 1^-, respectively, and the excited spin doublet $\{D_1, D_2\}$, with the quantum numbers 1^+ and 2^+, respectively, are of interest. The latter pair has a light quark with $j_l^P = 3/2^-$ that allows for a decay into $D^{(*)}\pi$ in the D wave only, which is the reason for their narrow widths of the order of 30 MeV. The other low-lying pair with positive parity, $\{D_0, D_1\}$ with quantum numbers 0^+ and 1^+, can decay to $D\pi$ in the S-wave, which explains their large widths of the order of 300 MeV. This width is too broad to allow $\{D_0, D_1\}$ to form molecular states. Accordingly we expect that molecular states with positive parity are significantly lighter than those with negative parity. The lightest negative-parity molecule can only be a $D_1\bar{D}$ bound state with quantum numbers $J^P = 1^-$. The nominal $D_1\bar{D}$ threshold is at $2420 + 1866 = 4286$ MeV and indeed, the lowest in mass candidate for an exotic vector state is $Y(4230)$, located only 50 MeV below this threshold — this connection was exploited for the first time in Ref. [185]. An additional consequence of assuming a molecular structure for the negative-parity exotic candidates is that the lightest exotic pseudoscalar needs to be heavier than the lightest vector by about the mass difference $M_{D^*} - M_D = 140$ MeV, since $J = 0$ can only be formed from $D_1\bar{D}^*$ and not from $D_1\bar{D}$. The resulting pattern of relevant thresholds is illustrated in Fig. 72. This figure clearly shows that, while all states below the lowest S-wave threshold for a the given quantum number show properties in line with the quark model, most of the exotic candidates occur close to or above the threshold.

The width of a constituent not only provides a natural scale for the width of the molecular state but it also has an impact on the line shapes of the molecule. Consider a decay chain of the resonance R containing an unstable constituent A, $R \to AB \to [cd]B$, and study the line shape in the channel cdB. The effect of the finite width of a molecular constituent on the resulting line shapes is exemplified in Fig. 79, where different line shapes are plotted for a pole located on the real axis 0.5 MeV below the AB threshold on the first (left panel) or second (right panel) sheet. The plots are generated for an additional width of 1.5 MeV, due to other decay channels of the resonance, employing the expressions of Ref. [561], which are applicable to narrow states (the formalism was generalised to allow for larger widths in Ref. [562]). The width assumed for the state A is 0, 0.1, and 1 MeV for the solid, dotted and dashed line, in order. A pole on the unphysical sheet can in general only show up as a structure at the nominal AB threshold or above. However, a pole on the physical sheet generates in addition to the AB continuum a structure in the data near the pole location, if sufficient strength from the finite width of the resonance A leaks there. In the inelastic channels, a pole on the physical AB sheet leads to a structure near the pole location, while a pole on the unphysical sheet gives also in this case a signal only at the nominal AB threshold.

The mass parameters of all Z states extracted in the experimental papers are above the corresponding continuum thresholds. However, this may in part be a consequence of parameter extractions using symmetric and energy-independent BW functions. For example, in Ref. [563] it was shown that the data existing at the time for the Z_b states were consistent with them being bound states. The more refined study of Ref. [299] identifies both states as virtual states. The inclusion of pion exchange non-perturbatively in the analysis leaves the pole of the $Z_b(10610)$ untouched within errors, while the pole related to the $Z_b(10650)$ might even be located slightly above the threshold [300]. Recent theoretical studies for the pole location of the $Z_c(3900)$ find that current data are also consistent with an above-threshold resonance [564] or a virtual state [565], however, in both cases the pole location is not well constrained.

- *Remarks on the role of the heavy-quark spin*

Four of the established charged states in the charmonium sector are prime candidates for hadronic molecules as was quickly recognised by many authors [110, 185, 566–569]. Indeed, they are located very close to S-wave thresholds of narrow resonances: The $Z_c(3900)$ lies at the $D^*\bar{D}$ threshold, the $Z_c(4020)$ is close to the $D^*\bar{D}^*$ one, the
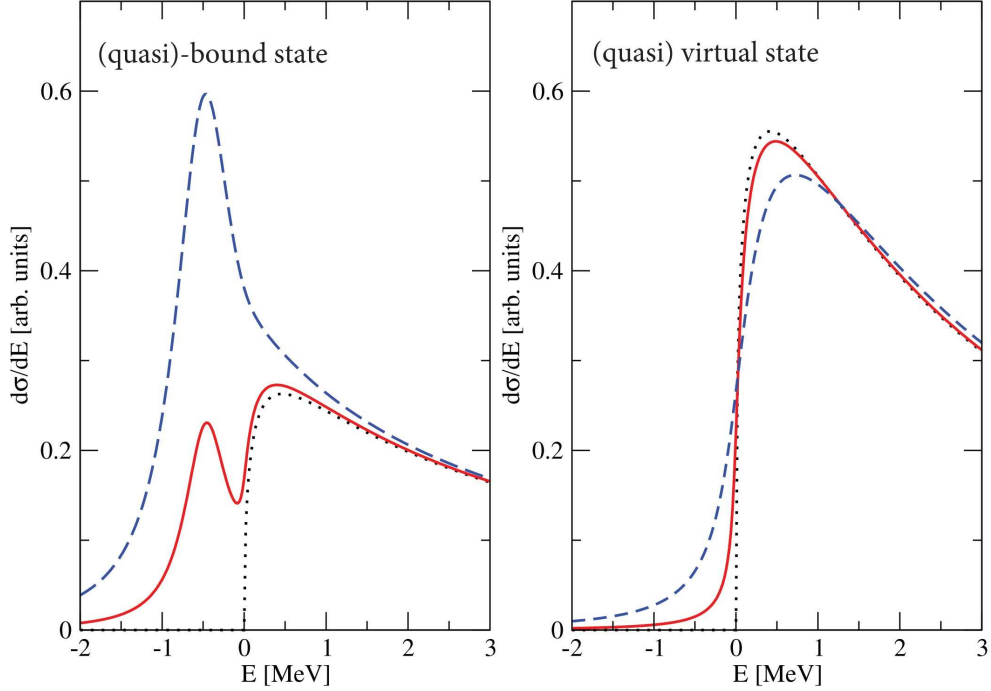
Figure 79: Line shapes for a quasibound (left panel) and virtual state (right panel) for different widths of one of the constituents: 0, 0.1, and 1 MeV as the dotted, solid, and dashed line in order. The mass of the state is 0.5 MeV below the threshold and an inelastic width of 1.5 MeV is added into the resonance propagator.

$Z_b(10610)$ and $Z_b(10650)$ reside near the $B^*\bar{B}$ and $B^*\bar{B}^*$ thresholds, respectively. For the Z_b states it is intriguing that they both are seen in three $\pi\Upsilon$ and two πh_b channels with a very similar strength in the two-pion transitions from the $\Upsilon(10860)$ bottomonium, although the initial state as well as the Υ's in the final states have a heavy-quark spin of 1 while the h_b's has a heavy-quark spin 0. This fact appears to be very unexpected since in heavy-quark systems the spin of the heavy quarks should be conserved given that spin-dependent interactions are suppressed as (Λ_{QCD}/m_h), where m_h denotes the heavy-quark mass (see Sec. 4.4.1). In addition, the interference patterns between the $Z_b(10610)$ and $Z_b(10650)$ appear to be different in the two types of channels: While in the former there appears to be a destructive interference between the two structures, it is constructive in the latter. Both features find a natural explanation if $Z_b(10610)$ and $Z_b(10650)$ are assumed to be $B^*\bar{B}$ and $B^*\bar{B}^*$ molecular states [566], for then one finds

$$Z_b(10610) \sim B^*\bar{B} - B\bar{B}^* = \frac{1}{\sqrt{2}}\left(0^-_{\bar{b}b} \otimes 1^-_{\bar{q}q} - 1^-_{\bar{b}b} \otimes 0^-_{\bar{q}q}\right),$$

$$Z_b(10650) \sim \quad B^*\bar{B}^* \quad = \frac{1}{\sqrt{2}}\left(0^-_{\bar{b}b} \otimes 1^-_{\bar{q}q} + 1^-_{\bar{b}b} \otimes 0^-_{\bar{q}q}\right). \tag{46}$$

For both states the first and second term in parentheses provide the coupling to the final state that contains h_b and Υ, respectively. An additional support for the molecular interpretation of all four Z's comes from the fact that they all decay, with a branching fraction larger than 80%, into the nearby open-flavor channel despite a very small phase space available in these decays while the phase space is wide open for their hidden-flavor channels. For a comparison of a molecular *versus* hadrocharmonium interpretation of the $Z_c(3900)$ we refer to Ref. [492].

If one admits that the charged states are good candidates for isovector hadronic molecules, it appears natural that there are also isoscalar hadronic molecules. Indeed, let us assume that the binding potential is provided by meson exchanges and that amongst those the most prominent one is an isovector meson exchange (this is an established picture for two-nucleon systems with the exchanged particle being the pion). For the exchange of such an isovector

particle between two isospin doublets the ratio of isospin factors of the isoscalar to the isovector channel is -3. An additional minus sign appears when switching the C-parity (clearly, for isovector states the C-parity is defined only for the neutral component). In particular, the picture just drawn would be consistent with a prominent isovector exchange potential if molecular states existed simultaneously in the $D^*\bar{D}$ system with $I = 0$ and $J^{PC} = 1^{++}$, and with $I = 1$ and $J^{PC} = 1^{+-}$. Furthermore, in this scenario there should not be any isovector (isoscalar) 1^{++} (1^{+-}) states. This naive pattern is in line with experimental observations. This is clearly different from the compact tetraquark picture, where each isoscalar state should be accompanied by its nearly degenerate isovector partner. However, this reasoning does not include that, e.g., pion exchange naturally provides large S-wave to D-wave transitions via its tensor force — as soon as those are included one-pion exchange can provide binding also in, e.g., isovector 1^{++} channels (see Refs. [570, 571] and the discussion in Sec. 4.4.5). In addition, the channel coupling driven by the tensor force of the one pion exchange also generates a transition of the $Z_b(10650)$ to the $B\bar{B}^*$ channel, which, however, is not seen in the data. It is shown in Ref. [300] that this transition is largely absorbed into a formally subleading counter term that needs to be promoted to leading order to render the calculation cut–off independent — this is discussed in some detail in Sec. 4.4.5.

The feature described above for the Z_b states, namely that molecules in the intermediate states evade the rule that the heavy-quark spin remains unchanged in a hadronic transition, is quite general. For example, in Ref. [482] the following decompositions of the above mentioned two-hadron states with the quantum numbers 1^{--} are given as

$$(D_1\bar{D} - \bar{D}_1 D) \quad : \quad \frac{1}{2\sqrt{2}}\psi_{11} + \frac{\sqrt{5}}{2\sqrt{2}}\psi_{12} + \frac{1}{2}\psi_{01}, \tag{47}$$

$$(D_1\bar{D}^* - \bar{D}_1 D^*) \quad : \quad \frac{3}{4}\psi_{11} - \frac{\sqrt{5}}{4}\psi_{12} + \frac{1}{2\sqrt{2}}\psi_{01}, \tag{48}$$

$$(D_1\bar{D} - \bar{D}_1 D) \quad : \quad \frac{\sqrt{5}}{4}\psi_{11} + \frac{1}{4}\psi_{12} - \frac{\sqrt{5}}{2\sqrt{2}}\psi_{01}, \tag{49}$$

where $\psi_{1J} = 1^{--}_{Q\bar{Q}} \otimes J^{++}_{q\bar{q}}$ and $\psi_{01} = 0^{-+}_{Q\bar{Q}} \otimes 1^{+-}_{q\bar{q}}$, where as before Q (q) denotes a heavy (light) quark. Accordingly, if there exist resonances generated as two-hadron states in these channels, one should expect a similar population for the final states with the total heavy-quark spin equal to 0 or 1. And indeed, in the mass range covered by the three corresponding thresholds, where at least three vector states[16], $Y(4230)$, $Y(4360)$ and $\psi(4415)$, coexist, one finds the $e^+e^- \to \pi\pi h_c$ cross section of the order of 60 pb and the $e^+e^- \to \pi\pi J/\psi$ cross section of the order of 80 pb — cf. Figs. 22 and 23. It should be stressed that those total cross sections have only a very small contribution from the Z_c states. Stated differently, the invariant mass spectrum that shows the Z_c states in the πh_c final state (cf. Fig. 55) shows also a strong non-resonant contribution. This is in contrast to the data on the Z_b's in the πh_b channels where the signal is resonant only which in the molecular picture is understood as a consequence of the large mass gap between the $\Upsilon(10860)$ and the first relevant two heavy-hadron S-wave threshold, $B_1\bar{B}$ at 11004 MeV.

Since in QCD the spin of the heavy quarks decouples from the interaction up to corrections of the order of $\Lambda_{\rm QCD}/m_h$, one can also predict spin partner states for hadronic molecules. It was stressed in Ref. [493] that the pattern of spin-symmetry breaking is very different between different models for the XYZ states. For example, to leading order in the $1/m_b$ expansion the Z_b-states and their spin partners form two multiplets: One doublet which contains the $J^{PC} = 1^{+-}$ state $Z_b(10650)$ and a 0^{++}, called W'_{b0}, and one quartet, which contains the $J^{PC} = 1^{+-}$ state $Z_b(10610)$ as well as the 0^{++}, 1^{++}, and 2^{++} states called W_{b0}, W_{b1}, and W_{b2}, respectively [567, 570, 572]. If one allows for spin-symmetry violation, whose leading effect for hadronic molecules is in this case driven by the B^*-B mass difference, the members of the multiplets follow the splitting of the thresholds — see Fig. 80. As soon as one–pion exchange is included, many additional partial waves need to be included in the calculation [573] since the tensor force provides strong S-D transitions. As a result of this, the spin-2 state acquires a width from the now allowed transition from $B^*\bar{B}^*(S\text{-wave}) \to B\bar{B}^{(*)}(D\text{-wave})$. Because of this additional transition there also appears a sizeable mass shift once pions are included. It was shown in Ref. [570] that the spectrum of spin partner states is very sensitive to the input masses used for the Z_b states. A more refined study using as input the masses determined directly from a fit to the Z_b

---

[16]Some analyses claim that even more are needed — see chapter 3.1.
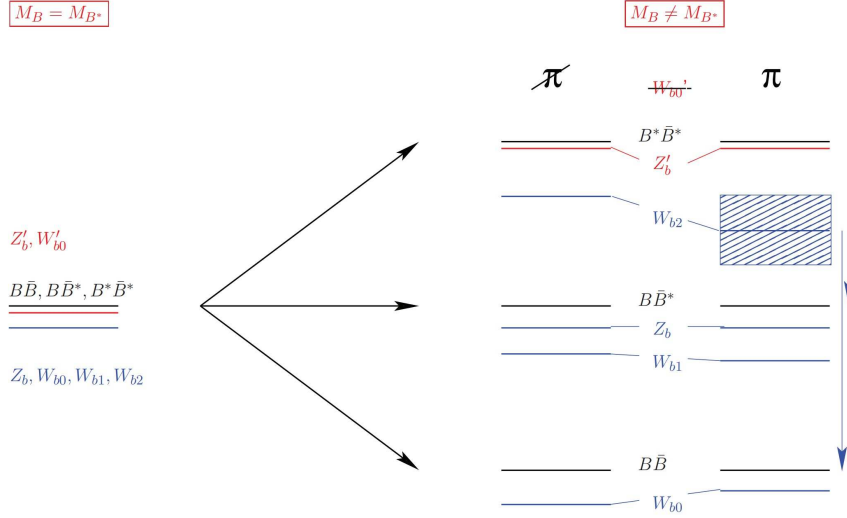
Figure 80: Sketch of the mass spectrum of $Z_b(10610)$ and $Z_b(10650)$ and their spin partner states in the spin-symmetric limit (left) and when the B^*-B mass splitting is included (right). In the latter case calculations with (marked by π) and without one-pion exchange (marked by $\not{\pi}$) in the potential are compared as detailed in the text. The results underlying the figure are from Ref. [570] based on the input masses for the Z_b states from Ref. [563].

line shapes is presented in Ref. [300] and will be discussed in more detail in Sec. 4.4.5. Moreover, the impact of the pions on the pole positions and the line shapes is important also for the spin partner states — in particular, while both Z_b's and their siblings W_{bJ} appear to be virtual states in the pionless theory, in the full EFT, including pions, most of these states turn to above-threshold resonances — see Ref. [571] for details.

A similar pattern of spin partner states is expected to also emerge in case of the isoscalar states in both the charm and the bottom sector. Thus, if the molecular picture is correct, then, in the strict spin-symmetry limit, the 1^{++} state $X(3872)$ should be a member of a multiplet together with one 1^{-+}, one 0^{++}, and one 2^{++} state. In addition, in this limit there could be a second multiplet with a 1^{-+} state and another 0^{++} state [574]. As mentioned above, the leading spin-symmetry-violating effect comes from the mass difference of the ground-state pseudoscalar and vector states, such that the interactions may be assumed spin symmetric. Still, to constrain all masses of the members of those multiplets, at least two states are needed as input. In Ref. [574] the masses of the $X(3872)$ and of the $X(3915)$, assumed to be a scalar $D^*\bar{D}^*$ molecular state, were employed, and, based on this, using a model with contact interactions only, in total four additional states were predicted. Note that an uncertainty estimate of these predictions is in general very difficult, since the $X(3915)$ is located 100 MeV below the relevant threshold and corrections to the pure contact interactions should be expected. However, it is interesting to observe that the spin partner of the $X(3872)$ with $J^{PC} = 2^{++}$ is generated from an interaction identical to that of the $X(3872)$ — thus, the small binding energy of this state with respect to the neutral $D\bar{D}^*$ threshold should directly translate to a small binding energy of the spin-2 state with respect to the $D^*\bar{D}^*$ threshold. This observation was confirmed by the explicit numerical calculations of Ref. [574]. Once one-pion exchange is included, transitions from the $D^*\bar{D}^*$ S-wave with spin 2 to the $D\bar{D}$ D-wave become possible which can lead to widths of a few MeV [575] to tens of MeV [573].

It is interesting to note that Refs. [574, 576, 577] all find a resonance with a mass about 3700 MeV that couples to $D\bar{D}$ strongly and is interpreted as a $D\bar{D}$ molecular state. Various reactions are proposed to look for this state, e.g. $e^+e^- \to J/\psi D\bar{D}$ [578] and radiative decays of heavier vector states [579]. While there are indications that this state might have left traces in the data, so far the analyses are not fully conclusive.

An SU(3)-flavor generalisation of the research of Ref. [574] is provided in Ref. [577]. Here the authors constrain the parameters by also investigating the decays of $X(3872)$ into $\rho J/\psi$ and $\omega J/\psi$, which constrains the isovector interaction, and propose that $X(4140)$ is a 0^{++} state (at the time of this work the Z_c states were not yet found). From this input they find that there should neither be a 1^{++} nor a 2^{++} isoscalar state with hidden strangeness. However, since

now the $X(4140)$ is established to be a 1^{++} state, this analysis should be redone. In contrast to Ref. [577], Ref. [580] finds a 2^{++} $D_s^* \bar{D}_s^*$ bound state at 4160 MeV, based on a similar construction but using vector-meson exchanges for the potential. Here more data, especially for states with different quantum numbers are needed before a clear theoretical understanding can emerge.

• $\chi_{c1}(3872)$ *aka X(3872) from a molecular perspective*

The probably most prominent example of a molecular state is the $X(3872)$, not only because its existence was predicted already in Refs. [534, 535] but also because its mass is incredibly close to the $D^0 \bar{D}^{0*}$ threshold. For a review with focus on the $X(3872)$ as a molecular state see Ref. [581]. Originally, the $X(3872)$ was claimed to be (predominantly) a bound state of $D^0 \bar{D}^{0*}$ [582, 583], which translates to an equal admixture of an isospin-1 and an isospin-0 component. However, this is at odds with experiments. From the first glance one might think that this is in line with the experimental observation that it decays at near equal rates into the $\rho^0 J/\psi$ and $\omega J/\psi$ final states (see section 3.1.1), the former having isospin 1, the latter isospin 0. However, this can only be understood, if the $X(3872)$ is predominantly an isoscalar state, since the formal $\rho^0 J/\psi$ threshold is located below the mass of the X while that of the $\omega J/\psi$ channel is 7 MeV above, which is almost as large as the width of the ω. Thus, the decay into the latter channel is heavily suppressed kinematically compared to that into the former, especially in light of the large width of the ρ^0 of the order of 150 MeV. Thus, had the $X(3872)$ been to 50% an isovector state it would have almost exclusively decayed into $\rho^0 J/\psi$. Moreover, it was shown in Ref. [584], and more recently in Ref. [585], that one can understand the apparent isospin violation in the $X(3872)$ decay quantitatively, if one considers in the decay the large isospin violation provided by the meson loops induced by a large coupling of the molecular state to the two–meson continuum according to Eq. (45): Meson loops in a relative S-wave show a strong mass dependence in form of a pronounced cusp structure exactly at the two–meson threshold, if there is a pole nearby (see Sec. 4.1). In isospin-violating transitions the loops in the neutral and the charged channel enter with a relative minus sign and equal coupling strength. Thus, if the masses of the meson pair in the two channels are equal, they cancel exactly as required by isospin symmetry. However, in reality the $D^\pm D^{*\mp}$ threshold is located 8 MeV above the $D^0 \bar{D}^{*0}$ threshold, which results in an enhanced isospin violation. A second argument in favor of a predominant isoscalar nature of the $X(3872)$ is given in Ref. [88], where it is shown that if there had been a sizeable $I = 1$ component in the wave function, then the $X(3872)$ should have copiously decayed into the $\pi^0 \chi_{cJ}$ channels — with the partial widths larger than the current upper limit of the $X(3872)$ total width. Finally, in Ref. [586] it is shown that a charged component in the $X(3872)$ is necessary to get a quantitative understanding of its radiative decays.

At present it is not known on which sheet the pole of the $X(3872)$ is located: It might be a shallow bound state (similar to the deuteron and hypertriton mentioned at the beginning of this chapter), which would imply a pole on the physical sheet, or a virtual state like the two-neutron state (or isovector nucleon-nucleon state), which would imply a pole on the unphysical sheet. It is generally believed that the latter scenario unambiguously points at a two-meson nature of the corresponding state. Unfortunately, an analysis of the currently existing data showed consistency with both scenarios [412, 561]. The latter reference stressed that in case of a bound state it is necessary to consider the width of the D^* meson and also provided analytic expressions for the resulting line shapes that can be used for narrow constituents. Since the width estimated for the neutral D^* is of the order of 0.1 MeV and the $X(3872)$ binding energy is 0.2 MeV or lower, one expects a structure below the $D^0 \bar{D}^{*0}$ threshold in the $D^0 \bar{D}^- \pi^+$ channel, if the $X(3872)$ is a bound state. This structure should be absent if the $X(3872)$ were a virtual state (cf. Fig. 79 and the corresponding discussion). If the transition rate $p\bar{p} \to X(3872)$ is large enough, there is hope that the PANDA experiment planned at the FAIR facility (see Sec. 5.1) could provide a direct measurement of this line shape. An alternative method to get high accuracy information of the pole location of $X(3872)$ has been provided recently based on the interplay of a triangle singularity and the corresponding pole [106] — this idea is discussed in more detail in Sec. 4.4.5.

• $\psi(4230)$ *aka Y(4230) as hadronic molecule*

Next we come back to the $Y(4260)$ and list some more properties that point at a $D_1 \bar{D}$ molecular nature of this state. The reasoning is based on the fact that a state that has a nearby two-hadron channel as its prominent molecular component will couple to it strongly. Accordingly, it appears natural in the molecular scenario for the $Y(4260)$ that the nominal $D_1 \bar{D}$ threshold leaves an imprint, for example, on its line shapes. This is shown in Fig. 81. In all panels the red solid line denotes the results of the full model of Ref. [154]. All model parameters were fixed in 2013 to the spectra
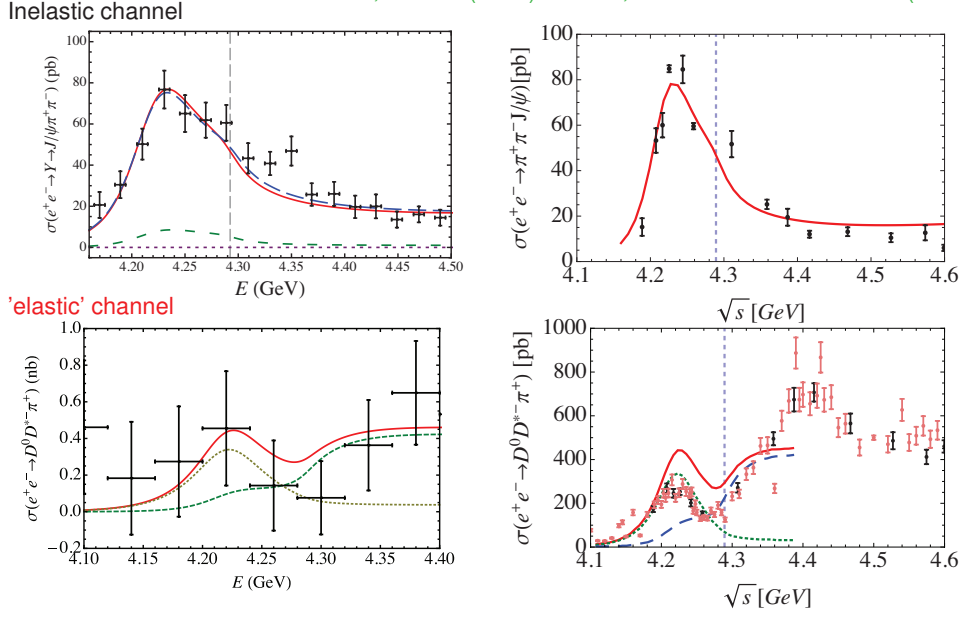
Figure 81: Lineshapes of the $\psi(4230)$ aka $Y(4230)$ in the $\pi\pi J/\psi$ channel (upper panel) and the $D\bar{D}^*\pi$ channel (lower panel). The left column shows the data available before 2014 from Belle [170] (lower panel) and [25] (upper panel) and the right column shows the very recent data from BESIII [73, 165]. In all panels the red lines show the results of the full model of Ref. [154] with its parameters fixed in 2013.
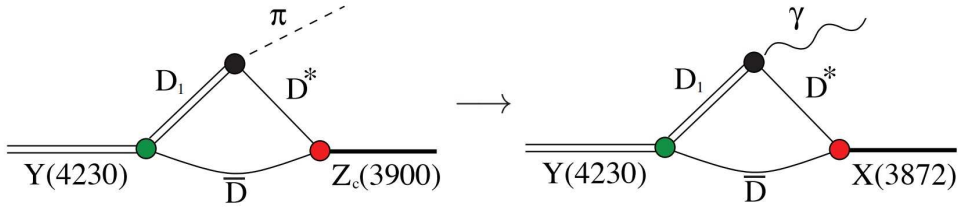
Figure 82: Triangle mechanisms driving both $Y(4230) \to \pi Z_c(3900)$ and $Y(4230) \to \gamma X(3872)$ decay in the molecular picture.

and angular distributions existing at that time. The results for the $\pi\pi J/\psi$ channel clearly show that the molecular model naturally generates asymmetric line shapes from just a single state. In contrast to this, the experimental analysis of the new data (upper right panel) generate the asymmetry from two BW resonances — see the discussion in Sec. 3.1 above. One conclusion from the molecular picture is that the structure known as $Y(4260)$ should be identified with the $Y(4230)$. We will use this name in the rest of this section.

Since the natural decay of a molecular state is into its constituents, and the strongest decay channel of the $D_1(2420)$ is $D^*\pi$, a $D_1\bar{D}$ molecular state must leave a strong imprint in the $\bar{D}D^*\pi$ final state. At the time when the model parameters of Ref. [154] were fixed, no high quality data in this channel were available and the results shown in the lower right panel of Fig. 81 came as a prediction. Also this calculation contains only one state — still the data and the calculation contain in addition to the peak of the $Y(4230)$ a second structure above the nominal $D_1\bar{D}$ threshold located at 4280 MeV — here a similarity of the red curve and the typical line shapes for molecules with unstable constituents shown in Fig. 79 should be emphasized. The missing strength to account for the data above 4350 MeV might come from the $\psi(4415)$ or $D_2\bar{D}^*$ channel missing in the model.

A $D_1\bar{D}$ molecular nature for the $Y(4230)$ also predicts peculiar decay patterns of this state. For example, it

was stressed in Ref. [185] that within this scenario it appears natural that the $Z_c(3900)$ envisioned as $D\bar{D}^*$ bound state gets excited in the $Y(4230)$ decay, since the prime decay channel of the $D_1(2420)$ is πD^* and, accordingly, the triangle mechanism shown in the left half of Fig. 82 provides an efficient source of low-energy $D^*\bar{D}$ pairs leading to a copious production of the related isovector molecular state. Moreover, the quark model predicts that the $D_1(2420)$ also decays into $D^*\gamma$ — thus, the very same triangle mechanism, shown in the right panel of Fig. 82, should again provide $D^*\bar{D}$ pairs, however, now with the opposite C-parity since π^0 and γ have $C = +$ and $C = -$, respectively. Accordingly, if the above explanation for the observation of the $Z_c(3900)$ in the decay $Y(4230) \to \pi Z_c(3900)$ is correct, necessarily $X(3872)$ must also be produced in the $Y(4230) \to \gamma X(3872)$ reaction [70]. This prediction was confirmed experimentally shortly after its publication — see Fig. 11.

As already mentioned above, the findings of Ref. [511], where the $\pi\pi$ spectra from $e^+e^- \to \pi^+\pi^- J/\psi$ in the 4260 MeV mass range were studied, that the source contains a sizeable flavor-octet component, are fully in line with a molecular as well as compact tetraquark interpretation of those states.

• *Closing remarks on hadronic molecules*

So far in this section we have focused on general properties of molecular states. To go beyond this and predict, for example, partner states that should exist given the symmetries of QCD, dynamical equations need to be solved. Those need as input phenomenological models like meson exchange models — see, for example, Refs. [201, 587–591]; many additional references are also provided in the review articles [84, 592]. Alternatively, one can construct the scattering potentials in an effective field theory framework. The latter method will be detailed in Sec. 4.4.5 below. Sometimes flavor SU(4) is used to constrain scattering potentials — see, for example, Refs. [568, 569, 580] — however, it should be stressed that such studies necessarily come with uncontrolled systematic uncertainties, since flavor SU(4) is not a symmetry of QCD (cf. chapter 16.4. of Ref. [593]). Note that some studies constructed on the basis of flavor SU(4) are in fact only sensitive to the flavor SU(3) subgroup and as such show a connection to QCD symmetries — see, e.g., the discussion in Sec. IIA of Ref. [594], where it is argued that in practice what is often employed is only the well established SU(2) symmetry.

From the molecular perspective, the $Z_c(4430)$ is the most problematic, since it is not close to any S-wave threshold[17] — see Fig. 72. The $Z_c(4430)$ could be a signature of the triangle singularity as originally proposed in Ref. [595]. If this were a proper explanation of these resonances, there should be no signal of the $Z_c(4430)$ in the $D^*\bar{D}$ channel, according to Schmid's theorem (see Sec. 4.4.5 for a more detailed discussion), which could be tested experimentally. A different set of triangle diagrams to explain both the $Z_c(4200)$ and the $Z_c(4430)$ was proposed in Ref. [596]. Here the latter (former) state emerges from the triangle $\bar{B}^0 \to \bar{K}^*(892)Y(4260) \to [K^-\pi^+]Y(4260) \to \pi^+\psi$ ($\bar{B}^0 \to \bar{K}_2^*(1430)\psi(3770) \to [K^-\pi^+]\psi(3770) \to \pi^+\psi$), where the ψ in the final state could be either J/ψ or $\psi(2S)$. For these transitions to be prominent there should be significant rates observable experimentally for $\bar{B}^0 \to \bar{K}^*(892)Y(4260)$ and $\bar{B}^0 \to \bar{K}_2^*(1430)\psi(3770)$, respectively, making also this prediction testable experimentally.

Since a state like $Z_c(4430)$ cannot be an S-wave bound state of a pair of ground-state mesons, Ref. [597] employs a one-pion exchange model to test the hypothesis whether this state could be a molecule of the $D^*\bar{D}(2S) - D^*(2S)\bar{D}$ system with the relevant thresholds assumed at 4509 MeV and 4590 MeV, respectively. The authors conclude that with their standard parameters they cannot get an isovector bound state in this system, however, they find significantly more deeply bound isoscalar states. If the pion coupling in the model is increased to a strength sufficient to get the $Z_c(4430)$ as a bound state, the isoscalar partner states appear to be at least 100 MeV more bound. Those states have not been seen experimentally.

Alternatively, also employing a one-pion exchange model, in Ref. [201] the $Z_c(4430)$ is proposed to be a P-wave $\bar{D}_1(2420)D^*$ resonance. In the same work $Y(4390)$ is explained as its isoscalar S-wave partner. In this calculation the excitation from the S- to the P-wave costs about 40 MeV. If this picture is correct, there should be a signature of the $Z_c(4430)$ in the $D^*\bar{D}\pi$ channel — a prediction that can be tested experimentally. Another candidate for a P-wave bound state, this time in the $D^*\bar{D}^*$ channel, could be the $Z_c(4100)$ if it has negative parity [286].

To summarise, the molecular model provides natural explanations for various observables, such as the masses, line shapes, and decay patterns, of various candidate exotic states. Based on the arguments presented above, for example,

---

[17]This state is located basically at the $D_2\bar{D}^*$ threshold, but here an S-wave calls for a negative parity at odds with the quantum numbers of the $Z_c(4430)$ determined by LHCb [38].

$X(3872)$, $Z_c(3900)$, $Z_c(4020)$, $Y(4230)$, and $Y(4360)$ in the charmonium sector, and $Z_b(10610)$ and $Z_b(10650)$ in the bottomonium sector are good candidates for states having a prominent molecular component. However, it should not remain unmentioned that also the molecular picture suffers from a few unresolved issues:

- At present it does not explain the relative strengths of the $Z_c(3900)$ and $Z_c(4020)$ at the various beam energies in the πh_c and $\pi J/\psi$ final states. While the anticipated production mechanism via a triangle might play an important role here as proposed in Refs. [185, 341], full understanding of all available data is still lacking.

- The state $Z_c(4430)$ is not located close to any S-wave threshold and thus calls for an alternative explanation. It is our understanding that so far no convincing explanation for this state in a two-hadron scenario has been provided.

- In addition, the interplay of the molecular states with compact quark states ($Q\bar{Q}$ quarkonia, $Q\bar{Q}g$ hybrids and so on) is not understood yet, although some efforts have already been taken in this direction [598].

4.3.5. Sum rules

Another non-perturbative approach often applied to both generic and exotic hadrons is the QCD sum rules method [599, 600]. A thorough description of the method and a comprehensive list of references on the subject can be found in the recent review [601], which is specifically devoted to the sum rules approach to exotic XYZ hadrons.

The cornerstone of the method is the quark–hadron duality conjecture, which allows one to relate observables for hadronic states with the properties of the non-perturbative QCD vacuum encoded in various local condensates. To this end one considers a correlation function of currents with the quantum numbers of the studied resonance and evaluates it in terms of local condensates of different dimensions using the operator product expansion. For example, for the two-point correlation function one has

$$\Pi(Q^2) = i \int d^4x \, e^{iqx} \, \langle 0|T[j(x)j^\dagger(0)]|0\rangle = \Pi^{\text{pert}}(Q^2) + C_3(Q^2)\langle \bar{q}q \rangle + C_4(Q^2)\langle g^2 \text{Tr}(F_{\mu\nu}F^{\mu\nu})\rangle + \dots, \tag{50}$$

where $j(x)$ is an interpolating current, $Q^2 = -q^2$, $\Pi^{\text{pert}}(Q^2)$ is the perturbative contribution to the correlation function, and $\langle \bar{q}q \rangle$, $\langle g^2 \text{Tr}(F_{\mu\nu}F^{\mu\nu}))\rangle$ and so on are the quark, gluon and so on local condensates characterising the QCD vacuum. Where to truncate the series in the right-hand side of Eq. (50) depends also on the resonance under study — typically the quark and the gluon condensates are sufficient to describe generic quarkonia, while one has to include higher-order condensates to provide a good convergence of the series for exotic states. The values of the condensates are assumed to be known and taken as input parameters. For example, the chiral condensate $\langle \bar{q}q \rangle$ is related with the light quark masses and the pion decay constant f_π through the Gell-Mann–Oakes–Renner relation [602]. One can also extract them from lattice QCD calculations of the same correlation functions in Euclidean spacetime — for recent determinations of the gluon condensate see Refs. [603, 604]. Finally, the numerical values of the condensates can be extracted from the sum rules applied to hadronic states with well established properties, such as the masses and the decay widths. It has to be remarked, however, that only a few low-dimension condensates are known and that additional assumptions need to be invoked to treat higher-dimension condensates. In particular, a factorisation hypothesis is usually employed, which implies that higher-dimension condensates are reduced to suitable powers of the lower-dimension ones. This results in a further error, difficult to assess precisely, that contributes to the overall uncertainty of the method. The Wilson coefficients $C_d(Q^2)$ of the expansion (50) can be expressed in terms of particular sets of Feynman diagrams and, as such, can be computed straightforwardly in perturbative QCD. Finally, the correlator $\Pi(Q^2)$ can be represented as a dispersive integral,

$$\Pi(Q^2) = \int_{s_{\min}}^\infty ds \, \frac{\rho(s)}{s - Q^2}, \qquad \rho(s) = \frac{1}{\pi}\text{Im}[\Pi(s)]. \tag{51}$$

This completes the first stage of the calculation based directly on QCD, and which involves only its fundamental degrees of freedom, i.e., quarks and gluons.

Alternatively, according to the quark–hadron duality conjecture, the correlation function (50) can be evaluated in terms of low-energy effective degrees of freedom, i.e., hadrons. In particular, this amounts to constructing the spectral density $\rho(s)$ as a suitable function that depends on the masses, coupling constants, and other parameters of the physical hadronic states. Generically, all hadronic states h, for which the matrix element does not vanish, contribute

to $\langle h|j(0)|0\rangle$ and, therefore, to the spectral density ρ. However, the contribution of high-lying broad hadronic states is usually taken into account effectively through a smooth continuum function added to the sharp contributions from the low-lying narrow states. This smooth function is expected to vanish below a certain threshold s_0.

To improve the convergence of the operator product expansion series by suppressing higher-order contributions, it is common to follow the original works [599, 600] and to employ a Borel transformation depending on a parameter M called the Borel mass. The typical value of this parameter is set by the mass scale of the hadronic system under study. The results can be regarded as reliable only if they are robust with respect to a variation of the parameter M in a sufficiently wide range — called the Borel window. Choosing a Borel parameter that is too small amounts to truncating the operator product expansion series before accounting for all contributions necessary to describe the hadronic system with enough precision. On the other hand, too large values of M would allow the poorly controlled continuum to contribute. Thus, the appropriate choice of the Borel parameter is a crucial point in the approach. Furthermore, consistency requires the lower bound of the continuum contribution s_0 to depend on the value of the Borel parameter M [605]. Indeed, it was noticed a long time ago that choosing a constant threshold s_0 results in an insufficient accuracy of the calculation [606].

Studying exotic hadronic states in the sum rules approach is more difficult than considering just generic quarkonia. On the one hand, as was mentioned above, the operator product expansion series has to be truncated at higher orders to provide a sufficient level of convergence. This implies that higher-order condensates need to be retained in the series. The evaluation of such higher-order condensates requires additional approximations, such as the factorisation assumption. For example, the quartic quark condensate is expressed as $\langle\bar{q}q\bar{q}q\rangle = \rho\langle\bar{q}q\rangle^2$, where the coefficient ρ is expected to be of order one. However, choosing the best value of ρ and estimating the corresponding uncertainty requires further theoretical assumptions. On the other hand, the interpolating current $j(x)$ entering the correlation function needs to be constructed in such a way that it overlaps with all relevant, ordinary and exotic, components of the hadronic state, hence, not only quark-antiquark components, but also hybrid, molecular, and compact tetraquark ones. The mixing angles between the different components in the interpolating current are additional parameters.

state	structure	J^{PC}
$\chi_{c1}(3872)$ aka $X(3872)$	mixed $\chi_{c1} - D\bar{D}^*$	1^{++}
$Z_c(3900)^+$	$D\bar{D}^*$	1^{+-}
$X(3940)$	mixed $\chi_{c0} - D^*\bar{D}^*$	0^{++}
$Z_c(4020)^+$	$D^*\bar{D}^*$	1^{+-} or 2^{++}
$Z_c(4100)^+$	$D_0^*\bar{D}_0^*$	0^{++}
$X(4160)$	$D_s^*\bar{D}_s^*$	2^{++}
$Z_c(4200)^+$	$[cs][\bar{c}\bar{s}]$	1^+
$X(4250)^+$	$D\bar{D}_1$	1^-
$\psi(4260)$ aka $Y(4260)$	mixed $J/\psi - [cq][\bar{c}\bar{q}]$	1^{--}
$\psi(4360)$ aka $Y(4360)$	$[cq][\bar{c}\bar{q}]$	1^{--}
$\psi(4660)$ aka $Y(4660)$	$[cs][\bar{c}\bar{s}]$	1^{--}

Table 11: Structures and quantum numbers of several charmonium-like states obtained within the sum rules approach (adapted from Ref. [601]). Only those states that appear in the listings of the PDG with the assumed or unknown quantum numbers are kept and listed using their official names.

The sum rule approach can be used not only to calculate masses but also to study three–point functions like for magnetic moments. For the evaluation of magnetic moments of the $Z(3900)$ state see, e.g., Refs. [327, 328].

To summarize, the sum rules approach to exotic hadrons is a strong analytical tool aimed at relating the properties of the hadronic states under study directly with intrinsic features of the QCD vacuum encoded in various local condensates. Shortcomings of this approach are the necessity of additional assumptions and approximations that can make systematic improvements and reliable uncertainty estimates difficult, especially for exotic near-threshold states. Predictions of the sum rules for the structures and quantum numbers of XYZ states in the charmonium spectrum are collected in Table 11, taken from the recent review [601]. There the interested reader can find further details of the method and its application to exotic hadrons. Results from sum rules for charmonium and bottomonium hybrids have been briefly summarized also in Sec. 4.4.4. For recent developments on the foundation of sum rules for compact

tetraquarks and their specific differences with respect to sum rules for ordinary quarkonia we refer to Ref. [607].

4.4. Effective field theories for QCD

In a physical system, the long-distance (or low-energy) dynamics usually does not depend on the details of the physics at short distances (or high energies). For example, the details of atomic physics are irrelevant to describe planetary motion; the only feature of the nucleus relevant to chemistry is its charge. Effective field theories (EFTs) are a theoretical tool that allows to put this generic observation into a rigorous framework. In particular, under some conditions, EFTs are able to describe systems characterized by several energy scales just in terms of a few relevant degrees of freedom. This description is improvable in a systematic way. It has, however, a limited, but well defined, range of applicability.

A necessary condition for the construction of an effective field theory is the existence of a hierarchy amongst the energy scales of the system. For instance, in the case of a system with two scales, Λ and Q, we can construct an EFT if $\Lambda \gg Q$. The effective field theory Lagrangian is then organized as an expansion in Q/Λ. Each term in the expansion is made of the fields describing the system at the low-energy scale Q, also called effective degrees of freedom. It can be any term as long as it is consistent with the symmetry principles. In turn, the resulting scattering matrix will be the most general one consistent with analyticity, perturbative unitarity, cluster decomposition and the symmetry principles [608].

Analytic terms in the expansion parameter Q/Λ are accounted for by the operators of the EFT. Non-analytic terms, carrying the contributions of the high-energy modes in the original, fundamental theory, which are no longer dynamical in the EFT, are encoded in the parameters multiplying the EFT operators. These parameters are the Wilson coefficients of the EFT, also called low-energy constants in hadronic EFTs like Chiral Perturbation Theory. Hence, EFTs automatically factorize, for any observable, high-energy from low-energy contributions. The Wilson coefficients of the EFT Lagrangian are fixed by matching to the fundamental theory, i.e. by requiring the EFT and the fundamental theory to describe the same physics (observables, Green functions, scattering matrices, ...) at any given order of the expansion parameter Q/Λ. Alternatively they can also be fixed from data. In case of hadronic EFTs they are fixed either from experimental data or from matching to results from lattice QCD.

To allow for controlled calculations based on the effective Lagrangian, operators, as well as the quantum corrections, are organized according to their expected importance. Operators in the Lagrangian are counted in powers of the small expansion parameter Q/Λ, whereas quantum corrections are either computed exactly or counted in powers of the coupling constant. EFTs are, in general, non-renormalizable, however, they are at each order in the expansion parameter. This leads eventually to finite results, whose different terms scale according to the power counting. The power counting may or may not be obvious. Nevertheless, once a power counting has been established, effective field theories prove to be very useful, sometimes the only tool, to compute in a systematic and rigorous fashion observables in multiscale systems.

One of the strengths of EFTs is that they enjoy at leading order a larger symmetry than the fundamental theory, as a consequence of the fact that some of the original degrees of freedom have been integrated out. For example, the heavy-quark symmetry of the Heavy Quark Effective Theory (see Sec. 4.4.1) is a hidden, approximate symmetry of the physical system that is made manifest by the EFT at leading order. Although higher-order terms in the EFT restore the symmetry of the full theory, having a more symmetric zeroth-order solution contributes to the predictive power of the EFT by reducing the number of its low-energy parameters.

The fundamental theory for hadronic physics is QCD. Its Lagrangian density reads (for simplicity gauge fixing, ghost fields and a possible θ-term are omitted) [1]

$$\mathcal{L}_{QCD} = \sum_{i=1}^{n_f} \bar{q}_i \left(i\gamma_\mu D^\mu - m_i \right) q_i - \frac{1}{4} F_{\mu\nu}^a F^{\mu\nu\,a} , \tag{52}$$

where the quark fields are denoted by q_i, the sum runs over the n_f quark flavors, m_i are the quark masses, the covariant derivative is $D^\mu = \partial^\mu - igA^\mu$, with $A^\mu = A^{\mu\,a}T^a$ the gluon fields and T^a the SU(3) generators, $F_{\mu\nu}^a$ is the field strength tensor, and g is the gauge coupling, related to the strong coupling via $\alpha_s = g^2/(4\pi)$. Of particular relevance in hadronic physics are the EFTs that can be constructed from QCD in the limit of small and large quark masses.

For light quarks we can expand the QCD Lagrangian for small masses and write at leading order

$$\mathcal{L}_{\text{QCD}} = \sum_{i=1}^{n_\ell} \bar{q}_{iL} \left(i\slashed{\partial} + g\slashed{A}^a T^a \right) q_{iL} + \bar{q}_{iR} \left(i\slashed{\partial} + g\slashed{A}^a T^a \right) q_{iR} - \frac{1}{4} F^a_{\mu\nu} F^{\mu\nu\, a}, \tag{53}$$

where q_{iR} (q_{iL}) are the right- (left-) handed components of the n_ℓ light-quark fields. In this limit, the Lagrangian is $U(1)_V \times SU(n_\ell)_V \times U(1)_A \times SU(n_\ell)_A$ invariant (V stands for vector, A for axial vector). However, the $SU(n_\ell)_V \times SU(n_\ell)_A$ symmetry is spontaneously broken to $SU(n_\ell)_V$, which has as a consequence that, at low energies, the effective degrees of freedom of QCD are the Goldstone bosons that emerge from the symmetry breaking rather than quarks and gluons. The effective field theory that describes QCD at low energies is called Chiral Perturbation Theory (ChPT) [609, 610]. Its effective degrees of freedom are the Goldstone bosons of the spontaneously broken $SU(n_\ell)_A$ symmetry. For $n_\ell = 2$ these are pions. The exploited hierarchy of scales is $\Lambda_\chi \gg M_\pi$, where M_π is the pion mass and $\Lambda_\chi \sim 4\pi f_\pi \sim 1$ GeV is the hadronic scale associated with the spontaneous breaking of the chiral symmetry; f_π is the pion decay constant. Hence ChPT is constructed as a perturbative expansion in powers of M_π/Λ_χ. Because ChPT is an EFT for degrees of freedom that live below the hadronic scale, its matching to QCD is non-perturbative. Chiral Perturbation Theory plays a crucial role in describing nuclei and hadronic molecules, see Refs. [611] and [531] and references therein. We will discuss it in this context in Sec. 4.4.5.

For hadrons made of one heavy quark, like heavy-light mesons and baryons, the proper EFT is called Heavy Quark Effective Theory (HQET). It exploits the hierarchy of scales $m_h \gg \Lambda_{\text{QCD}}$, where m_h is the heavy quark mass and Λ_{QCD} is the typical, hadronic scale, of the same order as Λ_χ, relevant for these systems. The condition $m_h \gg \Lambda_{\text{QCD}}$ is fulfilled by the charm, bottom, and top quarks.[18] In a sense, the HQET describes QCD in the opposite limit of ChPT, however, the HQET is not the large mass limit of QCD. We will discuss the HQET in the following Sec. 4.4.1. If we consider systems made of more than one heavy quark, like quarkonia or quarkonium-like states or doubly-heavy baryons, then more scales become relevant. These are the scales of the heavy-quark-heavy-(anti)quark interaction, i.e., the typical momentum transfer, $m_h v$, and the typical binding energy $m_h v^2$, where v is the relative velocity of the heavy quarks. At each of these scales one can construct an EFT, specifically, NRQCD at the scale $m_h v$, which will be discussed in Sec. 4.4.2, and potential NRQCD (pNRQCD) at the scale $m_h v^2$, which will be discussed in Sec. 4.4.3. The version of pNRQCD suited to deal with systems made of two or more heavy quarks bound with some light degrees of freedom, like light quarks or gluons, is called Born–Oppenheimer EFT and will be presented in Sec. 4.4.4. Finally, effective field theories at the hadron level are described in Sec. 4.4.5.

4.4.1. Heavy Quark Effective Field Theory

The HQET is the EFT suited to describe hadrons made of one heavy particle and light degrees of freedom, also called heavy-light hadrons [612–615] (for an early review see, for instance, Ref. [616], for a textbook see Ref. [617]). The heavy particle was originally designated to be a heavy quark. However, under some circumstances, it can be also a composite particle made by more than one heavy quark; this is the case when the internal modes of the composite heavy particle may be ignored. The light degrees of freedom are made by quarks and gluons. Among the light quarks we may distinguish between valence quarks and sea quarks, where the first ones are those that establish, together with the heavy degrees of freedom, the quantum numbers of the heavy-light hadron.

The HQET exploits the hierarchy $m_h \gg \Lambda_{\text{QCD}}$ that characterizes heavy-light hadrons made by a heavy quark of mass m_h. High-energy degrees of freedom that live at the energy scale m_h are integrated out from QCD. The resulting EFT is made of low-energy degrees of freedom living at the scale Λ_{QCD}. These are the low-energy modes of the heavy quark (antiquark), described by a Pauli spinor ψ (χ) that annihilates (creates) the heavy quark (antiquark), and low-energy gluons and light quarks. The HQET is constructed as an expansion in $1/m_h$: the heavy quark expansion. Matrix elements of operators of dimension d are of order Λ_{QCD}^d, hence the higher the dimension of the operator the higher the suppression in Λ_{QCD}/m_h. In the rest frame of the heavy-light hadron, the HQET Lagrangian density for a

---

[18] Top quarks will not play any role in the following, as this review focuses on hadrons and the top quark has no time to form any before decaying weakly into a b quark.

heavy quark reads up to order $1/m_h^2$ (the HQET Lagrangian including $1/m_h^4$ terms has been derived in Refs. [618, 619])

$$\mathcal{L}_{\text{HQET}} = \psi^\dagger \left\{ iD_0 + \frac{\boldsymbol{D}^2}{2m_h} - c_F \frac{\boldsymbol{\sigma} \cdot g\boldsymbol{B}}{2m_h} - c_D \frac{[\boldsymbol{D}\cdot, g\boldsymbol{E}]}{8m_h^2} - ic_S \frac{\boldsymbol{\sigma} \cdot [\boldsymbol{D}\times, g\boldsymbol{E}]}{8m_h^2} \right\} \psi$$

$$- \frac{1}{4} F_{\mu\nu}^a F^{a\mu\nu} + \frac{d_2}{m_h^2} F_{\mu\nu}^a D^2 F^{a\mu\nu} - \frac{d_3}{m_h^2} g f_{abc} F_{\mu\nu}^a F_{\mu\alpha}^b F_{\nu\alpha}^c + \sum_{\ell=1}^{n_\ell} \bar{q}_\ell \left(i\gamma_\mu D^\mu - m_\ell \right) q_\ell, \tag{54}$$

where $[\boldsymbol{D}\cdot, g\boldsymbol{E}] = \boldsymbol{D} \cdot g\boldsymbol{E} - g\boldsymbol{E} \cdot \boldsymbol{D}$ and $[\boldsymbol{D}\times, g\boldsymbol{E}] = \boldsymbol{D} \times g\boldsymbol{E} - g\boldsymbol{E} \times \boldsymbol{D}$, $E^i = F^{i0}$ is the chromoelectric field, $B^i = -\epsilon_{ijk} F^{jk}/2$ the chromomagnetic one with the totally antisymmetric tensor ϵ_{ijk} ($\epsilon_{123} = 1$), and $\boldsymbol{\sigma}$ are the Pauli matrices. The fields q_ℓ stand for n_ℓ light-quark fields, i.e., the mass m_ℓ is much smaller than Λ_{QCD} and may be set to zero in many applications. On the other hand, m_h has to be understood as the heavy quark pole mass, hence not the mass in the QCD Lagrangian. The coefficients c_F, c_D, c_S, d_2, and d_3 are Wilson coefficients of the EFT. They encode the contributions of the high-energy modes that have been integrated out from QCD. Since the high-energy scale, m_h, is larger than Λ_{QCD}, the Wilson coefficients may be computed in perturbation theory and organized as an expansion in α_s (at a typical scale of order m_h). The coefficients c_F, c_D, and c_S are 1 at leading order, while the perturbative series of the coefficients d_2 and d_3 starts at order α_s. The one-loop expression of the coefficients may be found in Ref. [620]. Some of the coefficients are known far beyond one loop. For instance, the Fermi coefficient c_F, which plays a crucial role in the spin splittings, is known up to three loops [621]. Not all the coefficients are independent. For instance, Poincaré invariance of QCD relates c_F and the spin-orbit coefficient c_S: $c_S = 2c_F - 1$ [620, 622, 623]. This relation is exact. The HQET Lagrangian for a heavy antiquark may be obtained from Eq. (54) by charge conjugation. In Eq. (54) we have not considered $1/m_h^2$ suppressed operators involving light quarks, since their impact is negligible in most hadronic observables. They have been considered first in Ref. [624]; for a recent calculation see Ref. [625].

The impact of the HQET on the physics involving heavy-light hadrons and, in particular, their weak decays has been enormous. The reason is that the leading-order HQET Lagrangian ($\mathcal{L}_{\text{HQET}} = \psi^\dagger iD_0 \psi - F_{\mu\nu}^a F^{a\mu\nu}/4$) makes manifest a hidden symmetry of heavy-light hadrons. This symmetry is the heavy-quark symmetry and stands for invariance with respect to the heavy-quark flavor and spin. Moreover, the leading-order HQET Lagrangian is exactly renormalizable. Higher-order operators in Eq. (54) break this symmetry (and exact renormalizability), however, they do it in a controlled, perturbative way. Hence, observables computed up to some order in the HQET expansion depend on fewer and more universal non-perturbative matrix elements than they would in a full QCD calculation. This makes the heavy quark expansion more predictive than a full QCD calculation. We will mention in the following a few implications of the heavy quark expansion for the spectrum of heavy-light hadrons.

Heavy-light meson masses, expressed in the HQET as an expansion up to order $1/m_h$ in the inverse of the heavy quark mass [626], read

$$M_{H^{(*)}} = m_h + \bar{\Lambda} + \frac{\mu_\pi^2}{2m_h} - d_{H^{(*)}} \frac{\mu_G^2(m_h)}{2m_h} + O(1/m_h^2), \tag{55}$$

where $M_{H^{(*)}}$ is the spin singlet (triplet) meson mass, m_h the heavy quark pole mass, $\bar{\Lambda}$ the binding energy in the static limit, of order Λ_{QCD}, $\mu_\pi^2/2m_h$ the kinetic energy of the heavy quark (μ_π^2 is the matrix element of $\psi^\dagger \boldsymbol{D}^2 \psi$), of order $\Lambda_{\text{QCD}}^2/m_h$, $d_{H^{(*)}}$ is 1 for H and $-1/3$ for H^*, and $d_{H^{(*)}} \mu_G^2(m_h)/2m_h$ is the matrix element of $c_F \psi^\dagger \boldsymbol{\sigma} \cdot g\boldsymbol{B}/(2m_h)\psi$, of order $\Lambda_{\text{QCD}}^2/m_h$. The heavy quark symmetry manifests itself through the universality of the leading term $M_{H^{(*)}} - m_h \approx \bar{\Lambda}$, as well as of the matrix elements μ_π^2 and $\mu_G^2(m_h)/c_F(m_h)$, which depend neither on the heavy quark flavor nor on the heavy quark spin. The flavor dependence of $\mu_G^2(m_h)$ comes entirely from the Wilson coefficient c_F, which depends on m_h through the running of the strong coupling.

A primary use of Eq. (55) is to determine the heavy quark masses from the (measured) meson masses. Since the relation between the $\overline{\text{MS}}$ mass (or any ultraviolet mass) and the pole mass is given by a poorly convergent perturbative series (at present, this relation is known up to four loops [627, 628]) [19], an intermediate step is necessary. This consists in rewriting Eq. (55) in a scheme that preserves the power counting of the EFT, which excludes a direct use of the $\overline{\text{MS}}$ scheme, and defines a mass that is related to the $\overline{\text{MS}}$ mass through a convergent perturbative series. There are many possibilities for such a scheme [630–635]. The approach favored by the recent lattice determination of Ref. [636]

---

[19] For model-dependent estimates of the five- and six- loop contributions see, for instance, Ref. [629].

is the minimal renormalon subtraction (MRS) scheme [635]. The obtained heavy quark masses from the D_s and B_s masses read

$$\overline{m}_c = 1273(4)_{\text{stat}}(1)_{\text{syst}}(10)_{\alpha_s}(0)_{f_{\pi,\text{PDG}}} \text{ MeV} = 1273(10) \text{ MeV}, \tag{56}$$

$$\overline{m}_b = 4201(12)_{\text{stat}}(1)_{\text{syst}}(8)_{\alpha_s}(1)_{f_{\pi,\text{PDG}}} \text{ MeV} = 4201(14) \text{ MeV}, \tag{57}$$

where $\overline{m}_h$ is the $\overline{\text{MS}}$ mass of the quark h at the scale of its $\overline{\text{MS}}$ mass, and the uncertainties are statistical, systematic, due to uncertainties in α_s and in the pion decay constant f_π from the PDG used to set the lattice scale.

The quantities $\bar{\Lambda}$, μ_π^2 and $\mu_G^2(m_h)$ are non-perturbative. The lattice determination of Ref. [636] finds

$$\bar{\Lambda}_{\text{MRS}} = 555(25)_{\text{stat}}(8)_{\text{syst}}(16)_{\alpha_s}(1)_{f_{\pi,\text{PDG}}} \text{ MeV}, \tag{58}$$

$$\mu_\pi^2 = 0.05(16)_{\text{stat}}(13)_{\text{syst}}(06)_{\alpha_s}(00)_{f_{\pi,\text{PDG}}} \text{ GeV}^2, \tag{59}$$

$$\mu_G^2(m_b) = 0.38(01)_{\text{stat}}(01)_{\text{syst}}(00)_{\alpha_s}(00)_{f_{\pi,\text{PDG}}} \text{ GeV}^2, \tag{60}$$

where $\bar{\Lambda}$ is in the MRS scheme and the quantity μ_G^2 has been evaluated for the b quark. At higher orders in the $1/m_h$ expansion, more matrix elements have to be determined, a fact that increasingly limits the predictive power of the HQET.

Clearly, Eq. (55) can be immediately extended to heavy-light baryons. What will change is the explicit value of the non-perturbative matrix elements, as the light degrees of freedom are different from the mesonic case. More interesting, from a conceptual point of view, is the case of doubly-heavy baryons. These systems are characterized by more energy scales than heavy-light hadrons. One of these scales is the inverse of the typical distance between the two heavy quarks. If it is much larger than Λ_{QCD}, a case more likely to be realized by doubly bottomed baryons than by doubly charmed baryons, then one can integrate out this scale. At the low-energy scale of the resulting EFT, one does not resolve the two heavy quarks anymore and the resulting EFT is just the HQET (for the heavy antiquark) with the role of the heavy antiquark given to an effective heavy diquark field with the same quantum numbers [637–646]. This is an appealing picture with predictive power, as it links the doubly-heavy baryon observables to the much better known heavy-light meson ones. Nevertheless, it has been also challenged by lattice data that, at least in the doubly charmed baryon spectrum, do not seem to fully support the diquark picture [647]. It is anyway clear that for any doubly-heavy baryon, and even more so for doubly charmed baryons, the heavy quark-quark dynamics provides a contribution that cannot be entirely neglected and that a diquark picture is theoretically justified only if the typical heavy quark distance is much smaller than $1/\Lambda_{\text{QCD}}$. Doubly charmed baryons have attracted more attention since the LHCb discovery of a resonance in the $\Lambda_c^+ K^- \pi^+ \pi^-$ mass spectrum at a mass of (3621.40 ± 0.78) MeV that is consistent with a Ξ_{cc}^{++} baryon [530, 648]. Earlier observations by the SELEX experiment remained unconfirmed by other experiments [649, 650] and show a huge isospin violation difficult to understand from an EFT point of view [651].

The heavy quark symmetry may be also applied to link doubly-heavy tetraquarks (tetraquarks made of two heavy quarks and two light anti-quarks) with heavy-light baryons sharing the same light-quark content [529, 643]. Even more relevant now that we have an experimental determination of a doubly-heavy baryon. In Ref. [529], using the mass formula in Eq. (55) and experimental input for heavy-light baryon and meson masses, the authors show evidence, at least from the HQET, that there are doubly bottomed tetraquark states $bb\bar{u}\bar{d}$, $bb\bar{u}\bar{s}$, and $bb\bar{d}\bar{s}$ that are stable against strong decays (these are states for which the decays into two heavy-light meson pairs, and a doubly-heavy baryon and a light antibaryon turn out to be kinematically forbidden), while the doubly charmed tetraquark $cc\bar{q}_\ell\bar{q}_{\ell'}$, mixed tetraquark $bc\bar{q}_\ell\bar{q}_{\ell'}$, and heavier doubly bottomed tetraquark states dissociate into pairs of heavy-light mesons. The existence of a stable doubly bottomed $I = 0$ tetraquark has been predicted by the quark model of Ref. [528], the lattice QCD calculations in Refs. [524, 525], and it is supported by the arguments of Ref. [525]. In Ref. [643] it has been pointed out that if the mass of this stable tetraquark is smaller than 10405 MeV (this is the case for the prediction in Ref. [528]), then the lowest-lying doubly bottomed tetraquark with quantum numbers $J^P = 1^+$ and $I = 1$ would also likely be stable against strong decays.

4.4.2. Non Relativistic QCD

Systems made of two or more non-relativistic particles, like two heavy quarks or a heavy quark and a heavy antiquark, are characterized by more energy scales than systems where just one particle is non-relativistic. These
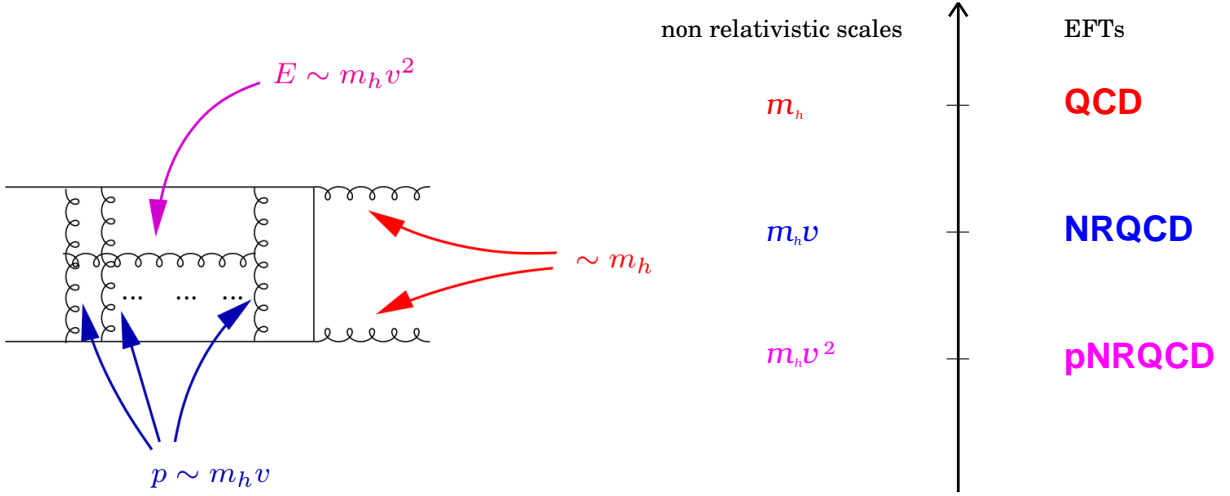
Figure 83: Left: Typical energy scales entangled in a quarkonium annihilation. Right: Hierarchy of energy scales and corresponding EFTs.

energy scales are the inverse radius (or radii) defining the size of the heavy particle system and the energy of the excitations of the heavy particle system. In the case of heavy quarks of mass m_h, the inverse size of the heavy quark system is of order $m_h v$ and the energy of its excitations is of order $m_h v^2$, where $v \ll 1$ is the velocity of the heavy quark relative to the c.m. frame (for simplicity, we do not distinguish here between heavy quarks of different flavor). This is analogous to what happens in the hydrogen atom, whose inverse Bohr radius is $m_e \alpha$ and whose energy levels are of order $m_e \alpha^2$, m_e being the mass of the electron and α the fine structure constant. The fine structure constant also provides the relative velocity of the electron in the atom. In QCD, the velocity v of the heavy quark may (for weakly-coupled bound states) or may not (for strongly-coupled bound states) be proportional to the strong coupling α_s. Regardless of this, the relative velocity of the heavy quark is much smaller than the velocity of light, and may serve to hierarchically order the non-relativistic energy scales:

$$m_h \gg m_h v \gg m_h v^2. \tag{61}$$

The non-relativistic energy scales are also correlated. The tower of hierarchically ordered energy scales in Eq. (61) calls for the construction of a tower of non-relativistic EFTs [652], see Fig. 83. In the last twenty years, the development of non-relativistic EFTs of QCD has been the major theoretical breakthrough in the description of quarkonium and quarkonium-like systems [12–14]. For a more historical perspective, see Ref. [653].

The EFT that follows from QCD by integrating out the energy scale of the heavy quark mass, m_h, which is the largest scale in Eq. (61), and that is suited to describe systems made of heavy quarks and heavy antiquarks, is NRQCD [654], see Fig. 84. Although the Lagrangian of the theory is identical to the one of the HQET in the two-fermion and gauge sectors, nevertheless the power counting is different. One consequence of this is that the leading-order NRQCD Lagrangian includes the kinetic energy operators, $\psi^\dagger \boldsymbol{\nabla}^2/(2m_h)\psi - \chi^\dagger \boldsymbol{\nabla}^2/(2m_h)\chi$. Therefore, differently from the HQET leading-order Lagrangian, it is not renormalizable.

Because of this seeming difficulty, NRQCD has been used first for lattice QCD calculations involving heavy quarks [655, 656]. The advantage there is that, once the heavy quark mass has been integrated out, the lattice spacing, a, is no more constrained to be smaller than $1/m_h$, which would amount to requiring a very fine lattice if the quark is very heavy. In lattice NRQCD the constraint is relaxed to $a < 1/(m_h v)$. Since at the same time the lattice size has to be large enough to include distances of the order of $1/\Lambda_{\rm QCD}$ for quenched calculations and $1/M_\pi$ for full calculations, simulations with very heavy quarks in full QCD are so far beyond reach for the required computational effort. Indeed, still nowadays, lattice NRQCD is the only way to compute non-perturbatively observables involving bottom quarks in full QCD (see, for instance, Refs. [657–661]).

Only after the development of the HQET, NRQCD has been systematically used for analytical calculations of quarkonium observables. In particular, NRQCD is well suited to describe heavy quark-antiquark annihilation pro-

Figure 84: Schematic matching of NRQCD; c is a Wilson coefficient of NRQCD, μ is the infrared renormalization scale of NRQCD.

cesses. These happen at the energy scale m_h, which is exactly the energy scale that has been integrated out from QCD. At the low-energy resolution of NRQCD no annihilation is possible and the numbe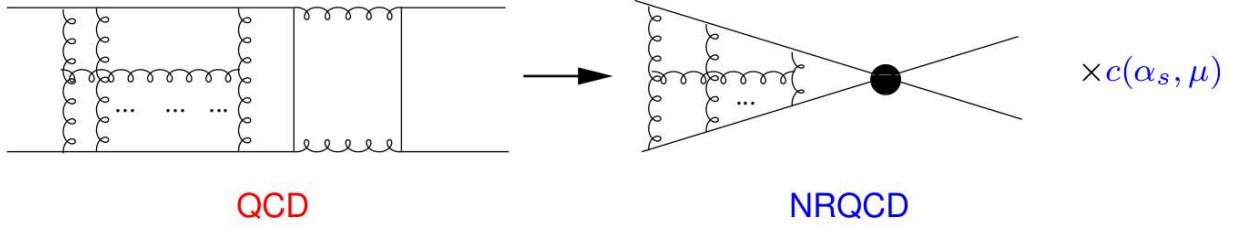r of heavy degrees of freedom is conserved. All the information about the annihilation goes instead into the (imaginary part) of the four-fermion Wilson coefficients of NRQCD, which may be computed in perturbative QCD, while the low-energy dynamics of the heavy quark-antiquark bound state is factorized into the matrix elements of the NRQCD operators. Processes involving heavy quark-antiquark annihilations are quarkonium decays [662, 663] and productions [663]. The large amount of data about quarkonium production in hadron and lepton colliders, together with the predictive power of NRQCD and its success in most of the predictions, has established NRQCD as a standard tool for studying quarkonium annihilation processes [12–14].

One novel feature of NRQCD with respect to the HQET is the presence of four-fermion operators in the Lagrangian. These are essential to describe annihilation processes, but also, more generally, to describe correctly the short-distance interaction between the heavy particles. Because also four-fermion operators projecting on color octet quark-antiquark states are possible, NRQCD naturally allows for production and decay of quark-antiquark states in a color octet configuration. Quark-antiquark states in a color octet configuration constitute a suppressed, in v, component of the Fock state describing a physical quarkonium. Four-fermion color octet matrix elements are necessary in the quarkonium phenomenology [12–14]. They are also necessary to cancel infrared divergences in quarkonium decay and production observables and provide eventually finite, physical results [662, 663]. It should be noted, however, that the NRQCD factorization has been rigorously proved only for quarkonium decay but not yet for quarkonium production (for progress in this direction see Refs. [664–668]). This unsolved issue may be related with the persisting difficulty in reconciling quarkonium polarization data with naive NRQCD expectations.

A last breakthrough in establishing NRQCD as a valuable tool for analytical calculations came when it was shown that the computation of the Wilson coefficients of NRQCD in dimensional regularization requires expanding in the heavy quark mass to avoid integrating over the high momentum region. The result is that, even if the power countings of NRQCD and the HQET are different, the matching to QCD proceeds in the same way, leading to the same Lagrangian in the two-fermion and gauge sectors [620].

The NRQCD Lagrangian density for systems made of a heavy quark and a heavy antiquark of equal masses m_h up to order $1/m_h^2$, and including the $1/m_h^3$ kinetic operator, is given by

$$
\begin{aligned}
\mathcal{L}_{\text{NRQCD}} = {} & \psi^\dagger \left\{ iD_0 + \frac{\boldsymbol{D}^2}{2m_h} + \frac{\boldsymbol{D}^4}{8m_h^3} - c_F \frac{\boldsymbol{\sigma} \cdot g\boldsymbol{B}}{2m_h} - c_D \frac{[\boldsymbol{D}\cdot, g\boldsymbol{E}]}{8m_h^2} - ic_S \frac{\boldsymbol{\sigma}\cdot[\boldsymbol{D}\times, g\boldsymbol{E}]}{8m_h^2} \right\} \psi \\
& + \chi^\dagger \left\{ iD_0 - \frac{\boldsymbol{D}^2}{2m_h} - \frac{\boldsymbol{D}^4}{8m_h^3} + c_F \frac{\boldsymbol{\sigma} \cdot g\boldsymbol{B}}{2m_h} - c_D \frac{[\boldsymbol{D}\cdot, g\boldsymbol{E}]}{8m_h^2} - ic_S \frac{\boldsymbol{\sigma}\cdot[\boldsymbol{D}\times, g\boldsymbol{E}]}{8m_h^2} \right\} \chi \\
& + \frac{f_1(^1S_0)}{m_h^2} \psi^\dagger\chi\chi^\dagger\psi + \frac{f_1(^3S_1)}{m_h^2} \psi^\dagger\boldsymbol{\sigma}\chi \cdot \chi^\dagger\boldsymbol{\sigma}\psi + \frac{f_8(^1S_0)}{m_h^2} \psi^\dagger\mathrm{T}^a\chi\chi^\dagger\mathrm{T}^a\psi + \frac{f_8(^3S_1)}{m_h^2} \psi^\dagger\mathrm{T}^a\boldsymbol{\sigma}\chi \cdot \chi^\dagger\mathrm{T}^a\boldsymbol{\sigma}\psi \\
& - \frac{1}{4} F_{\mu\nu}^a F^{a\mu\nu} + \frac{d_2}{m_h^2} F_{\mu\nu}^a D^2 F^{a\mu\nu} - \frac{d_3}{m_h^2} g f_{abc} F_{\mu\nu}^a F_{\mu\alpha}^b F_{\nu\alpha}^c + \sum_{\ell=1}^{n_\ell} \bar{q}_\ell \left(i\gamma_\mu D^\mu - m_\ell \right) q_\ell,
\end{aligned} \tag{62}
$$

where, as in the HQET case, m_h has to be understood as the pole mass. The first line of Eq. (62) is the two-fermion part of the NRQCD Lagrangian. As discussed above, it coincides, both in the operators and in the Wilson coefficients, with

the two-fermion part of the HQET Lagrangian shown in Eq. (54). The second line of Eq. (62) is the two-antifermion part of the NRQCD Lagrangian and it is the charge conjugated of the two-fermion part. The two-(anti)fermion sector of the HQET/NRQCD Lagrangian is known up to terms of order $1/m_h^4$ [618, 619]. The third line of Eq. (62) is made of all possible four-fermion operators of dimension 6. The corresponding Wilson coefficients are $f_1(^1S_0)$, $f_1(^3S_1)$, $f_8(^1S_0)$, and $f_8(^3S_1)$. The operator associated to the first (second) Wilson coefficient projects on a heavy quark-antiquark pair in a color singlet configuration with quantum numbers $^1S_0$ ($^3S_1$), whereas the operator associated to the third (fourth) Wilson coefficient projects on a heavy quark-antiquark pair in a color octet configuration with quantum numbers $^1S_0$ ($^3S_1$). The four-fermion Wilson coefficients have been computed in Refs. [663, 669]. They have a real part that starts at order α_s for $f_8(^3S_1)$ and at order α_s^2 for the other coefficients, and they have also an imaginary part, coming from one loop or higher annihilation diagrams, which is of order α_s^2 for Im $f_1(^1S_0)$, Im $f_8(^1S_0)$, and Im $f_8(^3S_1)$, and of order α_s^3 for Im $f_1(^3S_1)$. A list of imaginary parts of four-fermion Wilson coefficients in NRQCD and related bibliography can be found in Ref. [670]. The four-fermion sector of the NRQCD Lagrangian has been derived up to order $1/m_h^4$ (complete) and orders $1/m_h^5$ and $1/m_h^6$ (partial) in Refs. [671–673]. Like for the Wilson coefficients in the two-fermion sector, also the Wilson coefficients in the four-fermion sector are not all independent, but some of them are related by Poincaré invariance [672, 673]. Sometimes it may be useful to isolate the electromagnetic component of the four-fermion operator and of its corresponding Wilson coefficient. This is the case when computing electromagnetic decay widths and photoproduction cross sections in NRQCD. The electromagnetic operators are obtained by projecting on an intermediate QCD vacuum state, $|0\rangle$, e.g., $\psi^\dagger \chi \chi^\dagger \psi \rightarrow \psi^\dagger \chi |0\rangle\langle 0| \chi^\dagger \psi$. Finally, the fourth line of Eq. (62) contains the gauge sector of the EFT and the light quark Lagrangian. It coincides with the equivalent second line of the HQET Lagrangian in Eq. (54). As in the HQET case, in Eq. (62) we have not considered $1/m_h^2$ suppressed operators involving light quarks (either with two light quark and two heavy quark fields or with four light quark fields, see Ref. [652]).

Differently from the HQET, the power counting of NRQCD is not unique. The reason is that, while the HQET is a one-scale theory, its only dynamical scale being Λ_{QCD}, NRQCD is a multiscale theory. The dynamical scales of NRQCD are, at least, $m_h v$, $m_h v^2$, and Λ_{QCD}. In more complicated settings, even more scales can be relevant. Hence, one can imagine different power countings, some more conservative, like assuming that the matrix elements scale according to the largest dynamical scale, i.e., $m_h v$, see, e.g., Ref. [674], some less conservative or closer to a perturbative counting, see, e.g., Ref. [663]. What all the power countings have in common is that the kinetic energy scales like the binding energy and that therefore $\psi^\dagger i\partial_0 \psi$ is of the same order as $\psi^\dagger \boldsymbol{\nabla}^2/(2m_h)\psi$, and analogously for the antiquark. This follows from the virial theorem and is an unavoidable consequence of the dynamics of a non-relativistic bound state. Therefore, the leading-order NRQCD Lagrangian reads $\mathcal{L}_{\text{NRQCD}} = \psi^\dagger \{iD_0 + \boldsymbol{\nabla}^2/(2m_h)\}\psi + \chi^\dagger \{iD_0 - \boldsymbol{\nabla}^2/(2m_h)\}\chi - F_{\mu\nu}^a F^{a\mu\nu}/4$, which is different from the leading-order HQET Lagrangian for a heavy quark and a heavy antiquark. In particular, the leading-order NRQCD Lagrangian violates the heavy-quark flavor symmetry, which means, for instance, that the bottomonium binding energy is different, even at leading order, from the charmonium one. In the power counting of Ref. [663] one further assumes: $D_0 \sim m_h v^2$ (when acting on ψ or χ), $\boldsymbol{D} \sim m_h v$ (when acting on ψ or χ), $g\boldsymbol{E} \sim m_h^2 v^3$, and $g\boldsymbol{B} \sim m_h^2 v^4$. A consequence is that the heavy-quark spin symmetry is a symmetry of the leading-order NRQCD Lagrangian. Because of the mentioned counting, we have added the operator $\psi^\dagger \boldsymbol{D}^4/(8m_h^3)\psi$ and its charge conjugated to the Lagrangian in Eq. (62). Indeed, this operator is of the same order as the operators on its right. Matrix elements of octet operators on quarkonium states are further suppressed by the fact that they project on a subleading component of the quarkonium state, the one made of a heavy quark-antiquark pair in a color octet configuration and gluons. The amount of suppression depends again on the adopted power counting.

4.4.3. Potential Non-Relativistic QCD

NRQCD is well suited to describe quarkonium annihilation. However, it is still a complicated theory to describe the quarkonium spectrum (masses, transitions, widths, ...). In this context it is only used in lattice calculations. The reason is that the non-relativistic bound state involves scales, $m_h v$, $m_h v^2$, and Λ_{QCD}, that are still dynamical and entangled in NRQCD (as an illustration, see the non-annihilation part of the diagram on the left of Fig. 83). A consequence of this is that, although the equations of motion that follow from the NRQCD Lagrangian as shown in Eq. (62) resemble a Schrödinger equation for non-relativistic bound states, they are not quite that. They involve gauge fields and do not supply a field theoretical definition and derivation of the potential that would appear in a Schrödinger equation. Nevertheless, we expect that, in some non-relativistic limit, a Schrödinger equation describing the quantum mechanics of the non-relativistic bound state should emerge from field theory, since field theory may be understood

as an extension of quantum mechanics that includes relativistic and radiative corrections. In particular, in the case of quarkonium, the Schrödinger equation describing the bound state should be the non-Abelian equivalent of the one describing positronium. Another consequence is that, as already remarked in the previous section, the power counting of NRQCD is not unique.

Since the scales $m_h v$ and $m_h v^2$ are hierarchically ordered, they may be disentangled by systematically integrating out modes associated with scales larger than the smallest scale, $m_h v^2$, and matching to a lower energy EFT, where only degrees of freedom resolved at distances of order $1/(m_h v^2)$ are left dynamical [652]. This EFT is pNRQCD [675, 676]. Because the scale $m_h v$ has been integrated out, the power counting of pNRQCD is less ambiguous than the one of NRQCD. In situations where we can neglect the hadronic scale Λ_{QCD}, the power counting of pNRQCD is indeed unique, as its only dynamical scale is $m_h v^2$. Having integrated out the scale $m_h v$, which is the scale of the inverse of the distance r between the heavy quark and antiquark in any matrix element of quarkonium wave functions, implies that pNRQCD is constructed as an expansion in r. This is analogous to how the HQET and NRQCD are constructed. There, having integrated out the heavy quark mass, m_h, the EFTs are organized as expansions in $1/m_h$, with the Wilson coefficients encoding the non-analytic contributions, typically under the form of logarithms of m_h. Here, having integrated out the dynamical scale $m_h v$, pNRQCD is organized as an expansion in r, with the Wilson coefficients encoding non-analytic contributions in r. Some of the Wilson coefficients of pNRQCD may be identified with the potentials in the Schrödinger equation of quarkonium.

The specific form of pNRQCD depends on the scale Λ_{QCD}. If $\Lambda_{QCD} \lesssim m_h v^2$, then one deals with weakly-coupled bound states and the EFT is called weakly-coupled pNRQCD. At distances of the order of or smaller than $1/(m_h v^2)$, one may still resolve colored degrees of freedom (gluons, quarks, and antiquarks), as color confinement has not yet set in. Hence gluons, quarks, and antiquarks are the degrees of freedom of weakly-coupled pNRQCD. Weakly-coupled pNRQCD is well suited to describe tightly bound quarkonia, like the bottomonium and (to a less extent) charmonium ground states, the B_c ground state, and threshold effects in $t\bar{t}$ production. If $\Lambda_{QCD} \gtrsim m_h v^2$, then one deals with strongly-coupled bound states and the EFT is called strongly-coupled pNRQCD. At distances of the order of $1/(m_h v^2)$, confinement has set in and the only available degrees of freedom are color singlets. These are, in principle, all, ordinary and exotic, heavy and light, hadrons that we might have in the spectrum. Strongly-coupled pNRQCD is suited to describe higher states in the bottomonium and charmonium spectra, as well as quarkonium exotica. If $m_h v \gg \Lambda_{QCD} \gg m_h v^2$, the matching to pNRQCD may be done in two steps, first integrating out (perturbatively) $m_h v$ then (non-perturbatively) Λ_{QCD}. The advantage is that contributions coming from these two scales will be automatically factorized in the pNRQCD observables.

$$\frac{1}{E - p^2/m - V(r, \mu', \mu)}$$
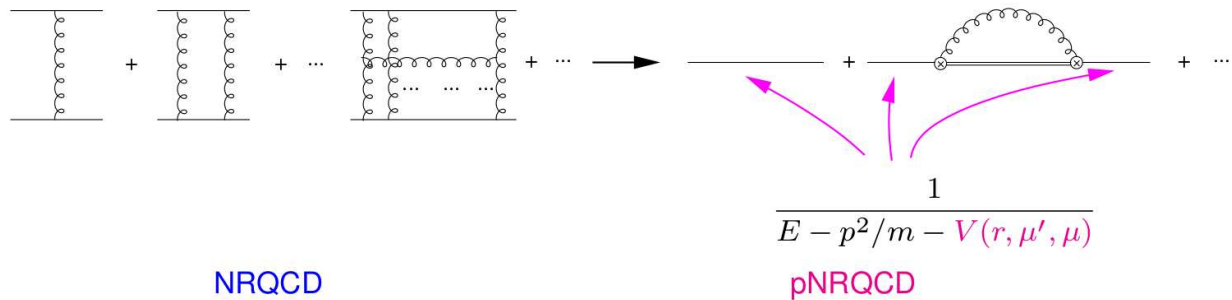
NRQCD

pNRQCD

Figure 85: Schematic matching of pNRQCD; V is a Wilson coefficient of pNRQCD, μ and μ' are the ultraviolet and infrared renormalization scales of pNRQCD, respectively. In the pNRQCD Feynman diagrams a single line stands for a singlet propagator, a double line for an octet propagator, curly lines for ultrasoft gluons, and a circle with a cross for a chromoelectric dipole interaction.

● *Weakly-coupled pNRQCD*

The degrees of freedom of weakly-coupled pNRQCD are heavy quarks and antiquarks of momentum $m_h v$ and energy $m_h v^2$, gluons of momentum and energy $m_h v^2$ (sometimes called ultrasoft gluons), and light quarks of momentum and energy $m_h v^2$. Weakly-coupled pNRQCD follows from integrating out gluons of energy or momentum $m_h v$

(sometimes called soft gluons) from NRQCD. Because at the scale $m_h v^2$ we cannot resolve the single heavy quark and antiquark, it may be useful to cast heavy quark and antiquark fields into bilocal fields that depend on time, t, the c.m. coordinate $\boldsymbol{R}$ and the relative coordinate $\boldsymbol{r}$. We call singlet, S, the color singlet component of the quark and antiquark field and octet, O, its color octet component, normalized as $S = \mathbb{1}_{3\times3}S/\sqrt{3}$ and $O = \sqrt{2}O^a T^a$. The distance r typically scales like $1/(m_h v)$, while the c.m. coordinate, R, and the time, t, typically scale like $1/(m_h v^2)$, as the quark-antiquark pair may only recoil against ultrasoft gluons. To ensure that gluons are ultrasoft in the pNRQCD Lagrangian, gauge fields are multipole expanded in $\boldsymbol{r}$. Hence gauge fields in the pNRQCD Lagrangian only depend on time and the c.m. coordinate. The matching of pNRQCD to NRQCD is schematically illustrated in Fig. 85. The pNRQCD Lagrangian is organized as a double expansion in $1/m_h$ and r. At order r in the multipole expansion and at leading order in $1/m_h$, the weakly-coupled pNRQCD Lagrangian density has the form [675, 676]

$$
\begin{aligned}
\mathcal{L}_{\text{pNRQCD}}^{\text{weak}} = \int d^3r \, \text{Tr} \Big\{ & S^\dagger (i\partial_0 - h_s) S + O^\dagger (iD_0 O - h_o) O \Big\} \\
& - V_A \text{Tr} \Big\{ O^\dagger \boldsymbol{r} \cdot g\boldsymbol{E}\, S + S^\dagger \boldsymbol{r} \cdot g\boldsymbol{E}\, O \Big\} - \frac{V_B}{2} \text{Tr} \Big\{ O^\dagger \boldsymbol{r} \cdot g\boldsymbol{E}\, O + O^\dagger O \boldsymbol{r} \cdot g\boldsymbol{E} \Big\} \\
& - \frac{1}{4} F_{\mu\nu}^a F^{\mu\nu a} + \sum_{\ell=1}^{n_\ell} \bar{q}_\ell \left(i\gamma_\mu D^\mu - m_\ell \right) q_\ell,
\end{aligned}
\tag{63}
$$

where (now writing also $1/m_h$, $1/m_h^2$, and $1/m_h^3$ terms in the kinetic energy and potentials)

$$
h_s = \frac{\boldsymbol{p}^2}{m_h} + \frac{\boldsymbol{P}^2}{4m_h} - \frac{\boldsymbol{p}^4}{4m_h^3} + \cdots + V_s, \qquad h_o = \frac{\boldsymbol{p}^2}{m_h} + \frac{\boldsymbol{P}^2}{4m_h} - \frac{\boldsymbol{p}^4}{4m_h^3} + \cdots + V_o,
\tag{64}
$$

$iD_0 O = i\partial_0 O + g[A_0(\boldsymbol{R}, t), O]$, $\boldsymbol{P} = -i\boldsymbol{D_R}$ is the c.m. momentum, $\boldsymbol{p} = -i\boldsymbol{\nabla}_r$ is the relative momentum, and h_s and h_o may be interpreted as the Hamiltonian for the color singlet and color octet heavy quark-antiquark fields. The dots in Eq. (64) stand for higher-order kinetic energy terms. The trace in Eq. (63) is understood both in spin and in color.

The quantities V_s, V_o, V_A, and V_B are Wilson coefficients of pNRQCD. They encode contributions from the soft gluons that have been integrated out from NRQCD. Because under the hierarchy of weakly-coupled pNRQCD the soft scale, $m_h v$, is larger than Λ_{QCD}, the Wilson coefficients may be computed in perturbation theory, order by order in α_s. The Wilson coefficients are, in general, functions of $\boldsymbol{r}$, as well as of the spin and momentum. At leading order, V_A and V_B are 1; they get possible first corrections at order α_s^2 [677]. The Wilson coefficients V_s and V_o may be identified with the color singlet and octet potentials, respectively. Indeed, at leading order $V_s^{(0)} = -4\alpha_s/(3r)$ and $V_o^{(0)} = \alpha_s/(6r)$, which are the Coulomb potentials in the color SU(3) fundamental and adjoint representation, respectively. The potentials V_s and V_o contain, however, also momentum- and spin-dependent corrections. To isolate the different corrections, it is useful to expand the potentials in powers of $1/m_h$. For the singlet case (the octet case is analogous) we can write up to order $1/m_h^2$:

$$
V_s = V_s^{(0)}(r) + \frac{V_s^{(1)}(r)}{m_h} + \frac{V_{\text{SI}}^{(2)}}{m_h^2} + \frac{V_{\text{SD}}^{(2)}}{m_h^2},
\tag{65}
$$

where, at order $1/m_h^2$ we have distinguished between spin-independent (SI) and spin-dependent (SD) terms. In turn, they can be organized as

$$
V_{\text{SI}}^{(2)} = V_r^{(2)}(r) + \frac{1}{4} V_{p^2,\text{CM}}^{(2)}(r)\boldsymbol{P}^2 + V_{L^2,\text{CM}}^{(2)}(r)\,(\boldsymbol{r} \times \boldsymbol{P})^2 + \frac{1}{2}\left\{V_{p^2}^{(2)}(r), \boldsymbol{p}^2\right\} + V_{L^2}^{(2)}(r)\,\boldsymbol{L}^2,
\tag{66}
$$

$$
V_{\text{SD}}^{(2)} = \frac{1}{2} V_{LS,\text{CM}}^{(2)}(r)\,(\boldsymbol{r} \times \boldsymbol{P}) \cdot (\boldsymbol{S}_1 - \boldsymbol{S}_2) + V_{LS}^{(2)}(r)\,\boldsymbol{L} \cdot \boldsymbol{S} + V_{S^2}^{(2)}(r)\,\boldsymbol{S}^2 + V_{S_{12}}^{(2)}(r)\,S_{12},
\tag{67}
$$

where $\boldsymbol{S} = \boldsymbol{S}_1 + \boldsymbol{S}_2 = (\boldsymbol{\sigma}_1 + \boldsymbol{\sigma}_2)/2$ is the total spin ($\boldsymbol{S}_i = \boldsymbol{\sigma}_i/2$ is the spin of the particle i), $\boldsymbol{L} = \boldsymbol{r} \times \boldsymbol{p}$ is the relative orbital angular momentum, and $S_{12} = 3(\hat{\boldsymbol{r}} \cdot \boldsymbol{\sigma}_1)(\hat{\boldsymbol{r}} \cdot \boldsymbol{\sigma}_2) - \boldsymbol{\sigma}_1 \cdot \boldsymbol{\sigma}_2$; $\{\,,\,\}$ stands for the anticommutator. The potential $V_s^{(0)}$ is the static potential, the potential proportional to $V_{LS}^{(2)}$ may be identified with the spin-orbit potential, the potential proportional to $V_{S^2}^{(2)}$ with the spin-spin potential and the potential proportional to $V_{S_{12}}^{(2)}$ with the spin tensor potential.

The above potentials read at leading (non-vanishing) order in perturbation theory (see, e.g., Ref. [652]):

$$V^{(1)}(r) = -\frac{2\alpha_s^2}{r^2}\,, \tag{68}$$

$$V_r^{(2)}(r) = \frac{4\pi}{3}\alpha_s\delta^{(3)}(\boldsymbol{r})\,, \qquad V_{p^2}^{(2)}(r) = -\frac{4\alpha_s}{3r}\,, \qquad V_{L^2}^{(2)}(r) = \frac{2\alpha_s}{3r^3}\,, \tag{69}$$

$$V_{LS}^{(2)}(r) = \frac{2\alpha_s}{r^3}\,, \qquad V_{S^2}^{(2)}(r) = \frac{16\pi\alpha_s}{9}\delta^{(3)}(\boldsymbol{r})\,, \qquad V_{S_{12}}^{(2)}(r) = \frac{\alpha_s}{3r^3}\,. \tag{70}$$

Beyond leading order, the static potential is known up to three-loop accuracy [678–680], and also subleading logarithms, showing up at four loops, have been computed [681]; the $1/m_h$ potential is known up to order α_s^3 [682] and $1/m_h^2$ potentials up to order α_s^2 (these potentials have a long history, see Ref. [683] and references therein). We have assumed that the heavy quark and antiquark have equal masses; for the case of a quark and an antiquark of different masses, we refer, for instance, to Refs. [623, 652, 684, 685]. The Wilson coefficients of pNRQCD inherit the Wilson coefficients of NRQCD. Hence, some of the couplings appearing in the expansion of the Wilson coefficients are naturally computed at the scale of NRQCD, m_h, while others, encoding the soft gluons, are naturally computed at the soft scale, $m_h v$. In weakly-coupled pNRQCD, because the leading potential is the Coulomb potential, the Bohr radius is proportional to $1/(m_h\alpha_s)$ and $v \sim \alpha_s$. Finally, like in any non relativistic EFT, also the Wilson coefficients of pNRQCD are related through constraints imposed by the relativistic invariance of the underlaying fundamental theory, QCD. These constraints fix, for instance, the coefficients of the kinetic terms appearing in Eq. (64) to be the ones coming from expanding the relativistic kinetic energies of a free quark and antiquark. Relations have been also found relating the potentials, e.g., $V_{LS,\mathrm{CM}} = -V_s^{(0)\prime}/(2r)$ (where $V' = dV/dr$), $V_{L^2,\mathrm{CM}} + r\,V_s^{(0)\prime}/2 = 0$, $V_{p^2,\mathrm{CM}} + V_{L^2,\mathrm{CM}} + V_s^{(0)}/2 = 0$ and many others [357, 358, 623, 673, 684]. These relations are exact, i.e., valid at any order in perturbation theory and, when applicable, also non-perturbatively.

From Eq. (63) we see that the relative coordinate $\boldsymbol{r}$ plays the role of a continuous parameter labeling different fields. The dynamical coordinates of the Lagrangian density are the time t and the coordinate $\boldsymbol{R}$, which, in the case of the fields S and O, is the c.m. coordinate. Having written the Lagrangian in terms of singlet and octet fields has made each term in Eq. (63) explicitly gauge invariant.

The power counting of pNRQCD is straightforward. We have already mentioned that $r \sim 1/(m_h v)$ and $t, R \sim 1/(m_h v^2)$. Momenta scale like $p \sim m_h v$ and $P \sim m_h v^2$. Gluon fields and light quark fields are ultrasoft and scale like $m_h v^2$ or Λ_{QCD} to their dimension. The leading-order Hamiltonian, $\boldsymbol{p}^2/m_h + V_s^{(0)}$, scales like $m_h v^2$ (and analogously in the octet case), which is the order of the Bohr levels. The potentials listed in Eqs. (68)-(70) scale like $m_h v^4$. The first correction to a pure potential picture of the quarkonium interaction comes from the chromoelectric dipole interaction terms in the second line of Eq. (63). These operators are of order $g(m_h v^2)^2/(m_h v) \sim g m_h v^3$. However, in order to project on singlet states the chromoelectric dipole interaction may enter only in loops (see the diagram in the right-hand side of Fig. 85). Such a loop diagram is of order $g^2(m_h v^2)^3/(m_h v)^2 \sim g^2 m_h v^4$. The coupling g^2 is computed at the ultrasoft scale. Hence, if $\Lambda_{\mathrm{QCD}} \ll m_h v^2$, the coupling is perturbative and the chromoelectric dipole loop diagram is suppressed with respect to the contributions coming from the potentials in Eqs. (68)-(70). Elsewhere, if $\Lambda_{\mathrm{QCD}} \sim m_h v^2$, it is of the same order.

At leading order in the multipole expansion, the equation of motion for the singlet field reads

$$i\partial_0 S = h_s S, \tag{71}$$

which is the Schrödinger equation that in quantum mechanics describes the evolution of a non-relativistic bound state. Potential NRQCD provides therefore a QCD foundation of the potential picture underlaying many phenomenological quark models, a rigorous QCD definition and derivation of the potentials and a range of validity for the Schrödinger equation itself (for the somehow paradoxical history that has led from the Lorentz covariant formulation of the bound state problem to the field theoretical foundation of the Schrödinger equation, see Ref. [653]). As we have seen, ultrasoft gluons start contributing, and therefore correcting the potential picture, for the spectrum, at order $m_h v^4$ or $m_h v^5$, in dependence of Λ_{QCD}. The potentials are Wilson coefficients of an EFT, they are regularized, undergo renormalization and satisfy renormalization group equations that allow to resum potentially large logarithms in their expressions [677, 678, 686–692]. The proper renormalization of the potentials, highly non-trivial, as it has to account for correlated renormalization scales originating in NRQCD and pNRQCD, guarantees, however, that the final physical

results are finite and scheme independent at any order in the expansion parameters of the EFT. This is not the case for phenomenological models.

Weakly-coupled pNRQCD requires the condition $\Lambda_{\text{QCD}} \lesssim m_h v^2$ to be fulfilled. This condition is realized if the size of the quarkonium is smaller and the revolution time not larger than the typical size of a heavy-light hadron. Examples are the bottomonium ground state, the ground state of the B_c system, and, to a somewhat lesser extent, the charmonium ground state, and the first bottomonium excited states. We recall that in a Coulombic system the size is proportional to the inverse of the mass and to the principal quantum number. The precise dependence on the latter follows from the precise definition of the size. A review on applications of weakly-coupled pNRQCD to several tightly bound quarkonia can be found in Ref. [693]. Weak-coupling determinations of the bottomonium ground state masses are typically used to extract the charm and bottom masses [633, 694–702]. Hence, they provide alternative observables for the extraction of the heavy quark masses to the heavy-light meson masses discussed in Sec. 4.4.1. The results are consistent with the ones presented in Sec. 4.4.1, but with some different systematics, although they face some similar issues, like the use of a proper subtraction scheme for the mass. Nowadays the precision is N^3LO, the determination of the bottom mass includes the effects due to a finite charm mass, and the observables used are not only the masses of the vector states, $\Upsilon(1S)$ and J/ψ, but also the masses of the pseudoscalar states, η_b following the BaBar discovery [703] and η_c, and the B_c ground state following the CDF discovery [704] and the latest LHCb precise measurements [705–708]. In Ref. [701] the bottom and charm masses have been extracted from a global fit up to $n = 3$ bottomonium states. On the other hand, once the heavy quark masses have been established on one set of spectroscopy observables, they can be used for others like the B_c mass or the B_c spectrum (see Ref. [709] for an early reference and Ref. [685] for a status of the art calculation at N^3LO). Fine and hyperfine splittings of charmonium and bottomonium have been computed perturbatively in Refs. [710, 711] and at to NLL accuracy in Ref. [712], similarly for the B_c^*-B_c hyperfine splitting in Ref. [713]. After an effort that lasted more than one decade the whole perturbative heavy quarkonium spectrum has been computed at N^3LO [687, 714–719]. Recently, this result has been further improved reaching N^3LL accuracy up to a missing contribution of the two-loop soft running [691, 692]. The N^3LL order represents the presently achievable precision of these calculations. Going beyond this precision will require a major computational effort, like the four-loop determination of the static potential, that appears beyond near reach. Electromagnetic decays of the bottomonium lowest levels have been computed including N^2LL corrections in Refs. [720, 721]. A different power counting that includes at leading order the exact static potential has been used for these quantities in Ref. [722]. Corrections to the wave function and leptonic decay width of the $\Upsilon(1S)$ at N^3LO have been computed in Refs. [723, 724]. Non-perturbative corrections in the form of condensates have been included in Refs. [725, 726]. Radiative quarkonium decays have been analyzed in Refs. [727–732]. Radiative and inclusive decays of the $\Upsilon(1S)$ may also serve as a determination of α_s at the bottom mass scale [733]. Radiative transitions, M1 and E1, at relative order v^2 in the velocity expansion have been computed in various power countings in Refs. [734–737]. Noteworthy, pNRQCD may explain the tiny $\Upsilon(2S) \to \gamma \eta_b(1S)$ branching fraction measured by BaBar [738]. Finally, the photon line shape in the radiative transition $J/\psi \to \gamma \eta_c(1S)$ has been studied in Ref. [739].

• *Strongly-coupled pNRQCD*

When the hierarchy of scales is $\Lambda_{\text{QCD}} \gg m_h v^2$, then the theory enters the strong-coupling regime. Such a regime may be appropriate to describe higher quarkonium states, and quarkonium exotica. Strongly-coupled pNRQCD is obtained by integrating out the hadronic scale Λ_{QCD}, which means that all colored degrees of freedom are absent [652, 674, 740–743]. Such an EFT may be constructed, in principle, for any hadron made of a heavy quark-antiquark pair, hence for both ordinary quarkonia and exotic states where the heavy quark-antiquark pair binds with valence light quarks or gluons.

Let us consider in this section the simplest case of strongly-coupled pNRQCD for ordinary quarkonia. Lattice QCD shows evidence that the quarkonium static energy is separated by a gap of order Λ_{QCD} from the energies of the gluonic excitations between the static quark-antiquark pair, see Fig. 86. If this condition is also fulfilled by the binding energies, i.e., if the binding energies of the states that can be constructed out of the quarkonium static energy are separated by a gap of order Λ_{QCD} from the binding energies of the states that can be constructed out of the static energies of the gluonic excitations, and from open-flavor states, then one can integrate out all these latter higher energy states. The resulting EFT is just made of a quark-antiquark color singlet field, whose modes are the quarkonium states, and light hadrons. The coupling of quarkonia with light hadrons has been considered in the framework of pNRQCD in
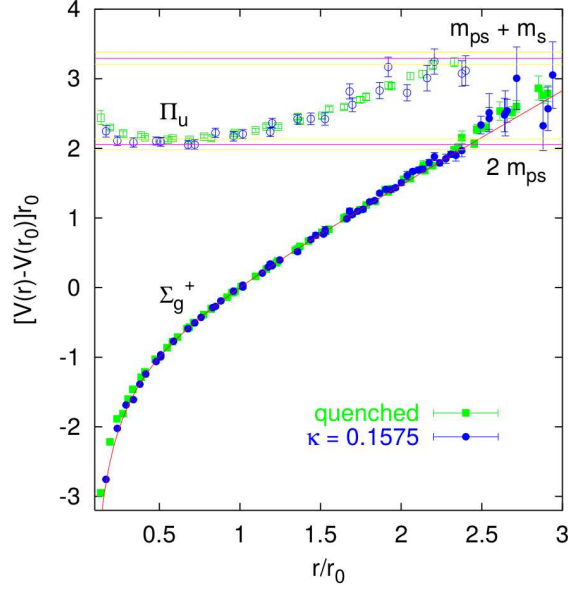
Figure 86: The quarkonium static energy (labeled Σ_g^+) vs the energy of the first gluonic excitation between a static quark-antiquark pair (labeled Π_u) as a function of the distance between the quark and the antiquark. The quenched (green) and two-flavor (blue) lattice data are from [744]. The unit r_0 is about 0.5 fm.

Ref. [745]. It impacts very mildly spectral properties (masses, widths) of quarkonia that lie well below the open-flavor threshold. If such quarkonia are our main concern, then we may neglect their coupling with light hadrons; under these circumstances the pNRQCD Lagrangian density assumes the particularly simple form:

$$\mathcal{L}_{\text{pNRQCD}}^{\text{strong}} = \int d^3 r \, \text{Tr} \left\{ S^\dagger \left(i\partial_0 - h_S \right) S \right\} . \tag{72}$$

The Hamiltonian, h_S, has the same form, given by Eqs. (64)-(67), as in weakly-coupled pNRQCD. The equation of motion is the Schrödinger equation (71), which provides a field theoretical foundation of potential models also in the strong-coupling regime. It also allows us to go systematically beyond the potential picture by including couplings with light degrees of freedom.

All the complications of the non-perturbative dynamics are encoded in the potentials, which at order $1/m_h$ is $V_s^{(1)}$ and at order $1/m_h^2$ are the spin-independent and spin-dependent terms identified in Eqs. (66) and (67). The crucial points about the EFT treatment that distinguish it from phenomenological potential models can be summarized as follows. *(i)* The potentials can be written as the products of Wilson coefficients, factorizing contributions from the high-energy scale, m_h, and low-energy matrix elements, encoding contributions coming from the scales $m_h v$ and Λ_{QCD}. The exact expressions follow from matching pNRQCD with its high-energy completion, which is NRQCD. *(ii)* The high-energy Wilson coefficients of pNRQCD are inherited from NRQCD. These are the Wilson coefficients listed up to order $1/m_h^2$ in the NRQCD Lagrangian (62). As we discussed there, they are known expansions in the strong coupling (up to the computed orders). Because the NRQCD Wilson coefficients have a real part and an imaginary part, also the pNRQCD potentials develop a real part, responsible for the quarkonium binding, and an imaginary part, responsible for the quarkonium annihilation. At higher orders, also contributions coming from the scale $\sqrt{m_h \Lambda_{\text{QCD}}}$ may become relevant; these contributions can be computed in perturbation theory as $\sqrt{m_h \Lambda_{\text{QCD}}} \gg \Lambda_{\text{QCD}}$ [743]. *(iii)* The low-energy matrix elements are non-perturbative. Their field-theoretical expressions, relevant for potentials up to order $1/m_h^2$, are known. The static potential is equal to $\lim_{T \to \infty} i \ln W/T$, where W is the expectation value of a rectangular Wilson loop of spatial extension r and temporal extension T [746–749]. Similarly, the low-energy real parts of the other potentials can be expressed in terms of Wilson loops and field insertions on them [356, 740, 741]. These Wilson loops may be computed in weak-coupling QCD giving back the weak-coupling potentials listed in

114

Eqs. (68)-(70) [750]. More relevant from the phenomenological point of view is, however, their numerical non-perturbative determination via lattice QCD. Indeed, the computation of these potentials has a long history that begins with the inception of lattice QCD. Their most recent determinations can be found in Refs. [359–361]. One should remark that lattice calculations of the quarkonium potentials have not included so far $1/m_h^2$ momentum- and spin-independent potentials, and have been limited to the pure SU(3) gauge theory. Potentials that have not been computed on the lattice may be estimated in the long distance using the effective string theory, which has also proved to be very successful in interpreting the existing long-distance data [355, 750–752]. The low-energy contributions to the imaginary parts of the potential are matrix elements of the NRQCD four-fermion operators. Hence they are local terms proportional to $\delta^3(\mathbf{r})$ or derivatives of it. Non-perturbative contributions are encoded into constants that may be expressed in terms of momenta of correlators of chromoelectric and/or chromomagnetic fields [674, 742]. They may be fixed on data or computed with lattice QCD, but lattice calculations have not been intensively pursued, so far, for these quantities. *(iv)* Finally, because pNRQCD retains the correct ultraviolet behaviour of the low-energy EFT, it is renormalizable order by order in the expansion parameters in both its weak-coupling and strong-coupling versions. In particular, quantum-mechanical perturbation theory can be implemented at any order without incurring into uncanceled divergences.

Applications of strongly-coupled pNRQCD have been limited so far to the computation of quarkonium decay widths, in particular for charmonium and bottomonium *P*-waves [12, 674, 742, 743]. The advantage with respect to the NRQCD approach is that, while the NRQCD four-fermion matrix elements depend on the quarkonium state, their pNRQCD expression factorizes all the quarkonium dependence into the wave function at the origin (or its derivatives) squared. The wave function at the origin squared gets multiplied by momenta of correlators of field-strength tensors, *F*, that are universal, quarkonium independent, constants. Schematically, one obtains for the expression of a generic NRQCD four-fermion matrix element in pNRQCD that $\langle \text{4-fermion} \rangle \sim |\text{wave-function}(0)|^2 \times \int dt \, \langle F(t) \cdots F(0) \rangle$. This leads to a significant reduction in the number of non-perturbative parameters and allows to use information gained in the charmonium sector to make predictions in the bottomonium one. Electroproduction of quarkonium may be treated in pNRQCD in the same way. Hadroproduction, instead, has not been formulated yet in the pNRQCD language, owing in part to the difficulty to state and prove rigorously the NRQCD factorization theorem in that context, see discussion and references in the previous section. Finally, very recently pNRQCD conbined with the multipole expansion has been used to compute quarkonium hadronic transitions [753].

- *pNRQCD for systems other than quarkonia*

Weakly-coupled pNRQCD, strongly-coupled pNRQCD or a mixture of the two can be used to describe systems with three valence quarks, two of them heavy [639, 640, 646, 754, 755]. The key observation is that the non-relativistic hierarchy of scales given in Eq. (61), where *v* is the relative heavy-quark velocity, is preserved. This allows one to systematically integrate out these scales to describe eventually the baryon with a suitable EFT. If the heavy quark-quark distance is of the order of $1/\Lambda_{\text{QCD}}$, then the valence light-quark affects the quark-quark potential. Elsewhere, if the heavy quark-quark distance is smaller than $1/\Lambda_{\text{QCD}}$, then we may disentangle the quark-quark dynamics, described by a perturbative quark-quark potential, from the coupling of the heavy-quark pair with the light quark. Since in this last case, the light quark sees the heavy-quark pair as a pointlike particle, its interaction with the heavy-quark pair is described by the HQET. Processes involving light hadrons in final or intermediate states may be described in the framework of the heavy-baryon chiral effective theory [756]. Similarly, one can devise EFTs for describing low-energy modes of baryons made of three heavy quarks. These states have not been discovered yet in experiments, but they offer a unique tool to study confinement and the transition region from the Coulomb regime to the confined one in a non-trivial geometrical setting [754]. These issues are already addressed by lattice computations of the three-quark static potential [757–759]. Higher-order potentials in the $1/m_h$ expansion have been defined in terms of Wilson loops and field insertions on them, as in the quarkonium case, and may be eventually computed on the lattice providing, for instance, first principle determinations of the heavy baryon fine and hyperfine splittings [754].

Possible bound states made of two quarkonia or of a quarkonium and a nucleon (hadroquarkonium, see Sec. 4.3.2) may be characterized by even lower energy scales than those characterizing the binding in quarkonia or baryons made of at least two heavy quarks. These lower energy scales are those associated with the pion exchanges responsible for the long-range interaction. One can treat these systems in an EFT framework by starting from the pNRQCD

description of the quarkonium and the heavy-baryon chiral effective theory description of the nucleon. The long-range pion exchange interaction sets the scale of the typical size of the system to be of the order of $1/M_\pi$, i.e., much larger than the size of the quarkonium and even larger than its typical time scale, which is of the order of the inverse of the binding energy. Once modes associated with the quarkonium binding energy and M_π have been integrated out, the quarkonium-quarkonium or the quarkonium-nucleon interaction is described by a potential that, in this way, has been systematically computed from QCD. The coupling of quarkonium with the pions is encoded in a Wilson coefficient that may be identified with the quarkonium chromoelectric polarizability. In the quarkonium-quarkonium system, the lowest energy EFT describing modes of energy and momentum of order $m_\pi^2/(2m_h)$ is called van der Waals EFT (WEFT) [490, 745]. The resulting potential is, in fact, the van der Waals potential. In the quarkonium-nucleon system, the lowest energy EFT describing modes of energy and momentum of order $M_\pi^2/(2\Lambda_\chi)$ has been dubbed potential quarkonium-nucleon EFT (pQNEFT) [491]. Interest in these systems has been renewed recently after the discovery by the LHCb Collaboration of the pentaquark states $P_c(4380)^+$ and $P_c(4450)^+$, with valence quark content $P_c^+ = \bar{c}cuud$, as intermediate resonant states in the weak decay process $\Lambda_b^0 \to J/\psi K^- p$ [36, 305], see Sec. 3.3.2.

In the next section, we will deal with higher excitations of a heavy quark-antiquark pair due to gluons (hybrids) and, on a more qualitative level, due to light quark pairs (generic tetraquarks, not assuming any kind of clustering). The framework will be that one of strongly-coupled pNRQCD. The specific application of strongly-coupled pNRQCD to these systems will require some extra assumptions that allow for further expansions in the EFT and, therefore, in the observables. In the case of molecular physics (i.e., QED), the leading-order term in the expansion corresponds to the Born–Oppenheimer approximation. Although this is no more the case in QCD, we will nevertheless call the resulting EFT, the Born–Oppenheimer effective field theory (BOEFT).

4.4.4. Born–Oppenheimer EFT

In the previous section, we have studied strongly-coupled quarkonia under the assumption that the quarkonium energy levels develop a mass gap of order $\Lambda_{\rm QCD}$ with respect to the spectrum of quarkonium hybrids, quarkonium plus glueballs and other exotic states. This assumption allows one to integrate out all degrees of freedom with the exception of the heavy quark-antiquark pair and cast their contribution into a potential. We may call this the Born–Oppenheimer assumption. If we extend it to hybrid (tetraquark) heavy quarkonium states, we may picture each hybrid (tetraquark) state as being a vibrational mode of a heavy quark-antiquark pair inside a potential. The hybrid (tetraquark) potential may be identified with the energy of a gluonic (light-quark pair) excitation between the heavy quark-antiquark pair with given quantum numbers. Ideally, gluonic (light-quark pair) excitations are separated from each other by a gap of order $\Lambda_{\rm QCD}$, while vibrational modes of a heavy quark-antiquark pair inside a given potential have a typical energy of order $m_h v^2$, which is assumed to be much smaller than $\Lambda_{\rm QCD}$. An illustration of the distribution of vibrational modes for the different quarkonium and hybrid (or tetraquark) potentials, under the above assumptions, is shown in Fig. 87. A Born–Oppenheimer picture to describe quarkonium hybrids has been suggested in Refs. [192, 469, 476]. An EFT for quarkonium hybrids in the framework of strongly-coupled pNRQCD under the Born–Oppenheimer assumption has been developed in Ref. [470] under the name of Born–Oppenheimer EFT (BOEFT). A similar approach is in Refs. [193, 471]. An extension to include excitations due to light quarks, i.e., tetraquarks, has been suggested in Refs. [467, 760], and more explicitly worked out in Refs. [467–469, 761]. For recent related work see Ref. [762].

● *Hybrids*

Hybrid potentials have been computed in the pure SU(3)-color gauge theory on the lattice for almost three decades [763–768]. The lowest static hybrid energy has been shown in Fig. 86 together with the heavy quark-antiquark static energy. Higher static hybrid energies are shown in Fig. 88. The gluonic static energies, E_Γ, are classified according to representations of the symmetry group $D_{\infty h}$, which is the symmetry group of diatomic molecules. They are labeled Λ_η^σ. The quantum number Λ is equal to $|\lambda|$, where λ are the eigenvalues of $\hat{r} \cdot K$, i.e., the angular momentum of the gluons, K, projected on the unit vector, $\hat{r}$, along the heavy-quark-antiquark axis. Λ may assume the values $0, 1, 2, \ldots$; these numbers are usually indicated with capital greek letters: $\Lambda = \Sigma, \Pi, \Delta, \ldots$. The quantum number η is the CP eigenvalue ($+1 \equiv g$ and $-1 \equiv u$), and σ is the eigenvalue of reflection with respect to a plane passing through the heavy quark-antiquark axis. The quantum number σ is relevant only for Σ states. The lowest state, with quantum numbers Σ_g^+, describes a static quark-antiquark pair in the color singlet representation. In general, there is more than one state for each irreducible representation of $D_{\infty h}$: higher states are denoted by primes, e.g., Π_u, Π_u', Π_u'', ... In
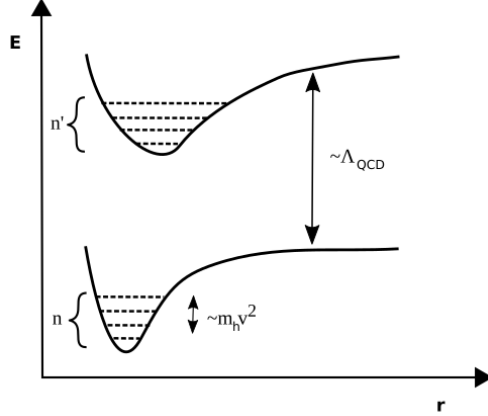
Figure 87: Schematic distribution of the hybrid or tetraquark energy levels in the Born–Oppenheimer picture.

the long range, the ordering of the hybrid static energies may be understood in terms of the effective string theory, see discussion in Ref. [766]. In the limit $r \to 0$, the group $D_{\infty h}$ becomes the more symmetric group O(3)×C. This means that several different Λ_η^σ representations reduce to the same J^{PC} representation in that limit and the corresponding static energies become degenerate [765]. Hybrid states in the $r \to 0$ limit are often called gluelumps. In particular, the gluelump multiplets (Σ_u^-, Π_u), $(\Sigma_g^{+\prime}, \Pi_g)$, $(\Sigma_g^-, \Pi_g', \Delta_g)$, $(\Sigma_u^+, \Pi_u', \Delta_u)$ are degenerate. Finally, in the very short range, $r\Lambda_{\text{QCD}} \ll 1$, all hybrid potentials behave like the Coulomb color-octet potential, which is the short-distance component of the potential between a static quark-antiquark pair in the adjoint representation. The symmetry O(3)×C is made manifest in pNRQCD. Hence pNRQCD is the suitable EFT framework for studying hybrids in the short range [676].

Figure 88 shows that close to their minimum the hybrid potentials tend, indeed, to cluster into the gluelump multiplets, i.e., according to the short-distance symmetry group O(3)×C. Hence, assuming that the physical hybrid states live close to their potential minimum, the simplified Born–Oppenheimer picture of Fig. 87 has to be modified by replacing single potentials with multiplets of nearly degenerate potentials. Because of the near degeneracy, vibrational modes associated to these potentials may have a significant mixing. Different multiplets are separated by a mass gap of order Λ_{QCD}.

Let us consider, in the following, hybrids that are vibrational modes of the lowest-lying static energies. According to Fig. 88, these are the static energies with quantum numbers Π_u and Σ_u^-. In the $r \to 0$ limit Π_u and Σ_u^- are degenerate and correspond to a gluonic operator with quantum numbers 1^{+-}. The Born–Oppenheimer EFT Lagrangian density describing hybrids that are vibrational modes of the static potentials Π_u and Σ_u^- is a generalization of the Lagrangian for strongly-coupled pNRQCD, Eq. (72), for nearly degenerate states. It reads [192, 470]:

$$\mathcal{L}_{\text{BOEFT for } 1^{+-}} = \int d^3 r \sum_{\lambda \lambda'} \text{Tr} \left\{ \Psi_{1^{+-}\lambda}^\dagger \left(i\partial_0 - V_{1^{+-}\lambda\lambda'}(r) + \hat{r}_\lambda^{i\dagger} \frac{\nabla_r^2}{m_h} \hat{r}_{\lambda'}^i \right) \Psi_{1^{+-}\lambda'} \right\}. \tag{73}$$

An equivalent Lagrangian is in Ref. [193]. The quantum number λ (and λ') may assume the values ± 1 and 0. The projectors to the eigenstates of the angular momentum of the gluons along the heavy-quark-antiquark axis are $\hat{r}_0^i = \hat{r}^i$ and $\hat{r}_{\pm 1}^i = \mp \left(\hat{\theta}^i \pm i\hat{\phi}^i \right) / \sqrt{2}$, where $\hat{r} = (\sin\theta\cos\phi, \sin\theta\sin\phi, \cos\theta)$, $\hat{\theta} = (\cos\theta\cos\phi, \cos\theta\sin\phi, -\sin\theta)$ and $\hat{\phi} = (-\sin\phi, \cos\phi, 0)$. The fields $\Psi_{1^{+-}\lambda}$ depend on time, the c.m. coordinate $\boldsymbol{R}$, and the relative coordinate $\boldsymbol{r}$. The modes of the fields $\Psi_{1^{+-}\lambda}$ are the hybrid eigenstates that may be built out of the hybrid potentials $V_{1^{+-}\lambda\lambda'}$. The hybrid potentials may be organized, like the quarkonium potentials, as an expansion in the inverse of the heavy quark mass, $1/m_h$. The static potential, $V_{1^{+-}\lambda\lambda'}^{(0)} = \delta_{\lambda\lambda'} V_{1^{+-}\lambda}^{(0)}$, coincides with the hybrid static energy: $V_{1^{+-}0}^{(0)} = E_{\Sigma_u^-}$ and $V_{1^{+-}\pm 1}^{(0)} = E_{\Pi_u}$. For what concerns hybrid potentials of higher order in $1/m_h$, there are no available lattice determinations. In the absence of them, these potentials have been modeled either using the short-distance multipole expansion [472], or both the short-distance multipole expansion and the long-range effective string theory [193, 471].
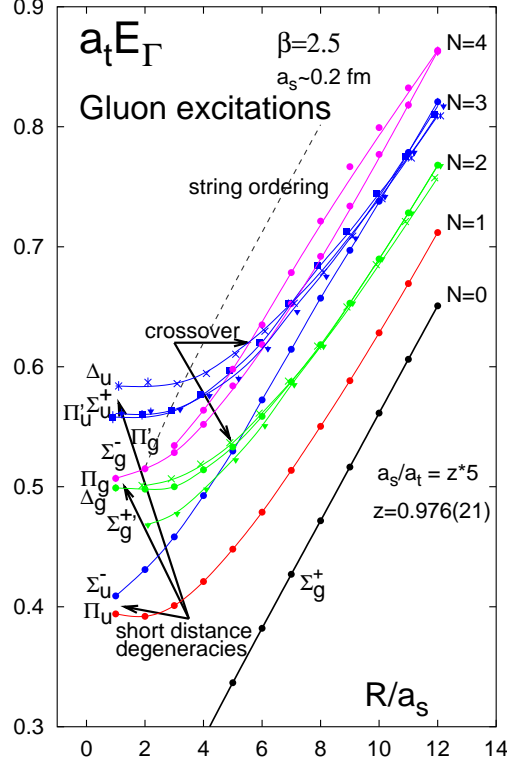
Figure 88: Hybrid static energies in the lattice units a_s and a_t from the quenched lattice simulations of Ref. [766] at the lattice coupling $\beta = 2.5$.

The term $\hat{r}_\lambda^{i\dagger}(\mathbf{\nabla}_r^2/m_h)\hat{r}_{\lambda'}^i$ in the Lagrangian (73) can be split into a kinetic operator acting on the heavy quark-antiquark field and a nonadiabatic coupling: $\hat{r}_\lambda^{i\dagger}(\mathbf{\nabla}_r^2/m_h)\hat{r}_{\lambda'}^i = \delta_{\lambda\lambda'}\mathbf{\nabla}_r^2/m_h + C_{1^{+-}\lambda\lambda'}^{\mathrm{nad}}$, with $C_{1^{+-}\lambda\lambda'}^{\mathrm{nad}} = \hat{r}_\lambda^{i\dagger}[\mathbf{\nabla}_r^2/m_h, \hat{r}_{\lambda'}^i]$ being the nonadiabatic coupling. Concerning the size of the different terms appearing in the Lagrangian (73), the temporal derivative, the kinetic term and the leading-order (static) potential (up to a constant shift) are of order $m_h v^2$. As discussed in Ref. [470], this is also the size of the nonadiabatic coupling. For diatomic molecules the counting is different, essentially because the size of the electron cloud and the distance of the two atoms are in the molecule of the same order, while for hybrids the distance of the heavy quark-antiquark pair is of order $1/(m_h v)$, i.e., smaller than the size of the hadron, which is of order Λ_{QCD}. As a consequence the adiabatic coupling may be treated as a perturbation in diatomic molecules, while it contributes at leading order to heavy quarkonium hybrids. Another consequence is that, since in diatomic molecules there is no special hierarchy between these two lengths, there is neither a special symmetry at short distances nor a corresponding degeneracy pattern, which are instead typical, as we have seen, of heavy quarkonium hybrids.

The leading-order equations of motion for the fields $\Psi_{1^{+-}\lambda}^\dagger$ that follow from the Lagrangian (73) are a set of coupled Schrödinger equations [192]

$$i\partial_0\Psi_{1^{+-}\lambda} = \left[\left(-\frac{\mathbf{\nabla}_r^2}{m_h} + V_{1^{+-}\lambda}^{(0)}\right)\delta_{\lambda\lambda'} - \sum_{\lambda'} C_{1^{+-}\lambda\lambda'}^{\mathrm{nad}}\right]\Psi_{\kappa\lambda'}, \tag{74}$$

which generalize Eq. (71). By solving them we obtain the eigenvalues $\mathcal{E}_N$ that give the masses M_N of the states

118

Multiplet	T	$J^{PC}(S=0)$	$J^{PC}(S=1)$	E_Γ
H_1	1	1^{--}	$(0,1,2)^{-+}$	$E_{\Sigma_u^-}, E_{\Pi_u}$
H_2	1	1^{++}	$(0,1,2)^{+-}$	E_{Π_u}
H_3	0	0^{++}	1^{+-}	$E_{\Sigma_u^-}$
H_4	2	2^{++}	$(1,2,3)^{+-}$	$E_{\Sigma_u^-}, E_{\Pi_u}$

Table 12: Lowest-lying quarkonium hybrid multiplets. The number labeling H reflects the order in which the state appears in the spectrum from lower to higher masses. S is the total spin of the quark-antiquark pair, and T is the sum of the orbital angular momentum of the quark-antiquark pair and the gluonic angular momentum. Note that the $T=0$ state is not the lowest mass state [192].
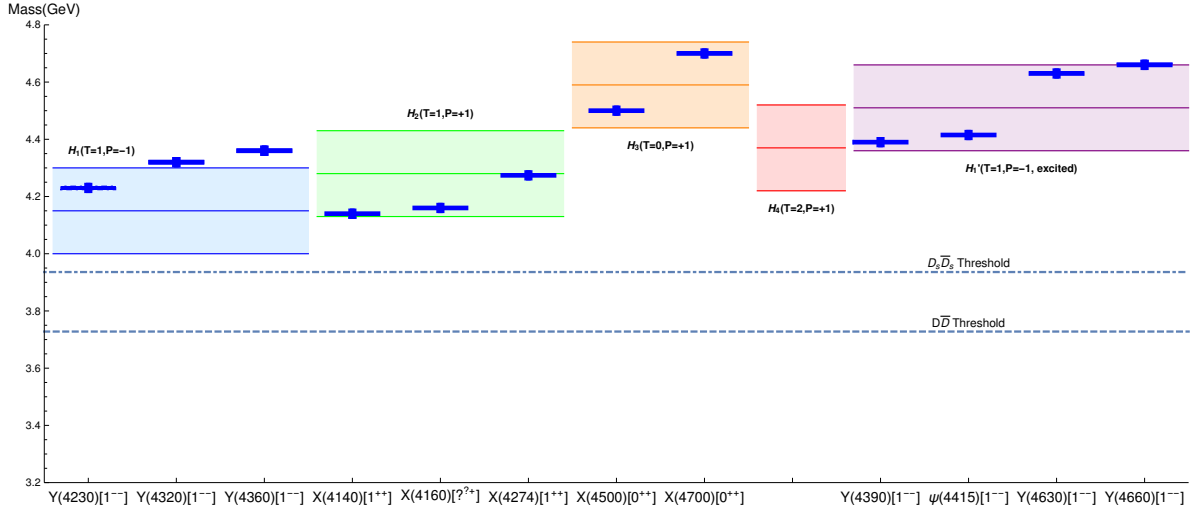

Figure 89: Mass spectrum of neutral exotic charmonium states obtained by solving Eqs. (74) according to Ref. [192]. The experimental states of Sec. 3.1 that have matching quantum numbers are plotted in solid blue lines. The spin-symmetry multiplets are labeled H_1 ($T = 1$, negative parity), H_2 ($T = 1$, positive parity), H_3 ($T = 0$, positive parity), H_4 ($T = 2$, positive parity), and H_1' (first radially excited state with $T = 1$ and negative parity). The multiplets have been plotted with error bands corresponding to a gluelump mass uncertainty of 0.15 GeV. Figure updated from Refs. [192, 470].

as $M_N = 2m_h + \mathcal{E}_N$. Keeping in the Eqs. (74) only the heavy quark-antiquark kinetic energy and the hybrid static energies, $E_{\Sigma_u^-}$ and E_{Π_u}, amounts to the Born–Oppenheimer approximation. Keeping only the diagonal terms amounts to the adiabatic approximation. As we argued above, the exact leading-order equations include both diagonal and off-diagonal terms of the so-called non-adiabatic coupling, as both diagonal and off-diagonal terms contribute at the same order to the energy levels of heavy quarkonium hybrids.

The coupled Schrödinger equations (74) mix states with the same parity. A physical consequence of this mixing is the so-called Λ-doubling, i.e., the lifting of degeneracy between states with opposite parity. The effect is also present in molecular physics, however, there Λ-doubling is a subleading effect, while it is a leading-order effect in the spectrum of quarkonium hybrids. The eigenstates of the Eqs. (74) are organized in the multiplets shown in Table 12. In the adiabatic approximation the multiplets H_1 and H_2 would be degenerate [467–469]. The solution of the full set of equations (74) is the spectrum shown in Fig. 89. The spectrum has been computed using for the charm quark the mass in the renormalon subtraction (RS) scheme $m_{c\,\mathrm{RS}} = 1.477(40)$ GeV [633, 767] (for more details about masses in renormalon subtraction schemes see also Sec. 4.4.1). The gluelump masses, which enter in the normalization of the hybrid potentials, have been computed in the same scheme and assigned an uncertainty of ± 0.15 GeV, which is the largest source of uncertainty in the hybrid masses [767]. Figure 89 clearly shows Λ-doubling, as the degeneracy between the H_1 and H_2 multiplets is lifted. The experimental states plotted in Fig. 89 are neutral isoscalar states in the charmonium sector taken from Sec. 3.1 with matching J^{PC} quantum numbers. The figure does not imply that all these states should be identified with hybrids. A critical analysis of their properties and different possible interpretations have been extensively presented in Sec. 3.1, and in Secs. 4.3.2, 4.3.3 and 4.3.4. Promising candidates for charmonium

hybrids or for states with a large hybrid component are the $Y(4230)$ and $Y(4390)$ because of their significant width into $\pi^+\pi^- h_c$. In the hybrid picture this decay does not need spin flipping of the heavy quark-antiquark pair, which is in a spin zero state. Spin-flipping terms are suppressed in the heavy quark limit. Nevertheless, it has been pointed out in Ref. [193] that mixing with spin one quarkonium states happens already at order $1/m_h$ (see below). This possibly large mixing may allow for significant widths also into final states with spin one quarkonia, in particular $\pi^+\pi^- J/\psi$. In Ref. [192] a similar study as the one summarized in Fig. 89 has been done for hybrids in the bottomonium [$(b\bar{c})$] sector: H_1 multiplets get a mass of (10.79 ± 0.15) GeV [(7.48 ± 0.15) GeV], H_2 multiplets a mass of (10.84 ± 0.15) GeV [(7.58 ± 0.15) GeV], H_3 multiplets a mass of (11.06 ± 0.15) GeV [(7.85 ± 0.15) GeV], H_4 multiplets a mass of (10.90 ± 0.15) GeV [(7.65 ± 0.15) GeV], and H_1' multiplets a mass of (10.98 ± 0.15) GeV [(7.76 ± 0.15) GeV]. The RS bottom mass has been fixed at $m_{b\,\mathrm{RS}} = 4.863(55)$ GeV. From the experimental side, candidate states of bottomonium hybrids in the H_1 or H_1' multiplets are the $\Upsilon(10860)$ [1^{--}], with a mass of $M_{\Upsilon(10860)} = (10891.1 \pm 3.2^{+0.6}_{-1.7})$ MeV and the $\Upsilon(11020)$ [1^{--}], with a mass of $M_{\Upsilon(11020)} = (10987.5^{+6.4}_{-2.5}{}^{+9.0}_{-2.1})$ MeV [296], see Sec. 3.2.3. To these we can add the recently observed signal by Belle with a mass of $M_{\Upsilon(10750)} = (10752.7 \pm 5.9^{+0.7}_{-1.1})$ MeV, which may also qualify as an H_1 multiplet bottomonium hybrid candidate [7].

The charmonium hybrid spectrum has been recently computed by the Hadron Spectrum Collaboration using dynamical lattice QCD simulations: in Ref. [130] using anisotropic lattices with $2+1$ flavors at a pion mass of 396 MeV, and in Ref. [131] in an improved setting at a pion mass of 236 MeV, see Fig. 96. Lattice data are consistent with the computations reported in Fig. 89, although the quoted lattice errors are somewhat smaller but these are only the statistical uncertainties — see Sec. 4.5.1 for a discussion of these lattice results and potential systematic uncertainties. In the case of the H_1 multiplet the smaller errors make the data sensitive to the spin splittings of the states inside the multiplet. The spin splittings provide relevant information on the heavy quarkonium hybrid spin interaction, as we will discuss at the end of this section. The bottomonium hybrid spectrum has been studied, so far, only on quenched lattices: in Ref. [476] using anisotropic lattices and treating the bottom-antibottom pair non relativistically in the framework of lattice NRQCD, and in Ref. [477] using anisotropic lattices and treating the bottom-antibottom pair fully relativistically. At the present state of our knowledge the results of Ref. [476] appear consistent with the mass values of the bottomonium hybrid multiplets reported above from Ref. [192], while those of Ref. [477] show some major discrepancies. We refer to Ref. [192] for a discussion.

The bottomonium and charmonium hybrid spectrum has been studied in the framework of QCD sum rules in Ref. [769] and the $b\bar{c}$ hybrid spectrum in Ref. [770]. Using hybrid operators and computing correlation functions and spectral functions up to dimension-six condensates, the sum rules stabilize and provide mass predictions. The masses for the H_1 hybrids are between 3.4 GeV and 4 GeV in the charmonium sector, between 9.7 GeV and 9.9 GeV in the bottomonium sector, and between 6.8 GeV and 7.2 GeV for the $c\bar{b}$ hybrids. Hence, for this multiplet they are somewhat smaller than in the analysis of Ref. [192]. The other multiplets are consistent with Ref. [192], although the 1^{++} state of the charmonium H_2 multiplet and the H_3 multiplet tend to be heavier. Similar observations also hold for the 1^+ state of the $b\bar{c}$ H_2 multiplet and the H_3 multiplet, while the bottomonium 0^{+-} hybrid state of the H_2 multiplet tends to be lighter.

As remarked above, the lattice data of Ref. [131] are sensitive to the charmonium hybrid spin splittings (but it is important to remember that these data suffer from systematic uncertainties). In Ref. [472], this information has been used to constrain the heavy quarkonium hybrid spin-dependent potential. The heavy quarkonium hybrid spin-dependent potential may be organized, like in the quarkonium case, as an expansion in $1/m_h$, see Eqs. (65) and (67). Differently from the quarkonium case, the hybrid potential gets a first contribution already at order $1/m_h$ [193]. For the implications of this term to the spin splittings see Ref. [471]; heavy quarkonium hybrid spin splittings in the Born–Oppenheimer framework with NRQCD have been also analyzed in Ref. [771]. The $1/m_h$ potential is the leading contribution to the spin-dependent potential. It stems from the expectation value of the chromomagnetic operator, $c_F \psi^\dagger \boldsymbol{\sigma} \cdot \boldsymbol{B}/(2m_h)\psi + $charge conjugation, on the hybrid state (the operator appears in the NRQCD Lagrangian (62)), and, in the framework of pNRQCD, among the operators listed in Ref. [623]). It is of order $\Lambda_{\mathrm{QCD}}^2/m_h$. The same operator does not contribute at leading order to matrix elements of quarkonium states as its projection on quark-antiquark color singlet states vanishes. Hence, spin splittings are remarkably less suppressed in heavy quarkonium hybrids than in heavy quarkonia. For the lowest-lying hybrid excitations of a gluonic operator with quantum numbers 1^{+-}, the $1/m_h$ spin-dependent potential takes the form

$$V^{(1)}_{1^{+-}\lambda\lambda'\,\mathrm{SD}}(\boldsymbol{r}) = V_{SK}(r)\left(\hat{r}^{i\dagger}_\lambda \boldsymbol{K}^{ij} \hat{r}^j_{\lambda'}\right)\cdot \boldsymbol{S} + V_{SKb}(r)\left[\left(\boldsymbol{r}\cdot\hat{\boldsymbol{r}}^\dagger_\lambda\right)\left(r^i \boldsymbol{K}^{ij} \hat{r}^j_{\lambda'}\right)\cdot \boldsymbol{S} + \left(r^i \boldsymbol{K}^{ij} \hat{r}^{j\dagger}_\lambda\right)\cdot \boldsymbol{S}\left(\boldsymbol{r}\cdot\hat{\boldsymbol{r}}_{\lambda'}\right)\right], \tag{75}$$
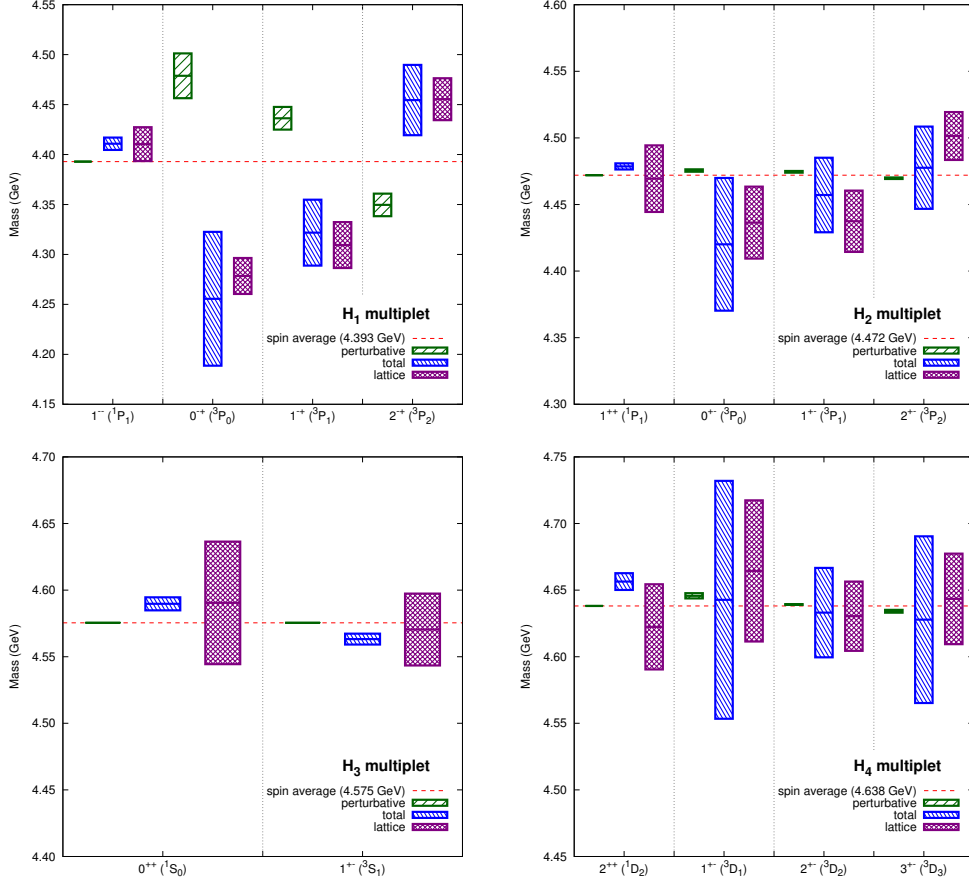
120

Figure 90: Spectrum of the four lowest-lying charmonium hybrid multiplets. The lattice results from Ref. [131] with $m_\pi \approx 240$ MeV are the most right (purple) boxes for each quantum number. The perturbative contributions to the spin-dependent operators added to the spin average of the lattice results (red dashed lines) are the most left (green) boxes. The central (blue) boxes for each quantum number are the full results from the spin-dependent operators including perturbative and non-perturbative contributions. The unknown non-perturbative matrix elements are fitted to reproduce the lattice data. Figure from Ref. [472].

where $\left(K^{ij}\right)^k = i\epsilon^{ikj}$ is the angular momentum operator of the spin one gluons. Also the $1/m_h^2$ spin-dependent potential presents some new structures with respect to the corresponding quarkonium potential (67):

$$
\begin{aligned}
V^{(2)}_{1^{+-}\lambda\lambda'\,\mathrm{SD}}(\boldsymbol{r}) = {} & V^{(2)}_{LS\,a}(r)\left(\hat{r}^{i\dagger}_\lambda \boldsymbol{L}\,\hat{r}^i_{\lambda'}\right)\cdot\boldsymbol{S} + V^{(2)}_{LS\,b}(r)\hat{r}^{i\dagger}_\lambda\left(L^i S^j + S^i L^j\right)\hat{r}^j_{\lambda'} \\
& + V^{(2)}_{S^2}(r)\boldsymbol{S}^2\delta_{\lambda\lambda'} + V^{(2)}_{S_{12}\,a}(r)S_{12}\delta_{\lambda\lambda'} + V^{(2)}_{S_{12}\,b}(r)\hat{r}^{i\dagger}_\lambda\hat{r}^j_{\lambda'}\left(S^i_1 S^j_2 + S^i_2 S^j_1\right),
\end{aligned}
\tag{76}
$$

where $\boldsymbol{L}$ is the orbital angular momentum of the heavy-quark-antiquark pair, and the spin operators are defined as after Eq. (67). The terms proportional to $V^{(2)}_{LS\,a}(r)$, $V^{(2)}_{S^2}(r)$, and $V^{(2)}_{S_{12}\,a}(r)$ are present also in the quarkonium case. The leading-order perturbative expressions of $V^{(2)}_{LS\,a}(r)$, $V^{(2)}_{S^2}(r)$, and $V^{(2)}_{S_{12}\,a}(r)$ follow from the perturbative expressions of the corresponding quarkonium potentials in Eq. (70) after replacing an overall factor $-4/3$ by $1/6$, which is the same change that relates the Coulomb potential in the SU(3) fundamental representation with the Coulomb potential in the SU(3) adjoint representation. The functions $V^{(2)}_{LS\,a}(r)$, $V^{(2)}_{S^2}(r)$, and $V^{(2)}_{S_{12}\,a}(r)$ also get non-perturbative contributions. Non-perturbative contributions are particularly important for $V_{SK}(r)$, $V_{SKb}(r)$, $V^{(2)}_{LS\,b}(r)$, and $V^{(2)}_{S_{12}\,b}(r)$, since these terms vanish at leading order in perturbation theory.

In Fig. 90, for each multiplet, the charmonium hybrid spin splittings computed in lattice QCD (purple, right boxes) are compared with leading-order perturbation theory (green, left boxes) and with a fit that allows for non-perturbative
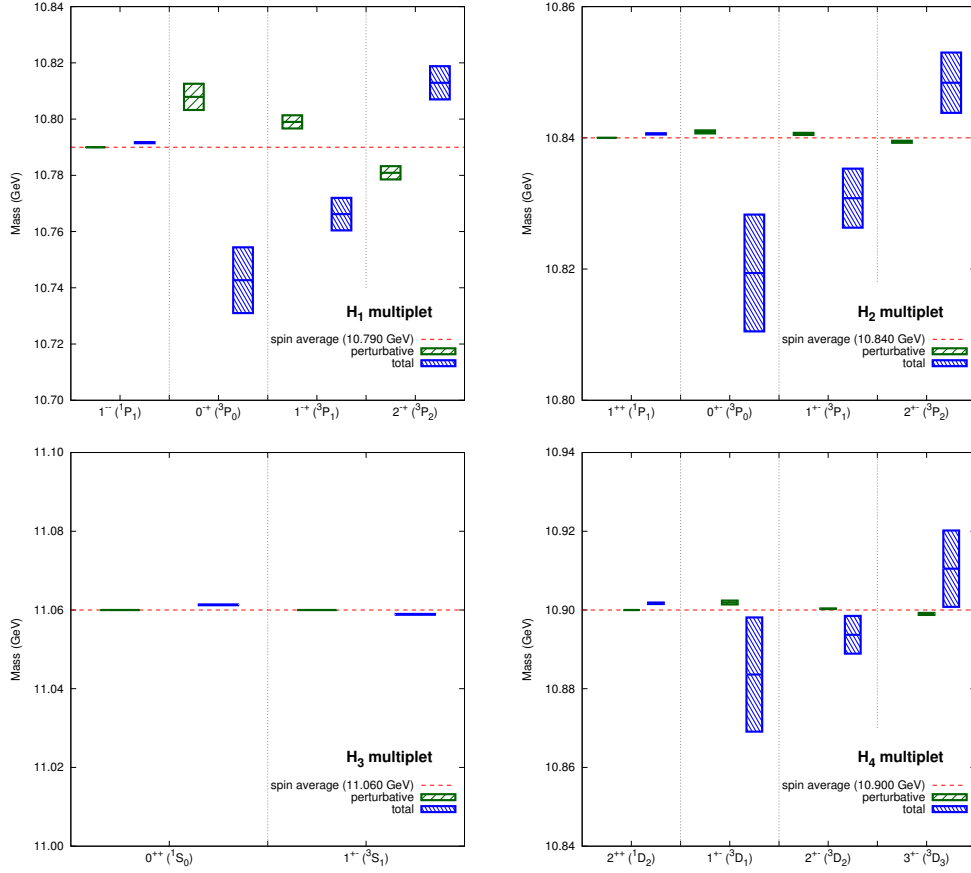
Figure 91: Spectrum of the four lowest-lying bottomonium hybrid multiplets computed by adding the spin-dependent contributions to the spectrum obtained in Ref. [192]. The non-perturbative contributions are determined from the fit of the charmonium hybrid spectrum of Ref. [131], see Fig. 90. The average mass for each multiplet is displayed as a red dashed line. The results with only the perturbative contributions included and the full results with perturbative and non-perturbative contributions included are shown for each quantum number by the left (green) and the right (blue) boxes, respectively. Figure from Ref. [472].

contributions to the potentials listed in Eqs. (75) and (76) (blue, central boxes). We see that the pattern of splittings induced by the perturbative contributions alone is opposite to the data. It is also opposite to the quarkonium case, as the signs of all spin-dependent potentials is reversed at leading order. Hence, non-perturbative contributions are crucial to bring the splittings in agreement with lattice data, consistently with the fact that the non-perturbative contribution proportional to $V_{SK}(r)$ is the dominant spin-dependent potential for hybrids. In Ref. [472], the fitted contributions turn out to scale, in powers of Λ_{QCD}, as expected by the power counting of the EFT. If the non-perturbative potentials may be organized according to the multipole expansion, then information gained from the charmonium hybrid spin splittings can be used to predict, for each multiplet, the bottomonium hybrid spin splittings. The predictions are shown in Fig. 91. We see again that the characteristic pattern of spin splittings induced by the perturbative contributions (green, left boxes) is reversed by the full result that includes the non-perturbative contributions (blue, right boxes).

A full theoretical description of hybrids, which may eventually lead to a certain identification of some of the X and Y quarkonium states, requires also the study of their decay properties. An early study is Ref. [188] that explains the apparent suppression of the decay $Y(4260) \to D^{(*)}\bar{D}^{(*)}$ with respect to the decay $Y(4260) \to \pi^+\pi^- J/\psi$ by interpreting the $Y(4260)$ (now $Y(4230)$) as a charmonium hybrid state with a magnetic constituent gluon, see Sec. 3.1.2. A relation of this model with the Born–Oppenheimer picture was first suggested in Refs. [452, 772]. Later it was worked out in Ref. [192], see Fig. 89 and the possible H_1 assignment of the $Y(4230)$. More recently, heavy quarkonium hybrid inclusive transitions into quarkonia have been studied in the BOEFT framework in Ref. [193]. The outcome of

122

$nL_T \to n'L'$	ΔE (MeV)	Γ (MeV)
$c\bar{c}$ sector		
$1P_0 \to 2S$	808	7.5(7.4)
$2(S/D)_1 \to 1P$	861	22(19)
$4(S/D)_1 \to 1P$	1224	23(15)
$b\bar{b}$ sector		
$1P_0 \to 1S$	1569	44(23)
$1P_0 \to 2S$	1002	15(9)
$2P_0 \to 2S$	1290	2.9(1.3)
$2P_0 \to 3S$	943	15(12)
$4P_0 \to 1S$	2337	53(25)
$4P_0 \to 2S$	1770	18(7)
$4P_0 \to 3S$	1423	7.4(4.1)
$2(S/D)_1 \to 1P$	977	17(8)
$3(S/D)_1 \to 1P$	1176	29(14)
$3(S/D)_1 \to 2P$	818	5(3)
$4(S/D)_1 \to 2P$	891	33(25)
$5(S/D)_1 \to 1P$	1376	18(7)
$5(S/D)_1 \to 2P$	1018	14(8)

Table 13: Decay widths for charmonium (above) and bottomonium (below) hybrids to lower-lying charmonia and bottomonia, respectively. n and n' are principal quantum numbers, $L(L + 1)$ and $L'(L' + 1)$ are eigenvalues of L^2, where L is the orbital angular momentum of the heavy quarks, and $T(T + 1)$ are eigenvalues of $(L + K)^2$, where K is the angular momentum of the gluons. ΔE is the energy difference between the hybrid and the quarkonium state. Mixing with quarkonia has been neglected. The hybrid states P_0 belong to the H_3 multiplet of Table 12 and the states $(S/D)_1$ to the H_1 multiplet. Table taken from Ref. [193].

that study is summarized in Table 13. The transition widths range from a few MeV to about 50 MeV. Moreover, in Ref. [193] it was emphasized that the same NRQCD operator responsible for the appearance of the $1/m_h$ spin-dependent potential (75) is also responsible for the appearance of a mixing potential between hybrids and ordinary quarkonia at order $1/m_h$. The mixing potential mixes spin 0 (1) hybrids with spin 1 (0) quarkonia and may explain, in dependence of the strength of the mixing, which is of order $\Lambda_{\text{QCD}}^2/m_h$ and non-perturbative, why some hybrid candidates appear to decay both into $\pi^+\pi^- J/\psi$ and $\pi^+\pi^- h_c$. This could be the case of the $Y(4230)$, which, according to Ref. [193], has a potentially large mixing with the ordinary charmonium $2D$, 1^{--}, state. Finally, selection rules for hadronic transitions of X, Y and Z mesons have been derived in Ref. [468]

● *Tetraquarks*

The BOEFT Lagrangian density in the isospin $I = 1$ sector, relevant for tetraquarks, may be constructed following the same line of reasoning that leads to the BOEFT for hybrids and to the heavy-hadron chiral effective Lagrangian [773]. Its form is very similar to the BOEFT Lagrangian for hybrids given in Eq. (73), but the isovector fields are 2×2 matrices:

$$Z_\kappa = Z_\kappa^i \sigma^i = \begin{pmatrix} Z_\kappa^0 & \sqrt{2}Z_\kappa^+ \\ \sqrt{2}Z_\kappa^- & -Z_\kappa^0 \end{pmatrix}, \tag{77}$$
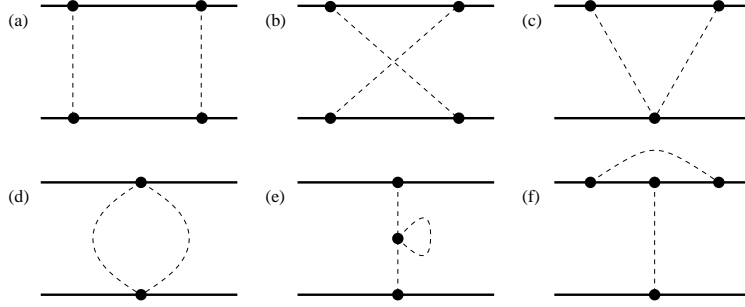
Figure 92: Topologies contributing at the leading one-loop level to the scattering of two heavy particles: the ladder diagram (a), the crossed box (b), the triangle (c), the football (d), the pion tadpole (e) and the vertex correction (f).

where σ^i are the isospin Pauli matrices. The BOEFT Lagrangian density in the $I = 1$ sector has the form [761]:

$$
\begin{aligned}
\mathcal{L}_{\text{BOEFT for } I=1} = & \int d^3r \, \text{Tr} \left\{ Z_{0^{+-}}^\dagger \left(iD_0 - V_{\Sigma_g^+}^{\text{tetra}}(r) + \frac{\boldsymbol{\nabla}_r^2}{m_h} \right) Z_{0^{+-}} \right\} \\
& + \int d^3r \sum_{\lambda\lambda'} \text{Tr} \left\{ Z_{1^{+-}\lambda}^\dagger \left(iD_0 - V_{1^{+-}\lambda\lambda'}^{\text{tetra}}(r) + \hat{r}_\lambda^{i\dagger} \frac{\boldsymbol{\nabla}_r^2}{m_h} \hat{r}_{\lambda'}^i \right) Z_{1^{+-}\lambda'} \right\} \\
& + \int d^3r \sum_{\lambda\lambda'} \text{Tr} \left\{ Z_{1^{--}\lambda}^\dagger \left(iD_0 - V_{1^{--}\lambda\lambda'}^{\text{tetra}}(r) + \hat{r}_\lambda^{i\dagger} \frac{\boldsymbol{\nabla}_r^2}{m_h} \hat{r}_{\lambda'}^i \right) Z_{1^{--}\lambda'} \right\} + \dots,
\end{aligned}
\tag{78}
$$

where the dots stand for terms involing higher orbital momentum and possibly mixing between states. The fields $Z_{1^{+-}\lambda}$, $Z_{1^{--}\lambda}$, and $Z_{0^{+-}}$ depend on time, the c.m. coordinate $\boldsymbol{R}$ and the relative coordinate $\boldsymbol{r}$. The trace is also over the isospin indices. The covariant derivative for the $I = 1$ fields reads $D_\mu Z_\kappa = \partial_\mu + [\Gamma_\mu, Z_\kappa]$ with $\Gamma_\mu = \left(u^\dagger \partial_\mu u + u \partial_\mu u^\dagger \right)/2$ and $u = \exp[i\pi^i \sigma^i/(2f_\pi)]$. The pion fields, π^i, depend on t and $\boldsymbol{R}$. The direct use of the effective Lagrangian (78) is limited by the fact that the potentials have not, even in their static limit, been measured on the lattice. For recent studies in this direction we refer to Sec. 4.5.3. Hence, the situation is different from the hybrid case, where static hybrid energies are known since long time. In particular, an analysis of the type performed for heavy quarkonium hybrids in the previous paragraphs is at the moment not possible for quarkonium tetraquarks. In Refs. [467, 469], to circumvent this difficulty, it was assumed that the tetraquark static energies have the same shape as the hybrid ones. In this way, it became possible for the authors to provide preliminary mass estimates and to make predictions on the ordering of the tetraquark spectrum. Clearly, the lattice computation of the tetraquark static energies would provide a major input for studies based on the Born–Oppenheimer picture.

4.4.5. Effective field theories at the hadron level

Effective field theories for few-hadron systems can be constructed along the lines of the analogous effective field theories for few-nucleon systems — see Ref. [611] for a comprehensive review of the subject. Here we will focus on the treatment of few-hadron bound systems. On the one hand, the formalism must be formulated non-perturbatively. But, on the other hand, in an effective field theory one needs to identify a proper expansion parameter in such a way that the results can be improved systematically by going to higher orders in this expansion. It was Weinberg in 1990 who argued that those seemingly contradictory requirements can be brought together, if one performs an expansion not of the full amplitude but only of the scattering potential which then should be resummed by some wave equations [774]. The argument is based on the following observation: Assume the scattering of two heavy particles interacting via the exchange of a light meson. As illustrated in Fig. 92, at the leading one-loop level the scattering potential contains six contributions: the ladder, the crossed box, the triangle, the football, the pion tadpole and the vertex correction. Clearly, the diagrams (a), (b) and (f) scale equally with respect to the coupling constants, however, a detailed analysis reveals that the ladder diagram scales with an additional factor $\pi(2\mu/p)$ compared to the other two, where μ denotes the reduced mass of the two heavy particles and p is the typical momentum of the two-hadron state.

This kind of kinematic enhancement is also absent in diagrams (c), (d) and (e). The enhancement factor comes from the two-hadron cut, which is present only in diagrams that have a time slice that cuts only two heavy hadron lines (in the language of few-body physics these kinds of diagrams are called two–body reducible). Thus, for momenta small compared to the masses of the two hadrons, the ladder diagram is enhanced compared to all the other one-loop diagrams. This remains true at higher orders in perturbation theory and thus justifies a resummation of at least part of the potential constructed to a given order in perturbation theory, where "potential" means all contributions that are two-hadron irreducible. In contrast to Weinberg's scheme, it was argued in Refs. [775, 776] that instead of the potential the full amplitude should be analyzed under the assumption that there is a pole present very near threshold. Within this scheme only a momentum-independent counterterm needs to be resummed while pion exchange is perturbative. However, in Ref. [777] it was shown that, as soon as the tensor force of the one-pion exchange contributes, the expansion that results from the scheme of Refs. [775, 776] does not converge at least for the two-nucleon system in the deuteron channel.

As in case of studies of the few-nucleon system, also for the interactions of heavy mesons both schools co-exist: While some authors propose that only contact terms need to be resummed and one-pion exchange should be treated perturbatively [110, 574, 577, 778–780], others call for a resummation of both contact terms and pion exchange [300, 537, 570, 573, 781]. For example, in Ref. [779] it is argued that the tensor force of the pion should be reduced significantly here compared to the two-nucleon system as a result of a smaller effective pion mass and a smaller coupling that invalidate the argument of Ref. [777]. However, in Ref. [300] it is shown that the fit to the line shapes of $Z_b(10610)$ and $Z_b(10650)$, especially in the lower elastic channel, improves once the tensor force of the pion is included, pointing at the need for a non-perturbative inclusion of the pion exchange — see Fig. 93 — and thus calling for an application of Weinberg's counting also in heavy meson systems. This work will be discussed in a little more detail below. From now on we only investigate two–hadron molecular states. The possible interplay of scales in meson containing three hadrons is discussed in Ref. [782] on the example for the $Y(4660)$.

The leading-order piece of the HQET Lagrangian shown in Eq. (54) is independent of the heavy-quark flavor. This is at the origin of the heavy-quark flavor symmetry, which is routinely employed to relate features from the c-quark sector to the b-quark sector, as long as there is only a single heavy quark involved. However, when it comes to doubly-heavy systems the flavor symmetry is no more a symmetry of the leading-order Lagrangian, since both the potential and the kinetic energy of the heavy particle are of the same order. See the discussion at the end of Sec. 4.4.2 for NRQCD, but the same reasoning applies to pNRQCD. It should be remarked, however, that, differently from (p)NRQCD, where the potential seen by the two heavy quarks is known at short distances and may be computed in perturbation theory, in the hadronic EFT this is not the case: The short distance interaction always contains counter terms at leading order. Hence, if one wants to construct an EFT that connects the c-quark with the b-quark sector, the scaling of these counter terms with the hadron mass, M, must be either derived or imposed. Clearly, different assumptions lead to different results: In Refs. [110, 783] the binding energy of the heavier systems is found larger than that of the lighter systems; the opposite is the case in Ref. [778], reflecting the fact that the former work assumes that the scattering potential of the two heavy-meson system is independent of the heavy meson-mass M, whereas the latter derives a $1/M$ scaling based on a renormalisation group argument. The role of the heavy flavor symmetry in the hadronic EFT was first studied systematically in Ref. [112], with the conclusion that no common effective field theory can be defined for bottomed and charmed molecular systems simultaneously, since the heavy meson mass cannot be removed consistently from the formalism. As we have remarked, this is the same situation that we face in (p)NRQCD for bottomonia and charmonia. On the other hand, as in case of (p)NRQCD, the heavy-particle spin symmetry holds at leading order also in any EFT for two–hadron systems.

The power counting to treat the heavy two-hadron systems is based on a velocity counting in a non relativistic scheme. The typical velocity for some intermediate state is estimated via

$$v \sim \sqrt{|M - M_1 - M_2|/\mu}, \tag{79}$$

where M denotes the total energy of the intermediate state that couples to the two mesons with masses M_1 and M_2; their reduced mass is denoted by μ. It may either be formulated based on a four-dimensional formalism or a three-dimensional formalism related to time-ordered perturbation theory (for a comparison of the two schemes we refer to Appendix E of Ref. [784]). For example, in the former scheme the integral measure counts as v^5, a heavy meson propagator as $1/v^2$ and a pion exchange (as long as one studies the scattering of two ground-state open-flavor mesons
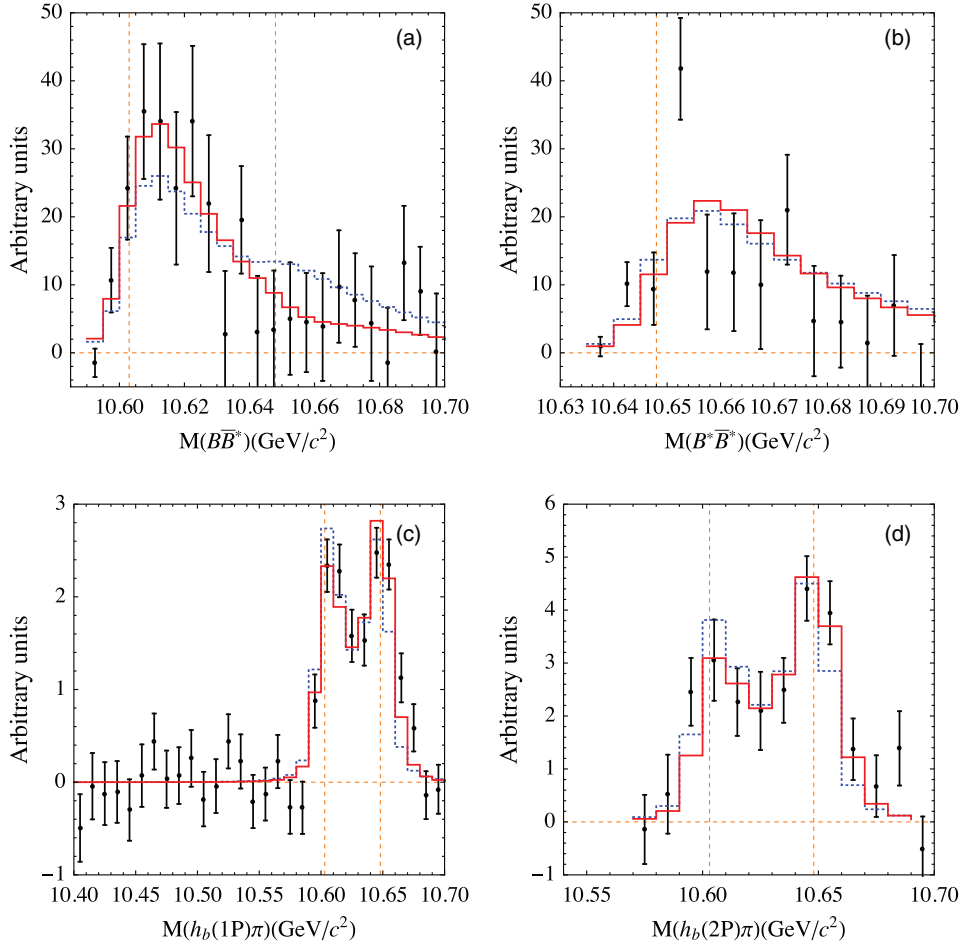
Figure 93: Results for the line shapes of the Z_b states reported in Ref. [300]: The red solid line (blue dotted line) is based on a calculation that includes one-pion exchange as well as contact interactions (only contact interactions).

off each other[20]) or a momentum-independent counter term as v^L, where L denotes the partial wave. In the latter case, the integral measure counts as v^3 and a time slice that cuts only heavy mesons counts as $1/v^2$. Pion exchange and contact terms are counted as in the four-dimensional formalism the same way. Accordingly, a meson bubble scales as $v^{(2L+1)}$ in both schemes. This shows that loops are most important for S-waves ($L = 0$), however, there is no parametric enhancement of the loops calling for their resummation (This statement is not in conflict with the observation made at the beginning of this section, namely that two–hadron reducible diagrams are parametrically enhanced compared to the irreducible ones). This is completely analogous to the situation in the two–nucleon system and we refer to Ref. [611] for a detailed discussion. What is generally done to arrive at a formalism where the heavy meson loops are resummed to all orders is to argue that the coupling constants that multiply each loop are sufficiently large to call for this or to simply impose it, since a resummation is necessary to generate bound states (see, e.g., Refs. [775, 776, 779]),

The same construction can also be applied to decays. Since for a molecular state its coupling to the molecule-forming channel is large, two-hadron loops always appear at leading order. However, whether a given decay is sensitive to the long-range part of the wave function, which contains the information on the molecular component, as

---

[20]Here the $1/v^2$ enhancement from the propagator gets balanced by the factor v^2 in the numerator since pions couple to heavy mesons in the P-wave.
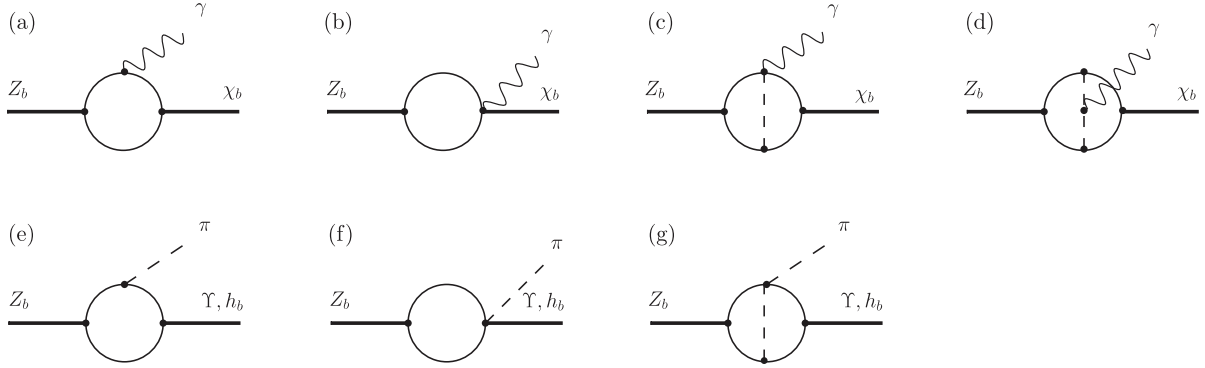
126

Figure 94: Diagrams contributing to various Z_b and Z'_b decays at leading (a,e) and subleading order (b,c,d,f,g). Thick (thin) solid lines denote the propagation of doubly (singly) heavy states, dashed lines show pions and wavy lines photons.

explained in Sec. 4.3.4, depends on the quantum numbers involved. As an example, we present here the reasoning of Ref. [785] where the decays of the Z_b states were investigated from an effective field theory point of view based on the non relativistic effective field theory introduced in Refs. [786, 787]. The relevant diagrams that appear at leading order as well as some subleading diagrams are displayed in Fig. 94.

We start with the radiative decays. Since the Z_b states carry the quantum numbers 1^{+-} and the photon is a vector with $J^{PC} = 1^{--}$, the quarkonium in the final state needs to have $C = +$ and $P = (-1)^{L+1}$, where L denotes the angular momentum between the outgoing quarkonium and the photon. To reach an allowed quark model bottomonium in the final state, the decay must happen in a P-wave ($L = 1$) and the final state should contain a χ_{bJ} state. The latter couples to a pair of B-mesons in an S-wave and, accordingly, all vertices inside the loop are S-wave ones. Then all decays must scale with the photon momentum q.[21] Adapting the rules outlined in the previous paragraph (we now use the four-dimensional counting only, although the two schemes naturally continue to give the same scaling) we find for diagram (a):

$$v^5 (1/v^2)^3 q = q/v. \tag{80}$$

It is shown in Ref. [788] (see also Ref. [531]) that the proper scale used for v in the triangle topology away from the Landau singularity (discussed in more detail at the end of this section) is the average of the two velocities appearing. Since the velocity of the B-meson pair right in front of the $\chi_{bJ}(mP)$-state [from Eq. (79) we find $v_\chi = 0.12, 0.26, 0.37$ for $m = 3, 2, 1$, respectively] is much larger than the one right after the Z_b decay ($v_z \sim 0.02$) due to the proximity of the Z_b states to the threshold, one may safely choose $v \sim v_\chi$ in Eq. (80). Note that as soon as one takes v_χ as the hard scale of the problem, a different power counting arises and the same factorisation theorem used for positronium decays may also be applied here — the two choices (v_χ as hard or soft scale) are contrasted on the example of pionic decays of $X(3872)$ in Ref. [88]. See also the discussion in Sec. 4.3.4.

For diagram (b) one finds

$$v_z^5 (1/v_z^2)^2 q = q v_z. \tag{81}$$

Thus diagram (a) is enhanced compared to diagram (b) by about one order of magnitude. Gauge invariance demands diagrams (c) and (d) to appear at the same order. For this diagram we find (the rules applied here are a simplified version of what is presented in Ref. [785] that, however, does not change the conclusions)

$$v_z^5 (1/v_z^2)^2 q v_\chi / v_\chi^2 v_\chi^5 (1/v_\chi^2)^2 = q v_z, \tag{82}$$

where we used that the pion momentum is controlled by the larger one of the two-loop momenta. Thus diagrams (c) and (d) are equally suppressed as diagram (b). Accordingly, diagram (a) allows one to estimate the decay rate with a 10% accuracy at the amplitude level, which translates to a 20% accuracy for the branching fraction.

---

[21]In Ref. [785] the photon energy was used, which is equivalent since the photon is on shell.

127

We now turn to the pionic decays of the Z_b states shown in the second line of Fig. 94. Parity conservation demands that the decay to the h_b states, which couple to the B-pairs in an S-wave, happens in a P-wave, while the decay to the Υ states, which couple in a P-wave to the B-meson pairs, happens in an S-wave. Accordingly, we estimate that

$$v^5 (1/v^2)^3 q = q/v. \tag{83}$$

for the h_b decays, where $v \sim v_h \sim v_\chi$ in line with the discussion above, and

$$v^5 (1/v^2)^3 v = 1. \tag{84}$$

for the Υ decays, where q denotes the outgoing pion momentum. Moreover, the latter loop is divergent while the former is convergent. Thus, there must be a counter term at leading order to render the calculation of the Υ-decays well defined, while there is no leading order counterterm for the h_b decays.

To estimate the diagram in Fig. 94(g) we need to use that the pion rescattering vertex scales with the pion energy (E_π) — an insight that may be adapted from effective field theory studies of the reaction $NN \to NN\pi$ [789] (for a recent review see Ref. [790]). Thus we find for this diagram with an h_b in the final state

$$v_z^5 (1/v_z^2)^2 (E_\pi/\Lambda_\chi) q/v_h^2 v_h^5 (1/v_h^2)^2 = q^2/(\Lambda_\chi) v_z/v_h, \tag{85}$$

where we introduced the typical hadronic scale $\Lambda_\chi \sim 1$ GeV to render the units equal and identified the pion energy with the pion momentum, since both are of the same order of magnitude. For the decay to the ground state h_b the pion momentum can be of the order of Λ_χ, however, the remaining factors are sufficient to provide a suppression of diagram (g) by more than one order of magnitude. For the Υ in the final state the analogous estimate gives

$$v_z^5 (1/v_z^2)^2 q v_h/v_h^2 v_h^5 (1/v_h^2)^2 v_h = q v_z v_h. \tag{86}$$

Thus also for the Υ final states the higher loop diagrams are suppressed. In Ref. [785] even higher loop diagrams are shown to be suppressed. Thus we may conclude that the effective field theory described here allows one to calculate the decays of the Z_b states to $\gamma\chi_{bJ}$ and πh_{bJ} in a controlled way (with a 10% uncertainty in the amplitude); these transitions are dominated by the light degrees of freedom and are, therefore, sensitive to the molecular component of the Z_b states. The same reasoning allows one to show that under certain conditions heavy meson loops can provide very prominent contributions in the transitions of regular heavy quarkonia [787, 791, 792]. In contrast to this, the decays to the $\pi\Upsilon$ final states acquire short-range contributions already at leading order. In this case, it is not possible to make quantitative predictions for the transitions within the molecular picture. An analogous reasoning allows one to conclude that the transitions $X(3872) \to \gamma J/\psi$ and $X(3872) \to \gamma\psi(2S)$ are sensitive to the short-range part of the X wave function and may not be used to draw conclusions on the molecular nature of the $X(3872)$ [85] — contrary to the claims of Refs. [83] where a particular model was employed to estimate the rates.

In Ref. [300] the line shapes of the Z_b states are studied within the effective field theory formalism sketched above. At the first stage, only the naive leading order diagrams were considered: Momentum independent counter terms as well as the one pion exchange. Note that, since the pion exchange with its sizeable tensor force can connect S- to D-waves, the basis needs to be enlarged compared to the inclusion of only S-waves commonly kept when studying heavy meson molecules. The typical momentum in the $B^*\bar{B}$ channel for the energies near the $B^*\bar{B}^*$ threshold is $p_{\text{typ}} \sim \sqrt{M_B\delta} \sim 500$ MeV, where $\delta = M_{B^*} - M_B \approx 45$ MeV. This implies, since $p_{\text{typ}}/M_\pi > 1$, that there is no suppression of higher partial waves. Moreover, the coupling to D-waves induces a sizeable regularisation scheme dependence — cf. first row of Fig. 95, where the scheme dependence is illustrated by the variation of a sharp cut-off employed to render the loop diagrams finite; for each value of the cut-off a refit to the data was performed, which is nothing but a numerical implementation of the renormalisation program. In a properly renormalised EFT the contact terms should be capable of absorbing the cut-off dependence. For the system at hand this appears possible only once a counter term that connects S- to D-waves is promoted to leading order as can be seen from the second row in Fig. 95.[22] It should be stressed, however, that not all pion effects were absorbed into the promoted counter term: Not only does

---

[22]For the nucleon–nucleon system a formal argument for the need to promote certain counter terms to lower order in the presence of the tensor force is provided in Ref. [793].
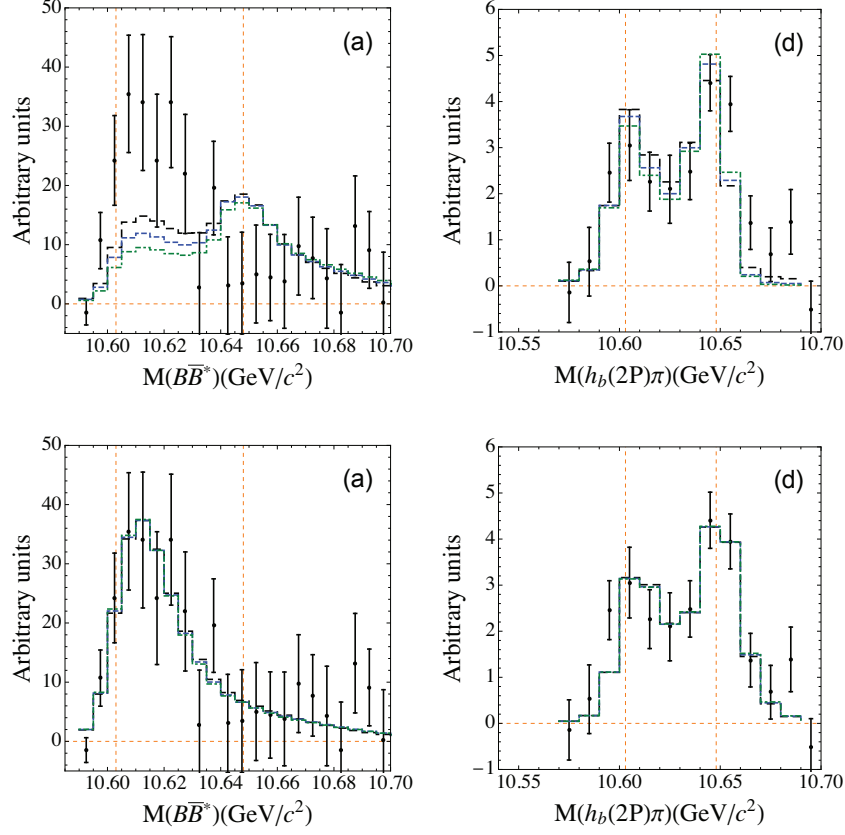
Figure 95: The fitted line shapes for a calculation employing only the formal leading order potential (upper line) and when the S-D counter term is added (lower line) in the elastic $B\bar{B}^*$ and inelastic $\pi h_b(2P)$ channels with sharp cut-offs 800 MeV (black long-dashed), 1000 MeV (blue dashed), and 1200 MeV (green dot-dashed), respectively. The experimental data are from Refs. [284, 295].

J^{PC}	State	Threshold	Im p_{in}	Im $p_{B\bar{B}}$	Im $p_{B\bar{B}^*}$	Im $p_{B^*\bar{B}^*}$	E_{pole} w.r.t. threshold (MeV)	Residue at E_{pole}
1^{+-}	Z_b	$B\bar{B}^*$	+		−	+	$(-0.9 \pm 0.4) + i(1.0 \pm 0.3)$	$(-1.4 \pm 0.2) + i(0.5 \pm 0.1)$
1^{+-}	Z'_b	$B^*\bar{B}^*$	+		+	−	$(-0.8 \pm 0.5) + i(1.3 \pm 0.4)$	$(-1.4 \pm 0.3) + i(0.7 \pm 0.1)$
0^{++}	W_{b0}	$B\bar{B}$	+	−		+	$(-1.0 \pm 0.6) + i(1.0 \pm 0.3)$	$(-1.4 \pm 0.3) + i(0.5 \pm 0.1)$
0^{++}	W'_{b0}	$B^*\bar{B}^*$	+	+		−	$(-1.2 \pm 0.6) + i(0.9 \pm 0.3)$	$(-1.4 \pm 0.3) + i(0.4 \pm 0.1)$
1^{++}	W_{b1}	$B\bar{B}^*$	+		−		$(-0.3 \pm 0.6) + i(1.6 \pm 0.8)$	$(-1.3 \pm 0.4) + i(0.9 \pm 0.1)$
2^{++}	W_{b2}	$B^*\bar{B}^*$	+			−	$(0.4 \pm 0.6) + i(1.9 \pm 0.9)$	$(-1.2 \pm 0.4) + i(1.3 \pm 0.2)$

Table 14: The pole positions and the residues g^2, normalized according to Eq. (87), in various S-wave $B^{(*)}\bar{B}^{(*)}$ channels for a potential with contact terms only. The energy E_{pole} is given relative to the nearest open-bottom threshold quoted in the third column. The Riemann Sheet (RS) is defined by the signs of the imaginary parts of the corresponding momenta (quoted in the columns 4-7); a missing sign indicates that this channel is uncoupled. Uncertainties correspond to a 1σ deviation in the parameters allowed by the fit to the data in the channels with $J^{PC} = 1^{+-}$ where the $Z_b^{(')}$ states reside [300]. The poles are calculated for the cutoff $\Lambda = 1$ GeV.

the inclusion of the one pion exchange improve the fit quality (compare red solid and blue dotted lines in Fig. 93), the convergence of the approach is improved as well: If momentum-dependent counter terms that connect S-to-S-waves are included in addition, fitting without one-pion exchange calls for those formally subleading terms to be larger than the leading ones. On the contrary, as soon as one pion exchange is included in the calculation, these additional terms provide a perturbative correction only.

J^{PC}	State	Threshold	Im p_{in}	Im $p_{B\bar{B}}$	Im $p_{B\bar{B}^*}$	Im $p_{B^*\bar{B}^*}$	E_{pole} w.r.t. threshold [MeV]	Residue at E_{pole}
1^{+-}	Z_b	$B\bar{B}^*$	–		–	+	$(-1.3 \pm 0.2) - i(0.6 \pm 0.1)$	$(-0.6 \pm 0.1) - i(0.1 \pm 0.1)$
1^{+-}	Z'_b	$B^*\bar{B}^*$	–		–	–	$(2.1 \pm 2.2) - i(12.9 \pm 2.4)$	$(0.8 \pm 0.1) - i(0.4 \pm 0.2)$
0^{++}	W_{b0}	$B\bar{B}$	+	–		+	$(-8.5 \pm 2.8) + i(1.5 \pm 0.2)$	$(-2.0 \pm 0.7) - i(0.1 \pm 0.3)$
0^{++}	W'_{b0}	$B^*\bar{B}^*$	–	–		–	$(-1.2 \pm 0.1) - i(0.7 \pm 0.3)$	$(-0.4 \pm 0.1) - i(0.2 \pm 0.1)$
1^{++}	W_{b1}	$B\bar{B}^*$	–		–	+	$(25.0 \pm 2.6) - i(20.5 \pm 3.3)$	$(0.9 \pm 0.1) - i(0.4 \pm 0.2)$
2^{++}	W_{b2}	$B^*\bar{B}^*$	–		–	–	$(4.0 \pm 2.1) - i(10.4 \pm 1.5)$	$(0.4 \pm 0.1) - i(0.2 \pm 0.1)$

Table 15: The same as in Table 14 but with pion exchange included.

The pole locations and residues that emerge from the described study of the Z_b states, as well as their spin partners W_{bJ}, are presented in Tab. 14 for a potential with contact terms only and in Tab. 15 for the fully renormalised potential including one pion exchange [571] — note that for the W_{bJ} states partial waves up to G-waves need to be included in order to render the potential consistent with the heavy quark spin symmetry [573]. In all cases, to reduce the complexity of the problem when extracting the poles and residues, the inelastic channels are lumped into a single effective channel. The sign convention of the energies is such that negative (positive) energies refer to below (above) threshold poles. Moreover, a negative (positive) imaginary part of a pole-momentum for a given channel refers to the unphysical (physical) sheet. Thus, in all cases the poles extracted from the analysis appear on the unphysical sheet very close to the threshold and the data are consistent with only a single near-threshold pole in line with a molecular interpretation for the states. Since all poles are on the unphysical sheets, the Weinberg criterion to measure the molecular admixture cannot be applied to the residues provided in the tables. However, we may still use Eq. (45) to estimate the order of magnitude of the residues one would expect for molecular states in the $B\bar{B}$ system bound by, say, 1 MeV only. The residues in the tables were extracted from the diagonal elements of the theoretical $B^{(*)}\bar{B}^{(*)}$ scattering amplitudes using the definition

$$T_{\alpha\alpha}(M) = \frac{g_\alpha^2}{2M(M - M_R)} \, , \tag{87}$$

in combination with a non relativistic normalisation of the fields. Thus g_{eff}^2 defined in Eq. (45) needs to be divided by a factor $(2M_1)(2M_2)$ to match this normalisation, and we get

$$\left. \frac{g_{\mathrm{eff}}^2}{4M_1 M_2} \right|_{E_b = 1 \, \mathrm{MeV}} \sim 0.7 \, .$$

In light of this number we should regard all residues listed in Tab. 14 and Tab. 15 as large and in this sense providing further evidence for a molecular interpretation of the Z_b states.

One feature, however, is special: When the pion exchange is included some states appear as above-threshold poles with a small imaginary part. This was commonly believed to be a signature for compact states, however, the proximity of the left–hand singularity from the pion exchange, which introduces an additional small scale, seems to be responsible for this finding. Here more research appears to be necessary — especially since all poles but that of the W_{b2} move below threshold in the formalism without one pion exchange and the latter pole moves below threshold as well as soon as the inelastic channels are switched off.

The effective field theory outlined in the chapter is based on the most general Lagrangian compatible with the QCD symmetries. As such, a priori it does not involve any assumption about the nature of the states that emerge once the dynamical equations are solved. However, an assumption enters as soon as the power counting is employed. As argued in the beginning of this section, the scheme is built on the assumption that the two-hadron relative momentum is the smallest scale of the problem. Then ladder diagrams are enhanced and a potential picture is justified. According to Weinberg's criterion we call states that emerge from the presence of the two-hadron cut hadronic molecules (see the discussion in Sec. 4.3.4). If there were an s-channel pole in the system (that could be generated from a nearby tetraquark state, for example), it would appear as a pole of the kind $1/(s - s_0)$. Employing a momentum/energy expansion of the counter terms means that those pole terms are effectively expanded in s/s_0. Thus, the effective field theory would signal a close by bare pole by a nonconvergence of the expansion of the contact terms. The analysis of,

e.g., the Z_b states presented in Ref. [300] shows that the currently existing data are consistent with the assumed power counting as soon as a properly renormalised one pion exchange is included in the formalism. It is therefore fair to say that the data are consistent with a molecular nature of the states. However, once the one pion exchange is omitted from the study, the expansion of contact terms seems to converge badly. Better data are necessary in order to allow one to draw more sound conclusions from the Z_b line shapes. In particular, data for the line shapes of the spin partner states would be extremely valuable. Theoretical predictions for these observables within the hadronic effective field theory outlined in this section are provided in Ref. [571].

It is important to note that under special kinematic circumstances the triangle diagrams shown in the first column of Fig. 94 may get enhanced significantly by the so-called triangle, or Landau, singularity [558]. For a detailed discussion we refer to Refs. [342, 531, 794, 795]. These logarithmic singularities can play an important role, whenever all intermediate states in the triangle can go (near) on-shell simultaneously and additional kinematic conditions are met. It should be stressed, however, that in many cases the inverse of the average velocity (see above) is a good approximation to the triangle diagram [531]. Triangle singularities might play an important role in different decays of vector mesons [341, 342, 796], and might explain the signal of the $Z_c(4430)$ [595, 797, 798] or the narrow pentaquark signal [799, 800]. In this context it is important to observe that the triangle singularities appear only under very special kinematic conditions. In particular, if a state is seen, e.g., from very different initial states or energies, one can assume that the triangle singularities are not operative for all of them. Moreover, when studying a three–body final state containing a particle pair that emerged from an elastic rescattering form a particle pair in the triangle, no logarithmic singularity can be present according to Schmid's theorem [801, 802] — in other words: Even when a triangle singularity is responsible for a structure that was interpreted as a resonance in some inelastic channels, in the corresponding elastic channel there should not be any signal. On the other hand: If there were a pole present it should naturally show up in all channels to which it can couple according to the selection rules. This feature can clearly be tested experimentally.

In Ref. [106] it was proposed to exploit the interplay of the triangle singularity in $D^*\bar{D}^* \rightarrow \gamma X(3872)$ (with a very low energy initial state as could be studied at LHCb) and the $X(3872)$ pole for a very high accuracy mass determination of the $X(3872)$. In this reference, it is shown that the resulting line shape is very sensitive to the relative location of the logarithmic Landau singularity and the pole.

4.5. Lattice QCD

Lattice QCD is a method which enables first-principles systematically-improvable calculations in QCD. The theory is discretised onto a four-dimensional spacetime lattice, a grid of points, of finite volume and quantities of interest are extracted from Euclidean (imaginary-time) correlation functions which are computed numerically using Monte-Carlo methods. For spectroscopy, the energy eigenstates of QCD in a finite volume follow from computations of two-point correlation functions, $\langle O_i(t) O_j^\dagger(0) \rangle$, where $O_i(t)$ is an interpolating operator at discrete time t with appropriate quantum numbers. The effect of working on a discrete lattice can be accounted for by performing calculations with a number of different lattice spacings and extrapolating to the continuum limit and, similarly, the effect of working in a finite volume can be taken into account by performing calculations with a number of different lattice volumes. Historically, calculations with light (up and down) quarks having their physical mass were too computationally expensive – unphysically-heavy light quarks were used, giving an unphysically-large π mass, M_π, and a 'chiral' extrapolation to physical M_π was performed. More recently, it has become feasible to calculate some quantities using physical-mass, or very close to physical-mass, light quarks.

Calculations of the masses of the lower-lying hadrons in each flavour sector which are stable within QCD, i.e., below the relevant thresholds for strong-decay, are now very mature and give precise results with the various systematic uncertainties quantified. See Refs. [803–817] for some recent work in the charmonium and bottomonium sectors. Computations have begun to include the effects of isospin breaking (different masses for the up and down quarks) and QED, for now mainly in the light-hadron sector, e.g., Refs. [818–829].

However, most hadrons are not stable in QCD but instead are resonances that decay to final states containing two or more lighter hadrons. In particular, the various charmonium and bottomonium-like X, Y, Z states that are the subjects of this report are resonances or have masses very close to threshold. These phenomena are more challenging to study in lattice QCD because it is not possible to compute scattering amplitudes or the properties of resonances directly from finite-volume Euclidean correlation functions – asymptotic states can not be defined in finite volume

and, in contrast to an infinite volume, the spectrum above threshold is discrete with allowed momenta quantised by the boundary conditions.

Nevertheless, infinite-volume scattering amplitudes can be determined indirectly from a relation between them and the discrete spectrum of finite-volume energy eigenstates. For elastic scattering, each energy level, E_{cm}, gives the scattering phase shift at that energy, $\delta(E_{cm})$. When more than one scattering channel or partial wave is relevant, each energy provides a constraint on the scattering amplitudes at that energy. Once the scattering amplitudes have been determined, analytically continuing to complex E_{cm}, their singularity content can be investigated and so the resonance and bound-state content inferred (including the mass and width of any resonance and its coupling to various hadron-hadron channels). This method was originally introduced by Lüscher, Refs. [830–833], and has subsequently been generalised by many others – it is now applicable to hadron-hadron scattering with arbitrary spin, arbitrary overall momentum with respect to the lattice, and with any number of coupled two-hadron scattering channels, Refs. [834–857]. Work is advancing to extend the approach to channels with three or more hadrons, see Refs. [858–877]. A related approach for connecting finite-volume lattice QCD calculations to infinite-volume scattering amplitudes, based on the same underlying ideas, is to consider an effective Hamiltonian describing hadron-hadron interactions in a finite volume, such as unitarised chiral perturbation theory, see e.g. Refs. [843, 844, 848, 878–885]. Other approaches include using an optical potential, Ref. [886], the histogram method in which a probability distribution connected to the cross section is computed, Refs. [887, 888], and a method, advocated by HAL QCD, where a non-relativistic hadron-hadron potential is computed from the Bethe–Salpeter wavefunction, Refs. [889–901]. Ref. [902] provides a more detailed review of the "Lüscher method" and applications, and discusses some of the other approaches.

To robustly determine scattering amplitudes using the Lüscher method, many finite-volume energies must be extracted across the energy range being considered. The reduced symmetry of the spatial lattice volume, usually a cubic or rectangular box, compared to the infinite-volume continuum, means that partial waves of different J can 'mix' and appear in the same spectrum – sufficient energies must be extracted across a number of different quantum-number channels in order to disentangle them. Achieving the required constraint generally necessitates the computation of many energies in a number of lattice volumes, for systems moving with respect to the lattice, and/or using "twisted boundary conditions" on the quark fields – these all modify the quantisation of momentum and so provide additional E_{cm}, which give extra constraints. Furthermore, this approach neglects corrections that are exponentially suppressed in the spatial extent L, $\sim e^{-M_\pi L}$, and so requires a large enough volume, $LM_\pi \gg 1$, for these to be negligible. In recent years, computational power and algorithms have advanced sufficiently to allow applications of this method to meaningfull computations of hadron-hadron scattering. However, it must be kept in mind that, unlike the lattice QCD studies of stable hadrons mentioned above, these investigations do not generally have quantitative control over all the systematic uncertainties (for example, those arising from working at a finite lattice spacing or with unphysically-heavy light quarks).

As discussed in Ref. [902], a number of light-hadron scattering channels have been studied in detail: many energy levels are extracted, the scattering amplitudes are robustly determined and the resonant content is inferred. For example, the ρ resonance in isospin-1 $\pi\pi$ scattering has been studied by a number of groups for various light-quark masses and lattice spacings, Refs. [903–918].

Lattice QCD calculations in the charmonium, bottomonium and related exotic-flavor sectors are, however, less advanced. We will discuss calculations with three levels of sophistication. The first class of calculations neglect the fact that hadrons above threshold are unstable and determine the energy eigenstates using solely fermion-bilinear operators (with a structure resembling a single meson) – the full finite-volume spectrum, which includes multihadron levels, is not extracted. As discussed in Refs. [130, 902, 919], these results should only be considered a guide to the pattern of narrow resonances, and the precise resonance mass and other properties can not be obtained. It is also unclear whether these calculations are sensitive to broad resonances and resonances where coupled-channel effects are important.

The second class of calculations include operators with relevant meson-meson-like structures and extract the finite-volume spectrum in the energy region considered (though they may neglect some potentially relevant meson-meson channels). However, these do not have enough constraints to robustly determine scattering amplitudes using the Lüscher method and are often limited to looking for the presence of extra levels in the spectrum compared to the spectrum if there were no meson-meson interactions. This is likely to give a reasonable guide to the presence of a narrow resonance in elastic scattering, but it is less clear for broader resonances and coupled-channel scattering, see Ref. [902]. The third class of calculations extract the complete finite-volume spectrum in the energy region
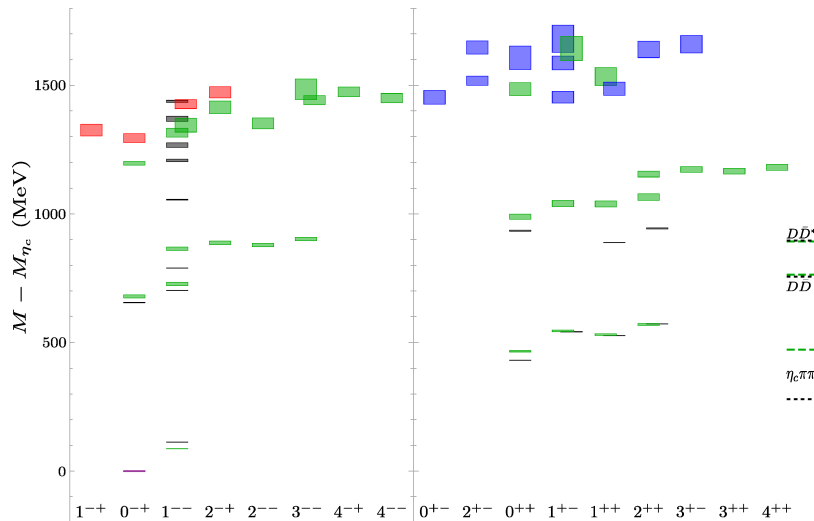
Figure 96: From Ref. [131]. Charmonium spectrum labeled by J^{PC} from a lattice calculation with $M_\pi \approx 240$ MeV where the unstable nature of states above threshold has been neglected. Green, red and blue boxes represent the computed masses and one-sigma statistical uncertainties, with red and blue boxes highlighting states identified as hybrid mesons; black boxes are experimental values. Some of the lower thresholds are shown as dashed lines on the right of the figure (green are using computed masses and black are using experimental masses).

considered and have enough constraints to determine the scattering amplitudes and hence the resonance content. Only these should be considered rigorous but the other less sophisticated calculations may provide useful qualitative guides.

We now discuss lattice QCD calculations of charmonia and related exotic-flavour hadrons before moving to bottomonia and then investigations using the potential between two infinitely-heavy (static) quarks. Unless otherwise stated, all the computations are performed for a single lattice spacing and have dynamical up, down, and strange quarks, i.e. they include the effects of these quarks in the sea, and the two light (up and down) quarks are degenerate. Some of the calculations have dynamical light quarks but quenched (not dynamical) strange quarks – this leads to a non-unitary theory and an unknown systematic uncertainty. The use of quenched charm (or bottom) quarks is not expected to have a significant effect far below *cccc* (or *bbbb*) threshold.

4.5.1. Charmonia and related flavour-exotic channels

Neglecting the fact that they are unstable, higher-lying charmonia have been studied in Refs. [130, 131, 920, 921]. The results presented in Refs. [130, 131], with $M_\pi \approx 390$ and 240 MeV, one lattice spacing and a few volumes, include hybrid mesons with exotic and non-exotic quantum numbers – see Fig. 96 for the results with $M_\pi \approx 240$ MeV. These suggest an interesting hybrid-meson phenomenology with the lightest hybrid multiplet being consistent with a quark-antiquark pair in an S wave coupled to a $J^{PC} = 1^{+-}$ gluonic excitation, and an energy scale of ~ 1.2 - 1.3 GeV. The results have been discussed in the context of Born–Oppenheimer effective field theory in Sec. 4.4.4. However, as mentioned above, these spectra should only be considered a guide to the pattern of narrow resonances.

One challenge that lattice QCD investigations of charmonium resonances face is the large number of channels to which such a resonance can potentially couple – all these channels need to be considered to reach robust conclusions. Currently, calculations are mostly limited to extracting finite-volume spectra and looking for the presence of extra levels, and they have generally been exploratory or inconclusive. More detailed computations are needed that extract a larger number of finite-volume energy levels and allow scattering amplitudes to be determined and hence the state content to be investigated robustly. All the following calculations neglect contributions where a charm quark and a charm antiquark annihilate – these are OZI suppressed and so expected to be small (see also Ref. [922]). In the NRQCD language of Sec. 4.4.2, quark-antiquark annihilation is described by four-fermion operators in the Lagrangian density, Eq. (62). These operators are of dimension 6 or higher, and they are therefore suppressed by powers of the quark mass in the power counting of the effective field theory.

In Refs. [923, 924] $I = 0$ $J^{PC} = 1^{++}$ $D\bar{D}^*$, $\omega J/\psi$, $\sigma\eta_c$, $\sigma\chi_{c1}$ scattering is investigated, neglecting potential coupling
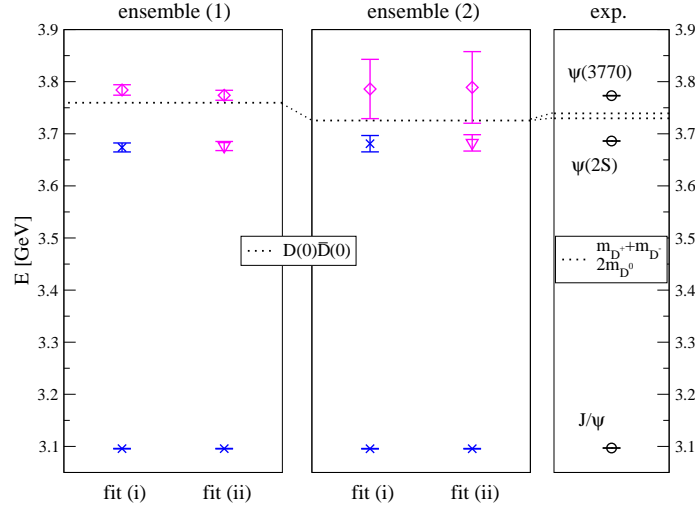
Figure 97: From Ref. [927]. Charmonium spectrum in the $J^{PC} = 1^{--}$ channel from lattice calculations with $M_\pi \approx 266$ MeV (ensemble 1) and $M_\pi \approx 156$ MeV (ensemble 2), compared to experimental results. Two different fit procedures have been used (fit i and fit ii) as described in Ref. [927].

to some other channels. Interpolating operators with diquark-antidiquark structure are used in addition to those with fermion-bilinear and meson-meson structures, though their inclusion is not found to have a significant impact on the results. Computations are performed with $M_\pi \approx 266$ MeV and dynamical light quarks (quenched strange quarks). One rather small volume, $M_\pi L \approx 2.7$, is employed with the system overall at rest leading to only a few energy levels being determined. A bound state is found just below $D\bar{D}^*$ threshold, a candidate for the $X(3872)$. Refs. [781, 925, 926] discuss how the binding energy of the $X(3872)$ is expected to depend on the light quark mass. A study of $\bar{c}c\bar{s}s$ ($D_s\bar{D}_s^*$, $\phi J/\psi$) in Ref. [924], neglecting coupling to the other $I = 0$ channels, finds no sign of a bound state or resonance, so no candidate for the $X(4140)$.

Ref. [927] studied P-wave $D\bar{D}$ (1^{--}) scattering and S-wave $\omega J/\psi$, $D\bar{D}$ (0^{++}) scattering, neglecting potential couplings to other channels. Two small lattices are used: one with $M_\pi \approx 266$ MeV, $M_\pi L \approx 2.7$ and dynamical light quarks, and the other with $M_\pi \approx 156$ MeV, $M_\pi L \approx 2.3$ and dynamical light and strange quarks, and a small number of energy levels extracted. A 1^{--} resonance is found and possibly a $\psi(3770)$ candidate as shown in Fig. 97. Assuming elastic $D\bar{D}$ scattering there is a suggestion of a narrow 0^{++} resonance slightly below 4 GeV – this does not appear to be in particularly good agreement with the experimental data in Ref. [134].

Low-energy $\phi(\bar{s}s) J/\psi$ scattering in S-wave and P-wave is investigated in Ref. [928] using a small volume, $M_\pi L \approx 2$, with $M_\pi \approx 156$ MeV. Other open channels are neglected as are contibutions where any quark and antiquark annihilate, leading to unquantified systematic uncertainties. Twisted boundary conditions are employed to extract a number of energy levels and determine the phase shifts close to threshold. However, the twisted boundary conditions are only applied to valence quarks, not sea quarks, leading to a non-unitary theory and another unknown systematic uncertainty. The extracted $S-$ and P-wave phase shifts are consistent with weak attraction and show no sign of a resonance such as a candidate for the $X(4140)$.

Moving to exotic-flavor channels, Ref. [929] investigates the doubly-charmed $I = 0$ channel (quark content $cc\bar{q}\bar{q}$ where q is an up or down quark) with $J^P = 0^+, 1^+, 2^+$ and the $I = 1/2$ channel (quark content $cc\bar{q}\bar{s}$) with $J^P = 0^+, 1^+$, and the hidden-charm $I = 1$ channel (quark content $c\bar{c}q\bar{q}$) with $I^G J^P = 1^+1^+, 1^-0^+, 1^-1^+$. Calculations are performed with $M_\pi \approx 390$ MeV on a single volume where $M_\pi L \approx 3.8$. Operators with both meson-meson and diquark-antidiquark structures are used, though the latter are found not to be important in determining the spectrum. In each channel studied, a number of energy levels are extracted and there is no sign of a bound state or narrow resonance.

In Ref. [930] (an extension of Ref. [931]), the hidden-charm $I^G = 1^+$, $J^P = 1^+$ channel is studied considering $D\bar{D}^*, \pi J/\psi, \rho\eta_c, D^*\bar{D}^*, \pi\psi(2S), \pi\psi(1D)$ scattering. A small lattice volume is used, $M_\pi L \approx 2.7$, with $M_\pi \approx 266$

MeV and dynamical light quarks (quenched strange quarks). Interpolating operators with meson-meson structure are employed along with a few having diquark-antidiquark structure. A number of energy levels are extracted – these only give evidence for at most weak interactions and there is no sign of a bound state or narrow resonance [e.g. the $Z_c(3900)^+$] up to ~ 4.2 GeV. Ref. [932] considers different possible scenarios for the $Z_c(3900)^+$ (resonance or virtual state) in comparison to these lattice results. A similar study of the $I^G = 1^-$ $J^P = 1^+$ channel ($D\bar{D}^*$, $\rho J/\psi$, $\pi\chi_{c0}$, $\pi\chi_{c1}$) is presented in Refs. [923, 924]. A few energy levels are determined for the system overall at rest and no evidence for a bound state or resonance is seen.

Ref. [933] investigates low-energy S-wave $D\bar{D}^*$ scattering with $I^G = 1^+$, $J^P = 1^+$, neglecting possibly couplings to other open channels. Computations are performed on three lattices with $M_\pi \approx 300, 420, 485$ MeV and $M_\pi L \approx 3.3$, 4.6, 5.3, respectively – these have dynamical light quarks (quenched strange quarks). Twisted boundary conditions are used to extract a number of energy levels but the twisting is only applied to valence quarks, not sea quarks, leading to a non-unitary theory and an unquantified systematic uncertainty. The phase shifts are found to correspond to weakly repulsive scattering and the scattering length and effective range are determined. There is no sign of a bound state or narrow resonance such as a $Z_c(3900)^+$ candidate.

The same setup, with the same limitations, is used in Ref. [934] to study low-energy S-wave $D^*\bar{D}^*$ scattering with $I^G = 1^+$, $J^P = 1^+$. Again, the interaction is found to be weakly repulsive, the scattering length and effective range are extracted, and there is no evidence for a bound state or narrow resonance such as the $Z_c(4020)^+$. A similar study of low-energy $D^*\bar{D}_1$ scattering in S-wave ($J^P = 0^-$) and P-wave ($J^P = 1^+$) with $I^G = 1^+$ is presented in Ref. [935], relevant for, inter-alia, the $Z_c(4430)^+$. In this case, the results suggest an attractive interaction but a definite conclusion on whether or not there is a bound state can not be reached.

The HAL QCD collaboration has pursued an alternative to the Lüscher approach in which lattice QCD is used to compute correlation functions involving spatially-displaced interpolating operators. These are related to Nambu–Bethe–Salpeter wave functions and in turn to non-relativistic potentials which are used in the Schrödinger equation, see Refs. [889–901]. There has been a lot of discussion as to the reliability of the HAL QCD approach and how it is employed. There is yet to be a successful demonstration of its application to the ρ resonance in $I = 1$ $\pi\pi$ scattering. For a number of baryon-baryon channels, there appears to be a discrepancy between results obtained using this method and results obtain using the Lüscher approach, though investigations using the latter method have their own limitations – see Refs. [898–900, 902, 936] and references therein. In Ref. [937] the HAL QCD potentials for baryon-baryon scattering are critically examined phenomenologically. It is found that especially in the ΩN and $\Omega\Omega$ channels, where one pion change is not forbidden in the scattering potential, the range of the potential reported by the HAL QCD studies is at odds with phenomenological expectations.

Ref. [938] investigates the flavor-exotic $cc\bar{u}\bar{d}$ and $cs\bar{u}\bar{d}$ channels. Reasonably large lattice volumes ($M_\pi L \gtrsim 6$) with $M_\pi \approx 410$ MeV, 570 MeV, 700 MeV are used. The HAL QCD method is used to extract S-wave potentials for DD, $\bar{K}D$, DD^*, and $\bar{K}D^*$, these potentials are fit and the corresponding Schrödinger equations are solved to compute the phase shifts. The $I = 0$ channels are found to be attractive, particularly $I = 0$ $J^P = 1^+$ DD^*, i.e. $cc\bar{u}\bar{d}$, and become more attractive as M_π decreases. However, there is no evidence for a bound state or resonance. The $I = 1$ channels are all found to be repulsive.

S-wave $\pi J/\psi$, $\rho\eta_c$, $\bar{D}D^*$ coupled-channel scattering with $I = 1$, $J^P = 1^+$ is studied in Ref. [939, 940] using the same lattices as above. The HAL QCD method is employed and the diagonal potentials are found to be weak, but the off-diagonal $\pi J/\psi - \bar{D}D^*$ and $\rho\eta_c - \bar{D}D^*$ potentials are strong. The S-matrix is computed from these potentials and poles are searched for: a pole is found on an unphysical sheet far below $D\bar{D}^*$ threshold with a large imaginary part and it is suggested that the $Z_c(3900)^+$ is a threshold cusp. These results are then used as an input to a phenomenological study of the invariant mass spectra in $Y(4230) \to \pi\pi J/\psi$ and $Y(4230) \to \pi D\bar{D}^*$.

Going beyond spectroscopy and studying transitions between mesons can provide a more stringent probe of their structure. Ref. [177] performed a quenched calculation of radiative transition amplitudes involving some excited, high spin and exotic charmonia, neglecting the unstable nature of states above threshold. One highlight was the radiative decay of an exotic $J^{PC} = 1^{-+}$ hybrid meson, η_{c1}, which was found to have a significant partial width, $\Gamma(\eta_{c1} \to J/\psi\gamma) \sim 100$ keV, supporting suggestions from models that the photocouplings between 1^{-+} hybrids and conventional mesons should be large. A large decay amplitude for the decay of a 1^{--} hybrid to η_c was found, again in line with phenomenological expectations. In addition, it was shown how the pattern of different multipole amplitudes in the radiative decay of 2^{++} charmonia to J/ψ can distinguish P wave and F wave tensor mesons. As well as studying the $\chi_{c2} \to J/\psi\gamma$ transition, Ref. [941] performed a quenched calculation of the $\eta_{c2}(2^{-+}) \to J/\psi\gamma$ transition amplitudes,
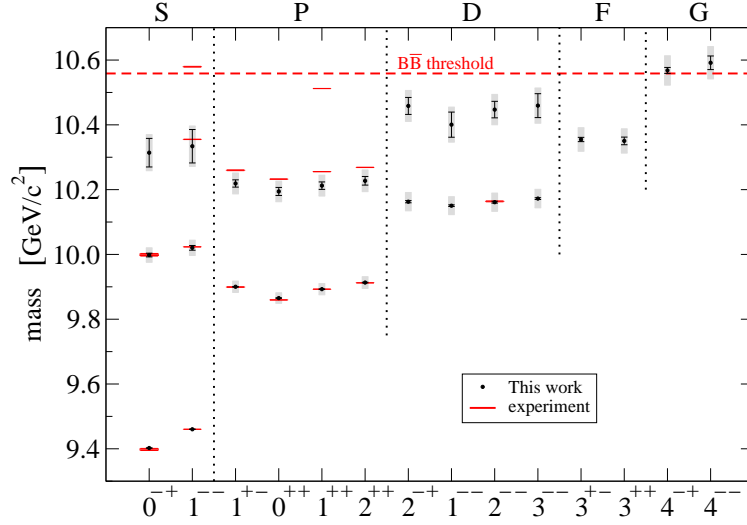
Figure 98: From Ref. [943]. Bottomonium spectrum labeled by J^{PC} from a lattice calculation with $M_\pi \approx 156$ MeV. Black points with errorbars are the lattice results with statistical uncertainties, and grey bands give an estimate of the combined systematic and statistical uncertainties. Red bands are experimental masses.

finding a small partial width and determining the three multipole amplitudes. These investigations demonstrate the feasibility of using lattice QCD to study transitions involving higher-lying charmonia and that such calculations can provide phenomenologically-interesting results – calculations with dynamical quarks allowing for the unstable nature of resonances are warranted.

In summary, there have been a number of lattice QCD studies of charmonium-like resonances and related scattering channels, but these all suffer from significant limitations. Candidates for conventional resonances and the $X(3872)$ have been seen. However, there is currently no clear evidence for a flavor-exotic hidden-charm or doubly-charmed state from lattice QCD calculations, in contrast to the various experimental signals for charged charmonium-like structures — see Sec. 3.2.

4.5.2. Bottomonia and related flavour-exotic channels

Some higher-lying S-, P-, D-, F- and G-wave bottomonia up to $B\bar{B}$ threshold have been studied in Refs. [942, 943] (along with B, B_s and B_c mesons). A single lattice volume was used with $M_\pi \approx 156$ MeV and NRQCD b quarks – the results were found to be in reasonable agreement with experiment – see Fig. 98.

Ref. [524] investigates the possibility of $J^P = 1^+$ flavor-exotic $I = 0$ $ud\bar{b}\bar{b}$ and $I = 1/2$ $qs\bar{b}\bar{b}$ systems. Three different light-quark masses are considered corresponding to $M_\pi \approx 164$, 299 and 415 MeV, each on one volume ($M_\pi L \approx 6.1$, 4.4, and 2.4, respectively), and NRQCD b quarks are employed. A small number of energy levels are computed using local meson-meson and diquark-antidiquark interpolating operators. These give some evidence for bound states for all three light-quark masses: $(189 \pm 10 \pm 3)$ MeV below the BB^* threshold for $ud\bar{b}\bar{b}$ and $(98 \pm 7 \pm 3)$ MeV below the $B_s B^*$ threshold for $qs\bar{b}\bar{b}$, though the robustness of the signal is not clear in all cases.

That investigation has recently been extended in Ref. [944], which studies $J^P = 1^+$ $ud\bar{b}\bar{b}'$ ($I = 0$), $ud\bar{b}'\bar{b}'$ ($I = 0$), $qs\bar{b}\bar{b}'$ and $qs\bar{b}'\bar{b}'$ for $M_\pi \approx 299$ MeV, where the mass of the b' quark ranges from 0.59 to 6.3 m_b. Evidence for binding is found in all cases and the dependence of the binding energy on $m_{b'}$ is fit to phenomenologically-motivated forms. Extrapolating to $m_{b'} = m_c$ appears to suggest that only $ud\bar{c}\bar{b}$ has a possibility of being bound. The $J^P = 1^+$ $I = 0$ $ud\bar{c}\bar{b}$ is then studied for all three M_π – the ground state is found to be consistent with threshold for $M_\pi = 415$ MeV and bound for $M_\pi = 163$ MeV and 299 MeV, with the binding energy estimated to be between 15 and 61 MeV. However, as the authors point out, unaccounted-for finite-volume effects may be significant.

In Ref. [945] a number of $J = 0, 1$ double-bottom channels are studied with three different lattice spacings ($a \approx$ 0.12, 0.09, 0.06 fm), each on a single volume, and with dynamical light, strange and charm quarks. The sea light-quark
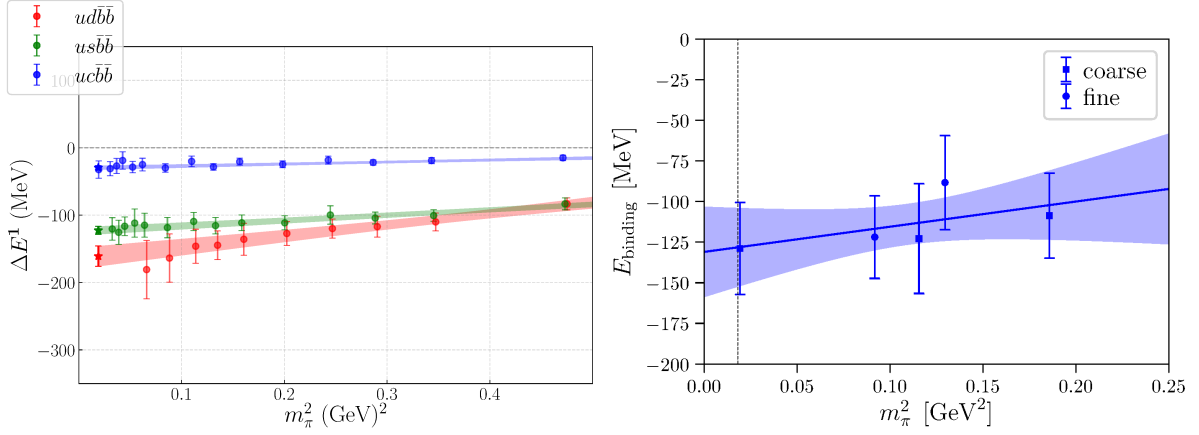
Figure 99: Left: Dependence of the binding energies in the $J^P = 1^+$ $ud\bar{b}\bar{b}$ ($I = 0$), $us\bar{b}\bar{b}$ and $uc\bar{b}\bar{b}$ channels on the valence M_π from Ref. [945] (the light sea-quark mass is fixed). Right: Dependence of the binding energy in the $J^P = 1^+$ $ud\bar{b}\bar{b}$ ($I = 0$) channel on M_π from Ref. [946].

mass corresponds to $M_\pi \sim 300$ MeV, but a different action is used for the light valence quarks with a range of masses corresponding to $M_\pi \approx 153$ to 689 MeV – this leads to a non-unitary theory and an unquantified systematic uncertainty. Local meson-meson and diquark-antidiquark operators are employed and a small number of levels extracted, though in some cases the quality of the signal is not that good. With $J^P = 1^+$, bound states are claimed in $ud\bar{b}\bar{b}$ ($I = 0$) and $us\bar{b}\bar{b}$ with respective masses 143 ± 34 MeV and 87 ± 32 MeV below BB^* threshold – see left panel of Fig. 99. For $uc\bar{b}\bar{b}$, $sc\bar{b}\bar{b}$, $ud\bar{c}\bar{c}$ ($I = 0$) and $us\bar{c}\bar{c}$, there is some suggestion of a close-to-threshold state but finite-volume effects may be important. The binding energy shows a general trend to increase as the light-quark masses decrease. There is no evidence for bound states with $J^P = 0^+$ for $uu\bar{b}\bar{b}$ ($I = 1$), $ss\bar{b}\bar{b}$, $cc\bar{b}\bar{b}$, $uu\bar{c}\bar{c}$ ($I = 1$) and $ss\bar{c}\bar{c}$.

Very recently, Ref. [946] has reported on a more detailed investigation of the $I = 0$ $J^P = 1^+$ $ud\bar{b}\bar{b}$ channel.[23] Five different lattices are used with dynamical light and strange quarks, a range of lattice spacings ($a \approx 0.083 - 0.114$ fm), volumes ($M_\pi L \approx 3.9$ to 5.8) and light-quark masses ($M_\pi \approx 139$ to 431 MeV); NRQCD b quarks are employed. Operators with a meson-meson-like structure (BB^* and B^*B^*) are used in addition to those with a local diquark-antidiquark structure, and a couple of energy levels are extracted on each lattice. The Lüscher method was used to determine the infinite-volume binding energy through a fit to an effective range expansion (though this was found to be consistent with the finite-volume binding energy), giving a bound state $128 \pm 24 \pm 10$ MeV below BB^* threshold, where the second error is an estimate of systematic uncertainties – see right panel of Fig. 99.

In an investigation of the $bb\bar{b}\bar{b}$ system, Ref. [948] uses four lattices with various light-quark masses (including one lattice with physical-mass light quarks) and lattice spacings ($a = 0.06 - 0.12$ fm), and NRQCD b quarks. A number of meson-meson and diquark-antidiquark operators are employed and no sign of a bound state is found with $J^{PC} = 0^{++}$, 1^{+-}, 2^{++}.

Turning briefly away from bottomonium-like systems, Ref. [249] investigates the exotic-flavor bottom-strange $I = 1$ $J^P = 0^+$ $\bar{b}s\bar{d}u$ channel relevant for the $X(5568)$ (see Sec. 3.2.1). A number of $B_s\pi$ and $B\bar{K}$ operators are employed in a calculation on small volume, $M_\pi L \approx 2.3$, using dynamical light and strange quarks with $M_\pi \approx 156$ MeV. A few energy levels are extracted and the results are compared with the levels expected if a $X(5568)$ were present. No signs of strong $B_s\pi$ interactions are found and there is no evidence for a $X(5568)$ candidate. Ref. [251] comments on some implications for the $X(5568)$ in light of these results.

To summarise, there have been few lattice QCD investigations of excited bottomonia. However, in contrast to the charm sector, there appears to be evidence for a double-bottom $J^P = 1^+$ bound state in $I = 0$ $ud\bar{b}\bar{b}$ and $I = 1/2$ $qs\bar{b}\bar{b}$,

---

[23]Some preliminary results from an early stage of this study appeared in Ref. [947] where, in addtion, b quarks with masses ranging from one to five times the physical b-quark mass were considered.

with the binding energy increasing if the light-quark mass decreases or m_b increases. However, confirmation of some of these results is required, and further work is needed to investigate a number of channels in more detail and assess some of the systematics. In the next section we discuss lattice QCD calculations of the potential between two static quarks – these support the presence of a $J^P = 1^+$ $I = 0$ $ud\bar{b}\bar{b}$ bound state for large m_b.

4.5.3. Static quark potentials

Refs. [949, 950] use lattice QCD to compute the potential between two infinitely-heavy static antiquarks $\bar{Q}$ in the presence of light quarks, fit to a phenomenologically-inspired form and then investigate whether a bound state is present by solving the Schrödinger equation. These calculations have dynamical light quarks (quenched strange quarks)[24] and two small lattice volumes are used: one with $M_\pi \approx 340$ MeV, $a \approx 0.079$ fm and $M_\pi L \approx 3.3$ for systems involving qq and another with $M_\pi \approx 352$ MeV, $a \approx 0.042$ fm and $M_\pi L \approx 2.4$ for systems involving ss or cc. They find evidence for a $J^P = 1^+$ bound state in $I = 0$ $qq\bar{Q}\bar{Q}$, and evidence against a bound state in $J^P = 0^+, 1^+$ or 2^+ for $I = 1$ $qq\bar{Q}\bar{Q}$, $ss\bar{Q}\bar{Q}$ and $cc\bar{Q}\bar{Q}$.

In Ref. [523], this work is extended by performing calculations with multiple light-quark masses, corresponding to $M_\pi \approx 340$ MeV, 480 MeV, and 650 MeV ($M_\pi L \approx 3.3$, 4.6, 6.3), and extrapolating to physical M_π. Again, evidence is found for a $J^P = 1^+$ $I = 0$ $qq\bar{Q}\bar{Q}$ bound state, with a mass 90^{+43}_{-36} MeV below threshold, and against a $J^P = 0^+, 1^+$ or 2^+ $I = 1$ $qq\bar{Q}\bar{Q}$ bound state. Ref. [525] makes an attempt to incorporate spin effects, computing static potentials for various light-quark spin combinations, interpreting in terms of BB, BB^* and B^*B^* meson pairs, then using in a coupled-channel Schrödinger equation. Following this procedure, evidence remains for a $I = 0$ $J^P = 1^+$ $qq\bar{Q}\bar{Q}$ bound state but the spin effects reduce the binding, giving a mass 59^{+30}_{-38} MeV below threshold. An extension in Ref. [951] investigates the possibility of resonances using the emergent wave method, predicting a $J^P = 1^-$ $I = 0$ $qq\bar{Q}\bar{Q}$ resonance but no $I = 1$ bound states or resonances.

An independent investigation presented in Ref. [952] employs a similar approach to calculate the static potential in $I = 0, 1$ $qq\bar{Q}\bar{Q}$ for a range of spin and parity channels. One lattice volume is used with $M_\pi \approx 380$ MeV and $M_\pi L \approx 6$. Results are consistent with those of Refs. [949, 950]: there is evidence for a $I = 0$ $J^P = 1^+$ bound state with a mass 50.0 ± 5.1 MeV below threshold.

As well as molecular mesons and tetraquarks, another proposed exotic multiquark structure is a hadroquarkonium state which has a compact $Q\bar{Q}$ core along with a more diffuse distribution of light quarks — see Sec. 4.3.2. Ref. [953] computes the static $Q\bar{Q}$ potential in the presence of a variety of light mesons and baryons, and compares with the static potential in vacuum. One lattice volume is used with $M_\pi \approx 223$ MeV and $M_\pi L \approx 4.6$. A suggestion of weak attraction, a shift in the potential $\lesssim$ a few MeV, is found for $Q\bar{Q}$ with π, K, ρ, K^*, ϕ, $N(1/2^+)$, $\Xi(1/2^+)$, $\Delta(3/2^+)$, $\Xi^*(3/2^+)$, $N(1/2^-)$, $\Xi(1/2^-)$ or $\Xi^*(3/2^+)$. Applying the results to a phenomenological study of charmonia (where the static approximation is not necessarily a good approximation), the energy shifts in the presence of a light hadron are found to be $\sim$ -0.9 to -2.6 MeV for $1S$ charmonia, -1 to -6.5 MeV for $2S$ charmonia and -1 to -4.9 MeV for $1P$ charmonia. Because the shifts are very small, the effects of having unphysical quark masses and working in a finite volume may be significant – these need to be checked before definite conclusions can be drawn.

Lattice calculations of hybrid static potentials, i.e. the potential between a static quark and antiquark in the presence of a gluonic excitation, in pure SU(3) gauge theory (no dynamical quarks) have a long history, Refs. [476, 744, 763, 765–768, 954–957] – the results of these calculations and their phenomenological implication were discussed above in Section 4.4.4. A related recent calculation of the color field density profiles of excited flux tubes between a static quark and antiquark is presented in Ref. [958].

In summary, lattice QCD calculations of the potential between static quarks can provide an interesting window on the physics of the strong interaction. They appear to support the existence of a bound state with $J^P = 1^+$ $I = 0$ $qq\bar{Q}\bar{Q}$ in line with the phenomenological findings outlined in Sec. 4.3.3. However, because the binding is sensitive to the light- and heavy-quark masses and spin effects, calculations with physical-mass quarks and addressing the various other systematics are necessary to draw stronger conclusions.

To conclude this section, Table 16 gives a summary of lattice studies where candidates for the $X(3872)$ and flavour exotics have been seen. In Sec. 5.3 we give an outlook on prospects for future lattice calculations.

---

[24]Because the twisted mass action is used for the quarks, isospin is broken and this has to be taken into account in the calculations.

State	Reference	Approx. M_π / MeV	$M_\pi L$	Binding Energy / MeV
$X(3872)\ I = 0\ J^{PC} = 1^{++}$	[923]	266	2.7	11 ± 7
	[924]	266	2.7	8 ± 15 or 9 ± 8
$ud\bar{c}\bar{b}\ I = 0\ J^P = 1^+$	[944]	extrap. of 164, 299, 415 MeV	2.4, 4.4, 6.1	$\sim 15 - 61$
$ud\bar{b}\bar{b}\ I = 0\ J^P = 1^+$	[524]	extrap. of 164, 299, 415 MeV	2.4, 4.4, 6.1	$189 \pm 10 \pm 3$
	[945]	extrap. of various valence quark masses	various	143 ± 34
	[946]	extrap. of various (139 to 431 MeV)	various	$128 \pm 24 \pm 10$
$qs\bar{b}\bar{b}\ I = 1/2\ J^P = 1^+$	[524]	extrap. of 164, 299, 415 MeV	2.4, 4.4, 6.1	$98 \pm 7 \pm 3$
	[945]	extrap. of various valence quark masses	various	87 ± 32
$ud\bar{Q}\bar{Q}\ I = 0\ J^P = 1^+$ (static quark potentials)	[952]	380	6	50 ± 5
	[949]	340	3.3	$\sim 30 - 57$
	[950]	340	3.3	90^{+46}_{-42} or 93^{+47}_{-43}
	[523]	extrap. of 340, 480, 650 MeV	3.3, 4.6, 6.3	90^{+43}_{-36}
	[525]	extrap. of 340, 480, 650 MeV	3.3, 4.6, 6.3	59^{+30}_{-38}

Table 16: Summary of lattice studies where candidates for the *X*(3872) and flavour exotics have been seen, and the binding energy below the relevant threshold. See the text for more details.

5. Summary and future prospects

With more and more experimental data available and the improvement of experimental techniques, a large number of *XYZ* states have been reported in the charmonium and bottomonium sectors which have properties at odds with the quark model description in terms of charm–anti-charm and bottom–anti-bottom systems, respectively. This suggests the existence of new kinds of hadrons and, in this report, we referred to any state that does not appear to fit with the expectations for an ordinary $\bar{Q}Q$ meson or qqq baryon as "exotic" or as an "exotic candidate".

For many states, their unambiguous identification as exotics, and even more their classification in a specific class of exotics, is still a matter of intense investigation both experimentally and theoretically. On one hand, experimental investigations aim to complete the phenomenological description of these states. On the other hand, theoretical studies aim to reduce the uncertainties in the computation of observables for ordinary quarkonia and exotics. A particular challenge for theoretical studies is to properly account for the mixing of exotics with ordinary quarkonia, which may play an important role for some states.

We have reported extensively on the latest experimental progress which in recent years has come mostly from the Belle, BESIII, and LHCb experiments. This report contains a description of all exotic candidates that have been observed up to the current date. On the theory side, only lattice QCD has the potential to perform full self-consistent calculations from first principles. Currently, however, lattice QCD calculations of exotics adopt approximations and have unquantified systematic uncertainties that reduce their reliability. Moreover, not all observables are currently accessible in lattice QCD calculations. For these reasons, also other methods are employed to describe exotics. Effective field theories allow to perform calculations of exotic states with a clear connection to QCD. They are limited by their specific ranges of applicability, and need to be supplemented by data or lattice QCD results. Nevertheless, they are systematically improvable and progress is steady. In addition to these systematic approaches there are various phenomenological models investigating different aspects of exotic states. While uncertainty estimates for their results are difficult if not impossible, phenomenological models can still provide valuable insights, in particular where other methods have not been applied yet. In the report, we have presented in some detail these different theoretical approaches.

To understand the existing *XYZ* states and finally understand the exotic hadrons, more efforts in both experiment and theory are needed. In experiment, we need to obtain more accurate information on the *XYZ*s, including lineshapes and the resonance parameters for various the J^{PC} quantum numbers, the production and decay modes and so on. Whereas, on the theoretical side, we need improved calculations to more cleanly discriminate exotic hadrons from conventional hadronic states. We close this report with a discussion of the experimental prospects before giving a theoretical outlook.

5.1. Ongoing and future experiments

It is expected that data samples accumulated at the *B* factory experiments (BaBar and Belle), τ-charm experiment (BESIII), and hadron machine experiments (CDF, D0, LHCb, ATLAS, CMS) will continue to be used for the study of the *XYZ* states. At the same time, the ongoing experiments will continue to accumulate more experimental data: LHCb just started exploration of its full RUN1 and RUN2 data and is upgrading for more luminosity; BESIII will continue its program with extended c.m. energy coverage and improved data taking strategy; the GlueX experiment started data taking in 2017 with an expectation to reach a higher sensitivity for the search for pentaquarks and other exotic mesons in photoproduction processes with more beam time available; Belle II has started its pioneering run with the full detector in April 2019 and is expecting its target integrated luminosity of 50 ab^{-1} in a few years. Furthermore, some new experiments are expected to join the effort of investigating the exotic hadrons in the future: the PANDA experiment at Darmstadt, Germany, the super τ-charm factories STCF (HIEPA) in Hefei, China, and SCTF in Novosibirsk, Russia. In this section, we give a brief description of future prospects at the ongoing and planned experiments.

• *The GlueX experiment*

The GlueX experiment, studying light meson spectroscopy with an emphasis on the search for light hybrid states, is the flagship experiment of the newly constructed Hall D at the Thomas Jefferson National Accelerator Facility (JLab) [959]. The experiment exploits photoproduction from a fixed hydrogen target, using both linearly polarized and unpolarized photons.

The GlueX detector is illustrated in Fig. 100. An electron beam of up to 12 GeV impinges on a thin diamond radiator which produces a coherent bremsstrahlung photon beam with a substantial linear polarization in a narrow energy range peaking at 9 GeV. With a collimator suppressing the incoherent bremsstrahlung spectrum, a linear polarization of 40% is achieved in the coherent peak at 9 GeV. The scattered electrons are used to tag the energy of the photon beam. The main detector, shown in Fig. 100, consists of a 2 T solenoid magnet with the central and forward drift chamber for charged particles, a lead/scintillating fiber barrel calorimeter and lead-glass forward calorimeter for neutral particles and electron detection, and a start counter and forward TOF wall for precision timing measurements. The angular coverage of the detector is complete down to opening angles from the beam of about two degrees. Pions are reconstructed for momenta down to 100 MeV and protons to 300 MeV with a resolution from 1% to 3%.
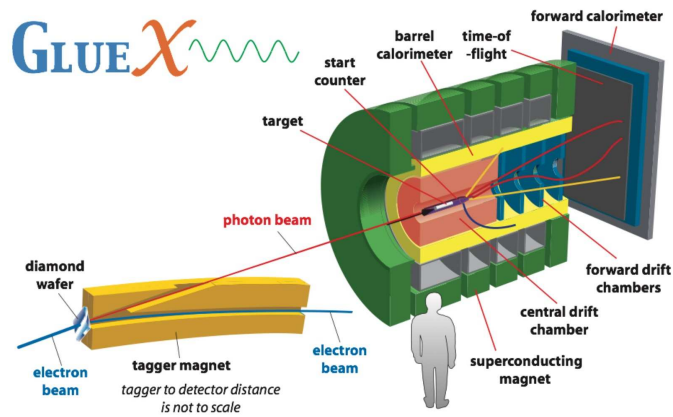

Figure 100: Schematic of the GlueX detector and the photon beam tagger [959].

The GlueX detector has been successfully commissioned and started its physics data taking in spring 2017. Based on the accumulated data, the analysis of a variety of physics topics is already ongoing. For example, the cross section of $\gamma p \rightarrow J/\psi p$ has been measured at $8.2 < E_\gamma < 11.8$ GeV using about 25% of the total data accumulated by the GlueX experiment from 2016 to date [322]. Although clear J/ψ signals were observed, no statistically significant evidence was found for the pentaquark observed by LHCb.

140

The observation of many well-known meson resonances as well as the first successful reconstruction of the J/ψ demonstrates good prospects for a broad physics program with initial GlueX data. The mapping of the entire light meson spectrum will be possible, with a precise measurement of the properties of known resonances and, ultimately, the candidates for exotic mesons. The completion of the initial GlueX running is expected in 2019, after which several upgrades are planned. A DIRC detector will be added in the forward region to improve pion and kaon separation [960]. This and a factor of five or more higher luminosity will allow to reach a higher sensitivity for the search for pentaquarks and other exotic mesons.

• *The BESIII experiment*

Since its commissioning in 2008, the BESIII detector has been operating successfully for more than 10 years. The end cap TOF system has been upgraded into a MRPC-based detector with improved particle identification capability. A cylindrical gas electron multiplier (CGEM) based inner detector CGEM-IT is being constructed to replace the inner MDC chamber with similar performance as the previous chamber.

The BEPCII has delivered more than 20 fb^{-1} integrated luminosity at different energy points in the last 10 years and the peak luminosity keeps on improving every year. BESIII is planning to take more data above 4 GeV, 500 pb^{-1} per point with a 10 MeV interval. The intervals were chosen to cover the possibility for studying narrow XYZ states. For example, the $e^+e^- \to \pi^+\pi^- J/\psi$ cross section has shown rapid changes between 4.20 and 4.23 GeV. The cross sections for other reactions are likely to have such rapidly changing features, which require fine energy scans. Figure 101 shows the data sets accumulated by BESIII, and possible future plan.
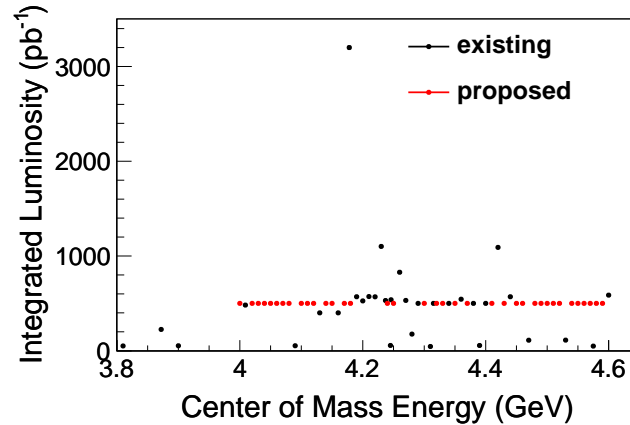

Figure 101: The data sets accumulated by BESIII mainly for the study of XYZ states, where the data sets collected are shown in black, and those considered in the near future for potential future measurements are shown in red.

To meet the requirement of the BESIII physics research, two aspects of the BEPCII upgrade have been considered: one is to increase the maximum c.m. energy from 4.6 to 4.9 GeV, and the other is the top-up injection in collision operation. The former will allow to fully cover the $Y(4630)$ and $Y(4660)$ resonances and a wide range of $e^+e^- \to K^+K^- J/\psi$ production, which may be a key mode of searching for the Z_{cs} state and might also provide deeper insights for the $Y(4660)$. The latter will increase the integrated luminosity by about 30% in the same period of data taking time. These upgrades are in progress and are expected to be completed in 2019.

In addition, an even more ambitious upgrading plan of increasing the peak luminosity by a factor of 10 has been proposed [961]. In this scheme, the Crab Waist collision with large Piwinski angle would be adopted together with significant modification of the BEPCII parameters. At the same time, BEPCII is also investigating a possibility of moderate improvement of the peak luminosity by increasing the number of bunches and the beam current, as well as installing more radio frequency cavities. This latter scenario may need much less machine shutdown time to accumulate similar amount of integrated luminosity in 5 to 10 years than the realisation of the Crab Waist scheme.

● *The Belle II experiment*

The Belle II detector is the sole experiment at the SuperKEKB e^+e^- collider in Tsukuba, Japan. The goal of the Belle II experiment, as a next generation flavor factory, is to search for new physics in the flavor sector at the intensity frontier, and to improve the precision of measurements of Standard Model parameters. It started to record data in April 2018 and is in a unique position regarding bottomonium physics, and an experiment with full capability to explore QCD phenomenology and study conventional/exotic states.

There are many experimental reasons that make Belle II perfectly suited to study exotic states: (1) Running at the $\Upsilon(4S)$ resonance produces a very clean sample of $B\bar{B}$ pairs. The low background environment allows for reconstruction of final states containing photons. (2) Due to low track multiplicities and detector occupancy, the reconstruction efficiency of $B-/D-$mesons is high and the trigger bias is very low. (3) Since the initial state is known, "missing mass" analyses can be performed to infer the existence of new particles via energy/momentum conservation rather than demanding full reconstruction of their final states. This gives the opportunity to measure the absolute branching fractions of the XYZ states. (4) Overcoming the statistical limitations of previous experiments, Belle II will be in a unique position to perform, for example, searches for resonant states via ISR processes, studies of quarkonium-like spectroscopy via bottomonium decays and bottomonium-like spectroscopy via hadronic and radiative transitions among bottomonia, and studies of QCD bound states like the deuteron and di-baryons.

The SuperKEKB accelerator is an upgrade of the KEKB B-factory running in the region of the Υ resonances with the beam energies of 7 GeV for the high energy ring and 4 GeV for the low energy ring. The target luminosity of SuperKEKB is a factor of 40 larger than that of KEKB, i.e., 8×10^{35} cm$^{-2}s^{-1}$. To achieve such a high luminosity, a nanobeam collision scheme is taken. The maximum c.m. energy in SuperKEKB is 11.24 GeV, just at the $\Lambda_b\bar{\Lambda}_b$ threshold which makes the possibility of studying the Λ_b decays very uncertain.

The Belle II detector is a hermetic magnetic spectrometer including several substantially upgraded or new subsystems. The new vertex detector (VXD) consists of two subdetectors: a Pixel Vertex Detector and a double-sided Silicon strip Vertex Detector. An improvement by a factor of 2 on the vertex resolution compared with the Belle vertex detector is obtained with this strategy. The central tracking system is a large volume CDC surrounding the VXD. To be able to operate at high event rates, the CDC has been modified with smaller cells. The particle identification system includes the Time-Of-Propagation system in the barrel region and the Aerogel Ring Image Cherenkov detector in the forward region to measure the time of propagation and the impact position of Cherenkov photons, the EMC based on CsI(Tl) crystals to detect photons and identify electrons, the K-Long and Muon detector. A full discussion can be found in the Technical Design Report [962].

The Belle II experiment started physics running with its full detector in March 2019. It is foreseen to run for 9 months/year with a three-month summer shutdown. It is planned to reach a peak luminosity of 8×10^{35} cm$^2s^{-1}$ by 2025 and continue running until 2027 to integrate more than 50 ab^{-1}. The planned integrated luminosity is shown in Fig. 102.
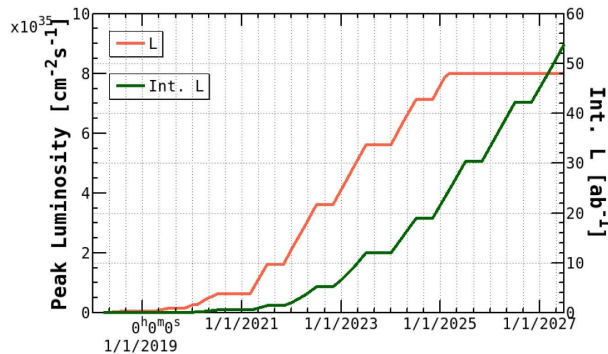

Figure 102: Plan of instantaneous and integrated luminosity at SuperKEKB.

In the near future, the study of XYZ particles will benefit a lot from the large data samples of the Belle II experiment

in many different ways [17], among which ISR can produce events in the same energy range covered by BESIII. Figure 103 shows the effective luminosity distribution in the Belle and Belle II data samples. We can see that, 50 ab^{-1} of Belle II data correspond to 2,000–2,800 pb^{-1} data for every 10 MeV from 4–5 GeV, similar statistics will be reached for modes like $e^+e^- \rightarrow \pi^+\pi^- J/\psi$ at Belle II and BESIII taking into account the fact that Belle II has lower efficiency. Belle II has the advantage that data at different energies will be accumulated at the same time, making the analysis much simpler than at BESIII where data are accumulated at many data points. Many ISR processes, like $e^+e^- \rightarrow \pi^+\pi^- J/\psi$, $\pi^+\pi^- \psi(2S)$, $K^+K^- J/\psi$, $K^+K^- \psi(2S)$, $\gamma X(3872)$, $\pi^+\pi^- \psi_2(1D)$, $\pi^+\pi^- h_c$, $\pi^+\pi^- h_c(2P)$, $\omega \chi_{cJ}$, $\phi \chi_{cJ}$, $\eta J/\psi$, $\eta' J/\psi$, $\eta \psi(2S)$, ηh_c, $(D\bar{D}^*)^{\pm}\pi^{\mp}$, $(D^*\bar{D}^*)^{\pm}\pi^{\mp}$, $\Lambda_c^+\bar{\Lambda}_c^-$, $\Lambda_c^+\bar{\Sigma}_c^-$, can be done at Belle II to search for more production and decay modes of known XYZ states or more new charmonium-like states.
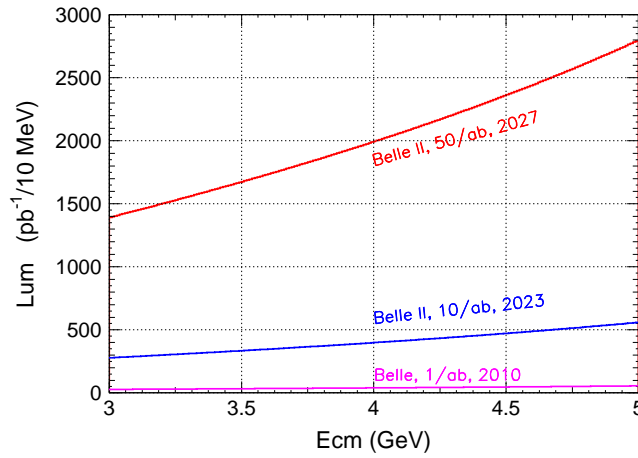

Figure 103: Effective luminosity at low energy in the Belle and Belle II $\Upsilon(4S)$ data samples.

● *The LHCb experiment*

The LHCb experiment has demonstrated itself as an ideal laboratory for flavor physics studies. The LHCb upgrade will fully exploit the flavor-physics opportunities of the high-luminosity large hadron collider (HL-LHC) to search for physics beyond the Standard Model in an approach complementary to the energy frontier. The timelines of operation and major shutdowns of the LHC, HL-LHC, and LHCb are illustrated in Fig. 104.

The LHCb Upgrade I is currently in progress and data taking will start in 2021 after the LHC Long Shutdown 2 (LS2). Consolidation of the LHCb Upgrade I detector is required during LS3. The preparatory work for the LHCb Upgrade II will also be carried out at this time. These changes are referred to as Upgrade Ib. During the period of LHCb Upgrade I, the detector will be operated with an instantaneous luminosity of 2×10^{33} cm$^{-2}s^{-1}$. A total integrated luminosity of around 23 fb^{-1} is anticipated by the end of Run 3 and 50 fb^{-1} by the end of Run 4 of the LHC. LHCb Upgrade II will be installed during LS4, which is expected to start data taking in 2031. At that time, the LHCb will operate with an instantaneous luminosity of up to 2×10^{34} cm$^{-2}s^{-1}$, an order of magnitude above Upgrade I. LHCb will accumulate a data sample corresponding to a minimum of 300 fb^{-1}. To meet such a high instantaneous luminosity, modest improvements of the Upgrade I and II detector will be performed during LS3 and LS4. New upgrades in some subdetector components include a pixel detector, a vertex detector, the RICH system, and so on. They will improve the intrinsic performance of the experiment in certain key areas. For more detail, we refer to Ref. [963].

The LHCb experiment has already strongly contributed to our understanding of the XYZ particles, e.g. via the determination of the quantum numbers of the $X(3872)$ [37, 58], and the observation of pentaquark candidates $P_c(4380)^+$
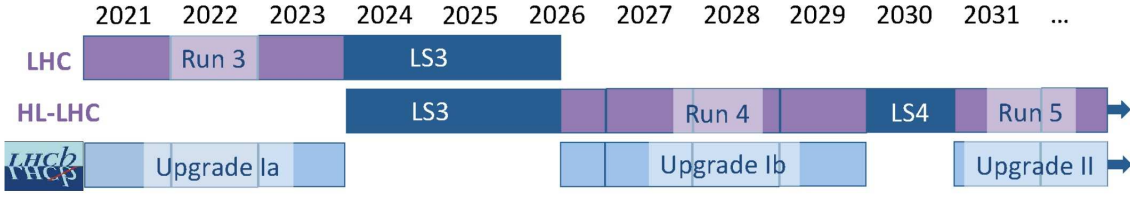
Figure 104: Timeline of accelerator and experiment operation of the LHC, HL-LHC, and LHCb over the decade 2021 to 2031 [963].

and $P_c(4450)^+$ [36] [recently LHCb found that the $P_c(4450)^+$ is composed of two narrow overlapping structures $P_c(4440)^+$ and $P_c(4457)^+$ [307]]. The large data set collected in the Upgrade II era will boost the sensitivity of searches for pentaquark multiplets and heavy exotic states with small production cross sections and low efficiency. For examples: (1) the observation of radiative decays involving exotic baryons will provide a new insight into the structure of the pentaquark candidates by performing an amplitude analysis of the $\Lambda_b \to J/\psi p \gamma K$ decay. The proposed improved EMC is crucial for the feasibility of such a measurement in a high-luminosity environment. (2) The neutral pentaquark candidates can be searched for in the $\Lambda_c^+ D^-$ system in the process $\Lambda_b^0 \to \Lambda_c^+ D^- \bar{K}^{*0}$. Such process suffers from the low detection efficiency and the small branching fractions of Λ_c^+ and D^- decays. Such channel needs very large data sets to compensate the low efficiency and small product branching fraction. (3) The pentaquark states with strangeness can be searched for in the $\Xi_b^- \to J/\psi \Lambda K^-$ process, which has been seen at LHCb using Run 1 data [964]. About 300 signal events were observed, thus no intermediate states were investigated. An increase of the integrated luminosity by a factor of 100 would allow detailed amplitude analyses with a similar sensitivity as in the pentaquark discovery channel.

The enhancements of the Upgrade I and II detector [963] together with the enormous sample sizes of Run 5 will ensure that LHCb maintains its position in exotic hadron studies, and provide a unique access to studies involving the production of B_c^+, Λ_b^0, and Ξ_b hadrons.

● *The PANDA experiment*

The PANDA (antiProton ANnihilation in DArmstadt) experiment under construction will be located at the FAIR (Facility for Antiproton and Ion Research) complex in Darmstadt, Germany. It is dedicated to study hadron physics. The FAIR accelerator complex will provide particle beams for four main experimental pillars, one of which is the PANDA experiment. At FAIR, a new proton LINAC will preaccelerate protons to 70 MeV, and ultimately accelerate them to about 30 GeV. The proton beam will hit a copper target acting as the antiproton production target. Magnetic horns are then used to filter the antiprotons of 3.7 GeV, which are collected and cooled in the Collector Ring (CR), then injected in the High Energy Storage Ring (HESR). Here, the antiprotons can be deaccelerated or further accelerated to a range of 1.5 GeV and 15 GeV, which correspond to c.m. energies in the range of 2.2 GeV and 5.5 GeV. The full setup is designed to provide an instantaneous peaking luminosity of 2×10^{32} cm$^{-2}s^{-1}$. The accumulated integrated luminosity can reach 2 fb^{-1} in about five months.

The proposed PANDA detector with a 4π geometrical acceptance is shown in Fig. 105. It consists of the target spectrometer surrounding the target area and the forward spectrometer for the detection of particles produced in the forward direction. The Micro Vertex Detector (MVD), surrounding the target region, will provide precise vertex position measurements with resolution of about 50 μm perpendicular to and 100 μm along the beam axis. It consists of silicon pixel and strip sensors. Tracking with a transverse momentum resolution better than 1% will be provided by Gas Electro Multiplier (GEM) planes and a Straw Tube Tracker (STT) combined with the MVD and the field of the 2 T solenoid magnet. Information from two Detection of Internally Reflected Cherenkov Light (DIRC) detectors and a Time-Of-Flight detector system (TOF) will be utilized to perform particle identification (PID). The Electromagnetic Calorimeter (EMC) will be used to detect photons. Muon PID will be provided by the muon detector system surrounding the solenoid magnet.

The forward spectrometer, which consists of a forward tracking system (FTS) of three pairs of straw tube planes, covers polar angles below 10 and 5 degrees in the horizontal and vertical planes, respectively. An Aerogel Ring

Imaging Cherenkov Counter (ARICH) and a Forward TOF system (FTOF) will be used for PID and the Forward Spectrometer Calorimeter (FSC) provides photon detection and electron/pion separation. A Forward Range System (FRS) and the Luminosity Detector (LMD) complete the forward spectrometer.

Three different scenarios for the different phases of the accelerator completion are expected and summarized in Table 17, where the momentum spreads dp/p, beam-energy resolutions dE_{cms}, and integrated luminosities $\mathcal{L}$ (at $\sqrt{s} = 3.872$ GeV) are given for three different HESR operation modes: The High Luminosity (HL), High Resolution (HR), and initial "Phase-1" (P1) [965].

HESR mode	dp/p	dE_{cms} (keV)	$\mathcal{L}$ [1/(day × nb)]
HL	1×10^{-4}	167.8	13680
HR	2×10^{-5}	33.6	1368
P1	5×10^{-5}	83.9	1170

Table 17: Momentum spreads dp/p, beam-energy resolutions dE_{cms}, and integrated luminosities $\mathcal{L}$ (at $\sqrt{s} = 3.872$ GeV) of the three different HESR operation modes [965].
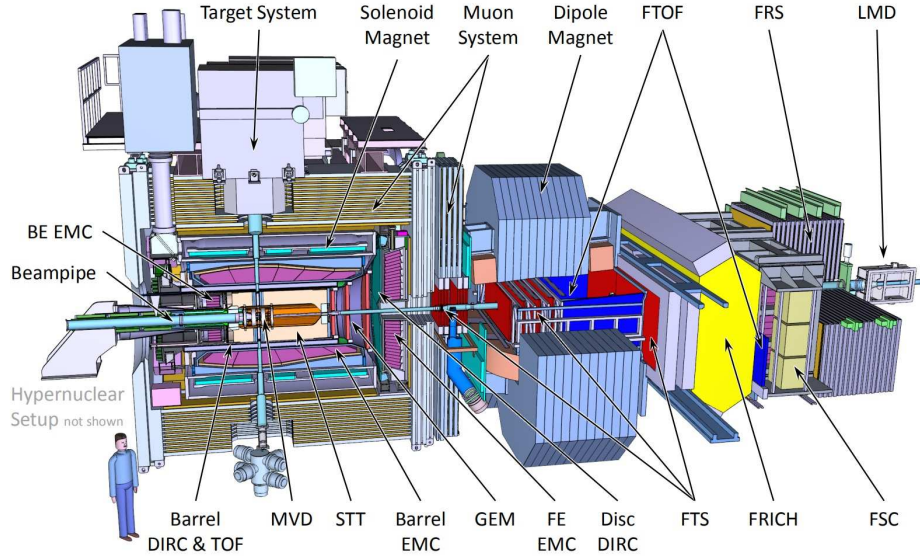

Figure 105: The proposed PANDA experimental setup [966].

For the PANDA experiment, a significant contribution to the study of the XYZ states will be the precise measurement of the energy-dependent cross section of a specific process over a certain range of c.m. energies by adjusting the beam momentum at high precision. This allows for the precise determination of some parameters for some XYZ states, for example the natural width and line-shape measurements of very narrow resonances. Recently PANDA used the $X(3872)$ as an example to study the achievable sensitivities of measuring its width, since an absolute width measurement is the key to understand the nature of the $X(3872)$ and distinguish between the various theoretical models. For such a narrow state with $J^{PC} = 1^{++}$, the PANDA experiment has a good ability to perform precise energy scans of the resonance regions. Based on a comprehensive MC simulation study, the achievable sensitivities of measuring $X(3872)$ width are achieved by assuming 40 energy scan points and data-taking time period of two days per point [966]. The outcome of the sensitivity study is very promising. For example, with an assumption of the BW shape of the $X(3872)$ and an input signal cross section of $\sigma(p\bar{p} \to X(3872)) = 50$ nb, a 3σ precision on the measured $X(3872)$ width (Γ_{mesa}), $\Delta\Gamma_{mesa}/\Gamma_{mesa}$ better than 33%, is achieved for an assumed natural decay width larger than about $\Gamma_0 = 40, 80,$ and 110 keV for HR, HL, and P1 running modes, respectively.

● *The Super-Charm-Tau and Super-Tau-Charm Factories*

For a decade, the Budker Institute of Nuclear Physics in Novosibirsk has been developing plans for a Super-Charm-Tau Factory (SCTF). SCTF is an e^+e^- collider complex for high-precision measurements between 2 and 6 GeV with instantaneous luminosity up to 10^{35} cm$^{-2}s^{-1}$ and longitudinal polarization of the initial e^- beam. The feasibility of constructing a collider with such instantaneous luminosity is based on the Crab-Waist scheme of collisions with large Piwinski angle experimentally tested at the ϕ-factory DAFNE in Frascati. The chosen collision scheme and machine lattice provide luminosity from 0.7 to 2×10^{35} cm$^{-2}s^{-1}$ at beam energies from 1 to 3 GeV. Such a facility should be a successor of the CLEO-c and BESIII experiments integrating their best features and increasing the useful yield of BESIII by two orders of magnitude. Integrated luminosity of ~ 10 ab^{-1} could be collected in 10 years. The energy range covers rich physics from light quark mesons to the $\tau^+\tau^-$ threshold, charm mesons, baryons, and exotic hadrons.

While SCTF cannot compete generally with Belle II and LHCb in the size of the data samples, the advantages of SCTF are: (1) Threshold production of pairs of τ leptons and charmed hadrons; (2) Longitudinal polarization of initial electrons facilitating searches for CP violation in decays of charm baryons and τ leptons; (3) Coherent production of $D^0\bar{D}^0$ mesons (measurement of phases); (4) Double tagging (measurement of absolute branching fractions).

More than 10 charmonium-(like) states discovered since 2003 remain unclassified; in other words, their origin is still unclear. Detailed studies of their properties that could lead to their final classification demand huge data samples. With such collected statistics coupled-channel analyses become possible, which result in a consistent set of resonance parameters. Various production mechanisms of such states exist:

1. All $\psi(Y)$ states with $J^{PC} = 1^{--}$ will be directly produced at $\sqrt{s} = M_Y$: $\psi(4260/4230)$, $\psi(4360)$, $\psi(4660)$
2. Charged Z_c states can be produced by scanning the $\sqrt{s}$ range and studying the $J/\psi\pi\pi$, $h_c\pi\pi$, $D^{(*)}\bar{D}^{(*)}$ final states
3. Neutral $c\bar{c}$ states with other quantum numbers can be studied in the recoil to $\pi\pi$, π^0, η, ω final states
4. $C = +1$ states can be also produced in $\gamma\gamma$ collisions
5. For the SCTF with the maximal energy higher than 6 GeV, between 6 and 7 GeV double $c\bar{c}$ production becomes possible

To accomplish the physical program of experiments at the SCTF a universal magnetic detector should be designed with the following features: (1) Digitizing electronics and a data acquisition system have to be capable of reading out events with a data rate of 300-400 kHz and average event size of 30 kB; (2) High efficiency for soft tracks; (3) Excellent momentum resolution for charged particles and good energy resolution for photons; (4) High-quality particle identification; (5) Trigger is capable of selecting events and rejecting background at high detector occupancy.

The detector includes a standard set of subsystems shown in Fig. 106: Beryllium beam pipe, inner tracker (time projection chamber with micropattern gaseous detectors, four-layer cylindrical GEM detector, stack of silicon strip layers), main tracker (drift chamber with traditional hexagonal cells, low-mass drift chamber with cluster counting), particle identification system (FARICH - Focusing aerogel-based ring imaging Cherenkov detector, ASHIPH - aerogel shifter photomultiplier system), EMC (CsI crystal counters, LYSO, Liquid Xenon), thin superconducting solenoid (thickness $0.1X_0$), iron yoke with a built-in muon system (scintillators, drift tubes).

It is believed that BEPCII will finish its mission in the next decade. After that, a super τ-charm factory, called High Intensity Electron Positron Accelerator (HIEPA), is being proposed in China. It will be a next generation electron-positron collider operating in the range of c.m. energies from 2 to 7 GeV with polarized electron beam in collision. The design peak luminosity is $(0.5 \sim 1) \times 10^{35}$ cm$^{-2}s^{-1}$ at $\sqrt{s} = 4$ GeV. The HIEPA detector is designed to consist of a small-cell MDC with 48 layers, an EMC, a cylindrical RICH for particle identification, and a muon detector using the muon telescope detector method. The SCTF and HIEPA share most of the common physics goals and interests – the approval of either one of them (or even better both) will make a dedicated high precision study of the physics in tau-charm energy region possible for another one to two decades.

5.2. Issues and opportunities in experiments

With the large data samples accumulated at the B factories, τ-charm facilities, and hadron machines, we have achieved a lot in the study of the exotic states recently: new charged charmonium-like states $Z_c(3900)$ and $Z_c(4020)$ were discovered; the spin-parity quantum numbers of the $X(3872)$, $Z_c(3900)$, and $Z_c(4430)$ were determined; the $Y(4260)$ structure was found to be dominated by the $Y(4230)$ with lower mass, narrower width, and more decay modes; and so on. However, an understanding of these XYZ states is still primarily at the level of conjecture. In view
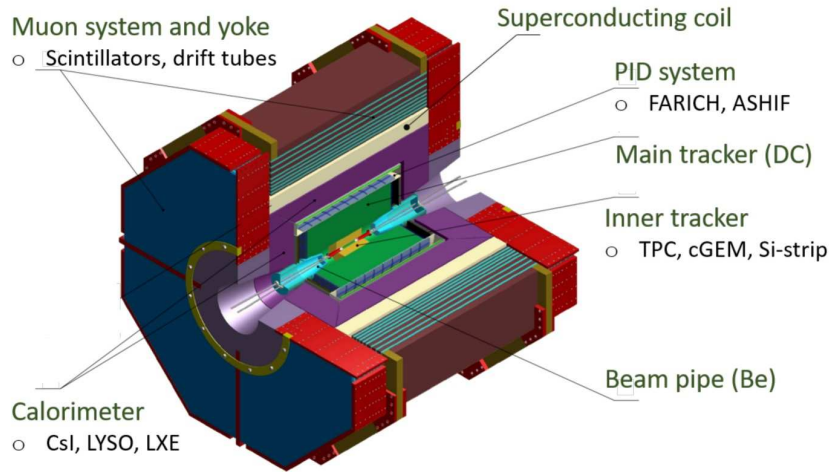
Figure 106: Detector for Novosibirsk SCTF

of this situation, there is still a lot to learn with the existing and coming data samples to understand these states better. We stress that the topics contained hereinafter are not meant to be comprehensive, but are offered as examples in the hope that progress will be spurred in various directions.

- In the X sector:

    - Search for more decay modes [including confirmation of $X(3872) \to \gamma\psi(2S)$], measure precisely its parameters and the absolute branching fractions for the $X(3872)$.

    - Measure the production cross section of $e^+e^- \to \gamma X(3872)$ and $\pi^+\pi^-\psi(1\,^3D_2)$ [possibly also $\pi^+\pi^-\psi(1\,^3D_3)$], determine whether they are from resonance decays or continuum production.

    - Study the other X states, such as $X(3915)$ and $X(4140)$, in e^+e^- annihilation and B decays.

    - Confirm some marginal states, such as $X(3940)$, $X(4160)$, and $X(4350)$.

    - Perform PWA analyses as much as possible with improved parameterizations of the data to determine J^P values and measure resonant parameters.

    - Search for flavor analog exotic states like the X_b [the bottomonium analog of the $X(3872)$].

    - Search for a charmonium/bottomonium-like state with exotic J^{PC}.

- In the Y sector:

    - Measure more precisely the line shapes of more final states in e^+e^- annihilation, including open-charm and charmonium final states.

    - Try coupled-channel analysis with more information.

    - Search for the Y states in B or other particle decays.

    - Search for the Y states in more processes, such as $Y \to D_s D_{s1}(2536)$, $D_s D_{s2}(2573)$, $D_s^* D_{s0}(2317)$, etc.

    - Search for the Y states in a higher mass region, such as above 4.7 GeV.

    - Search for quantum number partners of the Y states.

- In the Z sector:

    - Measure the Z_c production cross section in e^+e^- annihilation, determine whether they are produced from resonance decays or continuum production.

- Search for Z_c production in B or other particle decays.

- Determine the quantum numbers, measure the Argand plot of the resonant amplitude, and search for more decay modes.

- Search for Z_{cs} states decaying into $K^\pm J/\psi$, $D_s^- D^{*0} + c.c.$, or $D_s^{*-} D^0 + c.c.$

- Search for more Z_c states and possible partners containing strangeness.

- Study in more detail the Z_b production from $\Upsilon(11020)$ which might highlight the role of the $B_1 \bar{B}$ channel in this transition.

- In the P_c sector:

  - Measure additional reactions to investigate the P_c, such as the J/ψ photoproduction off a nucleon using the $\gamma p \to J/\psi p$ reaction.

  - Confirm the P_c via other final states, for examples $\Lambda_b^0 \to \psi(2S)pK^-$, $J/\psi\pi^+\pi^- pK^-$, $\chi_{c1}pK^-$, and $\chi_{c2}pK^-$.

  - Search for the P_c states in B decays, baryon decays, quarkonium decays, and e^+e^- annihilation.

5.3. Issues and opportunities in theory

In this section, we briefly outline possible developments in the theoretical approaches discussed in the main body of the review, and in particular in Sec. 4, that may improve our understanding of the exotic XYZ states. In general, we regard it as crucial that, within each existing approach, as many observables as possible are evaluated, since different features show up most prominently in different observables. In particular, different assumptions about the underlying structure of the states lead to quite different predictions for the masses of states other than the ones used to fix the parameters of a given scheme.

We start by considering phenomenological approaches. As emphasized in Sec. 4.2, the main virtue of the quark model is that it allows a first classification of states and the computation of some observables by means of a simple theoretical apparatus. The quark model has turned out to be quite useful in identifying possible exotic states close to or above open heavy-flavor thresholds, where more rigorous alternatives are often absent. The very notion "exotic" is based on the observation of whether or not the studied resonance fits into the quark-model scheme. It is natural to expect that the quark model will continue to play a role in the identification of ordinary quarkonium states and, climbing up in the spectra, of the XYZ states. For the identification of states, such as the XYZ, close to or above open-flavor thresholds, its most important evolution should consist of incorporating more and more realistically the effects due to the coupling of the heavy quark-antiquark pair with hadron pairs. The inclusion of these effects goes under the generic name of unquenching the quark model. Unquenching the quark model is not without difficulties. The reason is that the results are extremely sensitive to the details of the particular model framework and to the values of the parameters used therein. Indeed, even small changes in the parameters may result in a sizeable shift in the nodes of the wave functions of the mesons involved and, therefore, their overlap. This, in turn, may result in sizeable changes of the mass shifts and decay widths of the hadrons under study. Besides this, as was stressed in Sec. 4.3, a proper inclusion of strong thresholds does not reduce to just a modification of the quark-model potential, but requires also an extension of the Fock space to multiparticle components and coupled channels. Multiparticle components include hybrids, hadroquarkonia, tetraquarks, hadronic molecules, and others.

Hybrids may be described in the quark model by extending it to include constituent gluons, see Sec. 4.3.1. The connection of the model parameters with QCD is however very feeble. This is more so for the constituent gluon than it is in general for the quark model, as gluons are exactly massless in the QCD Lagrangian due to the gauge symmetry. Hence, although it is reasonable to expect that the quark model with constituent gluons will continue to serve as a reference in identifying hybrid state candidates, it will not, by its own definition, be improvable in a significant way. Even for what concerns the classification of states, we have seen that the degeneracy patterns of higher multiplets may be different in other approaches.

Hadroquarkonium and related research have been presented in Sec. 4.3.2. To deepen our understanding of the hadroquarkonium dynamics it would be important to clarify under which circumstances the QCD van der Waals forces generate binding and when not. For example, in certain cases spin symmetry can be employed to predict additional, as yet unobserved states. Those predictions allow for a non-trivial test or falsifications of the approach as detailed in Sec. 4.3.2.

If there exist compact tetraquarks with compact diquarks in the color antitriplet configuration as building blocks, as discussed in Sec. 4.3.3, the most striking problem is the abundance of predicted states that, at least at present, vastly exceeds the number of observations. Although there are attempts to explain why compact tetraquarks with masses near thresholds are produced more abundantly, further work is required. It would be very valuable if within the compact tetraquark approach predictions for line shapes were also provided.

In analogy to the nucleon-nucleon system, the two most popular approaches to hadronic molecules are phenomenological as well as EFT approaches. Phenomenological approaches have been presented in Sec. 4.3.4. The form of the phenomenological potentials is typically deduced from various meson exchanges. Although such models are rather attractive, since the potentials allow for a straightforward interpretation, they have serious shortcomings. To begin with, the potentials constructed and used in these models need regularisation at short distances, which calls for additional modelling. This results in significant differences from work to work, thus giving rise to different, sometimes controversial, predictions. Also, quantum-mechanical calculations employing a static potential inevitably ignore multiparticle unitarity, which might play an important, sometimes crucial, role in some systems.

Despite some advantages, phenomenological approaches, and the quark model in particular, have some obvious limitations. The most important one is that phenomenological models are not derived from QCD. Hence they may miss relevant degrees of freedom and their parameters do not have a field-theoretical definition. As a result, even in cases where phenomenological models catch the main physical features of the system under study, they are not improvable in a systematic fashion. This is why crucial progress may be expected if phenomenological approaches get embedded in or substituted by suitable effective field theories of QCD. The ones relevant for the *XYZ* states have been extensively presented in Sec. 4.4. Effective field theories provide proper definitions of the potentials, couplings, low-energy constants and matrix elements describing the systems of interest. They are supposed to include in their description all relevant degrees of freedom, and are equipped by a power counting that allows, on one hand, to assess the accuracy of each prediction and, on the other one, to systematically improve it.

States below threshold are well described by pNRQCD (see Sec. 4.4.3). Potentials can be computed at short distances in perturbative QCD, and we have documented the progress made in this direction in the last years allowing computations with (almost) N^3LL accuracy. At large distances the effective string theory provides valuable analytical tools. Nevertheless, the most straightforward way to compute the potentials from QCD is numerically via lattice QCD. Despite many decades of work, still several improvements and even first-time calculations are possible in this direction. The precision of the already computed potentials (spin- and momentum-dependent ones) should be improved, as some of them do not match properly with short-distance expectations. Further, they should be computed (ideally) in 2+1+1 flavor lattice simulations. For the time being only the static potential is available on dynamical lattices. Finally, some potentials should be computed for the first time, in particular the $1/m_h^2$ spin- and momentum-independent ones, where m_h is the heavy-quark mass. These are crucial to have eventually wave functions that include consistently all leading relativistic corrections.

An effective field theory for hybrids and, still to be fully developed, for tetraquarks is the BOEFT reviewed in Sec. 4.4.4. To be fully predictive, this EFT requires input from lattice QCD. Hybrid potentials have been computed, also recently, but in the pure gauge theory. Full QCD lattice calculations are still missing. Even more urgent than the calculation of the dynamical hybrid potentials is the calculation of the leading spin-dependent potential and quarkonium-hybrid mixing potential. Both depend on the same $1/m_h$ suppressed operator. Their determination would allow a consistent determination of the fine structure of the hybrid spectrum and of mixing with quarkonium states of different spin. The mixing of spin 0 (1) hybrids with spin 1 (0) quarkonium states may be crucial to identify those hybrid candidate states that have been detected in both $\pi^+\pi^- J/\psi$ and $\pi^+\pi^- h_c$ decay channels. Potentials in the isospin 1 (tetraquark) sector are even less known than in the hybrid sector. However, several groups are working in this direction and first results have appeared recently. These studies will allow, for the first time, to put on a solid ground the dynamics of systems made of two heavy and two light quarks, also by highlighting possible analogies and symmetry relations with hybrid systems.

As we mentioned above, hadronic molecules have been studied not only within phenomenological approaches but also, more recently, with EFTs at the hadron level. In both cases, a Schrödinger or Schrödinger-like equation is solved for a system of two hadrons connected by a potential. The differences are, however, in the choice of the potential and in the regularisation of the equations. A detailed discussion of the EFT approach for hadronic molecules and a comprehensive list of relevant references can be found in Sec. 4.4.5. Further theoretical developments of the EFT approach for molecules should include a systematic improvement in the theoretical accuracy by considering

higher orders in the EFT expansion, extension to the SU(3) flavor group for light quarks and tests of the accuracy of the various approximate symmetries employed to construct the EFT potential. For example, systematic studies of the breaking patterns of the heavy-quark spin symmetry appear to be very important especially for the charm-quark sector. Moreover, since within the EFT the light-quark mass dependence is under control (see, e.g., Ref. [781]), it should be possible to provide more predictions for the pole trajectories as a function of the light-quark masses. These contain important information on the nature of the states [788] and can be compared to lattice QCD evaluations.

Other rigorous approaches to the physics of XYZ states are sum rules, briefly reviewed in Sec. 4.3.5 and direct determinations by lattice QCD, discussed in Sec. 4.5. As we have seen, lattice QCD plays an important role in providing the crucial non-perturbative input to EFTs. The combination of suitable EFTs with lattice QCD has the potential to access all relevant observables. Nevertheless, lattice QCD alone may also provide direct determinations of many observables.

In recent years there have been significant advances in first-principles lattice QCD calculations of excited hadrons, near-threshold states and resonances. However, as summarised in Sec. 4.5, progress in studying resonances and other phenomena relevant for the XYZs in the charmonium, bottomonium and related exotic flavor sectors has been generally limited to extracting finite-volume energy levels rather than robustly determining infinite-volume scattering amplitudes.

No clear sign of any charged charmonium- or bottomonium-like state has been seen in lattice calculations, in contrast to the various experimental signals for such structures. A candidate for the $X(3872)$ has been found, Refs. [923, 924], but more detailed calculations are necessary. This is a case where precision lattice calculations will be particularly difficult: the $X(3872)$ is very close to threshold and isospin breaking effects are significant, so the quark masses will need to be very precisely tuned and QED effects included — such effects have begun to be included in some calculations as mentioned in Sec. 4.5. Furthermore, because the $X(3872)$ is above three-hadron thresholds, three-hadron scattering channels will need to be incorporated into the analysis.

As discussed in Sec. 4.5.2, there appears to be accumulating evidence for a double-bottom $J^P = 1^+$ bound state in $I = 0$ $ud\bar{b}\bar{b}$ and $I = 1/2$ $qs\bar{b}\bar{b}$, with the binding getting stronger as the light-quark mass decreases or the bottom-quark mass increases. This is supported by calculations involving static quarks, Sec. 4.5.3, and phenomenological studies, Sec. 4.3.3. Investigating similar exotic $\bar{b}b$ states is more challenging, but this is another area where we can expect progress.

One useful probe that is available to lattice QCD calculations, and not possible in experiment, is to observe how phenomena evolve as the quark masses are varied — this can provide insight into the structure of states and provide a window on the underlying physics. For example, a conventional charmonium or bottomonium resonance would be expected to vary little in mass as the light-quark mass changes, though the relative position of thresholds will change. On the other hand, a state where compact tetraquark or meson-meson configurations are important would behave in a very different way. As a concrete example of this in the light-meson sector, compare the behaviour of the σ and κ resonances with the ρ resonance in unitarised chiral perturbation theory, Refs. [878, 967]. The fact that states predicted in a simple model may become broad when analyzed more closely, and thus build the continuum, while others survive as new hadrons, was pointed out already in Ref. [968].

One reason that progress has been slower here than in the light-meson sector is that many hadron-hadron channels become kinematically open relatively close together in energy, including those involving hadrons with non-zero spin — this leads to numerous finite-volume energy levels that must all be extracted and a number of coupled scattering amplitudes that must be constrained simultaneously. Techniques to extract coupled-channel scattering amplitudes, which have been demonstrated for light mesons, Refs. [909, 969–974], suggest that there are good prospects for progress in the near future. Another issue is the presence of three-hadron thresholds relatively low in energy. To date, no scattering amplitudes involving more than two hadrons have been extracted from lattice QCD calculations. Recent computations of finite-volume energy levels involving three hadrons and developments in the formalism for relating these to infinite-volume scattering amplitudes suggest that we can expect the first lattice determinations of these in the not-too-distant future. However, it is likely to take longer to see realistic applications in the charmonium and bottomonium sectors. These are areas where the challenges overlap with those encountered when analysing experimental data, the techniques developed there may be useful and it may be fruitful to work together with the amplitude analysis community.

Studying transitions enables more stringent probes of the structure of the XYZs, both theoretically and experimentally, than is possible solely from spectroscopy. Following the first calculations of radiative transition amplitudes

involving a resonance, $\rho \to \pi\gamma$, Refs. [975–977], this is another area where lattice QCD calculations can be expected to make progress.

With the ongoing and planned experiments, and theoretical approaches being developed, there are good prospects for increasing our understanding of the XYZ states and exotic hadrons in the near future.

Acknowledgements

References

[1] H. Fritzsch, M. Gell-Mann, H. Leutwyler, Advantages of the Color Octet Gluon Picture, Phys. Lett. 47B (1973) 365. doi:10.1016/0370-2693(73)90625-4.

[2] D. J. Gross, F. Wilczek, Ultraviolet Behavior of Nonabelian Gauge Theories, Phys. Rev. Lett. 30 (1973) 1343. doi:10.1103/PhysRevLett.30.1343.

[3] H. D. Politzer, Reliable Perturbative Results for Strong Interactions?, Phys. Rev. Lett. 30 (1973) 1346. doi:10.1103/PhysRevLett.30.1346.

[4] M. Gell-Mann, A Schematic Model of Baryons and Mesons, Phys. Lett. 8 (1964) 214. doi:10.1016/S0031-9163(64)92001-3.

[5] S. K. Choi, et al., Observation of a narrow charmonium-like state in exclusive $B^\pm \to K^\pm \pi^+ \pi^- J/\psi$ decays, Phys. Rev. Lett. 91 (2003) 262001. arXiv:hep-ex/0309032, doi:10.1103/PhysRevLett.91.262001.

[6] M. Tanabashi, et al., Review of Particle Physics, Phys. Rev. D98 (2018) 030001. doi:10.1103/PhysRevD.98.030001.

[7] R. Mizuk, et al., Observation of a new structure near 10.75 GeV in the energy dependence of the $e^+e^- \to \Upsilon(nS)\pi^+\pi^-$ ($n = 1, 2, 3$) cross sections, JHEP 10 (2019) 220. arXiv:1905.05521, doi:10.1007/JHEP10(2019)220.

[8] H.-M. Chan, M. Fukugita, T. Hansson, H. Hoffman, K. Konishi, H. Hogaasen, S. T. Tsou, Color Chemistry: A Study of Metastable Multi - Quark Molecules, Phys. Lett. B 76 (1978) 634–640. doi:10.1016/0370-2693(78)90872-9.

[9] M. Gavela, A. Le Yaouanc, L. Oliver, O. Pene, J. Raynal, S. Sood, Exact Selection Rules for 'Chromo - Harmonic' Diquonium Decay Into Mesons, Phys. Lett. B 79 (1978) 459–463. doi:10.1016/0370-2693(78)90406-9.

[10] M. Anselmino, E. Predazzi, S. Ekelin, S. Fredriksson, D. B. Lichtenberg, Diquarks, Rev. Mod. Phys. 65 (1993) 1199–1234. doi:10.1103/RevModPhys.65.1199.

[11] J.-M. Richard, A. Valcarce, J. Vijande, Few-body quark dynamics for doubly heavy baryons and tetraquarks, Phys. Rev. C97 (3) (2018) 035211. arXiv:1803.06155, doi:10.1103/PhysRevC.97.035211.

[12] N. Brambilla, et al., Heavy quarkonium physics arXiv:hep-ph/0412158.

[13] N. Brambilla, et al., Heavy quarkonium: progress, puzzles, and opportunities, Eur. Phys. J. C71 (2011) 1534. arXiv:1010.5827, doi:10.1140/epjc/s10052-010-1534-9.

[14] N. Brambilla, et al., QCD and Strongly Coupled Gauge Theories: Challenges and Perspectives, Eur. Phys. J. C74 (2014) 2981. arXiv:1404.3723, doi:10.1140/epjc/s10052-014-2981-5.

[15] A. Abashian, et al., The Belle Detector, Nucl. Instrum. Meth. A479 (2002) 117. doi:10.1016/S0168-9002(01)02013-7.

[16] S. Kurokawa, E. Kikutani, Overview of the KEKB accelerators, Nucl. Instrum. Meth. A499 (2003) 1. doi:10.1016/S0168-9002(02)01771-0.

[17] A. J. Bevan, et al., The Physics of the B Factories, Eur. Phys. J. C74 (2014) 3026. arXiv:1406.6311, doi:10.1140/epjc/s10052-014-3026-9.

[18] B. Aubert, et al., The BABAR detector, Nucl. Instrum. Meth. A479 (2002) 1. arXiv:hep-ex/0105044, doi:10.1016/S0168-9002(01)02012-5.

[19] B. Aubert, et al., The BABAR Detector: Upgrades, Operation, and Performance, Nucl. Instrum. Meth. A729 (2013) 615. arXiv:1305.3560, doi:10.1016/j.nima.2013.05.107.

[20] M. Ablikim, et al., Design and Construction of the BESIII Detector, Nucl. Instrum. Meth. A614 (2010) 345. arXiv:0911.4960, doi:10.1016/j.nima.2009.12.050.

[21] D. M. Asner, et al., Physics at BES-III, Int. J. Mod. Phys. A24 (2009) S1. arXiv:0809.1869.

[22] M. Ablikim, et al., Observation of a Charged Charmoniumlike Structure in $e^+e^- \to \pi^+\pi^- J/\psi$ at $\sqrt{s}$ = 4.26 GeV, Phys. Rev. Lett. 110 (2013) 252001. arXiv:1303.5949, doi:10.1103/PhysRevLett.110.252001.

[23] M. Ablikim, et al., Luminosity measurements for the R scan experiment at BESIII, Chin. Phys. C41 (2017) 063001. arXiv:1702.04977, doi:10.1088/1674-1137/41/6/063001.

[24] M. Ablikim, et al., Precision measurement of the integrated luminosity of the data taken by BESIII at center-of-mass energies between 3.810 GeV and 4.600 GeV, Chin. Phys. C39 (2015) 093001. arXiv:1503.03408, doi:10.1088/1674-1137/39/9/093001.

[25] C. Z. Yuan, et al., Measurement of the $e^+e^- \to \pi^+\pi^- J/\psi$ Cross Section Via Initial-State Radiation at Belle, Phys. Rev. Lett. 99 (2007) 182004. arXiv:0707.2541, doi:10.1103/PhysRevLett.99.182004.

[26] F. Abe, et al., The CDF Detector: An Overview, Nucl. Instrum. Meth. A271 (1988) 387. doi:10.1016/0168-9002(88)90298-7.

[27] S. Abachi, et al., The D0 Detector, Nucl. Instrum. Meth. A338 (1994) 185. doi:10.1016/0168-9002(94)91312-9.

[28] F. Abe, et al., Observation of top quark production in $\bar{p}p$ collisions, Phys. Rev. Lett. 74 (1995) 2626. arXiv:hep-ex/9503002, doi:10.1103/PhysRevLett.74.2626.

[29] S. Abachi, et al., Observation of the top quark, Phys. Rev. Lett. 74 (1995) 2632. arXiv:hep-ex/9503003, doi:10.1103/PhysRevLett.74.2632.

[30] T. E. W. Group, Combination of CDF and D0 results on the mass of the top quark using up 9.7 fb^{-1} at the TevatronarXiv:1608.01881.

[31] D. Acosta, et al., Measurement of the lifetime difference between B_s mass eigenstates, Phys. Rev. Lett. 94 (2005) 101803. arXiv:hep-ex/0412057, doi:10.1103/PhysRevLett.94.101803.

[32] T. Aaltonen, et al., Precision Measurement of the $X(3872)$ Mass in $J/\psi\pi^+\pi^-$ Decays, Phys. Rev. Lett. 103 (2009) 152001. arXiv:0906.5218, doi:10.1103/PhysRevLett.103.152001.

[33] T. Aaltonen, et al., Evidence for a Narrow Near-Threshold Structure in the $J/\psi\phi$ Mass Spectrum in $B^+ \to J/\psi\phi K^+$ Decays, Phys. Rev. Lett. 102 (2009) 242002. arXiv:0903.2229, doi:10.1103/PhysRevLett.102.242002.

[34] V. M. Abazov, et al., Evidence for a $B_s^0\pi^\pm$ state, Phys. Rev. Lett. 117 (2016) 022003. arXiv:1602.07588, doi:10.1103/PhysRevLett.117.022003.

[35] A. A. Alves Jr, et al., The LHCb Detector at the LHC, JINST 3 (2008) S08005. doi:10.1088/1748-0221/3/08/S08005.

[36] R. Aaij, et al., Observation of $J/\psi p$ Resonances Consistent with Pentaquark States in $\Lambda_b^0 \to J/\psi K^- p$ Decays, Phys. Rev. Lett. 115 (2015) 072001. arXiv:1507.03414, doi:10.1103/PhysRevLett.115.072001.

[37] R. Aaij, et al., Determination of the $X(3872)$ meson quantum numbers, Phys. Rev. Lett. 110 (2013) 222001. arXiv:1302.6269, doi:10.1103/PhysRevLett.110.222001.

[38] R. Aaij, et al., Observation of the resonant character of the $Z(4430)^-$ state, Phys. Rev. Lett. 112 (2014) 222002. arXiv:1404.1903, doi:10.1103/PhysRevLett.112.222002.

[39] R. Aaij, et al., Observation of $J/\psi\phi$ structures consistent with exotic states from amplitude analysis of $B^+ \to J/\psi\phi K^+$ decays, Phys. Rev. Lett. 118 (2017) 022003. arXiv:1606.07895, doi:10.1103/PhysRevLett.118.022003.

[40] R. Aaij, et al., LHCb Detector Performance, Int. J. Mod. Phys. A30 (2015) 1530022. arXiv:1412.6352, doi:10.1142/S0217751X15300227.

[41] S. Chatrchyan, et al., A New Boson with a Mass of 125 GeV Observed with the CMS Experiment at the Large Hadron Collider, Science 338 (2012) 1569. doi:10.1126/science.1230816.

[42] G. Aad, et al., A particle consistent with the Higgs Boson observed with the ATLAS Detector at the Large Hadron Collider, Science 338 (2012) 1576. doi:10.1126/science.1232005.

[43] V. Bhardwaj, et al., Evidence of a new narrow resonance decaying to $\chi_{c1}\gamma$ in $B \to \chi_{c1}\gamma K$, Phys. Rev. Lett. 111 (2013) 032001. arXiv:1304.3975, doi:10.1103/PhysRevLett.111.032001.

[44] M. Suzuki, Search of $^1P_1$ charmonium in B decay, Phys. Rev. D66 (2002) 037503. arXiv:hep-ph/0204043, doi:10.1103/PhysRevD.66.037503.

[45] P. Colangelo, F. De Fazio, T. N. Pham, $B^- \to K^-\chi_{c0}$ decay from charmed meson rescattering, Phys. Lett. B542 (2002) 71. arXiv:hep-ph/0207061, doi:10.1016/S0370-2693(02)02306-7.

[46] M. Ablikim, et al., Observation of the $\psi(1^3D_2)$ state in $e^+e^- \to \pi^+\pi^-\gamma\chi_{c1}$ at BESIII, Phys. Rev. Lett. 115 (2015) 011803. arXiv:1503.08203, doi:10.1103/PhysRevLett.115.011803.

[47] S. Godfrey, N. Isgur, Mesons in a Relativized Quark Model with Chromodynamics, Phys. Rev. D32 (1985) 189. doi:10.1103/PhysRevD.32.189.

[48] D. Ebert, R. N. Faustov, V. O. Galkin, Properties of heavy quarkonia and B_c mesons in the relativistic quark model, Phys. Rev. D67 (2003) 014027. arXiv:hep-ph/0210381, doi:10.1103/PhysRevD.67.014027.

[49] E. J. Eichten, K. Lane, C. Quigg, Charmonium levels near threshold and the narrow state $X(3872) \to \pi^+\pi^- J/\psi$, Phys. Rev. D69 (2004) 094019. arXiv:hep-ph/0401210, doi:10.1103/PhysRevD.69.094019.

[50] M. Blank, A. Krassnigg, Bottomonium in a Bethe-Salpeter-equation study, Phys. Rev. D84 (2011) 096014. arXiv:1109.6509, doi:10.1103/PhysRevD.84.096014.

[51] W. Kwong, J. L. Rosner, C. Quigg, Heavy Quark Systems, Ann. Rev. Nucl. Part. Sci. 37 (1987) 325. doi:10.1146/annurev.ns.37.120187.001545.

[52] C.-F. Qiao, F. Yuan, K.-T. Chao, A crucial test for color octet production mechanism in Z^0 decays, Phys. Rev. D55 (1997) 4001. arXiv:hep-ph/9609284, doi:10.1103/PhysRevD.55.4001.

[53] R. Aaij, et al., Near-threshold $D\bar{D}$ spectroscopy and observation of a new charmonium state, JHEP 07 (2019) 035. arXiv:1903.12240, doi:10.1007/JHEP07(2019)035.

[54] D. Acosta, et al., Observation of the narrow state $X(3872) \to J/\psi\pi^+\pi^-$ in $\bar{p}p$ collisions at $\sqrt{s}$ = 1.96 TeV, Phys. Rev. Lett. 93 (2004) 072001. arXiv:hep-ex/0312021, doi:10.1103/PhysRevLett.93.072001.

[55] V. M. Abazov, et al., Observation and properties of the $X(3872)$ decaying to $J/\psi\pi^+\pi^-$ in $p\bar{p}$ collisions at $\sqrt{s}$ = 1.96 TeV, Phys. Rev. Lett. 93 (2004) 162002. arXiv:hep-ex/0405004, doi:10.1103/PhysRevLett.93.162002.

[56] B. Aubert, et al., Study of the $B^- \to J/\psi K^-\pi^+\pi^-$ decay and measurement of the $B^- \to X(3872)K^-$ branching fraction, Phys. Rev. D71 (2005) 071103. arXiv:hep-ex/0406022, doi:10.1103/PhysRevD.71.071103.

[57] A. Abulencia, et al., Analysis of the quantum numbers J^{PC} of the $X(3872)$, Phys. Rev. Lett. 98 (2007) 132002. arXiv:hep-ex/0612053,

`doi:10.1103/PhysRevLett.98.132002`.

[58] R. Aaij, et al., Quantum numbers of the $X(3872)$ state and orbital angular momentum in its $\rho^0 J/\psi$ decay, Phys. Rev. D92 (2015) 011102. `arXiv:1504.06339`, `doi:10.1103/PhysRevD.92.011102`.

[59] R. Aaij, et al., Observation of $X(3872)$ production in pp collisions at $\sqrt{s}$ = 7 TeV, Eur. Phys. J. C72 (2012) 1972. `arXiv:1112.5310`, `doi:10.1140/epjc/s10052-012-1972-7`.

[60] S. Chatrchyan, et al., Measurement of the $X(3872)$ production cross section via decays to $J/\psi\pi^+\pi^-$ in pp collisions at $\sqrt{s}$ = 7 TeV, JHEP 04 (2013) 154. `arXiv:1302.3968`, `doi:10.1007/JHEP04(2013)154`.

[61] M. Aaboud, et al., Measurements of $\psi(2S)$ and $X(3872) \to J/\psi\pi^+\pi^-$ production in pp collisions at $\sqrt{s}$ = 8 TeV with the ATLAS detector, JHEP 01 (2017) 117. `arXiv:1610.09303`, `doi:10.1007/JHEP01(2017)117`.

[62] C. P. Shen, et al., Search for charmonium and charmonium-like states in $\Upsilon(1S)$ radiative decays, Phys. Rev. D82 (2010) 051504. `arXiv:1008.1774`, `doi:10.1103/PhysRevD.82.051504`.

[63] X. L. Wang, et al., Search for charmonium and charmonium-like states in $\Upsilon(2S)$ radiative decays, Phys. Rev. D84 (2011) 071107. `arXiv:1108.4514`, `doi:10.1103/PhysRevD.84.071107`.

[64] C. P. Shen, et al., Search for XYZ states in $\Upsilon(1S)$ inclusive decays, Phys. Rev. D93 (2016) 112013. `arXiv:1605.00990`, `doi:10.1103/PhysRevD.93.112013`.

[65] M. Ablikim, et al., Observation of $e^+e^- \to \gamma X(3872)$ at BESIII, Phys. Rev. Lett. 112 (2014) 092001. `arXiv:1310.4101`, `doi:10.1103/PhysRevLett.112.092001`.

[66] E. A. Kuraev, V. S. Fadin, On Radiative Corrections to e^+e^- Single Photon Annihilation at High-Energy, Sov. J. Nucl. Phys. 41 (1985) 466, [Yad. Fiz. 41 (1985) 733].

[67] S. Actis, et al., Quest for precision in hadronic cross sections at low energy: Monte Carlo tools vs. experimental data, Eur. Phys. J. C66 (2010) 585. `arXiv:0912.0749`, `doi:10.1140/epjc/s10052-010-1251-4`.

[68] Z. Q. Liu, et al., Study of $e^+e^- \to \pi^+\pi^- J/\psi$ and Observation of a Charged Charmoniumlike State at Belle, Phys. Rev. Lett. 110 (2013) 252002. `arXiv:1304.0121`, `doi:10.1103/PhysRevLett.110.252002`.

[69] T. Xiao, S. Dobbs, A. Tomaradze, K. K. Seth, Observation of the charged hadron $Z_c^\pm(3900)$ and evidence for the neutral $Z_c^0(3900)$ in $e^+e^- \to \pi\pi J/\psi$ at $\sqrt{s}$ = 4170 MeV, Phys. Lett. B727 (2013) 366. `arXiv:1304.3036`, `doi:10.1016/j.physletb.2013.10.041`.

[70] F-K. Guo, C. Hanhart, U.-G. Meißner, Q. Wang, Q. Zhao, Production of the $X(3872)$ in charmonia radiative decays, Phys. Lett. B725 (2013) 127. `arXiv:1306.3096`, `doi:10.1016/j.physletb.2013.06.053`.

[71] M. Ablikim, et al., Observation of the decay $X(3872) \to \pi^0\chi_{c1}(1P)$, Phys. Rev. Lett. 122 (2019) 202001. `arXiv:1901.03992`, `doi:10.1103/PhysRevLett.122.202001`.

[72] A. Bala, et al., Observation of $X(3872)$ in $B \to X(3872)K\pi$ decays, Phys. Rev. D91 (2015) 051101. `arXiv:1501.06867`, `doi:10.1103/PhysRevD.91.051101`.

[73] M. Ablikim, et al., Precise measurement of the $e^+e^- \to \pi^+\pi^- J/\psi$ cross section at center-of-mass energies from 3.77 to 4.60 GeV, Phys. Rev. Lett. 118 (2017) 092001. `arXiv:1611.01317`, `doi:10.1103/PhysRevLett.118.092001`.

[74] M. Ablikim, et al., Study of $e^+e^- \to \gamma\omega J/\psi$ and Observation of $X(3872) \to \omega J/\psi$, Phys. Rev. Lett. 122 (2019) 232002. `arXiv:1903.04695`, `doi:10.1103/PhysRevLett.122.232002`.

[75] R. Aaij, et al., Observation of the $\Lambda_b^0 \to \chi_{c1}(3872)pK^-$ decay, JHEP 09 (2019) 028. `arXiv:1907.00954`, `doi:10.1007/JHEP09(2019)028`.

[76] B. A. Li, Is $X(3872)$ a possible candidate as a hybrid meson?, Phys. Lett. B605 (2005) 306. `arXiv:hep-ph/0410264`, `doi:10.1016/j.physletb.2004.11.062`.

[77] X.-H. Liu, Q. Zhao, F. E. Close, Search for tetraquark candidate $Z(4430)$ in meson photoproduction, Phys. Rev. D77 (2008) 094005. `arXiv:0802.2648`, `doi:10.1103/PhysRevD.77.094005`.

[78] J. He, X. Liu, Discovery potential for charmonium-like state $Y(3940)$ by the meson photoproduction, Phys. Rev. D80 (2009) 114007. `arXiv:0910.5867`, `doi:10.1103/PhysRevD.80.114007`.

[79] M. Aghasyan, et al., Search for muoproduction of $X(3872)$ at COMPASS and indication of a new state $\widetilde{X}(3872)$, Phys. Lett. B783 (2018) 334. `arXiv:1707.01796`, `doi:10.1016/j.physletb.2018.07.008`.

[80] B. Aubert, et al., Evidence for $X(3872) \to \psi(2S)\gamma$ in $B^\pm \to X(3872)K^\pm$ decays, and a study of $B \to c\bar{c}\gamma K$, Phys. Rev. Lett. 102 (2009) 132001. `arXiv:0809.0042`, `doi:10.1103/PhysRevLett.102.132001`.

[81] V. Bhardwaj, et al., Observation of $X(3872) \to J/\psi\gamma$ and search for $X(3872) \to \psi'\gamma$ in B decays, Phys. Rev. Lett. 107 (2011) 091803. `arXiv:1105.0177`, `doi:10.1103/PhysRevLett.107.091803`.

[82] R. Aaij, et al., Evidence for the decay $X(3872) \to \psi(2S)\gamma$, Nucl. Phys. B886 (2014) 665. `arXiv:1404.0275`, `doi:10.1016/j.nuclphysb.2014.06.011`.

[83] E. S. Swanson, Diagnostic decays of the $X(3872)$, Phys. Lett. B598 (2004) 197. `arXiv:hep-ph/0406080`, `doi:10.1016/j.physletb.2004.07.059`.

[84] H.-X. Chen, W. Chen, X. Liu, S.-L. Zhu, The hidden-charm pentaquark and tetraquark states, Phys. Rept. 639 (2016) 1. `arXiv:1601.02092`, `doi:10.1016/j.physrep.2016.05.004`.

[85] F.-K. Guo, C. Hanhart, Yu. S. Kalashnikova, U.-G. Meißner, A. V. Nefediev, What can radiative decays of the $X(3872)$ teach us about its nature?, Phys. Lett. B742 (2015) 394. `arXiv:1410.6712`, `doi:10.1016/j.physletb.2015.02.013`.

[86] S. Dubynskiy, M. B. Voloshin, Pionic transitions from $X(3872)$ to χ_{cJ}, Phys. Rev. D77 (2008) 014013. `arXiv:0709.4474`, `doi:10.1103/PhysRevD.77.014013`.

[87] S. Fleming, T. Mehen, Hadronic decays of the $X(3872)$ to χ_{cJ} in effective field theory, Phys. Rev. D78 (2008) 094019. `arXiv:0807.2674`, `doi:10.1103/PhysRevD.78.094019`.

[88] T. Mehen, Hadronic loops versus factorization in effective field theory calculations of $X(3872) \to \chi_{cJ}\pi^0$, Phys. Rev. D92 (2015) 034019. `arXiv:1503.02719`, `doi:10.1103/PhysRevD.92.034019`.

[89] V. Bhardwaj, et al., Inclusive and exclusive measurements of B decays to χ_{c1} and χ_{c2} at Belle, Phys. Rev. D93 (2016) 052016. `arXiv:1512.02672`, `doi:10.1103/PhysRevD.93.052016`.

153

[90] V. Bhardwaj, et al., Search for $X(3872)$ and $X(3915)$ decay into $\chi_{c1}\pi^0$ in B decays at Belle, Phys. Rev. D99 (2019) 111101. arXiv:1904.07015, doi:10.1103/PhysRevD.99.111101.

[91] P. del Amo Sanchez, et al., Evidence for the decay $X(3872) \to J/\psi\omega$, Phys. Rev. D82 (2010) 011101. arXiv:1005.5190, doi:10.1103/PhysRevD.82.011101.

[92] K. Abe, et al., Evidence for $X(3872) \to \gamma J/\psi$ and the sub-threshold decay $X(3872) \to \omega J/\psi$, in: Lepton and photon interactions at high energies. Proceedings, 22nd International Symposium, LP 2005, Uppsala, Sweden, June 30-July 5, 2005. arXiv:hep-ex/0505037.

[93] G. Gokhroo, et al., Observation of a Near-threshold $D^0\bar{D}^0\pi^0$ Enhancement in $B \to D^0\bar{D}^0\pi^0 K$ Decay, Phys. Rev. Lett. 97 (2006) 162002. arXiv:hep-ex/0606055, doi:10.1103/PhysRevLett.97.162002.

[94] B. Aubert, et al., Study of resonances in exclusive B decays to $\bar{D}^{(*)}D^{(*)}K$, Phys. Rev. D77 (2008) 011102. arXiv:0708.1565, doi:10.1103/PhysRevD.77.011102.

[95] T. Aushev, et al., Study of the $B \to X(3872)(\to D^{*0}\bar{D}^0)K$ decay, Phys. Rev. D81 (2010) 031103. arXiv:0810.0358, doi:10.1103/PhysRevD.81.031103.

[96] R. Aaij, et al., Observation of $\eta_c(2S) \to p\bar{p}$ and search for $X(3872) \to p\bar{p}$ decays, Phys. Lett. B769 (2017) 305. arXiv:1607.06446, doi:10.1016/j.physletb.2017.03.046.

[97] R. Aaij, et al., Study of charmonium production in b-hadron decays and first evidence for the decay $B_s^0 \to \phi\phi\phi$, Eur. Phys. J. C77 (2017) 609. arXiv:1706.07013, doi:10.1140/epjc/s10052-017-5151-8.

[98] B. Aubert, et al., Measurements of the absolute branching fractions of $B^\pm \to K^\pm X_{c\bar{c}}$, Phys. Rev. Lett. 96 (2006) 052002. arXiv:hep-ex/0510070, doi:10.1103/PhysRevLett.96.052002.

[99] Y. Kato, et al., Measurements of the absolute branching fractions of $B^+ \to X_{c\bar{c}}K^+$ and $B^+ \to \bar{D}^{(*)0}\pi^+$ at Belle, Phys. Rev. D97 (2018) 012005. arXiv:1709.06108, doi:10.1103/PhysRevD.97.012005.

[100] C.-Z. Yuan, Exotic Hadrons, in: 29th International Conference on Physics in Collision (PIC 2009) Kobe, Japan, August 30-September 2, 2009. arXiv:0910.3138.

[101] J. H. Kühn, J. Kaplan, E. G. O. Safiani, Electromagnetic Annihilation of e^+e^- Into Quarkonium States with Even Charge Conjugation, Nucl. Phys. B157 (1979) 125. doi:10.1016/0550-3213(79)90055-5.

[102] N. Kivel, M. Vanderhaeghen, $\chi_{cJ} \to e^+e^-$ decays revisited, JHEP 02 (2016) 032. arXiv:1509.07375, doi:10.1007/JHEP02(2016)032.

[103] H. Czyż, J. H. Kühn, S. Tracz, χ_{c1} and χ_{c2} production at e^+e^- colliders, Phys. Rev. D94 (2016) 034033. arXiv:1605.06803, doi:10.1103/PhysRevD.94.034033.

[104] A. Denig, F.-K. Guo, C. Hanhart, A. V. Nefediev, Direct $X(3872)$ production in e^+e^- collisions, Phys. Lett. B736 (2014) 221. arXiv:1405.3404, doi:10.1016/j.physletb.2014.07.027.

[105] M. Ablikim, et al., An improved limit for Γ_{ee} of $X(3872)$ and Γ_{ee} measurement of $\psi(3686)$, Phys. Lett. B749 (2015) 414. arXiv:1505.02559, doi:10.1016/j.physletb.2015.08.013.

[106] F.-K. Guo, Novel Method for Precisely Measuring the $X(3872)$ Mass, Phys. Rev. Lett. 122 (2019) 202002. arXiv:1902.11221, doi:10.1103/PhysRevLett.122.202002.

[107] D. Ebert, R. N. Faustov, V. O. Galkin, Masses of heavy tetraquarks in the relativistic quark model, Phys. Lett. B634 (2006) 214. arXiv:hep-ph/0512230, doi:10.1016/j.physletb.2006.01.026.

[108] W.-S. Hou, Searching for the bottom counterparts of $X(3872)$ and $Y(4260)$ via $\pi^+\pi^-\Upsilon$, Phys. Rev. D74 (2006) 017504. arXiv:hep-ph/0606016, doi:10.1103/PhysRevD.74.017504.

[109] A. Ali, C. Hambrock, I. Ahmed, M. J. Aslam, A case for hidden $b\bar{b}$ tetraquarks based on $e^+e^- \to b\bar{b}$ cross section between $\sqrt{s} = 10.54$ and 11.20 GeV, Phys. Lett. B684 (2010) 28. arXiv:0911.2787, doi:10.1016/j.physletb.2009.12.053.

[110] F.-K. Guo, C. Hidalgo-Duque, J. Nieves, M. P. Valderrama, Consequences of Heavy Quark Symmetries for Hadronic Molecules, Phys. Rev. D88 (2013) 054007. arXiv:1303.6608, doi:10.1103/PhysRevD.88.054007.

[111] M. Karliner, S. Nussinov, The doubly heavies: $\bar{Q}Q\bar{q}q$ and $QQ\bar{q}\bar{q}$ tetraquarks and QQq baryons, JHEP 07 (2013) 153. arXiv:1304.0345, doi:10.1007/JHEP07(2013)153.

[112] V. Baru, E. Epelbaum, J. Gegelia, C. Hanhart, U.-G. Meißner, A. V. Nefediev, Remarks on the Heavy-Quark Flavour Symmetry for doubly heavy hadronic molecules, Eur. Phys. J. C79 (2019) 46. arXiv:1810.06921, doi:10.1140/epjc/s10052-019-6560-7.

[113] F.-K. Guo, U.-G. Meißner, W. Wang, Z. Yang, Production of the bottom analogs and the spin partner of the $X(3872)$ at hadron colliders, Eur. Phys. J. C74 (2014) 3063. arXiv:1402.6236, doi:10.1140/epjc/s10052-014-3063-4.

[114] Q. Wu, G. Li, F. Shao, Q. Wang, R. Wang, Y. Zhang, Y. Zheng, Production of X_b in $\Upsilon(5S, 6S) \to \gamma X_b$ radiative decays, Adv. High Energy Phys. 2016 (2016) 3729050. arXiv:1606.05118, doi:10.1155/2016/3729050.

[115] G. Li, W. Wang, Hunting for the X_b via radiative decays, Phys. Lett. B733 (2014) 100. arXiv:1402.6463, doi:10.1016/j.physletb.2014.04.029.

[116] G. Li, Z. Zhou, Hunting for the X_b via hidden bottomonium decays, Phys. Rev. D91 (2015) 034020. arXiv:1502.02936, doi:10.1103/PhysRevD.91.034020.

[117] G. Aad, et al., Search for the X_b and other hidden-beauty states in the $\pi^+\pi^-\Upsilon(1S)$ channel at ATLAS, Phys. Lett. B740 (2015) 199. arXiv:1410.4409, doi:10.1016/j.physletb.2014.11.055.

[118] S. Chatrchyan, et al., Search for a new bottomonium state decaying to $\Upsilon(1S)\pi^+\pi^-$ in pp collisions at $\sqrt{s} = 8$ TeV, Phys. Lett. B727 (2013) 57. arXiv:1309.0250, doi:10.1016/j.physletb.2013.10.016.

[119] X. H. He, et al., Observation of $e^+e^- \to \pi^+\pi^-\pi^0\chi_{bJ}$ and search for $X_b \to \omega\Upsilon(1S)$ at $\sqrt{s} = 10.867$ GeV, Phys. Rev. Lett. 113 (2014) 142001. arXiv:1408.0504, doi:10.1103/PhysRevLett.113.142001.

[120] Z.-Y. Zhou, D.-Y. Chen, Z. Xiao, Does the bottomonium counterpart of $X(3872)$ exist?, Phys. Rev. D99 (2019) 034005. arXiv:1810.03452, doi:10.1103/PhysRevD.99.034005.

[121] S. Uehara, et al., Observation of a charmonium-like enhancement in the $\gamma\gamma \to \omega J/\psi$ process, Phys. Rev. Lett. 104 (2010) 092001. arXiv:0912.4451, doi:10.1103/PhysRevLett.104.092001.

[122] J. P. Lees, et al., Study of $X(3915) \to J/\psi\omega$ in two-photon collisions, Phys. Rev. D86 (2012) 072002. arXiv:1207.2651, doi:10.1103/PhysRevD.86.072002.

[123] C. P. Shen, et al., Evidence for a new resonance and search for the $Y(4140)$ in the $\gamma\gamma \to \phi J/\psi$ process, Phys. Rev. Lett. 104 (2010) 112004. arXiv:0912.2383, doi:10.1103/PhysRevLett.104.112004.

[124] K. Abe, et al., Observation of a near-threshold $\omega J/\psi$ mass enhancement in exclusive $B \to K\omega J/\psi$ decays, Phys. Rev. Lett. 94 (2005) 182002. arXiv:hep-ex/0408126, doi:10.1103/PhysRevLett.94.182002.

[125] B. Aubert, et al., Observation of $Y(3940) \to J/\psi\omega$ in $B \to J/\psi\omega K$ at BABAR, Phys. Rev. Lett. 101 (2008) 082001. arXiv:0711.2047, doi:10.1103/PhysRevLett.101.082001.

[126] F.-K. Guo, U.-G. Meißner, Where is the $\chi_{c0}(2P)$?, Phys. Rev. D86 (2012) 091501. arXiv:1208.1134, doi:10.1103/PhysRevD.86.091501.

[127] S. L. Olsen, Is the $X(3915)$ the $\chi_{c0}(2P)$?, Phys. Rev. D91 (2015) 057501. arXiv:1410.6534, doi:10.1103/PhysRevD.91.057501.

[128] Z.-Y. Zhou, Z. Xiao, H.-Q. Zhou, Could the $X(3915)$ and the $X(3930)$ Be the Same Tensor State?, Phys. Rev. Lett. 115 (2015) 022001. arXiv:1501.00879, doi:10.1103/PhysRevLett.115.022001.

[129] A. Vinokurova, et al., Search for B decays to final states with the η_c meson, JHEP 06 (2015) 132, [Erratum: JHEP 02 (2017) 088]. arXiv:1501.06351, doi:10.1007/JHEP06(2015)132,10.1007/JHEP02(2017)088.

[130] L. Liu, G. Moir, M. Peardon, S. M. Ryan, C. E. Thomas, P. Vilaseca, J. J. Dudek, R. G. Edwards, B. Joo, D. G. Richards, Excited and exotic charmonium spectroscopy from lattice QCD, JHEP 07 (2012) 126. arXiv:1204.5425, doi:10.1007/JHEP07(2012)126.

[131] G. K. C. Cheung, C. O'Hara, G. Moir, M. Peardon, S. M. Ryan, C. E. Thomas, D. Tims, Excited and exotic charmonium, D_s and D meson spectra for two light quark masses from lattice QCD, JHEP 12 (2016) 089. arXiv:1610.01073, doi:10.1007/JHEP12(2016)089.

[132] K. Abe, et al., Observation of a new charmonium state in double charmonium production in e^+e^- annihilation at $\sqrt{s} \approx 10.6$ GeV, Phys. Rev. Lett. 98 (2007) 082001. arXiv:hep-ex/0507019, doi:10.1103/PhysRevLett.98.082001.

[133] P. Pakhlov, et al., Production of New Charmoniumlike States in $e^+e^- \to J/\psi D^{(*)}\bar{D}^{(*)}$ at $\sqrt{s} \approx 10$ GeV, Phys. Rev. Lett. 100 (2008) 202001. arXiv:0708.3812, doi:10.1103/PhysRevLett.100.202001.

[134] K. Chilikin, et al., Observation of an alternative $\chi_{c0}(2P)$ candidate in $e^+e^- \to J/\psi D\bar{D}$, Phys. Rev. D95 (2017) 112003. arXiv:1704.01872, doi:10.1103/PhysRevD.95.112003.

[135] K.-T. Chao, Interpretations for the $X(4160)$ observed in the double charm production at B factories, Phys. Lett. B661 (2008) 348. arXiv:0707.3982, doi:10.1016/j.physletb.2008.02.039.

[136] S. Uehara, et al., Observation of a χ'_{c2} candidate in $\gamma\gamma \to D\bar{D}$ production at Belle, Phys. Rev. Lett. 96 (2006) 082003. arXiv:hep-ex/0512035, doi:10.1103/PhysRevLett.96.082003.

[137] B. Aubert, et al., Observation of the $\chi_{c2}(2p)$ meson in the reaction $\gamma\gamma \to D\bar{D}$ at BABAR, Phys. Rev. D81 (2010) 092003. arXiv:1002.0281, doi:10.1103/PhysRevD.81.092003.

[138] C. P. Shen, *XYZ* particles at Belle, Chin. Phys. C34 (2010) 615. arXiv:0912.2386, doi:10.1088/1674-1137/34/6/001.

[139] J. P. Lees, et al., Study of $B^{\pm,0} \to J/\psi K^+ K^- K^{\pm,0}$ and search for $B^0 \to J/\psi\phi$ at BABAR, Phys. Rev. D91 (2015) 012003. arXiv:1407.7244, doi:10.1103/PhysRevD.91.012003.

[140] R. Aaij, et al., Search for the $X(4140)$ state in $B^+ \to J/\psi\phi K^+$ decays, Phys. Rev. D85 (2012) 091103. arXiv:1202.5087, doi:10.1103/PhysRevD.85.091103.

[141] T. Aaltonen, et al., Observation of the $Y(4140)$ structure in the $J/\psi\phi$ mass spectrum in $B^\pm \to J/\psi\phi K^\pm$ decays, Mod. Phys. Lett. A32 (2017) 1750139. arXiv:1101.6058, doi:10.1142/S0217732317501395.

[142] S. Chatrchyan, et al., Observation of a peaking structure in the $J/\psi\phi$ mass spectrum from $B^\pm \to J/\psi\phi K^\pm$ decays, Phys. Lett. B734 (2014) 261. arXiv:1309.6920, doi:10.1016/j.physletb.2014.05.055.

[143] V. M. Abazov, et al., Search for the $X(4140)$ state in $B^+ \to J/\psi\phi K^+$ decays with the D0 detector, Phys. Rev. D89 (2014) 012004. arXiv:1309.6580, doi:10.1103/PhysRevD.89.012004.

[144] V. M. Abazov, et al., Inclusive Production of the $X(4140)$ State in $p\bar{p}$ Collisions at D0, Phys. Rev. Lett. 115 (2015) 232001. arXiv:1508.07846, doi:10.1103/PhysRevLett.115.232001.

[145] M. Ablikim, et al., Search for the $Y(4140)$ via $e^+e^- \to \gamma\phi J/\psi$ at $\sqrt{s}$=4.23 , 4.26 and 4.36 GeV, Phys. Rev. D91 (2015) 032002. arXiv:1412.1867, doi:10.1103/PhysRevD.91.032002.

[146] M. Ablikim, et al., Observation of $e^+e^- \to \phi\chi_{c1}$ and $\phi\chi_{c2}$ at $\sqrt{s}$=4.600 GeV, Phys. Rev. D97 (2018) 032008. arXiv:1712.09240, doi:10.1103/PhysRevD.97.032008.

[147] R. Aaij, et al., Amplitude analysis of $B^+ \to J/\psi\phi K^+$ decays, Phys. Rev. D95 (2017) 012002. arXiv:1606.07898, doi:10.1103/PhysRevD.95.012002.

[148] E. Wang, J.-J. Xie, L.-S. Geng, E. Oset, Analysis of the $B^+ \to J/\psi\phi K^+$ data at low $J/\psi\phi$ invariant masses and the $X(4140)$ and $X(4160)$ resonances, Phys. Rev. D97 (2018) 014017. arXiv:1710.02061, doi:10.1103/PhysRevD.97.014017.

[149] B. Aubert, et al., Observation of a broad structure in the $\pi^+\pi^- J/\psi$ mass spectrum around 4.26 GeV/c^2, Phys. Rev. Lett. 95 (2005) 142001. arXiv:hep-ex/0506081, doi:10.1103/PhysRevLett.95.142001.

[150] B. Aubert, et al., Evidence of a broad structure at an invariant mass of 4.32 GeV/c^2 in the reaction $e^+e^- \to \pi^+\pi^-\psi(2S)$ measured at BABAR, Phys. Rev. Lett. 98 (2007) 212001. arXiv:hep-ex/0610057, doi:10.1103/PhysRevLett.98.212001.

[151] X. L. Wang, et al., Observation of Two Resonant Structures in $e^+e^- \to \pi^+\pi^-\psi(2S)$ via Initial State Radiation at Belle, Phys. Rev. Lett. 99 (2007) 142002. arXiv:0707.3699, doi:10.1103/PhysRevLett.99.142002.

[152] V. N. Baier, V. S. Fadin, Radiative corrections to the resonant particle production, Phys. Lett. B27 (1968) 223. doi:10.1016/0370-2693(68)90279-7.

[153] J. P. Lees, et al., Study of the reaction $e^+e^- \to J/\psi\pi^+\pi^-$ via initial-state radiation at BABAR, Phys. Rev. D86 (2012) 051102. arXiv:1204.2158, doi:10.1103/PhysRevD.86.051102.

[154] M. Cleven, Q. Wang, F.-K. Guo, C. Hanhart, U.-G. Meißner, Q. Zhao, $Y(4260)$ as the first S-wave open charm vector molecular state?, Phys. Rev. D90 (2014) 074039. arXiv:1310.2190, doi:10.1103/PhysRevD.90.074039.

[155] X. L. Wang, et al., Measurement of $e^+e^- \to \pi^+\pi^-\psi(2S)$ via Initial State Radiation at Belle, Phys. Rev. D91 (2015) 112007. arXiv:1410.7641, doi:10.1103/PhysRevD.91.112007.

[156] J. P. Lees, et al., Study of the reaction $e^+e^- \to \psi(2S)\pi^+\pi^-$ via initial-state radiation at BABAR, Phys. Rev. D89 (2014) 111103. arXiv:

1211.6271, doi:10.1103/PhysRevD.89.111103.

[157] M. Ablikim, et al., Observation of $e^+e^- \to \pi^0\pi^0 h_c$ and a Neutral Charmoniumlike Structure $Z_c(4020)^0$, Phys. Rev. Lett. 113 (2014) 212002. arXiv:1409.6577, doi:10.1103/PhysRevLett.113.212002.

[158] M. Ablikim, et al., Observation of a Charged Charmoniumlike Structure $Z_c(4020)$ and Search for the $Z_c(3900)$ in $e^+e^- \to \pi^+\pi^- h_c$, Phys. Rev. Lett. 111 (2013) 242001. arXiv:1309.1896, doi:10.1103/PhysRevLett.111.242001.

[159] M. Ablikim, et al., Evidence of Two Resonant Structures in $e^+e^- \to \pi^+\pi^- h_c$, Phys. Rev. Lett. 118 (2017) 092002. arXiv:1610.07044, doi:10.1103/PhysRevLett.118.092002.

[160] M. Ablikim, et al., Study of $e^+e^- \to \omega\chi_{cJ}$ at center-of-mass energies from 4.21 to 4.42 GeV, Phys. Rev. Lett. 114 (2015) 092003. arXiv:1410.6538, doi:10.1103/PhysRevLett.114.092003.

[161] C. Z. Yuan, P. Wang, X. H. Mo, The $Y(4260)$ as an $\omega\chi_{c1}$ molecular state, Phys. Lett. B634 (2006) 399. arXiv:hep-ph/0511107, doi:10.1016/j.physletb.2006.01.031.

[162] L. Y. Dai, M. Shi, G.-Y. Tang, H. Q. Zheng, Nature of $X(4260)$, Phys. Rev. D92 (2015) 014020. arXiv:1206.6911, doi:10.1103/PhysRevD.92.014020.

[163] M. Ablikim, et al., Observation of $e^+e^- \to \omega\chi_{c1,2}$ near $\sqrt{s}$ = 4.42 and 4.6 GeV, Phys. Rev. D93 (2016) 011102. arXiv:1511.08564, doi:10.1103/PhysRevD.93.011102.

[164] M. Ablikim, et al., Cross section measurements of $e^+e^- \to \omega\chi_{c0}$ from $\sqrt{s}$ = 4.178 to 4.278 GeV, Phys. Rev. D99 (2019) 091103. arXiv:1903.02359, doi:10.1103/PhysRevD.99.091103.

[165] M. Ablikim, et al., Evidence of a resonant structure in the $e^+e^- \to \pi^+ D^0 D^{*-}$ cross section between 4.05 and 4.60 GeV, Phys. Rev. Lett. 122 (2019) 102002. arXiv:1808.02847, doi:10.1103/PhysRevLett.122.102002.

[166] M. Ablikim, et al., Measurement of $e^+e^- \to \pi^+\pi^-\psi(3686)$ from 4.008 to 4.600 GeV and observation of a charged structure in the $\pi^\pm\psi(3686)$ mass spectrum, Phys. Rev. D96 (2017) 032004. arXiv:1703.08787, doi:10.1103/PhysRevD.96.032004.

[167] K. Abe, et al., Measurement of the near-threshold $e^+e^- \to D^{(*)\pm} D^{(*)\mp}$ cross section using initial-state radiation, Phys. Rev. Lett. 98 (2007) 092001. arXiv:hep-ex/0608018, doi:10.1103/PhysRevLett.98.092001.

[168] G. Pakhlova, et al., Measurement of $e^+e^- \to D_s^{(*)+} D_s^{(*)-}$ cross sections near threshold using initial-state radiation, Phys. Rev. D83 (2011) 011101. arXiv:1011.4397, doi:10.1103/PhysRevD.83.011101.

[169] S.-R. Xue, H.-J. Jing, F.-K. Guo, Q. Zhao, Disentangling the role of the $Y(4260)$ in $e^+e^- \to D^*\bar{D}^*$ and $D_s^*\bar{D}_s^*$ via line shape studies, Phys. Lett. B779 (2018) 402. arXiv:1708.06961, doi:10.1016/j.physletb.2018.02.027.

[170] G. Pakhlova, et al., Measurement of the $e^+e^- \to D^0 D^{*-}\pi^+$ cross section using initial-state radiation, Phys. Rev. D80 (2009) 091101. arXiv:0908.0231, doi:10.1103/PhysRevD.80.091101.

[171] X. Y. Gao, C. P. Shen, C. Z. Yuan, Resonant parameters of the $Y(4220)$, Phys. Rev. D95 (2017) 092007. arXiv:1703.10351, doi:10.1103/PhysRevD.95.092007.

[172] Y. Chen, W.-F. Chiu, M. Gong, L.-C. Gui, Z. Liu, Exotic vector charmonium and its leptonic decay width, Chin. Phys. C40 (2016) 081002. arXiv:1604.03401, doi:10.1088/1674-1137/40/8/081002.

[173] W. Qin, S.-R. Xue, Q. Zhao, Production of $Y(4260)$ as a hadronic molecule state of $\bar{D}D_1 + c.c.$ in e^+e^- annihilations, Phys. Rev. D94 (2016) 054035. arXiv:1605.02407, doi:10.1103/PhysRevD.94.054035.

[174] L. Maiani, V. Riquer, R. Faccini, F. Piccinini, A. Pilloni, A. D. Polosa, A J^{PG} = 1^{++} Charged Resonance in the $Y(4260) \to \pi^+\pi^- J/\psi$ Decay?, Phys. Rev. D87 (2013) 111102. arXiv:1303.6857, doi:10.1103/PhysRevD.87.111102.

[175] X.-G. Wu, C. Hanhart, Q. Wang, Q. Zhao, Probing the nature of $Y(4260)$ in the isospin violating process $Y(4260) \to J/\psi\eta\pi^0$, Phys. Rev. D89 (2014) 054038. arXiv:1312.5621, doi:10.1103/PhysRevD.89.054038.

[176] M. Ablikim, et al., Search for the isospin violating decay $Y(4260) \to J/\psi\eta\pi^0$, Phys. Rev. D92 (2015) 012008. arXiv:1505.00539, doi:10.1103/PhysRevD.92.012008.

[177] J. J. Dudek, R. Edwards, C. E. Thomas, Exotic and excited-state radiative transitions in charmonium from lattice QCD, Phys. Rev. D79 (2009) 094504. arXiv:0902.2241, doi:10.1103/PhysRevD.79.094504.

[178] M. Ablikim, et al., Evidence for $e^+e^- \to \gamma\eta_c(1S)$ at center-of-mass energies between 4.01 and 4.60 GeV, Phys. Rev. D96 (2017) 051101. arXiv:1705.06853, doi:10.1103/PhysRevD.96.051101.

[179] M. Ablikim, et al., Precision measurements of $\sigma_B(e^+e^- \to K_S^0 K^\pm\pi^\mp)$ at center-of-mass energies between 3.8 and 4.6 GeV, Phys. Rev. D99 (2019) 072005. arXiv:1808.08733, doi:10.1103/PhysRevD.99.072005.

[180] M. Ablikim, et al., Measurements of $e^+e^- \to K_S^0 K^\pm\pi^\mp\pi^0$ and $K_S^0 K^\pm\pi^\mp\eta$ at center-of-mass energies from 3.90 to 4.60 GeV, Phys. Rev. D99 (2019) 012003. arXiv:1810.09395, doi:10.1103/PhysRevD.99.012003.

[181] B. Aubert, et al., Study of $J/\psi\pi^+\pi^-$ states produced in $B^0 \to J/\psi\pi^+\pi^- K^0$ and $B^- \to J/\psi\pi^+\pi^- K^-$, Phys. Rev. D73 (2006) 011101. arXiv:hep-ex/0507090, doi:10.1103/PhysRevD.73.011101.

[182] R. Garg, et al., Search for the $B \to Y(4260)K$, $Y(4260) \to J/\psi\pi^+\pi^-$ decays, Phys. Rev. D99 (2019) 071102. arXiv:1901.06470, doi:10.1103/PhysRevD.99.071102.

[183] V. M. Abazov, et al., Evidence for $Z_c^\pm(3900)$ in semi-inclusive decays of b-flavored hadrons, Phys. Rev. D98 (2018) 052010. arXiv:1807.00183, doi:10.1103/PhysRevD.98.052010.

[184] G.-J. Ding, Are $Y(4260)$ and $Z_2^+(4250)$ are $D_1 D$ or $D_0 D^*$ hadronic molecules?, Phys. Rev. D79 (2009) 014001. arXiv:0809.4818, doi:10.1103/PhysRevD.79.014001.

[185] Q. Wang, C. Hanhart, Q. Zhao, Decoding the riddle of $Y(4260)$ and $Z_c(3900)$, Phys. Rev. Lett. 111 (2013) 132003. arXiv:1303.6355, doi:10.1103/PhysRevLett.111.132003.

[186] S.-L. Zhu, The possible interpretations of $Y(4260)$, Phys. Lett. B625 (2005) 212. arXiv:hep-ph/0507025, doi:10.1016/j.physletb.2005.08.068.

[187] F. E. Close, P. R. Page, Gluonic charmonium resonances at BaBar and Belle?, Phys. Lett. B628 (2005) 215. arXiv:hep-ph/0507199, doi:10.1016/j.physletb.2005.09.016.

[188] E. Kou, O. Pene, Suppressed decay into open charm for the $Y(4260)$ being an hybrid, Phys. Lett. B631 (2005) 164. arXiv:hep-ph/0507119, doi:10.1016/j.physletb.2005.09.013.

156

[189] L. Maiani, F. Piccinini, A. D. Polosa, V. Riquer, The $Z(4430)$ and a New Paradigm for Spin Interactions in Tetraquarks, Phys. Rev. D89 (2014) 114010. arXiv:1405.1551, doi:10.1103/PhysRevD.89.114010.

[190] S. Dubynskiy, M. B. Voloshin, Hadro-Charmonium, Phys. Lett. B666 (2008) 344. arXiv:0803.2224, doi:10.1016/j.physletb.2008.07.086.

[191] X. Li, M. B. Voloshin, $Y(4260)$ and $Y(4360)$ as mixed hadrocharmonium, Mod. Phys. Lett. A29 (2014) 1450060. arXiv:1309.1681, doi:10.1142/S0217732314500606.

[192] M. Berwein, N. Brambilla, J. Tarrús Castellà, A. Vairo, Quarkonium Hybrids with Nonrelativistic Effective Field Theories, Phys. Rev. D92 (2015) 114019. arXiv:1510.04299, doi:10.1103/PhysRevD.92.114019.

[193] R. Oncala, J. Soto, Heavy quarkonium hybrids: spectrum, decay and mixing, Phys. Rev. D96 (2017) 014004. arXiv:1702.03900, doi:10.1103/PhysRevD.96.014004.

[194] D.-Y. Chen, C.-Q. Pang, J. He, Z.-Y. Zhou, D-wave charmonia, Phys. Rev. D100 (2019) 074016. arXiv:1804.00614, doi:10.1103/PhysRevD.100.074016.

[195] T. Bhavsar, M. Shah, P. C. Vinodkumar, Status of quarkonia-like negative and positive parity states in a relativistic confinement scheme, Eur. Phys. J. C78 (2018) 227. arXiv:1803.07249, doi:10.1140/epjc/s10052-018-5694-3.

[196] Z.-G. Wang, Analysis of the vector tetraquark states with P-waves between the diquarks and antidiquarks via the QCD sum rules, Eur. Phys. J. C79 (2019) 29. arXiv:1811.02726, doi:10.1140/epjc/s10052-019-6568-z.

[197] Z.-G. Wang, Vector tetraquark state candidates: $Y(4260/4220)$, $Y(4360/4320)$, $Y(4390)$ and $Y(4660/4630)$, Eur. Phys. J. C78 (2018) 518. arXiv:1803.05749, doi:10.1140/epjc/s10052-018-5996-5.

[198] J. Ferretti, η_c- and J/ψ-isoscalar meson bound states in the hadro-charmonium picture, Phys. Lett. B782 (2018) 702. arXiv:1805.04717, doi:10.1016/j.physletb.2018.06.032.

[199] Q. Wang, M. Cleven, F.-K. Guo, C. Hanhart, U.-G. Meißner, X.-G. Wu, Q. Zhao, $Y(4260)$: hadronic molecule versus hadro-charmonium interpretation, Phys. Rev. D89 (2014) 034001. arXiv:1309.4303, doi:10.1103/PhysRevD.89.034001.

[200] D.-Y. Chen, C.-J. Xiao, J. He, Hidden-charm decays of $Y(4390)$ in a hadronic molecular scenario, Phys. Rev. D96 (2017) 054017. doi:10.1103/PhysRevD.96.054017.

[201] J. He, D.-Y. Chen, Interpretation of $Y(4390)$ as an isoscalar partner of $Z(4430)$ from $D^*(2010)\bar{D}_1(2420)$ interaction, Eur. Phys. J. C77 (2017) 398. arXiv:1704.08776, doi:10.1140/epjc/s10052-017-4973-8.

[202] R. F. Lebed, Spectroscopy of exotic hadrons formed from dynamical diquarks, Phys. Rev. D96 (2017) 116003. arXiv:1709.06097, doi:10.1103/PhysRevD.96.116003.

[203] D.-Y. Chen, X. Liu, T. Matsuki, Interference effect as resonance killer of newly observed charmoniumlike states $Y(4320)$ and $Y(4390)$, Eur. Phys. J. C78 (2018) 136. arXiv:1708.01954, doi:10.1140/epjc/s10052-018-5635-1.

[204] G. Pakhlova, et al., Observation of a near-threshold enhancement in the $e^+e^- \to \Lambda_c^+\bar{\Lambda}_c^-$ cross section using initial-state radiation, Phys. Rev. Lett. 101 (2008) 172001. arXiv:0807.4458, doi:10.1103/PhysRevLett.101.172001.

[205] M. Ablikim, et al., Precision measurement of the $e^+e^- \to \Lambda_c^+\bar{\Lambda}_c^-$ cross section near threshold, Phys. Rev. Lett. 120 (2018) 132001. arXiv:1710.00150, doi:10.1103/PhysRevLett.120.132001.

[206] D. V. Bugg, An alternative fit to Belle mass spectra for $D\bar{D}$, $D^*\bar{D}^*$ and $\Lambda_c\bar{\Lambda}_c$, J. Phys. G36 (2009) 075002. arXiv:0811.2559, doi:10.1088/0954-3899/36/7/075002.

[207] G. Cotugno, R. Faccini, A. D. Polosa, C. Sabelli, Charmed Baryonium, Phys. Rev. Lett. 104 (2010) 132005. arXiv:0911.2178, doi:10.1103/PhysRevLett.104.132005.

[208] F.-K. Guo, J. Haidenbauer, C. Hanhart, U.-G. Meißner, Reconciling the $X(4630)$ with the $Y(4660)$, Phys. Rev. D82 (2010) 094008. arXiv:1005.2055, doi:10.1103/PhysRevD.82.094008.

[209] F.-K. Guo, C. Hanhart, U.-G. Meißner, Evidence that the $Y(4660)$ is a $f_0(980)\psi'$ bound state, Phys. Lett. B665 (2008) 26. arXiv:0803.1392, doi:10.1016/j.physletb.2008.05.057.

[210] F.-K. Guo, C. Hanhart, U.-G. Meißner, Implications of heavy quark spin symmetry on heavy meson hadronic molecules, Phys. Rev. Lett. 102 (2009) 242004. arXiv:0904.3338, doi:10.1103/PhysRevLett.102.242004.

[211] Y. B. Li, et al., Observation of $\Xi_c(2930)^0$ and updated measurement of $B^- \to K^-\Lambda_c^+\bar{\Lambda}_c^-$ at Belle, Eur. Phys. J. C78 (2018) 252. arXiv:1712.03612, doi:10.1140/epjc/s10052-018-5720-5.

[212] Y. B. Li, et al., Evidence of a structure in $\bar{K}^0\Lambda_c^+$ consistent with a charged $\Xi_c(2930)^+$, and updated measurement of $\bar{B}^0 \to \bar{K}^0\Lambda_c^+\bar{\Lambda}_c^-$ at Belle, Eur. Phys. J. C78 (2018) 928. arXiv:1806.09182, doi:10.1140/epjc/s10052-018-6425-5.

[213] T. E. Coan, et al., Charmonium decays of $Y(4260)$, $\psi(4160)$ and $\psi(4040)$, Phys. Rev. Lett. 96 (2006) 162003. arXiv:hep-ex/0602034, doi:10.1103/PhysRevLett.96.162003.

[214] C. Z. Yuan, et al., Observation of $e^+e^- \to K^+K^-J/\psi$ via initial state radiation at Belle, Phys. Rev. D77 (2008) 011105. arXiv:0709.2565, doi:10.1103/PhysRevD.77.011105.

[215] C. P. Shen, et al., Updated cross section measurement of $e^+e^- \to K^+K^-J/\psi$ and $K_S^0K_S^0J/\psi$ via initial state radiation at Belle, Phys. Rev. D89 (2014) 072015. arXiv:1402.6578, doi:10.1103/PhysRevD.89.072015.

[216] M. Ablikim, et al., Observation of $e^+e^- \to K\bar{K}J/\psi$ at center-of-mass energies from 4.189 to 4.600 GeV, Phys. Rev. D97 (2018) 071101. arXiv:1802.01216, doi:10.1103/PhysRevD.97.071101.

[217] X. L. Wang, et al., Observation of $\psi(4040)$ and $\psi(4160)$ decay into $\eta J/\psi$, Phys. Rev. D87 (2013) 051101. arXiv:1210.7550, doi:10.1103/PhysRevD.87.051101.

[218] M. Ablikim, et al., Observation of $e^+e^- \to \eta J/\psi$ at center-of-mass energy $\sqrt{s}$ = 4.009 GeV, Phys. Rev. D86 (2012) 071101. arXiv:1208.1857, doi:10.1103/PhysRevD.86.071101.

[219] M. Ablikim, et al., Measurement of the $e^+e^- \to \eta J/\psi$ cross section and search for $e^+e^- \to \pi^0 J/\psi$ at center-of-mass energies between 3.810 and 4.600 GeV, Phys. Rev. D91 (2015) 112005. arXiv:1503.06644, doi:10.1103/PhysRevD.91.112005.

[220] M. Ablikim, et al., Observation of $e^+e^- \to \eta' J/\psi$ at center-of-mass energies between 4.189 and 4.600 GeV, Phys. Rev. D94 (2016) 032009. arXiv:1605.03256, doi:10.1103/PhysRevD.94.032009.

[221] M. Ablikim, et al., Observation of $e^+e^- \to \eta h_c$ at center-of-mass energies from 4.085 to 4.600 GeV, Phys. Rev. D96 (2017) 012001.

arXiv:1704.08033, doi:10.1103/PhysRevD.96.012001.

[222] T. K. Pedlar, et al., Observation of the $h_c(1P)$ using e^+e^- collisions above $D\bar{D}$ threshold, Phys. Rev. Lett. 107 (2011) 041803. arXiv:1104.2025, doi:10.1103/PhysRevLett.107.041803.

[223] M. Ablikim, et al., Study of $e^+e^- \to \pi^+\pi^-\pi^0\eta_c$ and evidence for $Z_c(3900)^\pm$ decaying into $\rho^\pm\eta_c$, Phys. Rev. D100 (2019) 111102. arXiv:1906.00831, doi:10.1103/PhysRevD.100.111102.

[224] S. Jia, et al., Search for the 0^{--} Glueball in $\Upsilon(1S)$ and $\Upsilon(2S)$ decays, Phys. Rev. D95 (2017) 012001. arXiv:1611.07131, doi:10.1103/PhysRevD.95.012001.

[225] C.-F. Qiao, L. Tang, Finding the 0^{--} Glueball, Phys. Rev. Lett. 113 (2014) 221601. arXiv:1408.3995, doi:10.1103/PhysRevLett.113.221601.

[226] L. Bellantuono, P. Colangelo, F. Giannuzzi, Holographic oddballs, JHEP 10 (2015) 137. arXiv:1507.07768, doi:10.1007/JHEP10(2015)137.

[227] V. M. Abazov, et al., Study of the $X^\pm(5568)$ state with semileptonic decays of the B_s^0 meson, Phys. Rev. D97 (2018) 092004. arXiv:1712.10176, doi:10.1103/PhysRevD.97.092004.

[228] R. Aaij, et al., Search for structure in the $B_s^0\pi^\pm$ invariant mass spectrum, Phys. Rev. Lett. 117 (2016) 152003, [Addendum: Phys. Rev. Lett. 118 (2017) 109904]. arXiv:1608.00435, doi:10.1103/PhysRevLett.118.109904,10.1103/PhysRevLett.117.152003.

[229] T. Aaltonen, et al., Search for the Exotic Meson $X(5568)$ with the Collider Detector at Fermilab, Phys. Rev. Lett. 120 (2018) 202006. arXiv:1712.09620, doi:10.1103/PhysRevLett.120.202006.

[230] A. M. Sirunyan, et al., Search for the $X(5568)$ state decaying into $B_s^0\pi^\pm$ in proton-proton collisions at $\sqrt{s}$ = 8 TeV, Phys. Rev. Lett. 120 (2018) 202005. arXiv:1712.06144, doi:10.1103/PhysRevLett.120.202005.

[231] M. Aaboud, et al., Search for a Structure in the $B_s^0\pi^\pm$ Invariant Mass Spectrum with the ATLAS Experiment, Phys. Rev. Lett. 120 (2018) 202007. arXiv:1802.01840, doi:10.1103/PhysRevLett.120.202007.

[232] S. S. Agaev, K. Azizi, H. Sundu, Mass and decay constant of the newly observed exotic $X(5568)$ state, Phys. Rev. D93 (2016) 074024. arXiv:1602.08642, doi:10.1103/PhysRevD.93.074024.

[233] S. S. Agaev, K. Azizi, H. Sundu, Width of the exotic $X_b(5568)$ state through its strong decay to $B_s^0\pi^+$, Phys. Rev. D93 (2016) 114007. arXiv:1603.00290, doi:10.1103/PhysRevD.93.114007.

[234] S. S. Agaev, K. Azizi, H. Sundu, Charmed partner of the exotic $X(5568)$ state and its properties, Phys. Rev. D93 (2016) 094006. arXiv:1603.01471, doi:10.1103/PhysRevD.93.094006.

[235] S. S. Agaev, K. Azizi, H. Sundu, Exploring $X(5568)$ as a meson molecule, Eur. Phys. J. Plus 131 (2016) 351. arXiv:1603.02708, doi:10.1140/epjp/i2016-16351-8.

[236] S. S. Agaev, K. Azizi, B. Barsbay, H. Sundu, Resonance $X(5568)$ as an exotic axial-vector state, Eur. Phys. J. A53 (2017) 11. arXiv:1608.04785, doi:10.1140/epja/i2017-12201-2.

[237] Z.-G. Wang, Analysis of the $X(5568)$ as scalar tetraquark state in the diquark-antidiquark model with QCD sum rules, Commun. Theor. Phys. 66 (2016) 335. arXiv:1602.08711, doi:10.1088/0253-6102/66/3/335.

[238] Z.-G. Wang, Analysis of the strong decay $X(5568) \to B_s^0\pi^+$ with QCD sum rules, Eur. Phys. J. C76 (2016) 279. arXiv:1603.02498, doi:10.1140/epjc/s10052-016-4133-6.

[239] W. Chen, H.-X. Chen, X. Liu, T. G. Steele, S.-L. Zhu, Decoding the $X(5568)$ as a fully open-flavor $su\bar{b}\bar{d}$ tetraquark state, Phys. Rev. Lett. 117 (2016) 022002. arXiv:1602.08916, doi:10.1103/PhysRevLett.117.022002.

[240] Y.-R. Liu, X. Liu, S.-L. Zhu, $X(5568)$ and its partner states, Phys. Rev. D93 (2016) 074023. arXiv:1603.01131, doi:10.1103/PhysRevD.93.074023.

[241] J. M. Dias, K. P. Khemchandani, A. Martnez Torres, M. Nielsen, C. M. Zanetti, A QCD sum rule calculation of the $X^\pm(5568) \to B_s^0\pi^\pm$ decay width, Phys. Lett. B758 (2016) 235. arXiv:1603.02249, doi:10.1016/j.physletb.2016.05.015.

[242] F. Stancu, $X(5568)$ as a $su\bar{d}\bar{b}$ tetraquark in a simple quark model, J. Phys. G43 (2016) 105001. arXiv:1603.03322, doi:10.1088/0954-3899/43/10/105001.

[243] J.-R. Zhang, J.-L. Zou, J.-Y. Wu, 0^+ tetraquark states from improved QCD sum rules: delving into $X(5568)$, Chin. Phys. C42 (2018) 043101. arXiv:1705.03741, doi:10.1088/1674-1137/42/4/043101.

[244] Z.-Y. Wang, J.-J. Qi, X.-H. Guo, Studying the Bound State of the $B\bar{K}$ System in the Bethe-Salpeter Formalism, Adv. High Energy Phys. 2019 (2019) 7576254. arXiv:1802.04566, doi:10.1155/2019/7576254.

[245] H.-W. Ke, X.-Q. Li, Estimating decay rate of $X^\pm(5568) \to B_s\pi^\pm$ while assuming them to be molecular states, Eur. Phys. J. C78 (2018) 364. arXiv:1801.00675, doi:10.1140/epjc/s10052-018-5834-9.

[246] W. Wang, R. Zhu, Can $X(5568)$ be a tetraquark state?, Chin. Phys. C40 (2016) 093101. arXiv:1602.08806, doi:10.1088/1674-1137/40/9/093101.

[247] M. Albaladejo, J. Nieves, E. Oset, Z.-F. Sun, X. Liu, Can $X(5568)$ be described as a $B_s\pi$, $B\bar{K}$ resonant state?, Phys. Lett. B757 (2016) 515. arXiv:1603.09230, doi:10.1016/j.physletb.2016.04.033.

[248] X.-W. Kang, J. A. Oller, P-wave coupled-channel scattering of $B_s\pi$, $B_s^*\pi$, $B\bar{K}$, $B^*\bar{K}$ and the puzzling $X(5568)$, Phys. Rev. D94 (2016) 054010. arXiv:1606.06665, doi:10.1103/PhysRevD.94.054010.

[249] C. B. Lang, D. Mohler, S. Prelovsek, $B_s\pi^+$ scattering and search for $X(5568)$ with lattice QCD, Phys. Rev. D94 (2016) 074509. arXiv:1607.03185, doi:10.1103/PhysRevD.94.074509.

[250] R. Chen, X. Liu, Is the newly reported $X(5568)$ a $B\bar{K}$ molecular state?, Phys. Rev. D94 (2016) 034006. arXiv:1607.05566, doi:10.1103/PhysRevD.94.034006.

[251] J.-X. Lu, X.-L. Ren, L.-S. Geng, $B_s\pi$-$B\bar{K}$ interactions in finite volume and $X(5568)$, Eur. Phys. J. C77 (2017) 94. arXiv:1607.06327, doi:10.1140/epjc/s10052-017-4660-9.

[252] X. Chen, J. Ping, Is the exotic $X(5568)$ a bound state?, Eur. Phys. J. C76 (2016) 351. arXiv:1604.05651, doi:10.1140/epjc/s10052-016-4210-x.

[253] F.-K. Guo, U.-G. Meißner, B.-S. Zou, How the $X(5568)$ challenges our understanding of QCD, Commun. Theor. Phys. 65 (2016) 593. arXiv:1603.06316, doi:10.1088/0253-6102/65/5/593.

158

[254] T. J. Burns, E. S. Swanson, Interpreting the $X(5568)$, Phys. Lett. B760 (2016) 627. arXiv:1603.04366, doi:10.1016/j.physletb.2016.07.049.

[255] H.-W. Ke, X.-Q. Li, How can $X^{\pm}(5568)$ escape detection?, Phys. Lett. B785 (2018) 301. arXiv:1802.08823, doi:10.1016/j.physletb.2018.07.071.

[256] R. Albuquerque, S. Narison, A. Rabemananjara, D. Rabetiarivony, Nature of the $X(5568)$-A critical Laplace sum rule analysis at N2LO, Int. J. Mod. Phys. A31 (2016) 1650093. arXiv:1604.05566, doi:10.1142/S0217751X16500937.

[257] A. Esposito, A. Pilloni, A. D. Polosa, Hybridized Tetraquarks, Phys. Lett. B758 (2016) 292. arXiv:1603.07667, doi:10.1016/j.physletb.2016.05.028.

[258] S. K. Choi, et al., Observation of a resonance-like structure in the $\pi^{\pm}\psi'$ mass distribution in exclusive $B \to K\pi^{\pm}\psi'$ decays, Phys. Rev. Lett. 100 (2008) 142001. arXiv:0708.1790, doi:10.1103/PhysRevLett.100.142001.

[259] K. Chilikin, et al., Experimental constraints on the spin and parity of the $Z(4430)^+$, Phys. Rev. D88 (2013) 074026. arXiv:1306.4894, doi:10.1103/PhysRevD.88.074026.

[260] R. Mizuk, et al., Observation of two resonance-like structures in the $\pi^+\chi_{c1}$ mass distribution in exclusive $\bar{B}^0 \to K^-\pi^+\chi_{c1}$ decays, Phys. Rev. D78 (2008) 072004. arXiv:0806.4098, doi:10.1103/PhysRevD.78.072004.

[261] K. Chilikin, et al., Observation of a new charged charmoniumlike state in $\bar{B}^0 \to J/\psi K^-\pi^+$ decays, Phys. Rev. D90 (2014) 112009. arXiv:1408.6457, doi:10.1103/PhysRevD.90.112009.

[262] R. Aaij, et al., Evidence for an $\eta_c(1S)\pi^-$ resonance in $B^0 \to \eta_c(1S)K^+\pi^-$ decays, Eur. Phys. J. C78 (2018) 1019. arXiv:1809.07416, doi:10.1140/epjc/s10052-018-6447-z.

[263] B. Aubert, et al., Search for the $Z(4430)^-$ at BABAR, Phys. Rev. D79 (2009) 112001. arXiv:0811.0564, doi:10.1103/PhysRevD.79.112001.

[264] R. Aaij, et al., Model-independent observation of exotic contributions to $B^0 \to J/\psi K^+\pi^-$ decays, Phys. Rev. Lett. 122 (2019) 152002. arXiv:1901.05745, doi:10.1103/PhysRevLett.122.152002.

[265] J. P. Lees, et al., Search for the $Z_1(4050)^+$ and $Z_2(4250)^+$ states in $\bar{B}^0 \to \chi_{c1}K^-\pi^+$ and $B^+ \to \chi_{c1}K_S^0\pi^+$, Phys. Rev. D85 (2012) 052003. arXiv:1111.5919, doi:10.1103/PhysRevD.85.052003.

[266] M. Ablikim, et al., Observation of a charged $(D\bar{D}^*)^{\pm}$ mass peak in $e^+e^- \to \pi D\bar{D}^*$ at $\sqrt{s}$ = 4.26 GeV, Phys. Rev. Lett. 112 (2014) 022001. arXiv:1310.1163, doi:10.1103/PhysRevLett.112.022001.

[267] M. Ablikim, et al., Confirmation of a charged charmoniumlike state $Z_c(3885)^{\mp}$ in $e^+e^- \to \pi^{\pm}(D\bar{D}^*)^{\mp}$ with double D tag, Phys. Rev. D92 (2015) 092006. arXiv:1509.01398, doi:10.1103/PhysRevD.92.092006.

[268] M. Ablikim, et al., Observation of a Neutral Structure near the $D\bar{D}^*$ Mass Threshold in $e^+e^- \to (D\bar{D}^*)^0\pi^0$ at $\sqrt{s}$ = 4.226 and 4.257 GeV, Phys. Rev. Lett. 115 (2015) 222002. arXiv:1509.05620, doi:10.1103/PhysRevLett.115.222002.

[269] M. Ablikim, et al., Determination of the Spin and Parity of the $Z_c(3900)$, Phys. Rev. Lett. 119 (2017) 072001. arXiv:1706.04100, doi:10.1103/PhysRevLett.119.072001.

[270] S. U. Chung, A General formulation of covariant helicity coupling amplitudes, Phys. Rev. D57 (1998) 431. doi:10.1103/PhysRevD.57.431.

[271] S. U. Chung, Helicity coupling amplitudes in tensor formalism, Phys. Rev. D48 (1993) 1225, [Erratum: Phys. Rev. D56 (1997) 4419]. doi:10.1103/PhysRevD.56.4419,10.1103/PhysRevD.48.1225.

[272] S.-U. Chung, J. Friedrich, Covariant helicity-coupling amplitudes: A new formulation, Phys. Rev. D78 (2008) 074027. arXiv:0711.3143, doi:10.1103/PhysRevD.78.074027.

[273] Q.-Y. Lin, X. Liu, H.-S. Xu, Charged charmoniumlike state $Z_c(3900)^{\pm}$ via meson photoproduction, Phys. Rev. D88 (2013) 114009. arXiv:1308.6345, doi:10.1103/PhysRevD.88.114009.

[274] C. Adolph, et al., Search for exclusive photoproduction of $Z_c^{\pm}(3900)$ at COMPASS, Phys. Lett. B742 (2015) 330. arXiv:1407.6186, doi:10.1016/j.physletb.2015.01.042.

[275] M. Ablikim, et al., Observation of a charged charmoniumlike structure in $e^+e^- \to (D^*\bar{D}^*)^{\pm}\pi^{\mp}$ at $\sqrt{s}$ = 4.26GeV, Phys. Rev. Lett. 112 (2014) 132001. arXiv:1308.2760, doi:10.1103/PhysRevLett.112.132001.

[276] M. Ablikim, et al., Observation of a neutral charmoniumlike state $Z_c(4025)^0$ in $e^+e^- \to (D^*\bar{D}^*)^0\pi^0$, Phys. Rev. Lett. 115 (2015) 182002. arXiv:1507.02404, doi:10.1103/PhysRevLett.115.182002.

[277] A. Esposito, A. L. Guerrieri, A. Pilloni, Probing the nature of $Z_c^{(')}$ states via the $\eta_c\rho$ decay, Phys. Lett. B746 (2015) 194. arXiv:1409.3551, doi:10.1016/j.physletb.2015.04.057.

[278] G. Li, X. H. Liu, Z. Zhou, More hidden heavy quarkonium molecules and their discovery decay modes, Phys. Rev. D90 (2014) 054006. arXiv:1409.0754, doi:10.1103/PhysRevD.90.054006.

[279] H.-W. Ke, Z.-T. Wei, X.-Q. Li, Is $Z_c(3900)$ a molecular state ?, Eur. Phys. J. C73 (2013) 2561. arXiv:1307.2414, doi:10.1140/epjc/s10052-013-2561-0.

[280] L. Ma, X.-H. Liu, X. Liu, S.-L. Zhu, Strong decays of the XYZ states, Phys. Rev. D91 (2015) 034032. arXiv:1406.6879, doi:10.1103/PhysRevD.91.034032.

[281] L. Ma, W.-Z. Deng, X.-L. Chen, S.-L. Zhu, Strong decay patterns of the hidden-charm tetraquarks arXiv:1512.01938.

[282] M. B. Voloshin, Radiative and ρ transitions between a heavy quarkonium and isovector four-quark states, Phys. Rev. D98 (2018) 034025. arXiv:1806.05651, doi:10.1103/PhysRevD.98.034025.

[283] A. Bondar, talk at the 9th international workshop on charm physics, may 21 to 25, 2018, novosibirsk, russia.
URL https://indico.inp.nsk.su/event/10/session/2/contribution/74/material/slides/0.pdf

[284] A. Bondar, et al., Observation of two charged bottomonium-like resonances in $\Upsilon(5S)$ decays, Phys. Rev. Lett. 108 (2012) 122001. arXiv:1110.2251, doi:10.1103/PhysRevLett.108.122001.

[285] L. Maiani, F. Piccinini, A. D. Polosa, V. Riquer, Diquark-antidiquarks with hidden or open charm and the nature of $X(3872)$, Phys. Rev. D71 (2005) 014028. arXiv:hep-ph/0412098, doi:10.1103/PhysRevD.71.014028.

[286] Q. Zhao, Some insights into the newly observed $Z_c(4100)$ in $B^0 \to \eta_c K^+\pi^-$ by LHCb arXiv:1811.05357.

[287] M. B. Voloshin, $Z_c(4100)$ and $Z_c(4200)$ as hadrocharmonium, Phys. Rev. D98 (2018) 094028. arXiv:1810.08146, doi:10.1103/

`PhysRevD.98.094028`.

[288] J. Wu, X. Liu, Y.-R. Liu, S.-L. Zhu, Systematic studies of charmonium-, bottomonium-, and B_c-like tetraquark states, Phys. Rev. D99 (2019) 014037. `arXiv:1810.06886`, `doi:10.1103/PhysRevD.99.014037`.

[289] Z.-G. Wang, Lowest vector tetraquark states: $Y(4260/4220)$ or $Z_c(4100)$, Eur. Phys. J. C78 (2018) 933. `arXiv:1809.10299`, `doi:10.1140/epjc/s10052-018-6417-5`.

[290] C.-Z. Yuan, Recent progress on the study of the charmoniumlike states, Int. J. Mod. Phys. A29 (2014) 1430046. `arXiv:1404.7768`, `doi:10.1142/S0217751X14300464`.

[291] S. J. Brodsky, R. F. Lebed, V. E. Lyubovitskij, QCD compositeness as revealed in exclusive vector boson reactions through double-photon annihilation: $e^+e^- \rightarrow \gamma\gamma^* \rightarrow \gamma V^0$ and $e^+e^- \rightarrow \gamma^*\gamma^* \rightarrow V^0V^0$, Phys. Lett. B764 (2017) 174. `arXiv:1609.06635`, `doi:10.1016/j.physletb.2016.11.009`.

[292] S. J. Brodsky, R. F. Lebed, QCD dynamics of tetraquark production, Phys. Rev. D91 (2015) 114025. `arXiv:1505.00803`, `doi:10.1103/PhysRevD.91.114025`.

[293] K. F. Chen, et al., Observation of anomalous $\Upsilon(1S)\pi^+\pi^-$ and $\Upsilon(2S)\pi^+\pi^-$ production near the $\Upsilon(5S)$ resonance, Phys. Rev. Lett. 100 (2008) 112001. `arXiv:0710.2577`, `doi:10.1103/PhysRevLett.100.112001`.

[294] P. Krokovny, et al., First observation of the $Z_b^0(10610)$ in a Dalitz analysis of $\Upsilon(10860) \rightarrow \Upsilon(nS)\pi^0\pi^0$, Phys. Rev. D88 (2013) 052016. `arXiv:1308.2646`, `doi:10.1103/PhysRevD.88.052016`.

[295] A. Garmash, et al., Observation of $Z_b(10610)$ and $Z_b(10650)$ Decaying to B Mesons, Phys. Rev. Lett. 116 (2016) 212001. `arXiv:1512.07419`, `doi:10.1103/PhysRevLett.116.212001`.

[296] D. Santel, et al., Measurements of the $\Upsilon(10860)$ and $\Upsilon(11020)$ resonances via $\sigma(e^+e^- \rightarrow \Upsilon(nS)\pi^+\pi^-)$, Phys. Rev. D93 (2016) 011101. `arXiv:1501.01137`, `doi:10.1103/PhysRevD.93.011101`.

[297] A. Abdesselam, et al., Energy scan of the $e^+e^- \rightarrow h_b(nP)\pi^+\pi^-$ ($n = 1, 2$) cross sections and evidence for $\Upsilon(11020)$ decays into charged bottomonium-like states, Phys. Rev. Lett. 117 (2016) 142001. `arXiv:1508.06562`, `doi:10.1103/PhysRevLett.117.142001`.

[298] A. Drutskoy, et al., Measurement of $\Upsilon(5S)$ decays to B^0 and B^+ mesons, Phys. Rev. D81 (2010) 112003. `arXiv:1003.5885`, `doi:10.1103/PhysRevD.81.112003`.

[299] F.-K. Guo, C. Hanhart, Yu. S. Kalashnikova, P. Matuschek, R. V. Mizuk, A. V. Nefediev, Q. Wang, J. L. Wynen, Interplay of quark and meson degrees of freedom in near-threshold states: A practical parametrization for line shapes, Phys. Rev. D93 (2016) 074031. `arXiv:1602.00940`, `doi:10.1103/PhysRevD.93.074031`.

[300] Q. Wang, V. Baru, A. A. Filin, C. Hanhart, A. V. Nefediev, J. L. Wynen, Line shapes of the $Z_b(10610)$ and $Z_b(10650)$ in the elastic and inelastic channels revisited, Phys. Rev. D98 (2018) 074023. `arXiv:1805.07453`, `doi:10.1103/PhysRevD.98.074023`.

[301] S. H. Lee, M. Nielsen, U. Wiedner, D_sD^* molecule as an axial meson, J. Korean Phys. Soc. 55 (2009) 424. `arXiv:0803.1168`, `doi:10.3938/jkps.55.424`.

[302] J. M. Dias, X. Liu, M. Nielsen, Prediction for the decay width of a charged state near the $D_s\bar{D}^*/D_s^*\bar{D}$ threshold, Phys. Rev. D88 (2013) 096014. `arXiv:1307.7100`, `doi:10.1103/PhysRevD.88.096014`.

[303] D.-Y. Chen, X. Liu, T. Matsuki, Predictions of Charged Charmoniumlike Structures with Hidden-Charm and Open-Strange Channels, Phys. Rev. Lett. 110 (2013) 232001. `arXiv:1303.6842`, `doi:10.1103/PhysRevLett.110.232001`.

[304] D.-Y. Chen, X. Liu, T. Matsuki, Two Charged Strangeonium-Like Structures Observable in the $Y(2175) \rightarrow \phi(1020)\pi^+\pi^-$ Process, Eur. Phys. J. C72 (2012) 2008. `arXiv:1112.3773`, `doi:10.1140/epjc/s10052-012-2008-z`.

[305] R. Aaij, et al., Model-independent evidence for $J/\psi p$ contributions to $\Lambda_b^0 \rightarrow J/\psi pK^-$ decays, Phys. Rev. Lett. 117 (2016) 082002. `arXiv:1604.05708`, `doi:10.1103/PhysRevLett.117.082002`.

[306] R. Aaij, et al., Study of the production of Λ_b^0 and $\overline{B}^0$ hadrons in pp collisions and first measurement of the $\Lambda_b^0 \rightarrow J/\psi pK^-$ branching fraction, Chin. Phys. C40 (2016) 011001. `arXiv:1509.00292`, `doi:10.1088/1674-1137/40/1/011001`.

[307] R. Aaij, et al., Observation of a narrow pentaquark state, $P_c(4312)^+$, and of two-peak structure of the $P_c(4450)^+$, Phys. Rev. Lett. 122 (2019) 222001. `arXiv:1904.03947`, `doi:10.1103/PhysRevLett.122.222001`.

[308] M. I. Eides, V. Yu. Petrov, M. V. Polyakov, Narrow nucleon-$\psi(2S)$ bound state and LHCb pentaquarks, Phys. Rev. D93 (2016) 054039. `arXiv:1512.00426`, `doi:10.1103/PhysRevD.93.054039`.

[309] R. Aaij, et al., Evidence for exotic hadron contributions to $\Lambda_b^0 \rightarrow J/\psi p\pi^-$ decays, Phys. Rev. Lett. 117 (2016) 082003, [Addendum: Phys. Rev. Lett. 118 (2017) 119901]. `arXiv:1606.06999`, `doi:10.1103/PhysRevLett.118.119901,10.1103/PhysRevLett.117.082003,10.1103/PhysRevLett.117.109902`.

[310] R. Aaij, et al., Search for weakly decaying b-flavored pentaquarks, Phys. Rev. D97 (2018) 032010. `arXiv:1712.08086`, `doi:10.1103/PhysRevD.97.032010`.

[311] R. Aaij, et al., Observation of the decay $\Lambda_b^0 \rightarrow \psi(2S)p\pi^-$, JHEP 08 (2018) 131. `arXiv:1806.08084`, `doi:10.1007/JHEP08(2018)131`.

[312] R. Aaij, et al., Observation of $\Lambda_b^0 \rightarrow \psi(2S)pK^-$ and $\Lambda_b^0 \rightarrow J/\psi\pi^+\pi^- pK^-$ decays and a measurement of the Λ_b^0 baryon mass, JHEP 05 (2016) 132. `arXiv:1603.06961`, `doi:10.1007/JHEP05(2016)132`.

[313] R. Aaij, et al., Observation of the decays $\Lambda_b^0 \rightarrow \chi_{c1}pK^-$ and $\Lambda_b^0 \rightarrow \chi_{c2}pK^-$, Phys. Rev. Lett. 119 (2017) 062001. `arXiv:1704.07900`, `doi:10.1103/PhysRevLett.119.062001`.

[314] Q. Wang, X.-H. Liu, Q. Zhao, Photoproduction of hidden charm pentaquark states $P_c^+(4380)$ and $P_c^+(4450)$, Phys. Rev. D92 (2015) 034022. `arXiv:1508.00339`, `doi:10.1103/PhysRevD.92.034022`.

[315] V. Kubarovsky, M. B. Voloshin, Search for Hidden-Charm Pentaquark with CLAS12`arXiv:1609.00050`.

[316] M. Karliner, J. L. Rosner, Photoproduction of Exotic Baryon Resonances, Phys. Lett. B752 (2016) 329. `arXiv:1508.01496`, `doi:10.1016/j.physletb.2015.11.068`.

[317] E. Ya. Paryev, Yu. T. Kiselev, The role of hidden-charm pentaquark resonance $P_c^+(4450)$ in J/ψ photoproduction on nuclei near threshold, Nucl. Phys. A978 (2018) 201. `arXiv:1810.01715`, `doi:10.1016/j.nuclphysa.2018.08.009`.

[318] Z. E. Meziani, et al., A Search for the LHCb Charmed 'Pentaquark' using Photo-Production of J/ψ at Threshold in Hall C at Jefferson Lab`arXiv:1609.00676`.

[319] A. N. Hiller Blin, C. Fernández-Ramírez, A. Jackura, V. Mathieu, V. I. Mokeev, A. Pilloni, A. P. Szczepaniak, Studying the $P_c(4450)$ reso-

nance in J/ψ photoproduction off protons, Phys. Rev. D94 (2016) 034002. arXiv:1606.08912, doi:10.1103/PhysRevD.94.034002.

[320] V. Kubarovsky, M. B. Voloshin, Formation of hidden-charm pentaquarks in photon-nucleon collisions, Phys. Rev. D92 (2015) 031502. arXiv:1508.00888, doi:10.1103/PhysRevD.92.031502.

[321] C. Fernández-Ramírez, A. N. H. Blin, A. Pilloni, Pentaquark photoproduction, J. Phys. Conf. Ser. 876 (2017) 012007. arXiv:1703.06928, doi:10.1088/1742-6596/876/1/012007.

[322] A. Ali, et al., First Measurement of Near-Threshold J/ψ Exclusive Photoproduction off the Proton, Phys. Rev. Lett. 123 (2019) 072001. arXiv:1905.10811, doi:10.1103/PhysRevLett.123.072001.

[323] B. Gittelman, K. M. Hanson, D. Larson, E. Loh, A. Silverman, G. Theodosiou, Photoproduction of the $\psi(3100)$ Meson at 11 GeV, Phys. Rev. Lett. 35 (1975) 1616. doi:10.1103/PhysRevLett.35.1616.

[324] U. Camerini, J. G. Learned, R. Prepost, C. M. Spencer, D. E. Wiser, W. Ash, R. L. Anderson, D. Ritson, D. Sherden, C. K. Sinclair, Photoproduction of the ψ Particles, Phys. Rev. Lett. 35 (1975) 483. doi:10.1103/PhysRevLett.35.483.

[325] S. J. Brodsky, E. Chudakov, P. Hoyer, J. M. Laget, Photoproduction of charm near threshold, Phys. Lett. B498 (2001) 23. arXiv:hep-ph/0010343, doi:10.1016/S0370-2693(00)01373-3.

[326] D. Kharzeev, H. Satz, A. Syamtomov, G. Zinovev, J/ψ-photoproduction and the gluon structure of the nucleon, Nucl. Phys. A661 (1999) 568. doi:10.1016/S0375-9474(99)85090-8.

[327] Z.-G. Wang, The magnetic moment of the $Z_c(3900)$ as an axialvector tetraquark state with QCD sum rules, Eur. Phys. J. C78 (2018) 297. arXiv:1712.05664, doi:10.1140/epjc/s10052-018-5794-0.

[328] U. Özdem, K. Azizi, Magnetic and quadrupole moments of the $Z_c(3900)$, Phys. Rev. D96 (2017) 074030. arXiv:1707.09612, doi:10.1103/PhysRevD.96.074030.

[329] G.-J. Wang, R. Chen, L. Ma, X. Liu, S.-L. Zhu, Magnetic moments of the hidden-charm pentaquark states, Phys. Rev. D94 (2016) 094018. arXiv:1605.01337, doi:10.1103/PhysRevD.94.094018.

[330] U. Özdem, K. Azizi, Electromagnetic multipole moments of the $P_c^+(4380)$ pentaquark in light-cone QCD, Eur. Phys. J. C78 (2018) 379. arXiv:1803.06831, doi:10.1140/epjc/s10052-018-5873-2.

[331] C. Hanhart, J. R. Peláez, G. Rios, Remarks on pole trajectories for resonances, Phys. Lett. B739 (2014) 375. arXiv:1407.7452, doi:10.1016/j.physletb.2014.11.011.

[332] D. V. Bugg, Reinterpreting several narrow 'resonances' as threshold cusps, Phys. Lett. B598 (2004) 8. arXiv:hep-ph/0406293, doi:10.1016/j.physletb.2004.07.047.

[333] D. V. Bugg, An Explanation of Belle states $Z_b(10610)$ and $Z_b(10650)$, Eur. Phys. Lett. 96 (2011) 11002. arXiv:1105.5492, doi:10.1209/0295-5075/96/11002.

[334] D.-Y. Chen, X. Liu, $Z_b(10610)$ and $Z_b(10650)$ structures produced by the initial single pion emission in the $\Upsilon(5S)$ decays, Phys. Rev. D84 (2011) 094003. arXiv:1106.3798, doi:10.1103/PhysRevD.84.094003.

[335] D.-Y. Chen, X. Liu, Predicted charged charmonium-like structures in the hidden-charm dipion decay of higher charmonia, Phys. Rev. D84 (2011) 034032. arXiv:1106.5290, doi:10.1103/PhysRevD.84.034032.

[336] D.-Y. Chen, X. Liu, T. Matsuki, Charged bottomonium-like structures in the hidden-bottom dipion decays of $\Upsilon(11020)$, Phys. Rev. D84 (2011) 074032. arXiv:1108.4458, doi:10.1103/PhysRevD.84.074032.

[337] D.-Y. Chen, X. Liu, T. Matsuki, Reproducing the $Z_c(3900)$ structure through the initial-single-pion-emission mechanism, Phys. Rev. D88 (2013) 036008. arXiv:1304.5845, doi:10.1103/PhysRevD.88.036008.

[338] E. S. Swanson, Z_b and Z_c Exotic States as Coupled Channel Cusps, Phys. Rev. D91 (2015) 034009. arXiv:1409.3291, doi:10.1103/PhysRevD.91.034009.

[339] F.-K. Guo, C. Hanhart, Q. Wang, Q. Zhao, Could the near-threshold XYZ states be simply kinematic effects?, Phys. Rev. D91 (2015) 051504. arXiv:1411.5584, doi:10.1103/PhysRevD.91.051504.

[340] E. S. Swanson, Cusps and Exotic Charmonia, Int. J. Mod. Phys. E25 (2016) 1642010. arXiv:1504.07952, doi:10.1142/S0218301316420106.

[341] Q. Wang, C. Hanhart, Q. Zhao, Systematic study of the singularity mechanism in heavy quarkonium decays, Phys. Lett. B725 (2013) 106. arXiv:1305.1997, doi:10.1016/j.physletb.2013.06.049.

[342] A. P. Szczepaniak, Triangle Singularities and XYZ Quarkonium Peaks, Phys. Lett. B747 (2015) 410. arXiv:1501.01691, doi:10.1016/j.physletb.2015.06.029.

[343] Q.-R. Gong, J.-L. Pang, Y.-F. Wang, H.-Q. Zheng, The $Z_c(3900)$ peak does not come from the "triangle singularity", Eur. Phys. J. C78 (2018) 276. arXiv:1612.08159, doi:10.1140/epjc/s10052-018-5690-7.

[344] E. van Beveren, G. Rupp, J. Segovia, A very broad $X(4260)$ and the resonance parameters of the $\psi(3D)$ vector charmonium state, Phys. Rev. Lett. 105 (2010) 102001. arXiv:1005.1010, doi:10.1103/PhysRevLett.105.102001.

[345] J.-M. Richard, An introduction to the quark model, in: Ferrara International School Niccol Cabeo 2012: Hadronic spectroscopy Ferrara, Italy, May 21-26, 2012, 2012. arXiv:1205.4326.

[346] J. Ferretti, G. Galatá, E. Santopinto, Interpretation of the $X(3872)$ as a charmonium state plus an extra component due to the coupling to the meson-meson continuum, Phys. Rev. C88 (2013) 015207. arXiv:1302.6857, doi:10.1103/PhysRevC.88.015207.

[347] J. Ferretti, E. Santopinto, Higher mass bottomonia, Phys. Rev. D90 (2014) 094022. arXiv:1306.2874, doi:10.1103/PhysRevD.90.094022.

[348] V. O. Galkin, A. Yu. Mishurov, R. N. Faustov, Meson masses in the relativistic quark model, Sov. J. Nucl. Phys. 55 (1992) 1207, [Yad. Fiz. 55, 2175 (1992)].

[349] D. Ebert, R. N. Faustov, V. O. Galkin, Quark-antiquark potential with retardation and radiative contributions and the heavy quarkonium mass spectra, Phys. Rev. D62 (2000) 034014. arXiv:hep-ph/9911283, doi:10.1103/PhysRevD.62.034014.

[350] D. Ebert, R. N. Faustov, V. O. Galkin, Spectroscopy and Regge trajectories of heavy quarkonia in the relativistic quark model, Phys. Atom. Nucl. 76 (2013) 1554. doi:10.1134/S1063778813110057.

[351] G. S. Bali, QCD forces and heavy quark bound states, Phys. Rept. 343 (2001) 1. arXiv:hep-ph/0001312, doi:10.1016/S0370-1573(00)00079-X.

[352] A. Bazavov, et al., Nonperturbative QCD simulations with 2+1 flavors of improved staggered quarks, Rev. Mod. Phys. 82 (2010) 1349. `arXiv:0903.3598`, `doi:10.1103/RevModPhys.82.1349`.

[353] E. Eichten, K. Gottfried, T. Kinoshita, K. D. Lane, T.-M. Yan, Charmonium: The Model, Phys. Rev. D17 (1978) 3090, [Erratum: Phys. Rev. D21 (1980) 313]. `doi:10.1103/PhysRevD.17.3090,10.1103/physrevd.21.313.2`.

[354] Y. Nambu, QCD and the string model, Phys. Lett. B80 (1979) 372. `doi:10.1016/0370-2693(79)91193-6`.

[355] N. Brambilla, M. Groher, H. E. Martinez, A. Vairo, Effective string theory and the long-range relativistic corrections to the quark-antiquark potential, Phys. Rev. D90 (2014) 114032. `arXiv:1407.7761`, `doi:10.1103/PhysRevD.90.114032`.

[356] E. Eichten, F. Feinberg, Spin dependent forces in QCD, Phys. Rev. D23 (1981) 2724. `doi:10.1103/PhysRevD.23.2724`.

[357] D. Gromes, Spin Dependent Potentials in QCD and the Correct Long Range Spin Orbit Term, Z. Phys. C26 (1984) 401. `doi:10.1007/BF01452566`.

[358] A. Barchielli, N. Brambilla, G. M. Prosperi, Relativistic corrections to the quark-antiquark potential and the quarkonium spectrum, Nuovo Cim. A103 (1990) 59. `doi:10.1007/BF02902620`.

[359] Y. Koma, M. Koma, H. Wittig, Nonperturbative determination of the QCD potential at $O(1/m)$, Phys. Rev. Lett. 97 (2006) 122003. `arXiv:hep-lat/0607009`, `doi:10.1103/PhysRevLett.97.122003`.

[360] Y. Koma, M. Koma, Spin-dependent potentials from lattice QCD, Nucl. Phys. B769 (2007) 79. `arXiv:hep-lat/0609078`, `doi:10.1016/j.nuclphysb.2007.01.033`.

[361] Y. Koma, M. Koma, H. Wittig, Relativistic corrections to the static potential at $O(1/m)$ and $O(1/m^2)$, PoS LATTICE2007 (2007) 111. `arXiv:0711.2322`, `doi:10.22323/1.042.0111`.

[362] Yu. A. Simonov, Nonperturbative dynamics of heavy quarkonia, Nucl. Phys. B324 (1989) 67. `doi:10.1016/0550-3213(89)90181-8`.

[363] N. Brambilla, A. Vairo, Heavy quarkonia: Wilson area law, stochastic vacuum model and dual QCD, Phys. Rev. D55 (1997) 3974. `arXiv:hep-ph/9606344`, `doi:10.1103/PhysRevD.55.3974`.

[364] M. Baker, J. S. Ball, N. Brambilla, A. Vairo, Nonperturbative evaluation of a field correlator appearing in the heavy quarkonium system, Phys. Lett. B389 (1996) 577. `arXiv:hep-ph/9609233`, `doi:10.1016/S0370-2693(96)01297-X`.

[365] N. Brambilla, A. Vairo, Quark confinement and the hadron spectrum, in: Strong interactions at low and intermediate energies. Proceedings, 13th Annual Hampton University Graduate Studies, HUGS'98, Newport News, USA, May 26-June 12, 1998, p. 151. `arXiv:hep-ph/9904330`.

[366] A. Di Giacomo, H. G. Dosch, V. I. Shevchenko, Yu. A. Simonov, Field correlators in QCD: Theory and applications, Phys. Rept. 372 (2002) 319. `arXiv:hep-ph/0007223`, `doi:10.1016/S0370-1573(02)00140-0`.

[367] A. M. Badalian, A. V. Nefediev, Yu. A. Simonov, Spin-dependent interactions in quarkonia, Phys. Rev. D78 (2008) 114020. `arXiv:0811.2599`, `doi:10.1103/PhysRevD.78.114020`.

[368] D. A. Varshalovich, A. N. Moskalev, V. K. Khersonsky, Quantum Theory of Angular Momentum: Irreducible Tensors, Spherical Harmonics, Vector Coupling Coefficients, 3nj Symbols, World Scientific, Singapore, 1988.

[369] L. Ya. Glozman, Chiral multiplets of excited mesons, Phys. Lett. B587 (2004) 69. `arXiv:hep-ph/0312354`, `doi:10.1016/j.physletb.2004.02.066`.

[370] L. Ya. Glozman, Restoration of chiral and $U(1)_A$ symmetries in excited hadrons, Phys. Rept. 444 (2007) 1. `arXiv:hep-ph/0701081`, `doi:10.1016/j.physrep.2007.04.001`.

[371] L. Ya. Glozman, A. V. Nefediev, Chiral symmetry, the angular content of the vector current in QED and QCD, and the holographic description of hadrons, Phys. Rev. D80 (2009) 057901. `arXiv:0904.3067`, `doi:10.1103/PhysRevD.80.057901`.

[372] L. Ya. Glozman, A. V. Nefediev, Chiral symmetry and the string description of excited hadrons, Phys. Rev. D76 (2007) 096004. `arXiv:0704.2673`, `doi:10.1103/PhysRevD.76.096004`.

[373] K. Heikkila, S. Ono, N. A. Tornqvist, Heavy $c\bar{c}$ and $b\bar{b}$ quarkonium states and unitarity effects, Phys. Rev. D29 (1984) 110, [Erratum: Phys. Rev. D29 (1984) 2136]. `doi:10.1103/PhysRevD.29.2136,10.1103/PhysRevD.29.110`.

[374] F. J. Llanes-Estrada, $Y(4260)$ and possible charmonium assignment, Phys. Rev. D72 (2005) 031503. `arXiv:hep-ph/0507035`, `doi:10.1103/PhysRevD.72.031503`.

[375] M. Shah, A. Parmar, P. C. Vinodkumar, Leptonic and digamma decay properties of S-wave quarkonia states, Phys. Rev. D86 (2012) 034015. `arXiv:1203.6184`, `doi:10.1103/PhysRevD.86.034015`.

[376] A. M. Badalian, B. L. G. Bakker, Leptonic widths of high ψ-resonances in a unitary coupled-channel model, Phys. Rev. D96 (2017) 014030. `arXiv:1702.06374`, `doi:10.1103/PhysRevD.96.014030`.

[377] H.-F. Fu, L. Jiang, Coupled-channel-induced $S-D$ mixing of Charmonia and testing possible assignments for $Y(4260)$ and $Y(4360)$, Eur. Phys. J. C79 (2019) 460. `arXiv:1812.00179`, `doi:10.1140/epjc/s10052-019-6976-0`.

[378] C. Bernard, T. Burch, C. E. DeTar, Z.-W. Fu, S. A. Gottlieb, E. Gregory, U. M. Heller, J. Osborn, R. L. Sugar, D. Toussaint, Static hybrid quarkonium potential with improved staggered quarks, Nucl. Phys. Proc. Suppl. 119 (2003) 598. `arXiv:hep-lat/0209051`, `doi:10.1016/S0920-5632(03)01632-3`.

[379] A. Duncan, E. Eichten, H. Thacker, String breaking in four-dimensional lattice QCD, Phys. Rev. D63 (2001) 111501. `arXiv:hep-lat/0011076`, `doi:10.1103/PhysRevD.63.111501`.

[380] G. S. Bali, H. Neff, T. Duessel, T. Lippert, K. Schilling, Observation of string breaking in QCD, Phys. Rev. D71 (2005) 114513. `arXiv:hep-lat/0505012`, `doi:10.1103/PhysRevD.71.114513`.

[381] A. M. Badalian, B. L. G. Bakker, Yu. A. Simonov, Light meson radial Regge trajectories, Phys. Rev. D66 (2002) 034026. `arXiv:hep-ph/0204088`, `doi:10.1103/PhysRevD.66.034026`.

[382] Yu. S. Kalashnikova, A. V. Nefediev, Yu. A. Simonov, QCD string in light-light and heavy-light mesons, Phys. Rev. D64 (2001) 014037. `arXiv:hep-ph/0103274`, `doi:10.1103/PhysRevD.64.014037`.

[383] Yu. A. Simonov, Nonperturbative corrections to the quark selfenergy, Phys. Lett. B515 (2001) 137. `arXiv:hep-ph/0105141`, `doi:10.1016/S0370-2693(01)00876-0`.

[384] E. Eichten, K. Gottfried, T. Kinoshita, K. D. Lane, T.-M. Yan, Interplay of Confinement and Decay in the Spectrum of Charmonium, Phys. Rev. Lett. 36 (1976) 500. `doi:10.1103/PhysRevLett.36.500`.

[385] E. Eichten, K. Gottfried, T. Kinoshita, K. D. Lane, T.-M. Yan, Effects of Coupling to Decay Channels in the Spectroscopy of the New Resonances, preprint: CLNS-316, 1975.

[386] E. Eichten, K. Gottfried, T. Kinoshita, K. D. Lane, T.-M. Yan, Charmonium: Comparison with experiment, Phys. Rev. D21 (1980) 203. `doi:10.1103/PhysRevD.21.203`.

[387] E. van Beveren, C. Dullemond, G. Rupp, Spectrum and strong decays of charmonium, Phys. Rev. D21 (1980) 772, [Erratum: Phys. Rev. D22 (1980) 787]. `doi:10.1103/PhysRevD.21.772,10.1103/physrevd.22.787.2`.

[388] N. A. Tornqvist, The meson mass spectrum and unitarity, Annals Phys. 123 (1979) 1. `doi:10.1016/0003-4916(79)90262-8`.

[389] E. van Beveren, G. Rupp, T. A. Rijken, C. Dullemond, Radial spectra and hadronic decay widths of light and heavy mesons, Phys. Rev. D27 (1983) 1527. `doi:10.1103/PhysRevD.27.1527`.

[390] S. Ono, N. A. Tornqvist, Continuum mixing and coupled channel effects in $c\bar{c}$ and $b\bar{b}$ quarkonium, Z. Phys. C23 (1984) 59. `doi:10.1007/BF01558041`.

[391] N. A. Tornqvist, P. Zenczykowski, Ground state baryon mass splittings from unitarity, Phys. Rev. D29 (1984) 2139. `doi:10.1103/PhysRevD.29.2139`.

[392] P. Zenczykowski, Baryon spectroscopy: Symmetries, symmetry breaking and hadronic loops, Annals Phys. 169 (1986) 453. `doi:10.1016/0003-4916(86)90176-4`.

[393] P. Geiger, N. Isgur, Quenched approximation in the quark model, Phys. Rev. D41 (1990) 1595. `doi:10.1103/PhysRevD.41.1595`.

[394] P. Geiger, N. Isgur, How the Okubo-Zweig-Iizuka rule evades large loop corrections, Phys. Rev. Lett. 67 (1991) 1066. `doi:10.1103/PhysRevLett.67.1066`.

[395] P. Geiger, N. Isgur, Reconciling the OZI rule with strong pair creation, Phys. Rev. D44 (1991) 799. `doi:10.1103/PhysRevD.44.799`.

[396] P. Geiger, N. Isgur, When can hadronic loops scuttle the OZI rule?, Phys. Rev. D47 (1993) 5050. `doi:10.1103/PhysRevD.47.5050`.

[397] D. Morel, S. Capstick, Baryon meson loop effects on the spectrum of nonstrange baryons`arXiv:nucl-th/0204014`.

[398] E. van Beveren, G. Rupp, Nonperturbative scalar meson resonances with open charm and beauty, in: CFIF Workshop on Time Asymmetric Quantum Theory: The Theory of Resonances Lisbon, Portugal, July 23-26, 2003. `arXiv:hep-ph/0312078`.

[399] E. van Beveren, G. Rupp, Continuum bound states K_L, $D_1(2420)$, $D_{s1}(2536)$ and their partners K_S, $D_1(2400)$, $D^*_{sJ}(2463)$, Eur. Phys. J. C32 (2004) 493. `arXiv:hep-ph/0306051`, `doi:10.1140/epjc/s2003-01465-0`.

[400] E. van Beveren, G. Rupp, Observed $D_s(2317)$ and tentative $D(2030)$ as the charmed cousins of the light scalar nonet, Phys. Rev. Lett. 91 (2003) 012003. `arXiv:hep-ph/0305035`, `doi:10.1103/PhysRevLett.91.012003`.

[401] E. van Beveren, G. Rupp, Multichannel calculation for D^*_s vector states and the $D_s(2632)$ resonance, Phys. Rev. Lett. 93 (2004) 202001. `arXiv:hep-ph/0407281`, `doi:10.1103/PhysRevLett.93.202001`.

[402] E. van Beveren, G. Rupp, Classification of the scalar mesons: A strange pole expedition into charm and beauty territory, Mod. Phys. Lett. A19 (2004) 1949. `arXiv:hep-ph/0406242`, `doi:10.1142/S0217732304015208`.

[403] D. S. Hwang, D.-W. Kim, Mass of $D^*_{sJ}(2317)$ and coupled channel effect, Phys. Lett. B601 (2004) 137. `arXiv:hep-ph/0408154`, `doi:10.1016/j.physletb.2004.09.040`.

[404] C. Amsler, N. A. Tornqvist, Mesons beyond the naive quark model, Phys. Rept. 389 (2004) 61. `doi:10.1016/j.physrep.2003.09.003`.

[405] Yu. S. Kalashnikova, Coupled-channel model for charmonium levels and an option for $X(3872)$, Phys. Rev. D72 (2005) 034010. `arXiv:hep-ph/0506270`, `doi:10.1103/PhysRevD.72.034010`.

[406] E. S. Swanson, Unquenching the quark model and screened potentials, J. Phys. G31 (2005) 845. `arXiv:hep-ph/0504097`, `doi:10.1088/0954-3899/31/7/025`.

[407] E. van Beveren, J. E. G. N. Costa, F. Kleefeld, G. Rupp, From the κ via the $D^*_{s0}(2317)$ to the χ_{c0}: Connecting light and heavy scalar mesons, Phys. Rev. D74 (2006) 037501. `arXiv:hep-ph/0509351`, `doi:10.1103/PhysRevD.74.037501`.

[408] E. J. Eichten, K. Lane, C. Quigg, New states above charm threshold, Phys. Rev. D73 (2006) 014014, [Erratum: Phys. Rev.D73,079903(2006)]. `arXiv:hep-ph/0511179`, `doi:10.1103/PhysRevD.73.014014,10.1103/PhysRevD.73.079903`.

[409] G. Rupp, E. van Beveren, Multichannel calculation of the very narrow $D^*_{s0}(2317)$ and the very broad $D^*_0(2300 - 2400)$, Eur. Phys. J. A31 (2007) 698. `arXiv:hep-ph/0610188`, `doi:10.1140/epja/i2006-10269-3`.

[410] E. van Beveren, G. Rupp, New BABAR state $D_{sJ}(2860)$ as the first radial excitation of the $D^*_{s0}(2317)$, Phys. Rev. Lett. 97 (2006) 202001. `arXiv:hep-ph/0606110`, `doi:10.1103/PhysRevLett.97.202001`.

[411] E. van Beveren, G. Rupp, Is the $Y(4260)$ just a coupled-channel signal?`arXiv:hep-ph/0605317`.

[412] C. Hanhart, Yu. S. Kalashnikova, A. E. Kudryavtsev, A. V. Nefediev, Reconciling the $X(3872)$ with the near-threshold enhancement in the $D^0\bar{D}^{*0}$ final state, Phys. Rev. D76 (2007) 034007. `arXiv:0704.0605`, `doi:10.1103/PhysRevD.76.034007`.

[413] Yu. S. Kalashnikova, $X(3872)$ as a near-threshold state in the coupled-channel model for charmonia levels, AIP Conf. Proc. 892 (2007) 318. `doi:10.1063/1.2714405`.

[414] M. R. Pennington, D. J. Wilson, Decay channels and charmonium mass-shifts, Phys. Rev. D76 (2007) 077502. `arXiv:0704.3384`, `doi:10.1103/PhysRevD.76.077502`.

[415] Y. Lu, M. N. Anwar, B.-S. Zou, How large is the contribution of excited mesons in coupled-channel effects?, Phys. Rev. D95 (2017) 034018. `arXiv:1701.00692`, `doi:10.1103/PhysRevD.95.034018`.

[416] Y. Lu, M. N. Anwar, B.-S. Zou, Coupled-Channel Effects for the Bottomonium with Realistic Wave Functions, Phys. Rev. D94 (2016) 034021. `arXiv:1606.06927`, `doi:10.1103/PhysRevD.94.034021`.

[417] B. Aubert, et al., Observation of a narrow meson decaying to $D^+_s\pi^0$ at a mass of 2.32 GeV/c^2, Phys. Rev. Lett. 90 (2003) 242001. `arXiv:hep-ex/0304021`, `doi:10.1103/PhysRevLett.90.242001`.

[418] D. Besson, et al., Observation of a narrow resonance of mass 2.46 GeV/c^2 decaying to $D^{*+}_s\pi^0$ and confirmation of the $D^*_{sJ}(2317)$ state, Phys. Rev. D68 (2003) 032002, [Erratum: Phys. Rev. D75 (2007) 119908]. `arXiv:hep-ex/0305100`, `doi:10.1103/PhysRevD.68.032002,10.1103/PhysRevD.75.119908`.

[419] S. Godfrey, R. Kokoski, Properties of P-wave mesons with one heavy quark, Phys. Rev. D43 (1991) 1679. `doi:10.1103/PhysRevD.43.1679`.

[420] F. E. Close, E. S. Swanson, Dynamics and decay of heavy-light hadrons, Phys. Rev. D72 (2005) 094004. `arXiv:hep-ph/0505206`,

     `doi:10.1103/PhysRevD.72.094004`.

[421] T. Barnes, E. S. Swanson, Hadron loops: General theorems and application to charmonium, Phys. Rev. C77 (2008) 055206. `arXiv:0711.2080`, `doi:10.1103/PhysRevC.77.055206`.

[422] L. Micu, Decay rates of meson resonances in a quark model, Nucl. Phys. B10 (1969) 521. `doi:10.1016/0550-3213(69)90039-X`.

[423] A. Le Yaouanc, L. Oliver, O. Pene, J. C. Raynal, Naive quark pair creation model of strong interaction vertices, Phys. Rev. D8 (1973) 2223. `doi:10.1103/PhysRevD.8.2223`.

[424] A. Le Yaouanc, L. Oliver, O. Pene, J. C. Raynal, Naive quark pair creation model and baryon decays, Phys. Rev. D9 (1974) 1415. `doi:10.1103/PhysRevD.9.1415`.

[425] A. Le Yaouanc, L. Oliver, O. Pene, J. C. Raynal, Resonant partial-wave amplitudes in $\pi N \to \pi\pi N$ according to the naive quark-pair-creation model, Phys. Rev. D11 (1975) 1272. `doi:10.1103/PhysRevD.11.1272`.

[426] J. W. Alcock, M. J. Burfitt, W. N. Cottingham, A string breaking model of heavy meson decays, Z. Phys. C25 (1984) 161. `doi:10.1007/BF01557474`.

[427] S. Kumano, V. R. Pandharipande, Decay of mesons in flux tube quark model, Phys. Rev. D38 (1988) 146. `doi:10.1103/PhysRevD.38.146`.

[428] P. Geiger, E. S. Swanson, Distinguishing among strong decay models, Phys. Rev. D50 (1994) 6855. `arXiv:hep-ph/9405238`, `doi:10.1103/PhysRevD.50.6855`.

[429] H. G. Blundell, S. Godfrey, $\xi(2220)$ reexamined: Strong decays of the 1^3F_2 and 1^3F_4 $s\bar{s}$ mesons, Phys. Rev. D53 (1996) 3700. `arXiv:hep-ph/9508264`, `doi:10.1103/PhysRevD.53.3700`.

[430] A. Le Yaouanc, L. Oliver, O. Pene, J. C. Raynal, Strong decays of $\psi''(4.028)$ as a radial excitation of charmonium, Phys. Lett. 71B (1977) 397. `doi:10.1016/0370-2693(77)90250-7`.

[431] A. Le Yaouanc, L. Oliver, O. Pene, J. C. Raynal, Why is $\psi''(4.414)$ so narrow?, Phys. Lett. 72B (1977) 57. `doi:10.1016/0370-2693(77)90062-4`.

[432] P. R. Page, Excited charmonium decays by flux tube breaking and the ψ' anomaly at CDF, Nucl. Phys. B446 (1995) 189. `arXiv:hep-ph/9502204`, `doi:10.1016/0550-3213(95)00171-N`.

[433] R. Kokoski, N. Isgur, Meson decays by flux tube breaking, Phys. Rev. D35 (1987) 907. `doi:10.1103/PhysRevD.35.907`.

[434] E. S. Ackleh, T. Barnes, E. S. Swanson, On the mechanism of open flavor strong decays, Phys. Rev. D54 (1996) 6811. `arXiv:hep-ph/9604355`, `doi:10.1103/PhysRevD.54.6811`.

[435] T. Barnes, F. E. Close, P. R. Page, E. S. Swanson, Higher quarkonia, Phys. Rev. D55 (1997) 4157. `arXiv:hep-ph/9609339`, `doi:10.1103/PhysRevD.55.4157`.

[436] J. Ferretti, G. Galata, E. Santopinto, A. Vassallo, Bottomonium self-energies due to the coupling to the meson-meson continuum, Phys. Rev. C86 (2012) 015204. `doi:10.1103/PhysRevC.86.015204`.

[437] I. K. Hammer, C. Hanhart, A. V. Nefediev, Remarks on meson loop effects on quark models, Eur. Phys. J. A52 (2016) 330. `arXiv:1607.06971`, `doi:10.1140/epja/i2016-16330-8`.

[438] B. Silvestre-Brac, C. Gignoux, Unitary effects in spin orbit splitting of P-wave baryons, Phys. Rev. D43 (1991) 3699. `doi:10.1103/PhysRevD.43.3699`.

[439] P. Geiger, N. Isgur, Strange hadronic loops of the proton: A quark model calculation, Phys. Rev. D55 (1997) 299. `arXiv:hep-ph/9610445`, `doi:10.1103/PhysRevD.55.299`.

[440] N. A. Tornqvist, M. Roos, Resurrection of the σ meson, Phys. Rev. Lett. 76 (1996) 1575. `arXiv:hep-ph/9511210`, `doi:10.1103/PhysRevLett.76.1575`.

[441] M. Boglione, M. R. Pennington, Unquenching the scalar glueball, Phys. Rev. Lett. 79 (1997) 1998. `arXiv:hep-ph/9703257`, `doi:10.1103/PhysRevLett.79.1998`.

[442] E. van Beveren, G. Rupp, Reconciling the light scalar mesons with Breit-Wigner resonances as well as the quark model, Int. J. Theor. Phys. Group Theor. Nonlin. Opt. 11 (2006) 179. `arXiv:hep-ph/0304105`.

[443] E. van Beveren, D. V. Bugg, F. Kleefeld, G. Rupp, The nature of σ, κ, $a_0(980)$ and $f_0(980)$, Phys. Lett. B641 (2006) 265. `arXiv:hep-ph/0606022`, `doi:10.1016/j.physletb.2006.08.051`.

[444] E. van Beveren, G. Rupp, Meson-meson interactions and Regge propagators, Annals Phys. 324 (2009) 1620. `arXiv:0809.1149`, `doi:10.1016/j.aop.2009.03.013`.

[445] G. Rupp, E. van Beveren, S. Coito, No serious meson spectroscopy without scattering, Acta Phys. Polon. Supp. 8 (2015) 139. `arXiv:1502.05250`, `doi:10.5506/APhysPolBSupp.8.139`.

[446] G. Rupp, S. Coito, E. van Beveren, Meson spectroscopy: too much excitement and too few excitations, Acta Phys. Polon. Supp. 5 (2012) 1007. `arXiv:1209.1475`, `doi:10.5506/APhysPolBSupp.5.1007`.

[447] T. Wolkanowski, F. Giacosa, D. H. Rischke, $a_0(980)$ revisited, Phys. Rev. D93 (2016) 014002. `arXiv:1508.00372`, `doi:10.1103/PhysRevD.93.014002`.

[448] A. A. Logunov, A. N. Tavkhelidze, Quasioptical approach in quantum field theory, Nuovo Cim. 29 (1963) 380. `doi:10.1007/BF02750359`.

[449] A. P. Martynenko, R. N. Faustov, Relativistic reduced mass and quasipotential equation, Theor. Math. Phys. 64 (1985) 765, [Teor. Mat. Fiz. 64 (1985) 179]. `doi:10.1007/BF01017955`.

[450] I. V. Danilkin, Yu. A. Simonov, Dynamical origin and the pole structure of $X(3872)$, Phys. Rev. Lett. 105 (2010) 102002. `arXiv:1006.0211`, `doi:10.1103/PhysRevLett.105.102002`.

[451] R. F. Lebed, E. S. Swanson, Quarkonium h states as arbiters of exoticity, Phys. Rev. D96 (2017) 056015. `arXiv:1705.03140`, `doi:10.1103/PhysRevD.96.056015`.

[452] A. Vairo, Quarkonia: a theoretical frame, in: 3rd International Workshop on Charm Physics (Charm 2009) Leimen, Germany, May 20-22, 2009. `arXiv:0912.4422`.

[453] F. E. Close, P. R. Page, The Production and decay of hybrid mesons by flux tube breaking, Nucl. Phys. B443 (1995) 233–254. `arXiv:hep-ph/9411301`, `doi:10.1016/0550-3213(95)00085-7`.

[454] T. Barnes, F. E. Close, E. S. Swanson, Hybrid and conventional mesons in the flux tube model: Numerical studies and their phenomenological

implications, Phys. Rev. D52 (1995) 5242. `arXiv:hep-ph/9501405`, `doi:10.1103/PhysRevD.52.5242`.

[455] S. R. Cotanch, F. J. Llanes-Estrada, Relativistic many body approach to exotic and charmed hybrid mesons, Nucl. Phys. A689 (2001) 481. `doi:10.1016/S0375-9474(01)00886-7`.

[456] I. J. General, S. R. Cotanch, F. J. Llanes-Estrada, QCD Coulomb gauge approach to hybrid mesons, Eur. Phys. J. C51 (2007) 347. `arXiv:hep-ph/0609115`, `doi:10.1140/epjc/s10052-007-0298-3`.

[457] F. J. Llanes-Estrada, S. R. Cotanch, Many body Coulomb gauge exotic and charmed hybrids, Phys. Lett. B504 (2001) 15. `arXiv:hep-ph/0008337`, `doi:10.1016/S0370-2693(01)00290-8`.

[458] E. Abreu, P. Bicudo, Glueball and hybrid mass and decay with string tension below Casimir scaling, J. Phys. G34 (2007) 195207. `arXiv:hep-ph/0508281`, `doi:10.1088/0954-3899/34/2/003`.

[459] D. Horn, J. Mandula, Model of mesons with constituent gluons, Phys. Rev. D17 (1978) 898. `doi:10.1103/PhysRevD.17.898`.

[460] F. Iddir, S. Safir, O. Pene, Do 1^- $c\bar{c}g$ hybrid mesons exist, do they mix with charmonium?, Phys. Lett. B433 (1998) 125. `arXiv:hep-ph/9803470`, `doi:10.1016/S0370-2693(98)00603-0`.

[461] Yu. A. Simonov, QCD and topics in hadron physics, in: QCD: Perturbative or nonperturbative? Proceedings, 17th Autumn School, Lisbon, Portugal, September 29-October 4, 1999, p. 60. `arXiv:hep-ph/9911237`.
URL `http://www.slac.stanford.edu/spires/find/books/www?cl=QCD161:A85:1999`

[462] Yu. A. Simonov, Mixing of meson, hybrid, and glueball states, Phys. Atom. Nucl. 64 (2001) 1876, [Yad. Fiz.64 (2001) 1959]. `arXiv:hep-ph/0110033`, `doi:10.1134/1.1414936`.

[463] Yu. S. Kalashnikova, D. S. Kuzmenko, Hybrid adiabatic potentials in the QCD string model, Phys. Atom. Nucl. 66 (2003) 955, [Yad. Fiz. 66 (2003) 988]. `arXiv:hep-ph/0203128`, `doi:10.1134/1.1577918`.

[464] F. Buisseret, V. Mathieu, C. Semay, B. Silvestre-Brac, Excited flux tube from $q\bar{q}g$ hybrid mesons, Eur. Phys. J. A32 (2007) 123. `arXiv:hep-ph/0703020`, `doi:10.1140/epja/i2007-10379-4`.

[465] Yu. S. Kalashnikova, A. V. Nefediev, Spectra and decays of hybrid charmonia, Phys. Rev. D77 (2008) 054025. `arXiv:0801.2036`, `doi:10.1103/PhysRevD.77.054025`.

[466] Yu. S. Kalashnikova, A. V. Nefediev, QCD string in excited heavy-light mesons and heavy-quark hybrids, Phys. Rev. D94 (2016) 114007. `arXiv:1611.10066`, `doi:10.1103/PhysRevD.94.114007`.

[467] E. Braaten, How the Z_c(3900) Reveals the Spectra of Quarkonium Hybrid and Tetraquarks, Phys. Rev. Lett. 111 (2013) 162003. `arXiv:1305.6905`, `doi:10.1103/PhysRevLett.111.162003`.

[468] E. Braaten, C. Langmack, D. H. Smith, Selection Rules for Hadronic Transitions of XYZ Mesons, Phys. Rev. Lett. 112 (2014) 222001. `arXiv:1401.7351`, `doi:10.1103/PhysRevLett.112.222001`.

[469] E. Braaten, C. Langmack, D. H. Smith, Born-Oppenheimer Approximation for the XYZ Mesons, Phys. Rev. D90 (2014) 014044. `arXiv:1402.0438`, `doi:10.1103/PhysRevD.90.014044`.

[470] N. Brambilla, G. Krein, J. Tarrús Castellà, A. Vairo, Born-Oppenheimer approximation in an effective field theory language, Phys. Rev. D97 (2018) 016016. `arXiv:1707.09647`, `doi:10.1103/PhysRevD.97.016016`.

[471] J. Soto, Heavy Quarkonium Hybrids, Nucl. Part. Phys. Proc. 294 (2018) 87. `arXiv:1709.08038`, `doi:10.1016/j.nuclphysbps.2018.03.020`.

[472] N. Brambilla, W. K. Lai, J. Segovia, J. Tarrús Castellà, A. Vairo, Spin structure of heavy-quark hybrids, Phys. Rev. D99 (2019) 014017. `arXiv:1805.07713`, `doi:10.1103/PhysRevD.99.014017`.

[473] C. Michael, Hybrid mesons from the lattice`arXiv:hep-ph/0308293`.

[474] Y. Liu, X.-Q. Luo, Estimate of the charmed 0^{--} hybrid meson spectrum from quenched lattice QCD, Phys. Rev. D73 (2006) 054510. `arXiv:hep-lat/0511015`, `doi:10.1103/PhysRevD.73.054510`.

[475] X.-Q. Luo, Y. Liu, Gluonic excitation of non-exotic hybrid charmonium from lattice QCD, Phys. Rev. D74 (2006) 034502, [Erratum: Phys. Rev. D74 (2006) 039902]. `arXiv:hep-lat/0512044`, `doi:10.1103/PhysRevD.74.034502,10.1103/PhysRevD.74.039902`.

[476] K. J. Juge, J. Kuti, C. J. Morningstar, Ab initio study of hybrid $\bar{b}bg$ mesons, Phys. Rev. Lett. 82 (1999) 4400. `arXiv:hep-ph/9902336`, `doi:10.1103/PhysRevLett.82.4400`.

[477] X. Liao, T. Manke, Relativistic bottomonium spectrum from anisotropic lattices, Phys. Rev. D65 (2002) 074508. `arXiv:hep-lat/0111049`, `doi:10.1103/PhysRevD.65.074508`.

[478] N. Isgur, J. E. Paton, Flux-tube model for hadrons in QCD, Phys. Rev. D31 (1985) 2910. `doi:10.1103/PhysRevD.31.2910`.

[479] F. Buisseret, V. Mathieu, Hybrid mesons and auxiliary fields, Eur. Phys. J. A29 (2006) 343. `arXiv:hep-ph/0607083`, `doi:10.1140/epja/i2006-10090-0`.

[480] Yu. S. Kalashnikova, Exotic hybrids and their nonexotic counterparts, Z. Phys. C62 (1994) 323. `doi:10.1007/BF01560246`.

[481] N. Isgur, R. Kokoski, J. Paton, Gluonic excitations of mesons: Why they are missing and where to find them, Phys. Rev. Lett. 54 (1985) 869, [AIP Conf. Proc.132 (1985) 242]. `doi:10.1103/PhysRevLett.54.869,10.1063/1.35357`.

[482] X. Li, M. B. Voloshin, Suppression of the S-wave production of $(3/2)^+ + (1/2)^-$ heavy meson pairs in e^+e^- annihilation, Phys. Rev. D88 (2013) 034012. `arXiv:1307.1072`, `doi:10.1103/PhysRevD.88.034012`.

[483] F. E. Close, New metastable charmonium and the ψ' anomaly at CDF, Phys. Lett. B342 (1995) 369. `arXiv:hep-ph/9409203`, `doi:10.1016/0370-2693(94)01360-O`.

[484] I. Dunietz, J. Incandela, F. D. Snider, H. Yamamoto, Large charmless yield in B decays and inclusive B decay puzzles, Eur. Phys. J. C1 (1998) 211. `arXiv:hep-ph/9612421`, `doi:10.1007/BF01245810`.

[485] F. E. Close, I. Dunietz, P. R. Page, S. Veseli, H. Yamamoto, Gluonic hadrons and charmless B decays, Phys. Rev. D57 (1998) 5653. `arXiv:hep-ph/9708265`, `doi:10.1103/PhysRevD.57.5653`.

[486] G. Chiladze, A. F. Falk, A. A. Petrov, Hybrid charmonium production in B decays, Phys. Rev. D58 (1998) 034013. `arXiv:hep-ph/9804248`, `doi:10.1103/PhysRevD.58.034013`.

[487] V. Zhukova, et al., Angular analysis of the $e^+e^- \to D^{(*)\pm}D^{*\mp}$ process near the open charm threshold using initial-state radiation, Phys. Rev. D97 (2018) 012002. `arXiv:1707.09167`, `doi:10.1103/PhysRevD.97.012002`.

[488] T. V. Uglov, Yu. S. Kalashnikova, A. V. Nefediev, G. V. Pakhlova, P. N. Pakhlov, Exclusive open-charm near-threshold cross sec-

tions in a coupled-channel approach, JETP Lett. 105 (2017) 1. `arXiv:1611.07582`, `doi:10.1134/S0021364017010064,10.7868/S0370274X17010015`.

[489] M. B. Voloshin, Charmonium, Prog. Part. Nucl. Phys. 61 (2008) 455. `arXiv:0711.4556`, `doi:10.1016/j.ppnp.2008.02.001`.

[490] N. Brambilla, V. Shtabovenko, J. Tarrús Castellà, A. Vairo, Effective field theories for van der Waals interactions, Phys. Rev. D95 (2017) 116004. `arXiv:1704.03476`, `doi:10.1103/PhysRevD.95.116004`.

[491] J. Tarrús Castellà, G. Krein, Effective field theory for the nucleon-quarkonium interaction, Phys. Rev. D98 (2018) 014029. `arXiv:1803.05412`, `doi:10.1103/PhysRevD.98.014029`.

[492] M. B. Voloshin, Z_c(3900) - what is inside?, Phys. Rev. D87 (2013) 091501. `arXiv:1304.0380`, `doi:10.1103/PhysRevD.87.091501`.

[493] M. Cleven, F.-K. Guo, C. Hanhart, Q. Wang, Q. Zhao, Employing spin symmetry to disentangle different models for the XYZ states, Phys. Rev. D92 (2015) 014005. `arXiv:1505.01771`, `doi:10.1103/PhysRevD.92.014005`.

[494] A. Martinez Torres, K. P. Khemchandani, D. Gamermann, E. Oset, The Y(4260) as a $J/\psi K\bar{K}$ system, Phys. Rev. D80 (2009) 094012. `arXiv:0906.5333`, `doi:10.1103/PhysRevD.80.094012`.

[495] L.-Y. Dai, J. Haidenbauer, U.-G. Meißner, Re-examining the X(4630) resonance in the reaction $e^+e^- \to \Lambda_c^+\bar{\Lambda}_c^-$, Phys. Rev. D96 (2017) 116001. `arXiv:1710.03142`, `doi:10.1103/PhysRevD.96.116001`.

[496] R. L. Jaffe, Multiquark hadrons. 1. Phenomenology of $Q^2\bar{Q}^2$ mesons, Phys. Rev. D15 (1977) 267. `doi:10.1103/PhysRevD.15.267`.

[497] A. Selem, F. Wilczek, Hadron systematics and emergent diquarks, in: Proceedings, Ringberg Workshop on New Trends in HERA Physics 2005: Ringberg Castle, Tegernsee, Germany, October 2-7, 2005, p. 337. `arXiv:hep-ph/0602128`, `doi:10.1142/9789812773524_0030`.
URL `http://www-library.desy.de/preparch/conf/ringberg/2005/wilczek.ps.gz`

[498] A. Ali, L. Maiani, A. D. Polosa, Multiquark Hadrons, Cambridge University Press, 2019. `doi:10.1017/9781316761465`.

[499] A. Esposito, A. Pilloni, A. D. Polosa, Multiquark Resonances, Phys. Rept. 668 (2017) 1–97. `arXiv:1611.07920`, `doi:10.1016/j.physrep.2016.11.002`.

[500] D. Ebert, R. N. Faustov, V. O. Galkin, Relativistic model of hidden bottom tetraquarks, Mod. Phys. Lett. A24 (2009) 567. `arXiv:0812.3477`, `doi:10.1142/S0217732309030357`.

[501] D. Ebert, R. N. Faustov, V. O. Galkin, W. Lucha, Masses of tetraquarks with two heavy quarks in the relativistic quark model, Phys. Rev. D76 (2007) 114015. `arXiv:0706.3853`, `doi:10.1103/PhysRevD.76.114015`.

[502] D. Ebert, R. N. Faustov, V. O. Galkin, Excited heavy tetraquarks with hidden charm, Eur. Phys. J. C58 (2008) 399. `arXiv:0808.3912`, `doi:10.1140/epjc/s10052-008-0754-8`.

[503] D. Ebert, R. N. Faustov, V. O. Galkin, Masses of tetraquarks with open charm and bottom, Phys. Lett. B696 (2011) 241. `arXiv:1011.2677`, `doi:10.1016/j.physletb.2010.12.033`.

[504] J. P. Ader, J. M. Richard, P. Taxil, Do narrow heavy multiquark states exist ?, Phys. Rev. D25 (1982) 2370. `doi:10.1103/PhysRevD.25.2370`.

[505] A. Czarnecki, B. Leng, M. B. Voloshin, Stability of tetrons, Phys. Lett. B778 (2018) 233. `arXiv:1708.04594`, `doi:10.1016/j.physletb.2018.01.034`.

[506] N. Ishii, W. Bentz, K. Yazaki, Solution of the relativistic three quark Faddeev equation in the Nambu-Jona-Lasinio (NJL) model, Phys. Lett. B318 (1993) 26. `doi:10.1016/0370-2693(93)91778-L`.

[507] C. Hanhart, S. Krewald, Faddeev approach to the octet and decuplet baryons, Phys. Lett. B344 (1995) 55. `arXiv:nucl-th/9501021`, `doi:10.1016/0370-2693(94)01532-H`.

[508] A. Ali, L. Maiani, A. V. Borisov, I. Ahmed, M. Jamil Aslam, A. Ya. Parkhomenko, A. D. Polosa, A. Rehman, A new look at the Y tetraquarks and Ω_c baryons in the diquark model, Eur. Phys. J. C78 (2018) 29. `arXiv:1708.04650`, `doi:10.1140/epjc/s10052-017-5501-6`.

[509] L. Maiani, A. D. Polosa, V. Riquer, A theory of X and Z multiquark resonances, Phys. Lett. B778 (2018) 247. `arXiv:1712.05296`, `doi:10.1016/j.physletb.2018.01.039`.

[510] S. J. Brodsky, D. S. Hwang, R. F. Lebed, Dynamical Picture for the Formation and Decay of the Exotic XYZ Mesons, Phys. Rev. Lett. 113 (11) (2014) 112001. `arXiv:1406.7281`, `doi:10.1103/PhysRevLett.113.112001`.

[511] Y.-H. Chen, L.-Y. Dai, F.-K. Guo, B. Kubis, Nature of the Y(4260): A light-quark perspective, Phys. Rev. D99 (2019) 074016. `arXiv:1902.10957`, `doi:10.1103/PhysRevD.99.074016`.

[512] G. 't Hooft, A Planar Diagram Theory for Strong Interactions, Nucl. Phys. B72 (1974) 461. `doi:10.1016/0550-3213(74)90154-0`.

[513] S. Coleman, Aspects of Symmetry, Cambridge University Press, Cambridge, U.K., 1985. `doi:10.1017/CBO9780511565045`.

[514] S. Weinberg, Tetraquark Mesons in Large-N Quantum Chromodynamics, Phys. Rev. Lett. 110 (2013) 261601. `arXiv:1303.0342`, `doi:10.1103/PhysRevLett.110.261601`.

[515] M. Knecht, S. Peris, Narrow Tetraquarks at Large-N, Phys. Rev. D88 (2013) 036016. `arXiv:1307.1273`, `doi:10.1103/PhysRevD.88.036016`.

[516] R. F. Lebed, Large-N Structure of Tetraquark Mesons, Phys. Rev. D88 (2013) 057901. `arXiv:1308.2657`, `doi:10.1103/PhysRevD.88.057901`.

[517] L. Maiani, A. D. Polosa, V. Riquer, Tetraquarks in the $1/N$ expansion and meson-meson resonances, JHEP 06 (2016) 160. `arXiv:1605.04839`, `doi:10.1007/JHEP06(2016)160`.

[518] L. Maiani, A. D. Polosa, V. Riquer, Tetraquarks in the $1/N$ expansion: A new appraisal, Phys. Rev. D98 (2018) 054023. `arXiv:1803.06883`, `doi:10.1103/PhysRevD.98.054023`.

[519] W. Lucha, D. Melikhov, H. Sazdjian, Tetraquark and two-meson states at large N_c, Eur. Phys. J. C77 (2017) 866. `arXiv:1710.08316`, `doi:10.1140/epjc/s10052-017-5437-x`.

[520] W. Lucha, D. Melikhov, H. Sazdjian, Are there narrow flavor-exotic tetraquarks in large-N_c QCD?, Phys. Rev. D98 (2018) 094011. `arXiv:1810.09986`, `doi:10.1103/PhysRevD.98.094011`.

[521] H. Sazdjian, Large-N_c QCD and tetraquarks, in: 13th Conference on Quark Confinement and the Hadron Spectrum (Confinement XIII) Maynooth, Ireland, July 31-August 6, 2018, 2018. `arXiv:1811.07613`.

[522] M.-L. Du, W. Chen, X.-L. Chen, S.-L. Zhu, Exotic $QQ\bar{q}\bar{q}$, $QQ\bar{q}\bar{s}$ and $QQ\bar{s}\bar{s}$ states, Phys. Rev. D87 (2013) 014003. `arXiv:1209.5134`,

doi:10.1103/PhysRevD.87.014003.

[523] P. Bicudo, K. Cichy, A. Peters, M. Wagner, *BB* interactions with static bottom quarks from lattice QCD, Phys. Rev. D93 (2016) 034501. arXiv:1510.03441, doi:10.1103/PhysRevD.93.034501.

[524] A. Francis, R. J. Hudspith, R. Lewis, K. Maltman, Lattice Prediction for Deeply Bound Doubly Heavy Tetraquarks, Phys. Rev. Lett. 118 (2017) 142001. arXiv:1607.05214, doi:10.1103/PhysRevLett.118.142001.

[525] P. Bicudo, J. Scheunert, M. Wagner, Including heavy spin effects in the prediction of a $b\bar{b}ud$ tetraquark with lattice QCD potentials, Phys. Rev. D95 (2017) 034502. arXiv:1612.02758, doi:10.1103/PhysRevD.95.034502.

[526] Y. Cui, X.-L. Chen, W.-Z. Deng, S.-L. Zhu, The Possible Heavy Tetraquarks $qQ\bar{q}\bar{Q}$, $qq\bar{Q}\bar{Q}$ and $qQ\bar{Q}\bar{Q}$, HEPNP 31 (2007) 7. arXiv:hep-ph/0607226.

[527] S.-Q. Luo, K. Chen, X. Liu, Y.-R. Liu, S.-L. Zhu, Exotic tetraquark states with the $qq\bar{Q}\bar{Q}$ configuration, Eur. Phys. J. C77 (2017) 709. arXiv:1707.01180, doi:10.1140/epjc/s10052-017-5297-4.

[528] M. Karliner, J. L. Rosner, Discovery of doubly-charmed Ξ_{cc} baryon implies a stable ($bb\bar{u}\bar{d}$) tetraquark, Phys. Rev. Lett. 119 (2017) 202001. arXiv:1707.07666, doi:10.1103/PhysRevLett.119.202001.

[529] E. J. Eichten, C. Quigg, Heavy-quark symmetry implies stable heavy tetraquark mesons $Q_iQ_j\bar{q}_k\bar{q}_l$, Phys. Rev. Lett. 119 (2017) 202002. arXiv:1707.09575, doi:10.1103/PhysRevLett.119.202002.

[530] R. Aaij, et al., Observation of the doubly charmed baryon Ξ_{cc}^{++}, Phys. Rev. Lett. 119 (2017) 112001. arXiv:1707.01621, doi:10.1103/PhysRevLett.119.112001.

[531] F.-K. Guo, C. Hanhart, U.-G. Meißner, Q. Wang, Q. Zhao, B.-S. Zou, Hadronic molecules, Rev. Mod. Phys. 90 (2018) 015004. arXiv:1705.00141, doi:10.1103/RevModPhys.90.015004.

[532] J. R. Peláez, From controversy to precision on the sigma meson: a review on the status of the non-ordinary $f_0(500)$ resonance, Phys. Rept. 658 (2016) 1. arXiv:1510.00653, doi:10.1016/j.physrep.2016.09.001.

[533] D. R. Tilley, C. M. Cheves, J. L. Godwin, G. M. Hale, H. M. Hofmann, J. H. Kelley, C. G. Sheu, H. R. Weller, Energy levels of light nuclei A=5, A=6, A=7, Nucl. Phys. A708 (2002) 3. doi:10.1016/S0375-9474(02)00597-3.

[534] M. B. Voloshin, L. B. Okun, Hadron Molecules and Charmonium Atom, JETP Lett. 23 (1976) 333, [Pisma Zh. Eksp. Teor. Fiz. 23 (1976) 369].

[535] N. A. Tornqvist, From the deuteron to deusons, an analysis of deuteron-like meson meson bound states, Z. Phys. C61 (1994) 525. arXiv:hep-ph/9310247, doi:10.1007/BF01413192.

[536] M. Suzuki, The X(3872) boson: Molecule or charmonium, Phys. Rev. D72 (2005) 114013. arXiv:hep-ph/0508258, doi:10.1103/PhysRevD.72.114013.

[537] V. Baru, A. A. Filin, C. Hanhart, Yu. S. Kalashnikova, A. E. Kudryavtsev, A. V. Nefediev, Three-body $D\bar{D}\pi$ dynamics for the X(3872), Phys. Rev. D84 (2011) 074029. arXiv:1108.5644, doi:10.1103/PhysRevD.84.074029.

[538] V. Baru, E. Epelbaum, A. A. Filin, F. K. Guo, H. W. Hammer, C. Hanhart, U. G. Meißner, A. V. Nefediev, Remarks on study of X(3872) from effective field theory with pion-exchange interaction, Phys. Rev. D91 (2015) 034002. arXiv:1501.02924, doi:10.1103/PhysRevD.91.034002.

[539] C. Bignamini, B. Grinstein, F. Piccinini, A. D. Polosa, C. Sabelli, Is the X(3872) Production Cross Section at Tevatron Compatible with a Hadron Molecule Interpretation?, Phys. Rev. Lett. 103 (2009) 162001. arXiv:0906.0882, doi:10.1103/PhysRevLett.103.162001.

[540] A. Esposito, A. L. Guerrieri, L. Maiani, F. Piccinini, A. Pilloni, A. D. Polosa, V. Riquer, Observation of light nuclei at ALICE and the X(3872) conundrum, Phys. Rev. D92 (2015) 034028. arXiv:1508.00295, doi:10.1103/PhysRevD.92.034028.

[541] A. Esposito, B. Grinstein, L. Maiani, F. Piccinini, A. Pilloni, A. D. Polosa, V. Riquer, Comment on Note on X(3872) production at hadron colliders and its molecular structure, Chin. Phys. C42 (2018) 114107. arXiv:1709.09631, doi:10.1088/1674-1137/42/11/114107.

[542] P. Artoisenet, E. Braaten, Production of the X(3872) at the Tevatron and the LHC, Phys. Rev. D81 (2010) 114018. arXiv:0911.2016, doi:10.1103/PhysRevD.81.114018.

[543] P. Artoisenet, E. Braaten, Estimating the production rate of loosely bound hadronic molecules using event generators, Phys. Rev. D83 (2011) 014019. arXiv:1007.2868, doi:10.1103/PhysRevD.83.014019.

[544] F.-K. Guo, U.-G. Meißner, W. Wang, Production of charged heavy quarkonium-like states at the LHC and the Tevatron, Commun. Theor. Phys. 61 (2014) 354. arXiv:1308.0193, doi:10.1088/0253-6102/61/3/14.

[545] M. Albaladejo, F.-K. Guo, C. Hanhart, U.-G. Meißner, J. Nieves, A. Nogga, Z. Yang, Note on X(3872) production at hadron colliders and its molecular structure, Chin. Phys. C41 (2017) 121001. arXiv:1709.09101, doi:10.1088/1674-1137/41/12/121001.

[546] W. Wang, On the production of hidden-flavored hadronic states at high energy, Chin. Phys. C42 (2018) 043103. arXiv:1709.10382, doi:10.1088/1674-1137/42/4/043103.

[547] E. Braaten, L.-P. He, K. Ingles, Estimates of the X(3872) cross section at a hadron collider, Phys. Rev. D100 (2019) 094024. arXiv:1811.08876, doi:10.1103/PhysRevD.100.094024.

[548] C. Hanhart, E. Klempt, Are the XYZ states unconventional states or conventional states with unconventional properties? arXiv:1906.11971.

[549] S. Weinberg, Evidence that the Deuteron Is Not an Elementary Particle, Phys. Rev. 137 (1965) B672. doi:10.1103/PhysRev.137.B672.

[550] L. D. Landau, Malye energii sviazi v kvantovoi teorii polia, Soviet Zh. Eksp. Teor. Fiz. 39 (1960) 1856, (in Russian).

[551] V. Baru, J. Haidenbauer, C. Hanhart, Yu. Kalashnikova, A. E. Kudryavtsev, Evidence that the $a_0(980)$ and $f_0(980)$ are not elementary particles, Phys. Lett. B586 (2004) 53. arXiv:hep-ph/0308129, doi:10.1016/j.physletb.2004.01.088.

[552] T. Sekihara, T. Hyodo, D. Jido, Comprehensive analysis of the wave function of a hadronic resonance and its compositeness, PTEP 2015 (2015) 063D04. arXiv:1411.2308, doi:10.1093/ptep/ptv081.

[553] D. Gamermann, J. Nieves, E. Oset, E. Ruiz Arriola, Couplings in coupled channels versus wave functions: Application to the X(3872) resonance, Phys. Rev. D81 (2010) 014029. arXiv:0911.4407, doi:10.1103/PhysRevD.81.014029.

[554] D. Morgan, Pole counting and resonance classification, Nucl. Phys. A543 (1992) 632. doi:10.1016/0375-9474(92)90550-4.

[555] D. Morgan, M. R. Pennington, New data on the $K\bar{K}$ threshold region and the nature of the $f_0(S^*)$, Phys. Rev. D48 (1993) 1185. doi:10.1103/PhysRevD.48.1185.

[556] V. Baru, J. Haidenbauer, C. Hanhart, A. E. Kudryavtsev, U.-G. Meißner, Flatté-like distributions and the $a_0(980)/f_0(980)$ mesons, Eur. Phys. J. A23 (2005) 523. arXiv:nucl-th/0410099, doi:10.1140/epja/i2004-10105-x.

[557] C. Hanhart, Yu. S. Kalashnikova, A. E. Kudryavtsev, A. V. Nefediev, Two-photon decays of hadronic molecules, Phys. Rev. D75 (2007) 074015. arXiv:hep-ph/0701214, doi:10.1103/PhysRevD.75.074015.

[558] L. D. Landau, On analytic properties of vertex parts in quantum field theory, Nucl. Phys. 13 (1959) 181. doi:10.1016/0029-5582(59)90154-3.

[559] A. A. Filin, A. Romanov, V. Baru, C. Hanhart, Yu. S. Kalashnikova, A. E. Kudryavtsev, U.-G. Meißner, A. V. Nefediev, Comment on 'Possibility of Deeply Bound Hadronic Molecules from Single Pion Exchange', Phys. Rev. Lett. 105 (2010) 019101. arXiv:1004.4789, doi:10.1103/PhysRevLett.105.019101.

[560] F.-K. Guo, U.-G. Meißner, More kaonic bound states and a comprehensive interpretation of the D_{sJ} states, Phys. Rev. D84 (2011) 014013. arXiv:1102.3536, doi:10.1103/PhysRevD.84.014013.

[561] E. Braaten, M. Lu, Line shapes of the $X(3872)$, Phys. Rev. D76 (2007) 094028. arXiv:0709.2697, doi:10.1103/PhysRevD.76.094028.

[562] C. Hanhart, Yu. S. Kalashnikova, A. V. Nefediev, Lineshapes for composite particles with unstable constituents, Phys. Rev. D81 (2010) 094028. arXiv:1002.4097, doi:10.1103/PhysRevD.81.094028.

[563] M. Cleven, F.-K. Guo, C. Hanhart, U.-G. Meißner, Bound state nature of the exotic Z_b states, Eur. Phys. J. A47 (2011) 120. arXiv:1107.0254, doi:10.1140/epja/i2011-11120-6.

[564] M. Albaladejo, F.-K. Guo, C. Hidalgo-Duque, J. Nieves, $Z_c(3900)$: What has been really seen?, Phys. Lett. B755 (2016) 337. arXiv:1512.03638, doi:10.1016/j.physletb.2016.02.025.

[565] A. Pilloni, C. Fernandez-Ramirez, A. Jackura, V. Mathieu, M. Mikhasenko, J. Nys, A. P. Szczepaniak, Amplitude analysis and the nature of the $Z_c(3900)$, Phys. Lett. B772 (2017) 200. arXiv:1612.06490, doi:10.1016/j.physletb.2017.06.030.

[566] A. E. Bondar, A. Garmash, A. I. Milstein, R. Mizuk, M. B. Voloshin, Heavy quark spin structure in Z_b resonances, Phys. Rev. D84 (2011) 054010. arXiv:1105.4473, doi:10.1103/PhysRevD.84.054010.

[567] T. Mehen, J. W. Powell, Heavy Quark Symmetry Predictions for Weakly Bound B-Meson Molecules, Phys. Rev. D84 (2011) 114013. arXiv:1109.3479, doi:10.1103/PhysRevD.84.114013.

[568] J. M. Dias, F. Aceti, E. Oset, Study of $B\bar{B}^*$ and $B^*\bar{B}^*$ interactions in $I = 1$ and relationship to the $Z_b(10610)$, $Z_b(10650)$ states, Phys. Rev. D91 (2015) 076001. arXiv:1410.1785, doi:10.1103/PhysRevD.91.076001.

[569] F. Aceti, M. Bayar, E. Oset, A. Martinez Torres, K. P. Khemchandani, J. M. Dias, F. S. Navarra, M. Nielsen, Prediction of an $I = 1$ $D\bar{D}^*$ state and relationship to the claimed $Z_c(3900)$, $Z_c(3885)$, Phys. Rev. D90 (2014) 016003. arXiv:1401.8216, doi:10.1103/PhysRevD.90.016003.

[570] V. Baru, E. Epelbaum, A. A. Filin, C. Hanhart, A. V. Nefediev, Spin partners of the $Z_b(10610)$ and $Z_b(10650)$ revisited, JHEP 06 (2017) 158. arXiv:1704.07332, doi:10.1007/JHEP06(2017)158.

[571] V. Baru, E. Epelbaum, A. Filin, C. Hanhart, A. Nefediev, Q. Wang, Spin partners W_{bJ} from the line shapes of the $Z_b(10610)$ and $Z_b(10650)$, Phys. Rev. D99 (2019) 094013. arXiv:1901.10319, doi:10.1103/PhysRevD.99.094013.

[572] M. B. Voloshin, Radiative transitions from $\Upsilon(5S)$ to molecular bottomonium, Phys. Rev. D84 (2011) 031502. arXiv:1105.5829, doi:10.1103/PhysRevD.84.031502.

[573] V. Baru, E. Epelbaum, A. A. Filin, C. Hanhart, U.-G. Meißner, A. V. Nefediev, Heavy-quark spin symmetry partners of the $X(3872)$ revisited, Phys. Lett. B763 (2016) 20. arXiv:1605.09649, doi:10.1016/j.physletb.2016.10.008.

[574] J. Nieves, M. P. Valderrama, The Heavy Quark Spin Symmetry Partners of the $X(3872)$, Phys. Rev. D86 (2012) 056004. arXiv:1204.2790, doi:10.1103/PhysRevD.86.056004.

[575] M. Albaladejo, F. K. Guo, C. Hidalgo-Duque, J. Nieves, M. P. Valderrama, Decay widths of the spin-2 partners of the $X(3872)$, Eur. Phys. J. C75 (2015) 547. arXiv:1504.00861, doi:10.1140/epjc/s10052-015-3753-6.

[576] D. Gamermann, E. Oset, D. Strottman, M. J. Vicente Vacas, Dynamically generated open and hidden charm meson systems, Phys. Rev. D76 (2007) 074016. arXiv:hep-ph/0612179, doi:10.1103/PhysRevD.76.074016.

[577] C. Hidalgo-Duque, J. Nieves, M. P. Valderrama, Light flavor and heavy quark spin symmetry in heavy meson molecules, Phys. Rev. D87 (2013) 076006. arXiv:1210.5431, doi:10.1103/PhysRevD.87.076006.

[578] D. Gamermann, E. Oset, Hidden charm dynamically generated resonances and the $e^+e^- \rightarrow J/\psi D\bar{D}$, $J/\psi D\bar{D}^*$ reactions, Eur. Phys. J. A36 (2008) 189. arXiv:0712.1758, doi:10.1140/epja/i2007-10580-5.

[579] C. W. Xiao, E. Oset, Three methods to detect the predicted $D\bar{D}$ scalar meson $X(3700)$, Eur. Phys. J. A49 (2013) 52. arXiv:1211.1862, doi:10.1140/epja/i2013-13052-5.

[580] R. Molina, E. Oset, The $Y(3940)$, $Z(3930)$ and the $X(4160)$ as dynamically generated resonances from the vector-vector interaction, Phys. Rev. D80 (2009) 114013. arXiv:0907.3043, doi:10.1103/PhysRevD.80.114013.

[581] Y. S. Kalashnikova, A. V. Nefediev, $X(3872)$ in the molecular model, Phys. Usp. 62 (2019) 568, [Usp. Fiz. Nauk 189 (2019) 603]. arXiv:1811.01324, doi:10.3367/UFNe.2018.08.038411.

[582] F. E. Close, P. R. Page, The $D^{*0}\bar{D}^0$ threshold resonance, Phys. Lett. B578 (2004) 119. arXiv:hep-ph/0309253, doi:10.1016/j.physletb.2003.10.032.

[583] E. Braaten, M. Kusunoki, S. Nussinov, Production of the $X(3870)$ in B meson decay by the coalescence of charm mesons, Phys. Rev. Lett. 93 (2004) 162001. arXiv:hep-ph/0404161, doi:10.1103/PhysRevLett.93.162001.

[584] D. Gamermann, E. Oset, Isospin breaking effects in the $X(3872)$ resonance, Phys. Rev. D80 (2009) 014003. arXiv:0905.0402, doi:10.1103/PhysRevD.80.014003.

[585] Z.-Y. Zhou, Z. Xiao, Comprehending isospin breaking effects of $X(3872)$ in a Friedrichs-model-like scheme, Phys. Rev. D97 (2018) 034011. arXiv:1711.01930, doi:10.1103/PhysRevD.97.034011.

[586] F. Aceti, R. Molina, E. Oset, $X(3872) \rightarrow J/\psi\gamma$ decay in the $D\bar{D}^*$ molecular picture, Phys. Rev. D86 (2012) 113007. arXiv:1207.2832, doi:10.1103/PhysRevD.86.113007.

[587] Y.-J. Zhang, H.-C. Chiang, P.-N. Shen, B.-S. Zou, Possible S-wave bound-states of two pseudoscalar mesons, Phys. Rev. D74 (2006)

014013. `arXiv:hep-ph/0604271`, `doi:10.1103/PhysRevD.74.014013`.

[588] G.-J. Ding, J.-F. Liu, M.-L. Yan, Dynamics of hadronic molecule in one-boson exchange approach and possible heavy flavor molecules, Phys. Rev. D79 (2009) 054005. `arXiv:0901.0426`, `doi:10.1103/PhysRevD.79.054005`.

[589] N. Li, Z.-F. Sun, X. Liu, S.-L. Zhu, Coupled-channel analysis of the possible $D^{(*)}D^{(*)}$, $\overline{B}^{(*)}\overline{B}^{(*)}$ and $D^{(*)}\overline{B}^{(*)}$ molecular states, Phys. Rev. D88 (2013) 114008. `arXiv:1211.5007`, `doi:10.1103/PhysRevD.88.114008`.

[590] L. Zhao, L. Ma, S.-L. Zhu, Spin-orbit force, recoil corrections, and possible $B\bar{B}^*$ and $D\bar{D}^*$ molecular states, Phys. Rev. D89 (2014) 094026. `arXiv:1403.4043`, `doi:10.1103/PhysRevD.89.094026`.

[591] M.-Z. Liu, T.-W. Wu, M. Pavon Valderrama, J.-J. Xie, L.-S. Geng, Heavy-quark spin and flavor symmetry partners of the X(3872) revisited: What can we learn from the one boson exchange model?, Phys. Rev. D99 (2019) 094018. `arXiv:1902.03044`, `doi:10.1103/PhysRevD.99.094018`.

[592] Y.-R. Liu, H.-X. Chen, W. Chen, X. Liu, S.-L. Zhu, Pentaquark and Tetraquark states, Prog. Part. Nucl. Phys. 107 (2019) 237. `arXiv:1903.11976`, `doi:10.1016/j.ppnp.2019.04.003`.

[593] H. Georgi, Lie algebras in particle physics, Front. Phys. 54 (1999) 1.

[594] S. Sakai, L. Roca, E. Oset, Charm-beauty meson bound states from $B(B^*)D(D^*)$ and $B(B^*)\bar{D}(\bar{D}^*)$ interaction, Phys. Rev. D96 (2017) 054023. `arXiv:1704.02196`, `doi:10.1103/PhysRevD.96.054023`.

[595] T. V. Uglov, P. N. Pakhlov, Z^+(4430): Nonexotic interpretation, Phys. Atom. Nucl. 79 (2016) 285, [Yad. Fiz. 79 (2016) 174]. `doi:10.1134/S1063778816020198`.

[596] S. X. Nakamura, K. Tsushima, Z_c(4430) and Z_c(4200) as triangle singularities, Phys. Rev. D100 (2019) 051502. `arXiv:1901.07385`, `doi:10.1103/PhysRevD.100.051502`.

[597] T. Barnes, F. E. Close, E. S. Swanson, Molecular Interpretation of the Supercharmonium State Z(4475), Phys. Rev. D91 (2015) 014004. `arXiv:1409.6651`, `doi:10.1103/PhysRevD.91.014004`.

[598] E. Cincioglu, J. Nieves, A. Ozpineci, A. U. Yilmazer, Quarkonium Contribution to Meson Molecules, Eur. Phys. J. C76 (2016) 576. `arXiv:1606.03239`, `doi:10.1140/epjc/s10052-016-4413-1`.

[599] M. A. Shifman, A. I. Vainshtein, V. I. Zakharov, QCD and Resonance Physics. Theoretical Foundations, Nucl. Phys. B147 (1979) 385. `doi:10.1016/0550-3213(79)90022-1`.

[600] M. A. Shifman, A. I. Vainshtein, V. I. Zakharov, QCD and Resonance Physics: Applications, Nucl. Phys. B147 (1979) 448. `doi:10.1016/0550-3213(79)90023-3`.

[601] R. M. Albuquerque, J. M. Dias, K. P. Khemchandani, A. Martinez Torres, F. S. Navarra, M. Nielsen, C. M. Zanetti, QCD sum rules approach to the X, Y and Z states, J. Phys. G46 (2019) 093002. `arXiv:1812.08207`, `doi:10.1088/1361-6471/ab2678`.

[602] M. Gell-Mann, R. J. Oakes, B. Renner, Behavior of current divergences under SU(3) × SU(3), Phys. Rev. 175 (1968) 2195. `doi:10.1103/PhysRev.175.2195`.

[603] G. S. Bali, C. Bauer, A. Pineda, Model-independent determination of the gluon condensate in four-dimensional SU(3) gauge theory, Phys. Rev. Lett. 113 (2014) 092001. `arXiv:1403.6477`, `doi:10.1103/PhysRevLett.113.092001`.

[604] L. Del Debbio, F. Di Renzo, G. Filaci, Non perturbative physics from NSPT: renormalons, the gluon condensate and all that, in: 36th International Symposium on Lattice Field Theory (Lattice 2018) East Lansing, MI, United States, July 22-28, 2018. `arXiv:1811.05427`.

[605] W. Lucha, D. Melikhov, S. Simula, Systematic uncertainties of hadron parameters obtained with QCD sum rules, Phys. Rev. D76 (2007) 036002. `arXiv:0705.0470`, `doi:10.1103/PhysRevD.76.036002`.

[606] P. Pascual, R. Tarrach, QCD: Renormalization for the practitioner, Lect. Notes Phys. 194 (1984) 1.

[607] W. Lucha, D. Melikhov, H. Sazdjian, Tetraquark-adequate formulation of QCD sum rules, Phys. Rev. D100 (2019) 014010. `arXiv:1901.03881`, `doi:10.1103/PhysRevD.100.014010`.

[608] S. Weinberg, Phenomenological Lagrangians, Physica A96 (1979) 327. `doi:10.1016/0378-4371(79)90223-1`.

[609] J. Gasser, H. Leutwyler, Chiral perturbation theory to one loop, Annals Phys. 158 (1984) 142. `doi:10.1016/0003-4916(84)90242-2`.

[610] H. Leutwyler, On the foundations of chiral perturbation theory, Annals Phys. 235 (1994) 165. `arXiv:hep-ph/9311274`, `doi:10.1006/aphy.1994.1094`.

[611] E. Epelbaum, H.-W. Hammer, U.-G. Meißner, Modern theory of nuclear forces, Rev. Mod. Phys. 81 (2009) 1773. `arXiv:0811.1338`, `doi:10.1103/RevModPhys.81.1773`.

[612] N. Isgur, M. B. Wise, Weak decays of heavy mesons in the static quark approximation, Phys. Lett. B232 (1989) 113. `doi:10.1016/0370-2693(89)90566-2`.

[613] N. Isgur, M. B. Wise, Weak Transition form-factors between heavy mesons, Phys. Lett. B237 (1990) 527. `doi:10.1016/0370-2693(90)91219-2`.

[614] N. Isgur, M. B. Wise, Spectroscopy with heavy quark symmetry, Phys. Rev. Lett. 66 (1991) 1130. `doi:10.1103/PhysRevLett.66.1130`.

[615] E. Eichten, B. R. Hill, An effective field theory for the calculation of matrix elements involving heavy quarks, Phys. Lett. B234 (1990) 511. `doi:10.1016/0370-2693(90)92049-0`.

[616] M. Neubert, Heavy quark symmetry, Phys. Rept. 245 (1994) 259. `arXiv:hep-ph/9306320`, `doi:10.1016/0370-1573(94)90091-4`.

[617] A. V. Manohar, M. B. Wise, Heavy quark physics, Camb. Monogr. Part. Phys. Nucl. Phys. Cosmol. 10 (2000) 1.

[618] A. Gunawardana, G. Paz, On HQET and NRQCD Operators of Dimension 8 and Above, JHEP 07 (2017) 137. `arXiv:1702.08904`, `doi:10.1007/JHEP07(2017)137`.

[619] A. Kobach, S. Pal, Hilbert series and operator basis for NRQED and NRQCD/HQET, Phys. Lett. B772 (2017) 225. `arXiv:1704.00008`, `doi:10.1016/j.physletb.2017.06.026`.

[620] A. V. Manohar, Heavy quark effective theory and nonrelativistic QCD Lagrangian to order α_s/m^3, Phys. Rev. D56 (1997) 230. `arXiv:hep-ph/9701294`, `doi:10.1103/PhysRevD.56.230`.

[621] A. G. Grozin, P. Marquard, J. H. Piclum, M. Steinhauser, Three-loop chromomagnetic interaction in HQET, Nucl. Phys. B789 (2008) 277. `arXiv:0707.1388`, `doi:10.1016/j.nuclphysb.2007.08.012`.

[622] M. E. Luke, A. V. Manohar, Reparametrization invariance constraints on heavy particle effective field theories, Phys. Lett. B286 (1992) 348. `arXiv:hep-ph/9205228`, `doi:10.1016/0370-2693(92)91786-9`.

[623] N. Brambilla, D. Gromes, A. Vairo, Poincaré invariance constraints on NRQCD and potential NRQCD, Phys. Lett. B576 (2003) 314. arXiv:hep-ph/0306107, doi:10.1016/j.physletb.2003.09.100.

[624] C. Balzereit, Spectator effects in heavy quark effective theory at $O(1/m_Q^3)$, Phys. Rev. D59 (1999) 094015. arXiv:hep-ph/9805503, doi:10.1103/PhysRevD.59.094015.

[625] D. Moreno, A. Pineda, Chromopolarizabilities of a heavy quark at weak coupling, Phys. Rev. D97 (2018) 016012, [Erratum: Phys. Rev. D98 (2018) 059902]. arXiv:1710.07647, doi:10.1103/PhysRevD.97.016012,10.1103/PhysRevD.98.059902.

[626] A. F. Falk, M. Neubert, Second-order power corrections in the heavy-quark effective theory. 1. Formalism and meson form factors, Phys. Rev. D47 (1993) 2965. arXiv:hep-ph/9209268, doi:10.1103/PhysRevD.47.2965.

[627] P. Marquard, A. V. Smirnov, V. A. Smirnov, M. Steinhauser, Quark Mass Relations to Four-Loop Order in Perturbative QCD, Phys. Rev. Lett. 114 (2015) 142002. arXiv:1502.01030, doi:10.1103/PhysRevLett.114.142002.

[628] P. Marquard, A. V. Smirnov, V. A. Smirnov, M. Steinhauser, D. Wellmann, $\overline{MS}$-on-shell quark mass relation up to four loops in QCD and a general SU(N) gauge group, Phys. Rev. D94 (2016) 074025. arXiv:1606.06754, doi:10.1103/PhysRevD.94.074025.

[629] A. L. Kataev, V. S. Molokoedov, Dependence of Five- and Six-Loop Estimated QCD Corrections to the Relation between Pole and Running Masses of Heavy Quarks on the Number of Light Flavors, JETP Lett. 108 (2018) 777. arXiv:1811.02867, doi:10.1134/S0021364018240050.

[630] N. Uraltsev, BLM resummation and OPE in heavy flavor transitions, Nucl. Phys. B491 (1997) 303. arXiv:hep-ph/9610425, doi:10.1016/S0550-3213(97)00121-1.

[631] M. Beneke, A quark mass definition adequate for threshold problems, Phys. Lett. B434 (1998) 115. arXiv:hep-ph/9804241, doi:10.1016/S0370-2693(98)00741-2.

[632] A. H. Hoang, $1S$ and $\overline{MS}$ bottom quark masses from Υ sum rules, Phys. Rev. D61 (2000) 034005. arXiv:hep-ph/9905550, doi:10.1103/PhysRevD.61.034005.

[633] A. Pineda, Determination of the bottom quark mass from the $\Upsilon(1S)$ system, JHEP 06 (2001) 022. arXiv:hep-ph/0105008, doi:10.1088/1126-6708/2001/06/022.

[634] A. H. Hoang, A. Jain, I. Scimemi, I. W. Stewart, Infrared Renormalization Group Flow for Heavy Quark Masses, Phys. Rev. Lett. 101 (2008) 151602. arXiv:0803.4214, doi:10.1103/PhysRevLett.101.151602.

[635] N. Brambilla, J. Komijani, A. S. Kronfeld, A. Vairo, Relations between heavy-light meson and quark masses, Phys. Rev. D97 (2018) 034503. arXiv:1712.04983, doi:10.1103/PhysRevD.97.034503.

[636] A. Bazavov, et al., Up-, down-, strange-, charm-, and bottom-quark masses from four-flavor lattice QCD, Phys. Rev. D98 (2018) 054517. arXiv:1802.04248, doi:10.1103/PhysRevD.98.054517.

[637] M. J. Savage, M. B. Wise, Spectrum of baryons with two heavy quarks, Phys. Lett. B248 (1990) 177. doi:10.1016/0370-2693(90)90035-5.

[638] W. A. Bardeen, E. J. Eichten, C. T. Hill, Chiral multiplets of heavy-light mesons, Phys. Rev. D68 (2003) 054024. arXiv:hep-ph/0305049, doi:10.1103/PhysRevD.68.054024.

[639] N. Brambilla, A. Vairo, T. Rosch, Effective field theory Lagrangians for baryons with two and three heavy quarks, Phys. Rev. D72 (2005) 034021. arXiv:hep-ph/0506065, doi:10.1103/PhysRevD.72.034021.

[640] S. Fleming, T. Mehen, Doubly heavy baryons, heavy quark-diquark symmetry and NRQCD, Phys. Rev. D73 (2006) 034502. arXiv:hep-ph/0509313, doi:10.1103/PhysRevD.73.034502.

[641] T. Mehen, B. C. Tiburzi, Doubly heavy baryons and quark-diquark symmetry in quenched and partially quenched chiral perturbation theory, Phys. Rev. D74 (2006) 054505. arXiv:hep-lat/0607023, doi:10.1103/PhysRevD.74.054505.

[642] Y.-L. Ma, M. Harada, Degeneracy of doubly heavy baryons from heavy quark symmetry, Phys. Lett. B754 (2016) 125. arXiv:1510.07481, doi:10.1016/j.physletb.2016.01.011.

[643] T. Mehen, Implications of heavy quark-diquark symmetry for excited doubly heavy baryons and tetraquarks, Phys. Rev. D96 (2017) 094028. arXiv:1708.05020, doi:10.1103/PhysRevD.96.094028.

[644] Y.-L. Ma, M. Harada, Chiral partner structure of doubly heavy baryons with heavy quark spin-flavor symmetry, J. Phys. G45 (2018) 075006. arXiv:1709.09746, doi:10.1088/1361-6471/aac86e.

[645] H.-Y. Cheng, Y.-L. Shi, Lifetimes of doubly charmed baryons, Phys. Rev. D98 (2018) 113005. arXiv:1809.08102, doi:10.1103/PhysRevD.98.113005.

[646] T. C. Mehen, A. Mohapatra, Perturbative corrections to heavy quark-diquark symmetry predictions for doubly heavy baryon hyperfine splittings, Phys. Rev. D100 (2019) 076014. arXiv:1905.06965, doi:10.1103/PhysRevD.100.076014.

[647] M. Padmanath, R. G. Edwards, N. Mathur, M. Peardon, Spectroscopy of doubly-charmed baryons from lattice QCD, Phys. Rev. D91 (2015) 094502. arXiv:1502.01845, doi:10.1103/PhysRevD.91.094502.

[648] R. Aaij, et al., Measurement of the Lifetime of the Doubly Charmed Baryon Ξ_{cc}^{++}, Phys. Rev. Lett. 121 (2018) 052002. arXiv:1806.02744, doi:10.1103/PhysRevLett.121.052002.

[649] M. Mattson, et al., First observation of the doubly charmed baryon Ξ_{cc}^+, Phys. Rev. Lett. 89 (2002) 112001. arXiv:hep-ex/0208014, doi:10.1103/PhysRevLett.89.112001.

[650] A. Ocherashvili, et al., Confirmation of the double charm baryon $\Xi_{cc}^+(3520)$ via its decay to pD^+K^-, Phys. Lett. B628 (2005) 18. arXiv:hep-ex/0406033, doi:10.1016/j.physletb.2005.09.043.

[651] S. J. Brodsky, F.-K. Guo, C. Hanhart, U.-G. Meißner, Isospin splittings of doubly heavy baryons, Phys. Lett. B698 (2011) 251. arXiv:1101.1983, doi:10.1016/j.physletb.2011.03.014.

[652] N. Brambilla, A. Pineda, J. Soto, A. Vairo, Effective field theories for heavy quarkonium, Rev. Mod. Phys. 77 (2005) 1423. arXiv:hep-ph/0410047, doi:10.1103/RevModPhys.77.1423.

[653] A. Vairo, Non-relativistic bound states: the long way back from the Bethe-Salpeter to the Schröedinger equation arXiv:0902.3346, doi:10.1142/9789814277839_0002.

[654] W. E. Caswell, G. P. Lepage, Effective Lagrangians for Bound State Problems in QED, QCD, and Other Field Theories, Phys. Lett. 167B (1986) 437. doi:10.1016/0370-2693(86)91297-9.

[655] B. A. Thacker, G. P. Lepage, Heavy quark bound states in lattice QCD, Phys. Rev. D43 (1991) 196. `doi:10.1103/PhysRevD.43.196`.

[656] G. P. Lepage, L. Magnea, C. Nakhleh, U. Magnea, K. Hornbostel, Improved nonrelativistic QCD for heavy quark physics, Phys. Rev. D46 (1992) 4052. `arXiv:hep-lat/9205007`, `doi:10.1103/PhysRevD.46.4052`.

[657] B. Colquhoun, R. J. Dowdall, C. T. H. Davies, K. Hornbostel, G. P. Lepage, Υ and Υ' Leptonic Widths, a_μ^b and m_b from full lattice QCD, Phys. Rev. D91 (2015) 074514. `arXiv:1408.5768`, `doi:10.1103/PhysRevD.91.074514`.

[658] C. Hughes, R. J. Dowdall, C. T. H. Davies, R. R. Horgan, G. von Hippel, M. Wingate, Hindered M1 Radiative Decay of $\Upsilon(2S)$ from Lattice NRQCD, Phys. Rev. D92 (2015) 094501. `arXiv:1508.01694`, `doi:10.1103/PhysRevD.92.094501`.

[659] B. Colquhoun, C. T. H. Davies, R. J. Dowdall, J. Koponen, G. P. Lepage, A. T. Lytle, Phenomenology with Lattice NRQCD b Quarks, PoS LATTICE2015 (2016) 334. `arXiv:1511.01852`.

[660] C. Hughes, C. T. H. Davies, C. J. Monahan, New methods for B meson decay constants and form factors from lattice NRQCD, Phys. Rev. D97 (2018) 054509. `arXiv:1711.09981`, `doi:10.1103/PhysRevD.97.054509`.

[661] A. Lytle, B. Colquhoun, C. Davies, J. Koponen, B_c spectroscopy using highly improved staggered quarks, in: 36th International Symposium on Lattice Field Theory (Lattice 2018) East Lansing, MI, United States, July 22-28, 2018. `arXiv:1811.09448`.

[662] G. T. Bodwin, E. Braaten, G. P. Lepage, Rigorous QCD predictions for decays of P-wave quarkonia, Phys. Rev. D46 (1992) R1914. `arXiv:hep-lat/9205006`, `doi:10.1103/PhysRevD.46.R1914`.

[663] G. T. Bodwin, E. Braaten, G. P. Lepage, Rigorous QCD analysis of inclusive annihilation and production of heavy quarkonium, Phys. Rev. D51 (1995) 1125, [Erratum: Phys. Rev. D55 (1997) 5853]. `arXiv:hep-ph/9407339`, `doi:10.1103/PhysRevD.55.5853,10.1103/PhysRevD.51.1125`.

[664] G. C. Nayak, J.-W. Qiu, G. F. Sterman, Fragmentation, factorization and infrared poles in heavy quarkonium production, Phys. Lett. B613 (2005) 45. `arXiv:hep-ph/0501235`, `doi:10.1016/j.physletb.2005.03.031`.

[665] G. C. Nayak, J.-W. Qiu, G. F. Sterman, Fragmentation, NRQCD and NNLO factorization analysis in heavy quarkonium production, Phys. Rev. D72 (2005) 114012. `arXiv:hep-ph/0509021`, `doi:10.1103/PhysRevD.72.114012`.

[666] Z.-B. Kang, Y.-Q. Ma, J.-W. Qiu, G. Sterman, Heavy Quarkonium Production at Collider Energies: Factorization and Evolution, Phys. Rev. D90 (2014) 034006. `arXiv:1401.0923`, `doi:10.1103/PhysRevD.90.034006`.

[667] Y.-Q. Ma, J.-W. Qiu, G. Sterman, H. Zhang, Factorized power expansion for high-p_T heavy quarkonium production, Phys. Rev. Lett. 113 (2014) 142002. `arXiv:1407.0383`, `doi:10.1103/PhysRevLett.113.142002`.

[668] Z.-B. Kang, Y.-Q. Ma, J.-W. Qiu, G. Sterman, Heavy Quarkonium Production at Collider Energies: Partonic Cross Section and Polarization, Phys. Rev. D91 (2015) 014030. `arXiv:1411.2456`, `doi:10.1103/PhysRevD.91.014030`.

[669] A. Pineda, J. Soto, Matching at one loop for the four quark operators in NRQCD, Phys. Rev. D58 (1998) 114011. `arXiv:hep-ph/9802365`, `doi:10.1103/PhysRevD.58.114011`.

[670] A. Vairo, A theoretical review of heavy quarkonium inclusive decays, Mod. Phys. Lett. A19 (2004) 253. `arXiv:hep-ph/0311303`, `doi:10.1142/S0217732304012927`.

[671] N. Brambilla, E. Mereghetti, A. Vairo, Electromagnetic quarkonium decays at order v^7, JHEP 08 (2006) 039, [Erratum: JHEP 04 (2011) 058]. `arXiv:hep-ph/0604190`, `doi:10.1088/1126-6708/2006/08/039,10.1007/JHEP04(2011)058`.

[672] N. Brambilla, E. Mereghetti, A. Vairo, Hadronic quarkonium decays at order v^7, Phys. Rev. D79 (2009) 074002, [Erratum: Phys. Rev. D83 (2011) 079904]. `arXiv:0810.2259`, `doi:10.1103/PhysRevD.83.079904`.

[673] M. Berwein, N. Brambilla, S. Hwang, A. Vairo, Poincaré invariance in NRQCD and pNRQCD revisited, Phys. Rev. D99 (2019) 094008. `arXiv:1811.05184`, `doi:10.1103/PhysRevD.99.094008`.

[674] N. Brambilla, D. Eiras, A. Pineda, J. Soto, A. Vairo, Inclusive decays of heavy quarkonium to light particles, Phys. Rev. D67 (2003) 034018. `arXiv:hep-ph/0208019`, `doi:10.1103/PhysRevD.67.034018`.

[675] A. Pineda, J. Soto, Effective field theory for ultrasoft momenta in NRQCD and NRQED, Nucl. Phys. Proc. Suppl. 64 (1998) 428. `arXiv:hep-ph/9707481`, `doi:10.1016/S0920-5632(97)01102-X`.

[676] N. Brambilla, A. Pineda, J. Soto, A. Vairo, Potential NRQCD: An Effective theory for heavy quarkonium, Nucl. Phys. B566 (2000) 275. `arXiv:hep-ph/9907240`, `doi:10.1016/S0550-3213(99)00693-8`.

[677] N. Brambilla, A. Vairo, X. Garcia i Tormo, J. Soto, QCD static energy at next-to-next-to-next-to leading-logarithmic accuracy, Phys. Rev. D80 (2009) 034016. `arXiv:0906.1390`, `doi:10.1103/PhysRevD.80.034016`.

[678] N. Brambilla, A. Pineda, J. Soto, A. Vairo, Infrared behavior of the static potential in perturbative QCD, Phys. Rev. D60 (1999) 091502. `arXiv:hep-ph/9903355`, `doi:10.1103/PhysRevD.60.091502`.

[679] C. Anzai, Y. Kiyo, Y. Sumino, Static QCD potential at three-loop order, Phys. Rev. Lett. 104 (2010) 112003. `arXiv:0911.4335`, `doi:10.1103/PhysRevLett.104.112003`.

[680] A. V. Smirnov, V. A. Smirnov, M. Steinhauser, Three-loop static potential, Phys. Rev. Lett. 104 (2010) 112002. `arXiv:0911.4742`, `doi:10.1103/PhysRevLett.104.112002`.

[681] N. Brambilla, X. Garcia i Tormo, J. Soto, A. Vairo, The Logarithmic contribution to the QCD static energy at N^4LO, Phys. Lett. B647 (2007) 185. `arXiv:hep-ph/0610143`, `doi:10.1016/j.physletb.2007.02.015`.

[682] B. A. Kniehl, A. A. Penin, M. Steinhauser, V. A. Smirnov, Non-Abelian $\alpha_s^3/(m_q r^2)$ heavy quark anti-quark potential, Phys. Rev. D65 (2002) 091503. `arXiv:hep-ph/0106135`, `doi:10.1103/PhysRevD.65.091503`.

[683] B. A. Kniehl, A. A. Penin, V. A. Smirnov, M. Steinhauser, Potential NRQCD and heavy quarkonium spectrum at next-to-next-to-next-to-leading order, Nucl. Phys. B635 (2002) 357. `arXiv:hep-ph/0203166`, `doi:10.1016/S0550-3213(02)00403-0`.

[684] N. Brambilla, D. Gromes, A. Vairo, Poincaré invariance and the heavy quark potential, Phys. Rev. D64 (2001) 076010. `arXiv:hep-ph/0104068`, `doi:10.1103/PhysRevD.64.076010`.

[685] C. Peset, A. Pineda, M. Stahlhofen, Potential NRQCD for unequal masses and the B_c spectrum at N^3LO, JHEP 05 (2016) 017. `arXiv:1511.08210`, `doi:10.1007/JHEP05(2016)017`.

[686] B. A. Kniehl, A. A. Penin, Ultrasoft effects in heavy quarkonium physics, Nucl. Phys. B563 (1999) 200. `arXiv:hep-ph/9907489`, `doi:10.1016/S0550-3213(99)00564-7`.

[687] N. Brambilla, A. Pineda, J. Soto, A. Vairo, The heavy quarkonium spectrum at order $m\alpha_s^5 ln\alpha_s$, Phys. Lett. B470 (1999) 215. `arXiv:`

`hep-ph/9910238`, `doi:10.1016/S0370-2693(99)01301-5`.

[688] A. Pineda, J. Soto, The Renormalization group improvement of the QCD static potentials, Phys. Lett. B495 (2000) 323. `arXiv:hep-ph/0007197`, `doi:10.1016/S0370-2693(00)01261-2`.

[689] A. Pineda, Renormalization group improvement of the NRQCD Lagrangian and heavy quarkonium spectrum, Phys. Rev. D65 (2002) 074007. `arXiv:hep-ph/0109117`, `doi:10.1103/PhysRevD.65.074007`.

[690] A. Pineda, Next-to-leading ultrasoft running of the heavy quarkonium potentials and spectrum: Spin-independent case, Phys. Rev. D84 (2011) 014012. `arXiv:1101.3269`, `doi:10.1103/PhysRevD.84.014012`.

[691] C. Peset, A. Pineda, J. Segovia, P-wave heavy quarkonium spectrum with next-to-next-to-next-to-leading logarithmic accuracy, Phys. Rev. D98 (2018) 094003. `arXiv:1809.09124`, `doi:10.1103/PhysRevD.98.094003`.

[692] C. Anzai, D. Moreno, A. Pineda, S-wave heavy quarkonium spectrum with next-to-next-to-next-to-leading logarithmic accuracy, Phys. Rev. D98 (2018) 114034. `arXiv:1810.11031`, `doi:10.1103/PhysRevD.98.114034`.

[693] A. Pineda, Review of heavy quarkonium at weak coupling, Prog. Part. Nucl. Phys. 67 (2012) 735. `arXiv:1111.0165`, `doi:10.1016/j.ppnp.2012.01.038`.

[694] N. Brambilla, Y. Sumino, A. Vairo, Quarkonium spectroscopy and perturbative QCD: A new perspective, Phys. Lett. B513 (2001) 381. `arXiv:hep-ph/0101305`, `doi:10.1016/S0370-2693(01)00611-6`.

[695] N. Brambilla, Y. Sumino, A. Vairo, Quarkonium spectroscopy and perturbative QCD: Massive quark loop effects, Phys. Rev. D65 (2002) 034001. `arXiv:hep-ph/0108084`, `doi:10.1103/PhysRevD.65.034001`.

[696] S. Recksiegel, Y. Sumino, Improved perturbative QCD prediction of the bottomonium spectrum, Phys. Rev. D67 (2003) 014004. `arXiv:hep-ph/0207005`, `doi:10.1103/PhysRevD.67.014004`.

[697] C. Ayala, G. Cvetic, A. Pineda, The bottom quark mass from the $\Upsilon(1S)$ system at NNNLO, JHEP 09 (2014) 045. `arXiv:1407.2128`, `doi:10.1007/JHEP09(2014)045`.

[698] M. Beneke, A. Maier, J. Piclum, T. Rauh, The bottom-quark mass from non-relativistic sum rules at NNNLO, Nucl. Phys. B891 (2015) 42. `arXiv:1411.3132`, `doi:10.1016/j.nuclphysb.2014.12.001`.

[699] Y. Kiyo, G. Mishima, Y. Sumino, Determination of m_c and m_b from quarkonium 1S energy levels in perturbative QCD, Phys. Lett. B752 (2016) 122, [Erratum: Phys. Lett. B772 (2017) 878]. `arXiv:1510.07072`, `doi:10.1016/j.physletb.2015.11.040,10.1016/j.physletb.2017.09.024`.

[700] C. Ayala, G. Cvetic, A. Pineda, Mass of the bottom quark from $\Upsilon(1S)$ at NNNLO: an update, J. Phys. Conf. Ser. 762 (2016) 012063. `arXiv:1606.01741`, `doi:10.1088/1742-6596/762/1/012063`.

[701] V. Mateu, P. G. Ortega, Bottom and charm mass determinations from global fits to $Q\bar{Q}$ bound states at N^{3}LO, JHEP 01 (2018) 122. `arXiv:1711.05755`, `doi:10.1007/JHEP01(2018)122`.

[702] C. Peset, A. Pineda, J. Segovia, The charm/bottom quark mass from heavy quarkonium at N^{3}LO, JHEP 09 (2018) 167. `arXiv:1806.05197`, `doi:10.1007/JHEP09(2018)167`.

[703] B. Aubert, et al., Observation of the bottomonium ground state in the decay $\Upsilon(3S) \to \gamma\eta_b$, Phys. Rev. Lett. 101 (2008) 071801, [Erratum: Phys. Rev. Lett. 102 (2009) 029901]. `arXiv:0807.1086`, `doi:10.1103/PhysRevLett.102.029901,10.1103/PhysRevLett.101.071801`.

[704] F. Abe, et al., Observation of the B_c meson in $p\bar{p}$ collisions at $\sqrt{s}$ = 1.8 TeV, Phys. Rev. Lett. 81 (1998) 2432. `arXiv:hep-ex/9805034`, `doi:10.1103/PhysRevLett.81.2432`.

[705] R. Aaij, et al., Measurements of B_c^+ production and mass with the $B_c^+ \to J/\psi\pi^+$ decay, Phys. Rev. Lett. 109 (2012) 232001. `arXiv:1209.5634`, `doi:10.1103/PhysRevLett.109.232001`.

[706] R. Aaij, et al., Observation of $B_c^+ \to J/\psi D_s^+$ and $B_c^+ \to J/\psi D_s^{*+}$ decays, Phys. Rev. D87 (2013) 112012, [Addendum: Phys. Rev. D89 (2014) 019901]. `arXiv:1304.4530`, `doi:10.1103/PhysRevD.87.112012,10.1103/PhysRevD.89.019901`.

[707] R. Aaij, et al., First observation of a baryonic B_c^+ decay, Phys. Rev. Lett. 113 (2014) 152003. `arXiv:1408.0971`, `doi:10.1103/PhysRevLett.113.152003`.

[708] R. Aaij, et al., Observation of $B_c^+ \to J/\psi D^{(*)}K^{(*)}$ decays, Phys. Rev. D95 (2017) 032005. `arXiv:1612.07421`, `doi:10.1103/PhysRevD.95.032005`.

[709] N. Brambilla, A. Vairo, The B_c mass up to order α_s^4, Phys. Rev. D62 (2000) 094019. `arXiv:hep-ph/0002075`, `doi:10.1103/PhysRevD.62.094019`.

[710] S. Recksiegel, Y. Sumino, Fine and hyperfine splittings of charmonium and bottomonium: An improved perturbative QCD approach, Phys. Lett. B578 (2004) 369. `arXiv:hep-ph/0305178`, `doi:10.1016/j.physletb.2003.10.070`.

[711] N. Brambilla, A. Vairo, 1P quarkonium fine splittings at next-to-leading order, Phys. Rev. D71 (2005) 034020. `arXiv:hep-ph/0411156`, `doi:10.1103/PhysRevD.71.034020`.

[712] B. A. Kniehl, A. A. Penin, A. Pineda, V. A. Smirnov, M. Steinhauser, $M(\eta_b)$ and α_s from nonrelativistic renormalization group, Phys. Rev. Lett. 92 (2004) 242001, [Erratum: Phys. Rev. Lett. 104 (2010) 199901]. `arXiv:hep-ph/0312086`, `doi:10.1103/PhysRevLett.92.242001,10.1103/PhysRevLett.104.199901`.

[713] A. A. Penin, A. Pineda, V. A. Smirnov, M. Steinhauser, $M(B_c^*) - M(B_c)$ splitting from nonrelativistic renormalization group, Phys. Lett. B593 (2004) 124, [Erratum: Phys. Lett. B677 (2009) 343]. `arXiv:hep-ph/0403080`, `doi:10.1016/j.physletb.2009.05.036,10.1016/j.physletb.2004.04.066,10.1016/j.physletb.2009.12.035`.

[714] A. A. Penin, M. Steinhauser, Heavy quarkonium spectrum at $O(\alpha_s^5 m_q)$ and bottom/top quark mass determination, Phys. Lett. B538 (2002) 335. `arXiv:hep-ph/0204290`, `doi:10.1016/S0370-2693(02)02040-3`.

[715] A. A. Penin, V. A. Smirnov, M. Steinhauser, Heavy quarkonium spectrum and production/annihilation rates to order $\beta_0^3\alpha_s^3$, Nucl. Phys. B716 (2005) 303. `arXiv:hep-ph/0501042`, `doi:10.1016/j.nuclphysb.2005.03.028`.

[716] M. Beneke, Y. Kiyo, K. Schuller, Third-order coulomb corrections to the S-wave Green function, energy levels and wave functions at the origin, Nucl. Phys. B714 (2005) 67. `arXiv:hep-ph/0501289`, `doi:10.1016/j.nuclphysb.2005.02.028`.

[717] M. Beneke, Y. Kiyo, K. Schuller, Third-order non-Coulomb correction to the S-wave quarkonium wave functions at the origin, Phys. Lett. B658 (2008) 222. `arXiv:0705.4518`, `doi:10.1016/j.physletb.2007.09.074`.

172

[718] Y. Kiyo, Y. Sumino, Perturbative heavy quarkonium spectrum at next-to-next-to-next-to-leading order, Phys. Lett. B730 (2014) 76. `arXiv:1309.6571`, `doi:10.1016/j.physletb.2014.01.030`.

[719] Y. Kiyo, Y. Sumino, Full Formula for Heavy Quarkonium Energy Levels at Next-to-next-to-next-to-leading Order, Nucl. Phys. B889 (2014) 156. `arXiv:1408.5590`, `doi:10.1016/j.nuclphysb.2014.10.010`.

[720] A. A. Penin, A. Pineda, V. A. Smirnov, M. Steinhauser, Spin dependence of heavy quarkonium production and annihilation rates: Complete next-to-next-to-leading logarithmic result, Nucl. Phys. B699 (2004) 183, [Erratum: Nucl. Phys. B829 (2010) 398]. `arXiv:hep-ph/0406175`, `doi:10.1016/j.nuclphysb.2009.12.009,10.1016/j.nuclphysb.2004.08.026`.

[721] A. Pineda, A. Signer, Heavy Quark Pair Production near Threshold with Potential Non-Relativistic QCD, Nucl. Phys. B762 (2007) 67. `arXiv:hep-ph/0607239`, `doi:10.1016/j.nuclphysb.2006.09.025`.

[722] Y. Kiyo, A. Pineda, A. Signer, New determination of inclusive electromagnetic decay ratios of heavy quarkonium from QCD, Nucl. Phys. B841 (2010) 231. `arXiv:1006.2685`, `doi:10.1016/j.nuclphysb.2010.08.007`.

[723] M. Beneke, Y. Kiyo, A. A. Penin, Ultrasoft contribution to quarkonium production and annihilation, Phys. Lett. B653 (2007) 53. `arXiv:0706.2733`, `doi:10.1016/j.physletb.2007.06.068`.

[724] M. Beneke, Y. Kiyo, P. Marquard, A. Penin, J. Piclum, D. Seidel, M. Steinhauser, Leptonic decay of the $\Upsilon(1S)$ meson at third order in QCD, Phys. Rev. Lett. 112 (2014) 151801. `arXiv:1401.3005`, `doi:10.1103/PhysRevLett.112.151801`.

[725] A. Pineda, Next-to-leading nonperturbative calculation in heavy quarkonium, Nucl. Phys. B494 (1997) 213. `arXiv:hep-ph/9611388`, `doi:10.1016/S0550-3213(97)00175-2`.

[726] T. Rauh, Higher-order condensate corrections to Υ masses, leptonic decay rates and sum rules, JHEP 05 (2018) 201. `arXiv:1803.05477`, `doi:10.1007/JHEP05(2018)201`.

[727] C. W. Bauer, C.-W. Chiang, S. Fleming, A. K. Leibovich, I. Low, Resumming the color octet contribution to radiative Υ decay, Phys. Rev. D64 (2001) 114014. `arXiv:hep-ph/0106316`, `doi:10.1103/PhysRevD.64.114014`.

[728] S. Fleming, A. K. Leibovich, Resummed Photon Spectrum in Radiative Υ Decays, Phys. Rev. Lett. 90 (2003) 032001. `arXiv:hep-ph/0211303`, `doi:10.1103/PhysRevLett.90.032001`.

[729] S. Fleming, A. K. Leibovich, The photon spectrum in Υ decays, Phys. Rev. D67 (2003) 074035. `arXiv:hep-ph/0212094`, `doi:10.1103/PhysRevD.67.074035`.

[730] X. Garcia i Tormo, J. Soto, Soft, collinear, and nonrelativistic modes in radiative decays of very heavy quarkonium, Phys. Rev. D69 (2004) 114006. `arXiv:hep-ph/0401233`, `doi:10.1103/PhysRevD.69.114006`.

[731] X. Garcia i Tormo, J. Soto, Semi-inclusive radiative decays of $\Upsilon(1S)$, Phys. Rev. D72 (2005) 054014. `arXiv:hep-ph/0507107`, `doi:10.1103/PhysRevD.72.054014`.

[732] X. Garcia i Tormo, J. Soto, Radiative decays and the nature of heavy quarkonia, Phys. Rev. Lett. 96 (2006) 111801. `arXiv:hep-ph/0511167`, `doi:10.1103/PhysRevLett.96.111801`.

[733] N. Brambilla, X. Garcia i Tormo, J. Soto, A. Vairo, Extraction of α_s from radiative $\Upsilon(1S)$ decays, Phys. Rev. D75 (2007) 074014. `arXiv:hep-ph/0702079`, `doi:10.1103/PhysRevD.75.074014`.

[734] N. Brambilla, Y. Jia, A. Vairo, Model-independent study of magnetic dipole transitions in quarkonium, Phys. Rev. D73 (2006) 054005. `arXiv:hep-ph/0512369`, `doi:10.1103/PhysRevD.73.054005`.

[735] N. Brambilla, P. Pietrulewicz, A. Vairo, Model-independent study of electric dipole transitions in quarkonium, Phys. Rev. D85 (2012) 094005. `arXiv:1203.3020`, `doi:10.1103/PhysRevD.85.094005`.

[736] A. Pineda, J. Segovia, Improved determination of heavy quarkonium magnetic dipole transitions in potential nonrelativistic QCD, Phys. Rev. D87 (2013) 074024. `arXiv:1302.3528`, `doi:10.1103/PhysRevD.87.074024`.

[737] J. Segovia, S. Steinbeier, A. Vairo, Electric dipole transitions of $1P$ bottomonia, Phys. Rev. D99 (2019) 074011. `arXiv:1811.07590`, `doi:10.1103/PhysRevD.99.074011`.

[738] B. Aubert, et al., Evidence for the $\eta_b(1S)$ meson in radiative $\Upsilon(2S)$ decay, Phys. Rev. Lett. 103 (2009) 161801. `arXiv:0903.1124`, `doi:10.1103/PhysRevLett.103.161801`.

[739] N. Brambilla, P. Roig, A. Vairo, Precise determination of the η_c mass and width in the radiative $J/\psi \to \eta_c\gamma$ decay, AIP Conf. Proc. 1343 (2011) 418. `arXiv:1012.0773`, `doi:10.1063/1.3575048`.

[740] N. Brambilla, A. Pineda, J. Soto, A. Vairo, QCD potential at $O(1/m)$, Phys. Rev. D63 (2001) 014023. `arXiv:hep-ph/0002250`, `doi:10.1103/PhysRevD.63.014023`.

[741] A. Pineda, A. Vairo, The QCD potential at $O(1/m^2)$: Complete spin dependent and spin independent result, Phys. Rev. D63 (2001) 054007, [Erratum: Phys. Rev. D64 (2001) 039902]. `arXiv:hep-ph/0009145`, `doi:10.1103/PhysRevD.64.039902,10.1103/PhysRevD.63.054007`.

[742] N. Brambilla, D. Eiras, A. Pineda, J. Soto, A. Vairo, New predictions for inclusive heavy quarkonium P-wave decays, Phys. Rev. Lett. 88 (2002) 012003. `arXiv:hep-ph/0109130`, `doi:10.1103/PhysRevLett.88.012003`.

[743] N. Brambilla, A. Pineda, J. Soto, A. Vairo, The $m\Lambda_{QCD}$ scale in heavy quarkonium, Phys. Lett. B580 (2004) 60. `arXiv:hep-ph/0307159`, `doi:10.1016/j.physletb.2003.11.031`.

[744] G. S. Bali, B. Bolder, N. Eicker, T. Lippert, B. Orth, P. Ueberholz, K. Schilling, T. Struckmann, Static potentials and glueball masses from QCD simulations with Wilson sea quarks, Phys. Rev. D62 (2000) 054503. `arXiv:hep-lat/0003012`, `doi:10.1103/PhysRevD.62.054503`.

[745] N. Brambilla, G. Krein, J. Tarrùs Castellà, A. Vairo, Long-range properties of $1S$ bottomonium states, Phys. Rev. D93 (2016) 054002. `arXiv:1510.05895`, `doi:10.1103/PhysRevD.93.054002`.

[746] K. G. Wilson, Confinement of Quarks, Phys. Rev. D10 (1974) 2445. `doi:10.1103/PhysRevD.10.2445`.

[747] L. Susskind, Coarse Grained Quantum Chromodynamics, in: Ecole d'Ete de Physique Theorique - Weak and Electromagnetic Interactions at High Energy Les Houches, France, July 5-August 14, 1976, p. 207.

[748] W. Fischler, Quark-antiquark potential in QCD, Nucl. Phys. B129 (1977) 157. `doi:10.1016/0550-3213(77)90026-8`.

[749] L. S. Brown, W. I. Weisberger, Remarks on the Static Potential in Quantum Chromodynamics, Phys. Rev. D20 (1979) 3239. `doi:10.1103/PhysRevD.20.3239`.

[750] C. Peset, A. Pineda, M. Stahlhofen, Relativistic corrections to the static energy in terms of Wilson loops at weak coupling, Eur. Phys. J. C77 (2017) 681. arXiv:1706.03971, doi:10.1140/epjc/s10052-017-5250-6.

[751] J. B. Kogut, G. Parisi, Long Range Spin Spin Forces in Gauge Theories, Phys. Rev. Lett. 47 (1981) 1089. doi:10.1103/PhysRevLett.47.1089.

[752] G. Perez-Nadal, J. Soto, Effective string theory constraints on the long distance behavior of the subleading potentials, Phys. Rev. D79 (2009) 114002. arXiv:0811.2762, doi:10.1103/PhysRevD.79.114002.

[753] A. Pineda, J. Tarrs Castell, Novel implementation of the multipole expansion to quarkonium hadronic transitions, Phys. Rev. D100 (2019) 054021. arXiv:1905.03794, doi:10.1103/PhysRevD.100.054021.

[754] N. Brambilla, J. Ghiglieri, A. Vairo, Three-quark static potential in perturbation theory, Phys. Rev. D81 (2010) 054031. arXiv:0911.3541, doi:10.1103/PhysRevD.81.054031.

[755] N. Brambilla, F. Karbstein, A. Vairo, Symmetries of the three-heavy-quark system and the color-singlet static energy at next-to-next-to-leading logarithmic order, Phys. Rev. D87 (2013) 074014. arXiv:1301.3013, doi:10.1103/PhysRevD.87.074014.

[756] E. E. Jenkins, A. V. Manohar, Baryon chiral perturbation theory using a heavy fermion Lagrangian, Phys. Lett. B255 (1991) 558. doi:10.1016/0370-2693(91)90266-S.

[757] T. T. Takahashi, H. Suganuma, Gluonic excitation of the three-quark system in SU(3) lattice QCD, Phys. Rev. Lett. 90 (2003) 182001. arXiv:hep-lat/0210024, doi:10.1103/PhysRevLett.90.182001.

[758] T. T. Takahashi, H. Suganuma, Detailed analysis of the gluonic excitation in the three-quark system in lattice QCD, Phys. Rev. D70 (2004) 074506. arXiv:hep-lat/0409105, doi:10.1103/PhysRevD.70.074506.

[759] Y. Koma, M. Koma, Precise determination of the three-quark potential in SU(3) lattice gauge theory, Phys. Rev. D95 (2017) 094513. arXiv:1703.06247, doi:10.1103/PhysRevD.95.094513.

[760] N. Brambilla, A. Vairo, A. Polosa, J. Soto, Round Table on Heavy Quarkonia and Exotic States, Nucl. Phys. Proc. Suppl. 185 (2008) 107. doi:10.1016/j.nuclphysbps.2008.10.011.

[761] J. Tarrs Castell, Heavy hybrids and tetraquarks in effective field theory, EPJ Web Conf. 202 (2019) 01005. arXiv:1901.09761, doi:10.1051/epjconf/201920201005.

[762] Y. Cai, T. Cohen, Narrow exotic hadrons in the heavy quark limit of QCD, Eur. Phys. J. A55 (2019) 206. arXiv:1901.05473, doi:10.1140/epja/i2019-12906-0.

[763] S. Perantonis, C. Michael, Static potentials and hybrid mesons from pure SU(3) lattice gauge theory, Nucl. Phys. B347 (1990) 854. doi:10.1016/0550-3213(90)90386-R.

[764] K. J. Juge, J. Kuti, C. J. Morningstar, Gluon excitations of the static quark potential and the hybrid quarkonium spectrum, Nucl. Phys. Proc. Suppl. 63 (1998) 326. arXiv:hep-lat/9709131, doi:10.1016/S0920-5632(97)00759-7.

[765] M. Foster, C. Michael, Hadrons with a heavy color adjoint particle, Phys. Rev. D59 (1999) 094509. arXiv:hep-lat/9811010, doi:10.1103/PhysRevD.59.094509.

[766] K. J. Juge, J. Kuti, C. Morningstar, Fine structure of the QCD string spectrum, Phys. Rev. Lett. 90 (2003) 161601. arXiv:hep-lat/0207004, doi:10.1103/PhysRevLett.90.161601.

[767] G. S. Bali, A. Pineda, QCD phenomenology of static sources and gluonic excitations at short distances, Phys. Rev. D69 (2004) 094001. arXiv:hep-ph/0310130, doi:10.1103/PhysRevD.69.094001.

[768] S. Capitani, O. Philipsen, C. Reisinger, C. Riehl, M. Wagner, Precision computation of hybrid static potentials in SU(3) lattice gauge theory, Phys. Rev. D99 (2019) 034502. arXiv:1811.11046, doi:10.1103/PhysRevD.99.034502.

[769] W. Chen, R. T. Kleiv, T. G. Steele, B. Bulthuis, D. Harnett, J. Ho, T. Richards, S.-L. Zhu, Mass Spectrum of Heavy Quarkonium Hybrids, JHEP 09 (2013) 019. arXiv:1304.4522, doi:10.1007/JHEP09(2013)019.

[770] W. Chen, T. G. Steele, S.-L. Zhu, Masses of the bottom-charm hybrid $\bar{b}Gc$ states, J. Phys. G41 (2014) 025003. arXiv:1306.3486, doi:10.1088/0954-3899/41/2/025003.

[771] R. F. Lebed, E. S. Swanson, Heavy-Quark Hybrid Mass Splittings: Hyperfine and "Ultrafine", Few Body Syst. 59 (2018) 53. arXiv:1708.02679, doi:10.1007/s00601-018-1376-9.

[772] A. Vairo, Heavy Hadron Spectroscopy, Int. J. Mod. Phys. A22 (2007) 5481. arXiv:hep-ph/0611310, doi:10.1142/S0217751X07038748.

[773] M. B. Wise, Chiral perturbation theory for hadrons containing a heavy quark, Phys. Rev. D45 (1992) R2188. doi:10.1103/PhysRevD.45.R2188.

[774] S. Weinberg, Nuclear forces from chiral Lagrangians, Phys. Lett. B251 (1990) 288. doi:10.1016/0370-2693(90)90938-3.

[775] D. B. Kaplan, M. J. Savage, M. B. Wise, A new expansion for nucleon-nucleon interactions, Phys. Lett. B424 (1998) 390. arXiv:nucl-th/9801034, doi:10.1016/S0370-2693(98)00210-X.

[776] D. B. Kaplan, M. J. Savage, M. B. Wise, Two nucleon systems from effective field theory, Nucl. Phys. B534 (1998) 329. arXiv:nucl-th/9802075, doi:10.1016/S0550-3213(98)00440-4.

[777] S. Fleming, T. Mehen, I. W. Stewart, NNLO corrections to nucleon-nucleon scattering and perturbative pions, Nucl. Phys. A677 (2000) 313. arXiv:nucl-th/9911001, doi:10.1016/S0375-9474(00)00221-9.

[778] M. T. AlFiky, F. Gabbiani, A. A. Petrov, X(3872): Hadronic molecules in effective field theory, Phys. Lett. B640 (2006) 238. arXiv:hep-ph/0506141, doi:10.1016/j.physletb.2006.07.069.

[779] S. Fleming, M. Kusunoki, T. Mehen, U. van Kolck, Pion interactions in the X(3872), Phys. Rev. D76 (2007) 034006. arXiv:hep-ph/0703168, doi:10.1103/PhysRevD.76.034006.

[780] M. P. Valderrama, Power Counting and Perturbative One Pion Exchange in Heavy Meson Molecules, Phys. Rev. D85 (2012) 114037. arXiv:1204.2400, doi:10.1103/PhysRevD.85.114037.

[781] V. Baru, E. Epelbaum, A. A. Filin, C. Hanhart, U.-G. Meißner, A. V. Nefediev, Quark mass dependence of the X(3872) binding energy, Phys. Lett. B726 (2013) 537. arXiv:1306.4108, doi:10.1016/j.physletb.2013.08.073.

[782] P. Hagen, H. W. Hammer, C. Hanhart, Two and three-body structure of the Y(4660), Phys. Lett. B696 (2011) 103. arXiv:1007.1126, doi:10.1016/j.physletb.2010.12.021.

174

[783] J. Nieves, M. P. Valderrama, Deriving the existence of $B\bar{B}^*$ bound states from the $X(3872)$ and Heavy Quark Symmetry, Phys. Rev. D84 (2011) 056015. arXiv:1106.0600, doi:10.1103/PhysRevD.84.056015.

[784] C. Hanhart, Meson production in nucleon-nucleon collisions close to the threshold, Phys. Rept. 397 (2004) 155. arXiv:hep-ph/0311341, doi:10.1016/j.physrep.2004.03.007.

[785] M. Cleven, Q. Wang, F.-K. Guo, C. Hanhart, U.-G. Meißner, Q. Zhao, Confirming the molecular nature of the $Z_b(10610)$ and the $Z_b(10650)$, Phys. Rev. D87 (2013) 074006. arXiv:1301.6461, doi:10.1103/PhysRevD.87.074006.

[786] F.-K. Guo, C. Hanhart, U.-G. Meißner, On the extraction of the light quark mass ratio from the decays $\psi' \to J/\psi\pi^0(\eta)$, Phys. Rev. Lett. 103 (2009) 082003, [Erratum: Phys. Rev. Lett. 104 (2010) 109901]. arXiv:0907.0521, doi:10.1103/PhysRevLett.103.082003, 10.1103/PhysRevLett.104.109901.

[787] F.-K. Guo, C. Hanhart, G. Li, U.-G. Meißner, Q. Zhao, Effect of charmed meson loops on charmonium transitions, Phys. Rev. D83 (2011) 034013. arXiv:1008.3632, doi:10.1103/PhysRevD.83.034013.

[788] F.-K. Guo, U.-G. Meißner, Light quark mass dependence in heavy quarkonium physics, Phys. Rev. Lett. 109 (2012) 062001. arXiv:1203.1116, doi:10.1103/PhysRevLett.109.062001.

[789] V. Lensky, V. Baru, J. Haidenbauer, C. Hanhart, A. E. Kudryavtsev, U. G. Meißner, Towards a field theoretic understanding of $NN \to NN\pi$, Eur. Phys. J. A27 (2006) 37. arXiv:nucl-th/0511054, doi:10.1140/epja/i2006-10002-4.

[790] V. Baru, C. Hanhart, F. Myhrer, Effective field theory calculations of $NN \to NN\pi$, Int. J. Mod. Phys. E23 (2014) 1430004. arXiv:1310.3505, doi:10.1142/S0218301314300045.

[791] F.-K. Guo, U.-G. Meißner, Z. Yang, Hindered magnetic dipole transitions between P-wave bottomonia and coupled-channel effects, Phys. Lett. B760 (2016) 417. arXiv:1604.00770, doi:10.1016/j.physletb.2016.07.023.

[792] F.-K. Guo, U.-G. Meißner, Examining coupled-channel effects in radiative charmonium transitions, Phys. Rev. Lett. 108 (2012) 112002. arXiv:1111.1151, doi:10.1103/PhysRevLett.108.112002.

[793] M. C. Birse, Deconstructing triplet nucleon-nucleon scattering, Phys. Rev. C76 (2007) 034002. arXiv:0706.0984, doi:10.1103/PhysRevC.76.034002.

[794] E. Wang, J.-J. Xie, W.-H. Liang, F.-K. Guo, E. Oset, Role of a triangle singularity in the $\gamma p \to K^+\Lambda(1405)$ reaction, Phys. Rev. C95 (2017) 015205. arXiv:1610.07117, doi:10.1103/PhysRevC.95.015205.

[795] M. Bayar, F. Aceti, F.-K. Guo, E. Oset, Discussion on triangle singularities in the $\Lambda_b \to J/\psi K^- p$ Reaction, Phys. Rev. D94 (2016) 074039. arXiv:1609.04133, doi:10.1103/PhysRevD.94.074039.

[796] A. E. Bondar, M. B. Voloshin, $\Upsilon(6S)$ and triangle singularity in $e^+e^- \to B_1(5721)\bar{B} \to Z_b(10610)\pi$, Phys. Rev. D93 (2016) 094008. arXiv:1603.08436, doi:10.1103/PhysRevD.93.094008.

[797] P. Pakhlov, Charged charmonium-like states as rescattering effects in $B \to D_{sJ}D^{(*)}$ decays, Phys. Lett. B702 (2011) 139. arXiv:1105.2945, doi:10.1016/j.physletb.2011.06.079.

[798] P. Pakhlov, T. Uglov, Charged charmonium-like $Z^+(4430)$ from rescattering in conventional B decays, Phys. Lett. B748 (2015) 183. arXiv:1408.5295, doi:10.1016/j.physletb.2015.06.074.

[799] F.-K. Guo, U.-G. Meißner, W. Wang, Z. Yang, How to reveal the exotic nature of the $P_c(4450)$, Phys. Rev. D92 (2015) 071502. arXiv:1507.04950, doi:10.1103/PhysRevD.92.071502.

[800] F.-K. Guo, U.-G. Meißner, J. Nieves, Z. Yang, Remarks on the P_c structures and triangle singularities, Eur. Phys. J. A52 (2016) 318. arXiv:1605.05113, doi:10.1140/epja/i2016-16318-4.

[801] C. Schmid, Final-State Interactions and the Simulation of Resonances, Phys. Rev. 154 (1967) 1363. doi:10.1103/PhysRev.154.1363.

[802] A. V. Anisovich, V. V. Anisovich, Rescattering effects in three particle states and the Schmid theorem, Phys. Lett. B345 (1995) 321. doi:10.1016/0370-2693(94)01671-X.

[803] A. Gray, I. Allison, C. T. H. Davies, E. Dalgic, G. P. Lepage, J. Shigemitsu, M. Wingate, Υ spectrum and m_b from full lattice QCD, Phys. Rev. D72 (2005) 094507. arXiv:hep-lat/0507013, doi:10.1103/PhysRevD.72.094507.

[804] T. Burch, C. DeTar, M. Di Pierro, A. X. El-Khadra, E. D. Freeland, S. Gottlieb, A. S. Kronfeld, L. Levkova, P. B. Mackenzie, J. N. Simone, Quarkonium mass splittings in three-flavor lattice QCD, Phys. Rev. D81 (2010) 034508. arXiv:0912.2701, doi:10.1103/PhysRevD.81.034508.

[805] S. Meinel, Bottomonium spectrum at order v^6 from domain-wall lattice QCD: Precise results for hyperfine splittings, Phys. Rev. D82 (2010) 114502. arXiv:1007.3966, doi:10.1103/PhysRevD.82.114502.

[806] Y. Namekawa, et al., Charm quark system at the physical point of 2+1 flavor lattice QCD, Phys. Rev. D84 (2011) 074505. arXiv:1104.4600, doi:10.1103/PhysRevD.84.074505.

[807] J. O. Daldrop, C. T. H. Davies, R. J. Dowdall, Prediction of the bottomonium D-wave spectrum from full lattice QCD, Phys. Rev. Lett. 108 (2012) 102003. arXiv:1112.2590, doi:10.1103/PhysRevLett.108.102003.

[808] D. Mohler, R. M. Woloshyn, D and D_s meson spectroscopy, Phys. Rev. D84 (2011) 054505. arXiv:1103.5506, doi:10.1103/PhysRevD.84.054505.

[809] R. J. Dowdall, et al., The Upsilon spectrum and the determination of the lattice spacing from lattice QCD including charm quarks in the sea, Phys. Rev. D85 (2012) 054509. arXiv:1110.6887, doi:10.1103/PhysRevD.85.054509.

[810] C. McNeile, C. T. H. Davies, E. Follana, K. Hornbostel, G. P. Lepage, Heavy meson masses and decay constants from relativistic heavy quarks in full lattice QCD, Phys. Rev. D86 (2012) 074503. arXiv:1207.0994, doi:10.1103/PhysRevD.86.074503.

[811] R. J. Dowdall, C. T. H. Davies, T. C. Hammant, R. R. Horgan, Precise heavy-light meson masses and hyperfine splittings from lattice QCD including charm quarks in the sea, Phys. Rev. D86 (2012) 094510. arXiv:1207.5149, doi:10.1103/PhysRevD.86.094510.

[812] G. C. Donald, C. T. H. Davies, R. J. Dowdall, E. Follana, K. Hornbostel, J. Koponen, G. P. Lepage, C. McNeile, Precision tests of the J/ψ from full lattice QCD: mass, leptonic width and radiative decay rate to η_c, Phys. Rev. D86 (2012) 094501. arXiv:1208.2855, doi:10.1103/PhysRevD.86.094501.

[813] Y. Aoki, N. H. Christ, J. M. Flynn, T. Izubuchi, C. Lehner, M. Li, H. Peng, A. Soni, R. S. Van de Water, O. Witzel, Nonperturbative tuning of an improved relativistic heavy-quark action with application to bottom spectroscopy, Phys. Rev. D86 (2012) 116003. arXiv:1206.2554, doi:10.1103/PhysRevD.86.116003.

[814] R. J. Dowdall, C. T. H. Davies, T. Hammant, R. R. Horgan, C. Hughes, Bottomonium hyperfine splittings from lattice nonrelativistic QCD including radiative and relativistic corrections, Phys. Rev. D89 (2014) 031502, [Erratum: Phys. Rev. D92 (2015) 039904]. `arXiv: 1309.5797`, `doi:10.1103/PhysRevD.92.039904,10.1103/PhysRevD.89.031502`.

[815] M. Kalinowski, M. Wagner, Masses of D mesons, D_s mesons and charmonium states from twisted mass lattice QCD, Phys. Rev. D92 (2015) 094508. `arXiv:1509.02396`, `doi:10.1103/PhysRevD.92.094508`.

[816] K. Cichy, M. Kalinowski, M. Wagner, Continuum limit of the D meson, D_s meson and charmonium spectrum from $N_f = 2 + 1 + 1$ twisted mass lattice QCD, Phys. Rev. D94 (2016) 094503. `arXiv:1603.06467`, `doi:10.1103/PhysRevD.94.094503`.

[817] C. DeTar, A. S. Kronfeld, S.-h. Lee, D. Mohler, J. N. Simone, Splittings of low-lying charmonium masses at the physical point, Phys. Rev. D99 (2019) 034509. `arXiv:1810.09983`, `doi:10.1103/PhysRevD.99.034509`.

[818] A. Duncan, E. Eichten, H. Thacker, Electromagnetic splittings and light quark masses in lattice QCD, Phys. Rev. Lett. 76 (1996) 3894. `arXiv:hep-lat/9602005`, `doi:10.1103/PhysRevLett.76.3894`.

[819] T. Blum, T. Doi, M. Hayakawa, T. Izubuchi, N. Yamada, Determination of light quark masses from the electromagnetic splitting of pseudoscalar meson masses computed with two flavors of domain wall fermions, Phys. Rev. D76 (2007) 114508. `arXiv:0708.0484`, `doi:10.1103/PhysRevD.76.114508`.

[820] T. Blum, R. Zhou, T. Doi, M. Hayakawa, T. Izubuchi, S. Uno, N. Yamada, Electromagnetic mass splittings of the low lying hadrons and quark masses from 2+1 flavor lattice QCD+QED, Phys. Rev. D82 (2010) 094508. `arXiv:1006.1311`, `doi:10.1103/PhysRevD.82.094508`.

[821] S. Aoki, et al., 1+1+1 flavor QCD + QED simulation at the physical point, Phys. Rev. D86 (2012) 034507. `arXiv:1205.2961`, `doi: 10.1103/PhysRevD.86.034507`.

[822] R. Horsley, J. Najjar, Y. Nakamura, D. Pleiter, P. E. L. Rakow, G. Schierholz, J. M. Zanotti, Isospin breaking in octet baryon mass splittings, Phys. Rev. D86 (2012) 114511. `arXiv:1206.3156`, `doi:10.1103/PhysRevD.86.114511`.

[823] G. M. de Divitiis, R. Frezzotti, V. Lubicz, G. Martinelli, R. Petronzio, G. C. Rossi, F. Sanfilippo, S. Simula, N. Tantalo, Leading isospin breaking effects on the lattice, Phys. Rev. D87 (2013) 114505. `arXiv:1303.4896`, `doi:10.1103/PhysRevD.87.114505`.

[824] S. Borsanyi, et al., Isospin splittings in the light baryon octet from lattice QCD and QED, Phys. Rev. Lett. 111 (2013) 252001. `arXiv: 1306.2287`, `doi:10.1103/PhysRevLett.111.252001`.

[825] S. Borsanyi, et al., Ab initio calculation of the neutron-proton mass difference, Science 347 (2015) 1452. `arXiv:1406.4088`, `doi: 10.1126/science.1257050`.

[826] R. Horsley, et al., Isospin splittings of meson and baryon masses from three-flavor lattice QCD + QED, J. Phys. G43 (2016) 10LT02. `arXiv:1508.06401`, `doi:10.1088/0954-3899/43/10/10LT02`.

[827] R. Horsley, et al., QED effects in the pseudoscalar meson sector, JHEP 04 (2016) 093. `arXiv:1509.00799`, `doi:10.1007/JHEP04(2016) 093`.

[828] D. Giusti, V. Lubicz, C. Tarantino, G. Martinelli, S. Sanfilippo, S. Simula, N. Tantalo, Leading isospin-breaking corrections to pion, kaon and charmed-meson masses with Twisted-Mass fermions, Phys. Rev. D95 (2017) 114504. `arXiv:1704.06561`, `doi:10.1103/PhysRevD. 95.114504`.

[829] S. Basak, et al., Lattice computation of the electromagnetic contributions to kaon and pion masses, Phys. Rev. D99 (2019) 034503. `arXiv: 1807.05556`, `doi:10.1103/PhysRevD.99.034503`.

[830] M. Lüscher, Volume Dependence of the Energy Spectrum in Massive Quantum Field Theories. 1. Stable Particle States, Commun. Math. Phys. 104 (1986) 177. `doi:10.1007/BF01211589`.

[831] M. Lüscher, Volume Dependence of the Energy Spectrum in Massive Quantum Field Theories. 2. Scattering States, Commun. Math. Phys. 105 (1986) 153. `doi:10.1007/BF01211097`.

[832] M. Lüscher, Two-particle states on a torus and their relation to the scattering matrix, Nucl. Phys. B354 (1991) 531. `doi:10.1016/ 0550-3213(91)90366-6`.

[833] M. Lüscher, Signatures of unstable particles in finite volume, Nucl. Phys. B364 (1991) 237. `doi:10.1016/0550-3213(91)90584-K`.

[834] K. Rummukainen, S. A. Gottlieb, Resonance scattering phase shifts on a nonrest frame lattice, Nucl. Phys. B450 (1995) 397. `arXiv: hep-lat/9503028`, `doi:10.1016/0550-3213(95)00313-H`.

[835] X. Li, C. Liu, Two particle states in an asymmetric box, Phys. Lett. B587 (2004) 100. `arXiv:hep-lat/0311035`, `doi:10.1016/j. physletb.2004.02.068`.

[836] P. F. Bedaque, Aharonov-Bohm effect and nucleon nucleon phase shifts on the lattice, Phys. Lett. B593 (2004) 82. `arXiv:nucl-th/ 0402051`, `doi:10.1016/j.physletb.2004.04.045`.

[837] X. Feng, X. Li, C. Liu, Two particle states in an asymmetric box and the elastic scattering phases, Phys. Rev. D70 (2004) 014505. `arXiv: hep-lat/0404001`, `doi:10.1103/PhysRevD.70.014505`.

[838] N. H. Christ, C. Kim, T. Yamazaki, Finite volume corrections to the two-particle decay of states with non-zero momentum, Phys. Rev. D72 (2005) 114506. `arXiv:hep-lat/0507009`, `doi:10.1103/PhysRevD.72.114506`.

[839] C. H. Kim, C. T. Sachrajda, S. R. Sharpe, Finite-volume effects for two-hadron states in moving frames, Nucl. Phys. B727 (2005) 218. `arXiv:hep-lat/0507006`, `doi:10.1016/j.nuclphysb.2005.08.029`.

[840] S. He, X. Feng, C. Liu, Two particle states and the S-matrix elements in multi-channel scattering, JHEP 07 (2005) 011. `arXiv:hep-lat/ 0504019`, `doi:10.1088/1126-6708/2005/07/011`.

[841] M. Lage, U.-G. Meißner, A. Rusetsky, A method to measure the antikaon-nucleon scattering length in lattice QCD, Phys. Lett. B681 (2009) 439. `arXiv:0905.0069`, `doi:10.1016/j.physletb.2009.10.055`.

[842] V. Bernard, M. Lage, U. G. Meißner, A. Rusetsky, Scalar mesons in a finite volume, JHEP 01 (2011) 019. `arXiv:1010.6018`, `doi: 10.1007/JHEP01(2011)019`.

[843] M. Döring, U.-G. Meißner, E. Oset, A. Rusetsky, Unitarized Chiral Perturbation Theory in a finite volume: Scalar meson sector, Eur. Phys. J. A47 (2011) 139. `arXiv:1107.3988`, `doi:10.1140/epja/i2011-11139-7`.

[844] M. Döring, U. G. Meißner, Finite volume effects in pion-kaon scattering and reconstruction of the $\kappa(800)$ resonance, JHEP 01 (2012) 009. `arXiv:1111.0616`, `doi:10.1007/JHEP01(2012)009`.

[845] Z. Fu, Rummukainen-Gottlieb's formula on two-particle system with different mass, Phys. Rev. D85 (2012) 014506. `arXiv:1110.0319`,

doi:10.1103/PhysRevD.85.014506.

[846] L. Leskovec, S. Prelovsek, Scattering phase shifts for two particles of different mass and non-zero total momentum in lattice QCD, Phys. Rev. D85 (2012) 114507. arXiv:1202.2145, doi:10.1103/PhysRevD.85.114507.

[847] M. Göckeler, R. Horsley, M. Lage, U. G. Meißner, P. E. L. Rakow, A. Rusetsky, G. Schierholz, J. M. Zanotti, Scattering phases for meson and baryon resonances on general moving-frame lattices, Phys. Rev. D86 (2012) 094513. arXiv:1206.4141, doi:10.1103/PhysRevD.86.094513.

[848] M. Döring, U. G. Meißner, E. Oset, A. Rusetsky, Scalar mesons moving in a finite volume and the role of partial wave mixing, Eur. Phys. J. A48 (2012) 114. arXiv:1205.4838, doi:10.1140/epja/i2012-12114-6.

[849] M. T. Hansen, S. R. Sharpe, Multiple-channel generalization of Lellouch-Lüscher formula, Phys. Rev. D86 (2012) 016007. arXiv:1204.0826, doi:10.1103/PhysRevD.86.016007.

[850] R. A. Briceno, Z. Davoudi, Moving multichannel systems in a finite volume with application to proton-proton fusion, Phys. Rev. D88 (2013) 094507. arXiv:1204.1110, doi:10.1103/PhysRevD.88.094507.

[851] P. Guo, J. Dudek, R. Edwards, A. P. Szczepaniak, Coupled-channel scattering on a torus, Phys. Rev. D88 (2013) 014501. arXiv:1211.0929, doi:10.1103/PhysRevD.88.014501.

[852] N. Li, C. Liu, Generalized Lscher formula in multichannel baryon-meson scattering, Phys. Rev. D87 (2013) 014502. arXiv:1209.2201, doi:10.1103/PhysRevD.87.014502.

[853] D. Agadjanov, U.-G. Meißner, A. Rusetsky, Partial twisting for scalar mesons, JHEP 01 (2014) 103. arXiv:1310.7183, doi:10.1007/JHEP01(2014)103.

[854] R. A. Briceno, Z. Davoudi, T. C. Luu, M. J. Savage, Two-Baryon Systems with Twisted Boundary Conditions, Phys. Rev. D89 (2014) 074509. arXiv:1311.7686, doi:10.1103/PhysRevD.89.074509.

[855] R. A. Briceno, Two-particle multichannel systems in a finite volume with arbitrary spin, Phys. Rev. D89 (2014) 074507. arXiv:1401.3312, doi:10.1103/PhysRevD.89.074507.

[856] N. Li, S.-Y. Li, C. Liu, Generalized Lschers formula in multichannel baryon-baryon scattering, Phys. Rev. D90 (2014) 034509. arXiv:1401.5569, doi:10.1103/PhysRevD.90.034509.

[857] F. X. Lee, A. Alexandru, Scattering phase-shift formulas for mesons and baryons in elongated boxes, Phys. Rev. D96 (2017) 054508. arXiv:1706.00262, doi:10.1103/PhysRevD.96.054508.

[858] R. A. Briceno, Z. Davoudi, Three-particle scattering amplitudes from a finite volume formalism, Phys. Rev. D87 (2013) 094507. arXiv:1212.3398, doi:10.1103/PhysRevD.87.094507.

[859] K. Polejaeva, A. Rusetsky, Three particles in a finite volume, Eur. Phys. J. A48 (2012) 67. arXiv:1203.1241, doi:10.1140/epja/i2012-12067-8.

[860] S. Kreuzer, H. W. Griesshammer, Three particles in a finite volume: The breakdown of spherical symmetry, Eur. Phys. J. A48 (2012) 93. arXiv:1205.0277, doi:10.1140/epja/i2012-12093-6.

[861] M. T. Hansen, S. R. Sharpe, Relativistic, model-independent, three-particle quantization condition, Phys. Rev. D90 (2014) 116003. arXiv:1408.5933, doi:10.1103/PhysRevD.90.116003.

[862] U.-G. Meißner, G. Rios, A. Rusetsky, Spectrum of three-body bound states in a finite volume, Phys. Rev. Lett. 114 (2015) 091602, [Erratum: Phys. Rev. Lett. 117 (2016) 069902]. arXiv:1412.4969, doi:10.1103/PhysRevLett.117.069902,10.1103/PhysRevLett.114.091602.

[863] M. T. Hansen, S. R. Sharpe, Expressing the three-particle finite-volume spectrum in terms of the three-to-three scattering amplitude, Phys. Rev. D92 (2015) 114509. arXiv:1504.04248, doi:10.1103/PhysRevD.92.114509.

[864] M. T. Hansen, S. R. Sharpe, Perturbative results for two and three particle threshold energies in finite volume, Phys. Rev. D93 (2016) 014506. arXiv:1509.07929, doi:10.1103/PhysRevD.93.014506.

[865] M. T. Hansen, S. R. Sharpe, Threshold expansion of the three-particle quantization condition, Phys. Rev. D93 (2016) 096006, [Erratum: Phys. Rev. D96 (2017) 039901(2017)]. arXiv:1602.00324, doi:10.1103/PhysRevD.96.039901,10.1103/PhysRevD.93.096006.

[866] M. T. Hansen, S. R. Sharpe, Applying the relativistic quantization condition to a three-particle bound state in a periodic box, Phys. Rev. D95 (2017) 034501. arXiv:1609.04317, doi:10.1103/PhysRevD.95.034501.

[867] R. A. Briceno, M. T. Hansen, S. R. Sharpe, Relating the finite-volume spectrum and the two-and-three-particle S matrix for relativistic systems of identical scalar particles, Phys. Rev. D95 (2017) 074510. arXiv:1701.07465, doi:10.1103/PhysRevD.95.074510.

[868] H.-W. Hammer, J.-Y. Pang, A. Rusetsky, Three-particle quantization condition in a finite volume: 1. The role of the three-particle force, JHEP 09 (2017) 109. arXiv:1706.07700, doi:10.1007/JHEP09(2017)109.

[869] H. W. Hammer, J. Y. Pang, A. Rusetsky, Three particle quantization condition in a finite volume: 2. general formalism and the analysis of data, JHEP 10 (2017) 115. arXiv:1707.02176, doi:10.1007/JHEP10(2017)115.

[870] M. Mai, M. Döring, Three-body Unitarity in the Finite Volume, Eur. Phys. J. A53 (2017) 240. arXiv:1709.08222, doi:10.1140/epja/i2017-12440-1.

[871] R. A. Briceno, M. T. Hansen, S. R. Sharpe, Three-particle systems with resonant subprocesses in a finite volume, Phys. Rev. D99 (2019) 014516. arXiv:1810.01429, doi:10.1103/PhysRevD.99.014516.

[872] R. A. Briceno, M. T. Hansen, S. R. Sharpe, Numerical study of the relativistic three-body quantization condition in the isotropic approximation, Phys. Rev. D98 (2018) 014506. arXiv:1803.04169, doi:10.1103/PhysRevD.98.014506.

[873] M. Mai, M. Döring, Finite-Volume Spectrum of $\pi^+\pi^+$ and $\pi^+\pi^+\pi^+$ Systems, Phys. Rev. Lett. 122 (2019) 062503. arXiv:1807.04746, doi:10.1103/PhysRevLett.122.062503.

[874] M. Döring, H. W. Hammer, M. Mai, J. Y. Pang, A. Rusetsky, J. Wu, Three-body spectrum in a finite volume: the role of cubic symmetry, Phys. Rev. D97 (2018) 114508. arXiv:1802.03362, doi:10.1103/PhysRevD.97.114508.

[875] M. T. Hansen, S. R. Sharpe, Lattice QCD and Three-Particle Decays of Resonances, Ann. Rev. Nucl. Part. Sci. 69 (2019) 65. arXiv:1901.00483, doi:10.1146/annurev-nucl-101918-023723.

[876] T. D. Blanton, F. Romero-Lpez, S. R. Sharpe, Implementing the three-particle quantization condition including higher partial waves, JHEP 03 (2019) 106. arXiv:1901.07095, doi:10.1007/JHEP03(2019)106.

[877] J.-Y. Pang, J.-J. Wu, H. W. Hammer, U.-G. Meißner, A. Rusetsky, Energy shift of the three-particle system in a finite volume, Phys. Rev. D99 (2019) 074513. arXiv:1902.01111, doi:10.1103/PhysRevD.99.074513.

[878] C. Hanhart, J. R. Peláez, G. Rios, Quark mass dependence of the rho and sigma from dispersion relations and Chiral Perturbation Theory, Phys. Rev. Lett. 100 (2008) 152001. arXiv:0801.2871, doi:10.1103/PhysRevLett.100.152001.

[879] G. Rios, A. Gomez Nicola, C. Hanhart, J. R. Peláez, Chiral extrapolation of the sigma and rho mesons from dispersion relations and Chiral Perturbation Theory, AIP Conf. Proc. 1030 (2008) 268. arXiv:0803.4318, doi:10.1063/1.2973511.

[880] M. Döring, J. Haidenbauer, U.-G. Meißner, A. Rusetsky, Dynamical coupled-channel approaches on a momentum lattice, Eur. Phys. J. A47 (2011) 163. arXiv:1108.0676, doi:10.1140/epja/i2011-11163-7.

[881] J. Nebreda, J. R. Peláez, G. Rios, Chiral extrapolation of pion-pion scattering phase shifts within standard and unitarized Chiral Perturbation Theory, Phys. Rev. D83 (2011) 094011. arXiv:1101.2171, doi:10.1103/PhysRevD.83.094011.

[882] H.-X. Chen, E. Oset, $\pi\pi$ interaction in the ρ channel in finite volume, Phys. Rev. D87 (2013) 016014. arXiv:1202.2787, doi:10.1103/PhysRevD.87.016014.

[883] M. Albaladejo, C. Hidalgo-Duque, J. Nieves, E. Oset, Hidden charm molecules in finite volume, Phys. Rev. D88 (2013) 014510. arXiv:1304.1439, doi:10.1103/PhysRevD.88.014510.

[884] E. J. Garzon, R. Molina, A. Hosaka, E. Oset, Strategies for an accurate determination of the X(3872) energy from QCD lattice simulations, Phys. Rev. D89 (2014) 014504. arXiv:1310.0972, doi:10.1103/PhysRevD.89.014504.

[885] J.-J. Wu, T. S. H. Lee, A. W. Thomas, R. D. Young, Finite-volume Hamiltonian method for coupled-channels interactions in lattice QCD, Phys. Rev. C90 (2014) 055206. arXiv:1402.4868, doi:10.1103/PhysRevC.90.055206.

[886] D. Agadjanov, M. Döring, M. Mai, U.-G. Meißner, A. Rusetsky, The Optical Potential on the Lattice, JHEP 06 (2016) 043. arXiv:1603.07205, doi:10.1007/JHEP06(2016)043.

[887] V. Bernard, M. Lage, U.-G. Meißner, A. Rusetsky, Resonance properties from the finite-volume energy spectrum, JHEP 08 (2008) 024. arXiv:0806.4495, doi:10.1088/1126-6708/2008/08/024.

[888] P. Giudice, D. McManus, M. Peardon, Comparison of analysis techniques for extracting resonance parameters from lattice Monte Carlo data, Phys. Rev. D86 (2012) 074516. arXiv:1204.2745, doi:10.1103/PhysRevD.86.074516.

[889] N. Ishii, S. Aoki, T. Hatsuda, Nuclear Force from Lattice QCD, Phys. Rev. Lett. 99 (2007) 022001. arXiv:nucl-th/0611096, doi:10.1103/PhysRevLett.99.022001.

[890] S. Aoki, T. Hatsuda, N. Ishii, Theoretical Foundation of the Nuclear Force in QCD and its applications to Central and Tensor Forces in Quenched Lattice QCD Simulations, Prog. Theor. Phys. 123 (2010) 89. arXiv:0909.5585, doi:10.1143/PTP.123.89.

[891] S. Aoki, N. Ishii, T. Doi, T. Hatsuda, Y. Ikeda, T. Inoue, K. Murano, H. Nemura, K. Sasaki, Extraction of Hadron Interactions above Inelastic Threshold in Lattice QCD, Proc. Japan Acad. B87 (2011) 509. arXiv:1106.2281, doi:10.2183/pjab.87.509.

[892] N. Ishii, S. Aoki, T. Doi, T. Hatsuda, Y. Ikeda, T. Inoue, K. Murano, H. Nemura, K. Sasaki, Hadronhadron interactions from imaginary-time NambuBetheSalpeter wave function on the lattice, Phys. Lett. B712 (2012) 437. arXiv:1203.3642, doi:10.1016/j.physletb.2012.04.076.

[893] S. Aoki, T. Doi, T. Hatsuda, Y. Ikeda, T. Inoue, N. Ishii, K. Murano, H. Nemura, K. Sasaki, Lattice QCD approach to Nuclear Physics, PTEP 2012 (2012) 01A105. arXiv:1206.5088, doi:10.1093/ptep/pts010.

[894] S. Aoki, B. Charron, T. Doi, T. Hatsuda, T. Inoue, N. Ishii, Construction of energy-independent potentials above inelastic thresholds in quantum field theories, Phys. Rev. D87 (2013) 034512. arXiv:1212.4896, doi:10.1103/PhysRevD.87.034512.

[895] S. Aoki, N. Ishii, T. Doi, Y. Ikeda, T. Inoue, Asymptotic behavior of Nambu-Bethe-Salpeter wave functions for multiparticles in quantum field theories, Phys. Rev. D88 (2013) 014036. arXiv:1303.2210, doi:10.1103/PhysRevD.88.014036.

[896] S. Aoki, Nucleon-nucleon interactions via Lattice QCD: Methodology, Eur. Phys. J. A49 (2013) 81. arXiv:1309.4150, doi:10.1140/epja/i2013-13081-0.

[897] Y. Namekawa, T. Yamazaki, Scattering amplitude from Bethe-Salpeter wave function inside the interaction range, Phys. Rev. D98 (2018) 011501. arXiv:1712.10141, doi:10.1103/PhysRevD.98.011501.

[898] T. Yamazaki, Y. Kuramashi, Relation between scattering amplitude and Bethe-Salpeter wave function in quantum field theory, Phys. Rev. D96 (2017) 114511. arXiv:1709.09779, doi:10.1103/PhysRevD.96.114511.

[899] S. Aoki, T. Doi, T. Hatsuda, N. Ishii, Comment on Relation between scattering amplitude and Bethe-Salpeter wave function in quantum field theory, Phys. Rev. D98 (2018) 038501. arXiv:1711.09344, doi:10.1103/PhysRevD.98.038501.

[900] T. Yamazaki, Y. Kuramashi, Reply to "Comment on 'Relation between scattering amplitude and Bethe-Salpeter wave function in quantum field theory'", Phys. Rev. D98 (2018) 038502. arXiv:1808.06299, doi:10.1103/PhysRevD.98.038502.

[901] T. Iritani, S. Aoki, T. Doi, S. Gongyo, T. Hatsuda, Y. Ikeda, T. Inoue, N. Ishii, H. Nemura, K. Sasaki, Systematics of the HAL QCD Potential at Low Energies in Lattice QCD, Phys. Rev. D99 (2019) 014514. arXiv:1805.02365, doi:10.1103/PhysRevD.99.014514.

[902] R. A. Briceno, J. J. Dudek, R. D. Young, Scattering processes and resonances from lattice QCD, Rev. Mod. Phys. 90 (2018) 025001. arXiv:1706.06223, doi:10.1103/RevModPhys.90.025001.

[903] S. Aoki, et al., Lattice QCD calculation of the ρ meson decay width, Phys. Rev. D76 (2007) 094506. arXiv:0708.3705, doi:10.1103/PhysRevD.76.094506.

[904] X. Feng, K. Jansen, D. B. Renner, Resonance parameters of the ρ meson from Lattice QCD, Phys. Rev. D83 (2011) 094505. arXiv:1011.5288, doi:10.1103/PhysRevD.83.094505.

[905] S. Aoki, et al., ρ Meson Decay in 2+1 Flavor Lattice QCD, Phys. Rev. D84 (2011) 094505. arXiv:1106.5365, doi:10.1103/PhysRevD.84.094505.

[906] C. B. Lang, D. Mohler, S. Prelovsek, M. Vidmar, Coupled channel analysis of the ρ meson decay in lattice QCD, Phys. Rev. D84 (2011) 054503, [Erratum: Phys. Rev. D89 (2014) 059903]. arXiv:1105.5636, doi:10.1103/PhysRevD.89.059903, 10.1103/PhysRevD.84.054503.

[907] J. J. Dudek, R. G. Edwards, C. E. Thomas, Energy dependence of the ρ resonance in $\pi\pi$ elastic scattering from lattice QCD, Phys. Rev. D87 (2013) 034505, [Erratum: Phys. Rev. D90 (2014) 099902]. arXiv:1212.0830, doi:10.1103/PhysRevD.87.034505, 10.1103/PhysRevD.90.099902.

[908] C. Pelissier, A. Alexandru, Resonance parameters of the rho-meson from asymmetrical lattices, Phys. Rev. D87 (2013) 014503. `arXiv:1211.0092`, `doi:10.1103/PhysRevD.87.014503`.

[909] D. J. Wilson, R. A. Briceno, J. J. Dudek, R. G. Edwards, C. E. Thomas, Coupled $\pi\pi, K\bar{K}$ scattering in P-wave and the ρ resonance from lattice QCD, Phys. Rev. D92 (2015) 094502. `arXiv:1507.02599`, `doi:10.1103/PhysRevD.92.094502`.

[910] G. S. Bali, S. Collins, A. Cox, G. Donald, M. Göckeler, C. B. Lang, A. Schfer, ρ and K^* resonances on the lattice at nearly physical quark masses and $N_f = 2$, Phys. Rev. D93 (2016) 054509. `arXiv:1512.08678`, `doi:10.1103/PhysRevD.93.054509`.

[911] D. R. Bolton, R. A. Briceno, D. J. Wilson, Connecting physical resonant amplitudes and lattice QCD, Phys. Lett. B757 (2016) 50. `arXiv:1507.07928`, `doi:10.1016/j.physletb.2016.03.043`.

[912] J. Bulava, B. Fahy, B. Horz, K. J. Juge, C. Morningstar, C. H. Wong, $I = 1$ and $I = 2 \pi - \pi$ scattering phase shifts from $N_{\mathrm{f}} = 2 + 1$ lattice QCD, Nucl. Phys. B910 (2016) 842. `arXiv:1604.05593`, `doi:10.1016/j.nuclphysb.2016.07.024`.

[913] D. Guo, A. Alexandru, R. Molina, M. Döring, Rho resonance parameters from lattice QCD, Phys. Rev. D94 (2016) 034501. `arXiv:1605.03993`, `doi:10.1103/PhysRevD.94.034501`.

[914] B. Hu, R. Molina, M. Döring, A. Alexandru, Two-flavor Simulations of the $\rho(770)$ and the Role of the $K\bar{K}$ Channel, Phys. Rev. Lett. 117 (2016) 122001. `arXiv:1605.04823`, `doi:10.1103/PhysRevLett.117.122001`.

[915] Z. Fu, L. Wang, Studying the ρ resonance parameters with staggered fermions, Phys. Rev. D94 (2016) 034505. `arXiv:1608.07478`, `doi:10.1103/PhysRevD.94.034505`.

[916] B. Hu, R. Molina, M. Döring, M. Mai, A. Alexandru, Chiral extrapolations of the $\rho(770)$ meson in $N_f = 2 + 1$ lattice QCD simulations, Phys. Rev. D96 (2017) 034520. `arXiv:1704.06248`, `doi:10.1103/PhysRevD.96.034520`.

[917] C. Alexandrou, L. Leskovec, S. Meinel, J. Negele, S. Paul, M. Petschlies, A. Pochinsky, G. Rendon, S. Syritsyn, P-wave $\pi\pi$ scattering and the ρ resonance from lattice QCD, Phys. Rev. D96 (2017) 034525. `arXiv:1704.05439`, `doi:10.1103/PhysRevD.96.034525`.

[918] C. Andersen, J. Bulava, B. Horz, C. Morningstar, The $I = 1$ pion-pion scattering amplitude and timelike pion form factor from $N_{\mathrm{f}} = 2 + 1$ lattice QCD, Nucl. Phys. B939 (2019) 145. `arXiv:1808.05007`, `doi:10.1016/j.nuclphysb.2018.12.018`.

[919] J. J. Dudek, R. G. Edwards, M. J. Peardon, D. G. Richards, C. E. Thomas, Toward the excited meson spectrum of dynamical QCD, Phys. Rev. D82 (2010) 034508. `arXiv:1004.4930`, `doi:10.1103/PhysRevD.82.034508`.

[920] G. S. Bali, S. Collins, C. Ehmann, Charmonium spectroscopy and mixing with light quark and open charm states from $n_F = 2$ lattice QCD, Phys. Rev. D84 (2011) 094506. `arXiv:1110.2381`, `doi:10.1103/PhysRevD.84.094506`.

[921] D. Mohler, S. Prelovsek, R. M. Woloshyn, $D\pi$ scattering and D meson resonances from lattice QCD, Phys. Rev. D87 (2013) 034501. `arXiv:1208.4059`, `doi:10.1103/PhysRevD.87.034501`.

[922] L. Levkova, C. DeTar, Charm annihilation effects on the hyperfine splitting in charmonium, Phys. Rev. D83 (2011) 074504. `arXiv:1012.1837`, `doi:10.1103/PhysRevD.83.074504`.

[923] S. Prelovsek, L. Leskovec, Evidence for $X(3872)$ from DD^* scattering on the lattice, Phys. Rev. Lett. 111 (2013) 192001. `arXiv:1307.5172`, `doi:10.1103/PhysRevLett.111.192001`.

[924] M. Padmanath, C. B. Lang, S. Prelovsek, $X(3872)$ and $Y(4140)$ using diquark-antidiquark operators with lattice QCD, Phys. Rev. D92 (2015) 034501. `arXiv:1503.03257`, `doi:10.1103/PhysRevD.92.034501`.

[925] V. Baru, E. Epelbaum, A. A. Filin, J. Gegelia, A. V. Nefediev, Binding energy of the $X(3872)$ at unphysical pion masses, Phys. Rev. D92 (2015) 114016. `arXiv:1509.01789`, `doi:10.1103/PhysRevD.92.114016`.

[926] M. Jansen, H. W. Hammer, Y. Jia, Finite volume corrections to the binding energy of the $X(3872)$, Phys. Rev. D92 (2015) 114031. `arXiv:1505.04099`, `doi:10.1103/PhysRevD.92.114031`.

[927] C. B. Lang, L. Leskovec, D. Mohler, S. Prelovsek, Vector and scalar charmonium resonances with lattice QCD, JHEP 09 (2015) 089. `arXiv:1503.05363`, `doi:10.1007/JHEP09(2015)089`.

[928] S. Ozaki, S. Sasaki, Lüscher's finite size method with twisted boundary conditions: An application to the J/ψ-ϕ system to search for a narrow resonance, Phys. Rev. D87 (2013) 014506. `arXiv:1211.5512`, `doi:10.1103/PhysRevD.87.014506`.

[929] G. K. C. Cheung, C. E. Thomas, J. J. Dudek, R. G. Edwards, Tetraquark operators in lattice QCD and exotic flavour states in the charm sector, JHEP 11 (2017) 033. `arXiv:1709.01417`, `doi:10.1007/JHEP11(2017)033`.

[930] S. Prelovsek, C. B. Lang, L. Leskovec, D. Mohler, Study of the Z_c^+ channel using lattice QCD, Phys. Rev. D91 (2015) 014504. `arXiv:1405.7623`, `doi:10.1103/PhysRevD.91.014504`.

[931] S. Prelovsek, L. Leskovec, Search for $Z_c^+(3900)$ in the 1^{+-} Channel on the Lattice, Phys. Lett. B727 (2013) 172. `arXiv:1308.2097`, `doi:10.1016/j.physletb.2013.10.009`.

[932] M. Albaladejo, P. Fernandez-Soler, J. Nieves, $Z_c(3900)$: Confronting theory and lattice simulations, Eur. Phys. J. C76 (2016) 573. `arXiv:1606.03008`, `doi:10.1140/epjc/s10052-016-4427-8`.

[933] Y. Chen, et al., Low-energy scattering of the $(D\bar{D}^*)^\pm$ system and the resonance-like structure $Z_c(3900)$, Phys. Rev. D89 (2014) 094506. `arXiv:1403.1318`, `doi:10.1103/PhysRevD.89.094506`.

[934] Y. Chen, et al., Low-energy Scattering of $(D^*\bar{D}^*)^\pm$ System and the Resonance-like Structure $Z_c(4025)$, Phys. Rev. D92 (2015) 054507. `arXiv:1503.02371`, `doi:10.1103/PhysRevD.92.054507`.

[935] T. Chen, et al., A Lattice Study of $(\bar{D}_1D^*)^\pm$ Near-threshold Scattering, Phys. Rev. D93 (2016) 114501. `arXiv:1602.00200`, `doi:10.1103/PhysRevD.93.114501`.

[936] T. Iritani, S. Aoki, T. Doi, T. Hatsuda, Y. Ikeda, T. Inoue, N. Ishii, H. Nemura, K. Sasaki, Consistency between Lschers finite volume method and HAL QCD method for two-baryon systems in lattice QCD, JHEP 03 (2019) 007. `arXiv:1812.08539`, `doi:10.1007/JHEP03(2019)007`.

[937] J. Haidenbauer, U.-G. Meißner, Phenomenological view on baryon-baryon potentials from lattice QCD simulations, Eur. Phys. J. A55 (2019) 70. `arXiv:1901.01801`, `doi:10.1140/epja/i2019-12736-0`.

[938] Y. Ikeda, B. Charron, S. Aoki, T. Doi, T. Hatsuda, T. Inoue, N. Ishii, K. Murano, H. Nemura, K. Sasaki, Charmed tetraquarks T_{cc} and T_{cs} from dynamical lattice QCD simulations, Phys. Lett. B729 (2014) 85. `arXiv:1311.6214`, `doi:10.1016/j.physletb.2014.01.002`.

[939] Y. Ikeda, S. Aoki, T. Doi, S. Gongyo, T. Hatsuda, T. Inoue, T. Iritani, N. Ishii, K. Murano, K. Sasaki, Fate of the Tetraquark Candidate $Z_c(3900)$ from Lattice QCD, Phys. Rev. Lett. 117 (2016) 242001. `arXiv:1602.03465`, `doi:10.1103/PhysRevLett.117.242001`.

[940] Y. Ikeda, The tetraquark candidate Z_c(3900) from dynamical lattice QCD simulations, J. Phys. G45 (2018) 024002. `arXiv:1706.07300`, `doi:10.1088/1361-6471/aa9afd`.

[941] Y.-B. Yang, Y. Chen, L.-C. Gui, C. Liu, Y.-B. Liu, Z. Liu, J.-P. Ma, J.-B. Zhang, Lattice study on η_{c2} and X(3872), Phys. Rev. D87 (2013) 014501. `arXiv:1206.2086`, `doi:10.1103/PhysRevD.87.014501`.

[942] R. Lewis, R. M. Woloshyn, Higher angular momentum states of bottomonium in lattice NRQCD, Phys. Rev. D85 (2012) 114509. `arXiv:1204.4675`, `doi:10.1103/PhysRevD.85.114509`.

[943] M. Wurtz, R. Lewis, R. M. Woloshyn, Free-form smearing for bottomonium and B meson spectroscopy, Phys. Rev. D92 (2015) 054504. `arXiv:1505.04410`, `doi:10.1103/PhysRevD.92.054504`.

[944] A. Francis, R. J. Hudspith, R. Lewis, K. Maltman, Evidence for charm-bottom tetraquarks and the mass dependence of heavy-light tetraquark states from lattice QCD, Phys. Rev. D99 (2019) 054505. `arXiv:1810.10550`, `doi:10.1103/PhysRevD.99.054505`.

[945] P. Junnarkar, N. Mathur, M. Padmanath, Study of doubly heavy tetraquarks in Lattice QCD, Phys. Rev. D99 (2019) 034507. `arXiv:1810.12285`, `doi:10.1103/PhysRevD.99.034507`.

[946] L. Leskovec, S. Meinel, M. Pflaumer, M. Wagner, Lattice QCD investigation of a doubly-bottom $\bar{b}\bar{b}ud$ tetraquark with quantum numbers $I(J^P) = 0(1^+)$, Phys. Rev. D100 (2019) 014503. `arXiv:1904.04197`, `doi:10.1103/PhysRevD.100.014503`.

[947] A. Peters, P. Bicudo, L. Leskovec, S. Meinel, M. Wagner, Lattice QCD study of heavy-heavy-light-light tetraquark candidates, PoS LAT-TICE2016 (2016) 104. `arXiv:1609.00181`, `doi:10.22323/1.256.0104`.

[948] C. Hughes, E. Eichten, C. T. H. Davies, Searching for beauty-fully bound tetraquarks using lattice nonrelativistic QCD, Phys. Rev. D97 (2018) 054505. `arXiv:1710.03236`, `doi:10.1103/PhysRevD.97.054505`.

[949] P. Bicudo, M. Wagner, Lattice QCD signal for a bottom-bottom tetraquark, Phys. Rev. D87 (2013) 114511. `arXiv:1209.6274`, `doi:10.1103/PhysRevD.87.114511`.

[950] P. Bicudo, K. Cichy, A. Peters, B. Wagenbach, M. Wagner, Evidence for the existence of $ud\bar{b}\bar{b}$ and the non-existence of $ss\bar{b}\bar{b}$ and $cc\bar{b}\bar{b}$ tetraquarks from lattice QCD, Phys. Rev. D92 (2015) 014507. `arXiv:1505.00613`, `doi:10.1103/PhysRevD.92.014507`.

[951] P. Bicudo, M. Cardoso, A. Peters, M. Pflaumer, M. Wagner, $ud\bar{b}\bar{b}$ tetraquark resonances with lattice QCD potentials and the Born-Oppenheimer approximation, Phys. Rev. D96 (2017) 054510. `arXiv:1704.02383`, `doi:10.1103/PhysRevD.96.054510`.

[952] Z. S. Brown, K. Orginos, Tetraquark bound states in the heavy-light heavy-light system, Phys. Rev. D86 (2012) 114506. `arXiv:1210.1953`, `doi:10.1103/PhysRevD.86.114506`.

[953] M. Alberti, G. S. Bali, S. Collins, F. Knechtli, G. Moir, W. Söldner, Hadroquarkonium from lattice QCD, Phys. Rev. D95 (2017) 074501. `arXiv:1608.06537`, `doi:10.1103/PhysRevD.95.074501`.

[954] L. A. Griffiths, C. Michael, P. E. L. Rakow, Mesons With Excited Glue, Phys. Lett. 129B (1983) 351. `doi:10.1016/0370-2693(83)90680-9`.

[955] N. A. Campbell, L. A. Griffiths, C. Michael, P. E. L. Rakow, Mesons with excited glue from SU(3) lattice gauge theory, Phys. Lett. 142B (1984) 291. `doi:10.1016/0370-2693(84)91200-0`.

[956] N. A. Campbell, A. Huntley, C. Michael, Heavy Quark Potentials and Hybrid Mesons From SU(3) Lattice Gauge Theory, Nucl. Phys. B306 (1988) 51. `doi:10.1016/0550-3213(88)90170-8`.

[957] C. Michael, S. J. Perantonis, Potentials and glueballs at large beta in SU(2) pure gauge theory, J. Phys. G18 (1992) 1725. `doi:10.1088/0954-3899/18/11/005`.

[958] P. Bicudo, N. Cardoso, M. Cardoso, Color field densities of the quark-antiquark excited flux tubes in SU(3) lattice QCD, Phys. Rev. D98 (2018) 114507. `arXiv:1808.08815`, `doi:10.1103/PhysRevD.98.114507`.

[959] H. Al Ghoul, et al., First Results from The GlueX Experiment, AIP Conf. Proc. 1735 (2016) 020001. `arXiv:1512.03699`, `doi:10.1063/1.4949369`.

[960] J. Stevens, et al., The GlueX DIRC Project, JINST 11 (2016) C07010. `arXiv:1606.05645`, `doi:10.1088/1748-0221/11/07/C07010`.

[961] A. Bogomyagkov, E. Levichev, P. Piminov, Final focus designs for crab waist colliders, Phys. Rev. Accel. Beams 19 (2016) 121005. `doi:10.1103/PhysRevAccelBeams.19.121005`.

[962] T. Abe, et al., Belle II Technical Design Report`arXiv:1011.0352`.

[963] R. Aaij, et al., Physics case for an LHCb Upgrade II - Opportunities in flavour physics, and beyond, in the HL-LHC era`arXiv:1808.08865`.

[964] R. Aaij, et al., Observation of the $\Xi_b^- \to J/\psi \Lambda K^-$ decay, Phys. Lett. B772 (2017) 265. `arXiv:1701.05274`, `doi:10.1016/j.physletb.2017.06.045`.

[965] A. Lehrach, O. Boine-Frankenheim, F. Hinterberger, R. Maier, D. Prasuhn, Beam performance and luminosity limitations in the high-energy storage ring (HESR), Nucl. Instrum. Meth. A561 (2006) 289. `arXiv:physics/0511165`, `doi:10.1016/j.nima.2006.01.017`.

[966] G. Barucca, et al., Precision resonance energy scans with the PANDA experiment at FAIR: Sensitivity study for width and line-shape measurements of the X(3872), Eur. Phys. J. A55 (2019) 42. `arXiv:1812.05132`, `doi:10.1140/epja/i2019-12718-2`.

[967] J. Nebreda, J. R. Peláez, Strange and nonstrange quark mass dependence of elastic light resonances from SU(3) unitarized chiral perturbation theory to one loop, Phys. Rev. D81 (2010) 054035. `arXiv:1001.5237`, `doi:10.1103/PhysRevD.81.054035`.

[968] R. L. Jaffe, F. E. Low, The Connection Between Quark Model Eigenstates and Low-Energy Scattering, Phys. Rev. D19 (1979) 2105–2118. `doi:10.1103/PhysRevD.19.2105`.

[969] J. J. Dudek, R. G. Edwards, C. E. Thomas, D. J. Wilson, Resonances in coupled $\pi K - \eta K$ scattering from quantum chromodynamics, Phys. Rev. Lett. 113 (2014) 182001. `arXiv:1406.4158`, `doi:10.1103/PhysRevLett.113.182001`.

[970] D. J. Wilson, J. J. Dudek, R. G. Edwards, C. E. Thomas, Resonances in coupled $\pi K, \eta K$ scattering from lattice QCD, Phys. Rev. D91 (2015) 054008. `arXiv:1411.2004`, `doi:10.1103/PhysRevD.91.054008`.

[971] G. Moir, M. Peardon, S. M. Ryan, C. E. Thomas, D. J. Wilson, Coupled-Channel $D\pi$, $D\eta$ and $D_s\bar{K}$ Scattering from Lattice QCD, JHEP 10 (2016) 011. `arXiv:1607.07093`, `doi:10.1007/JHEP10(2016)011`.

[972] J. J. Dudek, R. G. Edwards, D. J. Wilson, An a_0 resonance in strongly coupled $\pi\eta$, $K\bar{K}$ scattering from lattice QCD, Phys. Rev. D93 (9) (2016) 094506. `arXiv:1602.05122`, `doi:10.1103/PhysRevD.93.094506`.

[973] R. A. Briceno, J. J. Dudek, R. G. Edwards, D. J. Wilson, Isoscalar $\pi\pi$, $K\bar{K}$, $\eta\eta$ scattering and the σ, f_0, f_2 mesons from QCD, Phys. Rev. D97 (2018) 054513. `arXiv:1708.06667`, `doi:10.1103/PhysRevD.97.054513`.

[974] A. Woss, C. E. Thomas, J. J. Dudek, R. G. Edwards, D. J. Wilson, Dynamically-coupled partial-waves in $\rho\pi$ isospin-2 scattering from lattice QCD, JHEP 07 (2018) 043. `arXiv:1802.05580`, `doi:10.1007/JHEP07(2018)043`.

[975] R. A. Briceno, J. J. Dudek, R. G. Edwards, C. J. Shultz, C. E. Thomas, D. J. Wilson, Resonant $\pi^+\gamma \to \pi^+\pi^0$ Amplitude from Quantum Chromodynamics, Phys. Rev. Lett. 115 (2015) 242001. `arXiv:1507.06622`, `doi:10.1103/PhysRevLett.115.242001`.

[976] R. A. Briceno, J. J. Dudek, R. G. Edwards, C. J. Shultz, C. E. Thomas, D. J. Wilson, $\pi\pi \to \pi\gamma^*$ amplitude and the resonant $\rho \to \pi\gamma^*$ transition from lattice QCD, Phys. Rev. D93 (2016) 114508. `arXiv:1604.03530`, `doi:10.1103/PhysRevD.93.114508`.

[977] C. Alexandrou, L. Leskovec, S. Meinel, J. Negele, S. Paul, M. Petschlies, A. Pochinsky, G. Rendon, S. Syritsyn, $\pi\gamma \to \pi\pi$ transition and the ρ radiative decay width from lattice QCD, Phys. Rev. D98 (2018) 074502. `arXiv:1807.08357`, `doi:10.1103/PhysRevD.98.074502`.